DEVELOPING NEW 3D HYDROGEL MODELS OF THE HUMAN MAMMARY GLAND TO INVESTIGATE BREAST CANCER INITIATION

A thesis submitted to the University of Manchester for the degree of

Doctor of Philosophy

in the Faculty of Biology, Medicine and Health

2022

ELIANA D. LINGARD

SCHOOL OF MEDICAL SCIENCES

Contents

Word count: 54,285 words.

Index of figures

Index of tables

Abstract

The breast extracellular matrix provides mammary epithelial cells with physical, biochemical, and mechanical cues that direct their fate and function. Individuals with dense breast tissue are at increased risk of developing breast cancer. Dense breast tissue is associated with increased extracellular collagen deposition and alignment, which studies have shown increases the mechanical stiffness of the breast matrix. This increased environmental stiffness is hypothesised to promote pro-oncogenic behaviours in mammary epithelial cells through mechanically driven signal transduction pathways. However, these mechanotransduction mechanisms are poorly defined. Investigating these mechanisms requires a consistent, defined and mechanically tuneable *in vitro* model of the breast microenvironment. Here, we show that synthetic peptide hydrogels can be mechanically and biochemically modified to recapitulate some of the key properties of the breast matrix. We demonstrate that laminin 111 is a major regulator of acinar morphogenesis in breast tissue that can be used to functionalise a negatively charged peptide hydrogel for mammary epithelial cell culture. Laminin 111 appears to direct acinar morphogenesis by stimulating cell adhesion formation and regulating cell proliferation. We also find evidence to suggest that oxidative stress in mammary epithelial cells can be regulated by matrix stiffness. We also show that we can collect accurate and reliable qualitative and quantitative data from peptide hydrogel-encapsulated mammary epithelial cells by adapting protocols to accommodate for their physical properties. Together, our findings show that we can use synthetic peptide hydrogels to accurately and consistently model breast matrix stiffness to investigate cryptic mechanosignalling mechanisms.

Declaration

No portion of the work referred to in the thesis has been submitted in support of an application for another degree or qualification of this or any other university or other institute of learning.

Copyright statement

Acknowledgements

I would first like to thank my supervisors Andrew Gilmore, Alberto Saiani, Joe Swift and Marco Domingos for their feedback and advice over the past few years. Their kindness, patience and support have been invaluable throughout my PhD studentship, and I would not be where I am today without them. I truly could not have asked for better supervisors and I hope I can thank them all in person soon.

Secondly, I would like to thank the past and present members of the Gilmore, Brennan, Swift, Ucar, Saiani and Domingos labs for their help and support. I particularly want to thank Matt Jones, Hannah Percival, Simon Saadati, Alis Hales, Bel Taylor-Hearn and Nathan Jariwala. Their support, assistance, and company kept me going through some challenging times and it was a pleasure working alongside them. Other notable mentions go to Rob Pedley, Ellie Appleton, Mel Kidd, and Anna Hoyle for their advice on mass spectrometry analysis; Helen Clough and Angela Imere for their feedback on my findings; and Cosimo Ligorio and Siyuan Dong for their assistance with oscillatory shear rheology.

Special thanks go to Craig Lawless for his invaluable support with my mass spectrometry analysis and for his endless patience with my many, many questions. My thanks also go to Aline Miller and Dammy Olayanju at Manchester BioGEL for their advice and constructive feedback on my findings. The results of my research are in good hands.

I thank my colleagues at Amega Sciences for providing a warm and friendly work environment that I am excited to return to. In particular, I thank Claire Forster and Chris Taylor for their support and understanding this past year. My thanks also go to the staff at Forge Coffee for providing me with a relaxing environment to write up in and for giving me an excuse to get out of the flat.

Thanks also go to my friends and family who made the sudden transition from Manchester to Northamptonshire as painless as possible. Special thanks go to Brenda Walker for providing me with my wonderful flat and for putting me forward for the part-time job at Amega. I could not have supported myself while writing without Brenda’s endless generosity and kindness and I am forever grateful. I would also like to thank my wonderful friends Colby Glover, Calum Bass-Twitchell, Catherine Butterworth, Ollie Smart, Jasmin Wächter and Sarah Gomes Munro for providing me with company, support and food when I most needed it over these past few years. Thank you also to my mum, who I am sure is looking forward to my having the time to clean my own flat again, and to my dad and my siblings Hanna, Freya, and Joe, who have cheered me on during the hardest periods of writing this year. To my lovely cat Jasper, thank you for your companionship and entertaining hijinks. You may be a bit of a croissant fiend, but I am very lucky to have you.

Finally, I thank the University of Manchester, the UK Regenerative Medicine Platform and Manchester BioGEL for funding this project and myself. Their financial support made it possible for me to work on this project and I am very grateful that I was given this incredible opportunity.

Thank you all.

Author Contributions

This thesis has been written in the journal format as this allowed me to construct a logical narrative from my findings. This thesis consists of an introduction section immediately followed its reference list, which is then followed by three chapters which are presented in the style of pre-publication journal articles. The first two chapters contain an abstract, an introduction, then a methods section, a results section, a discussion section, an acknowledgements section, and a reference section followed by supplementary materials. The third chapter is presented as a methodology paper, where the results and discussion sections are combined into one. There is also no supplementary section in the third chapter. The thesis concludes with a final discussion chapter and its reference section.

The following figures have been produced in collaboration with others:

Paper 1 (Mammary epithelial organoids cultured in a self-assembling peptide hydrogel exhibit stiffness-induced remodelling): Amplitude sweep measurements of Alpha4 hydrogels were performed with the assistance of Siyuan Dong (Fig. 3A, Fig. 4A, Fig. S1). Matrigel-alginate gels were made by Hannah Percival (Fig. 4B, Fig. S2). Mass spectrometry data analysis was performed with the help of Craig Lawless (Table 4, Figs. 7 – 10). All other work presented in this paper were performed by me.

Paper 2 (Functionalising a negatively charged self-assembling peptide hydrogel for mammary epithelial cell culture with laminin 111): Collagen I hydrogels were made by Alis Hales (Fig. 2A). Mass spectrometry data analysis was performed with the help of Craig Lawless (Figs. 6 – 8). All other work presented in this paper were performed by me.

Paper 3 (Optimising experimental procedures for self-assembling peptide hydrogels): Fluorescent MCF10a cell lines were made by Alis Hales and Isobel Taylor-Hearn with the assistance of Gareth Howell (Fig. 3). Amplitude sweep measurements of Alpha4 hydrogels were performed with the assistance of Siyuan Dong (Fig. 8A). Peptide hydrogel AFM was carried out with the help of Will Williams and Nigel Hodson (Figs. 8B – C). All other work presented in this paper were performed by me.

Abbreviations

- 2D - two-dimensional
- 3D - three-dimensional
- AEC - alveolar epithelial cell
- AFM - atomic force microscopy
- Akt - protein kinase B
- BioID - proximity-dependent biotin identification
- BM - basement membrane
- BSA - bovine serum albumin
- C - concentration
- Ca^{2+} - calcium cation
- $CaSO_4$ - calcium sulphate
- CGC - critical gelation content
- CS - chondroitin sulphate
- DAPI - 4′,6-diamidino-2-phenylindole
- dECM - decellularised ECM
- DMEM - Dulbecco's modified eagle medium
- DS - dermatan sulphate
- DTT - dithiothreitol
- EBP - elastin binding protein
- ECM - extracellular matrix
- EGF - epidermal growth factor
- EHS - Engelbreth-Holm-Swarm
- ERK - MAP kinase 1
- FACIT - fibril-associated collagens with interrupted triple helices
- FACS - fluorescence-activated cell sorting
- FAK - focal adhesion kinase
- FGF - fibroblast growth factor
- FGF-7 - keratinocyte growth factor
- FN - fibronectin
- GAG - glycosaminoglycan
- G-block - guluronic acid-rich regions
- GFP - green fluorescent protein
- GlcA - glucuronic acid
- GlcNAc - acetylglucosamine
- Gly - glycine
- GPI - glycosyl-phosphatidylinositol
- GSK - glycogen synthase kinase

- H2B - histone 2B
- HA - hyaluronan
- hPro - hydroxyproline
- HS - heparan sulphate
- HSer - horse serum
- IF - immunofluorescence
- kDa - kilodaltons
- kPa - kilopascals
- KS - keratan sulphate
- L4 - laminin IV domain
- LC-MS/MS - liquid chromatography-coupled tandem mass spectrometry
- LDV - lactate dehydrogenase-elevating virus
- LE - laminin-type epidermal growth factor-like domain
- LF - laminin IV domain
- LG - laminin globular domain
- LN - laminin N-terminal domain
- LOX - lysyl oxidase
- lrECM - laminin-rich extracellular matrix
- MAPK - Ras–mitogen-activated protein kinase
- MEC - mammary epithelial cell
- MMP - matrix metalloproteinase
- MVEC - microvascular endothelial cell
- NaOH - sodium hydroxide
- Pa - Pascals
- PAM - polyacrylamide
- PBS - phosphate-buffered saline
- PEG - polyethylene-glycol
- PI3K - phosphoinositide-3 kinase
- PLA - polylactic acid
- Pro - proline
- PTM - post-translational modification
- RALA - Ras-related protein Ral-A
- rBM - reconstituted basement membrane
- RFP - red fluorescent protein
- RIPA - radioimmunoprecipitation assay buffer
- ROCK - Rho-associated coiled-coil containing protein kinase
- ROS - reactive oxygen species
- RPMI - Roswell Park Memorial Institute
- RTK - receptor tyrosine kinase

- SAPH - self-assembling peptide hydrogel
- SD - standard deviation
- SDS - sodium dodecyl sulphate
- SEM - standard error of mean
- SLRP - short leucine-rich proteoglycan
- SFK - Src-family kinase
- TGF-β - transforming growth factor-β
- TNF - tumour necrosis factor
- VEGF - vascular endothelial growth factor
- W - Watts

General introduction

The extracellular matrix (ECM) is the non-cellular component of tissues that surrounds cells as a three-dimensional (3D), hydrated scaffold, providing cells with structural and functional support [1, 2]. ECM scaffolds are composed of macromolecules such as collagens, laminins, fibronectins, elastic fibres, and proteoglycans, which vary in abundance and composition between and within tissues [3]. The ECM also acts as a reservoir of bioactive molecules such as growth factors and matrix metalloproteases [4-6]. Together, the ECM network and its soluble factors supply cells with biophysical and biochemical cues which regulate their adhesion, growth, survival, motility, and differentiation [1, 2, 7].

The collective regulation of cell behaviour in tissues by the ECM directs tissue development, morphology, and homeostasis [2]. Since these processes are dynamic and require specific cell behaviours, the ECM is frequently remodelled in tissues to regulate cell organisation and fate. Here, reciprocal signalling interactions between the ECM and its cells remodel the ECM through changes in matrix protein organisation, synthesis, and degradation [8-10]. These remodelling events alter the biochemical and biomechanical properties of the ECM by changing the abundance and expression of matrix proteins and growth factors, which cells detect via cell-surface receptors [8, 11-14]. Following detection of these environmental changes, the cells process these cues through intracellular signal transduction pathways and adjust their behaviour accordingly.

Since the biochemical and biomechanical properties of the ECM have a profound effect on tissue function, these remodelling and homeostatic mechanisms are tightly controlled to ensure that tissues remain healthy and functional [9]. Dysfunctional matrix regulatory systems result in the development of diseases such as cancer, fibrosis, or connective tissue disorders [11, 15-18]. Although the underlying causes of some diseases have been linked to specific genetic mutations that contribute to improper ECM organisation and function, other initiators of ECM dysregulation that are responsible for driving tissue dysfunction are poorly defined, making some diseases challenging to prevent and treat [14, 19-24].

The development of 3D tissue models has benefited research into ECM dysfunction and its influence on cell behaviour. A range of 3D cell culture scaffolds exist that can be used to identify the molecular mechanisms that drive ECM dysfunction and examine their role in disease initiation and progression [25-31]. Using these 3D models, researchers can identify molecular targets for therapeutic interventions [32-34].

Here we describe the key components of the ECM, focusing on collagens and laminins, and cover the differences in structure and function between the two types of ECM: the interstitial matrix and basement membranes. We then discuss how mechanical forces influence tissue structure and function, and present case studies of *in vitro* ECM models that have been used to investigate how the biochemical and biophysical properties of tissue ECMs regulate tissue organisation and function in

health and disease. We evaluate the strengths and limitations of established models and cover promising new scaffolds for cell culture that can be used to model tissue ECMs and enhance our understanding of the dynamic molecular events between cells and their environment that collectively regulate tissue fate.

A range of macromolecules regulate ECM form and function

The ECM is composed of a complex mixture of macromolecules which entangle and interact with one another to form a 3D network [6, 35]. Although the composition and organisation of these macromolecules are unique within individual tissues, there are several classes of matrix macromolecules that are near-ubiquitously expressed within tissues, which we here refer to as the core matrisome [12]. The core matrisome includes collagens, glycoproteins such as laminins, elastins, proteoglycans and glycosaminoglycans (GAG) [3, 36]. Many matrix proteins share characteristic arrangements of domains, although the function of a given domain can vary wildly between different ECM proteins [37]. Many of these conserved ECM domains emerged in multicellular organisms approximately 700 million years ago, which shows that they are essential for ECM function and fundamental to metazoan life [38]. Together, these macromolecules interact with each other to form extracellular scaffolds that provide cells with essential structural support and biochemical cues that direct their fate (Fig. 1).

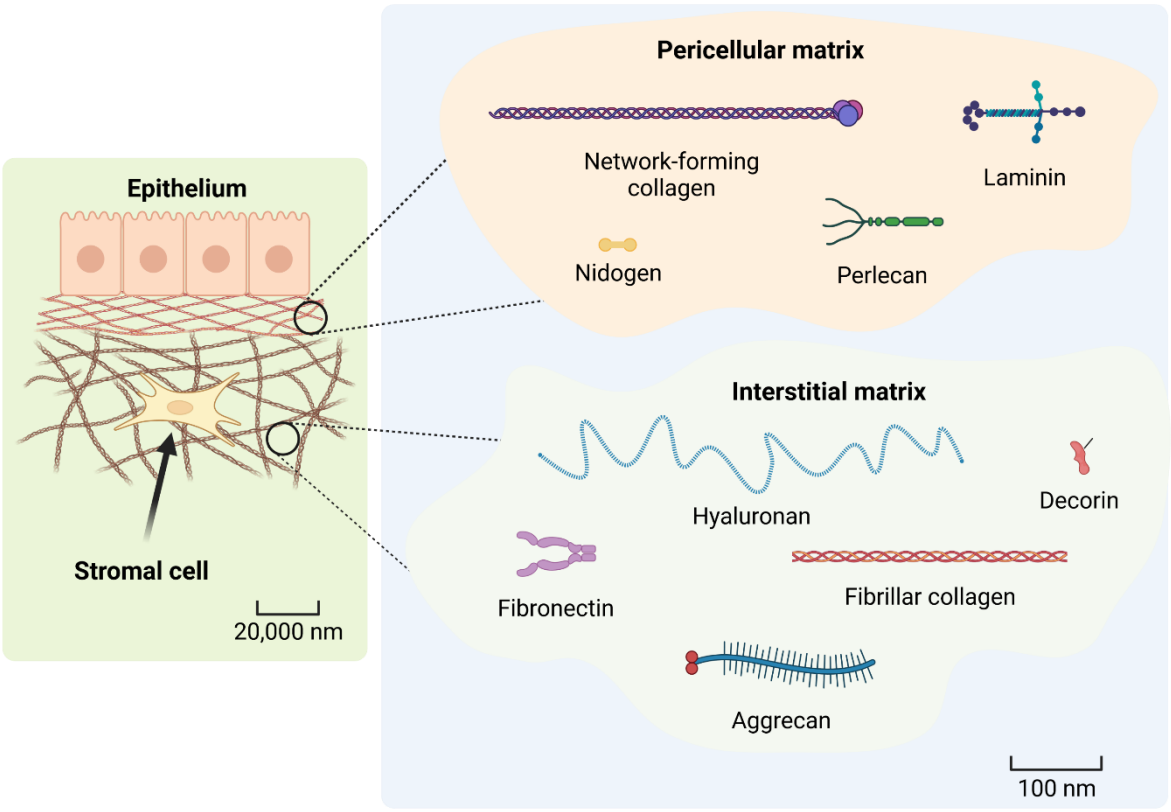

Fig. 1. Overview of extracellular matrices, some key matrix components and their comparative shapes and sizes. ECMs are divided into two matrix types: the pericellular matrix and the interstitial matrix. In epithelial tissues, the pericellular matrix separates epithelial cells from the surrounding interstitial matrix. Adapted from [3, 39]. Created with BioRender.com.

Collagens

Collagens are proteins that are present within all ECMs, providing essential structural support and mechanical strength to tissues [12, 40]. They are typically synthesised by specialised cells such as fibroblasts, osteoblasts, and chondrocytes, although some epithelial, endothelial, and parenchymal cells are also capable of synthesising collagens [36, 41]. Various supramolecular structures can be assembled from collagens to provide tissues with appropriate structural and functional scaffolding. Assembly of these supramolecular structures depends on the unique structural and functional properties of different collagen isoforms, which are localised to different tissues to provide tissue-specific mechanical, structural and functional properties [2, 42, 43]. Collagens consist of three polypeptide chains (α-chains) and bear a distinctive, rope-like triple-helix structure, although the prevalence of this structure within collagens ranges from 96% (collagen I) to <10% (collagen XII) [44, 45]. Many α-chain variants exist and consequently 29 collagens have been identified, each composed of a unique trimeric configuration of α-chains that govern their assembly and organisation into supramolecular structures (Table 1) [36, 43, 45, 46].

Assembly of the triple-helix structure (collagen domain) is initiated by the terminal ends of collagen molecules and stabilised by the glycine- (Gly)-X-Y amino acid motif within the α-chains, where the X and Y positions are often occupied by proline (Pro) and 4- hydroxyproline (hPro), respectively [36, 47-51]. Collagen domains are flanked and can be interrupted by other non-collagenous domains that give collagen molecules additional functionality, with increasing interruptions to the triple-helix motif increasing collagen flexibility [46, 51-56]. For example, fibril-associated collagens with interrupted triple helices (FACIT) have multiple interruptions between triple-helical motifs which enable them to associate with, organise and functionalise collagen fibrils [43]. Together, these domains give collagens their ability to assemble into supramolecular structures that impart tensile strength and anchorage sites to cells (Fig. 2) [36, 44, 45]. Consequently, alterations to these conserved domains, whether via genetic mutations or impaired amino acid modifications, result in impaired collagen assembly and ECM organisation, which leads to disease states such as scurvy or Alport syndrome [57-62].

Several other factors influence supramolecular collagen assembly and organisation, which in turn affect the mechanical and biochemical properties that collagen imparts within the ECM. Protease-mediated cleavage of the terminal ends of fibril-forming collagen molecules is critical for driving their self-assembly into fibrils, while incomplete cleavage of C- and N- termini in collagen types III, V and XI plays a key role in the regulation of fibril diameter in tendon and corneal tissues, and the intact N-terminus of collagen type IV is necessary for driving network formation in basement membranes [46, 54, 63-66]. Collagen organisation is not purely self-directed, however. Fibroblasts not only secrete collagen, but help direct its alignment, which influences tissue strength and structure [1]. Cross-linking enzymes such as lysyl oxidase (LOX) generate stabilising covalent bonds within collagen fibres, networks and filaments, and matrix glycoproteins such as fibronectin are crucial for fibril and filament assembly [67-70].

Collagen type	Chain configurations	Supramolecular structure	Tissue distribution
I	$[\alpha1(I)]_2\alpha2(I)]$ $[\alpha1(I)]_3$	Large diameter 67 nm banded fibrils 67 nm banded fibrils	Skin, cornea, tendon, bone, brain and spinal cord dura Dermis, tumours, bone
II	$[\alpha1(II)]_3$	67 nm banded fibrils	Cartilage, intervertebral disc, vitreous
III	$[\alpha1(III)]_3$	Small diameter 67 nm banded fibrils	Co-distribution with collagen I, skin, tendon, blood vessels, uterus, liver, spleen, around internal organs
IV	$[\alpha1(IV)_2\alpha2(IV)]$ also, α3(IV), α4(IV), α5(IV), α6(IV)	Nonfibrillar mesh	Basement membranes
V	$[\alpha1(V)]_2\alpha2(V)]$ $[\alpha1(V)\alpha2(V)\alpha3(V)]$ $[\alpha1(V)]_3$	9 nm diameter banded fibrils	Co-distribution with collagen I, dermis, cornea, bone, placenta, embryonic tissues, cell surfaces
VI	$[\alpha1(VI)\alpha2(VI)\alpha3(VI)]$	5-10 nm diameter beaded microfibrils	Dermis, cartilage, bone, muscle, uterus
VII	$[\alpha1(VII)]_3$	Anchoring fibrils	Skin, cornea, mucosal epithelium, amniotic membrane, bladder
VIII	$[\alpha1(VIII)]_2\alpha2(VIII)]$	Nonfibrillar, hexagonal lattice	Endothelial cells, Descemet's membrane
IX	$[\alpha1(IX)\alpha2(IX)\alpha3(IX)]$	Nonfibrillar, FACIT	Cartilage, tendon, vitreous, co-distribution with collagen II
X	$[\alpha1(X)]_3$	Nonfibrillar, hexagonal lattice	Calcifying cartilage
XI	$[\alpha1(XI)\alpha2(XI)\alpha3(XI)]$	Fine fibrils like those of collagen V	Cartilage, intervertebral disc
XII	$[\alpha1(XII)]_3$	Nonfibrillar, FACIT	Dermis, tendon, cartilage
XIII	$[\alpha1(XIII)]_3$	Transmembrane	Neuromuscular junctions, epidermis, endothelial cells, heart, eye
XIV	$[\alpha1(XIV)]_3$	Nonfibrillar, FACIT	Dermis, tendon, cartilage, bone
XV	$[\alpha1(XV)]_3$	Nonfibrillar, Multiplexin	Basement membranes, eye, placenta, kidney, heart, ovary, testis
XVI	$[\alpha1(XVI)]_3$	Nonfibrillar, FACIT	Dermis, kidney, heart, muscle
XVII	$[\alpha1\ (XVII)]_3$	Membrane intercalated	Skin hemidesmosomes, specialised epithelia
XVIII	$[\alpha1(XVIII)]_3$	Nonfibrillar, Multiplexin	Basement membranes, kidney, liver
XIX	$[\alpha1(XIX)]_3$	Nonfibrillar, FACIT	Basement membranes, muscle cells, interneurons, developing hippocampal synapses, embryonic tissues, rhabdomyosarcoma
XX	$[\alpha1(XX)]_3$	FACIT	Tendon, embryonic skin, corneal epithelium, sternal cartilage
XXI	$[\alpha1(XXI)]_3$	FACIT	Kidney, blood vessel walls, stomach, secreted by smooth muscle cells
XXII	$[\alpha1(XXII)]_3$	FACIT	Tissue junctions
XXIII	$[\alpha1(XXIII)]_3$	Transmembrane	Heart, retina, prostate tumours
XXIV	$[\alpha1(XXIV)]_3$	Fibrillar, fibril-associated	Associated with collagen I fibrillogenesis, differentiating osteoblasts
XXV	$[\alpha1(XXV)]_3$	Transmembrane	Brain, heart, testis
XXVI	$[\alpha1(XXVI)]_3$	FACIT	Ovary, testis
XXVII	$[\alpha1(XXVII)]_3$	Thin, nonstriated fibrils	Hypertrophic cartilage
XXVIII	$[\alpha1(XXVIII)]_3$	Beaded filaments	Dermis, Schwann cell basement membranes, peripheral nervous system
XXIX	$[\alpha1(XXIX)]_3$	Nonfibrillar	Suprabasal cells in epidermis, lung, colon, small intestine, and testis

Table 1. Collagen family member characteristics and tissue distribution. FACIT, fibril-associated collagens with interrupted triple helices. Adapted from [3, 43].

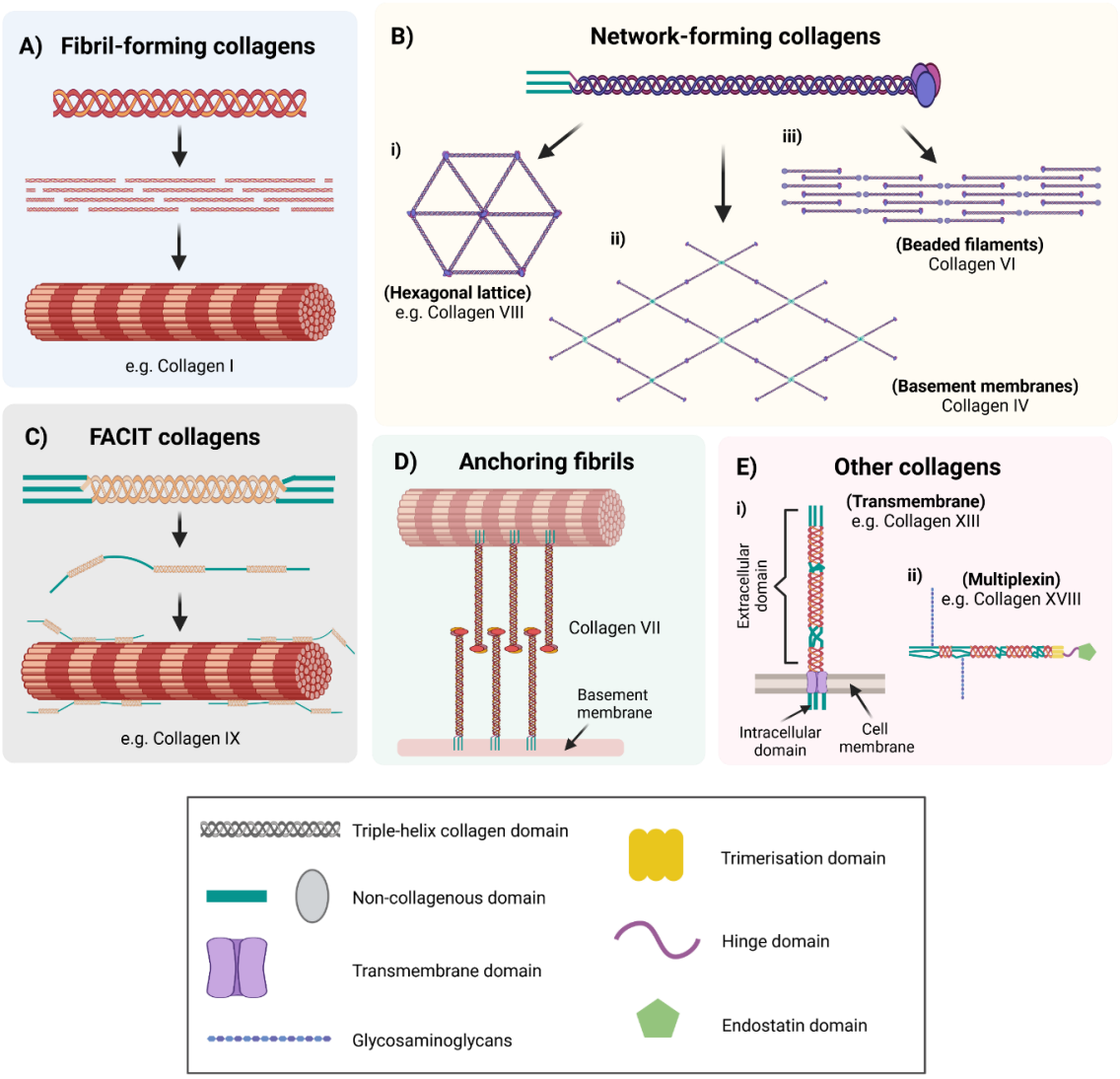

Fig. 2. Collagen subfamilies and their supramolecular assemblies. The collagen subfamilies are grouped according to structural homology and their assembly into distinct supramolecular structures. A) Fibril-forming collagens, such as collagen I, undergo terminal end processing which creates an uninterrupted triple-helical collagen domain. These processed collagens spontaneously assemble into staggered fibrils. These fibrils then fuse to create collagen bundles that are heavily cross-linked. B) Network-forming collagens. i) The non-collagenous domains (oval) of collagen VIII multimerise to create hexagonal lattices. ii) Collagen IV molecules assemble into a lattice in basement membranes. The non-collagenous C-terminal domains (oval) of collagen IV dimerise while their N-terminal domains (teal line) facilitate tetramerisation. End-to-end and lateral interactions between collagen IV dimers and tetramers finalise their assembly into a network. iii) Collagen VI molecules form disulphide-bonded, staggered dimers. These dimers laterally align to form tetramers, which then assemble into a microfibrillar network through end-to-end interactions between tetramers. C) The collagen domains (triple helix) of fibril-associated collagens with interrupted triple helices (FACIT), such as collagen IX, are interrupted by non-collagenous domains (teal line). FACITs associate with fibril-forming collagens. D) Collagen VII forms anchoring fibrils that tether basement membranes to collagen fibrils. Collagen VII molecules assemble into staggered dimers via C-terminal, non-collagenous domain (oval) interactions, which then laterally interact with other collagen VII dimers to create stable anchoring fibrils. E) Other collagens. i) Transmembrane collagens span cell membranes as they possess a hydrophobic transmembrane domain. They also have a large, C-terminal extracellular domain composed of repeat collagen domains (triple helix) interrupted with non-collagenous domains (teal line) and some, like collagen XIII, also have a smaller intracellular domain. ii) Multiplexin collagens such as collagen XVIII are composed of tandem collagen domain repeats that are interrupted by non-collagenous domains and sequences (teal line). They have glycosaminoglycan attachment sites at their N-terminal region, and they also have a distinctive C-terminus, which is comprised of a trimerisation domain, a hinge domain and an endostatin domain. The hinge domain can be cleaved to release the endostatin domain. Adapted from [36]. Created with BioRender.com.

Together, these regulatory factors help create diverse collagen scaffolds that meet the functional demands of tissues, whether that is forming a strong, crystallised matrix in bone tissue through calcification, aligning into cross-linked bundles of rigid fibrils in tendons or assembling into a highly ordered lattice of thin fibrils in the cornea [64, 71-73].

Laminins

Laminins are a family of glycoproteins that play key roles in ECM assembly and function. They are synthesised by many different cell types across tissues, including epithelial cells, endothelial cells, myocytes, and bone marrow cells [41, 74, 75]. Laminins are heterotrimeric, heavily glycated proteins that are composed of one α-, β- and γ-subunit each. Over 16 laminins are known to exist, which are made up from unique assemblies of the five α- (1-5), three β- (1-3) and three γ- (1-3) subunit isoforms (Table 2) [2, 3]. Laminins are named according to their subunit configuration, hence a laminin trimer with the subunit configuration α2β1γ1 is called laminin 211.

Laminin type	Subunit configuration	Tissue distribution
111	α1β1γ1	Embryonic epithelial tissue, brain, blood vessels and breast, kidney, liver, ovary, and testis epithelial tissue
121	α1β2γ1	Placenta
211	α2β1γ1	Heart, muscle, peripheral nerves, testis
212	α2β1γ2	Peripheral nerve
213	α2β1γ3	Placenta, testis
221	α2β2γ1	Heart, muscle, peripheral nerves, neuromuscular junctions
311 (3a11)	α3Aβ1γ1	Epidermis, amniotic membrane
321 (3a21)	α3Aβ2γ1	Epidermis, amniotic membrane
332 (3a32) 3b32	α3Aβ3γ2 α3Bβ3γ2	Skin, placenta, breast, lung, oesophagus Skin, breast, uterus, lung, oesophagus, blood vessel
411	α4β1γ1	Endothelial tissue, smooth muscle, fat, peripheral nerve
421	α4β2γ1	Endothelial tissue, smooth muscle, neuromuscular junction
423	α4β2γ3	Retina, central nervous system
511	α5β1γ1	Epithelial tissue, endothelial tissue, smooth muscle
521	α5β2γ1	Epithelial tissue, endothelial tissue, smooth muscle, neuromuscular junction, glomerular basement membrane
522	α5β2γ2	Bone marrow
523	α5β2γ3	Retina, central nervous system

Table 2. Laminin family member configurations and tissue distribution. '3a' and 'α3A' denote truncated α3 subunit, '3b' and 'α3B' denote full-length α3 subunit. Adapted from [76, 77].

With a few exceptions, all laminin subunits bear a conserved, globular laminin N-terminal (LN) domain that facilitates their polymerisation into supramolecular structures, in addition to repeat laminin-type epidermal growth factor-like (LE) domains that do not have defined functions but can bind other glycoproteins such as nidogens [3, 78, 79]. The C-termini of α-subunits also bear 5 modules called laminin globular (LG) domains, which together form a large, globular domain that interacts with cell-surface receptors and matrix proteins such as integrins, sulphated glycolipids and α-dystroglycan [80-83]. The three laminin subunits assemble through disulphide-bond interactions between their C-terminus coiled-coil domains to form trimers that often resemble a cruciform, although variations in subunit length and flexibility can result in the assembly of T-, Y- or I-shaped structures (Fig. 3) [2, 36, 78, 82, 84, 85]. Through interactions with cell surface moieties at their C-terminus and ECM

molecules via their N-terminal ‘arms’, laminins direct ECM organisation and facilitate communication between cells and their environment, which serves to regulate both cell and ECM function [3, 85].

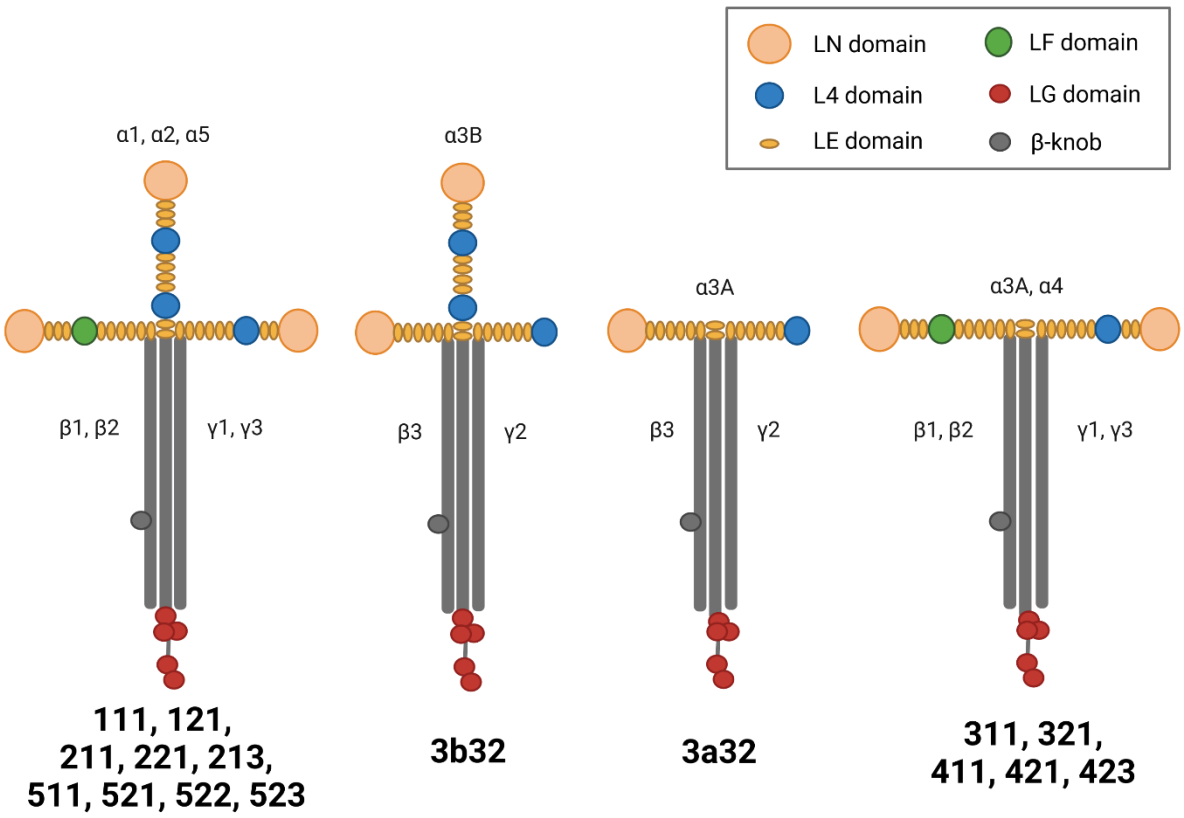

Fig. 3. Laminin heterotrimers and their major functional domains. The Greek letters α, β and γ denote subunits. Numbers below the heterotrimers indicate laminin trimers and their subunit composition. Major functional domains within the subunits are depicted. LN domain, laminin N-terminal domain; L4 domain, laminin IV domain; LE domain, laminin-type epidermal growth factor-like domain; LF domain, laminin IV domain; LG domain, laminin globular domain. Adapted from [82, 85]. Created with BioRender.com.

Laminins show tissue- and development-specific distribution [77, 85]. For example, laminin 111 is ubiquitous in embryonic epithelial tissues but is often replaced by other laminins such as laminin 511 and 521 as tissues mature, and laminin 332 is localised to epithelial basement membranes [41, 80, 86, 87]. This specificity is regulated by both cells and the ECM, as laminin synthesis is controlled by various environmental cues such as growth factor- and hormone- mediated signalling, integrin expression, and matrix stiffness [88-95]. Temporal- and tissue-specific laminin expression is essential for tissue function, as unique domain configurations within laminin subunit isoforms influence laminin glycosylation, polymerisation and substrate binding, which ultimately affect laminin’s interactions with cells and the ECM [82, 92, 96]. For example, most laminins bear three LN domains which collectively facilitate their homo-polymerisation into sheet-like networks that bind to the cell surface and provide cells with structural support and functional cues [97, 98]. Network-forming homo-polymers of laminin 3b32 (‘b’ here denotes a full-length α3 subunit) surround cells in the follicular epidermis and breast tissue and provide them with spatial cues that help direct their differentiation into specialised, functional structures [99-101]. Other domains present in the N-terminus of subunit isoforms confer additional functionality to laminins, as evidenced by the integrin-binding RGD motifs in the laminin α5 subunit that promote cell adhesion and migration [92, 102, 103]. Laminins that lack all three LN

domains cannot polymerise into networks and often bind cell surface or matrix proteins as monomers, although laminin 3a11 ('a' here denotes a truncated α3 subunit) can assemble into fibres with the help of β1 integrins [82, 101, 104-106]. In the lung alveolar ECM, these fibres closely associate with alveolar cells to facilitate alveolar stretch-relaxation cycles during ventilation [107].

The vital role laminins play in regulating cell organisation and behaviour means that defects in laminin synthesis, processing and assembly have severe impacts on tissue function and organismal health. Laminin 221 is a major component of the neuromuscular ECM and promotes muscle adhesion and stability, so partial or complete reduction in laminin α2 expression leads to muscular dystrophy [108]. Chronic skin blisters of varying severity can be caused by missense or deleterious laminin 3b32 subunit mutations, while impaired processing of the α3 and γ2 subunits prevents laminin 3b32 polymerisation and impairs hemidesmosome formation which results in the development of benign but persistent tumours [109, 110]. Laminin 3a32 (laminin 332) is a vital basement membrane component of mammary ductal structures that regulates epithelial cell homeostasis, differentiation, migration, and adhesion, and both its overexpression and absence have been implicated in the development of various breast cancers [111-115]. Impaired glycosylation events are suspected to promote metastasis in some tumours and heavy glycosylation of network-forming laminins appears to inhibit laminin network assembly and ligand binding, which have been proposed as causative mechanisms for tissue dysfunction in uncontrolled diabetes [96, 116-118]. Laminin 111 is often overexpressed by malignant cells as several of its domains promote cell migration and growth [119]. The variety and severity of diseases attributed to laminin dysfunction demonstrate their importance in tissue homeostasis, morphogenesis, and development.

Other glycoproteins

In addition to laminins, approximately 200 other glycoproteins are included in the human core matrisome [12]. Glycoproteins can play key roles in matrix organisation, mediate signalling events between cells and matrix components and control the release of soluble matrix factors such as transforming growth factor-β (TGF-β) [36, 120].

Fibronectin (FN) is an essential matrix glycoprotein which is ubiquitously expressed in tissues [121]. 20 isoforms of FN exist in humans, all of which are composed of two near-identical subunits that are covalently bound to each other at their C-termini via disulphide bridges to form flexible molecules that can extend to reveal various binding sites for cell-surface receptors and ECM molecules [121-123]. Their binding partners include integrins, collagens, heparins, fibrillins, laminins and other FN molecules, the latter of which allows FN to assemble into interconnected fibrillar networks between cells via integrin α5β1-RGD binding events [124, 125]. Through these interactions with cell-surface receptors and ECM molecules, FN regulates cell adhesion, migration and differentiation, and guides matrix assembly and organisation [69, 126, 127]. FN is so crucial for matrix and cell function that its absence in murine embryos causes developmental abnormalities, and several mutations that impair FN's ability to bind cell-surface receptors have been found to play a role in the development of some skeletal dysplasias [128, 129].

Fibrillins are large glycoproteins that assemble into microfibrils within tissues and are responsible for imparting tensile strength and elasticity to non-elastic and elastic tissues, respectively [130, 131]. Their assembly into microfibrils is driven by disulphide-bond interactions between their cysteine-rich domains and through binding interactions with integrins and heparins [130, 132-134]. The resultant microfibrils can associate with elastin to direct the formation of elastic fibres in lung, skin and blood vessel tissues which help them to withstand significant mechanical forces [120, 135]. In non-elastic tissues, fibrillin microfibrils frequently act as anchoring fibrils and can also control the release of growth factors that regulate cell survival and differentiation [36, 136, 137]. Because fibrillins provide numerous tissues with mechanical strength and flexibility, mutations in these glycoproteins or their absence cause a range of disorders that commonly affect the lungs, heart, skeleton, eyes and skin [136, 138].

Other key matrix glycoproteins include the tenascins, which are large multidomain proteins that regulate cell proliferation, adhesion and migration through their interactions with growth factors, integrins, FN, and heparin [139, 140]. There is also evidence that they regulate ECM organisation, as fibrillar collagen deposition is inhibited when tenascin-X is knocked out in mice [141]. Nidogens (formerly known as entactins) are sulphated glycoproteins that interact with laminins, collagens and proteoglycans to assist basement membrane assembly and maintain their integrity [142-144]. Recent *in vitro* and *in vivo* studies have provided insight into the functions of less-defined matrix glycoproteins such as SCO-spondin and hemicentins, demonstrating that hemicentins contribute to ECM stability and integrity by complexing with adhesive matrix factors to keep cells and tissues anchored together, and revealing that SCO-spondin assembles into dynamic, thread-like structures within cerebrospinal fluid that sequester and transport soluble factors throughout the central nervous system to regulate homeostasis and morphogenesis [145-147]. Although this is by no means an exhaustive list of matrix glycoproteins, the above examples illustrate their functional diversity within ECMs and highlights their importance for healthy tissue function.

Glycosaminoglycans and proteoglycans

GAGs are long, unbranched, charged polysaccharides that are found in all vertebrate tissues and play a variety of important roles as ECM macromolecules [148, 149]. Five members of the GAG family exist, four of which are covalently attached to proteins following their synthesis to create proteoglycans [149]. The exception to this is hyaluronan (HA), which is also the largest and only non-sulphated GAG [149]. HA is composed of repeating acetylglucosamine (GlcNAc) and glucuronic acid (GlcA) disaccharides and its functions are tied to its physical properties, which are regulated by several factors [150]. HA's size and molecular weight is predominantly controlled by biosynthetic and degradative enzymes, where high molecular weight HA isoforms are highly hydrated and viscous, acting as insulators and shock absorbers, while lower molecular weight HA isoforms assemble into permeable networks that are more permissive to the diffusion and exchange of molecules within matrices [151-154]. Interactions with cell surface receptors, such as CD44 receptors, serve to enhance or modify the functions of HA, hence it can stimulate cell adhesion, migration, proliferation or differentiation depending on its molecular weight, its concentration in the matrix and receptor type

[150, 153]. Associations with other matrix components such as collagens, proteoglycans and TGS-6 and post-synthesis covalent modifications allow HA to organise the ECM in various ways and help dictate its biochemical and biomechanical properties [149, 152, 155]. The diversity of modifications made to HA structure that regulate its interactions with other extracellular components make it a potent mediator of inflammation, morphogenesis, and homeostasis [156]. Given the major role that HA plays in regulating tissue structure and function, it is unsurprising that dysfunctional HA metabolism has been linked to cancer progression, pro-inflammatory diseases and tissue fibrosis [150, 153, 157, 158].

The four remaining GAGs (heparan sulphate (HS) and its heavily sulphated variant heparin, chondroitin sulphate (CS), dermatan sulphate (DS) and keratan sulphate (KS)) are covalently attached to proteins to form proteoglycans [148, 149]. Variations in disaccharide repeats and number mean that GAGs exhibit high structural and size heterogeneity, which helps give proteoglycans diverse properties that aid their functions as structural proteins and receptors [3]. Proteoglycans are present within many tissues and can be grouped into one of several categories depending on either their localisation within the extracellular space of tissues or their interacting partners (Fig. 4) [155]. Aggrecan, brevican, neurocan and versican are structural proteoglycans that are defined by their ability to form large complexes with HA through their N-terminal domains and subsequently create hydrated gels [159]. These proteoglycans are often extremely hydrophilic thanks to their high CS and KS content, so they are prevalent in the ECM of viscoelastic, hydrated tissues such as cartilage, brain, cornea, and intervertebral discs [3, 159, 160]. However, there is striking variation in the number and size of CS chains attached to brevican, which appears to be developmentally regulated and allows brevican to control neuron development and maturation in brain tissue [159, 161-163]. Through their ability to associate with HA, tenascins, cell-surface glycolipids and other proteoglycans such as phosphacan, this group of proteoglycans are key regulators of ECM organisation and its biophysical properties, which in turn regulates cell behaviour and fate [159, 164-166].

Another group of proteoglycans that are rich in HS include perlecan, agrin, cell-membrane bound glypicans and the membrane-spanning syndecans [160, 167-169]. Their diverse structures and localisations within the extracellular space of tissues reflect their ability to regulate various aspects of tissue behaviour. Syndecans bear several HS chains on their extracellular domains that interact with a vast array of growth factors, cytokines, cell-surface receptors and matrix proteins which drive cell signalling events that mediate survival, adhesion, migration and proliferation [170-172]. The extracellular domains of syndecans can also be cleaved by matrix metalloproteinases (MMP) and shed into the ECM during traumatic events to mediate tissue responses to injury and inflammation [172, 173]. The large, secreted HS proteoglycan perlecan mediates various aspects of tissue development, morphogenesis and homeostasis [174]. Perlecan is a ubiquitous proteoglycan that is often localised to the basement membrane of tissues where it associates with laminins, collagen IV, nidogens, dystroglycan and integrins to help stabilise the network and facilitate cell signalling events [175-179]. Perlecan bears five domains that enable it to perform other, and at times contradictory, functions within tissues such as aiding fibril formation, controlling the release of growth factors and

cytokines, and driving and suppressing morphogenic events [174, 180-182]. Finally, glypicans are bound to the cell surface via a glycosyl-phosphatidylinositol (GPI) anchor, where they bind morphogens and growth factors such as TGF-β, bone morphogenic proteins and Wnt to help regulate cell growth and differentiation [183, 184]. Because they are predominantly involved in regulating tissue development, their expression can be highly localised and transient [185, 186].

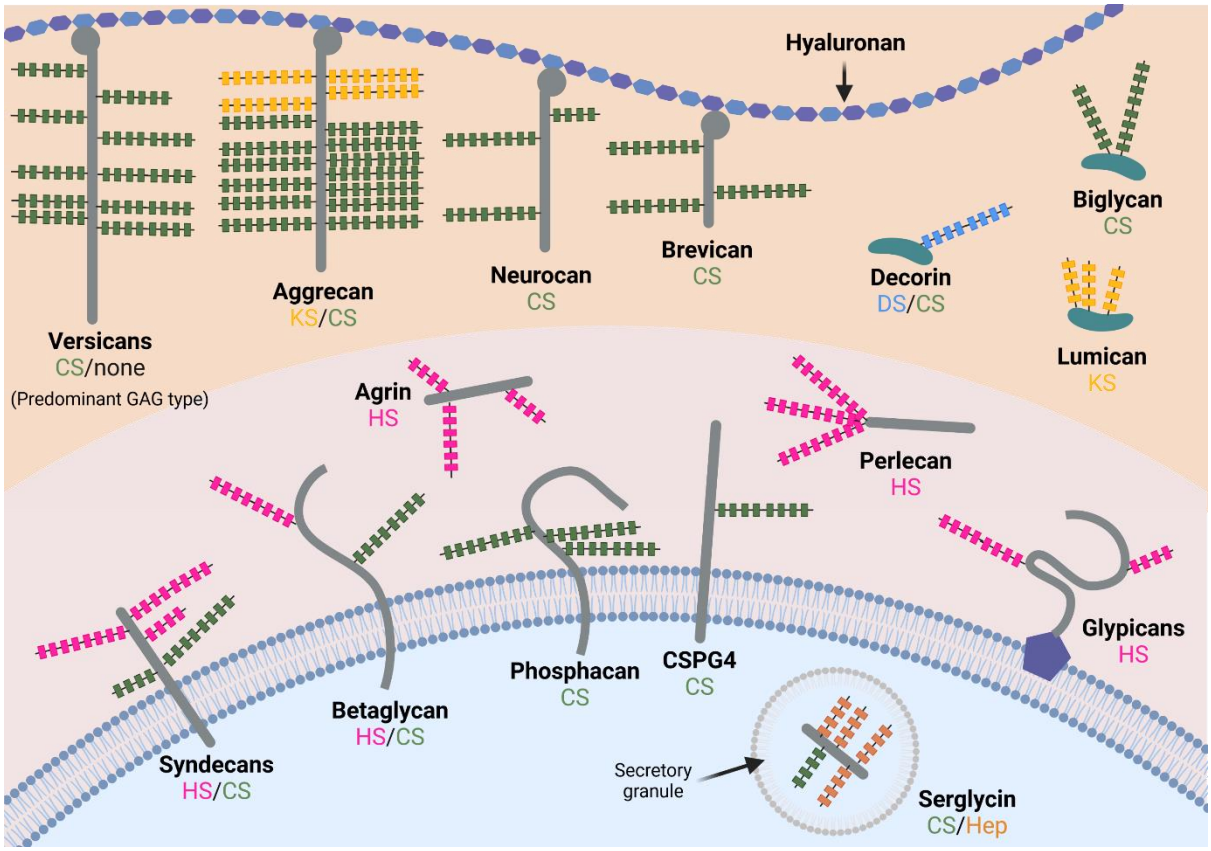

Fig. 4. Schematic representation of proteoglycans and their localisation. Extracellular proteoglycans (orange zone) include the hyalectans versican, aggrecan, neurocan and brevican, which interact with hyaluronan, and the short, leucine-rich proteoglycans decorin, biglycan and lumican. Pericellular proteoglycans (pink zone) include agrin and perlecan. Cell-surface proteoglycans (blue bilayer) comprise syndecans, betaglycan, phosphacan and CSPG4. Glypicans are also found at the cell surface, where they are anchored to glycosyl-phosphatidylinositol lipids. Serglycin is the only identified intracellular proteoglycan (blue zone) and is found in secretory granules. Adapted from [3]. Created with BioRender.com.

Short, leucine-rich proteoglycans (SLRP) such as decorin, biglycan and lumican comprise the largest family of proteoglycans [187]. They are commonly composed of a short protein core that bears multiple leucine-rich repeat motifs, and while some members of this large family do not have attached GAG chains, they still share structural and functional homologies with the GAG-decorated members of this family, hence they are included [160]. A well-documented function of many SLRPs is their ability to associate with collagen fibrils and maintain their organisation by regulating fibre diameter and aggregation [3, 71, 188, 189]. This function can be driven either by GAG chains or the core protein, as the KS chains of lumican and decorin's core protein were found to be important mediators of collagen fibril assembly in corneal and tendon tissue, respectively [188, 190-193]. Some SLRPs can also bind growth factors such as TGF-β and are therefore involved in the regulation of cell growth and motility and ECM remodelling events [189, 194, 195]. Many SLRPs also interact with immune

receptors and receptor tyrosine kinases (RTK) which can either stimulate or inhibit cell migration, growth and adhesion depending on the specific SLRP involved [3, 196, 197]. Although the specific mechanisms of action and targets may differ between members of the SLRP family, they all ultimately regulate matrix structure and cell behaviour in tissue- and cell-specific ways to promote healthy tissue function.

While more comprehensive reviews of proteoglycan structures and functions can be found elsewhere, the above examples illustrate the structural and functional diversity of proteoglycans and their constituent GAG chains in the ECM [148, 160].

Elastin

Elastin is an extremely stable and flexible biopolymer that forms the core of elastic fibres, providing elastic recoil to tissues that are subjected to elastic stress [198]. Elastin is synthesised by many tissues early on during development, where it is secreted into the extracellular space as a highly hydrophobic, flexible and extensible polypeptide (called tropoelastin) that polymerises with other tropoelastin molecules into aggregates that align themselves along fibrillar glycoproteins to form elastin fibres [198-201]. Elastin fibre assembly is driven by interactions between the hydrophobic domains of tropoelastin and via LOX-mediated cross-links between lysine residues [201, 202]. Cells and ECM components such as elastin binding proteins (EBP) also guide elastin fibre assembly, with tissue-specific receptors and matrix factors providing specific cues that dictate elastin organisation [200, 203-205].

The abundance and organisation of elastin fibres varies between tissues to meet their mechanical requirements. For example, elastin fibres in the lung can be found arranged into lattices that encircle alveoli which provide them with the ability to withstand elastic recoil forces as the diaphragm moves, and they are also present within the pulmonary arteries, where they are organised around the vascular endothelium circumference as concentric rings that help distribute elastic stress evenly throughout the arterial wall [206-208]. In tendons, elastin fibres can make up to 10% of the tissue dry weight depending on the amount of strain it is routinely subjected to, and they tend to be distributed along the tendon axis [209, 210]. Tissue- and disease-specific expression of different elastin splice isoforms has also been found to influence elastin fibre assembly and organisation, and subsequently its physical properties [211-214]. Elastin fibres can also modulate cell adhesion, migration and proliferation through interactions with cell-surface moieties such as integrins and GAGs [200, 203, 215-218]. MMP- and elastase-mediated cleavage of elastin fibres releases soluble elastin monomers (elastokines) into the extracellular space where they can stimulate cell apoptosis, migration and proliferation [219, 220]. Given that elastin fibres are not subject to turnover and the activity of these enzymes is often activated in response to pro-inflammatory signals, elastin fibre degradation is frequently associated with the development and progression of various diseases, including emphysema, cancer, and atherosclerosis [206, 220-222].

While this is by no means an exhaustive list of ECM macromolecules and their isoforms, the examples described here highlight their structural and functional diversity and demonstrates their

importance for ECM function. Indeed, their structures are integral to their functions as initiators, organisers, and regulators of the ECM scaffold, collaborating with each other to create intricate, highly organised, and tightly regulated matrices that help dictate tissue form and function. As such, impaired synthesis or assembly of ECM components often have severe, pathological consequences.

Soluble factors are also important regulators of matrix structure and function

ECMs are also home to many soluble and secreted factors that interact with matrix components and cell surface moieties to regulate tissue development, growth, morphogenesis and repair [223]. Some of these factors are derivatives of matrix macromolecules which can stimulate or inhibit tissue remodelling events such as angiogenesis [219, 224-227]. Their cleavage into bioactive fragments is mediated by the activity of matrix-dwelling proteolytic enzymes such as MMPs. MMPs target all ECM components and therefore can effect various changes within tissues such as altering cell-matrix interactions, releasing sequestered growth factors, and altering matrix organisation [227, 228]. These changes elicit various cell behaviours, and as such MMPs regulate tissue homeostasis, growth, development, inflammation, and repair. Indeed, their targets and effects are so diverse and essential to healthy tissue function that dysregulated MMP activity has been shown to drive the development and progression of many diseases throughout most, if not all, tissues [229, 230]. For example, MMP-10 and MMP-2 are frequently overexpressed in cancers, as their activity suppresses apoptosis and stimulates metastasis and angiogenesis by cleaving matrix macromolecules to facilitate cell migration and release pro-angiogenic factors [231-233].

Other enzymes that inhabit the ECM include cross-linking enzymes such as LOX, protease inhibitors, and glycan and GAG-specific enzymes. Members of the LOX family catalyse the formation of covalent cross links between the fibrous matrix proteins collagens and elastin to generate stable fibres [234]. Their activity is essential for providing these fibres with their mechanical strength and integrity and their activity is tightly regulated within tissues to maintain optimal matrix tension [235, 236]. Tissue fibrosis and cancer, which are both associated with pathological matrix stiffness, are diseases that have been linked to dysfunctional LOX activity [237-240]. For example, increased LOX-mediated collagen cross-linking helps drive breast cancer progression, as the stiffened matrix promotes cell proliferation, growth and migration via focal adhesion and integrin signal transduction pathways [241, 242]. Many enzymes involved in GAG remodelling are also present in ECMs, which alter the structure and functions of proteoglycans and HA to regulate growth factor activity, matrix density and modulate receptor binding [243, 244]. Consequently, their uninhibited activity can also stimulate malignant behaviours in cells and facilitate tumour metastasis, which has made them attractive targets for anti-cancer therapies [244-248].

Growth factors are abundant within ECMs, where they directly stimulate a variety of signalling pathways within cells to regulate their behaviour. Although there are conflicting definitions for the term ‘growth factor’ in the literature, for the purposes of brevity all secreted, bioactive molecules will be referred to as growth factors here. Growth factors are a large, diverse group of soluble signalling molecules and here include interleukins, interferons, tumour necrosis factors (TNF), chemokines and the epidermal growth factor (EGF), vascular endothelial growth factor (VEGF), fibroblast growth factor

(FGF) and TGF families [249-252]. These growth factors bind various cell-surface receptors and proteoglycans to trigger signalling cascades that affect cell behaviour [252, 253]. Depending on the growth factor, its target receptors and environmental context, the responses they can elicit in cells encompass the stimulation or suppression of matrix deposition and organisation, and cell growth, proliferation, survival, migration, adhesion and differentiation [250, 253-255]. Given their ability to induce a variety of cell behaviours, growth factors are responsible for driving both beneficial and pathogenic remodelling events in tissues. For instance, wound healing in the skin is partially driven by increased keratinocyte deposition of laminin 332, which in turn is stimulated by multiple growth factors including members of the TGF family, EGF and interferon-γ [88]. In contrast, asthma development is associated with increased matrix deposition in the bronchus, which cysteinyl leukotrienes have been found to promote [256]. Since they are such potent mediators of cell behaviour and fate, growth factor signalling is highly controlled in tissues. In healthy tissues, growth factor signalling is regulated via sequestration, where cell-surface and matrix proteoglycans capture free growth factors and keep them away from cell-surface receptors to suppress their activity or create morphogenic gradients that regulate tissue organisation [170, 227]. Their release is mediated by matrix proteases and shedding events which, depending on the environmental context, can either help maintain healthy tissue function or drive tissue pathogenesis [173, 228, 255, 257, 258].

This intricate interplay between growth factors, matrix enzymes and soluble matrix fragments, and their interactions with the insoluble components of the ECM further illustrates the structural and functional complexity of tissue matrices and highlights how tenuous this balance is.

Two structurally distinct types of ECM are essential for tissue function

The composition and organisation of ECM macromolecules and soluble factors vary across tissues to meet their structural, mechanical, and biochemical requirements. However, this variation is also present within tissues, which often contain two structurally and functionally distinct forms of ECM. These are the pericellular and interstitial matrices, which are present in all triploblastic multicellular organisms and have gradually evolved into more complex structures over time due to the requirement for specialised tissues in higher-order organisms [259]. Some of the core components and base structures of interstitial and pericellular matrices are so conserved that they have been identified in simple, primitive multicellular organisms such as sponges and hydra [260-262]. This indicates that these two forms of ECM are essential for life in complex multicellular organisms, with changes in their components and organisation reflecting the unique functional requirements of different tissues.

Pericellular matrices

Pericellular matrices, also called basement membranes, are thin, dense sheets of matrix macromolecules that directly contact the basolateral surface of endothelial and epithelial cell monolayers to provide them with structural support and biochemical cues that direct cell behaviour (Fig. 5) [97, 263-265]. They also surround muscle fibres, adipose and Schwann cells, wrap around tissues, and bridge tissue junctions such as neuromuscular synapses [177, 266]. Knockout studies have shown that basement membrane formation is initiated by the self-assembly of laminin 111 into a

polymeric network [267, 268]. Laminin 111 self-assembly appears to require binding events between the LG domains of laminin α1 subunits and cell surface moieties, namely sulphated glycolipids, integrins and dystroglycans [83, 90, 104, 105, 269, 270]. The laminin 111 scaffold recruits collagen IV, which polymerises into a cross-linked lattice over the laminin scaffold to create a dense mesh that imparts mechanical strength to the basement membrane [266, 271, 272]. Nidogens and perlecan are also key components of basement membranes, as they bind to laminin, collagen IV, and each other to stimulate further recruitment of macromolecules and form bridges between the laminin and collagen lattices to create a stable, cohesive membrane [105, 142, 144, 180, 263, 270, 273, 274]. The formation of this dense, cross-linked macromolecular network creates a robust molecular sieve that performs a variety of essential functions, including modulating the diffusion and activity of soluble factors, regulating cell polarity, adhesion, and differentiation, and providing mechanical integrity and support to cells [263].

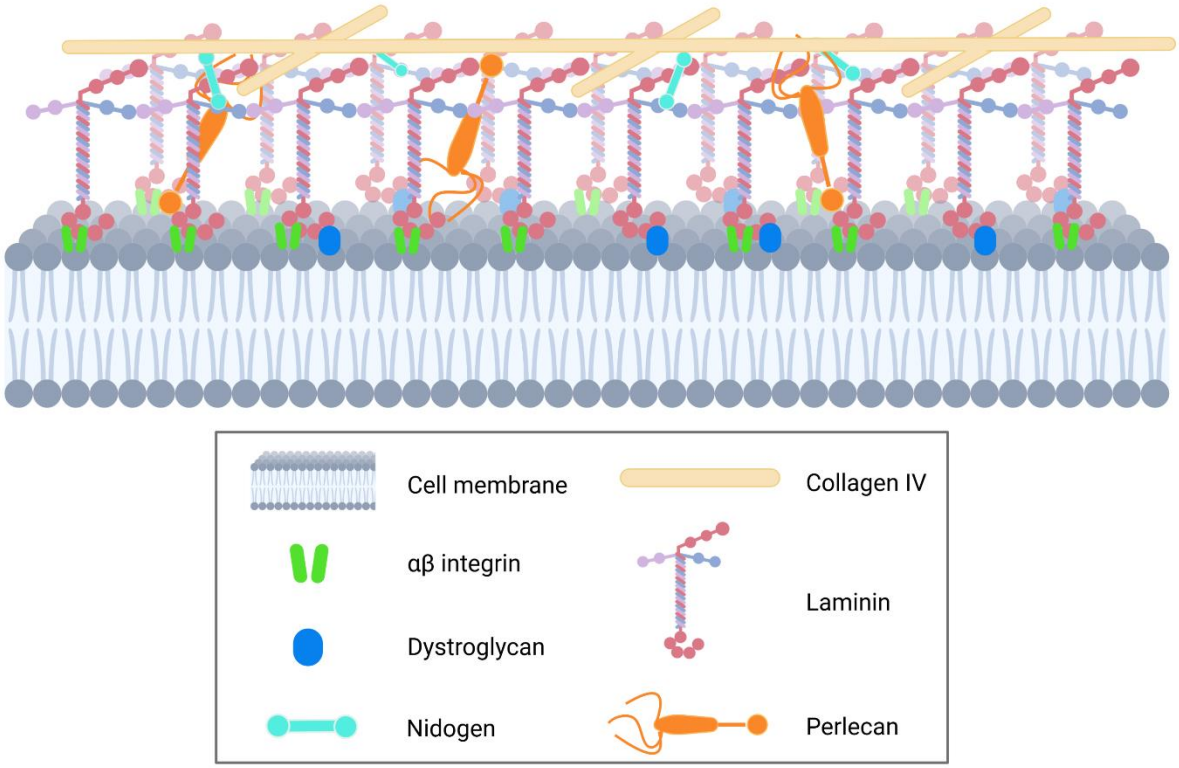

Fig. 5. Organisation of and interactions between core basement membrane proteins. Laminins self-assemble into a network at the cell surface by binding receptors such as integrins and dystroglycans. The formation of the laminin network drives the assembly of a separate collagen IV network. Interactions between these two networks are strengthened by nidogens and perlecan, creating a functional basement membrane. Adapted from [144]. Created with BioRender.com.

While all basement membranes contain laminin, collagen IV, perlecan and nidogen, tissue-specific isoforms of these macromolecules, development-dependent changes to basement membrane composition, and the integration of other components give rise to highly specialised basement membranes [82, 87, 263, 268, 270, 275]. For example, basement membranes underlying vascular endothelial cells in blood vessel walls contain laminin 511, which helps stabilise tight junctions between the cells to maintain vascular integrity and mediates arterial vasodilation in response to shear stress [276, 277]. Laminin 411, perlecan, agrin, nidogen, truncated collagen XVIII and the

[α1(IV)$_2$α2(IV)] isoform of collagen IV are also key components of vascular basement membranes and help regulate vessel growth, permeability, and integrity by regulating growth factor activity, controlling immune cell infiltration, and stabilising adherens junctions [278-284]. Laminin 111 is often replaced by other laminin isoforms in the basement membrane as tissues mature, but it remains expressed as a basement membrane protein at various developmental stages in the mammary gland as it stimulates and maintains the differentiation of mammary epithelial cells (MEC) into hollow, polarised alveoli (acini) that secrete milk during lactation [112, 270, 285-290]. Collagen IV (isoform [α1(IV)$_2$α2(IV)]), laminin 3a32, perlecan, nidogen and fibronectin are also incorporated in the basement membrane of mammary acini, where they aid acinar morphogenesis and function and maintain basement membrane integrity [290-295]. Finally, the kidney glomerulus basement membrane is highly specialised, containing the heavily cross-linked collagen IV (isoform [α3(IV)α4(IV)α5(IV)]), collagen XVIII, fibulin-1, nidogen, agrin and perlecan, which together form a thick basement membrane that, in conjunction with laminin 521, acts as a selective, semi-permeable barrier that facilitates plasma filtration [54, 263, 296-300].

Since basement membranes are essential for directing and maintaining tissue organisation and function, impaired basement membrane assembly has severe consequences. Impaired laminin 111 synthesis and assembly are developmentally lethal as early basement membranes cannot properly assemble [267, 301-303]. Mutations in the gene that codes for the laminin β2 subunit have widespread, pathological effects as laminins 221, 421 and 521 are all affected and are responsible for maintaining basement membrane integrity in the eye, glomerulus and neuromuscular junction basement membranes [177, 304, 305]. Alport syndrome is a progressive kidney disease caused by mutations in any of the three chains of collagen IV (isoform [α3(IV)α4(IV)α5(IV)]), which results in weakened glomerular basement membranes that cannot function correctly, in addition to defects in ocular basement membranes [62, 306]. As perlecan is ubiquitous in basement membranes, structural defects arising from mutations in the perlecan gene can be developmentally lethal or cause defects in cartilage development and neuromuscular function [307]. Dysfunctional basement membrane organisation and function also occurs during the onset and progression of various diseases such as cancer, atherosclerosis, and diabetes. Increased collagen IV and laminin deposition occurs as diabetic retinopathy develops, which thickens the glomerular basement membrane and impairs its filtration abilities [308-310]. Similarly, atherosclerosis is associated with abnormally thick vascular basement membranes caused by remodelling events that increase collagen IV and laminin deposition, which subsequently leads to inflammation, impaired vessel elasticity and wall leakage [311-313]. Cancer development and progression are also linked to basement membrane dysfunction, where basement membrane degradation is associated with cancer cells' invasive potential, while overexpression of basement membrane proteins such as laminins, collagen IV and nidogen can also promote tumour metastasis [114, 314-323]. These examples show that basement membranes are highly-specialised structures whose assembly and maintenance must be tightly regulated to ensure that tissues can organise and function correctly.

Interstitial matrices

In contrast to the dense, sheet-like meshwork of proteins that constitutes basement membranes, the interstitial matrix typically forms a hydrated, porous and fibrous macromolecular network that constitutes the extracellular bulk of tissues [124]. Interstitial matrices are primarily composed of fibrillar collagens, elastin, laminins, glycoproteins, GAGs and proteoglycans, although the organisation and abundance of these components within tissues varies widely depending on the specific biochemical and biomechanical requirements of tissues [9, 41, 124]. For example, the mammary interstitial matrix is a hydrated, loose mesh of type I and III collagen fibres, FN, tenascins and proteoglycans, where the fibres attach to cells and regulate their behaviour via cell-surface moieties such as integrins and syndecans [1, 324-327]. These cell-matrix contacts, paired with the controlled release of sequestered growth factors and the orientation of these fibres within a compliant matrix, help facilitate and direct mammary gland development and homeostasis [328-330]. The brain interstitial matrix is rich in proteoglycans and HA, which form an amorphous network through their interactions with each other and tenascins [331-333]. The resulting matrix can control neuronal and glial growth, differentiation and regeneration, modulate angiogenesis and regulate neuronal plasticity due to the multifunctional natures of its resident proteoglycans and GAGs, which interact with a variety of growth factors, matrix proteins, enzymes and their inhibitors [159, 163, 332, 334]. In contrast, the interstitial matrix of bone tissue is predominantly composed of stacked, mineralised type collagen I fibrils which are organised into various higher-order structures depending on their location within the bone tissue to provide optimal resilience in response to local mechanical forces [335-337]. FN is another key matrix protein in bone tissue, where it mediates osteoblast survival, growth, and differentiation in conjunction with collagen I [338-341].

Interstitial matrices can be remarkably heterogeneous within tissues to provide localised mechanical and biochemical cues, as evidenced by the altered organisation of collagen I within the inner and outer layers of mature long bones [342, 343]. The thin, dense outer layer (cortical, or compact, bone) is composed of concentric arrays of mineralised collagen fibres which are carefully oriented to withstand compressive loading, while the interior (trabecular bone) is a porous lattice of mineralised collagen fibrils that run parallel to high-stress areas of the bone to support its mechanical resilience while also providing a physical scaffold for blood vessels, bone cells and bone marrow [336, 337, 342, 344]. Interstitial matrices are also frequently remodelled to regulate tissue development, morphogenesis, and homeostasis. Nascent interstitial matrices are relatively simple and begin with the synthesis and secretion of scaffolding macromolecules such as collagens, laminins, FN, and elastin, which help define tissue boundaries, provide mechanical integrity to developing tissues and help direct tissue morphogenesis [8, 124, 128, 200, 331, 343, 345, 346]. Their organisation becomes more complex over time as differentiated cells such as osteoblasts, fibroblasts, immune cells, and adipocytes secrete tissue-specific matrix components and help direct their organisation within the extracellular space [347, 348]. During tendon development, growth factors such as sonic hedgehog, TGF-β and FGF stimulate the differentiation of mesenchymal stems into tendon fibroblasts (tenocytes), which then secrete fibrillar collagens, laminins, thrombospondins, and organisational

factors such as cross-linking collagens, proteoglycans, and tenascin-C [349, 350]. Self-regulated and mechanically driven interactions between these factors lead to the parallel assembly of groups of cross-linked collagen fibrils which can transmit mechanical forces from muscles to bones [351-356]. As force-sensitive structures, the tendon matrix is frequently remodelled in response to changing mechanical cues, which requires tight regulation of matrix-modifying factors to prevent tissue dysfunction [357]. Increased mechanical loading results in the controlled release of TGF-β from the matrix by proteases, which stimulates matrix production in tenocytes and increases fibre thickness, increasing tendon resilience to repeat cycles of mechanical loading and thus reducing the likelihood of fatigue and injury [349, 358-363]. However, tendon injuries disrupt matrix organisation which promotes the excessive release of sequestered TGF-β from the disrupted matrix, which kills tenocytes and leads to impaired fibril assembly [358]. The development of scar tissue and adhesions in injured tendons is also linked to dysregulated matrix remodelling [364]. For example, TGF-β signalling can prevent fibrin clot degradation by suppressing MMP activity and by promoting collagen deposition, which can create fibrotic adhesions that limit tendon functionality [364-368].

The specific structural and compositional characteristics of basement membranes and interstitial matrices give tissues their bulk mechanical properties and scaffolding. They also contribute to tissue heterogeneity by creating biochemical gradients and assembling into various supramolecular structures, which provide cells with highly localised biochemical, physical and mechanical cues that collectively orchestrate tissue function. As illustrated here, basement membranes and interstitial matrices are dynamic extracellular structures. They are often remodelled by their own matrix components and cells to drive tissue development and maintain tissue homeostasis. Defects in matrix synthesis, assembly and remodelling have severe impacts on tissue function and health, hence these processes are strictly regulated by both matrix components and resident cells.

Mechanical forces help direct tissue structure and function

Tissues are sensitive to mechanical forces which govern many aspects of tissue development, morphogenesis, and homeostasis [369, 370]. Here, we define force as a vector that has magnitude and direction, which can be applied or measured [370]. Synovial joint development during embryogenesis requires transcriptional activation of the Wnt signalling pathway, which is stimulated by muscular contractions [371-373]. Blood flow through veins and arteries creates circumferential hydrostatic pressure and generates shear stress (force per unit area) along the vessel walls, and differences in flow magnitude, frequency and direction affect lumen diameter and elasticity [374, 375]. Reduced mechanical loading on the musculoskeletal system in zero gravity results in reduced muscle mass and bone density [376-378]. However, tissue structure and function are not regulated purely by external mechanical forces, but also by mechanical cues that are generated by cells and matrix components (intrinsic mechanical forces) [379-381]. Indeed, mechanical forces can be acted upon at every level of the tissue architecture, as nano- and microscale, mechanically driven interactions between and within cells and the ECM ultimately coordinate how tissues respond to mechanical cues (Fig. 6) [382-384].

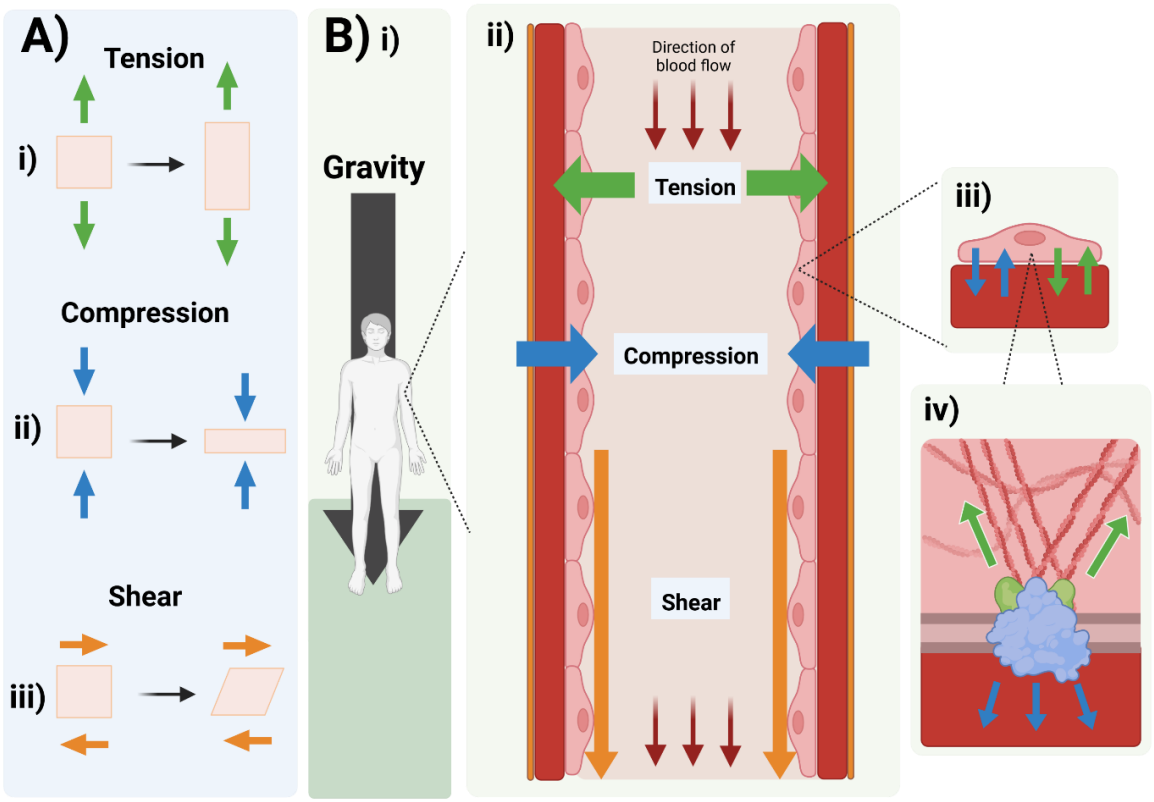

Fig. 6. Mechanical forces vary in their magnitude and direction within tissues. A) Diagrams depicting the effects of different mechanical forces on a block of material before (left) and after (right) deformation. i) Tensile forces stretch the surface they act on. ii) Compressive forces squash the surface they act on. iii) Shear forces deform parallel surfaces. Adapted from [382]. B) Schematic illustrating the direction and magnitude of mechanical forces. i) Gravity is a unidirectional force that acts on the entire body. ii) The vascular endothelium is subjected to tensile, compressive and shear forces as blood flows through the vessel lumen. Endothelial cells are subjected to shear stress on their lumen-facing surfaces, while hydrostatic pressure creates tensile stress that deforms the endothelium outwards. The elastic vessel wall generates elastic recoil in response to the hydrostatic pressure of blood flow, which compresses the vessel. iii) Individual endothelial cells and their basement membrane exert reciprocal tensile and compressive forces on one another. iv) The cell cytoskeleton and its attached membrane-spanning proteins transmit nano-scale mechanical forces onto their substrate. Created with BioRender.com.

Cells detect and convert physical forces into intracellular biochemical signals through mechanotransduction mechanisms, which ultimately trigger changes in cell behaviour [384, 385]. The specific signalling pathways that are stimulated in response to mechanical cues (mechanosignalling pathways) vary depending on the cell types, matrix components and mechanical forces involved, but the general principles remain the same (Fig. 7). In essence, mechanical cues are detected by force-sensitive structures (mechanosensors) that undergo molecular changes when mechanical force is applied to them [369, 386, 387]. Examples of force-sensitive structures include cell-surface moieties such as the lipid bilayer, integrins and ion channels, and intracellular structures such as actomyosin filaments [375, 382, 388-391]. Interestingly, ECM components that undergo conformational changes in response to mechanical forces such as fibrillar collagens, FN fibrils and elastin fibres are not considered to be force sensors in the wider literature, perhaps because they do not have an active role in responding to these mechanical cues unlike cells [392-397]. Resulting changes in the conformation, binding affinities, localisation, or enzymatic activities of these force-sensitive structures activate intracellular biochemical signalling cascades that alter gene expression, metabolic activity,

and cell contractility to effect appropriate changes in cell behaviour and matrix organisation [386, 387, 398-405].

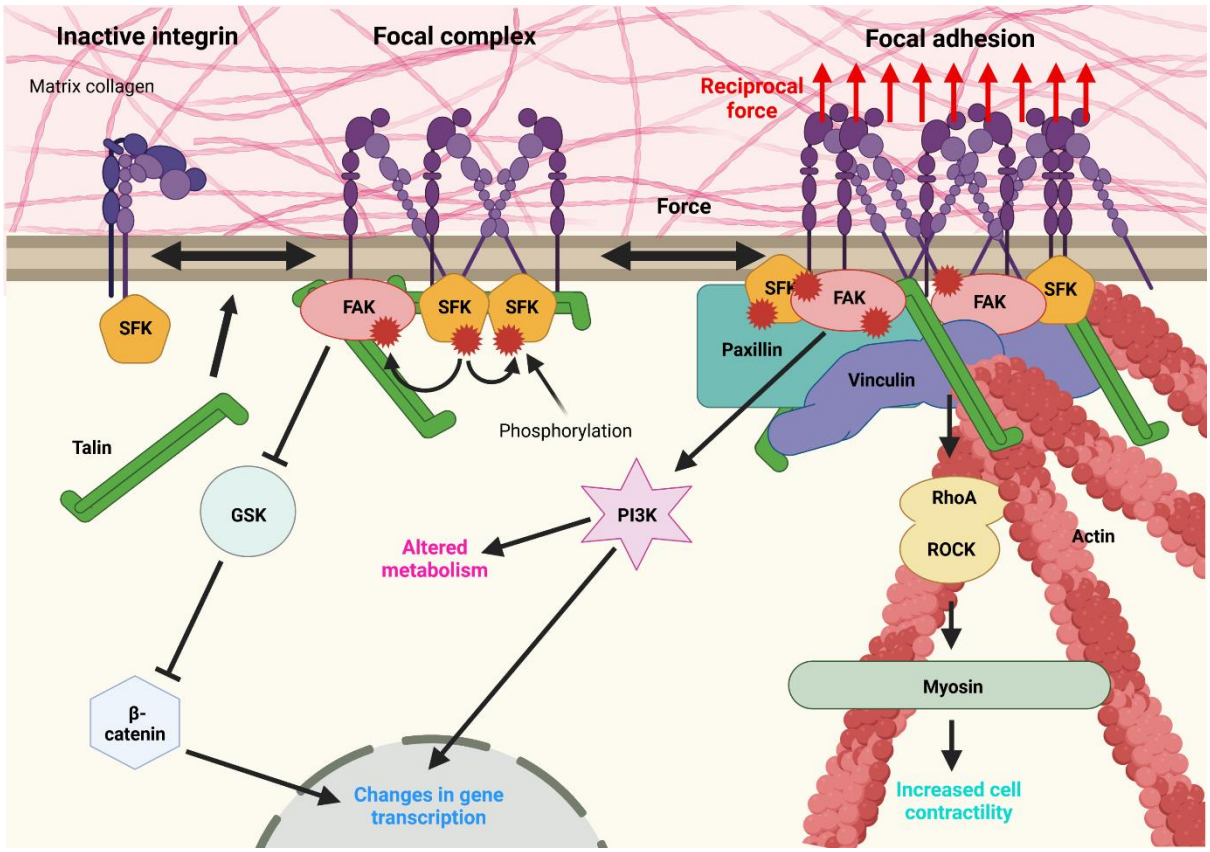

Fig. 7. Diagram depicting the key events of mechanotransduction and their effects on cell behaviour. Extracellular forces such as matrix stiffening prompt integrins at the cell surface to form active heterodimers. Persistent integrin activation in response to prolonged extracellular force stimulates integrin clustering and the unfolding and recruitment of mechanosensitive intracellular proteins such as talin and vinculin. These assemblies stimulate Src-family kinase (SFK) and focal adhesion kinase (FAK) signalling cascades, which alter gene transcription and cell metabolism. Continued detection of environmental force by these integrin clusters prompts their maturation into focal adhesions which enhances their influence on cell behaviour as further mechanosensitive proteins are recruited. For example, paxillin can be recruited to facilitate cross-talking between focal adhesions and other signalling platforms. Actin is assembled at focal adhesions through SFK-FAK signalling events, which stimulates stress-fibre formation and enhances cell contractility. Consequently, these force-sensitive structures stimulate changes in cell growth, differentiation, and migration in response to environmental forces. GSK, glycogen synthase kinase; PI3K, phosphoinositide-3 kinase; ROCK, Rho-associated kinase. Adapted from [399]. Created with BioRender.com.

While some mechanotransduction pathways have been characterised, many remain poorly defined [406]. This is hardly surprising given the diversity of mechanosensors and their downstream intracellular signalling pathways, which can interact with other signalling pathways and elicit a range of cell responses depending on the context [407-411]. Indeed, cells often respond to external mechanical cues by exerting their own forces onto the ECM and vice versa, which generates reciprocal, self-regulating mechanical dynamics between cells and the ECM that can be challenging to recapitulate and dissect *in vitro* [386, 412-415]. This complexity is exacerbated by the fact that tissues are subjected to multiple and specific mechanical forces, which vary in origin, frequency, direction, and magnitude [399, 416]. For example, gravity is a constant, macroscale force that affects all tissues, but its effects are notably profound in the musculoskeletal system which bears most of its perpendicular compressive and tensile forces and requires its constant presence to maintain

homeostasis [376, 377, 399, 417]. In contrast, the mechanical forces that primarily regulate breast tissue function are nanoscale tensile, contractile, and compressive forces generated by interactions between cells and their ECM until lactation, where these mechanical cues work in tandem with the external tensile stress produced during suckling to force milk towards the nipple [399]. All these factors combine to create incredibly complex, tissue-specific interplays of mechanically driven molecular interactions between cells and their ECM which collectively regulate tissue structure and function. As a result, identifying specific mechanotransduction mechanisms that regulate discrete aspects of tissue structure and function requires that we recapitulate the key properties of tissue ECMs *in vitro*.

How can *in vitro* models help us uncover the relationship between cells and the ECM?

In vitro models have been used to investigate *in vivo* signalling events between cells and their environment for decades, as they offer researchers greater control over experimental variables and permit visualisation and quantification of individual signalling steps [418]. The importance of providing cells with a 3D environment *in vitro* was established over 50 years ago, as two-dimensional (2D) surfaces fail to mimic the complex, 3D environment of tissues *in vivo* [419, 420]. Since many cell functions and behaviours depend on cell-cell and cell-matrix contacts and cues that can only occur in 3D environments, cells cultured on top of flat surfaces lose many of their *in vivo* phenotypes which affects their responses to various stimuli [419, 421-425]. This creates misleading experimental outcomes that do not represent how cells would behave *in vivo* [424, 426-428].

Many established 3D cell culture systems grow cells on or within a scaffold to provide them with a 3D environment that simulates the key physical, mechanical, and biochemical properties of native tissue [429, 430]. These scaffolds are typically hydrogels, which are water-swollen polymeric networks that recapitulate the 3D, viscoelastic nature of tissues [431, 432]. The most well-established hydrogels for 3D cell culture are composed of organic polymers such as collagen, GAGs, or alginate as their natural origins make them inherently biocompatible and encourage cell interaction [419, 433]. Indeed, the earliest 3D *in vitro* model of the breast matrix showed that MECs cultured on floating collagen I hydrogels form polarised structures that resemble mammary acini, whereas mouse MECs cultured on top of plastic and glass surfaces formed undifferentiated monolayers [434]. They also found that MECs cultured on anchored collagen I gels also failed to differentiate, demonstrating the importance of mechanical cues in regulating cell behaviour. Furthermore, studies in the 1980s and 1990s revealed that embedding human or mouse MECs into the reconstituted basement membrane (rBM) extract Matrigel stimulates the formation of polarised acini that secrete milk, which shows that cells mimic *in vivo* behaviours when grown in 3D environments [290, 315, 435, 436].

These studies pioneered the development of 3D organoid models, which have since been used to simulate numerous tissue and organ systems [30, 34, 437-441]. The definition of ‘organoid’ varies between studies, but they typically assert that organoids are 3D, self-organising, tissue-specific structures that are derived from primary tissue or stem cells [420, 442-445]. However, such definitions are considerably restrictive as they insist that organoids must be generated from stem cells or primary tissues, despite multiple studies showing that organoids can be grown from single cell lines [420, 446-

449]. Therefore, we here define organoids as 3D, self-assembling, *in vivo*-like structures that can be reproducibly generated from single cells, cell clusters or tissue fragments. Since stimulating organoid development *in vitro* often requires a combination of *in vivo*-like spatial, biochemical, and mechanical cues, both the development and use of 3D organoid models have provided important insights into how ECM composition, organisation and mechanics regulate cell behaviour and vice versa.

In vitro models of lung alveoli

Modelling tissues *in vitro* is challenging, as tissues are complex, intricate structures that perform specialised functions which are tightly regulated by various biochemical, physical, and mechanical cues. For example, gas exchange between air and blood in the lungs is facilitated by alveoli, which are multicellular structures that depend on specialised cells, their ECM, and cyclic, external physical forces to function properly. Here, we provide examples of several *in vitro* models of lung alveoli to demonstrate how we can recapitulate the organisation and function of complex and dynamic tissues *in vitro*.

Lung alveoli are vascularised, hollow spheroidal structures composed of type I and type II alveolar epithelial cells (AEC) that are surrounded by a relaxed meshwork of elastin and collagen I and III fibres that is filled by supportive, water-absorbing proteoglycans (Fig. 8) [450-454]. This matrix and its resident myofibroblasts connect the alveoli to the capillary endothelium, which enables gas exchange between alveolar airspaces and the pulmonary vasculature [451]. In addition to forming a diffusion barrier between alveoli and capillaries, the alveolar matrix provides mechanical stability and elastic recoil which allows alveoli to withstand cycles of expansion and contraction during respiration, which is aided by the lipid-rich surfactant secreted by type II AECs [450, 451, 453, 455-458]. Surfactant secretion is vital as it reduces alveolar surface tension, preventing the alveoli from collapsing during expiration [451]. Changes to organisation and composition of the alveolar interstitial matrix during the progression of diseases such as infection, emphysema and fibrosis affect the ability of the alveoli to withstand mechanical forces and facilitate gas exchange [455, 459-465]. Consequently, ensuring that the biochemical and mechanical properties of the alveolar interstitial ECM are recapitulated *in vitro* is important.

A study performed in 1987 showed that type II rat AECs cultured on top of Matrigel formed aggregates that retained some of their differentiated characteristics, revealing that the composition of Matrigel recapitulates some of the key properties of the lung ECM [466]. Later studies showed that more *in vivo*-like alveolar organoids could be consistently grown in Matrigel when primary or immortalised AECs were co-cultured with lung fibroblasts [467-470]. The presence of lung fibroblasts in these cultures promoted the formation of self-renewing alveolar organoids that contained both type I and II AECs and expressed surfactant proteins, which suggested that *in vivo* alveolar development and function requires fibroblast-derived matrix factors. Indeed, multiple *in vitro* and *in vivo* studies have demonstrated that soluble, fibroblast-derived growth factors such as keratinocyte growth factor (FGF-7) are important regulators of alveolar differentiation [471-479]. For example, one 3D *in vitro* study showed that supplying lung epithelial progenitor cells with stromal cell-conditioned media

promoted alveolar organoid formation [480]. The findings obtained from these 3D alveolar organoid models indicate that soluble factors secreted by stromal cells, such as fibroblasts, in the alveolar ECM are primarily responsible for stimulating alveolar morphogenesis and function, which is not surprising given that growth factors such as FGFs regulate epithelial cell differentiation, proliferation, and migration [481-483]. Furthermore, these studies show that complex behaviours such as AEC differentiation and alveolar development can be recapitulated *in vitro* by providing AECs with a 3D, bioactive environment that contains lung fibroblast-derived growth factors.

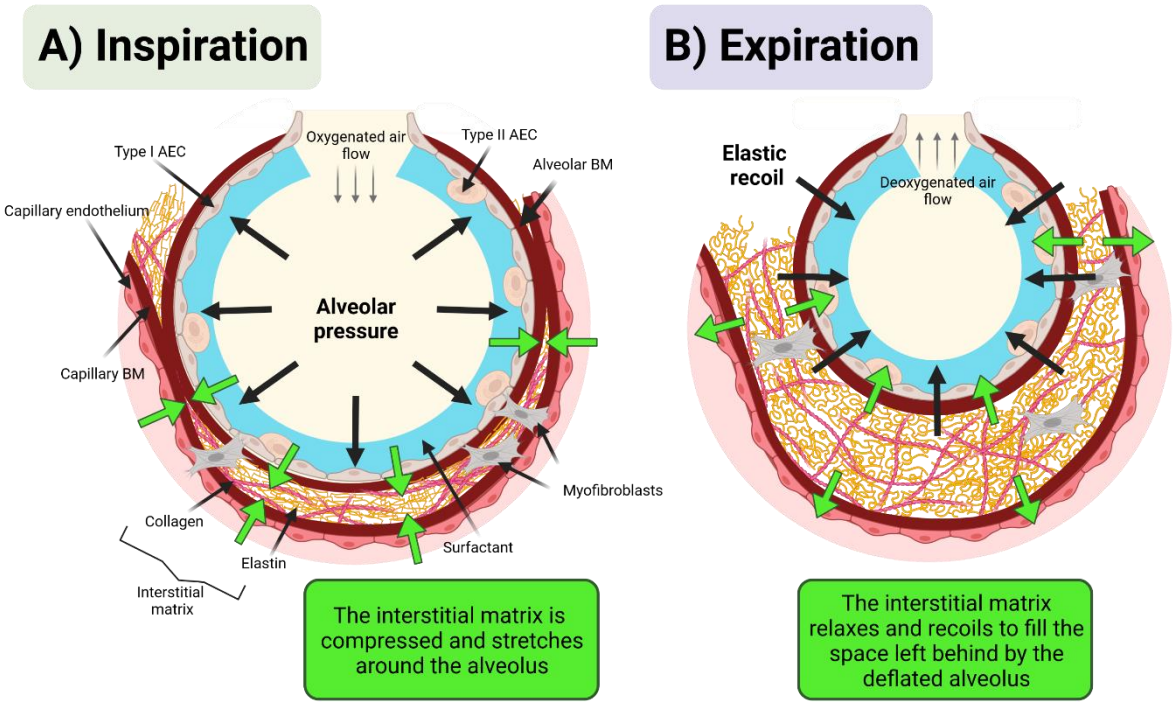

Fig. 8. An elastic and supportive extracellular matrix and the maintenance of an air-liquid interface permit cycles of alveolar inflation and deflation during respiration. A) During inspiration, oxygenated air fills the alveolar space which creates pressure. The increase in air pressure within the alveolar air space inflates the alveolus. As the alveolus inflates, its surrounding basement membrane (BM) keeps the structure intact while the interstitial matrix stretches to accommodate the increased alveolar volume. A network of elastin fibres that surrounds the alveolar BM deforms and stretches as alveolar volume increases, bearing most of the elastic strain. The collagen fibres within the matrix network also stretch, and their strong tensile properties help stabilise the alveolus by preventing over-inflation. B) As air is forced out of the lungs during exhalation, alveolar pressure quickly declines, and the alveolus deflates. The deformed and stretched interstitial matrix relaxes as alveolar pressure is reduced, springing back into its relaxed state and compressing the alveolar walls which drives more air out of the alveolus. The surfactant secreted by type II alveolar epithelial cells (AEC) creates a liquid barrier that prevents the AECs from sticking together due to surface tension as the alveolus deflates, thereby preventing the alveolus from collapsing. This air-liquid interface between the AECs and the alveolar airspace ensures that the alveolus continues to inflate during inspiration with each respiration cycle. Created with BioRender.com.

Although these 3D organoid models can support *in vivo* alveolar differentiation and functions, they do not provide the mechanical forces necessary to stimulate the cyclic changes in alveolar volume that occur during respiration [451, 458]. These changes in alveolar volume impose mechanical strain onto the alveolar cells and their underlying matrix, distending them [458]. *In vitro* monolayer studies have shown that this cyclic, distending stress regulates AEC migration, differentiation, surfactant secretion and permeability [484-491]. These findings prompted the development of lung-on-chip models, which are microfluidic devices that recapitulate key functional, mechanical, and structural features of lung

tissue [440, 492-495]. The alveolar-capillary interface is typically modelled by culturing primary AECs and microvascular endothelial cells (MVEC) on opposing sides of a thin, ECM-coated, porous membrane and introducing air and fluid into the epithelial and endothelial compartments, respectively, which mimics the air-liquid interface of vascularised alveoli (Fig. 9A) [440, 493, 496]. Cyclic mechanical strain is generated by applying vacuum pressure to the device, which subjects the cells to cyclic stretch-relaxation events that mimic the changes in mechanical pressure generated during respiration. Studies employing this mechanically dynamic model have shown that the AECs and MVECs secrete surfactant and display structural integrity, respectively, demonstrating that simulating mechanical forces *in vitro* is important for stimulating *in vivo* cell behaviours [440]. They have also shown that introducing interleukins, bacteria and TNF-α into this model stimulates changes in cell adhesion, epithelial-endothelial barrier integrity and immune cell infiltration, effectively mimicking the *in vivo* responses of AECs and MVECs to pathological stimuli [440, 496].

However, since alveoli *in vivo* are 3D structures, recapitulation of the alveolar environment *in vitro* requires a 3D model that applies cyclic, multi-dimensional mechanical stress to cells [458, 497, 498]. While the lung-on-chip model traditionally utilises monolayer cultures to mimic the alveolar-capillary interface, its simple design can be modified to create 3D structures that provide a more *in vivo*-like environment. For example, one study engineered a hollow, 3D, MVEC-populated tube surrounded by AECs using the principles developed by the original lung-on-chip model to create a more physiologically representative alveolar-capillary interface (Fig. 9B) [493]. The study found that culturing MVECs in a 3D environment that was subjected to shear fluidic forces directed *in vivo*-like blood clot formation and morphology in a way that had previously never been recapitulated *in vitro* [499, 500]. The 3D geometry of alveoli has also been recapitulated in a sophisticated organoid-on-chip model, where a gelatin-based hydrogel was modified to contain uniform, interconnecting pores that were populated with human AECs to create alveolar-like sacs [494]. These hydrogels recapitulated the bulk stiffness of lung tissue and, following their encapsulation within a mechanically tuneable chip, enabled alveolar sac expansion and contraction, which was shown to promote tight junction formation between AECs and therefore help maintain alveolar integrity [494, 501, 502].

Together, these *in vitro* models of lung alveoli demonstrate that alveolar tissue structure and functions can be recapitulated *in vitro* by providing AECs with stromal growth factors, simulating the air-liquid interface with AECs and MVECs and subjecting the cells to cyclic tensile strain. These models also show that biochemical, physical, and mechanical cues collectively regulate the ability of vascularised alveoli to facilitate gas exchange between air and blood, and demonstrate that it is possible to simulate complex biological processes such as tissue development and disease progression *in vitro*.

3D organoid models of breast tissue

3D organoid models are valuable tools for investigating and defining cell-ECM interactions that regulate tissue structure and function. Their relative simplicity, consistency and definition compared to tissues, which are complex and variable, permit researchers to identify and isolate signalling

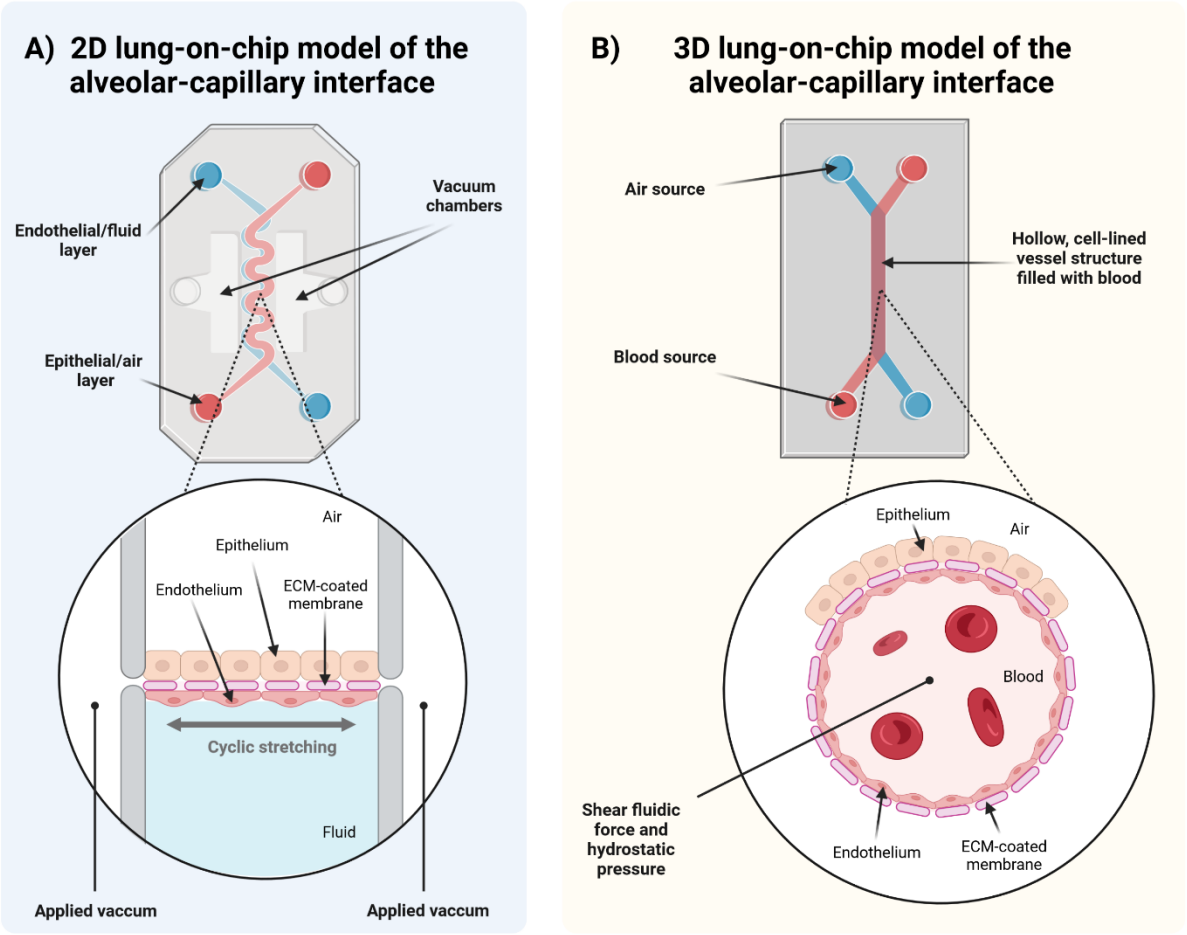

Fig. 9. Micro-engineered models of the alveolar-capillary interface. A) 2D lung-on-chip models are typically composed of three aligned layers to create two (top and bottom) chambers that are separated by a flexible, porous membrane coated with extracellular matrix (ECM). Alveolar epithelial cells (AEC) are cultured on top of the membrane while blood vessel endothelial cells are cultured on the bottom side of the membrane to create a cell bilayer that mimics the alveolar-capillary interface. Once the cells are confluent, air is introduced into the top chamber while the bottom chamber remains filled with fluid to simulate the alveolar airspace and blood, respectively. Air and fluid flow can be controlled independently. Two large side chambers are connected to either side of the ECM-coated membrane. Vacuum can be repeatedly applied to these chambers to stretch the membrane to simulate the cyclic distension and relaxation of the alveolus during breathing. Adapted from [440]. B) A 3D adaption of the lung-on-chip model was created by Jain et al. [493]. A porous, ECM-coated membrane is manipulated into a hollow tube and lined with endothelial cells to form a lumen. AECs are cultured on top of the tube. Blood is perfused through the lumen of the vessel-like tube while air surrounds its exterior. Created with BioRender.com.

mechanisms that drive specific tissue processes. Indeed, various 3D organoid models have been used to investigate how the biochemical, physical, and mechanical properties of the breast ECM regulate mammary gland organisation and function in healthy and cancerous breast tissue.

The primary function of the mammary gland is to secrete milk during lactation, which mammary acini are responsible for synthesising [503]. Acini are hollow, bi-layered spheroids that are composed of luminal epithelial cells surrounded by flattened myoepithelial cells and a laminin-rich basement membrane, which separates the acini from the collagen-rich, loose interstitial matrix of the mammary gland [504, 505]. Milk proteins such as β-casein and lipids are secreted into the lumen by the luminal epithelial cells, and myoepithelial contractions force the milk out of the acini and into the mammary ducts towards to the nipple [503, 506, 507]. Since milk production is only required during lactation,

acinar structure and function is tightly regulated by extracellular cues that are generated during puberty, pregnancy, lactation, and involution [286, 324, 327].

Acinar development begins in humans during puberty, where environmental factors such as hormonal cues, growth factors, MMPs and fibronectin drive ductal elongation and branching which leads to the formation of ducts terminating in clusters of immature acini that cannot synthesise or secrete milk [503, 506-512]. Pregnancy hormones such as progesterone and prolactin stimulate the differentiation of immature acini into vascularised acini that synthesise and secrete milk (called secretory acini) [505-507, 513]. Acinar morphogenesis is also aided by the basement membrane, which provides both mechanical stability to the acinar structures and supplies the cells with biochemical cues that direct cell differentiation, survival, and proliferation [286, 291, 327, 436, 506, 514]. Following childbirth, reduced progesterone levels paired with increased prolactin and insulin signalling stimulate an increase in acinar milk production, and suckling stimulates the release of oxytocin, which promotes myoepithelial contractions that force milk out of the acini [506, 515, 516]. Consistent loss of suckling-generated mechanical cues prompts mammary gland involution, where the luminal epithelial cells undergo apoptosis and most acini subsequently collapse and are eventually cleared, with only a few remaining after the remodelling process is complete [506, 507]. Through these remodelling events, acinar development, organisation, and function are controlled to ensure that milk production only occurs when necessary. The dynamic nature of acini, paired with their reliance on biochemical and biomechanical matrix cues to direct their organisation and function, makes them important structures to examine *in vitro*.

While early *in vitro* studies showed that floating collagen I gels could support the organisation of primary mouse MECs into polarised clusters and stimulate casein protein secretion, truly *in vivo*-like acinar structures could only be generated when culturing MECs on Matrigel, a basement membrane extract [290, 434, 517, 518]. MECs cultured on top of Matrigel differentiated into polarised, hollow spheroids that were surrounded by a laminin-rich basement membrane and secreted both casein and whey milk proteins into the lumen in response to pro-lactogenic stimulation, thereby recapitulating the key properties of secretory acini [290, 435, 519, 520]. These findings indicated that mammary ECM composition directs acinar differentiation [434]. They also revealed that the mechanical properties of the matrix also regulate MEC fate, as collagen I gels attached to petri dishes were unable to promote MEC organisation into acinar-like structures, stimulate MEC differentiation or support milk protein synthesis. 3D *in vitro* organoid model studies demonstrated that mammary acinar formation is primarily driven by the acinar basement membrane, as single MECs differentiated into polarised acini following their encapsulation in Matrigel, whereas MECs encapsulated in collagen I gels formed clusters that displayed reverse polarity, lacked a basement membrane, and did not form lumen and therefore were not *in vivo*-like acini [315, 436, 521]. Further studies showed that the basement membrane protein laminin 111, which is primarily secreted by myoepithelial cells *in vivo*, promotes MEC differentiation, directs acinar polarity and stimulates β-casein secretion *in vitro*, identifying laminin 111 as a key regulator of acinar development, maintenance, and function [288, 521]. These studies also demonstrated that Matrigel, which is primarily composed of laminin 111, recapitulates the

key biochemical properties of the basement membrane that surrounds mammary ducts and acini [522]. Matrigel's ability to stimulate *in vivo* MEC behaviours made it an established scaffold for 3D *in vitro* studies into MEC behaviour, as numerous Matrigel-based *in vitro* models have been used to elucidate cell-matrix signalling mechanisms involved in regulating MEC organisation and function [523-527]. For example, multiple studies have identified matrix-integrin interactions as crucial regulators of MEC polarity, survival, β-casein synthesis, and basement membrane formation through various signal transduction pathways that affect the activity of transcription factors such as p53 and Stat5 [436, 446, 528-532]. These studies also found that reduced expression of α3 and β1 integrins can stimulate malignant behaviours in MECs, such as reduced sensitivity to pro-apoptotic signals and loss of polarity, which demonstrates that MEC organisation and function depend on the ability of MECs to communicate with their ECM.

Increased appreciation of the role mechanical cues play in regulating cell behaviour prompted numerous studies into how breast matrix stiffness (defined here as the resistance of the ECM to deformation) regulates MEC organisation and function [533, 534]. There is currently no consensus on how stiff healthy human breast tissue is, as studies have employed different force measurement techniques to characterise the mechanical properties of breast tissue which have yielded a variety of results that appear to contradict one another, likely because some studies have subjected breast tissue to non-physiological forces [94, 242, 399, 535-540]. There is also significant variation in breast tissue stiffness between individuals as various factors including hormones, age, and number of pregnancies collectively regulate breast matrix composition and organisation and therefore the mechanical properties of the breast matrix [22, 541, 542]. Nonetheless, studies performed on human and mouse breast tissue explants have consistently shown that tumorigenic breast interstitial matrix is stiffer than healthy breast interstitial matrix [94, 536, 543]. It has also been established that individuals with denser, stiffer breast tissue are at increased risk of developing breast cancer than individuals with soft breast tissue [544]. Increased interstitial matrix stiffness in breast tissue is correlated with increased fibrillar collagen deposition around ducts and acini, as well as increased collagen fibril diameter, cross-linking and linearisation, increasing the density of the interstitial matrix (Fig. 10) [21, 545-551]. However, the mechanisms responsible for promoting breast matrix stiffness and the pro-oncogenic mechanosignalling events that subsequently occur are poorly understood and require interrogation using mechanically modifiable models of the breast ECM [552].

In vitro studies employing collagen I gels to simulate the breast interstitial matrix have shown that increased collagen I fibril density and local collagen cross-linking stimulates MEC growth and invasion through activation of Ras–mitogen-activated protein kinase (MAPK) and focal adhesion kinase (FAK) signalling pathways, and increased expression of matrix-remodelling enzymes such as MMPs and LOXs [21, 551, 553]. Increased collagen I density was also found to stimulate vinculin and FAK localisation to intracellular adhesion sites and increase Rho and Rho-associated coiled-coil containing protein kinase (ROCK) activity in MECs, which decreased cell contractility and subsequently led to the formation of proliferative, disorganised structures that exhibited pro-invasive behaviour [554]. These findings also demonstrated that cells sense matrix density and stiffness independently of one another,

as MECs could invade porous collagen I gels without depending on MMP activity, showing that MECs integrate physical and mechanical cues from their environment to modulate their behaviour.

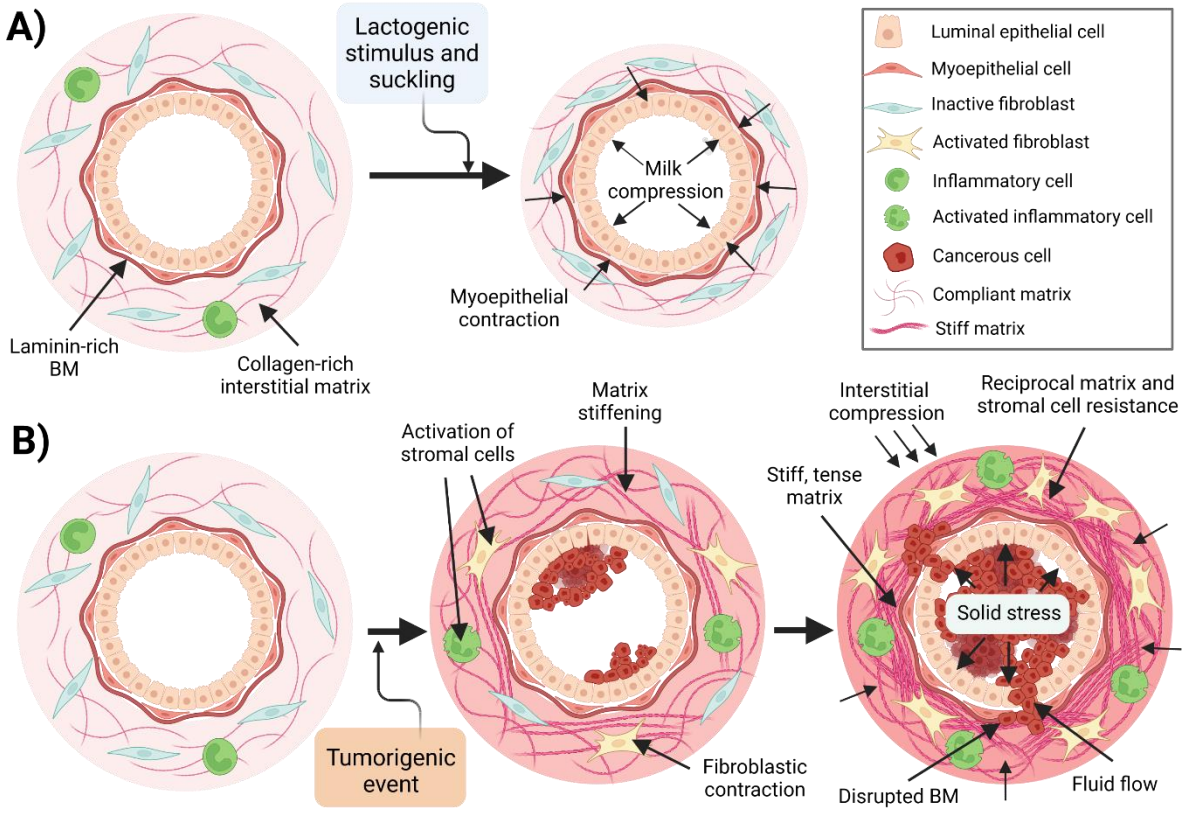

Fig. 10. The human mammary gland is sensitive to mechanical forces. A) During lactation, mammary luminal epithelial cells and their basement membrane are subjected to compressive stress as milk accumulates in alveoli (acini), distending them. Suckling and oxytocin stimulation creates inward tensile forces on the luminal epithelial cells as the myoepithelium contracts. The contractions force milk out of the acini towards the nipple. Absence of these lactogenic stimuli leads to milk accumulation within the acini, which exerts an outwards compressive force onto the luminal epithelium. A reciprocal, inward-projecting compressive force is generated by the interstitial matrix and the myoepithelium, which eventually disrupts tight junctions between the acinar cells. Prolonged exposure to these forces sensitises the cells to apoptosis, leading to involution. B) The healthy mammary gland is composed of ductal structures that terminate in acini, which are surrounded by a compliant, open-meshwork interstitial matrix. Fibroblasts reside in the interstitial matrix where they regulate matrix organisation, and inflammatory (immune) cells patrol the interstitial matrix. Mammary epithelial cells (MEC) that accumulate pro-oncogenic genetic mutations and epigenetic transformations along with altered matrix organisation and composition become uncontrollably proliferative and ignore pro-apoptotic signals. The malignant cells eventually fill the lumen of the gland and exert outwards compressive stress onto the basement membrane (BM), the myoepithelium and the interstitial matrix, which reciprocate this force. The malignant cells secrete various soluble factors that stimulate immune cell activation and infiltration and fibroblast activation. Activated fibroblasts (myofibroblasts) remodel the interstitial matrix by increasing matrix production and upregulating the activity of matrix organising and modifying factors such as cross-linking enzymes. The interstitial matrix gradually stiffens due to its altered composition and organisation, unregulated inflammation and myofibroblastic contractions. Interstitial fluid pressure from compromised lymph and blood vessels also increases. This increased stiffness exerts more and more resistance onto the malignant mammary gland structure. Eventually, the BM degrades due to elevated matrix metalloproteinase (MMP) activity and dysfunctional BM synthesis and assembly. The malignant cells exhibit dysfunctional tensional homeostasis responses and respond to the increased environmental forces by breaking through the compromised BM and invading the matrix. Adapted from [399]. Created with BioRender.com.

However, given that luminal MECs, which are commonly employed in *in vitro* studies, only have direct contact with their basement membrane and myoepithelial cells, encapsulating non-myoepithelial MECs in collagen I gels does not provide them with the biochemical cues they would receive *in vivo*

[514, 555]. As a result of this, several 3D, mechanically modifiable organoid models have been created using Matrigel. Chaudhuri's group developed a model that utilises different calcium ion concentrations to cross-link the alginate network interpenetrating Matrigel hydrogels and generate hydrogels of different stiffnesses that mimic normal, pre-malignant and malignant breast tissue (Fig. 11) [556].

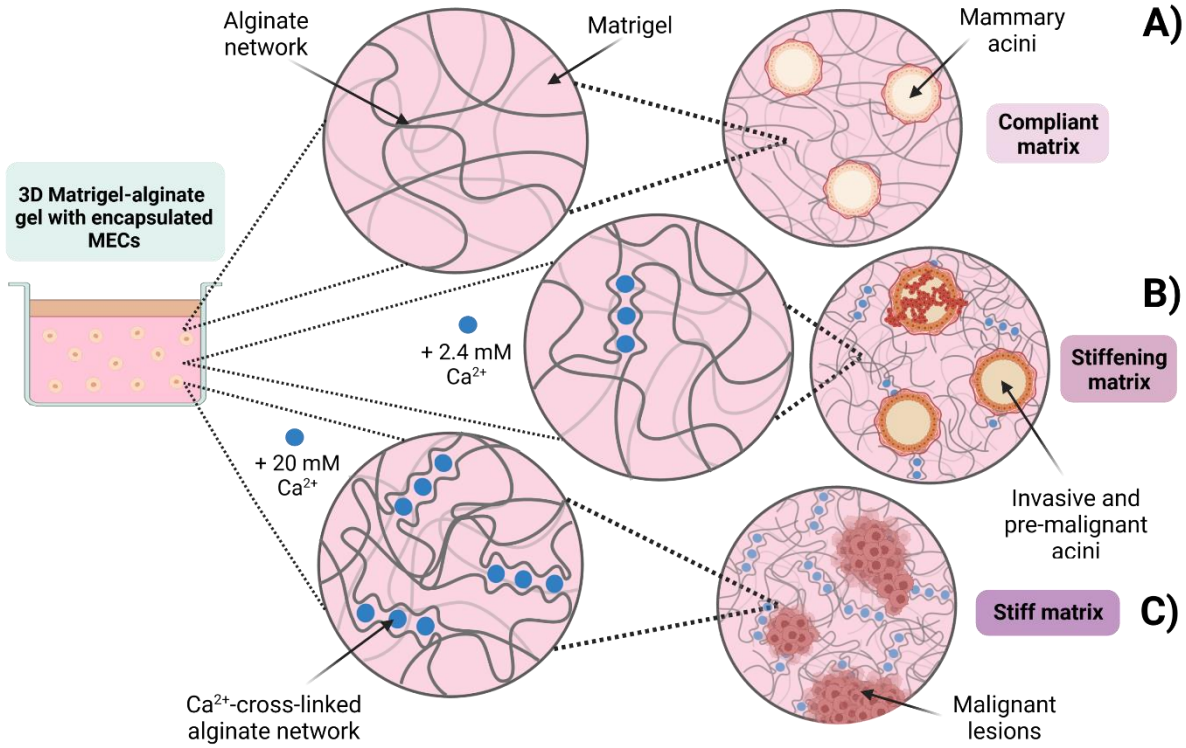

Fig. 11. 3D Matrigel-alginate hydrogels can be mechanically modified to mimic the stiffness of healthy, pre-tumorigenic and tumorigenic breast matrices. A) Single mammary epithelial cells (MEC) encapsulated in Matrigel-alginate gels are surrounded by a compliant matrix consisting of Matrigel and an interpenetrating alginate network. The lack of tension in the unmodified Matrigel-alginate matrix, paired with Matrigel's bioactivity, permits the cells to differentiate into mammary acini. B) Adding calcium cations (Ca^{2+}) into Matrigel-alginate gels stiffens the gel. The cations cross-link the alginate network by interacting with guluronic acid-rich (G-block) regions within alginate (zig-zag regions connected by blue dots), which associate with neighbouring G-block regions. These cross-links increase the stiffness of the hydrogel by increasing the resistance of the hydrogel matrix to deformation. These cross-links do not alter the porosity or architecture of Matrigel-alginate gels as the G-block regions are intrinsic features of alginate. Single MECs encapsulated in Matrigel-alginate gels with a Ca^{2+} concentration of 2.4 mM organise into acini that display some malignant phenotypes. Acini form invasive structures, lose their cell polarity, and proliferate uncontrollably, which resembles how tumorigenic acini initially behave *in vivo*. C) Increasing the concentration of Ca^{2+} increases Matrigel-alginate gel stiffness as more cross-links form within the interpenetrating alginate network. MECs encapsulated in Matrigel-alginate gels stiffened with 20 mM Ca^{2+} do not form acini. The cells grow and proliferate uncontrollably and invade their surrounding matrix, which recapitulates how tumorigenic MEC lesions behave *in vivo*. Created with BioRender.com.

Using this model, studies have found that increased breast matrix stiffness alters chromatin accessibility, aldehyde metabolism and hemidesmosome formation in MECs, with stiffness induced malignant MEC behaviours being linked to increased activation of pro-tumorigenic transcription factors, increased DNA damage caused by reactive aldehydes and altered α6β4 integrin and plectin localisation, respectively [556-559]. Increased Matrigel-alginate stiffness has also been found to inhibit invasive behaviours in tumorigenic MECs, which supports the findings obtained from collagen I-

based models that emphasised collagen matrix density as the driving force behind MEC invasion [21, 551, 553, 560]. Another 3D organoid model of the breast matrix combines collagen I and Matrigel to recapitulate both the basement membrane and interstitial matrix environments of the breast ECM, where hydrogel stiffness can be altered by changing Matrigel and collagen I concentration or by incorporating cross-linkers such as ribose into the gel [545, 553, 561, 562]. Increasing Matrigel-collagen I gel stiffness was shown to disrupt acinar formation, MEC polarity and adhesion and stimulate unrestrained MEC growth and invasion [94, 553]. Stiff Matrigel-collagen I matrices were also found to stimulate secretion of matrix factors such as MMP-14 and laminin and promote expression of the oncogene ZNF217, which stimulates MEC proliferation and suppresses apoptosis through protein kinase B (Akt) signalling [545, 562]. These findings indicate that matrix stiffness regulates MEC behaviour and matrix composition in what may well be a mechanically stimulated positive-feedback loop, which correlates with matrix remodelling events that arise during breast cancer progression [543, 546, 548].

Together, these 3D *in vitro* organoid models indicate that breast matrix composition predominantly drives acinar formation and function while breast matrix stiffness regulates maintenance of *in vivo* MEC behaviours and matrix organisation.

Established scaffolds used in 3D organoid models are limited in their ability to simulate tissue ECMs accurately and reliably

Matrigel is frequently used to simulate tissue ECMs in 3D organoid models due to its ability to stimulate *in vivo* behaviours in a variety of cell types [435, 563-565]. However, Matrigel suffers from numerous limitations that affect its ability to accurately and consistently model tissue ECMs. Matrigel is a basement membrane extract obtained from murine Engelbreth-Holm-Swarm (EHS) tumours that is predominantly composed of laminin 111, collagen IV, nidogen and perlecan, in addition to numerous matrix- and tumour-derived factors such as VEGF, EGF, FGF, cytokines, interleukins and MMPs [522, 564, 566-571]. Matrigel's complex composition of matrix proteins and bioactive soluble factors gives it similar functional properties to early basement membranes which allows it to maintain stem cell pluripotency and stimulate the development of epithelial organoids and endothelial tubules, but it lacks some tissue- and development-specific matrix factors that are required to support the formation of truly *in vivo*-like organoids in some models [567, 572-574]. For example, intestinal organoids grown in Matrigel lack luminal villous protrusions, as their formation requires the basement membrane protein laminin 511 which is not enriched in Matrigel [575-577]. Matrigel's complexity makes it difficult to identify whether changes in cell behaviour are due to controlled variables or Matrigel-derived, independent factors, which is of particular concern for studies investigating tumour development and progression since Matrigel contains many poorly defined pro-tumorigenic factors [567, 578-581]. Matrigel may also contain xenogenic contaminants, which limits Matrigel's ability to accurately simulate human ECMs [582-584]. Additionally, Matrigel is a soft substrate that often needs to be stiffened to mimic the mechanical properties of tissues, but its mechanical and physical properties are difficult to independently modify and the range of Matrigel stiffnesses that can be generated using conventional modification techniques is limited [556, 573, 585, 586]. All these

limitations are exacerbated by Matrigel's biochemical and mechanical batch-to-batch variability, which makes it difficult to create reproducible, Matrigel-based models of tissue ECMs [567, 570, 587, 588].

Alternative bioactive 3D scaffolds to Matrigel include hydrogels composed of organic polymers such as collagen I or HA, which can support some *in vivo* cell behaviours while being well defined substrates, providing greater reproducibility in studies [589-592]. Decellularised ECMs (dECM) obtained from tissue explants are also popular for 3D *in vitro* studies, as these scaffolds supply cells with tissue-specific environments and can also provide *in vivo* spatial and physical cues which stimulate more *in vivo* cell behaviours than single-polymer scaffolds or Matrigel [26, 573, 593-597]. For example, human MECs formed branching, hollow ducts within decellularised human breast tissue reminiscent of mammary ducts *in vivo* [598]. However, these scaffolds also suffer from limitations. Collagen I and HA gels can be xenogenic and do not provide cells with all the biochemical cues they need to behave as they do *in vivo*, which has led to some studies incorporating other bioactive materials, such as Matrigel, into the scaffolds which increases their complexity and makes them harder to reproduce [412, 599-602]. In contrast, dECMs can support many *in vivo* cell behaviours due to their tissue-derived origins but this comes at the expense of their poor definition, which is exacerbated by tissue heterogeneity between individuals and cryptic diseases that affect tissue composition and organisation [26, 573, 593, 598, 603]. The complexity and heterogeneity of dECMs can make it challenging to identify matrix factors responsible for stimulating cell functions, which makes it difficult to isolate and examine specific signalling mechanisms [596, 604]. Furthermore, organic and dECM scaffolds are difficult to modify mechanically and physically as their physical integrity and mechanical properties are weak and difficult to independently modify, which limits their ability to simulate stiff or diseased tissues [94, 433, 573, 585, 605]. Therefore, the applications of organic scaffolds for 3D *in vitro* studies are limited, particularly with regards to mechanotransduction studies given the challenges in mechanically modifying organic substrates.

Synthetic scaffolds are more consistent, defined, and amenable to chemical and mechanical modifications. Synthetic scaffolds are typically created by creating physical or chemical cross-links between synthetic monomers such as acrylamides, acrylates and glycols to form water-swollen, cross-linked polymer networks [606]. Polyacrylamide (PAM) hydrogels are commonly used as cell scaffolds for *in vitro* studies because they are easy and cheap to make, and their simple composition allows researchers to create well defined, reproducible *in vitro* models that can be chemically and mechanically modified to improve their biocompatibility and provide cells with more *in vivo*-like environments [433, 607-610]. For example, PAM hydrogels are uncharged and lack cell adhesion motifs, but studies have shown that they can be coated with matrix proteins to support cell viability and stimulate *in vivo* cell behaviours while also remaining mechanically tuneable [94, 433, 545, 559, 611-613]. However, PAM hydrogels are not compatible for 3D cell culture as the precursors used to make the gels are toxic to cells, which limits their ability to provide cells with appropriate physical and mechanical cues [433, 614]. Synthetic hydrogels that are suitable for cell encapsulation can be made from polymers such as polyethylene-glycol (PEG) or polylactic acid (PLA) [615-618]. The physical and mechanical properties of these chemically well-defined hydrogels can be precisely modified to create

hydrogels with different porosities, stiffnesses and elasticities [616, 619, 620]. Stimulus-sensitive cross-linkers can also be integrated into synthetic hydrogels to create responsive hydrogels with controlled mechanical and physical properties that recapitulate the dynamic extracellular environment in healthy and diseased tissues [606, 621-624]. Additionally, the viscoelasticity and mechanical stability of synthetic hydrogels can allow them to be physically manipulated to create intricate structures that mimic key spatial properties of tissues through techniques such as bioprinting [618, 620, 625-627]. For example, the topology of lung air ducts, their alveoli and the surrounding vasculature were patterned into PEG hydrogels to create a mechanically sensitive and structurally representative model of the lung airway that could be perfused with air and blood to investigate how the cyclic distention of alveoli influences blood flow and gas exchange [615]. However, since these hydrogels are also biologically inert, they must be functionalised with peptide motifs, matrix proteins, growth factors or polysaccharides to support cell proliferation, adhesion, differentiation, matrix secretion, long-term survival and organoid formation [625, 627-633]. Although functionalising synthetic hydrogels provides researchers with greater control over the biochemical properties of their scaffold, modifying synthetic hydrogels can be expensive, time-consuming and challenging [634]. Furthermore, some synthetic hydrogels are formed using cytotoxic precursors, or release toxic compounds over time, which can be off-putting to researchers who are unfamiliar with polymer chemistry [573].

The limitations of established organic and synthetic scaffolds as 3D *in vitro* organoid models emphasise the need for mechanically tuneable cell scaffolds that are inherently biocompatible, defined, and reproducible.

Self-assembling peptide hydrogels are attractive scaffolds for 3D *in vitro* organoid models

An attractive group of hydrogels for 3D cell culture are self-assembling peptide hydrogels (SAPH) because they are intrinsically biocompatible, can polymerise without needing intrusive cross-linkers and are also defined, reproducible and tuneable [635, 636]. SAPHs are composed of short (typically 2-30 amino acids long), synthetic peptides which self-assemble into supramolecular structures through non-covalent hydrogen bonding, pi-bonding, electrostatic interactions, van der Waals interactions or hydrophobic interactions between peptides and their aqueous environment [636-639]. These non-covalent interactions are driven by hydrophilic and hydrophobic residue patterns within the peptide sequence, which create distinctive charged and hydrophobic domains that direct peptide self-assembly into secondary structures such as β-sheets, β-hairpins, α-helices or collagen-like triple-helices [637, 640-643]. Hydrophobic and electrostatic interactions between the secondary structures drive their assembly into higher-order structures such as cylindrical, tape- or ribbon-like nanofibres, or collagen-like fibrils which become entangled or aggregate in solution to form hydrated scaffolds [637, 641, 642, 644, 645]. Peptide self-assembly and gelation is also regulated by factors such as peptide concentration, temperature, pH, and ions, which provides researchers with precise control over scaffold density, stiffness, and organisation [637, 638, 640, 641, 646, 647].

Since SAPHs are composed of synthetic peptides that self-assemble into hierarchical protein structures, they can recapitulate key aspects of ECM assembly and architecture while remaining

defined and consistent [638, 640, 644, 648, 649]. For example, some SAPHs have been designed to mimic fibrillar collagen matrices by incorporating the Gly-Pro-hPro motif or adhesive terminal motifs into synthetic peptides to promote triple helix and fibril assembly [650-654]. Fibroblasts and mesenchymal stem cells seeded into collagen-like SAPHs were morphologically identical to their counterparts encapsulated in organic collagen I gels and responded to increased SAPH stiffness [650, 651]. In addition, the peptide-based composition of SAPHs makes them intrinsically biocompatible and biodegradable, which allows them to support various *in vivo* cell behaviours without being biochemically modified [655-659]. Furthermore, peptide sequences can be modified to control SAPH architecture, mechanical properties, and bioactivity which allows researchers to independently control the structural, mechanical and biochemical properties of their SAPH while keeping it defined and reproducible [644, 660-664]. For example, various biomimetic sequences present in matrix proteins and soluble factors such as RGD and IKVAV motifs can be incorporated into synthetic peptides to promote cell proliferation, adhesion, migration, differentiation and morphogenesis [644, 665-668]. However, functionalising SAPHs with peptide motifs can be expensive, particularly if multiple motifs are required to stimulate desirable cell behaviours in a scaffold [669].

PeptiGels® are a family of β-sheet forming, nanofibrillar SAPHs that can be used to create 3D, reproducible and mechanically-tuneable organoid models that support *in vivo* cell behaviours (Fig. 12) [670]. Their design is based upon the amphipathic, β-sheet forming peptides pioneered by Zhang's group, where polypeptide self-assembly is primarily driven by the shielding of hydrophobic residues from solvent, which creates β-sheet fibres that have hydrophobic cores and hydrophilic faces [636, 671]. These fibres form inter-molecular non-covalent bonds that drive the formation of a hydrated network of entangled fibres. Several ready-to-use PeptiGels® with unique mechanical, biomimetic and charge properties have been designed by Manchester BioGEL, which allows researchers to explore scaffold compatibility for specific cell cultures without having to design and create the hydrogel themselves [670]. However, their novelty as 3D, synthetic cell scaffolds can present challenges for researchers looking to isolate biological material from PeptiGel®-encapsulated cells to examine cell behaviour, as conventional protocols may require optimisation which can be time-consuming and expensive [672, 673]. Nonetheless, multiple studies have demonstrated that 3D PeptiGels® support cell viability, growth, proliferation, differentiation and matrix and growth factor secretion [656, 657, 674-677]. 3D PeptiGels® that mimicked the stiffness of healthy and fibrotic liver tissue were shown to modulate vesicular transport and the secretion of pro-fibrotic factors by hepatic stellate cells through integrin signalling events in a stiffness-dependent manner [678]. Furthermore, PeptiGel®-encapsulated human induced pluripotent stem cells organised into heterogenous kidney organoids which were viable for at least 24 days and produced their own basement membrane [679]. These studies demonstrate that PeptiGels® can recapitulate key properties of tissue ECMs to support *in vivo* cell behaviours. PeptiGels® are also amenable to mechanical modifications and biochemical functionalisation [680]. The addition of growth factor-conjugated graphene oxide flakes to PeptiGels® was shown to affect the bulk mechanical properties of the hydrogel and enhance the viability of encapsulated cells [681-683]. Additionally, the viscoelastic and shear-thinning properties of

PeptiGels® make them amenable to bioprinting, which allows researchers to generate reproducible 3D structures with precisely controlled geometry without having to mechanically optimise the hydrogel for bioprinting applications [657, 682, 684-686].

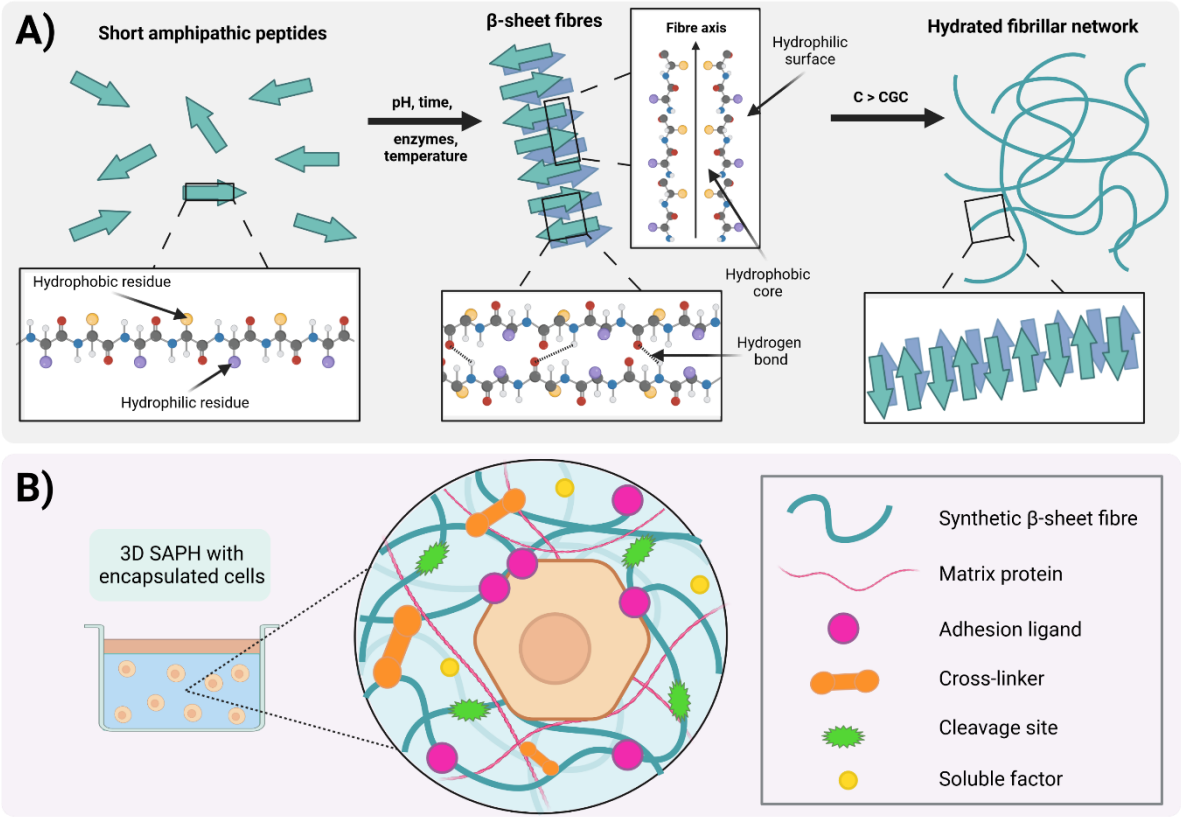

Fig. 12. β-sheet forming, self-assembling peptide hydrogels can be functionalised to provide a physiologically representative environment for encapsulated cells. A) Short, β-sheet forming peptides are composed of alternating hydrophobic and hydrophilic amino acids. Under the right environmental conditions, the peptides assemble into β-sheet fibres that have a hydrophilic, solvent-presenting face and a hydrophobic core. The hydrophobic residues are packed into the centre of the fibre where they interact with other hydrophobic residues while the hydrophilic residues are exposed to the solvent and shield the hydrophobic residues. Non-covalent hydrogen bonds and ionic interactions stabilise these fibres. When the peptide concentration (C) is greater than the critical gelation content (CGC), the β-sheet fibres entangle with one another to form a hydrated, fibrillar network. B) Self-assembling peptide hydrogels (SAPH) can be functionalised for cell culture in various ways. Matrix proteins such as collagens, laminins, proteoglycans, and fibronectin can be added into SAPHs to provide cells with tissue-specific cues that direct cell growth, proliferation, adhesion, or differentiation. Adhesion motifs can also be integrated into the peptide sequence of SAPHS. SAPHs can be cross-linked physically, through peptide interactions, or covalently using photo- and chemical-sensitive cross-linkers. Cleavage motifs can be incorporated into the peptide sequence which permit controlled matrix degradation through passive (hydrolysis) cell-directed (matrix proteases) or user-directed (photo-degradation) means. Soluble, bioactive factors such as growth factors can also be incorporated into SAPHs to elicit *in vivo* cell responses. Adapted from [433]. Created with BioRender.com.

SAPHs are biocompatible, well defined, reproducible, and tuneable hydrogels. Their hierarchical self-assembly into polypeptide fibres and fibrils recapitulates the structure and organisation of key ECM proteins such as collagens, which have been shown to stimulate *in vivo* cell behaviours. Moreover, the peptide sequences of SAPHs can be modified to include functional motifs that are present within native ECM proteins and soluble factors, which provides cells with a more *in vivo*-like environment. Finally, the mechanical properties of SAPHs can be fine-tuned to provide cells with tissue- and disease-specific mechanical cues that can be interrogated *in vitro* to identify mechanosignalling

pathways. Therefore, SAPHs are well-suited to simulating tissue ECMs in 3D *in vitro* organoid models.

Concluding remarks

Decades of research into ECM structure and function have shown that ECMs are essential for the health and survival of multicellular organisms. ECMs keep tissues and organs connected, provide structural support and bulk to tissues, and regulate tissue organisation and function. Numerous studies have shown that ECM composition and organisation is complex and tissue-specific because the ECM constituents provide physical, mechanical, and biochemical cues that regulate the fate and behaviour of resident cells. Cells can also respond to environmental cues by remodelling their environment by exerting their own forces or secreting factors that alter matrix architecture. Through dynamic and intricate signalling mechanisms, cells and their ECM collectively dictate the fate and behaviour of tissues.

Breast cancer is associated with aberrant breast matrix composition and organisation, which have been shown to trigger dysfunctional MEC behaviours via intricate signal transduction mechanisms. Established models of the breast matrix such as Matrigel-alginate gels have shown that some of these signalling cascades are stimulated by changes in breast matrix stiffness, which occurs as the ECM is remodelled during breast cancer development and progression. However, Matrigel is limited in its ability to create accurate, consistent, and mechanically tuneable models of breast matrix stiffness and the mechanotransduction mechanisms responsible for regulating MEC behaviour are still poorly defined. Since SAPHs such as PeptiGels® are defined, consistent and tuneable, it is possible that they can be functionalised for MEC culture to provide a synthetic alternative to Matrigel. This ‘synthetic Matrigel’ could be used to model breast matrix stiffness to investigate pro-oncogenic mechanosignalling events in MECs and help identify molecular targets for preventative and curative breast cancer therapies.

Project aims and objectives

Breast matrix stiffness regulates mammary epithelial cell fate through mechanosensitive signal transduction events, and increased matrix stiffness has been shown to trigger pro-oncogenic behaviours in mammary epithelial cells. However, the mechanotransduction events involved in driving mammary epithelial cell malignancy are poorly defined. Investigating these mechanosignalling events *in vitro* requires a 3D model that recapitulates the key biochemical properties of the human breast matrix and is amenable to mechanical modifications. Established 3D cell scaffolds are limited in their ability to accurately and reproducibly model human breast matrix stiffness. However, synthetic self-assembling peptide hydrogels such as PeptiGels® are a promising alternative to conventional cell scaffolds because they are biocompatible, well-defined, reproducible, and tuneable. Therefore, this thesis aims to investigate whether SAPHs can be used to generate 3D, mechanically tuneable *in vitro* organoid models of breast matrix stiffness.

The aims of this project are to:

- Investigate how human mammary epithelial cells respond to encapsulation in self-assembling peptide hydrogels of different stiffnesses by examining their ability to differentiate into polarised acini and comparing changes in protein expression between hydrogels of different stiffnesses and composition.
- Biochemically functionalise self-assembling peptide hydrogels for 3D mammary epithelial cell culture using breast matrix proteins to create a reproducible and accurate model of the breast matrix.
- Optimise experimental protocols for 3D self-assembling peptide hydrogel models of breast matrix stiffness to obtain clear and consistent data that will allow us to elucidate pro-oncogenic mechanosignalling events.

To address these aims, one or more self-assembling peptide hydrogels will need to be evaluated as scaffolds for 3D mammary epithelial cell culture. Here, I will be using PeptiGels® Alpha4 and Alpha7, which are self-assembling peptide hydrogels manufactured by Manchester BioGEL. To investigate how breast matrix composition and stiffness affect acinar development, I will be using non-transformed, immortalised human mammary epithelial MCF10a cells as they differentiate into polarised acini in hydrogels that recapitulate the key properties of the breast matrix. To assess their suitability as models of the human breast matrix, the responses of MCF10a cells to encapsulation within Alpha4 and Alpha7 will be compared against the behaviour of MCF10a cells encapsulated within the reconstituted basement membrane extract Matrigel, which is an established model of the breast matrix.

It is hoped that this research will offer insights into how breast matrix stiffness and composition affect mammary epithelial cell behaviour and demonstrate how self-assembling peptide hydrogels might be functionalised for mammary epithelial cell culture. This research will also reveal novel techniques for obtaining qualitative and quantitative data from 3D self-assembling peptide hydrogel cultures.

References

1. Frantz, C., K.M. Stewart, and V.M. Weaver, *The extracellular matrix at a glance.* Journal of Cell Science, 2010. **123**(24): p. 4195.
2. Karamanos, N.K., et al., *A guide to the composition and functions of the extracellular matrix.* The FEBS Journal, 2021. **288**(24): p. 6850-6912.
3. Theocharis, A.D., et al., *Extracellular matrix structure.* Advanced Drug Delivery Reviews, 2016. **97**: p. 4-27.
4. Löffek, S., O. Schilling, and C.W. Franzke, *Biological role of matrix metalloproteinases: a critical balance.* European Respiratory Journal, 2011. **38**(1): p. 191.
5. Taipale, J. and J. Keski-Oja, *Growth factors in the extracellular matrix.* The FASEB Journal, 1997. **11**(1): p. 51-59.
6. Yue, B., *Biology of the extracellular matrix: an overview.* Journal of glaucoma, 2014. **23**(8 Suppl 1): p. S20-S23.
7. Dolega, M.E., et al., *Extracellular matrix in multicellular aggregates acts as a pressure sensor controlling cell proliferation and motility.* eLife, 2021. **10**: p. e63258.
8. Daley, W.P., S.B. Peters, and M. Larsen, *Extracellular matrix dynamics in development and regenerative medicine.* Journal of Cell Science, 2008. **121**(3): p. 255-264.
9. Lu, P., et al., *Extracellular matrix degradation and remodeling in development and disease.* Cold Spring Harbor perspectives in biology, 2011. **3**(12): p. 10.1101/cshperspect.a005058 a005058.
10. Pompili, S., et al., *The Charming World of the Extracellular Matrix: A Dynamic and Protective Network of the Intestinal Wall.* Frontiers in medicine, 2021. **8**: p. 610189-610189.
11. Handorf, A.M., et al., *Tissue stiffness dictates development, homeostasis, and disease progression.* Organogenesis, 2015. **11**(1): p. 1-15.
12. Hynes, R.O. and A. Naba, *Overview of the matrisome--an inventory of extracellular matrix constituents and functions.* Cold Spring Harbor perspectives in biology, 2012. **4**(1): p. a004903-a004903.
13. Kim, S.-H., J. Turnbull, and S. Guimond, *Extracellular matrix and cell signalling: the dynamic cooperation of integrin, proteoglycan and growth factor receptor.* Journal of Endocrinology, 2011. **209**(2): p. 139-151.
14. Lukashev, M.E. and Z. Werb, *ECM signalling: orchestrating cell behaviour and misbehaviour.* Trends in Cell Biology, 1998. **8**(11): p. 437-441.
15. Burgess, J.K. and M.C. Harmsen, *Chronic lung diseases: entangled in extracellular matrix.* European Respiratory Review, 2022. **31**(163): p. 210202.
16. Cohen, J.C. and J.E. Larson, *Cystic fibrosis transmembrane conductance regulator (CFTR) dependent cytoskeletal tension during lung organogenesis.* Developmental Dynamics, 2006. **235**(10): p. 2736-2748.
17. Iozzo, R.V. and M.A. Gubbiotti, *Extracellular matrix: The driving force of mammalian diseases.* Matrix biology : journal of the International Society for Matrix Biology, 2018. **71-72**: p. 1-9.
18. Theocharis, A.D., D. Manou, and N.K. Karamanos, *The extracellular matrix as a multitasking player in disease.* The FEBS Journal, 2019. **286**(15): p. 2830-2869.
19. Cox, T.R. and J.T. Erler, *Remodeling and homeostasis of the extracellular matrix: implications for fibrotic diseases and cancer.* Disease models & mechanisms, 2011. **4**(2): p. 165-178.
20. Izzi, V., M.N. Davis, and A. Naba, *Pan-Cancer Analysis of the Genomic Alterations and Mutations of the Matrisome.* Cancers, 2020. **12**(8).
21. Provenzano, P.P., et al., *Matrix density-induced mechanoregulation of breast cell phenotype, signaling and gene expression through a FAK–ERK linkage.* Oncogene, 2009. **28**: p. 4326.
22. Sherratt, M.J., J.C. McConnell, and C.H. Streuli, *Raised mammographic density: causative mechanisms and biological consequences.* Breast cancer research : BCR, 2016. **18**(1): p. 45-45.
23. Gorski, J.P. and B.R. Olsen, *Mutations in extracellular matrix molecules.* Current Opinion in Cell Biology, 1998. **10**(5): p. 586-593.
24. Lamandé, S.R. and J.F. Bateman, *Genetic Disorders of the Extracellular Matrix.* Anatomical record (Hoboken, N.J. : 2007), 2020. **303**(6): p. 1527-1542.
25. Ma, X., et al., *3D bioprinting of functional tissue models for personalized drug screening and in vitro disease modeling.* Advanced drug delivery reviews, 2018. **132**(1872-8294 (Electronic)): p. 235-251.
26. Landberg, G., et al., *Patient-derived scaffolds uncover breast cancer promoting properties of the microenvironment.* Biomaterials, 2020. **235**.

27. Lee, J.Y. and O. Chaudhuri, *Regulation of Breast Cancer Progression by Extracellular Matrix Mechanics: Insights from 3D Culture Models.* ACS Biomaterials Science & Engineering, 2018. **4**(2): p. 302-313.
28. Rios de la Rosa, J.M., et al., *Colorectal tumor 3D in vitro models: advantages of biofabrication for the recapitulation of early stages of tumour development.* Biomedical Physics & Engineering Express, 2018. **4**(4): p. 045010.
29. Tian, A., J. Muffat, and Y. Li, *Studying Human Neurodevelopment and Diseases Using 3D Brain Organoids.* The Journal of Neuroscience, 2020. **40**(6): p. 1186.
30. Wong, C.-W., et al., *Biomaterial substrate-derived compact cellular spheroids mimicking the behavior of pancreatic cancer and microenvironment.* Biomaterials, 2019. **213**: p. 119202.
31. Chaicharoenaudomrung, N., P. Kunhorm, and P. Noisa, *Three-dimensional cell culture systems as an in vitro platform for cancer and stem cell modeling.* World journal of stem cells, 2019. **11**(12): p. 1065-1083.
32. Gaggar, A., et al., *The role of matrix metalloproteinases in cystic fibrosis lung disease.* European Respiratory Journal, 2011. **38**(3): p. 721.
33. Cuzick, J., et al., *Tamoxifen-Induced Reduction in Mammographic Density and Breast Cancer Risk Reduction: A Nested Case–Control Study.* JNCI: Journal of the National Cancer Institute, 2011. **103**(9): p. 744-752.
34. Yan, Y., et al., *The Use of Pluripotent Stem Cell-Derived Organoids to Study Extracellular Matrix Development during Neural Degeneration.* Cells, 2019. **8**(3): p. 2073-4409
35. Muncie, J.M. and V.M. Weaver, *Chapter One - The Physical and Biochemical Properties of the Extracellular Matrix Regulate Cell Fate*, in *Current Topics in Developmental Biology*, E.S. Litscher and P.M. Wassarman, Editors. 2018, Academic Press. p. 1-37.
36. Kaur, J. and D.P. Reinhardt, *Chapter 3 - Extracellular Matrix (ECM) Molecules*, in *Stem Cell Biology and Tissue Engineering in Dental Sciences*, A. Vishwakarma, et al., Editors. 2015, Academic Press: Boston. p. 25-45.
37. Engel, J., *Domain organizations of modular extracellular matrix proteins and their evolution.* Matrix Biology, 1996. **15**(5): p. 295-299.
38. Hohenester, E. and J. Engel, *Domain structure and organisation in extracellular matrix proteins.* Matrix Biology, 2002. **21**(2): p. 115-128.
39. Alberts, B., et al., *'The Extracellular Matrix of Animals'*, in *Molecular Biology of the Cell*. 2002, Garland Science: New York.
40. Kadler, K.E., et al., *Collagens at a glance.* Journal of Cell Science, 2007. **120**(12): p. 1955-1958.
41. Bosman, F.T. and I. Stamenkovic, *Functional structure and composition of the extracellular matrix.* The Journal of Pathology, 2003. **200**(4): p. 423-428.
42. Koch, M., et al., *A Novel Marker of Tissue Junctions, Collagen XXII.* Journal of Biological Chemistry, 2004. **279**(21): p. 22514-22521.
43. Sorushanova, A., et al., *The Collagen Suprafamily: From Biosynthesis to Advanced Biomaterial Development.* Advanced Materials, 2019. **31**(1): p. 1801651.
44. Brodsky, B. and A.V. Persikov, *Molecular Structure of the Collagen Triple Helix*, in *Advances in Protein Chemistry*. 2005, Academic Press. p. 301-339.
45. Ricard-Blum, S., *The collagen family.* Cold Spring Harbor perspectives in biology, 2011. **3**(1): p. 1943-0264 (Electronic).
46. Birk, D.E. and P. Brückner, *Collagens, Suprastructures, and Collagen Fibril Assembly*, in *The Extracellular Matrix: an Overview*, R.P. Mecham, Editor. 2011, Springer Berlin Heidelberg: Berlin, Heidelberg. p. 77-115.
47. Bretscher, L.E., et al., *Conformational Stability of Collagen Relies on a Stereoelectronic Effect.* Journal of the American Chemical Society, 2001. **123**(4): p. 777-778.
48. Berg, R.A. and D.J. Prockop, *The thermal transition of a non-hydroxylated form of collagen. Evidence for a role for hydroxyproline in stabilizing the triple-helix of collagen.* Biochemical and Biophysical Research Communications, 1973. **52**(1): p. 115-120.
49. Chow, W.Y., et al., *Proline provides site-specific flexibility for in vivo collagen.* Scientific Reports, 2018. **8**(1): p. 13809.
50. Shoulders, M.D. and R.T. Raines, *Collagen structure and stability.* Annual review of biochemistry, 2009. **78**: p. 1545-4509 (Electronic).
51. Khoshnoodi, J., et al., *Molecular Recognition in the Assembly of Collagens: Terminal Noncollagenous Domains Are Key Recognition Modules in the Formation of Triple Helical Protomers.* Journal of Biological Chemistry, 2006. **281**(50): p. 38117-38121.

52. Xu, E.-R., et al., *Structural analyses of von Willebrand factor C domains of collagen 2A and CCN3 reveal an alternative mode of binding to bone morphogenetic protein-2.* Journal of Biological Chemistry, 2017. **292**(30): p. 12516-12527.
53. Onursal, C., et al., *Collagen Biosynthesis, Processing, and Maturation in Lung Ageing.* Frontiers in Medicine, 2021. **8**.
54. Khoshnoodi, J., V. Pedchenko, and B.G. Hudson, *Mammalian collagen IV.* Microscopy research and technique, 2008. **71**(5): p. 357-370.
55. Mohs, A., et al., *Conformational Features of a Natural Break in the Type IV Collagen Gly-X-Y Repeat.* Journal of Biological Chemistry, 2006. **281**(25): p. 17197-17202.
56. Bella, J., et al., *Conformational Effects of Gly–X–Gly Interruptions in the Collagen Triple Helix.* Journal of Molecular Biology, 2006. **362**(2): p. 298-311.
57. Butterfield, R.J., et al., *Position of glycine substitutions in the triple helix of COL6A1, COL6A2, and COL6A3 is correlated with severity and mode of inheritance in collagen VI myopathies.* Human mutation, 2013. **34**(11): p. 1098-1004 (Electronic).
58. Cardinale, G.J. and S. Udenfriend, *Prolyl Hydroxylase.* Advances in Enzymology and Related Areas of Molecular Biology, 1974: p. 245-300.
59. Myllyharju, J. and K.I. Kivirikko, *Collagens, modifying enzymes and their mutations in humans, flies and worms.* Trends in Genetics, 2004. **20**(1): p. 33-43.
60. Peterkofsky, B., *Ascorbate requirement for hydroxylation and secretion of procollagen: relationship to inhibition of collagen synthesis in scurvy.* The American Journal of Clinical Nutrition, 1991. **54**(6): p. 1135S-1140S.
61. Hudson, B.G., et al., *Alport's Syndrome, Goodpasture's Syndrome, and Type IV Collagen.* New England Journal of Medicine, 2003. **348**(25): p. 2543-2556.
62. Cosgrove, D. and S. Liu, *Collagen IV diseases: A focus on the glomerular basement membrane in Alport syndrome.* Matrix Biology, 2017. **57-58**: p. 45-54.
63. Holmes, D.F., et al., *Chapter Three - Collagen Fibril Assembly and Function*, in *Current Topics in Developmental Biology*, E.S. Litscher and P.M. Wassarman, Editors. 2018, Academic Press. p. 107-142.
64. Canty, E.G. and K.E. Kadler, *Procollagen trafficking, processing and fibrillogenesis.* Journal of Cell Science, 2005. **118**(7): p. 1341-1353.
65. Linsenmayer, T.F., et al., *Type V collagen: molecular structure and fibrillar organization of the chicken alpha 1(V) NH2-terminal domain, a putative regulator of corneal fibrillogenesis.* Journal of Cell Biology, 1993. **121**(5): p. 1181-1189.
66. Von Der Mark, K., *CHAPTER 1 - Structure, Biosynthesis and Gene Regulation of Collagens in Cartilage and Bone*, in *Dynamics of Bone and Cartilage Metabolism (Second Edition)*, M.J. Seibel, S.P. Robins, and J.P. Bilezikian, Editors. 2006, Academic Press: Burlington. p. 3-40.
67. Revell, C.K., et al., *Collagen fibril assembly: New approaches to unanswered questions.* Matrix Biology Plus, 2021. **12**: p. 100079.
68. Smith-Mungo, L.I. and H.M. Kagan, *Lysyl oxidase: Properties, regulation and multiple functions in biology.* Matrix Biology, 1998. **16**(7): p. 387-398.
69. Kadler, K.E., A. Hill, and E.G. Canty-Laird, *Collagen fibrillogenesis: fibronectin, integrins, and minor collagens as organizers and nucleators.* Current Opinion in Cell Biology, 2008. **20**(5): p. 495-501.
70. McDonald, J.A., D.G. Kelley, and T.J. Broekelmann, *Role of fibronectin in collagen deposition: Fab' to the gelatin-binding domain of fibronectin inhibits both fibronectin and collagen organization in fibroblast extracellular matrix.* Journal of Cell Biology, 1982. **92**(2): p. 485-492.
71. Meek, K.M., *Corneal collagen-its role in maintaining corneal shape and transparency.* Biophysical reviews, 2009. **1**(2): p. 1867-2450 (Print).
72. Thorpe, C.T. and H.R.C. Screen, *Tendon Structure and Composition*, in *Metabolic Influences on Risk for Tendon Disorders*, P.W. Ackermann and D.A. Hart, Editors. 2016, Springer International Publishing: Cham. p. 3-10.
73. Viguet-Carrin, S., P. Garnero, and P.D. Delmas, *The role of collagen in bone strength.* Osteoporosis International, 2006. **17**(3): p. 319-336.
74. Rayagiri, S.S., et al., *Basal lamina remodeling at the skeletal muscle stem cell niche mediates stem cell self-renewal.* Nature Communications, 2018. **9**(1): p. 1075.
75. Siler, U., et al., *Characterization and functional analysis of laminin isoforms in human bone marrow.* Blood, 2000. **96**(13): p. 4194-4203.
76. Aumailley, M., et al., *A simplified laminin nomenclature.* Matrix Biology, 2005. **24**(5): p. 326-332.
77. Durbeej, M., *Laminins.* Cell and Tissue Research, 2009. **339**(1): p. 259.

78. Hohenester, E., *Structural biology of laminins.* Essays in Biochemistry, 2019. **63**(3): p. 285-295.
79. Mayer, U., et al., *A single EGF-like motif of laminin is responsible for high affinity nidogen binding.* The EMBO Journal, 1993. **12**(5): p. 1879-1885.
80. Rasmussen, D.G.K. and M.A. Karsdal, *Chapter 29 - Laminins*, in *Biochemistry of Collagens, Laminins and Elastin (Second Edition)*, M.A. Karsdal, Editor. 2019, Academic Press. p. 209-263.
81. Timpl, R., et al., *Structure and function of laminin LG modules.* Matrix Biology, 2000. **19**(4): p. 309-317.
82. Hamill, K.J., et al., *Laminin deposition in the extracellular matrix: a complex picture emerges.* Journal of Cell Science, 2009. **122**(24): p. 4409-4417.
83. Li, S., et al., *Laminin-sulfatide binding initiates basement membrane assembly and enables receptor signaling in Schwann cells and fibroblasts.* The Journal of cell biology, 2005. **169**(1): p. 179-189.
84. Macdonald, P.R., et al., *Laminin chain assembly is regulated by specific coiled-coil interactions.* Journal of Structural Biology, 2010. **170**(2): p. 398-405.
85. Aumailley, M., *The laminin family.* Cell adhesion & migration, 2013. **7**(1): p. 48-55.
86. Miner, J.H., et al., *The Laminin α Chains: Expression, Developmental Transitions, and Chromosomal Locations of α1-5, Identification of Heterotrimeric Laminins 8–11, and Cloning of a Novel α3 Isoform.* Journal of Cell Biology, 1997. **137**(3): p. 685-701.
87. Rousselle, P. and K. Beck, *Laminin 332 processing impacts cellular behavior.* Cell Adhesion & Migration, 2013. **7**(1): p. 122-134.
88. Amano, S., et al., *Increase of laminin 5 synthesis in human keratinocytes by acute wound fluid, inflammatory cytokines and growth factors, and lysophospholipids.* British Journal of Dermatology, 2004. **151**(5): p. 961-970.
89. Anderson, C., S.I. Thorsteinsdóttir, and A.-G.I. Borycki, *Sonic hedgehog-dependent synthesis of laminin α1 controls basement membrane assembly in the myotome.* Development, 2009. **136**(20): p. 3495-3504.
90. Aumailley, M., et al., *Altered synthesis of laminin 1 and absence of basement membrane component deposition in (beta)1 integrin-deficient embryoid bodies.* Journal of Cell Science, 2000. **113**(2): p. 259-268.
91. Eisenberg, J.L., et al., *Substrate stiffness regulates extracellular matrix deposition by alveolar epithelial cells.* Research and Reports in Biology, 2011. **2**(1179-7274 (Print)): p. 1–12.
92. Hallmann, R., et al., *Expression and Function of Laminins in the Embryonic and Mature Vasculature.* Physiological Reviews, 2005. **85**(3): p. 979-1000.
93. Li, X., et al., *Fibroblast Growth Factor Signaling and Basement Membrane Assembly Are Connected during Epithelial Morphogenesis of the Embryoid Body.* Journal of Cell Biology, 2001. **153**(4): p. 811-822.
94. Paszek, M.J., et al., *Tensional homeostasis and the malignant phenotype.* Cancer Cell, 2005. **8**(3): p. 241-254.
95. deHart, G.W., K.E. Healy, and J.C.R. Jones, *The role of α3β1 integrin in determining the supramolecular organization of laminin-5 in the extracellular matrix of keratinocytes.* Experimental Cell Research, 2003. **283**(1): p. 67-79.
96. Kariya, Y., et al., *N-Glycosylation of Laminin-332 Regulates Its Biological Functions: A NOVEL FUNCTION OF THE BISECTING GlcNAc.* Journal of Biological Chemistry, 2008. **283**(48): p. 33036-33045.
97. Timpl, R. and J.C. Brown, *Supramolecular assembly of basement membranes.* BioEssays, 1996. **18**(2): p. 123-132.
98. Cheng, Y.-S., et al., *Self-assembly of Laminin Isoforms.* Journal of Biological Chemistry, 1997. **272**(50): p. 31525-31532.
99. Yamada, T., et al., *Laminin-332 regulates differentiation of human interfollicular epidermal stem cells.* Mechanisms of Ageing and Development, 2018. **171**: p. 37-46.
100. Plachot, C., et al., *Factors necessary to produce basoapical polarity in human glandular epithelium formed in conventional and high-throughput three-dimensional culture: example of the breast epithelium.* BMC Biology, 2009. **7**(1): p. 77.
101. Hamill, K.J., A.S. Paller, and J.C.R. Jones, *Adhesion and Migration, the Diverse Functions of the Laminin α3 Subunit.* Dermatologic Clinics, 2010. **28**(1): p. 79-87.
102. Sasaki, T. and R. Timpl, *Domain IVa of laminin α5 chain is cell-adhesive and binds β1 and αVβ3 integrins through Arg-Gly-Asp.* FEBS Letters, 2001. **509**(2): p. 181-185.
103. Pouliot, N. and N. Kusuma, *Laminin-511.* Cell Adhesion & Migration, 2013. **7**(1): p. 142-149.

104. Hohenester, E. and P.D. Yurchenco, *Laminins in basement membrane assembly.* Cell adhesion & migration, 2013. **7**(1): p. 56-63.
105. McKee, K.K., et al., *Role of Laminin Terminal Globular Domains in Basement Membrane Assembly.* Journal of Biological Chemistry, 2007. **282**(29): p. 21437-21447.
106. DeBiase, P.J., et al., *Laminin-311 (Laminin-6) Fiber Assembly by Type I-like Alveolar Cells.* Journal of Histochemistry & Cytochemistry, 2006. **54**(6): p. 665-672.
107. Jones, J.C.R., et al., *Laminin-6 assembles into multimolecular fibrillar complexes with perlecan and participates in mechanical-signal transduction via a dystroglycan-dependent, integrin-independent mechanism.* Journal of Cell Science, 2005. **118**(12): p. 2557-2566.
108. Durbeej, M., *Chapter Two - Laminin-α2 Chain-Deficient Congenital Muscular Dystrophy: Pathophysiology and Development of Treatment*, in *Current Topics in Membranes*, J.H. Miner, Editor. 2015, Academic Press. p. 31-60.
109. McGowan, K.A. and M.P. Marinkovich, *Laminins and human disease.* Microscopy Research and Technique, 2000. **51**(3): p. 262-279.
110. Tunggal, L., et al., *Defective Laminin 5 Processing in Cylindroma Cells.* The American Journal of Pathology, 2002. **160**(2): p. 459-468.
111. Rousselle, P. and J.Y. Scoazec, *Laminin 332 in cancer: When the extracellular matrix turns signals from cell anchorage to cell movement.* Seminars in Cancer Biology, 2020. **62**: p. 149-165.
112. Furuta, S., et al., *Laminin signals initiate the reciprocal loop that informs breast-specific gene expression and homeostasis by activating NO, p53 and microRNAs.* eLife, 2018. **7**: p. e26148.
113. Martin, K.J., et al., *Down-regulation of laminin-5 in breast carcinoma cells. Molecular medicine*, 1998. **4**(9): p. 602–613.
114. Carpenter, P.M., et al., *Motility Induction in Breast Carcinoma by Mammary Epithelial Laminin 332 (Laminin 5).* Molecular Cancer Research, 2009. **7**(4): p. 462-475.
115. Kwon, S.-Y., et al., *Laminin 332 Expression in Breast Carcinoma.* Applied Immunohistochemistry & Molecular Morphology, 2012. **20**(2).
116. Gu, J., et al., *Potential roles of N-glycosylation in cell adhesion.* Glycoconjugate Journal, 2012. **29**(8): p. 599-607.
117. Charonis, A.S., et al., *Laminin Alterations After In Vitro Nonenzymatic Glycosylation.* Diabetes, 1990. **39**(7): p. 807-814.
118. Tarsio, J.F., L.A. Reger, and L.T. Furcht, *Molecular Mechanisms in Basement Membrane Complications of Diabetes: Alterations in Heparin, Laminin, and Type IV Collagen Association.* Diabetes, 1988. **37**(5): p. 532-539.
119. Kikkawa, Y., et al., *Laminin-111-derived peptides and cancer.* Cell Adhesion & Migration, 2013. **7**(1): p. 150-159.
120. Hubmacher, D. and D.P. Reinhardt, *Microfibrils and Fibrillin*, in *The Extracellular Matrix: an Overview*, R.P. Mecham, Editor. 2011, Springer Berlin Heidelberg: Berlin, Heidelberg. p. 233-265.
121. Potts, J.R. and I.D. Campbell, *Fibronectin structure and assembly.* Current Opinion in Cell Biology, 1994. **6**(5): p. 648-655.
122. Pankov, R. and K.M. Yamada, *Fibronectin at a glance.* Journal of Cell Science, 2002. **115**(20): p. 3861.
123. Romberger, D.J., *Fibronectin.* The International Journal of Biochemistry & Cell Biology, 1997. **29**(7): p. 939-943.
124. Singh, P., C. Carraher, and J.E. Schwarzbauer, *Assembly of Fibronectin Extracellular Matrix.* Annual Review of Cell and Developmental Biology, 2010. **26**(1): p. 397-419.
125. Ruoslahti, E. and B. Öbrink, *Common Principles in Cell Adhesion.* Experimental Cell Research, 1996. **227**(1): p. 1-11.
126. Sabatier, L., et al., *Fibrillin Assembly Requires Fibronectin.* Molecular Biology of the Cell, 2008. **20**(3): p. 846-858.
127. Proctor, R.A., *Fibronectin: A Brief Overview of Its Structure, Function, and Physiology.* Reviews of Infectious Diseases, 1987. **9**(Supplement_4): p. S317-S321.
128. George, E.L., et al., *Defects in mesoderm, neural tube and vascular development in mouse embryos lacking fibronectin.* Development, 1993. **119**(4): p. 1079-1091.
129. Lee, C.S., et al., *Mutations in Fibronectin Cause a Subtype of Spondylometaphyseal Dysplasia with "Corner Fractures".* The American Journal of Human Genetics, 2017. **101**(5): p. 815-823.

130. Ramirez, F. and L. Pereira, *The fibrillins.* The International Journal of Biochemistry & Cell Biology, 1999. **31**(2): p. 255-259.
131. Kumra, H. and D.P. Reinhardt, *Chapter 13 - Fibrillins*, in *Methods in Cell Biology*, R.P. Mecham, Editor. 2018, Academic Press. p. 223-246.
132. Reinhardt, D.P., et al., *Initial Steps in Assembly of Microfibrils: FORMATION OF DISULFIDE-CROSS-LINKED MULTIMERS CONTAINING FIBRILLIN-1.* Journal of Biological Chemistry, 2000. **275**(3): p. 2205-2210.
133. Kielty, C.M. and C.A. Shuttleworth, *Fibrillin-containing microfibrils: Structure and function in health and disease.* The International Journal of Biochemistry & Cell Biology, 1995. **27**(8): p. 747-760.
134. Tiedemann, K., et al., *Interactions of Fibrillin-1 with Heparin/Heparan Sulfate, Implications for Microfibrillar Assembly.* Journal of Biological Chemistry, 2001. **276**(38): p. 36035-36042.
135. Wagenseil, J.E. and R.P. Mecham, *New insights into elastic fiber assembly.* Birth Defects Research Part C: Embryo Today: Reviews, 2007. **81**(4): p. 229-240.
136. Neptune, E.R., et al., *Dysregulation of TGF-β activation contributes to pathogenesis in Marfan syndrome.* Nature Genetics, 2003. **33**(3): p. 407-411.
137. Ramirez, F. and D.B. Rifkin, *Extracellular microfibrils: contextual platforms for TGFβ and BMP signaling.* Current Opinion in Cell Biology, 2009. **21**(5): p. 616-622.
138. Hubmacher, D., K. Tiedemann, and D.P. Reinhardt, *Fibrillins: From Biogenesis of Microfibrils to Signaling Functions*, in *Current Topics in Developmental Biology*. 2006, Academic Press. p. 93-123.
139. Chiquet-Ehrismann, R. and M. Chiquet, *Tenascins: regulation and putative functions during pathological stress.* The Journal of Pathology, 2003. **200**(4): p. 488-499.
140. Tucker, R.P. and R. Chiquet-Ehrismann, *Tenascin-C: Its functions as an integrin ligand.* The International Journal of Biochemistry & Cell Biology, 2015. **65**: p. 165-168.
141. Mao, J.R., et al., *Tenascin-X deficiency mimics Ehlers-Danlos syndrome in mice through alteration of collagen deposition.* Nature Genetics, 2002. **30**(4): p. 421-425.
142. Aumailley, M., et al., *Nidogen mediates the formation of ternary complexes of basement membrane components.* Kidney International, 1993. **43**(1): p. 7-12.
143. Kohfeldt, E., et al., *Nidogen-2: a new basement membrane protein with diverse binding properties11Edited by I. B. Holland.* Journal of Molecular Biology, 1998. **282**(1): p. 99-109.
144. Zhou, S., et al., *Nidogen: A matrix protein with potential roles in musculoskeletal tissue regeneration.* Genes & Diseases, 2022. **9**(3): p. 598-609.
145. Welcker, D., et al., *Hemicentin-1 is an essential extracellular matrix component of the dermal–epidermal and myotendinous junctions.* Scientific Reports, 2021. **11**(1): p. 17926.
146. Morrissey, Meghan A., et al., *B-LINK: A Hemicentin, Plakin, and Integrin-Dependent Adhesion System that Links Tissues by Connecting Adjacent Basement Membranes.* Developmental Cell, 2014. **31**(3): p. 319-331.
147. Sepúlveda, V., et al., *SCO-spondin, a giant matricellular protein that regulates cerebrospinal fluid activity.* Fluids and Barriers of the CNS, 2021. **18**(1): p. 45.
148. Hardingham, T.I.M., *CHAPTER 5 - Proteoglycans and Glycosaminoglycans*, in *Dynamics of Bone and Cartilage Metabolism (Second Edition)*, M.J. Seibel, S.P. Robins, and J.P. Bilezikian, Editors. 2006, Academic Press: Burlington. p. 85-98.
149. Richter, R.P., et al., *Glycosaminoglycans in extracellular matrix organisation: are concepts from soft matter physics key to understanding the formation of perineuronal nets?* Current Opinion in Structural Biology, 2018. **50**: p. 65-74.
150. Kobayashi, T., T. Chanmee, and N. Itano, *Hyaluronan: Metabolism and Function.* Biomolecules, 2020. **10**(11).
151. Monslow, J., P. Govindaraju, and E. Puré, *Hyaluronan – A Functional and Structural Sweet Spot in the Tissue Microenvironment.* Frontiers in Immunology, 2015. **6**.
152. Garantziotis, S. and R.C. Savani, *Hyaluronan biology: A complex balancing act of structure, function, location and context.* Matrix Biology, 2019. **78-79**: p. 1-10.
153. Amorim, S., et al., *Extracellular Matrix Mimics Using Hyaluronan-Based Biomaterials.* Trends in Biotechnology, 2021. **39**(1): p. 90-104.
154. Cyphert, J.M., C.S. Trempus , and S. Garantziotis, *Size Matters: Molecular Weight Specificity of Hyaluronan Effects in Cell Biology.* International Journal of Cell Biology, 2015. **2015**.
155. Couchman, J.R. and C.A. Pataki, *An Introduction to Proteoglycans and Their Localization.* Journal of Histochemistry & Cytochemistry, 2012. **60**(12): p. 885-897.
156. Toole, B.P., *Hyaluronan in morphogenesis.* Seminars in Cell & Developmental Biology, 2001. **12**(2): p. 79-87.

157. Herrera, J., C.A. Henke, and P.B. Bitterman, *Extracellular matrix as a driver of progressive fibrosis.* The Journal of clinical investigation, 2018. **128**(1): p. 45-53.
158. Toole, B.P., T.N. Wight, and M.I. Tammi, *Hyaluronan-Cell Interactions in Cancer and Vascular Disease.* Journal of Biological Chemistry, 2002. **277**(7): p. 4593-4596.
159. Yamaguchi, Y., *Lecticans: organizers of the brain extracellular matrix.* Cellular and Molecular Life Sciences CMLS, 2000. **57**(2): p. 276-289.
160. Iozzo, R.V. and L. Schaefer, *Proteoglycan form and function: A comprehensive nomenclature of proteoglycans.* Matrix Biology, 2015. **42**: p. 11-55.
161. Fryer, H.J., et al., *The high molecular weight Cat-301 chondroitin sulfate proteoglycan from brain is related to the large aggregating proteoglycan from cartilage, aggrecan.* Journal of Biological Chemistry, 1992. **267**(14): p. 9874-9883.
162. Frischknecht, R. and C.I. Seidenbecher, *Brevican: A key proteoglycan in the perisynaptic extracellular matrix of the brain.* The International Journal of Biochemistry & Cell Biology, 2012. **44**(7): p. 1051-1054.
163. Yamada, H., et al., *The Brain Chondroitin Sulfate Proteoglycan Brevican Associates with Astrocytes Ensheathing Cerebellar Glomeruli and Inhibits Neurite Outgrowth from Granule Neurons.* The Journal of Neuroscience, 1997. **17**(20): p. 7784.
164. Howell, M.D. and P.E. Gottschall, *Lectican proteoglycans, their cleaving metalloproteinases, and plasticity in the central nervous system extracellular microenvironment.* Neuroscience, 2012. **217**: p. 6-18.
165. Bekku, Y., et al., *Brevican distinctively assembles extracellular components at the large diameter nodes of Ranvier in the CNS.* Journal of Neurochemistry, 2009. **108**(5): p. 1266-1276.
166. Attili, S. and R.P. Richter, *Self-assembly and elasticity of hierarchical proteoglycan–hyaluronan brushes.* Soft Matter, 2013. **9**(44): p. 10473-10483.
167. Schwartz, N.B. and M.S. Domowicz, *Proteoglycans in brain development and pathogenesis.* FEBS Letters, 2018. **592**(23): p. 3791-3805.
168. Kirkpatrick, C.A. and S.B. Selleck, *Heparan sulfate proteoglycans at a glance.* Journal of Cell Science, 2007. **120**(11): p. 1829-1832.
169. Sarrazin, S., W.C. Lamanna, and J.D. Esko, *Heparan Sulfate Proteoglycans.* Cold Spring Harbor Perspectives in Biology, 2011. **3**(7).
170. Couchman, J.R., et al., *Fell-Muir Lecture: Syndecans: from peripheral coreceptors to mainstream regulators of cell behaviour.* International Journal of Experimental Pathology, 2015. **96**(1): p. 1-10.
171. Stepp, M.A., et al., *Syndecan-1 and Its Expanding List of Contacts.* Advances in Wound Care, 2014. **4**(4): p. 235-249.
172. Gondelaud, F. and S. Ricard-Blum, *Structures and interactions of syndecans.* The FEBS Journal, 2019. **286**(15): p. 2994-3007.
173. Manon-Jensen, T., Y. Itoh, and J.R. Couchman, *Proteoglycans in health and disease: the multiple roles of syndecan shedding.* The FEBS Journal, 2010. **277**(19): p. 3876-3889.
174. Gubbiotti, M.A., T. Neill, and R.V. Iozzo, *A current view of perlecan in physiology and pathology: A mosaic of functions.* Matrix Biology, 2017. **57-58**: p. 285-298.
175. Murdoch, A.D., et al., *Widespread expression of perlecan proteoglycan in basement membranes and extracellular matrices of human tissues as detected by a novel monoclonal antibody against domain III and by in situ hybridization.* Journal of Histochemistry & Cytochemistry, 1994. **42**(2): p. 239-249.
176. Whitelock, J.M., J. Melrose, and R.V. Iozzo, *Diverse Cell Signaling Events Modulated by Perlecan.* Biochemistry, 2008. **47**(43): p. 11174-11183.
177. Yurchenco, P.D. and B.L. Patton, *Developmental and pathogenic mechanisms of basement membrane assembly.* Current pharmaceutical design, 2009. **15**(12): p. 1277-1294.
178. Nicole, S., et al., *Perlecan, the major proteoglycan of basement membranes, is altered in patients with Schwartz-Jampel syndrome (chondrodystrophic myotonia).* Nature Genetics, 2000. **26**(4): p. 480-483.
179. Costell, M., et al., *Perlecan maintains the integrity of cartilage and some basement membranes.* The Journal of cell biology, 1999. **147**(5): p. 1109-1122.
180. Iozzo, R.V., *Basement membrane proteoglycans: from cellar to ceiling.* Nature Reviews Molecular Cell Biology, 2005. **6**(8): p. 646-656.
181. Hayes, A.J., et al., *Colocalization in vivo and association in vitro of perlecan and elastin.* Histochemistry and Cell Biology, 2011. **136**(4): p. 437.

182. Knox, S.M. and J.M. Whitelock, *Perlecan: how does one molecule do so many things?* Cellular and Molecular Life Sciences CMLS, 2006. **63**(21): p. 2435-2445.
183. Filmus, J., M. Capurro, and J. Rast, *Glypicans.* Genome Biology, 2008. **9**(5): p. 224.
184. De Cat, B. and G. David, *Developmental roles of the glypicans.* Seminars in Cell & Developmental Biology, 2001. **12**(2): p. 117-125.
185. Watanabe, K., H. Yamada, and Y. Yamaguchi, *K-glypican: a novel GPI-anchored heparan sulfate proteoglycan that is highly expressed in developing brain and kidney.* Journal of Cell Biology, 1995. **130**(5): p. 1207-1218.
186. Stipp, C.S., E.D. Litwack, and A.D. Lander, *Cerebroglycan: an integral membrane heparan sulfate proteoglycan that is unique to the developing nervous system and expressed specifically during neuronal differentiation.* Journal of Cell Biology, 1994. **124**(1): p. 149-160.
187. Schaefer, L. and R.V. Iozzo, *Biological Functions of the Small Leucine-rich Proteoglycans: From Genetics to Signal Transduction.* Journal of Biological Chemistry, 2008. **283**(31): p. 21305-21309.
188. Chen, S. and D.E. Birk, *The regulatory roles of small leucine-rich proteoglycans in extracellular matrix assembly.* The FEBS Journal, 2013. **280**(10): p. 2120-2137.
189. Ameye, L. and M.F. Young, *Mice deficient in small leucine-rich proteoglycans: novel in vivo models for osteoporosis, osteoarthritis, Ehlers-Danlos syndrome, muscular dystrophy, and corneal diseases.* Glycobiology, 2002. **12**(9): p. 107R-116R.
190. Hayashida, Y., et al., *Matrix morphogenesis in cornea is mediated by the modification of keratan sulfate by GlcNAc 6-O-sulfotransferase.* Proceedings of the National Academy of Sciences, 2006. **103**(36): p. 13333-13338.
191. Ying, S., et al., *Characterization and Expression of the Mouse Lumican Gene.* Journal of Biological Chemistry, 1997. **272**(48): p. 30306-30313.
192. Reese, S.P., C.J. Underwood, and J.A. Weiss, *Effects of decorin proteoglycan on fibrillogenesis, ultrastructure, and mechanics of type I collagen gels.* Matrix Biology, 2013. **32**(7): p. 414-423.
193. Scott, J.E. and C.R. Orford, *Dermatan sulphate-rich proteoglycan associates with rat tail-tendon collagen at the d band in the gap region.* Biochemical Journal, 1981. **197**(1): p. 213-216.
194. Nikitovic, D., et al., *Lumican regulates osteosarcoma cell adhesion by modulating TGFβ2 activity.* The International Journal of Biochemistry & Cell Biology, 2011. **43**(6): p. 928-935.
195. Kolb, M., et al., *Proteoglycans decorin and biglycan differentially modulate TGF-β-mediated fibrotic responses in the lung.* American Journal of Physiology-Lung Cellular and Molecular Physiology, 2001. **280**(6): p. L1327-L1334.
196. Iozzo, R.V., et al., *Decorin Is a Biological Ligand for the Epidermal Growth Factor Receptor.* Journal of Biological Chemistry, 1999. **274**(8): p. 4489-4492.
197. Appunni, S., et al., *Small Leucine Rich Proteoglycans (decorin, biglycan and lumican) in cancer.* Clinica Chimica Acta, 2019. **491**: p. 1-7.
198. Debelle, L. and A.M. Tamburro, *Elastin: molecular description and function.* The International Journal of Biochemistry & Cell Biology, 1999. **31**(2): p. 261-272.
199. Davidson, J.M., et al., *Regulation of Elastin Synthesis in Pathological States.* Ciba Foundation Symposium 192 - The Molecular Biology and Pathology of Elastic Tissues, 2007: p. 81-99.
200. Ozsvar, J., et al., *Tropoelastin and Elastin Assembly.* Frontiers in Bioengineering and Biotechnology, 2021. **9**.
201. Tarakanova, A., et al., *Coarse-grained model of tropoelastin self-assembly into nascent fibrils.* Materials Today Bio, 2019. **3**: p. 100016.
202. Kagan, H.M. and K.A. Sullivan, *[35] Lysyl oxidase: Preparation and role in elastin biosynthesis*, in *Methods in Enzymology*. 1982, Academic Press. p. 637-650.
203. Broekelmann, T.J., et al., *Tropoelastin Interacts with Cell-surface Glycosaminoglycans via Its COOH-terminal Domain.* Journal of Biological Chemistry, 2005. **280**(49): p. 40939-40947.
204. Nakamura, T., et al., *Fibulin-5/DANCE is essential for elastogenesis in vivo.* Nature, 2002. **415**(6868): p. 171-175.
205. Yanagisawa, H. and E.C. Davis, *Unraveling the mechanism of elastic fiber assembly: The roles of short fibulins.* The International Journal of Biochemistry & Cell Biology, 2010. **42**(7): p. 1084-1093.
206. Mecham, R.P., *Elastin in lung development and disease pathogenesis.* Matrix Biology, 2018. **73**: p. 6-20.
207. Mithieux, S.M. and A.S. Weiss, *Elastin*, in *Advances in Protein Chemistry*. 2005, Academic Press. p. 437-461.

208. Kelleher, C.M., S.E. McLean, and R.P. Mecham, *Vascular Extracellular Matrix and Aortic Development*, in *Current Topics in Developmental Biology*. 2004, Academic Press. p. 153-188.
209. Hill, J.R., et al., *Elastic fibers in orthopedics: Form and function in tendons and ligaments, clinical implications, and future directions.* Journal of Orthopaedic Research, 2020. **38**(11): p. 2305-2317.
210. Grant, T.M., et al., *Elastic fibres are broadly distributed in tendon and highly localized around tenocytes.* Journal of Anatomy, 2013. **222**(6): p. 573-579.
211. Reichheld, S.E., et al., *Sequence variants of human tropoelastin affecting assembly, structural characteristics and functional properties of polymeric elastin in health and disease.* Matrix Biology, 2019. **84**: p. 68-80.
212. Yeo, G.C., et al., *Subtle balance of tropoelastin molecular shape and flexibility regulates dynamics and hierarchical assembly.* Science Advances, 2016. **2**(2): p. e1501145.
213. Muiznieks, L.D., et al., *Proline-poor hydrophobic domains modulate the assembly and material properties of polymeric elastin.* Biopolymers, 2015. **103**(10): p. 563-573.
214. Kozel, B.A., et al., *Domains in Tropoelastin That Mediate Elastin Depositionin Vitro and in Vivo.* Journal of Biological Chemistry, 2003. **278**(20): p. 18491-18498.
215. Lee, P., et al., *A Novel Cell Adhesion Region in Tropoelastin Mediates Attachment to Integrin αVβ5.* Journal of Biological Chemistry, 2014. **289**(3): p. 1467-1477.
216. Senior, R.M., et al., *Val-Gly-Val-Ala-Pro-Gly, a repeating peptide in elastin, is chemotactic for fibroblasts and monocytes.* Journal of Cell Biology, 1984. **99**(3): p. 870-874.
217. Karnik, S.K., et al., *A critical role for elastin signaling in vascular morphogenesis and disease.* Development, 2003. **130**(2): p. 411-423.
218. Yeo, G.C. and A.S. Weiss, *Soluble matrix protein is a potent modulator of mesenchymal stem cell performance.* Proceedings of the National Academy of Sciences, 2019. **116**(6): p. 2042-2051.
219. Cocciolone, A.J., et al., *Elastin, arterial mechanics, and cardiovascular disease.* American Journal of Physiology-Heart and Circulatory Physiology, 2018. **315**(2): p. H189-H205.
220. Heinz, A., *Elastases and elastokines: elastin degradation and its significance in health and disease.* Critical Reviews in Biochemistry and Molecular Biology, 2020. **55**(3): p. 252-273.
221. Rønnow, S.R., et al., *Specific elastin degradation products are associated with poor outcome in the ECLIPSE COPD cohort.* Scientific Reports, 2019. **9**(1): p. 4064.
222. Ayala, P., et al., *Elastin degradation products in acute lung injury induced by gastric contents aspiration.* Respiratory Research, 2018. **19**(1): p. 165.
223. Naba, A., et al., *The matrisome: in silico definition and in vivo characterization by proteomics of normal and tumor extracellular matrices.* Molecular & cellular proteomics : MCP, 2012. **11**(4): p. M111.014647-M111.014647.
224. Mongiat, M., et al., *Endorepellin, a Novel Inhibitor of Angiogenesis Derived from the C Terminus of Perlecan.* Journal of Biological Chemistry, 2003. **278**(6): p. 4238-4249.
225. Hangai, M., et al., *Matrix Metalloproteinase-9-Dependent Exposure of a Cryptic Migratory Control Site in Collagen is Required before Retinal Angiogenesis.* The American Journal of Pathology, 2002. **161**(4): p. 1429-1437.
226. Manon-Jensen, T., H.A.B. Multhaupt, and J.R. Couchman, *Mapping of matrix metalloproteinase cleavage sites on syndecan-1 and syndecan-4 ectodomains.* The FEBS Journal, 2013. **280**(10): p. 2320-2331.
227. Mott, J.D. and Z. Werb, *Regulation of matrix biology by matrix metalloproteinases.* Current Opinion in Cell Biology, 2004. **16**(5): p. 558-564.
228. Yu, Q. and I. Stamenkovic, *Cell surface-localized matrix metalloproteinase-9 proteolytically activates TGF-beta and promotes tumor invasion and angiogenesis.* Genes and Development, 2000. **14**(2): p. 163–176.
229. Noël, A., *New and Paradoxical Roles of Matrix Metalloproteinases in the Tumor Microenvironment.* Frontiers in Pharmacology, 2012. **3**.
230. Mittal, R., et al., *Intricate Functions of Matrix Metalloproteinases in Physiological and Pathological Conditions.* Journal of Cellular Physiology, 2016. **231**(12): p. 2599-2621.
231. Zhang, G., et al., *Matrix metalloproteinase-10 promotes tumor progression through regulation of angiogenic and apoptotic pathways in cervical tumors.* BMC Cancer, 2014. **14**(1): p. 310.
232. Duffy, M.J., et al., *Metalloproteinases: role in breast carcinogenesis, invasion and metastasis.* Breast Cancer Research, 2000. **2**(4): p. 252.
233. Quintero-Fabián, S., et al., *Role of Matrix Metalloproteinases in Angiogenesis and Cancer.* Frontiers in Oncology, 2019. **9**.

234. Vallet, S.D. and S. Ricard-Blum, *Lysyl oxidases: from enzyme activity to extracellular matrix cross-links.* Essays in Biochemistry, 2019. **63**(3): p. 349-364.
235. Saini, K., et al., *Tension in fibrils suppresses their enzymatic degradation – A molecular mechanism for 'use it or lose it'.* Matrix Biology, 2020. **85-86**: p. 34-46.
236. Amendola, P.G., R. Reuten, and J.T. Erler, *Interplay Between LOX Enzymes and Integrins in the Tumor Microenvironment.* Cancers, 2019. **11**(5).
237. Afratis, N.A., et al., *The apparent competitive action of ECM proteases and cross-linking enzymes during fibrosis: Applications to drug discovery.* Advanced Drug Delivery Reviews, 2018. **129**: p. 4-15.
238. Philp, C.J., et al., *Extracellular Matrix Cross-Linking Enhances Fibroblast Growth and Protects against Matrix Proteolysis in Lung Fibrosis.* American Journal of Respiratory Cell and Molecular Biology, 2017. **58**(5): p. 594-603.
239. Pehrsson, M., et al., *Enzymatic cross-linking of collagens in organ fibrosis – resolution and assessment.* Expert Review of Molecular Diagnostics, 2021. **21**(10): p. 1049-1064.
240. Setargew, Y.F.I., et al., *Targeting Lysyl Oxidase Family Meditated Matrix Cross-Linking as an Anti-Stromal Therapy in Solid Tumours.* Cancers, 2021. **13**(3).
241. Insua-Rodríguez, J. and T. Oskarsson, *The extracellular matrix in breast cancer.* Advanced Drug Delivery Reviews, 2016. **97**: p. 41-55.
242. Levental, K.R., et al., *Matrix Crosslinking Forces Tumor Progression by Enhancing Integrin Signaling.* Cell, 2009. **139**(5): p. 891-906.
243. Lamanna, W.C., et al., *Sulf Loss Influences N-, 2-O-, and 6-O-Sulfation of Multiple Heparan Sulfate Proteoglycans and Modulates Fibroblast Growth Factor Signaling.* Journal of Biological Chemistry, 2008. **283**(41): p. 27724-27735.
244. Piperigkou, Z., et al., *Key Matrix Remodeling Enzymes: Functions and Targeting in Cancer.* Cancers, 2021. **13**(6).
245. Jordan, A.R., et al., *Antitumor activity of sulfated hyaluronic acid fragments in pre-clinical models of bladder cancer.* Oncotarget; Vol 8, No 15, 2016.
246. Fink, S.P., et al., *Induction of KIAA1199/CEMIP is associated with colon cancer phenotype and poor patient survival.* Oncotarget; Vol 6, No 31, 2015.
247. Junliang, L., et al., *High-molecular-weight hyaluronan produced by activated pancreatic stellate cells promotes pancreatic cancer cell migration via paracrine signaling.* Biochemical and Biophysical Research Communications, 2019. **515**(3): p. 493-498.
248. Dredge, K., et al., *A Phase I study of the novel immunomodulatory agent PG545 (pixatimod) in subjects with advanced solid tumours.* British Journal of Cancer, 2018. **118**(8): p. 1035-1041.
249. Dinarello, C.A., *Historical insights into cytokines.* European Journal of Immunology, 2007. **37**(S1): p. S34-S45.
250. Kelso, A., *Cytokines: Principles and prospects.* Immunology & Cell Biology, 1998. **76**(4): p. 300-317.
251. Mina, M., *Chapter 7 - Growth Factors: Biochemical Signals for Tissue Engineering*, in *Stem Cell Biology and Tissue Engineering in Dental Sciences*, A. Vishwakarma, et al., Editors. 2015, Academic Press: Boston. p. 85-97.
252. Schönherr, E. and H.-J. Hausser, *Extracellular Matrix and Cytokines: A Functional Unit.* Developmental Immunology, 2000. **7**: p. 031748.
253. Hynes, R.O., *The Extracellular Matrix: Not Just Pretty Fibrils.* Science, 2009. **326**(5957): p. 1216.
254. Clark, D.A. and R. Coker, *Molecules in focus Transforming growth factor-beta (TGF-β).* The International Journal of Biochemistry & Cell Biology, 1998. **30**(3): p. 293-298.
255. Semkova, M.E. and J.J. Hsuan, *TGFβ-1 Induced Cross-Linking of the Extracellular Matrix of Primary Human Dermal Fibroblasts.* International Journal of Molecular Sciences, 2021. **22**(3).
256. Altraja, S., et al., *Synthesis of tenascin and laminin beta2 chain in human bronchial epithelial cells is enhanced by cysteinyl leukotrienes via CysLT1 receptor.* Respiratory Research, 2008. **9**(1): p. 44.
257. Turner, P.A., J.S. Thiele, and J.P. Stegemann, *Growth factor sequestration and enzyme-mediated release from genipin-crosslinked gelatin microspheres.* Journal of Biomaterials Science, Polymer Edition, 2017. **28**(16): p. 1826-1846.
258. Vlodavsky, I., et al., *Extracellular sequestration and release of fibroblast growth factor: a regulatory mechanism?* Trends in Biochemical Sciences, 1991. **16**: p. 268-271.
259. Huxley-Jones, J., D.L. Robertson, and R.P. Boot-Handford, *On the origins of the extracellular matrix in vertebrates.* Matrix Biology, 2007. **26**(1): p. 2-11.

260. Boute, N., et al., *Type IV collagen in sponges, the missing link in basement membrane ubiquity.* Biology of the Cell, 1996. **88**(1-2): p. 37-44.
261. Day, R.M. and H.M. Lenhoff, *Hydra Mesoglea: a Model for Investigating Epithelial Cell—Basement Membrane Interactions.* Science, 1981. **211**(4479): p. 291-294.
262. Exposito, J.Y. and R. Garrone, *Characterization of a fibrillar collagen gene in sponges reveals the early evolutionary appearance of two collagen gene families.* Proceedings of the National Academy of Sciences, 1990. **87**(17): p. 6669-6673.
263. LeBleu, V.S., B. MacDonald, and R. Kalluri, *Structure and Function of Basement Membranes.* Experimental Biology and Medicine, 2007. **232**(9): p. 1121-1129.
264. Jayadev, R. and D.R. Sherwood, *Basement membranes.* Current Biology, 2017. **27**(6): p. R207-R211.
265. Khalilgharibi, N. and Y. Mao, *To form and function: on the role of basement membrane mechanics in tissue development, homeostasis and disease.* Open Biology, 2021. **11**(2): p. 200360.
266. Morrissey, M.A. and D.R. Sherwood, *An active role for basement membrane assembly and modification in tissue sculpting.* Journal of Cell Science, 2015. **128**(9): p. 1661–1668.
267. Smyth, N., et al., *Absence of basement membranes after targeting the LAMC1 gene results in embryonic lethality due to failure of endoderm differentiation.* The Journal of cell biology, 1999. **144**(1): p. 151-160.
268. Pöschl, E., et al., *Collagen IV is essential for basement membrane stability but dispensable for initiation of its assembly during early development.* Development, 2004. **131**(7): p. 1619-1628.
269. Matsubayashi, Y., et al., *A Moving Source of Matrix Components Is Essential for De Novo Basement Membrane Formation.* Current Biology, 2017. **27**(22): p. 3526-3534.e4.
270. Sasaki, T., R. Fässler, and E. Hohenester, *Laminin : the crux of basement membrane assembly.* Journal of Cell Biology, 2004. **164**(7): p. 959-963.
271. Than, M.E., et al., *The 1.9-Å crystal structure of the noncollagenous (NC1) domain of human placenta collagen IV shows stabilization via a novel type of covalent Met-Lys cross-link.* Proceedings of the National Academy of Sciences, 2002. **99**(10): p. 6607-6612.
272. Vanacore, R., et al., *A Sulfilimine Bond Identified in Collagen IV.* Science, 2009. **325**(5945): p. 1230-1234.
273. Kohfeldt, E., et al., *Nidogen-2: a new basement membrane protein with diverse binding properties.* Journal of Molecular Biology, 1998. **282**(1): p. 99-109.
274. Behrens, D.T., et al., *The Epidermal Basement Membrane Is a Composite of Separate Laminin- or Collagen IV-containing Networks Connected by Aggregated Perlecan, but Not by Nidogens.* Journal of Biological Chemistry, 2012. **287**(22): p. 18700-18709.
275. Saarela, J., et al., *The Short and Long Forms of Type XVIII Collagen Show Clear Tissue Specificities in Their Expression and Location in Basement Membrane Zones in Humans.* The American Journal of Pathology, 1998. **153**(2): p. 611-626.
276. Di Russo, J., et al., *Endothelial basement membrane laminin 511 is essential for shear stress response.* The EMBO Journal, 2017. **36**(2): p. 183-201.
277. Song, J., et al., *Endothelial Basement Membrane Laminin 511 Contributes to Endothelial Junctional Tightness and Thereby Inhibits Leukocyte Transmigration.* Cell Reports, 2017. **18**(5): p. 1256-1269.
278. Thomsen, M.S., L.J. Routhe, and T. Moos, *The vascular basement membrane in the healthy and pathological brain.* Journal of Cerebral Blood Flow & Metabolism, 2017. **37**(10): p. 3300-3317.
279. Mutgan, A.C., K. Jandl, and G. Kwapiszewska, *Endothelial Basement Membrane Components and Their Products, Matrikines: Active Drivers of Pulmonary Hypertension?* Cells, 2020. **9**(9).
280. Parkin, J.D., et al., *Mapping structural landmarks, ligand binding sites, and missense mutations to the collagen IV heterotrimers predicts major functional domains, novel interactions, and variation in phenotypes in inherited diseases affecting basement membranes.* Human Mutation, 2011. **32**(2): p. 127-143.
281. Steiner, E., et al., *The heparan sulfate proteoglycan agrin contributes to barrier properties of mouse brain endothelial cells by stabilizing adherens junctions.* Cell and Tissue Research, 2014. **358**(2): p. 465-479.
282. Gustafsson, E., et al., *Perlecan Maintains Microvessel Integrity In Vivo and Modulates Their Formation In Vitro.* PLOS ONE, 2013. **8**(1): p. e53715.

283. Gould, D.B., et al., *Mutations in Col4a1 Cause Perinatal Cerebral Hemorrhage and Porencephaly.* Science, 2005. **308**(5725): p. 1167-1171.
284. Moulton, K.S., et al., *Loss of Collagen XVIII Enhances Neovascularization and Vascular Permeability in Atherosclerosis.* Circulation, 2004. **110**(10): p. 1330-1336.
285. Sternlicht, M.D., *Key stages in mammary gland development: The cues that regulate ductal branching morphogenesis.* Breast Cancer Research, 2005. **8**(1): p. 201.
286. Weigelt, B. and M.J. Bissell, *Unraveling the microenvironmental influences on the normal mammary gland and breast cancer.* Seminars in Cancer Biology, 2008. **18**(5): p. 311-321.
287. Bissell, M.J., et al., *The organizing principle: microenvironmental influences in the normal and malignant breast.* Differentiation, 2002. **70**(9): p. 537-546.
288. Streuli, C.H., et al., *Laminin mediates tissue-specific gene expression in mammary epithelia.* The Journal of cell biology, 1995. **129**(3): p. 591-603.
289. Kent, A.J., et al., *The microstructure of laminin-111 compensates for dystroglycan loss in mammary epithelial cells in downstream expression of milk proteins.* Biomaterials, 2019. **218**: p. 119337-119337.
290. Li, M.L., et al., *Influence of a reconstituted basement membrane and its components on casein gene expression and secretion in mouse mammary epithelial cells.* Proceedings of the National Academy of Sciences of the United States of America, 1987. **84**(1): p. 136-140.
291. Gaiko-Shcherbak, A., et al., *The Acinar Cage: Basement Membranes Determine Molecule Exchange and Mechanical Stability of Human Breast Cell Acini.* PLOS ONE, 2015. **10**(12): p. e0145174.
292. Magdaleno, C., et al., *Fibronectin assembly regulates lumen formation in breast acini.* Journal of Cellular Biochemistry, 2021. **122**(5): p. 524-537.
293. Williams, C.M., et al., *Fibronectin expression modulates mammary epithelial cell proliferation during acinar differentiation.* Cancer research, 2008. **68**(9): p. 3185-3192.
294. Fabris, G., et al., *Nanoscale Topography and Poroelastic Properties of Model Tissue Breast Gland Basement Membranes.* Biophysical Journal, 2018. **115**(9): p. 1770-1782.
295. Wang, H., et al., *Rotational motion during three-dimensional morphogenesis of mammary epithelial acini relates to laminin matrix assembly.* Proceedings of the National Academy of Sciences, 2013. **110**(1): p. 163-168.
296. Miner, J.H., *The glomerular basement membrane.* Experimental Cell Research, 2012. **318**(9): p. 973-978.
297. Suh, J.H. and J.H. Miner, *The glomerular basement membrane as a barrier to albumin.* Nature Reviews Nephrology, 2013. **9**(8): p. 470-477.
298. Naylor, R.W., M.R.P.T. Morais, and R. Lennon, *Complexities of the glomerular basement membrane.* Nature Reviews Nephrology, 2021. **17**(2): p. 112-127.
299. de Vega, S., T. Iwamoto, and Y. Yamada, *Fibulins: Multiple roles in matrix structures and tissue functions.* Cellular and Molecular Life Sciences, 2009. **66**(11): p. 1890-1902.
300. Gunwar, S., et al., *Glomerular Basement Membrane: IDENTIFICATION OF A NOVEL DISULFIDE-CROSS-LINKED NETWORK OF α3, α4, AND α5 CHAINS OF TYPE IV COLLAGEN AND ITS IMPLICATIONS FOR THE PATHOGENESIS OF ALPORT SYNDROME.* Journal of Biological Chemistry, 1998. **273**(15): p. 8767-8775.
301. Miner, J.H., et al., *Compositional and structural requirements for laminin and basement membranes during mouse embryo implantation and gastrulation.* Development, 2004. **131**(10): p. 2247-2256.
302. Heng, C., et al., *Functional role of laminin α1 chain during cerebellum development.* Cell Adhesion & Migration, 2011. **5**(6): p. 480-489.
303. Kao, G., et al., *The role of the laminin β subunit in laminin heterotrimer assembly and basement membrane function and development in C. elegans.* Developmental Biology, 2006. **290**(1): p. 211-219.
304. Chew, C. and R. Lennon, *Basement Membrane Defects in Genetic Kidney Diseases.* Frontiers in Pediatrics, 2018. **6**.
305. Miner, J.H., et al., *Transgenic isolation of skeletal muscle and kidney defects in lamininβ2 mutant mice: implications for Pierson syndrome.* Development, 2006. **133**(5): p. 967-975.
306. Kashtan, C.E., et al., *Alport syndrome, basement membranes and collagen.* Pediatric Nephrology, 1990. **4**(5): p. 523-532.
307. Arikawa-Hirasawa, E., et al., *Structural and Functional Mutations of the Perlecan Gene Cause Schwartz-Jampel Syndrome, with Myotonic Myopathy and Chondrodysplasia.* The American Journal of Human Genetics, 2002. **70**(5): p. 1368-1375.

308. Leclech, C., C.F. Natale, and A.I. Barakat, *The basement membrane as a structured surface – role in vascular health and disease.* Journal of Cell Science, 2020. **133**(18): p. jcs239889.
309. Das, A., et al., *Increases in collagen type IV and laminin in galactose-induced retinal capillary basement membrane thickening—Prevention by an aldose reductase inhibitor.* Experimental Eye Research, 1990. **50**(3): p. 269-280.
310. Tsilibary, E.C., *Microvascular basement membranes in diabetes mellitus.* The Journal of Pathology, 2003. **200**(4): p. 537-546.
311. Begieneman, M.P.V., et al., *The Basement Membrane of Intramyocardial Capillaries Is Thickened in Patients with Acute Myocardial Infarction.* Journal of Vascular Research, 2010. **47**(1): p. 54-60.
312. Holm Nielsen, S., et al., *Markers of Basement Membrane Remodeling Are Associated With Higher Mortality in Patients With Known Atherosclerosis.* Journal of the American Heart Association, 2018. **7**(21): p. e009193.
313. Xu, J. and G.-P. Shi, *Vascular wall extracellular matrix proteins and vascular diseases.* Biochimica et Biophysica Acta (BBA) - Molecular Basis of Disease, 2014. **1842**(11): p. 2106-2119.
314. Bosnian, F.T., M. Havenith, and J.P.M. Cleutjens, *Basement Membranes in Cancer.* Ultrastructural Pathology, 1985. **8**(4): p. 291-304.
315. Petersen, O.W., et al., *Interaction with basement membrane serves to rapidly distinguish growth and differentiation pattern of normal and malignant human breast epithelial cells.* Proceedings of the National Academy of Sciences, 1992. **89**(19): p. 9064.
316. Öhlund, D., et al., *Type IV collagen stimulates pancreatic cancer cell proliferation, migration, and inhibits apoptosis through an autocrine loop.* (1471-2407 (Electronic)).
317. Engbring, J.A. and H.K. Kleinman, *The basement membrane matrix in malignancy.* The Journal of Pathology, 2003. **200**(4): p. 465-470.
318. Chia, J., et al., *Evidence for a Role of Tumor-Derived Laminin-511 in the Metastatic Progression of Breast Cancer.* The American Journal of Pathology, 2007. **170**(6): p. 2135-2148.
319. Chang, J. and O. Chaudhuri, *Beyond proteases: Basement membrane mechanics and cancer invasion.* Journal of Cell Biology, 2019. **218**(8): p. 2456-2469.
320. Kleinman, H.K., et al., *Role of Basement Membrane in Tumor Growth and Metastasis.* Surgical Oncology Clinics of North America, 2001. **10**(2): p. 329-338.
321. Ishikawa, T., et al., *Laminins 411 and 421 differentially promote tumor cell migration via α6β1 integrin and MCAM (CD146).* Matrix Biology, 2014. **38**: p. 69-83.
322. Alečković, M., et al., *Identification of Nidogen 1 as a lung metastasis protein through secretome analysis.* Genes and Development, 2017. **31**(14): p. 1439–1455.
323. Albrechtsen, R., et al., *Basement Membrane Changes in Breast Cancer Detected by Immunohistochemical Staining for Laminin.* Cancer Research, 1981. **41**(12 Part 1): p. 5076.
324. Fata, J.E., Z. Werb, and M.J. Bissell, *Regulation of mammary gland branching morphogenesis by the extracellular matrix and its remodeling enzymes.* Breast Cancer Research, 2003. **6**(1): p. 1.
325. Zipfel, W.R., et al., *Live tissue intrinsic emission microscopy using multiphoton-excited native fluorescence and second harmonic generation.* Proceedings of the National Academy of Sciences, 2003. **100**(12): p. 7075-7080.
326. Aranda-Gutierrez, A. and H.M. Diaz-Perez, *Histology, Mammary Glands*. 2022, Treasure Island (FL): StatPearls Publishing.
327. Schedin, P., et al., *Mammary ECM composition and function are altered by reproductive state.* Molecular Carcinogenesis, 2004. **41**(4): p. 207-220.
328. Nelson, C.M. and M.J. Bissell, *Of extracellular matrix, scaffolds, and signaling: tissue architecture regulates development, homeostasis, and cancer.* Annual review of cell and developmental biology, 2006. **22**: p. 287-309.
329. Brownfield, Douglas G., et al., *Patterned Collagen Fibers Orient Branching Mammary Epithelium through Distinct Signaling Modules.* Current Biology, 2013. **23**(8): p. 703-709.
330. Muschler, J. and C.H. Streuli, *Cell-matrix interactions in mammary gland development and breast cancer.* Cold Spring Harbor perspectives in biology, 2010. **2**(10): p. a003202-a003202.
331. Mouw, J.K., G. Ou, and V.M. Weaver, *Extracellular matrix assembly: a multiscale deconstruction.* Nature Reviews Molecular Cell Biology, 2014. **15**(12): p. 771-785.
332. Bandtlow, C.E. and D.R. Zimmermann, *Proteoglycans in the Developing Brain: New Conceptual Insights for Old Proteins.* Physiological Reviews, 2000. **80**(4): p. 1267-1290.
333. Ruoslahti, E., *Brain extracellular matrix.* Glycobiology, 1996. **6**(5): p. 489-492.

334. Lau, L.W., et al., *Pathophysiology of the brain extracellular matrix: a new target for remyelination.* Nature Reviews Neuroscience, 2013. **14**(10): p. 722-729.
335. Young, M.F., *Bone matrix proteins: their function, regulation, and relationship to osteoporosis.* Osteoporosis International, 2003. **14**(3): p. 35-42.
336. Kane, R. and P.X. Ma, *Mimicking the nanostructure of bone matrix to regenerate bone.* Materials Today, 2013. **16**(11): p. 418-423.
337. Rho, J.-Y., L. Kuhn-Spearing, and P. Zioupos, *Mechanical properties and the hierarchical structure of bone.* Medical Engineering & Physics, 1998. **20**(2): p. 92-102.
338. Globus, R.K., et al., *Fibronectin is a survival factor for differentiated osteoblasts.* Journal of Cell Science, 1998. **111**(10): p. 1385-1393.
339. Moursi, A.M., et al., *Fibronectin regulates calvarial osteoblast differentiation.* Journal of Cell Science, 1996. **109**(6): p. 1369-1380.
340. Couchourel, D., et al., *Effects of fibronectin on hydroxyapatite formation.* Journal of Inorganic Biochemistry, 1999. **73**(3): p. 129-136.
341. Lynch, M.P., et al., *The Influence of Type I Collagen on the Development and Maintenance of the Osteoblast Phenotype in Primary and Passaged Rat Calvarial Osteoblasts: Modification of Expression of Genes Supporting Cell Growth, Adhesion, and Extracellular Matrix Mineralization.* Experimental Cell Research, 1995. **216**(1): p. 35-45.
342. Safadi, F.F., et al., *Bone Structure, Development and Bone Biology*, in *Bone Pathology*, J.S. Khurana, Editor. 2009, Humana Press: Totowa, NJ. p. 1-50.
343. Olszta, M.J., et al., *Bone structure and formation: A new perspective.* Materials Science and Engineering: R: Reports, 2007. **58**(3): p. 77-116.
344. Keaveny, T.M., et al., *Biomechanics of Trabecular Bone.* Annual Review of Biomedical Engineering, 2001. **3**(1): p. 307-333.
345. Latimer, A. and J.R. Jessen, *Extracellular matrix assembly and organization during zebrafish gastrulation.* Matrix Biology, 2010. **29**(2): p. 89-96.
346. Snow, C.J., et al., *Muscle development is disrupted in zebrafish embryos deficient for fibronectin.* Developmental Dynamics, 2008. **237**(9): p. 2542-2553.
347. Zhu, J., et al., *Integrated extracellular matrix signaling in mammary gland development and breast cancer progression.* Histology and histopathology, 2014. **29**(9): p. 1083-1092.
348. Ingman, W.V., et al., *Macrophages promote collagen fibrillogenesis around terminal end buds of the developing mammary gland.* Developmental Dynamics, 2006. **235**(12): p. 3222-3229.
349. Subramanian, A. and T.F. Schilling, *Tendon development and musculoskeletal assembly: emerging roles for the extracellular matrix.* Development, 2015. **142**(24): p. 4191-4204.
350. Berthet, E., et al., *Smad3 binds scleraxis and mohawk and regulates tendon matrix organization.* Journal of Orthopaedic Research, 2013. **31**(9): p. 1475-1483.
351. Birch, H.L., A.P. Thorpe Ct Fau - Rumian, and A.P. Rumian, *Specialisation of extracellular matrix for function in tendons and ligaments.* Muscles, Ligaments and Tendons Journal, 2013. **3**(1): p. 12-22.
352. Schwartz, A.G., et al., *Muscle loading is necessary for the formation of a functional tendon enthesis.* Bone, 2013. **55**(1): p. 44-51.
353. KjÆR, M., *Role of Extracellular Matrix in Adaptation of Tendon and Skeletal Muscle to Mechanical Loading.* Physiological Reviews, 2004. **84**(2): p. 649-698.
354. Subramanian, A., et al., *Mechanical force regulates tendon extracellular matrix organization and tenocyte morphogenesis through TGFbeta signaling.* eLife, 2018. **7**: p. e38069.
355. Herchenhan, A., et al., *In vitro tendon tissue development from human fibroblasts demonstrates collagen fibril diameter growth associated with a rise in mechanical strength.* Developmental Dynamics, 2013. **242**(1): p. 2-8.
356. Frolova, E.G., et al., *Control of organization and function of muscle and tendon by thrombospondin-4.* Matrix Biology, 2014. **37**: p. 35-48.
357. Sharir, A. and E. Zelzer, *Tendon Homeostasis: The Right Pull.* Current Biology, 2011. **21**(12): p. R472-R474.
358. Maeda, T., et al., *Conversion of Mechanical Force into TGF- β- Mediated Biochemical Signals.* Current Biology, 2011. **21**(11): p. 933-941.
359. Rullman, E., et al., *Endurance exercise activates matrix metalloproteinases in human skeletal muscle.* Journal of Applied Physiology, 2009. **106**(3): p. 804-812.
360. Heinemeier, K.M., et al., *Expression of collagen and related growth factors in rat tendon and skeletal muscle in response to specific contraction types.* The Journal of Physiology, 2007. **582**(3): p. 1303-1316.

361. Heinemeier, K.M., et al., *Uphill running improves rat Achilles tendon tissue mechanical properties and alters gene expression without inducing pathological changes.* Journal of Applied Physiology, 2012. **113**(5): p. 827-836.
362. Buchanan, C.I. and R.L. Marsh, *Effects of long-term exercise on the biomechanical properties of the Achilles tendon of guinea fowl.* Journal of Applied Physiology, 2001. **90**(1): p. 164-171.
363. Svensson, R.B., et al., *Effect of aging and exercise on the tendon.* Journal of Applied Physiology, 2016. **121**(6): p. 1353-1362.
364. Farhat, Y.M., et al., *TGF-β1 Suppresses Plasmin and MMP Activity in Flexor Tendon Cells via PAI-1: Implications for Scarless Flexor Tendon Repair.* Journal of Cellular Physiology, 2015. **230**(2): p. 318-326.
365. Toriseva, M. and V.M. Kähäri, *Proteinases in cutaneous wound healing.* Cellular and Molecular Life Sciences, 2009. **66**(2): p. 203-224.
366. Katzel, E.B., et al., *Impact of Smad3 loss of function on scarring and adhesion formation during tendon healing.* Journal of Orthopaedic Research, 2011. **29**(5): p. 684-693.
367. Oshiro, W., et al., *Flexor tendon healing in the rat: a histologic and gene expression study.* Journal of Hand Surgery, 2003. **28**(5): p. 814-823.
368. Chang, J., et al., *Studies in Flexor Tendon Wound Healing: Neutralizing Antibody to TGF-β1 Increases Postoperative Range of Motion.* Plastic and Reconstructive Surgery, 2000. **105**(1).
369. Orr, A.W., et al., *Mechanisms of Mechanotransduction.* Developmental Cell, 2006. **10**(1): p. 11-20.
370. Chen, C.S., *Mechanotransduction – a field pulling together?* Journal of Cell Science, 2008. **121**(20): p. 3285-3292.
371. Kahn, J., et al., *Muscle Contraction Is Necessary to Maintain Joint Progenitor Cell Fate.* Developmental Cell, 2009. **16**(5): p. 734-743.
372. Hartmann, C. and C.J. Tabin, *Wnt-14 Plays a Pivotal Role in Inducing Synovial Joint Formation in the Developing Appendicular Skeleton.* Cell, 2001. **104**(3): p. 341-351.
373. Guo, X., et al., *Wnt/beta-catenin signaling is sufficient and necessary for synovial joint formation.* Genes and Development, 2004. **18**(19): p. 2404–2417.
374. García-Cardeña, G., et al., *Biomechanical activation of vascular endothelium as a determinant of its functional phenotype.* Proceedings of the National Academy of Sciences, 2001. **98**(8): p. 4478-4485.
375. Davies, P.F., *Flow-mediated endothelial mechanotransduction.* Physiological Reviews, 1995. **75**(3): p. 519-560.
376. Shigematsu, T., et al., *Changes in bone and calcium metabolism with space flight.* Osteoporosis International, 1997. **7**(3): p. 63-67.
377. Najrana, T. and J. Sanchez-Esteban, *Mechanotransduction as an Adaptation to Gravity.* Frontiers in Pediatrics, 2016. **4**.
378. Vico, L., M.H. Lafage-Proust, and C. Alexandre, *Effects of Gravitational Changes on the Bone System In Vitro and In Vivo.* Bone, 1998. **22**(5, Supplement 1): p. 95S-100S.
379. Engler, A.J., et al., *Matrix Elasticity Directs Stem Cell Lineage Specification.* Cell, 2006. **126**(4): p. 677-689.
380. Stopak, D. and A.K. Harris, *Connective tissue morphogenesis by fibroblast traction: I. Tissue culture observations.* Developmental Biology, 1982. **90**(2): p. 383-398.
381. Wozniak, M.A. and C.S. Chen, *Mechanotransduction in development: a growing role for contractility.* Nature Reviews Molecular Cell Biology, 2009. **10**(1): p. 34-43.
382. Davidson, L., M. von Dassow, and J. Zhou, *Multi-scale mechanics from molecules to morphogenesis.* The International Journal of Biochemistry & Cell Biology, 2009. **41**(11): p. 2147-2162.
383. DuFort, C.C., M.J. Paszek, and V.M. Weaver, *Balancing forces: architectural control of mechanotransduction.* Nature Reviews Molecular Cell Biology, 2011. **12**(5): p. 308-319.
384. Ogawa, R., *Chapter 9 - Mechanobiology and Mechanotherapy in Tissue Engineering*, in *In Situ Tissue Regeneration*, S.J. Lee, J.J. Yoo, and A. Atala, Editors. 2016, Academic Press: Boston. p. 165-181.
385. Huang, C., S. Akaishi, and R. Ogawa, *Mechanosignaling pathways in cutaneous scarring.* Archives of Dermatological Research, 2012. **304**(8): p. 589-597.
386. Vogel, V. and M. Sheetz, *Local force and geometry sensing regulate cell functions.* Nature Reviews Molecular Cell Biology, 2006. **7**(4): p. 265-275.
387. Lim, C.-G., J. Jang, and C. Kim, *Cellular machinery for sensing mechanical force.* BMB reports, 2018. **51**(12): p. 623-629.

388. Martinac, B., *Mechanosensitive ion channels: molecules of mechanotransduction.* Journal of Cell Science, 2004. **117**(12): p. 2449-2460.
389. Katsumi, A., et al., *Integrins in Mechanotransduction.* Journal of Biological Chemistry, 2004. **279**(13): p. 12001-12004.
390. Anishkin, A., et al., *Feeling the hidden mechanical forces in lipid bilayer is an original sense.* Proceedings of the National Academy of Sciences, 2014. **111**(22): p. 7898-7905.
391. Chanet, S. and A.C. Martin, *Mechanical force sensing in tissues.* Progress in molecular biology and translational science, 2014. **126**: p. 317-352.
392. Humphrey, J.D., E.R. Dufresne, and M.A. Schwartz, *Mechanotransduction and extracellular matrix homeostasis.* Nature Reviews Molecular Cell Biology, 2014. **15**: p. 802.
393. Kielty, C.M., *Fell-Muir Lecture: Fibrillin microfibrils: structural tensometers of elastic tissues?* International Journal of Experimental Pathology, 2017. **98**(4): p. 172-190.
394. Saini, K. and N. Kumar, *Mechanical response of collagen molecule under hydrostatic compression.* Materials Science and Engineering: C, 2015. **49**: p. 720-726.
395. Klotzsch, E., et al., *Fibronectin forms the most extensible biological fibers displaying switchable force-exposed cryptic binding sites.* Proceedings of the National Academy of Sciences, 2009. **106**(43): p. 18267-18272.
396. Vogel, V., *Unraveling the Mechanobiology of Extracellular Matrix.* Annual Review of Physiology, 2018. **80**(1): p. 353-387.
397. Kubow, K.E., et al., *Mechanical forces regulate the interactions of fibronectin and collagen I in extracellular matrix.* Nature Communications, 2015. **6**(1): p. 8026.
398. Vogel, V., *MECHANOTRANSDUCTION INVOLVING MULTIMODULAR PROTEINS: Converting Force into Biochemical Signals.* Annual Review of Biophysics and Biomolecular Structure, 2006. **35**(1): p. 459-488.
399. Butcher, D.T., T. Alliston, and V.M. Weaver, *A tense situation: forcing tumour progression.* Nature Reviews Cancer, 2009. **9**: p. 108.
400. Dupont, S., et al., *Role of YAP/TAZ in mechanotransduction.* Nature, 2011. **474**: p. 179.
401. Kruger, T.M., et al., *Reduced Extracellular Matrix Stiffness Prompts SH-SY5Y Cell Softening and Actin Turnover To Selectively Increase Aβ(1–42) Endocytosis.* ACS Chemical Neuroscience, 2019. **10**(3): p. 1284-1293.
402. Park, J.S., et al., *Mechanical regulation of glycolysis via cytoskeleton architecture.* Nature, 2020. **578**(7796): p. 621-626.
403. Kim, J., et al., *Stress-induced plasticity of dynamic collagen networks.* Nature Communications, 2017. **8**(1): p. 842.
404. Leung, D.Y.M., S. Glagov, and M.B. Mathews, *Cyclic Stretching Stimulates Synthesis of Matrix Components by Arterial Smooth Muscle Cells in Vitro.* Science, 1976. **191**(4226): p. 475-477.
405. Ge, H., et al., *Extracellular Matrix Stiffness: New Areas Affecting Cell Metabolism.* Frontiers in Oncology, 2021. **11**.
406. Shamsan, G.A. and D.J. Odde, *Emerging technologies in mechanotransduction research.* Current Opinion in Chemical Biology, 2019. **53**: p. 125-130.
407. Huang, H., R.D. Kamm, and R.T. Lee, *Cell mechanics and mechanotransduction: pathways, probes, and physiology.* American Journal of Physiology-Cell Physiology, 2004. **287**(1): p. C1-C11.
408. Lavoie, H., J. Gagnon, and M. Therrien, *ERK signalling: a master regulator of cell behaviour, life and fate.* Nature Reviews Molecular Cell Biology, 2020. **21**(10): p. 607-632.
409. Gortazar, A.R., et al., *Crosstalk between Caveolin-1/Extracellular Signal-regulated Kinase (ERK) and β -Catenin Survival Pathways in Osteocyte Mechanotransduction.* Journal of Biological Chemistry, 2013. **288**(12): p. 8168-8175.
410. Vermeulen, S., et al., *Mechanotransduction is a context-dependent activator of TGF-β signaling in mesenchymal stem cells.* Biomaterials, 2020. **259**: p. 120331.
411. Martino, F., et al., *Cellular Mechanotransduction: From Tension to Function.* Frontiers in Physiology, 2018. **9**.
412. Anguiano, M., et al., *The use of mixed collagen-Matrigel matrices of increasing complexity recapitulates the biphasic role of cell adhesion in cancer cell migration: ECM sensing, remodeling and forces at the leading edge of cancer invasion.* PLOS ONE, 2020. **15**(1): p. e0220019.
413. Boyle, S.T. and M.S. Samuel, *Mechano-reciprocity is maintained between physiological boundaries by tuning signal flux through the Rho-associated protein kinase.* Small GTPases, 2016. **7**(3): p. 139-146.

414. Choquet, D., D.P. Felsenfeld, and M.P. Sheetz, *Extracellular Matrix Rigidity Causes Strengthening of Integrin & Cytoskeleton Linkages.* Cell, 1997. **88**(1): p. 39-48.
415. Discher, D.E., P. Janmey, and Y.-l. Wang, *Tissue Cells Feel and Respond to the Stiffness of Their Substrate.* Science, 2005. **310**(5751): p. 1139.
416. Hamill, O.P. and B. Martinac, *Molecular Basis of Mechanotransduction in Living Cells.* Physiological Reviews, 2001. **81**(2): p. 685-740.
417. Takahashi, K., et al., *Gravity sensing in plant and animal cells.* Microgravity, 2021. **7**(1): p. 2.
418. Katt, M.E., et al., *In Vitro Tumor Models: Advantages, Disadvantages, Variables, and Selecting the Right Platform.* Frontiers in Bioengineering and Biotechnology, 2016. **4**.
419. Baker, B.M. and C.S. Chen, *Deconstructing the third dimension: how 3D culture microenvironments alter cellular cues.* Journal of cell science, 2012. **125**(Pt 13): p. 3015-3024.
420. Simian, M. and M.J. Bissell, *Organoids: A historical perspective of thinking in three dimensions.* Journal of Cell Biology, 2016. **216**(1): p. 31-40.
421. Bissell, M.J., A. Rizki, and I.S. Mian, *Tissue architecture: the ultimate regulator of breast epithelial function.* Current Opinion in Cell Biology, 2003. **15**(6): p. 753-762.
422. Von Der Mark, K., et al., *Relationship between cell shape and type of collagen synthesised as chondrocytes lose their cartilage phenotype in culture.* Nature, 1977. **267**(5611): p. 531-532.
423. Jeanes, A.I., A. Maya-Mendoza, and C.H. Streuli, *Cellular Microenvironment Influences the Ability of Mammary Epithelia to Undergo Cell Cycle.* PLOS ONE, 2011. **6**(3): p. e18144.
424. Dhiman, H.K., A.R. Ray, and A.K. Panda, *Three-dimensional chitosan scaffold-based MCF-7 cell culture for the determination of the cytotoxicity of tamoxifen.* Biomaterials, 2005. **26**(9): p. 979-986.
425. Gómez-Lechón, M.J., et al., *Long-term expression of differentiated functions in hepatocytes cultured in three-dimensional collagen matrix.* Journal of Cellular Physiology, 1998. **177**(4): p. 553-562.
426. Fraley, S.I., et al., *A distinctive role for focal adhesion proteins in three-dimensional cell motility.* Nature Cell Biology, 2010. **12**(6): p. 598-604.
427. Cukierman, E., et al., *Taking Cell-Matrix Adhesions to the Third Dimension.* Science, 2001. **294**(5547): p. 1708-1712.
428. Asghar, W., et al., *Engineering cancer microenvironments for in vitro 3-D tumor models.* Materials today (Kidlington, England), 2015. **18**(10): p. 539-553.
429. Edmondson, R., et al., *Three-Dimensional Cell Culture Systems and Their Applications in Drug Discovery and Cell-Based Biosensors.* Assay and Drug Development Technologies, 2014. **12**(4): p. 207-218.
430. Carletti, E., A. Motta, and C. Migliaresi, *Scaffolds for Tissue Engineering and 3D Cell Culture*, in *3D Cell Culture: Methods and Protocols*, J.W. Haycock, Editor. 2011, Humana Press: Totowa, NJ. p. 17-39.
431. Ahmed, E.M., *Hydrogel: Preparation, characterization, and applications: A review.* Journal of Advanced Research, 2015. **6**(2): p. 105-121.
432. Appel, E.A., et al., *Supramolecular polymeric hydrogels.* Chemical Society Reviews, 2012. **41**(18): p. 6195-6214.
433. Caliari, S.R. and J.A. Burdick, *A practical guide to hydrogels for cell culture.* Nature Methods, 2016. **13**: p. 405.
434. Emerman, J.T. and D.R. Pitelka, *Maintenance and induction of morphological differentiation in dissociated mammary epithelium on floating collagen membranes.* 1977(0073-5655 (Print)).
435. Barcellos-Hoff, M.H., et al., *Functional differentiation and alveolar morphogenesis of primary mammary cultures on reconstituted basement membrane.* Development, 1989. **105**(2): p. 223.
436. Streuli, C.H., N. Bailey, and M.J. Bissell, *Control of mammary epithelial differentiation: basement membrane induces tissue-specific gene expression in the absence of cell-cell interaction and morphological polarity.* The Journal of cell biology, 1991. **115**(5): p. 1383-1395.
437. Baptista, L.S., et al., *Adult Stem Cells Spheroids to Optimize Cell Colonization in Scaffolds for Cartilage and Bone Tissue Engineering.* International journal of molecular sciences, 2018. **19**(5): p. 1285.
438. Barros da Silva, P., et al., *Reshaping in vitro Models of Breast Tissue: Integration of Stromal and Parenchymal Compartments in 3D Printed Hydrogels.* Frontiers in Bioengineering and Biotechnology, 2020. **8**: p. 494.

439. Charoen, K.M., et al., *Embedded multicellular spheroids as a biomimetic 3D cancer model for evaluating drug and drug-device combinations.* Biomaterials, 2014. **35**(7): p. 2264-2271.
440. Huh, D., et al., *Reconstituting Organ-Level Lung Functions on a Chip.* Science, 2010. **328**(5986): p. 1662-1668.
441. Hu, H., et al., *Long-Term Expansion of Functional Mouse and Human Hepatocytes as 3D Organoids.* Cell, 2018. **175**(6): p. 1591-1606.e19.
442. Kim, J., B.-K. Koo, and J.A. Knoblich, *Human organoids: model systems for human biology and medicine.* Nature Reviews Molecular Cell Biology, 2020. **21**(10): p. 571-584.
443. Fatehullah, A., S.H. Tan, and N. Barker, *Organoids as an in vitro model of human development and disease.* Nature Cell Biology, 2016. **18**(3): p. 246-254.
444. Lancaster, M.A. and J.A. Knoblich, *Organogenesis in a dish: Modeling development and disease using organoid technologies.* Science, 2014. **345**(6194): p. 1247125.
445. Clevers, H., *Modeling Development and Disease with Organoids.* Cell, 2016. **165**(7): p. 1586-1597.
446. Weaver, V.M., et al., *Reversion of the malignant phenotype of human breast cells in three-dimensional culture and in vivo by integrin blocking antibodies.* The Journal of cell biology, 1997. **137**(1): p. 231-245.
447. Debnath, J., S.K. Muthuswamy, and J.S. Brugge, *Morphogenesis and oncogenesis of MCF-10A mammary epithelial acini grown in three-dimensional basement membrane cultures.* Methods, 2003. **30**(3): p. 256-268.
448. Imbalzano, K.M., et al., *Increasingly transformed MCF-10A cells have a progressively tumor-like phenotype in three-dimensional basement membrane culture.* Cancer Cell International, 2009. **9**(1): p. 7.
449. Hall, B.R., et al., *Utilizing cell line-derived organoids to evaluate the efficacy of a novel LIFR-inhibitor, EC359 in targeting pancreatic tumor stroma.* Genes and Cancer, 2019. **10**(1-2): p. 1-10.
450. Nadkarni, R.R., S. Abed, and J.S. Draper, *Organoids as a model system for studying human lung development and disease.* Biochemical and Biophysical Research Communications, 2016. **473**(3): p. 675-682.
451. Knudsen, L. and M. Ochs, *The micromechanics of lung alveoli: structure and function of surfactant and tissue components.* Histochemistry and Cell Biology, 2018. **150**(6): p. 661-676.
452. Beretta, E., et al., *Pulmonary Interstitial Matrix and Lung Fluid Balance From Normal to the Acutely Injured Lung.* Frontiers in Physiology, 2021. **12**.
453. Burgstaller, G., et al., *The instructive extracellular matrix of the lung: basic composition and alterations in chronic lung disease.* European Respiratory Journal, 2017. **50**(1): p. 1601805.
454. Suki, B., et al., *Biomechanics of the lung parenchyma: critical roles of collagen and mechanical forces.* Journal of Applied Physiology, 2005. **98**(5): p. 1892-1899.
455. Faffe, D.S. and W.A. Zin, *Lung Parenchymal Mechanics in Health and Disease.* Physiological Reviews, 2009. **89**(3): p. 759-775.
456. Yuan, H., et al., *Effects of collagenase and elastase on the mechanical properties of lung tissue strips.* Journal of Applied Physiology, 2000. **89**(1): p. 3-14.
457. Cavalcante, F.S.A., et al., *Mechanical interactions between collagen and proteoglycans: implications for the stability of lung tissue.* Journal of Applied Physiology, 2005. **98**(2): p. 672-679.
458. Roan, E. and C.M. Waters, *What do we know about mechanical strain in lung alveoli?* American Journal of Physiology-Lung Cellular and Molecular Physiology, 2011. **301**(5): p. L625-L635.
459. Ingenito, E.P., L. Mark, and B. Davison, *Effects of acute lung injury on dynamic tissue properties.* Journal of Applied Physiology, 1994. **77**(6): p. 2689-2697.
460. Karlinsky, J.B., *Stress-strain characteristics of normal and emphysematous hamster lung strips.* Respiration Physiology, 1992. **90**(3): p. 251-260.
461. Suki, B. and J.H.T. Bates, *Extracellular matrix mechanics in lung parenchymal diseases.* Respiratory Physiology & Neurobiology, 2008. **163**(1): p. 33-43.
462. Kononov, S., et al., *Roles of Mechanical Forces and Collagen Failure in the Development of Elastase-induced Emphysema.* American Journal of Respiratory and Critical Care Medicine, 2001. **164**(10): p. 1920-1926.
463. Ito, S., et al., *Early Emphysema in the Tight Skin and Pallid Mice.* American Journal of Respiratory Cell and Molecular Biology, 2006. **34**(6): p. 688-694.

464. Ebihara, T., et al., *Changes in Extracellular Matrix and Tissue Viscoelasticity in Bleomycin–induced Lung Fibrosis.* American Journal of Respiratory and Critical Care Medicine, 2000. **162**(4): p. 1569-1576.
465. Melo, E., et al., *Inhomogeneity of local stiffness in the extracellular matrix scaffold of fibrotic mouse lungs.* Journal of the Mechanical Behavior of Biomedical Materials, 2014. **37**: p. 186-195.
466. Shannon, J.M., R.J. Mason, and S.D. Jennings, *Functional differentiation of alveolar type II epithelial cells in vitro: Effects of cell shape, cell-matrix interactions and cell-cell interactions.* Biochimica et Biophysica Acta (BBA) - Molecular Cell Research, 1987. **931**(2): p. 143-156.
467. Barkauskas, C.E., et al., *Type 2 alveolar cells are stem cells in adult lung.* The Journal of Clinical Investigation, 2013. **123**(7): p. 3025-3036.
468. Kong, J., et al., *Lung organoids, useful tools for investigating epithelial repair after lung injury.* Stem Cell Research & Therapy, 2021. **12**(1): p. 95.
469. Gotoh, S., et al., *Generation of Alveolar Epithelial Spheroids via Isolated Progenitor Cells from Human Pluripotent Stem Cells.* Stem Cell Reports, 2014. **3**(3): p. 394-403.
470. Tran, E., et al., *Development of human alveolar epithelial cell models to study distal lung biology and disease.* iScience, 2022. **25**(2): p. 103780.
471. Chen, H., et al., *Airway Epithelial Progenitors Are Region Specific and Show Differential Responses to Bleomycin-Induced Lung Injury.* Stem Cells, 2012. **30**(9): p. 1948-1960.
472. Yu, W., et al., *Formation of Cysts by Alveolar Type II Cells in Three-dimensional Culture Reveals a Novel Mechanism for Epithelial Morphogenesis.* Molecular Biology of the Cell, 2007. **18**(5): p. 1693-1700.
473. Lee, J.-H., et al., *Surfactant Protein–C Chromatin-Bound Green Fluorescence Protein Reporter Mice Reveal Heterogeneity of Surfactant Protein C–Expressing Lung Cells.* American Journal of Respiratory Cell and Molecular Biology, 2013. **48**(3): p. 288-298.
474. Jacob, A., et al., *Differentiation of Human Pluripotent Stem Cells into Functional Lung Alveolar Epithelial Cells.* Cell Stem Cell, 2017. **21**(4): p. 472-488.e10.
475. Rabata, A., et al., *3D Cell Culture Models Demonstrate a Role for FGF and WNT Signaling in Regulation of Lung Epithelial Cell Fate and Morphogenesis.* Frontiers in Cell and Developmental Biology, 2020. **8**.
476. Huang, S.X.L., et al., *Efficient generation of lung and airway epithelial cells from human pluripotent stem cells.* Nature Biotechnology, 2014. **32**(1): p. 84-91.
477. Dye, B.R., et al., *In vitro generation of human pluripotent stem cell derived lung organoids.* eLife, 2015. **4**: p. e05098.
478. Ulich, T.R., et al., *Keratinocyte growth factor is a growth factor for type II pneumocytes in vivo.* The Journal of Clinical Investigation, 1994. **93**(3): p. 1298-1306.
479. Weinstein, M., et al., *FGFR-3 and FGFR-4 function cooperatively to direct alveogenesis in the murine lung.* Development, 1998. **125**(18): p. 3615-3623.
480. Leeman, K.T., et al., *Mesenchymal Stem Cells Increase Alveolar Differentiation in Lung Progenitor Organoid Cultures.* Scientific Reports, 2019. **9**(1): p. 6479.
481. Rubin, J.S., et al., *Keratinocyte growth factor.* Cell Biology International, 1995. **19**(5): p. 399-411.
482. Desai, T.J. and W.V. Cardoso, *Growth factors in lung development and disease: friends or foe?* Respiratory Research, 2001. **3**(1): p. 2.
483. White, E.S., *Lung Extracellular Matrix and Fibroblast Function.* Annals of the American Thoracic Society, 2015. **12**(Supplement 1): p. S30-S33.
484. Fredberg, J.J. and R.D. Kamm, *STRESS TRANSMISSION IN THE LUNG: Pathways from Organ to Molecule.* Annual Review of Physiology, 2006. **68**(1): p. 507-541.
485. Sanchez-Esteban, J., et al., *Mechanical stretch promotes alveolar epithelial type II cell differentiation.* Journal of Applied Physiology, 2001. **91**(2): p. 589-595.
486. Cohen, T.S., K.J. Cavanaugh, and S.S. Margulies, *Frequency and peak stretch magnitude affect alveolar epithelial permeability.* European Respiratory Journal, 2008. **32**(4): p. 854.
487. Cavanaugh, K.J., J. Oswari, and S.S. Margulies, *Role of Stretch on Tight Junction Structure in Alveolar Epithelial Cells.* American Journal of Respiratory Cell and Molecular Biology, 2001. **25**(5): p. 584-591.
488. Arold, S.P., E. Bartolák-Suki, and B. Suki, *Variable stretch pattern enhances surfactant secretion in alveolar type II cells in culture.* American Journal of Physiology-Lung Cellular and Molecular Physiology, 2009. **296**(4): p. L574-L581.
489. Hammerschmidt, S., et al., *Stretch-Induced Alveolar Type II Cell Apoptosis.* American Journal of Respiratory Cell and Molecular Biology, 2007. **37**(6): p. 699-705.

490. Tschumperlin, D.J., J. Oswari, and A.S.S. Margulies, *Deformation-Induced Injury of Alveolar Epithelial Cells.* American Journal of Respiratory and Critical Care Medicine, 2000. **162**(2): p. 357-362.
491. Edwards, Y.S., *Stretch stimulation: its effects on alveolar type II cell function in the lung.* Comparative Biochemistry and Physiology Part A: Molecular & Integrative Physiology, 2001. **129**(1): p. 245-260.
492. Benam, K.H., et al., *Small airway-on-a-chip enables analysis of human lung inflammation and drug responses in vitro.* Nature Methods, 2016. **13**(2): p. 151-157.
493. Jain, A., et al., *Primary Human Lung Alveolus-on-a-chip Model of Intravascular Thrombosis for Assessment of Therapeutics.* Clinical Pharmacology & Therapeutics, 2018. **103**(2): p. 332-340.
494. Huang, D., et al., *Reversed-engineered human alveolar lung-on-a-chip model.* Proceedings of the National Academy of Sciences, 2021. **118**(19): p. e2016146118.
495. Kumar Mahto, S., J. Tenenbaum-Katan, and J. Sznitman, *Respiratory Physiology on a Chip.* Scientifica, 2012. **2012**: p. 364054.
496. Huh, D., et al., *A Human Disease Model of Drug Toxicity–Induced Pulmonary Edema in a Lung-on-a-Chip Microdevice.* Science Translational Medicine, 2012. **4**(159): p. 159ra147-159ra147.
497. Mead, J., T. Takishima, and D. Leith, *Stress distribution in lungs: a model of pulmonary elasticity.* Journal of Applied Physiology, 1970. **28**(5): p. 596-608.
498. Sarabia-Vallejos, M.A., M. Zuñiga, and D.E. Hurtado, *The role of three-dimensionality and alveolar pressure in the distribution and amplification of alveolar stresses.* Scientific Reports, 2019. **9**(1): p. 8783.
499. Colace, T., et al., *Analysis of Morphology of Platelet Aggregates Formed on Collagen Under Laminar Blood Flow.* Annals of Biomedical Engineering, 2011. **39**(2): p. 922-929.
500. Neeves, K.B., et al., *Sources of Variability in Platelet Accumulation on Type 1 Fibrillar Collagen in Microfluidic Flow Assays.* PLOS ONE, 2013. **8**(1): p. e54680.
501. Sicard, D., et al., *Aging and anatomical variations in lung tissue stiffness.* American Journal of Physiology-Lung Cellular and Molecular Physiology, 2018. **314**(6): p. L946-L955.
502. Polio, S.R., et al., *Cross-platform mechanical characterization of lung tissue.* PLOS ONE, 2018. **13**(10): p. e0204765.
503. Anderson, S.M., et al., *Key stages in mammary gland development. Secretory activation in the mammary gland: it's not just about milk protein synthesis!* Breast Cancer Research, 2007. **9**(1): p. 204.
504. Adriance, M.C., et al., *Myoepithelial cells: good fences make good neighbors.* Breast Cancer Research, 2005. **7**(5): p. 190.
505. Macias, H. and L. Hinck, *Mammary gland development.* Wiley interdisciplinary reviews. Developmental biology, 2012. **1**(4): p. 533-557.
506. Richert, M.M., et al., *An Atlas of Mouse Mammary Gland Development.* Journal of Mammary Gland Biology and Neoplasia, 2000. **5**(2): p. 227-241.
507. Inman, J.L., et al., *Mammary gland development: cell fate specification, stem cells and the microenvironment.* Development, 2015. **142**(6): p. 1028.
508. Sakai, T., M. Larsen, and K.M. Yamada, *Fibronectin requirement in branching morphogenesis.* Nature, 2003. **423**(6942): p. 876-881.
509. Wiseman, B.S., et al., *Site-specific inductive and inhibitory activities of MMP-2 and MMP-3 orchestrate mammary gland branching morphogenesis.* Journal of Cell Biology, 2003. **162**(6): p. 1123-1133.
510. Weaver, M., N.R. Dunn, and B.L. Hogan, *Bmp4 and Fgf10 play opposing roles during lung bud morphogenesis.* Development, 2000. **127**(12): p. 2695-2704.
511. Williams, J.M. and C.W. Daniel, *Mammary ductal elongation: Differentiation of myoepithelium and basal lamina during branching morphogenesis.* Developmental Biology, 1983. **97**(2): p. 274-290.
512. Ronnov-Jessen, L., O.W. Petersen, and M.J. Bissell, *Cellular changes involved in conversion of normal to malignant breast: importance of the stromal reaction.* Physiological Reviews, 1996. **76**(1): p. 69-125.
513. Medina, D., *The mammary gland: A unique organ for the study of development and tumorigenesis.* Journal of Mammary Gland Biology and Neoplasia, 1996. **1**(1): p. 5-19.
514. Streuli, C.H., *Preface: Cell Adhesion in Mammary Gland Biology and Neoplasia.* Journal of Mammary Gland Biology and Neoplasia, 2003. **8**(4): p. 375-381.

515. Pillay, J. and T.J. Davis, *Physiology, Lactation*. 2022, Treasure Island, FL: StatPearls Publishing.
516. Lee, Y.-J., et al., *Extracellular matrix controls insulin signaling in mammary epithelial cells through the RhoA/Rok pathway.* Journal of Cellular Physiology, 2009. **220**(2): p. 476-484.
517. Emerman, J.T., S.J. Burwen, and D.R. Pitelka, *Substrate properties influencing ultrastructural differentiation of mammary epithelial cells in culture.* Tissue and Cell, 1979. **11**(1): p. 109-119.
518. Lee, E.Y., G. Parry, and M.J. Bissell, *Modulation of secreted proteins of mouse mammary epithelial cells by the collagenous substrata.* Journal of Cell Biology, 1984. **98**(1): p. 146-155.
519. Aggeler, J., et al., *Cytodifferentiation of mouse mammary epithelial cells cultured on a reconstituted basement membrane reveals striking similarities to development in vivo.* Journal of Cell Science, 1991. **99**: p. 407-417
520. Chen, L.H. and M.J. Bissell, *A novel regulatory mechanism for whey acidic protein gene expression.* Cell Regulation, 1989. **1**(1): p. 45-54.
521. Gudjonsson, T., et al., *Normal and tumor-derived myoepithelial cells differ in their ability to interact with luminal breast epithelial cells for polarity and basement membrane deposition.* Journal of cell science, 2002. **115**(Pt 1): p. 39-50.
522. Corning. *Corning® Matrigel® Matrix: Frequently Asked Questions*. [PDF] 2021 [cited 20/02/2022]; Available from: https://www.corning.com/catalog/cls/documents/faqs/CLS-DL-CC-026.pdf.
523. Muthuswamy, S.K., et al., *ErbB2, but not ErbB1, reinitiates proliferation and induces luminal repopulation in epithelial acini.* Nature cell biology, 2001. **3**(9): p. 785-792.
524. Shaw, K.R.M., C.N. Wrobel, and J.S. Brugge, *Use of Three-Dimensional Basement Membrane Cultures to Model Oncogene-Induced Changes in Mammary Epithelial Morphogenesis.* Journal of Mammary Gland Biology and Neoplasia, 2004. **9**(4): p. 297-310.
525. Beliveau, A., et al., *Raf-induced MMP9 disrupts tissue architecture of human breast cells in three-dimensional culture and is necessary for tumor growth in vivo.* Genes & development, 2010. **24**(24): p. 2800-2811.
526. Fiore, A.P.Z.P., et al., *Laminin-111 and the Level of Nuclear Actin Regulate Epithelial Quiescence via Exportin-6.* Cell Reports, 2017. **19**(10): p. 2102-2115.
527. Walker, S., et al., *Oncogenic activation of FAK drives apoptosis suppression in a 3D-culture model of breast cancer initiation.* Oncotarget, 2016. **7**(43): p. 70336-70352.
528. Zutter, M.M., et al., *Re-expression of the alpha 2 beta 1 integrin abrogates the malignant phenotype of breast carcinoma cells.* Proceedings of the National Academy of Sciences, 1995. **92**(16): p. 7411-7415.
529. Akhtar, N. and C.H. Streuli, *Rac1 links integrin-mediated adhesion to the control of lactational differentiation in mammary epithelia.* The Journal of cell biology, 2006. **173**(5): p. 781-793.
530. Akhtar, N. and C.H. Streuli, *An integrin–ILK–microtubule network orients cell polarity and lumen formation in glandular epithelium.* Nature Cell Biology, 2013. **15**(1): p. 17-27.
531. Seewaldt, V.L., et al., *Suppression of p53 function in normal human mammary epithelial cells increases sensitivity to extracellular matrix–induced apoptosis.* Journal of Cell Biology, 2001. **155**(3): p. 471-486.
532. Naylor, M.J., et al., *Ablation of beta1 integrin in mammary epithelium reveals a key role for integrin in glandular morphogenesis and differentiation.* The Journal of cell biology, 2005. **171**(4): p. 717-728.
533. Wells, R.G., *Tissue mechanics and fibrosis.* Biochimica et Biophysica Acta (BBA) - Molecular Basis of Disease, 2013. **1832**(884-890).
534. Provenzano, P.P. and P.J. Keely, *Mechanical signaling through the cytoskeleton regulates cell proliferation by coordinated focal adhesion and Rho GTPase signaling.* Journal of cell science, 2011. **124**(Pt 8): p. 1195-1205.
535. Ramião, N.G., et al., *Biomechanical properties of breast tissue, a state-of-the-art review.* Biomechanics and Modeling in Mechanobiology, 2016. **15**(5): p. 1307-1323.
536. McConnell, J.C., et al., *Increased peri-ductal collagen micro-organization may contribute to raised mammographic density.* Breast Cancer Research, 2016. **18**(1): p. 5.
537. Samani, A., J. Zubovits, and D. Plewes, *Elastic moduli of normal and pathological human breast tissues: an inversion-technique-based investigation of 169 samples.* Physics in Medicine and Biology, 2007. **52**(6): p. 1565-1576.
538. Umemoto, T., et al., *Ex Vivo and In Vivo Assessment of the Non-linearity of Elasticity Properties of Breast Tissues for Quantitative Strain Elastography.* Ultrasound in Medicine & Biology, 2014. **40**(8): p. 1755-1768.

539. McKnight, A.L., et al., *MR Elastography of Breast Cancer: Preliminary Results.* American Journal of Roentgenology, 2002. **178**(6): p. 1411-1417.
540. Lopez, J.I., et al., *In situ force mapping of mammary gland transformation.* Integrative biology : quantitative biosciences from nano to macro, 2011. **3**(9): p. 910-921.
541. Burton, A., et al., *Mammographic density and ageing: A collaborative pooled analysis of cross-sectional data from 22 countries worldwide.* PLOS Medicine, 2017. **14**(6): p. e1002335.
542. Martin, L.J. and N.F. Boyd, *Mammographic density. Potential mechanisms of breast cancer risk associated with mammographic density: hypotheses based on epidemiological evidence.* Breast Cancer Research, 2008. **10**(1): p. 201.
543. Acerbi, I., et al., *Human breast cancer invasion and aggression correlates with ECM stiffening and immune cell infiltration.* Integrative biology : quantitative biosciences from nano to macro, 2015. **7**(10): p. 1120-1134.
544. Boyd, N.F., et al., *Mammographic Density and the Risk and Detection of Breast Cancer.* New England Journal of Medicine, 2007. **356**(3): p. 227-236.
545. Northey, J.J., et al., *Stiff stroma increases breast cancer risk by inducing the oncogene ZNF217.* The Journal of Clinical Investigation, 2020.
546. Huo, C.W., et al., *High mammographic density is associated with an increase in stromal collagen and immune cells within the mammary epithelium.* Breast Cancer Research, 2015. **17**(1): p. 79.
547. Provenzano, P.P., et al., *Collagen density promotes mammary tumor initiation and progression.* BMC medicine, 2008. **6**: p. 11-11.
548. Alowami, S., et al., *Mammographic density is related to stroma and stromal proteoglycan expression.* Breast Cancer Research, 2003. **5**(5): p. R129.
549. Guo, Y.-P., et al., *Growth Factors and Stromal Matrix Proteins Associated with Mammographic Densities.* Cancer Epidemiology Biomarkers & Prevention, 2001. **10**(3): p. 243.
550. Bredfeldt, J.S., et al., *Automated quantification of aligned collagen for human breast carcinoma prognosis.* Journal of pathology informatics, 2014. **5**(1): p. 28-28.
551. Koorman, T., et al., *Spatial collagen stiffening promotes collective breast cancer cell invasion by reinforcing extracellular matrix alignment.* Oncogene, 2022. **41**(17): p. 2458-2469.
552. Nazari, S.S. and P. Mukherjee, *An overview of mammographic density and its association with breast cancer.* Breast Cancer, 2018. **25**(3): p. 259-267.
553. Carey, S., K. E. Martin, and C. Reinhart-King, *Three-dimensional collagen matrix induces a mechanosensitive invasive epithelial phenotype*. Vol. 7. 2017. 42088.
554. Wozniak, M.A., et al., *ROCK-generated contractility regulates breast epithelial cell differentiation in response to the physical properties of a three-dimensional collagen matrix.* The Journal of Cell Biology, 2003. **163**(3): p. 583.
555. Keely, P.J., J.E. Wu, and S.A. Santoro, *The spatial and temporal expression of the α2β1 integrin and its ligands, collagen I, collagen IV, and laminin, suggest important roles in mouse mammary morphogenesis.* Differentiation, 1995. **59**(1): p. 1-13.
556. Chaudhuri, O., et al., *Extracellular matrix stiffness and composition jointly regulate the induction of malignant phenotypes in mammary epithelium.* Nature Materials, 2014. **13**: p. 970.
557. Stowers, R.S., et al., *Matrix stiffness induces a tumorigenic phenotype in mammary epithelium through changes in chromatin accessibility.* Nature Biomedical Engineering, 2019.
558. Wood, A., et al., *Increased microenvironment stiffness leads to altered aldehyde metabolism and DNA damage in mammary epithelial cells through a RhoA-dependent mechanism.* bioRxiv, 2020: p. 2020.10.06.327726.
559. Lee, J.Y., et al., *YAP-independent mechanotransduction drives breast cancer progression.* Nature Communications, 2019. **10**(1): p. 1848.
560. Chang, J., et al., *Increased Stiffness Inhibits Invadopodia Formation and Cell Migration in 3D.* Biophysical Journal, 2020. **119**(4): p. 726-736.
561. Maller, O., H. Martinson, and P. Schedin, *Extracellular Matrix Composition Reveals Complex and Dynamic Stromal-Epithelial Interactions in the Mammary Gland.* Journal of Mammary Gland Biology and Neoplasia, 2010. **15**(3): p. 301-318.
562. Lance, A., et al., *Increased extracellular matrix density decreases MCF10A breast cell acinus formation in 3D culture conditions.* Journal of Tissue Engineering and Regenerative Medicine, 2016. **10**(1): p. 71-80.
563. Jun, D.-Y., et al., *Tubular organotypic culture model of human kidney.* PloS one, 2018. **13**(10): p. e0206447-e0206447.

564. Kleinman, H.K. and G.R. Martin, *Matrigel: Basement membrane matrix with biological activity.* Seminars in Cancer Biology, 2005. **15**(5): p. 378-386.
565. Seino, T., et al., *Human Pancreatic Tumor Organoids Reveal Loss of Stem Cell Niche Factor Dependence during Disease Progression.* Cell Stem Cell, 2018. **22**(3): p. 454-467.e6.
566. Orkin, R.W., et al., *A murine tumor producing a matrix of basement membrane.* The Journal of experimental medicine, 1977. **145**(1): p. 204-220.
567. Hughes, C.S., L.M. Postovit, and G.A. Lajoie, *Matrigel: A complex protein mixture required for optimal growth of cell culture.* PROTEOMICS, 2010. **10**(9): p. 1886-1890.
568. Gillette, K.M., I. Forbes K Fau - Sehgal, and I. Sehgal, *Detection of matrix metalloproteinases (MMP), tissue inhibitor of metalloproteinase-2, urokinase and plasminogen activator inhibitor-1 within matrigel and growth factor-reduced matrigel basement membrane.* 2003(0300-8916 (Print)).
569. Mackay, A.R., et al., *Identification of the 72-kDa (MMP-2) and 92-kDa (MMP-9) gelatinase/type IV collagenase in preparations of laminin and Matrigel.* BioTechniques, 1993. **15**(6): p. 1048-1051.
570. Talbot, N.C. and T.J. Caperna, *Proteome array identification of bioactive soluble proteins/peptides in Matrigel: relevance to stem cell responses.* Cytotechnology, 2015. **67**(5): p. 873-883.
571. Hansen, K.C., et al., *An in-solution ultrasonication-assisted digestion method for improved extracellular matrix proteome coverage.* Molecular & cellular proteomics : MCP, 2009. **8**(7): p. 1648-1657.
572. Benton, G., et al., *Matrigel: From discovery and ECM mimicry to assays and models for cancer research.* Advanced Drug Delivery Reviews, 2014. **79-80**: p. 3-18.
573. Kozlowski, M.T., C.J. Crook, and H.T. Ku, *Towards organoid culture without Matrigel.* Communications Biology, 2021. **4**(1): p. 1387.
574. Vaillant, F., G.J. Lindeman, and J.E. Visvader, *Jekyll or Hyde: does Matrigel provide a more or less physiological environment in mammary repopulating assays?* Breast Cancer Research, 2011. **13**(3): p. 108.
575. Gjorevski, N., A. Ranga, and M.P. Lutolf, *Bioengineering approaches to guide stem cell-based organogenesis.* Development, 2014. **141**(9): p. 1794-1804.
576. Mahoney, Z.X., T.S. Stappenbeck, and J.H. Miner, *Laminin α5 influences the architecture of the mouse small intestine mucosa.* Journal of Cell Science, 2008. **121**(15): p. 2493-2502.
577. Sato, T., et al., *Single Lgr5 stem cells build crypt-villus structures in vitro without a mesenchymal niche.* Nature, 2009. **459**(7244): p. 262-265.
578. Vukicevic, S., et al., *Identification of multiple active growth factors in basement membrane matrigel suggests caution in interpretation of cellular activity related to extracellular matrix components.* Experimental Cell Research, 1992. **202**(1): p. 1-8.
579. Polykandriotis, E., et al., *To matrigel or not to matrigel.* The American journal of pathology, 2008. **172**(5): p. 1441-1442.
580. Prokhorova, T.A., et al., *Teratoma Formation by Human Embryonic Stem Cells Is Site Dependent and Enhanced by the Presence of Matrigel.* Stem Cells and Development, 2008. **18**(1): p. 47-54.
581. Mullen, P., et al., *Effect of matrigel on the tumorigenicity of human breast and ovarian carcinoma cell lines.* International Journal of Cancer, 1996. **67**(6): p. 816-820.
582. Riley, V., et al., *The LDH Virus: An Interfering Biological Contaminant.* Science, 1978. **200**(4338): p. 124-126.
583. Peterson, N.C., *From Bench to Cageside: Risk Assessment for Rodent Pathogen Contamination of Cells and Biologics.* ILAR Journal, 2008. **49**(3): p. 310-315.
584. Villa-Diaz, L.G., et al., *Concise Review: The Evolution of human pluripotent stem cell culture: From feeder cells to synthetic coatings.* STEM CELLS, 2013. **31**(1): p. 1-7.
585. Slater, K., Partridge, J. and Nandivada, H. , *Tuning the Elastic Moduli of Corning® Matrigel®and Collagen I 3D Matrices by Varying the Protein Concentration*, in *Corning Application Note*. 2018.
586. Chaudhuri, O., *Viscoelastic hydrogels for 3D cell culture.* Biomaterials Science, 2017. **5**(8): p. 1480-1490.
587. Soofi, S.S., et al., *The elastic modulus of Matrigel™ as determined by atomic force microscopy.* Journal of Structural Biology, 2009. **167**(3): p. 216-219.
588. Reed, J., et al., *In Situ Mechanical Interferometry of Matrigel Films.* Langmuir, 2009. **25**(1): p. 36-39.

589. Wullkopf, L., et al., *Cancer cells' ability to mechanically adjust to extracellular matrix stiffness correlates with their invasive potential.* Molecular Biology of the Cell, 2018. **29**(20): p. 2378-2385.
590. Jee, J.H., et al., *Development of Collagen-Based 3D Matrix for Gastrointestinal Tract-Derived Organoid Culture.* Stem Cells International, 2019. **2019**: p. 8472712.
591. Chung, C. and J.A. Burdick, *Influence of Three-Dimensional Hyaluronic Acid Microenvironments on Mesenchymal Stem Cell Chondrogenesis.* Tissue Engineering Part A, 2008. **15**(2): p. 243-254.
592. Hempel, U., et al., *Artificial extracellular matrices composed of collagen I and sulfated hyaluronan with adsorbed transforming growth factor β1 promote collagen synthesis of human mesenchymal stromal cells.* Acta Biomaterialia, 2012. **8**(2): p. 659-666.
593. Giobbe, G.G., et al., *Extracellular matrix hydrogel derived from decellularized tissues enables endodermal organoid culture.* Nature Communications, 2019. **10**(1): p. 5658.
594. Schwartz, D.M., et al., *Spray Delivery of Intestinal Organoids to Reconstitute Epithelium on Decellularized Native Extracellular Matrix.* Tissue Engineering Part C: Methods, 2017. **23**(9): p. 565-573.
595. Baptista, P.M., et al., *The use of whole organ decellularization for the generation of a vascularized liver organoid.* Hepatology, 2011. **53**(2): p. 604-617.
596. Lewis, P.L., et al., *Complex bile duct network formation within liver decellularized extracellular matrix hydrogels.* Scientific Reports, 2018. **8**(1): p. 12220.
597. Bruno, R.D., et al., *Mammary extracellular matrix directs differentiation of testicular and embryonic stem cells to form functional mammary glands in vivo.* Scientific Reports, 2017. **7**: p. 40196.
598. Mollica, P.A., et al., *3D bioprinted mammary organoids and tumoroids in human mammary derived ECM hydrogels.* Acta biomaterialia, 2019. **95**: p. 201-213.
599. Sokol, E.S., et al., *Growth of human breast tissues from patient cells in 3D hydrogel scaffolds.* Breast cancer research : BCR, 2016. **18**(1): p. 19-19.
600. Curvello, R., et al., *A thermo-responsive collagen-nanocellulose hydrogel for the growth of intestinal organoids.* Materials Science and Engineering: C, 2021. **124**: p. 112051.
601. Yazdani, M., et al., *A Hyaluronan Hydrogel Scaffold for Culture of Human Oral Mucosal Epithelial Cells in Limbal Stem-Cell Therapy.* Bioengineering, 2019. **6**(4).
602. Nguyen, E.H., et al., *Versatile synthetic alternatives to Matrigel for vascular toxicity screening and stem cell expansion.* Nature Biomedical Engineering, 2017. **1**(7): p. 0096.
603. Cho, A.-N., et al., *Microfluidic device with brain extracellular matrix promotes structural and functional maturation of human brain organoids.* Nature Communications, 2021. **12**(1): p. 4730.
604. Finkbeiner, S.R., et al., *Generation of tissue-engineered small intestine using embryonic stem cell-derived human intestinal organoids.* Biology Open, 2015. **4**(11): p. 1462-1472.
605. Engler, A., et al., *Substrate compliance versus ligand density in cell on gel responses.* Biophysical journal, 2004. **86**(1 Pt 1): p. 617-628.
606. Madduma-Bandarage, U.S.K. and S.V. Madihally, *Synthetic hydrogels: Synthesis, novel trends, and applications.* Journal of Applied Polymer Science, 2021. **138**(19): p. 50376.
607. Charrier, E.E., et al., *A novel method to make viscoelastic polyacrylamide gels for cell culture and traction force microscopy.* APL Bioengineering, 2020. **4**(3): p. 036104.
608. Díaz-Bello, B., et al., *Method for the Direct Fabrication of Polyacrylamide Hydrogels with Controlled Stiffness in Polystyrene Multiwell Plates for Mechanobiology Assays.* ACS Biomaterials Science & Engineering, 2019. **5**(9): p. 4219-4227.
609. Mouw, J.K., et al., *Tissue mechanics modulate microRNA-dependent PTEN expression to regulate malignant progression.* Nature Medicine, 2014. **20**(4): p. 360-367.
610. Lee, I.N., et al., *Photoresponsive Hydrogels with Photoswitchable Mechanical Properties Allow Time-Resolved Analysis of Cellular Responses to Matrix Stiffening.* ACS Applied Materials & Interfaces, 2018. **10**(9): p. 7765-7776.
611. Rowlands, A.S., P.A. George, and J.J. Cooper-White, *Directing osteogenic and myogenic differentiation of MSCs: interplay of stiffness and adhesive ligand presentation.* American Journal of Physiology-Cell Physiology, 2008. **295**(4): p. C1037-C1044.
612. Aisenbrey, E.A. and W.L. Murphy, *Synthetic alternatives to Matrigel.* Nature Reviews Materials, 2020. **5**(7): p. 539-551.
613. Zhang, K., et al., *Mechanical signals regulate and activate SNAIL1 protein to control the fibrogenic response of cancer-associated fibroblasts.* Journal of Cell Science, 2016. **129**(10): p. 1989-2002.

614. Duval, K., et al., *Modeling Physiological Events in 2D vs. 3D Cell Culture.* Physiology, 2017. **32**(4): p. 266-277.
615. Grigoryan, B., et al., *Multivascular networks and functional intravascular topologies within biocompatible hydrogels.* Science, 2019. **364**(6439): p. 458-464.
616. Zustiak, S.P. and J.B. Leach, *Hydrolytically Degradable Poly(Ethylene Glycol) Hydrogel Scaffolds with Tunable Degradation and Mechanical Properties.* Biomacromolecules, 2010. **11**(5): p. 1348-1357.
617. Lopes, M.S., A.L. Jardini, and R.M. Filho, *Poly (Lactic Acid) Production for Tissue Engineering Applications.* Procedia Engineering, 2012. **42**: p. 1402-1413.
618. Culenova, M., et al., *In Vitro Characterization of Poly(Lactic Acid)/ Poly(Hydroxybutyrate)/ Thermoplastic Starch Blends for Tissue Engineering Application.* Cell Transplantation, 2021. **30**: p. 09636897211021003.
619. Bryant, S.J., et al., *Crosslinking Density Influences Chondrocyte Metabolism in Dynamically Loaded Photocrosslinked Poly(ethylene glycol) Hydrogels.* Annals of Biomedical Engineering, 2004. **32**(3): p. 407-417.
620. Biagini, G., et al., *3D Poly(Lactic Acid) Scaffolds Promote Different Behaviors on Endothelial Progenitors and Adipose-Derived Stromal Cells in Comparison With Standard 2D Cultures.* Frontiers in Bioengineering and Biotechnology, 2021. **9**(700862).
621. Patterson, J. and J.A. Hubbell, *Enhanced proteolytic degradation of molecularly engineered PEG hydrogels in response to MMP-1 and MMP-2.* Biomaterials, 2010. **31**(30): p. 7836-7845.
622. McKinnon, D.D., et al., *Biophysically Defined and Cytocompatible Covalently Adaptable Networks as Viscoelastic 3D Cell Culture Systems.* Advanced Materials, 2014. **26**(6): p. 865-872.
623. LeValley, P.J. and A.M. Kloxin, *Chemical Approaches to Dynamically Modulate the Properties of Synthetic Matrices.* ACS Macro Letters, 2019. **8**(1): p. 7-16.
624. Qin, X.-H., et al., *Near-Infrared Light-Sensitive Polyvinyl Alcohol Hydrogel Photoresist for Spatiotemporal Control of Cell-Instructive 3D Microenvironments.* Advanced Materials, 2018. **30**(10): p. 1705564.
625. Narayanan, L.K., et al., *3D-Bioprinting of Polylactic Acid (PLA) Nanofiber–Alginate Hydrogel Bioink Containing Human Adipose-Derived Stem Cells.* ACS Biomaterials Science & Engineering, 2016. **2**(10): p. 1732-1742.
626. Unagolla, J.M. and A.C. Jayasuriya, *Hydrogel-based 3D bioprinting: A comprehensive review on cell-laden hydrogels, bioink formulations, and future perspectives.* Applied Materials Today, 2020. **18**: p. 100479.
627. Skardal, A., J. Zhang, and G.D. Prestwich, *Bioprinting vessel-like constructs using hyaluronan hydrogels crosslinked with tetrahedral polyethylene glycol tetracrylates.* Biomaterials, 2010. **31**(24): p. 6173-6181.
628. Weber, L.M., et al., *The effects of cell–matrix interactions on encapsulated β-cell function within hydrogels functionalized with matrix-derived adhesive peptides.* Biomaterials, 2007. **28**(19): p. 3004-3011.
629. Livingston, M.K., et al., *Evaluation of PEG-based hydrogel influence on estrogen receptor driven responses in MCF7 breast cancer cells.* ACS biomaterials science & engineering, 2019. **5**(11): p. 6089-6098.
630. Ziemkiewicz, N., et al., *Laminin-111 functionalized polyethylene glycol hydrogels support myogenic activity in vitro.* Biomedical Materials, 2018. **13**(6): p. 065007.
631. Ng, S.S., et al., *Human iPS derived progenitors bioengineered into liver organoids using an inverted colloidal crystal poly (ethylene glycol) scaffold.* Biomaterials, 2018. **182**: p. 299-311.
632. Gjorevski, N., et al., *Designer matrices for intestinal stem cell and organoid culture.* Nature, 2016. **539**(7630): p. 560-564.
633. Poudel, H., et al., *Synthetic Matrices for Intestinal Organoid Culture: Implications for Better Performance.* ACS Omega, 2022. **7**(1): p. 38-47.
634. Smithmyer, M.E., L.A. Sawicki, and A.M. Kloxin, *Hydrogel scaffolds as in vitro models to study fibroblast activation in wound healing and disease.* Biomaterials Science, 2014. **2**(5): p. 634-650.
635. Du, X., et al., *Supramolecular Hydrogelators and Hydrogels: From Soft Matter to Molecular Biomaterials.* Chemical Reviews, 2015. **115**(24): p. 13165-13307.
636. Zhang, S., *Fabrication of novel biomaterials through molecular self-assembly.* Nature Biotechnology, 2003. **21**(10): p. 1171-1178.
637. Chen, J. and X. Zou, *Self-assemble peptide biomaterials and their biomedical applications.* Bioactive Materials, 2019. **4**: p. 120-131.

638. Fu, K., H. Wu, and Z. Su, *Self-assembling peptide-based hydrogels: Fabrication, properties, and applications.* Biotechnology Advances, 2021. **49**: p. 107752.
639. Li, L., et al., *Self-Assembly Dipeptide Hydrogel: The Structures and Properties.* Frontiers in Chemistry, 2021. **9**.
640. Yang, Z., H. Xu, and X. Zhao, *Designer Self-Assembling Peptide Hydrogels to Engineer 3D Cell Microenvironments for Cell Constructs Formation and Precise Oncology Remodeling in Ovarian Cancer.* Advanced Science, 2020. **7**(9): p. 1903718.
641. Zhang, S., *Emerging biological materials through molecular self-assembly.* Biotechnology Advances, 2002. **20**(5): p. 321-339.
642. Matson, J.B. and S.I. Stupp, *Self-assembling peptide scaffolds for regenerative medicine.* Chemical Communications, 2012. **48**(1): p. 26-33.
643. Aggeli, A., et al., *Responsive gels formed by the spontaneous self-assembly of peptides into polymeric β-sheet tapes.* Nature, 1997. **386**(6622): p. 259-262.
644. Zhou, M., et al., *Self-assembled peptide-based hydrogels as scaffolds for anchorage-dependent cells.* Biomaterials, 2009. **30**(13): p. 2523-2530.
645. Aggeli, A., et al., *Hierarchical self-assembly of chiral rod-like molecules as a model for peptide beta -sheet tapes, ribbons, fibrils, and fibers.* Proceedings of the National Academy of Sciences of the United States of America, 2001. **98**(21): p. 11857-11862.
646. Yamada, Y., et al., *Design of a Peptide-Based Electronegative Hydrogel for the Direct Encapsulation, 3D Culturing, in Vivo Syringe-Based Delivery, and Long-Term Tissue Engraftment of Cells.* ACS Applied Materials & Interfaces, 2019. **11**(38): p. 34688-34697.
647. Guan, T., et al., *Self-Assembling Peptide-Based Hydrogels for Wound Tissue Repair.* Advanced Science, 2022. **9**(10): p. 2104165.
648. Webber, M.J., et al., *Supramolecular nanostructures that mimic VEGF as a strategy for ischemic tissue repair.* Proceedings of the National Academy of Sciences, 2011. **108**(33): p. 13438-13443.
649. Catoira, M.C., et al., *Overview of natural hydrogels for regenerative medicine applications.* Journal of Materials Science: Materials in Medicine, 2019. **30**(10): p. 115.
650. Hu, J., et al., *Design Strategies to Tune the Structural and Mechanical Properties of Synthetic Collagen Hydrogels.* Biomacromolecules, 2021. **22**(8): p. 3440-3450.
651. Hogrebe, N.J. and K.J. Gooch, *Direct influence of culture dimensionality on human mesenchymal stem cell differentiation at various matrix stiffnesses using a fibrous self-assembling peptide hydrogel.* Journal of Biomedical Materials Research Part A, 2016. **104**(9): p. 2356-2368.
652. O'Leary, L.E.R., et al., *Multi-hierarchical self-assembly of a collagen mimetic peptide from triple helix to nanofibre and hydrogel.* Nature Chemistry, 2011. **3**(10): p. 821-828.
653. Luo, T. and K.L. Kiick, *Collagen-like peptides and peptide–polymer conjugates in the design of assembled materials.* European Polymer Journal, 2013. **49**(10): p. 2998-3009.
654. Fallas, J.A., et al., *Structural Insights into Charge Pair Interactions in Triple Helical Collagen-like Proteins.* Journal of Biological Chemistry, 2012. **287**(11): p. 8039-8047.
655. Kumar, D., et al., *Peptide Hydrogels—A Tissue Engineering Strategy for the Prevention of Oesophageal Strictures.* Advanced Functional Materials, 2017. **27**(38): p. 1702424.
656. Imere, A., et al., *Engineering a cell-hydrogel-fibre composite to mimic the structure and function of the tendon synovial sheath.* Acta Biomaterialia, 2021. **119**: p. 140-154.
657. Raphael, B., et al., *3D cell bioprinting of self-assembling peptide-based hydrogels.* Materials Letters, 2017. **190**: p. 103-106.
658. Holmes, T.C., et al., *Extensive neurite outgrowth and active synapse formation on self-assembling peptide scaffolds.* Proceedings of the National Academy of Sciences, 2000. **97**(12): p. 6728-6733.
659. Wan, S., et al., *Self-assembling peptide hydrogel for intervertebral disc tissue engineering.* Acta Biomaterialia, 2016. **46**: p. 29-40.
660. Gao, J., et al., *Controlling Self-Assembling Peptide Hydrogel Properties through Network Topology.* Biomacromolecules, 2017. **18**(3): p. 826-834.
661. Jia, P., et al., *The RGD-modified self-assembling D-form peptide hydrogel enhances the therapeutic effects of mesenchymal stem cells (MSC) for hindlimb ischemia by promoting angiogenesis.* Chemical Engineering Journal, 2022. **450**: p. 138004.
662. Gelain, F., Z. Luo, and S. Zhang, *Self-Assembling Peptide EAK16 and RADA16 Nanofiber Scaffold Hydrogel.* Chemical Reviews, 2020. **120**(24): p. 13434-13460.
663. Caplan, M.R., et al., *Control of self-assembling oligopeptide matrix formation through systematic variation of amino acid sequence.* Biomaterials, 2002. **23**(1): p. 219-227.

664. Caplan, M.R., et al., *Effects of systematic variation of amino acid sequence on the mechanical properties of a self-assembling, oligopeptide biomaterial.* Journal of Biomaterials Science, Polymer Edition, 2002. **13**(3): p. 225-236.
665. Horii, A., et al., *Biological Designer Self-Assembling Peptide Nanofiber Scaffolds Significantly Enhance Osteoblast Proliferation, Differentiation and 3-D Migration.* PLOS ONE, 2007. **2**(2): p. e190.
666. Yan, M., P.L. Lewis, and R.N. Shah, *Tailoring nanostructure and bioactivity of 3D-printable hydrogels with self-assemble peptides amphiphile (PA) for promoting bile duct formation.* Biofabrication, 2018. **10**(3): p. 035010.
667. Liu, X., et al., *In vivo studies on angiogenic activity of two designer self-assembling peptide scaffold hydrogels in the chicken embryo chorioallantoic membrane.* Nanoscale, 2012. **4**(8): p. 2720-2727.
668. Gao, X.-r., et al., *Mesenchymal stem cell transplantation carried in SVVYGLR modified self-assembling peptide promoted cardiac repair and angiogenesis after myocardial infarction.* Biochemical and Biophysical Research Communications, 2017. **491**(1): p. 112-118.
669. Collier, J.H. and T. Segura, *Evolving the use of peptides as components of biomaterials.* Biomaterials, 2011. **32**(18): p. 4198-4204.
670. BioGEL, M. *PeptiGels for 2D and 3D Cell Culture*. 2021 [cited 06/03/2022]; Available from: https://manchesterbiogel.com/products/peptigels.
671. Zhang, S., et al., *Unusually stable β-sheet formation in an ionic self-complementary oligopeptide.* Biopolymers, 1994. **34**(5): p. 663-672.
672. Burgess, K., et al., *Western blot analysis of cells encapsulated in self-assembling peptide hydrogels.* BioTechniques, 2017. **63**.
673. Burgess, K.A., et al., *RNA extraction from self-assembling peptide hydrogels to allow qPCR analysis of encapsulated cells.* PLOS ONE, 2018. **13**(6): p. e0197517.
674. Mujeeb, A., et al., *Self-assembled octapeptide scaffolds for in vitro chondrocyte culture.* Acta Biomaterialia, 2013. **9**(1): p. 4609-4617.
675. Castillo Diaz, L.A., et al., *Osteogenic differentiation of human mesenchymal stem cells promotes mineralization within a biodegradable peptide hydrogel.* Journal of Tissue Engineering, 2016. **7**: p. 2041731416649789.
676. Faroni, A., et al., *Self-Assembling Peptide Hydrogel Matrices Improve the Neurotrophic Potential of Human Adipose-Derived Stem Cells.* Advanced Healthcare Materials, 2019. **8**(17): p. 1900410.
677. Clough, H.C., et al., *Neutrally charged self-assembling peptide hydrogel recapitulates in vitro mechanisms of breast cancer progression.* Materials Science and Engineering: C, 2021. **127**: p. 112200.
678. Lachowski, D., et al., *Substrate Stiffness-Driven Membrane Tension Modulates Vesicular Trafficking via Caveolin-1.* ACS Nano, 2022. **16**(3): p. 4322-4337.
679. Treacy, N.J., et al., *Growth and differentiation of human induced pluripotent stem cell (hiPSC)-derived kidney organoids using fully synthetic peptide hydrogels.* Bioactive Materials, 2022. **21**: p. 142-156.
680. Burgess, K.A., et al., *Functionalised peptide hydrogel for the delivery of cardiac progenitor cells.* Materials Science and Engineering: C, 2021. **119**: p. 111539.
681. Wychowaniec, J.K., et al., *Designing Peptide/Graphene Hybrid Hydrogels through Fine-Tuning of Molecular Interactions.* Biomacromolecules, 2018. **19**(7): p. 2731-2741.
682. Ligorio, C., et al., *Graphene oxide containing self-assembling peptide hybrid hydrogels as a potential 3D injectable cell delivery platform for intervertebral disc repair applications.* Acta Biomaterialia, 2019. **92**: p. 92-103.
683. Ligorio, C., et al., *TGF-β3-loaded graphene oxide - self-assembling peptide hybrid hydrogels as functional 3D scaffolds for the regeneration of the nucleus pulposus.* Acta Biomaterialia, 2021. **127**: p. 116-130.
684. Chiesa, I., et al., *Modeling the Three-Dimensional Bioprinting Process of β-Sheet Self-Assembling Peptide Hydrogel Scaffolds.* Frontiers in Medical Technology, 2020. **2**(571626).
685. Belgodere, J.A., et al., *Engineering Breast Cancer Microenvironments and 3D Bioprinting.* Frontiers in bioengineering and biotechnology, 2018. **6**: p. 66-66.
686. Melchels, F.P.W., et al., *Additive manufacturing of tissues and organs.* Progress in Polymer Science, 2012. **37**(8): p. 1079-1104.

Lingard et al. 2022

Mammary epithelial organoids cultured in a self-assembling peptide hydrogel exhibit stiffness-induced remodelling

Eliana Lingard[1,2], Craig Lawless[1], Siyuan Dong[3,4], Aline F. Miller[4,5], Marco Domingos[6,7], Joe Swift[1,8], Alberto Saiani[3,4], Andrew Gilmore[1,2]

Affiliations

[1]Wellcome Centre for Cell-Matrix Research, Oxford Road, Manchester, M13 9PT, UK.

[2]Division of Cancer Sciences, School of Medical Sciences, Faculty of Biology, Medicine and Health, Manchester Academic Health Science Centre, University of Manchester, Manchester, M13 9PL, UK.

[3]School of Materials, Faculty of Science and Engineering, The University of Manchester, Oxford Road, Manchester, UK.

[4]Manchester Institute of Biotechnology, The University of Manchester, Oxford Road, Manchester, UK.

[5]School of Chemical Engineering and Analytical Sciences, Faculty of Science and Engineering, The University of Manchester, Oxford Road, Manchester M13 9PL, UK.

[6]Department of Mechanical, Aerospace and Civil Engineering, School of Engineering, Faculty of Science and Engineering, The University of Manchester, Manchester, UK.

[7]The Henry Royce Institute, Department of Materials, the University of Manchester, Manchester, UK.

[8]Division of Cell Matrix Biology and Regenerative Medicine, School of Biological Sciences, Faculty of Biology, Medicine and Health, Manchester Academic Health Science Centre, University of Manchester, Manchester, M13 9PL, UK.

Abstract

Breast tissue stiffness is known to play a role in driving breast cancer development and progression via mechanosensitive signalling pathways, but the specific mechanosignalling events involved are poorly understood. Three-dimensional (3D) organoid models can assist with the identification of molecular mechanisms that promote these phenomena, but there remains a need for model systems that reproducibly replicate the biochemical and mechanical properties of the mammary extracellular matrix (ECM). Here we demonstrate that a synthetic peptide hydrogel can support human mammary epithelial cell (MEC) viability and formation of organoids over a period of three weeks. Moreover, we show that the stiffness of the peptide hydrogels can be readily tuned between 150 – 400 Pascals (Pa). We also demonstrate that cells and their proteins can be extracted from hydrogel culture systems and analysed using mass spectrometry; here, we found that MECs encapsulated in the peptide hydrogel Alpha4 synthesise basement membrane proteins. We also found that increased Alpha4 matrix stiffness reduced MEC viability and increased inflammatory, immune and antioxidant responses. These findings demonstrate the potential of Alpha4 as a model of matrix stiffness that can be used to examine pro-oncogenic mechanosignalling events.

Keywords

Self-assembling peptide hydrogel // mammary epithelial cells // organoid culture // mass spectrometry proteomics

Abbreviations

- 3D - three-dimensional
- ECM - extracellular matrix
- MEC - mammary epithelial cell
- Pa - Pascals
- 2D - two-dimensional
- PAM - polyacrylamide
- PEG - polyethylene-glycol
- SAPH - self-assembling peptide hydrogel
- DMEM - Dulbecco’s modified eagle medium
- HSer - horse serum
- EGF - epidermal growth factor
- PBS - phosphate-buffered saline
- BSA - bovine serum albumin
- DAPI - 4′,6-diamidino-2-phenylindole
- RIPA - radioimmunoprecipitation assay buffer
- SDS - sodium dodecyl sulphate
- W - Watts
- DTT - dithiothreitol
- PTM - post-translational modification

- LC-MS/MS - liquid chromatography-coupled tandem mass spectrometry
- SD - standard deviation
- SEM - standard error of mean
- $CaSO_4$ - calcium sulphate
- RALA - Ras-related protein Ral-A

Introduction

The breast ECM is a crucial regulator of MEC behaviour, influencing cell survival, growth, motility, polarity, and differentiation [1-5]. For decades, 3D models of breast tissue have been used to explore the relationship between the breast environment and MEC behaviour and fate [6-11]. Tissue derived hydrogels such as collagen I and the reconstituted basement membrane extract Matrigel are established scaffolds for modelling the breast matrix as they provide cells with a bioactive, 3D environment that can support complex, *in vivo*-like cell behaviours [12-14]. For example, culturing MECs on top of or encapsulating them within these organic hydrogels stimulates their differentiation into polarised, hollow organoids called acini [11, 14-17]. Using these bioactive models of the breast ECM, researchers have elucidated numerous molecular mechanisms that govern key aspects of MEC organisation and function [8, 18-21].

Breast tissue stiffness is a significant risk factor for breast cancer development, as individuals with stiff breast tissue are 4-6 times more likely to develop breast cancer than individuals with soft breast tissue [22-25]. Caused by increased ECM protein deposition and organisation, breast matrix stiffness drives cancer initiation and progression via mechanosensitive, pro-oncogenic signal transduction pathways [26-30]. These mechanosignalling pathways stimulate malignant cell behaviours by inducing changes in gene and protein expression as well as stimulating epigenetic changes [31-33]. For example, pro-oncogenic mechanotransduction targets that have been identified in breast tissue include the ZNF217 gene and the transcription factor TWIST-1, which stimulate MEC proliferation and epithelial-mesenchymal transition, respectively [34, 35]. However, many mechanotransduction events remain poorly defined, and the role that mechanotransduction mechanisms play in promoting breast cancer initiation are poorly understood. Using 3D models of the breast matrix, individual mechanosignalling events can be identified and examined in the context of cancer development [32, 36, 37].

Exploring the pro-oncogenic mechanosignalling mechanisms that arise in stiff breast tissue requires that the cells are cultured in a mechanically tuneable substrate that replicates the key properties of human breast tissue. Collagen I hydrogels can be stiffened by simply increasing the collagen concentration to create gels of variable stiffness, while the stiffness of Matrigel can be modified by mixing it with alginate or collagen to enhance its weak mechanical properties and create a mechanically modifiable model of breast matrix stiffness [14, 32, 37-42]. Studies employing these models have identified multiple mechanosignalling mechanisms responsible for promoting malignant phenotypes in MECs, such as stiffness-driven alterations to chromatin site accessibility, recruitment and activation of pro-oncogenic transcription factors and hyper-activation of Rho-mediated signalling pathways that stimulate cell growth and proliferation. However, organic hydrogel models suffer from many limitations that hinder their ability to accurately and reliably model breast matrix stiffness. They cannot be directly mechanically modified without significantly altering other physical aspects of the ECM, meaning that confounding factors are unavoidable in these models unless additional components are added to independently regulate their mechanical properties [38, 43-45]. Furthermore, the bioactivity of tissue-derived scaffolds often comes at the cost of being a complex,

xenogenic and poorly defined material that suffers from batch-to-batch variability in both composition and stiffness [46-50].

The limitations of tissue-derived scaffolds have prompted the development of synthetic scaffolds for cell culture such as polyacrylamide (PAM) and polyethylene-glycol (PEG) gels. PAM and PEG are reproducible and can be biologically and mechanically functionalised in various ways to meet the demands for specific cell culture requirements and experimental parameters [49, 51-57]. However, PAM gels are restricted to 2D culture applications as cells cannot survive encapsulation within them and PEG is ill-suited to modelling soft tissues like the breast matrix due to its non-degradable nature [48, 58, 59]. An alternative group of synthetic scaffolds that have been developed in the past decade are self-assembling peptide hydrogels (SAPH) [60-64]. SAPHs are intrinsically biocompatible, well-defined, and amenable to functionalisation, making them promising candidates for *in vitro* tissue modelling. One of the most well-established SAPH scaffold designs utilises short, amphipathic peptides that self-assemble into entangled β-sheet fibres to form 3D, hydrated fibrillar networks [65, 66]. The resulting hydrogels are chemically simple, viscoelastic, biodegradable, responsive to various physical and chemical stimuli, immunologically inert, and easy to physically and chemically modify for cell culture [67-71]. For example, incorporation of biomimetic peptides into the SAPH matrix is a non-invasive and effective way of stimulating *in vivo* cell behaviours [72-74]. Due to these properties, SAPHs have been successfully used and functionalised for various cell culture applications, including the creation of 3D tissue models to explore breast cancer development *in vitro* [60-62, 75-79].

Here we investigated the ability of the β-sheet forming SAPH PeptiGel® Alpha4 to support *in vivo* MEC behaviours and mimic different breast matrix stiffnesses. We found that Alpha4 supports long-term human MEC viability and ECM production, and that the bulk stiffness of Alpha4 can be modified to create hydrogels that have similar mechanical properties to Matrigel. We also found that we could extract protein lysates from 3D Matrigel and Alpha4 cultures to obtain information on how matrix stiffness influences production of ECM and cell proteins.

Materials and Methods

Materials

PeptiGel® Alpha4 was purchased from Manchester BioGEL (Alderley Park, UK). Sterile alginate was purchased from Novamatrix (Sandvika, Norway). Matrigel was bought from Corning (Glendale, US).

Mammary epithelial cell maintenance and passaging

Immortalised, non-tumorigenic human mammary epithelial cells (MCF10a) were sourced from ATCC and maintained in monolayer culture using Dulbecco's modified eagle medium (DMEM)-F12 media supplemented with 5% filtered horse serum (HSer) (v/v), 10 µg/mL insulin, 0.5 µg/mL hydrocortisone, 100 ng/mL cholera toxin and 20 ng/mL epidermal growth factor (EGF). The cells were passaged at 70-90% confluency using 1X trypsin/EDTA solution and the cell suspension was collected in a 15 mL falcon tube. Cells were recovered by centrifuging the suspension at 350 xg for 5 minutes to obtain a cell pellet, which was resuspended in 1 mL of resuspension media (DMEM-F12 containing 1.8% HSer (v/v), 10 µg/mL insulin, 0.5 µg/mL hydrocortisone, 100 ng/µL cholera toxin and 5 ng/mL EGF).

Mammary epithelial cell encapsulation in Matrigel

MCF10a cells were resuspended in 1 mL of resuspension media (DMEM-F12 containing 1.8% HSer (v/v), 10 µg/mL insulin, 0.5 µg/mL hydrocortisone, 100 ng/µL cholera toxin and 5 ng/mL EGF). Appropriate volumes of cell suspension were mixed into blank DMEM to give a volume of 49.5 µL per gel. 50.6 µL of 8.9 mg/mL Matrigel was then pipetted into the cell-DMEM mixture to give a final total protein concentration of 4.5 mg/mL and a seeding density of 0.5×10^5 cells per 100 µL of gel. Wells of a 24-well plate were coated with a 50 µL layer of undiluted Matrigel before 100 µL of the Matrigel-cell-DMEM solution was then pipetted into each well and gently spread to ensure even coverage before being left to polymerise at 37°C (5% CO_2) for 30 minutes. After the gels had polymerised, MCF10a cultures were bathed in assay media (DMEM-F12 supplemented with 2% HSer (v/v), 10 µg/mL insulin, 0.5 µg/mL hydrocortisone, 100 ng/µL cholera toxin and 5 ng/mL EGF). The gels were then incubated at 37°C (5% CO_2). Media was refreshed every 2-4 days.

Cell encapsulation in Matrigel-alginate hydrogels

Matrigel-alginate gels were made following the protocol created by the Chaudhuri lab [38]. To create 250 µL gels with a final concentration of 4.5 mg/mL Matrigel and 5 mg/mL alginate, appropriate volumes of cell suspension and DMEM were mixed before 50 µL of 25 mg/mL alginate was added. An appropriate volume of Matrigel (minimum 9.8 mg/mL, maximum 10.9 mg/mL) was then pipetted into this mixture. A 1.22 M stock solution of calcium sulphate ($CaSO_4$) in sterile water was diluted 10-fold in blank DMEM and then diluted further to make final concentrations. 50 µL of either diluted $CaSO_4$ solution (2.4 mM and 20 mM final $CaSO_4$ concentrations) or blank DMEM (0 mM final $CaSO_4$ concentration) was transferred to a 1 mL syringe, and 200 µL of the Matrigel-alginate-cell mixture was transferred to another syringe. The syringes were connected using a female-female luer-lock

connector and the solutions were mixed with 7 pumps before being deposited into wells of a 24-well plate precoated with 50 µL of undiluted Matrigel. The gels were left to polymerise at 37°C (5% CO_2) for 30 minutes. Following polymerisation, the gels were bathed in assay media and incubated at 37°C (5% CO_2). Media was refreshed every 2-4 days.

Cell encapsulation in peptide hydrogels

PeptiGels® were pre-warmed to room temperature before 50 µL of gel was spread over the bottom surface of wells in 24-well plates. MCF10a cells were encapsulated via gentle pipetting and mixing of cell suspension, as per the manufacturer's directions, into appropriate volumes of gel. Volumes of cell suspension used were calculated to ensure a final cell density of 0.5×10^5 cells per mL unless otherwise specified. Following encapsulation, 100 µL aliquots of cell-laden hydrogels were pipetted into wells and carefully spread on top of the gel layer. After 5 minutes recovery, 1 mL of assay media was added to each well and the cultures were incubated at 37°C (5% CO_2). Media was changed the following day and every 3-4 days thereafter.

Preparation of peptide hydrogel dilutions

PeptiGels® were equilibrated at room temperature before set volumes of phosphate-buffered saline (PBS) was pipetted on top of set volumes of gel (Table 1). The mixtures were then vortexed for 60 seconds until they were homogenous and left to recover for 5 minutes. Cells were encapsulated in the gels as described above.

Alpha4 dilution (%) and stiffness	Volume of Alpha4 per 100 µL	Volume of cell suspension and/or PBS per 100 µL
100% gel (Very stiff)	100	0
90% gel (Stiff)	90	10
75% gel (Medium)	75	25
50% gel (Soft)	50	50

Table 1. Alpha4 dilution formulas.

Organoid extraction from Matrigel and peptide hydrogels

Matrigel and peptide hydrogel cultures were washed with 1 mL of PBS following removal of media and then depolymerised using 1 mL of ice-cold cell recovery solution (Corning). After being incubated on an orbital shaker for 1 hour at 4°C, the freed well contents were resuspended and collected into falcon tubes pre-coated with 1% bovine serum albumin (BSA) in PBS (w/v) and washed via centrifugation in PBS at 70 xg for 3 minutes (4°C). The supernatants were discarded, and the pellets could then be resuspended for re-encapsulation or fixed for staining.

Immunofluorescent staining of extracted organoids

Extracted organoids were fixed for 45 minutes in 4% formaldehyde in PBS (v/v) at room temperature. The fixative was then diluted with 10 mL of PBS and the suspension was centrifuged at 70 xg for 3

minutes (4°C). After discarding the supernatants, pellets were resuspended in 1 mL of organoid wash buffer (PBS containing 0.1% Triton-X-100 and 0.2% BSA), transferred to pre-coated, low adherent 24-well plates (Greiner Bio-One, UK) and left to block at room temperature for 15 minutes. After blocking, excess buffer was carefully removed to leave 200 µL of liquid in each well and the clusters were incubated with primary antibodies (Table 2) in organoid wash buffer overnight on an orbital shaker (100 RPM) at 4°C. The plates were retrieved, and after being left to settle at room temperature for 10 minutes, the organoids were washed three times in 1 mL of organoid wash buffer for 1 hour each time on an orbital shaker at 4°C. After removing the excess buffer to leave 200 µL of liquid in each well, the clusters were incubated with secondary antibodies (Table 3) in organoid wash buffer overnight on an orbital shaker at 4°C. The organoids were then left to settle at room temperature for 10 minutes before excess liquid was removed to leave 200 µL of liquid per well. The organoids were then incubated with 200 µL of 2 µg/mL 4′,6-diamidino-2-phenylindole (DAPI) in PBS for 10 minutes on an orbital shaker at 4°C before being washed 3 times with organoid wash buffer for 1 hour each time as described above. Following the final wash, the organoids were diluted in PBS and transferred to 6-well plates.

Antigen	Host	Source	Catalogue number	Dilution
Active caspase-3	Rabbit	R&D Systems	AF835	1:200
Laminin α3 chain	Mouse	R&D Systems	MAB21441	1:200
Collagen IV	Rabbit	Abcam	ab6586	1:200
β-catenin	Mouse	BD Biosciences	610154	1:200

Table 2. Primary antibodies for immunofluorescence.

Antigen	Conjugate dye	Host	Source	Catalogue number	Dilution
Anti-mouse	AlexaFluor 594	Donkey	Invitrogen	A21203	1:250
Anti-rabbit	AlexaFluor 488	Donkey	Invitrogen	A21206	1:250

Table 3. Secondary antibodies for immunofluorescence.

Fluorescent microscope imaging

Confocal images were collected on a Leica TCS SP8 AOBS upright confocal using a 63x/0.90 water immersion objective. The confocal settings were as follows, pinhole 1 airy unit, scan speed 400 Hz unidirectional, format 1024 x 1024. Images were collected using hybrid and photomultiplier detectors with the following detection mirror settings; DAPI 410-475 nm; Alexa-488 507-580 nm; Alexa-594 605-750 nm using the 405 nm (50%), 490 nm (30%) and 590 nm (30%) laser lines respectively. When it was not possible to eliminate crosstalk between channels, the images were collected sequentially. The acquired images were processed using ImageJ.

Brightfield microscope imaging

Brightfield images were collected on a Leica DMIL LED inverted brightfield microscope connected to a xiQ USB3.0 Vision camera using a 20x objective. The acquired images were processed using ImageJ.

Organoid analysis in Matrigel and peptide hydrogels

To assess organoid area and circularity, 20x brightfield images of organoids encapsulated in Matrigel and peptide hydrogels were analysed in ImageJ. Clusters in focus were traced around their periphery using the freehand tool (to measure circularity) or the freehand line tool (to measure area). The tracing was done by hand using a Wacom One drawing tablet and pen. Measurements were exported to GraphPad Prism.

To assess organoid density, Matrigel- and peptide hydrogel-encapsulated MCF10a organoids were prepared in triplicate in 96-well plates, following the techniques described above. The gels were cultured for a maximum of 21 days and fixed with 4% formaldehyde in PBS for 30 minutes at room temperature. The fixative was washed out using PBS and then permeabilised for 5 minutes with 0.5% Triton-X-100. After being washed with 3D IF wash buffer (PBS containing 0.1% BSA, 0.2% Triton-X-100 and 0.05% Tween-20) for 30 minutes, the clusters were blocked in 10% HSer in 3D IF wash buffer for 90 minutes. The clusters were then stained with 1 µg/mL DAPI in PBS for 10 minutes before being washed with 3D IF wash buffer for 10 minutes and then double-distilled water overnight.

Fluorescent images of DAPI-stained clusters grown in Matrigel and peptide hydrogels were collected as Z-stacks on the EVOS M7000 Imaging system (Thermo Fisher Scientific, MA) using a 4x objective. 50% of each well area was imaged and 12 Z-planes were collected each time. Images were collected using the DAPI light source channel. The acquired images were processed in QuPath v0.2.3 by manually counting fluorescent nuclei. Measurements were exported to GraphPad Prism.

Protein extraction from Matrigel and peptide hydrogels for mass spectrometry analysis

Peptide hydrogel-encapsulated cells were washed in 1X PBS for 15 minutes and then lysed in 100 µL of 1X radioimmunoprecipitation assay buffer (RIPA) (50 mM Tris-HCL (pH 7.4), 150 mM sodium chloride, 1% IGEPAL, 0.1% (w/v) sodium dodecyl sulphate (SDS), 1% sodium deoxycholate, 20 mM sodium fluoride, 2 mM sodium orthovanadate, 1X mM protease inhibitor cocktail). Matrigel-encapsulated cells were extracted as described previously in the organoid extraction section and then resuspended in 100 µL of 1X RIPA buffer. Following 15 minutes incubation on ice, the samples were sonicated for 180 seconds at 10 Watts (W) using a Covaris S220 ultrasonicator before being centrifuged at 3220 xg for 5 minutes at 4°C. Lysates were stored at -20°C.

In-gel digestion of lysates

Lysates were mixed with 4X Laemmli buffer (Bio-Rad, CA) and heated at 95°C for 5 minutes. The samples were then allowed to migrate past the wells of a pre-cast 4-20% polyacrylamide gel (Bio-

Rad) before being stained with InstantBlue for 1 hour. The samples were then left to de-stain in de-ionised water overnight. Following de-staining, the sample bands were excised from the gel and dehydrated using acetonitrile before being subjected to vacuum centrifugation. The dried samples were reduced with 10 mM dithiothreitol (DTT) and alkylated using 55 mM iodoacetamide and then washed with 25 mM ammonium bicarbonate and then acetonitrile twice. The samples were dried again using vacuum centrifugation and digested in trypsin overnight at 37°C.

Liquid chromatography-coupled tandem mass spectrometry

Digested samples were analysed by liquid chromatography tandem-coupled mass spectrometry (LC-MS/MS) using an UltiMate® 3000 Rapid Separation LC (Dionex Corporation, CA) coupled to a Orbitrap Elite (Thermo Fisher Scientific, MA) mass spectrometer.

Peptide mixtures were separated using a gradient from 92% A (0.1% FA in water) and 8% B (0.1% FA in acetonitrile) to 33% B, in 44 min at 300 nL min^{-1}, using a 75 mm x 250 µm i.d. 1.7 mM BEH C18 analytical column (Waters). Peptides were selected for fragmentation automatically by data dependant analysis.

Liquid chromatography-coupled tandem mass spectrometry data acquisition

Mass spectrometry data was acquired in a data-directed manner for 60 minutes in positive mode, where peptides were selected for fragmentation automatically by data-dependent analysis on a basis of the top 12 peptides with m/z between 300 to 1750 Th and a charge state of 2, 3 or 4 with a dynamic exclusion set at 15 seconds. The MS Resolution was set at 120,000 with an AGC target of 3e6 and a maximum fill time set at 20 ms. The MS2 Resolution was set to 30,000, with an AGC target of 2e5, a maximum fill time of 45 ms, an isolation window of 1.3 Th and a collision energy of 28. The resulting data were searched using Mascot (Matrix Science, UK), against the Swissprot and Trembl databases with human taxonomy selected. The data were validated using Scaffold (Proteome Software, OR).

MaxQuant processing of raw peptide data

All raw MS data files were processed in MaxQuant (v2.0.1.0, [80]). Spectra were searched against the Human (Homo Sapiens) reference proteome obtained from Uniprot (June 2021, [81]). This proteome was modified to include the following murine peptide sequences obtained from the Mouse (Mus Musculus) proteome (July 2021): LAMA1_MOUSE, LAMB1_MOUSE, LAMC1_MOUSE, CO4A1_MOUSE, CO4A2_MOUSE, CO4A3_MOUSE, CO4A4_MOUSE and NID1_MOUSE. Methionine oxidation and N-terminal acetylation were set as variable modifications and cysteine carbamidomethylation was set as a fixed modification. Precursor tolerance for the first and main searches was set at 20 ppm and 4.5 ppm, respectively. MS/MS tolerance was set at 20 ppm, with a maximum of two missed cleavages allowed. The false discovery rate of PSM and protein were set at 0.01 and “Match between runs” was enabled.

Analysis of mass spectrometry data

MaxQuant output files were filtered through the Matrisome Project [82] and processed. Differential expression was performed in R (release 4.1.2) using the MSqRob package (v0.7.7, [83]), using a false discovery rate of 0.05 for significantly changing proteins. Functional analysis was performed using the packages ClusterProfiler (v4.2.2, [84]) and ReactomePA (v1.38.0, [85]), with significantly over-represented functional terms taken at adjusted p-value < 0.05. Significant functional terms were visualised using enrichplot (v1.14.2).

Oscillatory shear rheometry

The storage modulus of gels was investigated using a Discovery HR-2 hybrid rheometer (TA Instruments, US) with a 20 mm parallel plate and a gap size of 500 µm. Samples were prepared by aliquoting 180 µL of gel into ThinCert well inserts (1 µm pore size, Greiner Bio-One). 900 µL of assay media was pipetted into the wells after 5 minutes and left to recover for 5 minutes before 100 µL of media was added to each insert. The gels were incubated at 37°C (5% CO_2) for at least 30 minutes prior to testing. Following media exposure, samples were removed from the inserts by peeling off the bottom membrane of the insert and transferred onto the rheometer plate as described by Ligorio et al. [64]. The upper rheometer head was then lowered to the gap size and samples were equilibrated for 3 minutes at 37°C. Oscillatory amplitude experiments were performed at 1 Hz frequency and within the linear viscoelastic region in the strain range: 0.01 to 20%. The mean storage modulus values described in the results section were obtained at 0.2% oscillation strain.

Statistical analysis

All data were analysed in GraphPad Prism v9.4.1. Quantitative values are presented as mean ± standard deviation (SD) or mean ± standard error of mean (SEM). Parametric data was analysed using one-way or two-way analysis of variance (ANOVA). Non-parametric data was analysed using Kruskal-Wallis one-way ANOVA with Dunn's multiple comparisons test or unpaired t-tests and Mann-Whitney tests corrected for multiple comparisons using the Holm-Šídák method. Four levels of significance (p-value <0.05 (*), p-value <0.01 (**), p-value <0.001 (***), and p-value <0.0001 (****)) were used.

Results

The self-assembling peptide hydrogel Alpha4 supports long-term viability of MCF10a cells and their organisation into clusters that can deposit a laminin 332-rich basement membrane

Encapsulation and long-term culture of human MECs in Matrigel prompts their assembly into viable, polarised acini, which resemble *in vivo* mammary acini [12, 86-88]. Since previous studies have shown that the SAPH Alpha4 can support the viability and *in vivo*-like behaviours of several cell types, we predicted that Alpha4 would support human MEC viability and acinar development [76, 89, 90]. To investigate Alpha4's suitability for long-term MEC culture, we encapsulated non-malignant, human MECs (MCF10a cells) into Alpha4 or Matrigel hydrogels and used brightfield and fluorescent imaging to monitor MCF10a viability, size, and shape over 21 days. To quantify the number of clusters growing within the gels, the cells were stained with DAPI at days 7, 14 and 21 and cell clusters were counted. MCF10a cells were viable in Alpha4 for at least 21 days and formed 3D clusters that appeared to resemble the acinar structures growing in Matrigel (Fig. 1A). We found that the number of acinar structures grown in Matrigel decreased over 21 days, with 1000 ± 60 organoids counted at day 7 compared to 400 ± 90 organoids counted in Matrigel on day 21 (Fig. 1B). In contrast, the number of clusters counted in Alpha4 increased over 21 days from 100 ± 20 clusters at day 7 to 300 ± 90 clusters at day 21. This comparatively modest cluster growth could be due to a lack of growth factors and matrix proteins in Alpha4, meaning that MCF10a cells would receive fewer environmental cues to proliferate and grow into clusters.

Acini develop into spherical organoids that undergo growth arrest approximately 14 days into development and do not exceed 10,000 μm^2 in size [38, 88, 91]. To determine whether MCF10a cells encapsulated in Alpha4 form growth arrested acini, we compared the morphology of MCF10a organoids grown in Alpha4 and Matrigel at days 7, 14 and 21 by obtaining brightfield images of encapsulated organoids and measuring their area and circularity. In Matrigel, MCF10a organoids stopped increasing in size by day 14 which indicates that they underwent growth arrest (Fig. 1C). None of the organoids grown in Matrigel exceeded 10,000 μm^2 in size, which is another key indicator that they were acini. However, MCF10a organoids grown in Alpha4 hydrogels did not appear to undergo growth arrest at any point during the 21-day culture period. By day 21, the organoids grown in Alpha4 were 60% larger than the acini grown in Matrigel, with some organoids found to be over 10,000 μm^2 in size. These results indicate that MCF10a organoids encapsulated in Alpha4 were not growth-arrested acini. Comparison of organoid morphology in Matrigel and Alpha4 cultures led us to the same conclusion (Fig. 1D). In Matrigel, organoid shape was consistently spherical throughout the 21-day culture period as the consistently high circularity score of 0.9 ± 0.01 was calculated at each time interval. In contrast, organoid circularity in Alpha4 gels decreased over the 21-day period as the organoids became increasingly more irregular in shape. However, as there was only a minor decrease in circularity between day 7 (0.9 ± 0.01) and day 21 (0.8 ± 0.01), the organoids grown in Alpha4 remained relatively spheroidal. Together, these results show that organoids growing in Alpha4 were mostly spheroidal in shape and mostly within the boundaries of typical acinar size. However,

their inability to undergo growth arrest, paired with their inconsistent morphology, indicate that the organoids growing in Alpha4 hydrogels were not acini.

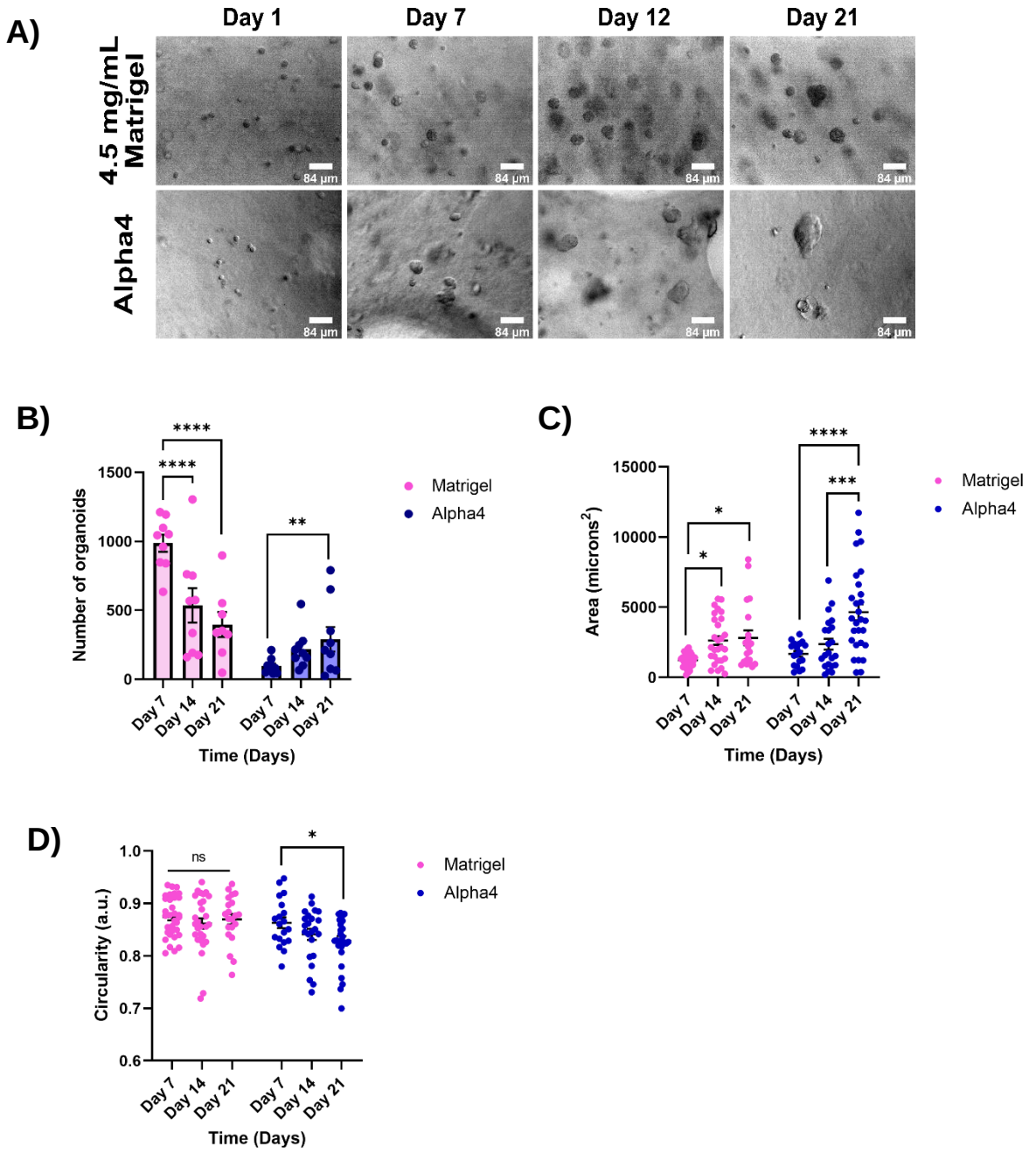

Fig. 1. MCF10a cells organise into organoids that remain viable in Alpha4 for 21 days. A) Brightfield images of MCF10a cells encapsulated in Matrigel and Alpha4 hydrogels at days 7, 14 and 21. B) Number of organoids counted in Matrigel and Alpha4 gels at days 7, 14 and 21. C) Area measurements of organoids cultured in Matrigel and Alpha4 gels at days 7, 14 and 21. D) Circularity measurements of organoids grown in Matrigel and Alpha4 gels at days 7, 14 and 21. All measurements were performed at least 3 times and data are shown as mean ± SEM (* p-value <0.05, ** p-value <0.01, *** p-value <0.001, **** p-value <0.0001).

We confirmed these findings by extracting organoids grown in Matrigel and Alpha4 at days 7, 12 and 21 and probing them with antibodies raised against key markers of acinar formation: luminal caspase-3-mediated apoptosis, the formation of a laminin 332- and collagen IV-rich basement membrane, and basolateral β-catenin expression [88, 92]. Organoids were extracted from Matrigel and Alpha4 at days

7, 12 and 21 (Fig. 2). Day 7 organoids extracted from Matrigel clearly displayed signs of luminal caspase-3 activity and cell polarisation (Fig. 2A). All the organoids extracted from Matrigel were also depositing the basement membrane proteins laminin 332 and collagen IV around their peripheries, which shows that they were immature acini. Day 7 Alpha4 organoids formed β-catenin cell-cell contacts, with 58% of the organoids depositing laminin 332 around their peripheries, but otherwise lacked the key markers of acinar development.100% of acini grown in Matrigel hydrogels at day 12 had formed a basement membrane and most were undergoing luminal apoptosis and forming polarised structures, while 46% of Alpha4-derived organoids still showed clear signs of peripheral laminin 332 deposition (Fig 2B). However, the organoids grown in Alpha4 remained unpolarised, did not form lumens and caspase-3 activity was not restricted to the centre of the organoids. At day 21, most of the acini growing in Matrigel hydrogels had finished maturing into hollow, polarised, spheroidal acini that all had laminin 332- and collagen IV-rich basement membranes and expressed β-catenin at cell junctions (Fig. 2C). In contrast, 44% of organoids extracted from Alpha4 at day 21 expressed laminin 332 and lacked signs of centralised apoptosis, cell polarisation or a collagen IV-rich basement membrane, which confirmed that they were not acini. However, the finding that some

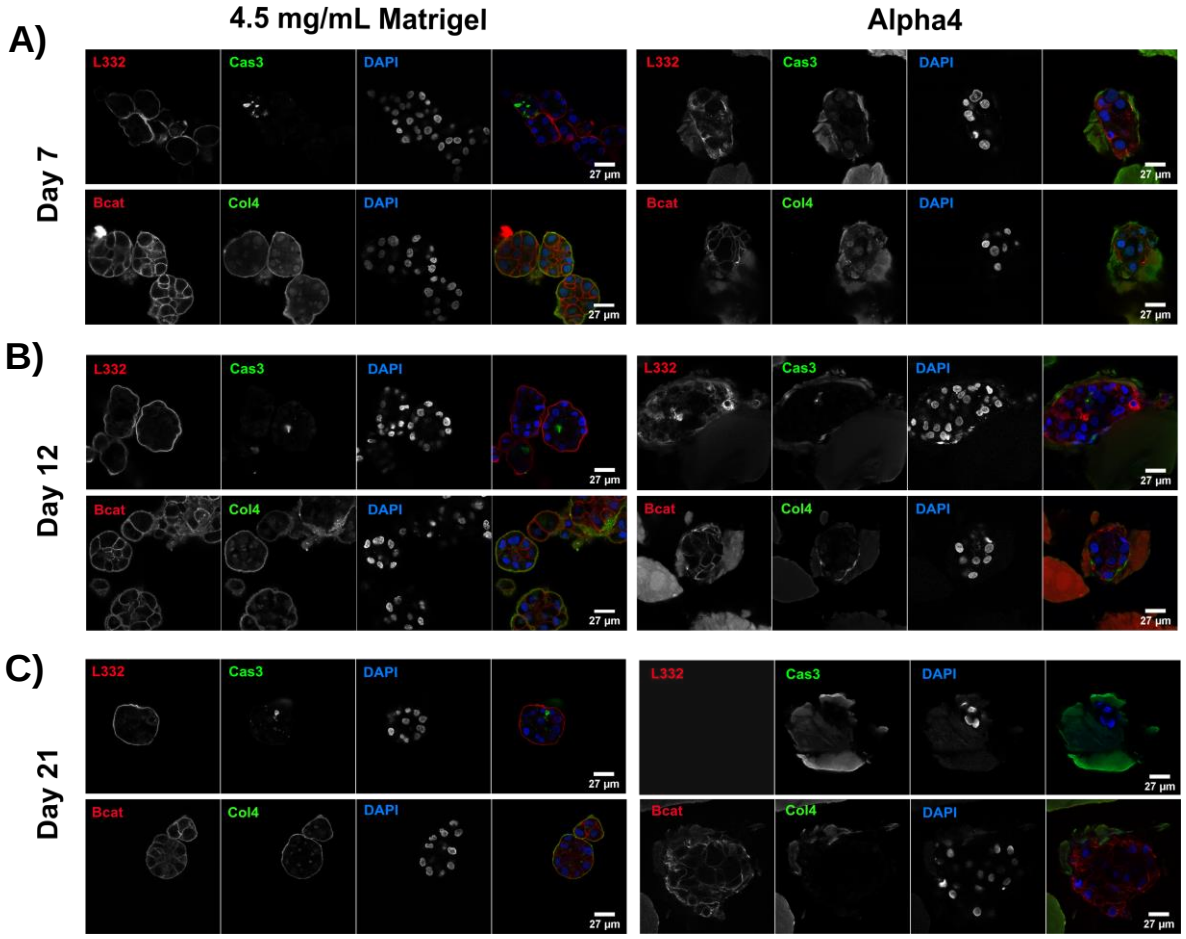

Fig. 2. MCF10a organoids growing in Alpha4 gels deposit a laminin 332-rich basement membrane. MCF10a cells encapsulated in Matrigel and Alpha4 gels were cultured for 21 days and stained with acinar markers: active caspase-3 (Cas3), laminin 332 (L332), collagen IV (Col4) and β-catenin (Bcat). IF images were taken of the extracted and stained organoids following their removal from the gels on days 7 (A), 12 (B) and 21 (C). Nuclei were stained with DAPI. 20 (day 7), 10 (day 12) and 11 (day 21) organoids were quantified for positive laminin 332 staining in Matrigel. 12 (day 7), 13 (day 12) and 9 (day 21) organoids were quantified for positive laminin 332 staining in Alpha4.

organoids extracted from Alpha4 deposited laminin 332 into their environment indicates that these organoids were communicating with, and modifying, their environment to create a niche in Alpha4.

To confirm this, mass spectrometry analysis was performed on MCF10a cell lysates obtained from day 7 Alpha4 cultures and a list of matrix and matrix-associated proteins detected in the samples was obtained. 54 proteins were identified (Table S1). Detected basement membrane components included the three subunits of laminin 332, agrin, the laminin γ1 subunit and the collagen α-1(XVII) chain, which forms the homotrimer collagen XVII (Table 4). Structural matrix components such as fibronectin, decorin and syndecans were also synthesised by Alpha4-encapsulated MCF10a cells, as were several cell-matrix bridging proteins such as vitronectin and desmoplakin. Many of these proteins have been shown to regulate various cell behaviours, including cell survival, proliferation, morphogenesis, and adhesion, which can have clinical consequences [93-97]. Together, these results indicate that MCF10a organoids were secreting and organising a complex extracellular niche that can stimulate *in vivo* MCF10a behaviours.

Matrix factor	Localisation	Function
Annexin A2	Cell membrane	Regulates cell proliferation, survival, motility and membrane trafficking
Fibronectin	Extracellular space	Initiates and regulates matrix assembly and organisation, regulates cell adhesion and migration
Annexin A1	Cell membrane	Regulates cell motility, cell adhesion, differentiation, survival, and proliferation
Galectin-1	Extracellular space	Regulates cell growth, adhesion, motility and differentiation
Laminin β3 subunit Laminin α3 subunit	Extracellular space	First two subunits of laminin 332 which regulates cell adhesion, motility and matrix assembly
Transforming growth factor-β-induced protein	Extracellular space	Soluble protein that regulates cell morphogenesis, adhesion, motility and is involved in matrix organisation
Desmoplakin	Intracellular	Desmosome component that regulates cell adhesion and facilitates cell-matrix communication
Laminin γ2 subunit	Extracellular space	The third subunit of laminin 332.
Syndecan-1 Syndecan-4	Cell surface	Connect cells to the matrix and regulate cell proliferation, motility, adhesion, and endocytosis
Vitronectin	Extracellular space	Connects cells to the matrix and regulates cell adhesion
Lactadherin	Extracellular space	Regulates cell adhesion and motility and regulates angiogenesis
Galectin-3	Extracellular space	Regulate cell adhesion, motility, survival, proliferation, and growth
Laminin γ1 subunit	Extracellular space	Regulates matrix assembly and organisation, cell adhesion, differentiation, survival, and polarity
Endorepellin	Extracellular space	Soluble fragment of perlecan that regulates cell motility and adhesion
Agrin	Extracellular space	Regulates matrix assembly and organisation
Decorin	Extracellular space	Regulates matrix organisation, cell growth, proliferation, adhesion, differentiation, and motility
Mucin-1	Transmembrane	Regulates cell adhesion and signalling events
Collagen α1(XVII) chain	Transmembrane	Structural component of hemidesmosomes, maintains cell adhesion to the matrix and cell junctions
Annexin A7	Cell membrane	Regulates membrane fusion and plays a role in exocytosis

Table 4. MCF10a cells encapsulated within Alpha4 gels secrete proteins that play key roles in acinar basement membrane development. Matrix-associated proteins synthesised by 7-day old MCF10a cells encapsulated in Alpha4 hydrogels. The seeding density used for this experiment was 2.5 x 10^5 cells per mL. Proteins are listed in descending order of peptide intensity (see Supplementary Table 1).

Overall, these findings reveal that Alpha4 supports the development and survival of organoids that secrete a complex, laminin 332-rich matrix reminiscent of a proto-basement membrane but does not support the growth of polarised acini.

Alpha4 can be mechanically tuned to create scaffolds of varying stiffnesses

Matrix stiffness, which we define here as the resistance of the matrix to deformation, affects cell behaviour, and stiff scaffolds have been shown to disrupt *in vivo* MEC behaviours [14, 32, 35, 38, 39, 42, 98]. Using shear oscillatory rheology, we compared the bulk elastic (storage modulus, G') and viscous (loss modulus, G") properties of Alpha4 and Matrigel hydrogels following assay media-conditioning [70]. Alpha4 is a viscoelastic gel (G' > G") that has a storage modulus of 400 ± 50 Pascals (Pa) following assay media-conditioning, which is within the storage modulus range reported by Manchester BioGEL (Fig. 3A) [99]. Matrigel is also a viscoelastic gel and has a storage modulus of 6 ± 4 Pa when its concentration is 4.5 mg/mL, which makes it 65-fold softer than Alpha4 (Fig. 3B). We therefore reasoned that the stiffness of Alpha4 might be responsible for the lack of *in vivo*-like MCF10a behaviours observed in the gels.

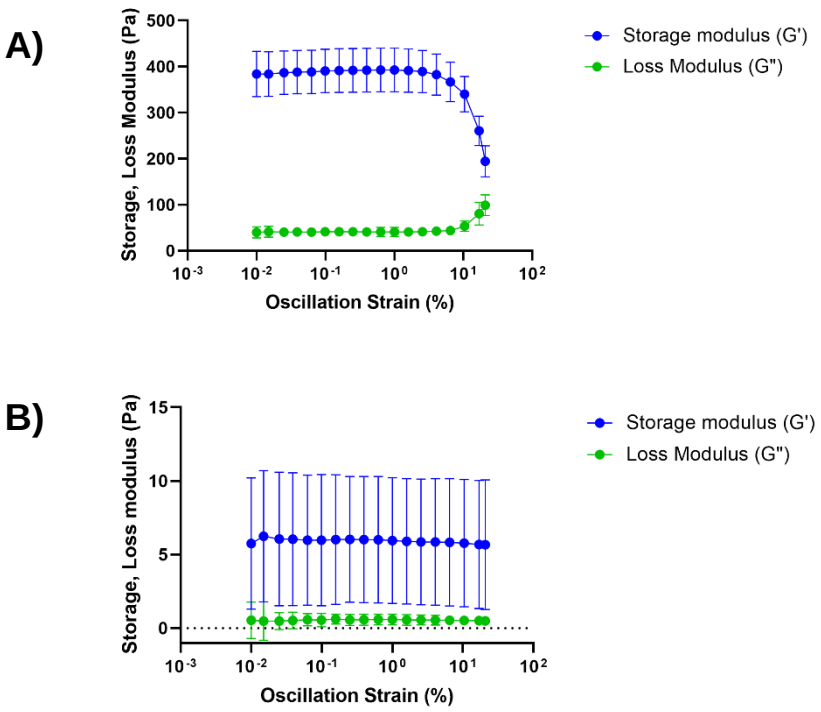

Fig. 3. Alpha4 is stiffer than Matrigel. A) Storage and loss moduli at 1 Hz of Alpha4 hydrogels. B) Storage and loss moduli at 1 Hz of 4.5 mg/mL Matrigel hydrogels. Means and ± SD are shown. All measurements were performed at least 3 times.

As Matrigel is a soft hydrogel that supports *in vivo* MEC behaviours such as acinar development, we reasoned that reducing the storage modulus of Alpha4 would provide MCF10a cells with more physiologically appropriate mechanical cues. Since Alpha4 is only composed of peptides and water, we hypothesised that we could reduce the storage modulus of Alpha4 by diluting it with the neutral,

non-cytotoxic isotonic salt solution PBS. To investigate this, we diluted Alpha4 hydrogels with different volumes of PBS (see Table 1) and measured the storage moduli of the diluted and assay media-conditioned Alpha4 hydrogels. We found that PBS can make up to 50% of the total hydrogel volume before the hydrogel begins to fragment and flow (G' < G"). We hypothesise that this dilution limit is caused by Alpha4's peptide network being unable to accommodate additional fluid once the amount added exceeds half of its total volume, resulting in network rupture and fragmentation. To maintain the integrity of Alpha4's peptide network, we did not exceed the 50% dilution limit and subsequently all diluted Alpha4 hydrogels made and measured in this study were viscoelastic gels (Fig. S1). Amplitude sweep experiments showed that diluting Alpha4 with up to 50% (v/v) PBS can reduce Alpha4's storage modulus 3-fold to create a hydrogel with a storage modulus of 150 ± 20 Pa (Fig. 4A). In contrast, the storage modulus of 90% (v/v) Alpha4 hydrogels was 350 ± 60 Pa, rendering it virtually the same stiffness as undiluted Alpha4 hydrogels. Similarly, the 75% (v/v) Alpha4 hydrogels had a storage modulus of 300 ± 30 Pa. Both the 90% (v/v) and 75% (v/v) Alpha4 hydrogels were 2-fold stiffer than the 50% (v/v) Alpha4 hydrogels, and there is a 1-fold difference in stiffness between the 90% (v/v) and 75% (v/v) Alpha4 hydrogels. These results reveal that Alpha4 can be accurately and consistently mechanically modified via dilution with PBS to create softer gels of consistent stiffnesses. Although there is a modest difference in stiffness between the 90% (v/v) and 75% (v/v) Alpha4 hydrogels, these results also indicate that these diluted hydrogels could be used to simulate different breast matrix stiffnesses.

Matrigel-alginate gels are an established model of breast matrix stiffness that are made by mixing Matrigel and alginate to create an interpenetrating alginate network which can then be crosslinked using calcium sulphate ($CaSO_4$) to stiffen the matrix [32, 37, 38, 40]. We reasoned that our diluted Alpha4 hydrogels should be equally as, if not more so, consistent in stiffness as Matrigel-alginate hydrogels are if we want to use them to model breast matrix stiffness. To characterise the storage moduli of Matrigel-alginate gels and compare their consistency to our diluted Alpha4 hydrogels, we conducted amplitude sweep experiments on assay media-conditioned soft (0 mM $CaSO_4$), medium (2.4 mM $CaSO_4$), and stiff (20 mM $CaSO_4$) Matrigel-alginate gels. During the study, we found that medium and stiff Matrigel-alginate gels were viscoelastic gels, but the soft Matrigel-alginate gels were less elastic and began to flow, indicating that their matrix was disrupted (Fig. S2). As expected, we found that the storage modulus of Matrigel-alginate gels increased as the concentration of $CaSO_4$ added to the matrix increased (Fig. 4B). This result had been previously reported by Chaudhuri, who also revealed the storage moduli of soft, medium and stiff Matrigel-alginate gels to be 30, 80 and 310 Pa, respectively [38]. However, our storage modulus measurements were much lower than these previously reported values [38]. Soft Matrigel-alginate gels had a storage modulus of 4 ± 3 Pa, making them almost 10-fold softer than the Matrigel-alginate gels in Chaudhuri's study. Similarly, medium Matrigel-alginate gels had a storage modulus of 9 ± 4 Pa, making them virtually indistinguishable from soft Matrigel-alginate gels in terms of stiffness and 8-fold softer than expected. While our stiff Matrigel-alginate gels were significantly stiffer than their soft and medium counterparts, they were almost 2-fold softer than what had been previously reported as they had a storage modulus of 170 ± 60 Pa. Interestingly, storage modulus comparison of our 4.5 mg/mL Matrigel samples with

Chaudhuri's 4.4 mg/mL Matrigel samples showed that our samples were 5-fold softer than theirs despite having a higher Matrigel concentration [38]. Therefore, these data suggest that Matrigel suffers from mechanical batch-to-batch variation and indicates that this variation independently affects the stiffness of gels that contain Matrigel. Paired with our data on Alpha4 stiffness, these results also indicate that Alpha4 can be mechanically tuned to create softer hydrogels that are more consistent than Matrigel-alginate gels.

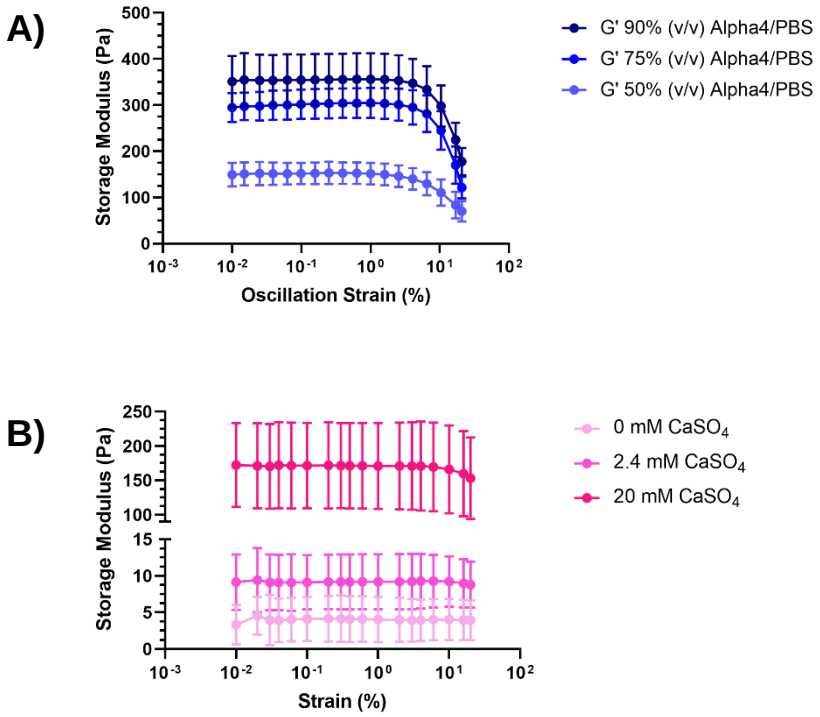

Fig. 4. Alpha4 can be mechanically tuned via dilution with PBS. A) Storage moduli at 1 Hz of Alpha4 gels diluted with different volumes of PBS. B) Storage moduli at 1 Hz of Matrigel-alginate gels stiffened using different concentrations of calcium sulphate ($CaSO_4$). Data are shown as mean ± SD. All measurements were performed at least three times, but underloading of five, 20 mM $CaSO_4$ Matrigel-alginate samples and of three 90% (v/v) Alpha4 samples led to their exclusion from analysis.

Soft Alpha4 gels stimulate increased MCF10a viability and cluster formation but do not stimulate acinar development

Since soft scaffolds support *in vivo* MEC behaviours such as acinar development, we next examined the behaviour of MCF10a cells encapsulated in soft (50% (v/v)) and medium (75% (v/v)) Alpha4 hydrogels to investigate if their behaviour and morphology changed in response to reduced Alpha4 matrix stiffness [38, 100, 101]. Brightfield images taken of encapsulated MCF10a cells at days 7, 12 and 21 showed that MCF10a cells remained viable and assembled into clusters in softened Alpha4 hydrogels for at least 21 days (Fig. 5A). We then quantified the number of organoids growing within the medium and soft Alpha4 hydrogels at days 7, 14 and 21 and measured their area and circularity. Although there was only a minimal increase in organoid number within each gel type over the 21-day culture period, there was a noticeable difference in organoid number between the medium and soft gels at each time point (Fig. 5B). By day 21, 90 ± 30 organoids were counted in medium Alpha4 gels

compared to 370 ± 40 organoids counted in soft Alpha4 gels. This 4-fold increase in organoid number in the soft Alpha4 gels indicates that softening Alpha4 increases MCF10a cell viability and cluster formation. Area measurements of organoids grown in medium and soft Alpha4 gels taken on days 7, 14 and 21 showed that there was virtually no difference in organoid area between organoids cultured in medium and soft Alpha4 gels at each time point (Fig. 5C). No signs of organoid growth arrest were detected in either hydrogel, as organoid size continually increased in both medium and soft hydrogels

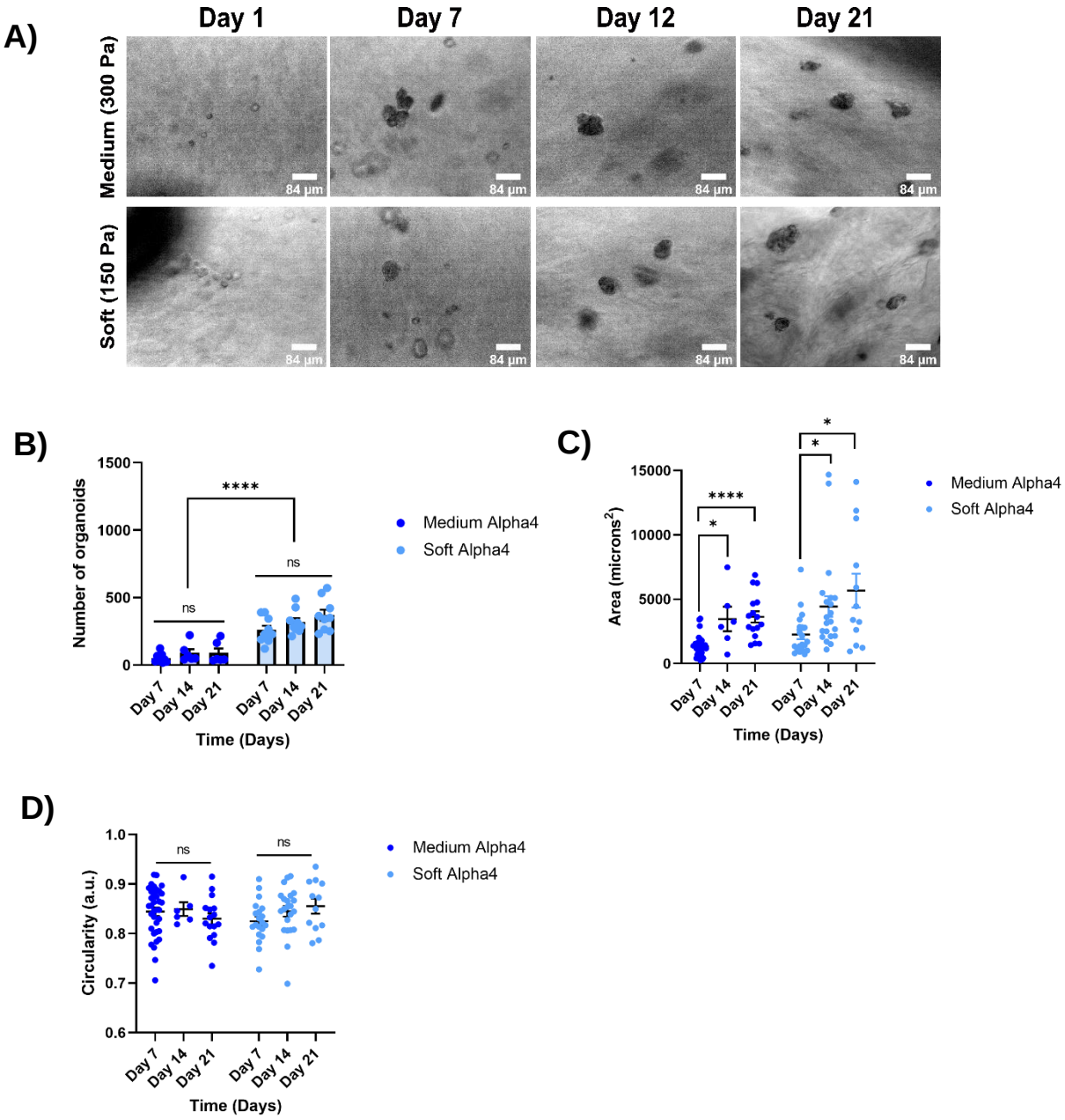

Fig. 5. Softening Alpha4 stimulates increased MCF10a cell viability and organoid formation. A) Brightfield images of MCF10a cells encapsulated in soft and medium Alpha4 hydrogels at days 7, 14 and 21. B) Number of organoids counted in medium and soft Alpha4 hydrogels at days 7, 14 and 21. C) Area measurements of organoids cultured in medium and soft Alpha4 hydrogels at days 7, 14 and 21. D) Circularity measurements of organoids grown in medium and soft Alpha4 hydrogels at days 7, 14 and 21. All measurements were performed at least three times, but several medium Alpha4 hydrogel cultures suffered infections during the experiment and were excluded from analysis. Data are shown as mean ± SEM (* p-value <0.05, **p-value <0.01, *** p-value <0.001, **** p-value <0.0001).

over the 21-day culture period with some organoids exceeding the 10,000 μm^2 area limit. The circularity measurements of organoids grown in medium and soft Alpha4 hydrogels showed that organoids in both hydrogels had a high circularity value of 0.8 ± 0.01 at day 7, which did not change by day 21 (Fig. 5D). This shows that the clusters had relatively regular, spheroid morphology. Together, these results indicate that softening Alpha4 stimulates increased MCF10a viability and organoid formation but does not stimulate the differentiation of MCF10a cells into growth-arrested acini.

We confirmed that the organoids growing in medium and soft Alpha4 hydrogels were not acini by extracting and probing the organoids with antibodies raised against active caspase-3, laminin 332, collagen IV and β-catenin at days 7, 12 and 21 (Fig. 6).

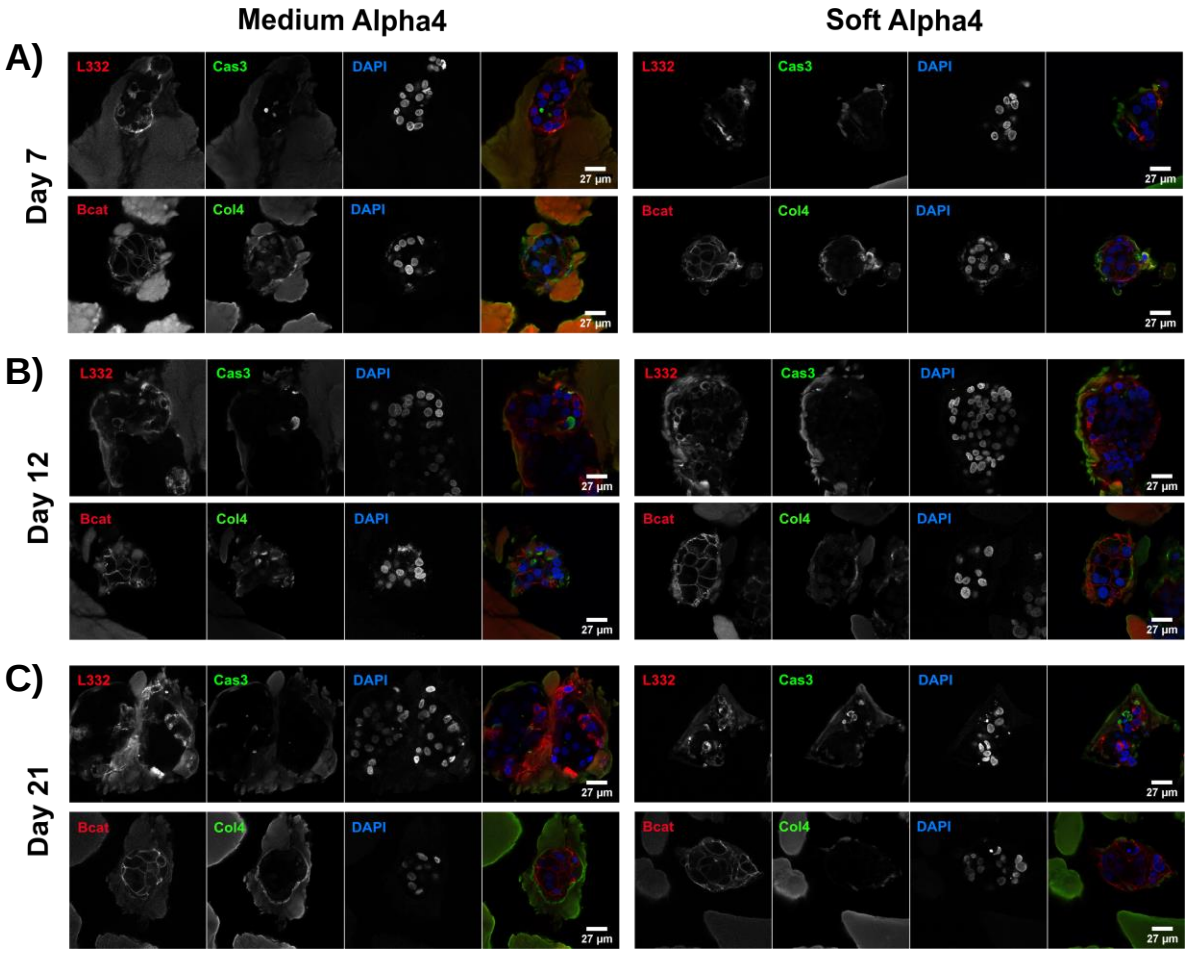

Fig. 6. Softening Alpha4 does not stimulate acinar development in MCF10a cells. MCF10a cells encapsulated in medium and soft Alpha4 gels were cultured for 21 days and stained with acinar markers: active caspase-3 (Cas3), laminin 332 (L332), collagen IV (Col4) and β-catenin (Bcat). IF images were taken of the extracted and stained organoids following their removal from the gels on days 7 (A), 12 (B) and 21 (C). Nuclei were stained with DAPI. 8 (day 7), 10 (day 12) and 4 (day 21) organoids were quantified for positive laminin 332 staining in medium Alpha4 gels. 1 (day 7), 8 (day 12) and 3 (day 21) organoids were quantified for positive laminin 332 staining in soft Alpha4 gels.

Day 7 organoids encapsulated in medium Alpha4 gels were not polarised or hollow, but 50% did deposit laminin 332 into their immediate environment (Fig. 6A). Organoids cultured in soft Alpha4 gels showed no signs of polarisation or luminal apoptosis but at least one had a laminin 332-rich matrix around its periphery at day 7. Day 12 organoids extracted from medium and soft Alpha4 hydrogels

continued to show no signs of cell polarisation or luminal apoptosis (Fig. 6B). However, 70% of organoids in medium gels and 50% of organoids found in the soft gels had a laminin 332-rich matrix. By day 21, the organoids extracted from medium and soft Alpha4 hydrogels remained unpolarised and still did not show any signs of luminal apoptosis (Fig. 6C). Nonetheless, 100% of the organoids in soft and medium hydrogels deposited laminin 332 around their peripheries. These results show that softening Alpha4 does not stimulate acinar formation in MCF10a cells. However, these results also show that softened Alpha4 gels can improve MCF10a viability and continue to support the formation of MCF10a organoids that deposit a laminin 332-rich basement membrane.

Alpha4-encapsulated MCF10a cells synthesise similar matrix proteins to Matrigel-encapsulated MCF10a cells

MECs secrete numerous matrix factors that help direct acinar formation by regulating MEC polarity, proliferation, and survival [15, 102-104]. Since Alpha4-encapsulated MCF10a cells produce a laminin 332-rich matrix, we asked whether they produce matrix proteins similar to matrix proteins produced by MECs *in vivo*. To investigate this, we obtained lysates from 14-day old MCF10a cells encapsulated in stiff, medium, and soft Alpha4 gels and submitted them for LC-MS/MS to obtain global qualitative and quantitative proteomic data. Since Matrigel stimulates acinar formation and contains a variety of matrix proteins, we also submitted 14-day old MCF10a lysates from Matrigel cultures to determine whether Alpha4-encapsulated MCF10a cells were synthesising the same matrix proteins as Matrigel-encapsulated cells or attempting to create a Matrigel-like environmental niche.

To control for proteins within assay media and Matrigel, we also submitted cell-free Matrigel and Alpha4 lysates that had been conditioned in assay media for 14 days. We expected to find matrix-derived proteins in our cell-free Matrigel samples as Matrigel is a complex, tissue-derived hydrogel that contains numerous matrix proteins and growth factors. However, since Alpha4 hydrogels are composed of peptides and water, we anticipated that we would not see many proteins in our cell-free Alpha4 samples. Contrary to our expectations, over 60 proteins were detected in all our cell-free samples, although we were unsurprised to find that the cell-free Matrigel samples contained the greatest number of proteins (Fig. 7A). We hypothesised that the high number of proteins present in our cell-free Alpha4 samples was caused by Matrigel contamination, as the cell-free Matrigel samples were the first samples to be analysed. To confirm this, we first screened our cell-free Matrigel sample data for matrix proteins and pulled out 45 matrix-associated proteins between all three replicates, 31 of which were present in all three replicates (Table S2). Included in this group were the two alpha chains of collagen IV isoform α1(IV),2α2(IV), two subunits of laminin 111, fibrinogen chains and fibronectin, which have all been previously detected in Matrigel [50, 105] (Fig. 7B). Several of these proteins were detected in some or all of our soft, medium, and stiff cell-free Alpha4 samples, which suggests that these proteins were contaminants from Matrigel (Table S3). Fewer matrix-associated proteins were detected in the cell-free Alpha4 samples than in the cell-free Matrigel samples, and included adiponectin, vitronectin and two subunits of laminin 332 (Fig. 7C). The plasma proteins

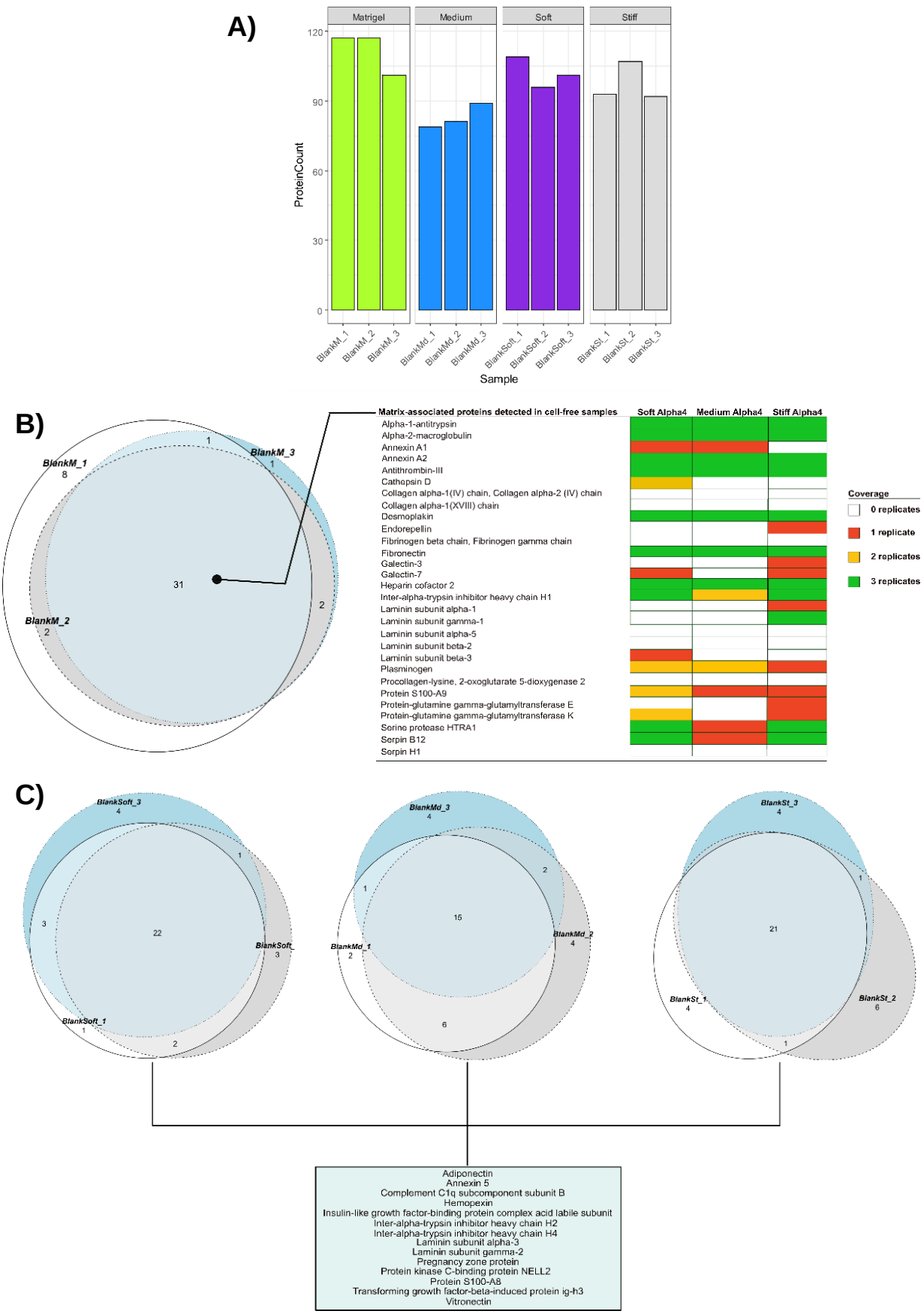

Fig. 7. Matrigel is a complex mixture of proteins that can contaminate other lysates during mass spectrometry analysis. A) Number of proteins quantified in cell-free Matrigel and soft, medium, and stiff Alpha4 samples. B) Comparison of matrix proteins detected in all cell-free Matrigel lysates and soft, medium, and stiff cell-free Alpha4 lysates. C) High-abundance matrix proteins detected in cell-free Alpha4 lysates. Three technical repeats per sample were prepared and submitted to obtain N=3.

hemopexin and a subunit of the C1 complement protein were also detected in these samples and are likely to be media proteins. Together, these results show that Matrigel is a protein-rich, complex substrate and suggest that most proteins detected in the cell-free hydrogel samples are contaminants from Matrigel. Indeed, we recommend that any study looking to analyse lysates obtained from Matrigel cultures ensure that Matrigel-derived lysates are the last samples to be run on the mass analyser to reduce sample contamination.

Significantly more proteins were detected in our cell-laden hydrogel samples than in our cell-free samples, which indicates that most proteins detected in the cell-laden samples originated from the lysed MCF10a cells (Fig. 8A). The number of proteins detected was highest in the Matrigel lysates, which could be due to the high protein content of Matrigel. However, the number of proteins detected in stiff Alpha4 lysates were unexpectedly few, which we attributed to unusually poor organoid growth during the experiment. Since peptide intensity normalisation also showed that stiff Alpha4 samples had abnormally low peptide intensities, we chose to exclude stiff Alpha4 samples from further analysis (Fig. 8B). We then compared matrix protein expression and intensity between our cell-free and cell-laden samples to determine what matrix proteins MCF10a cells were synthesising in Matrigel and soft and medium Alpha4 gels. We found that MCF10a cells encapsulated in Matrigel synthesised 47 matrix and matrix-associated proteins that were not previously detected in the cell-free Matrigel samples (Fig. 8C). These included the basement membrane proteins agrin and the laminin α3 and γ2 subunits, in addition to vitronectin and several enzymes that catalyse collagen crosslinking and hydroxylation. Matrix and matrix-associated proteins that showed an increase in intensity in the cell-laden Matrigel samples included the two chains of the collagen IV isoform α1(IV),2α2(IV), desmoplakin and the laminin β3 subunit, which together indicate that the MCF10a cells encapsulated in Matrigel were synthesising laminin 332- and collagen IV-rich basement membranes and forming contacts with the matrix. More matrix-associated proteins were also detected in the cell-laden medium Alpha4 samples than the cell-free samples, with all three subunits of laminin 332 detected, and upregulated matrix proteins included desmoplakin and various annexins (Fig. 8D). Two subunits of laminin 332 were also detected in cell-laden soft Alpha4 samples, along with the laminin γ1 subunit and fibronectin (Fig. 8E). Both medium and soft cell-laden Alpha4 samples, but not Matrigel samples, also contained metalloproteinase inhibitor-1 and elafin, which suggests that the MCF10a cells encapsulated in soft and medium Alpha4 gels were actively regulating matrix degradation.

Overall, fewer matrix proteins were detected in cell-laden soft and medium Alpha4 hydrogels when compared against the cell-laden Matrigel samples but given that MCF10a cells in Matrigel are more viable and exhibit more *in vivo*-like behaviours, this was expected. However, these results also indicate that MCF10a cells encapsulated in soft and medium Alpha4 gels are interacting with their environment and producing similar matrix proteins to those produced by Matrigel-encapsulated cells.

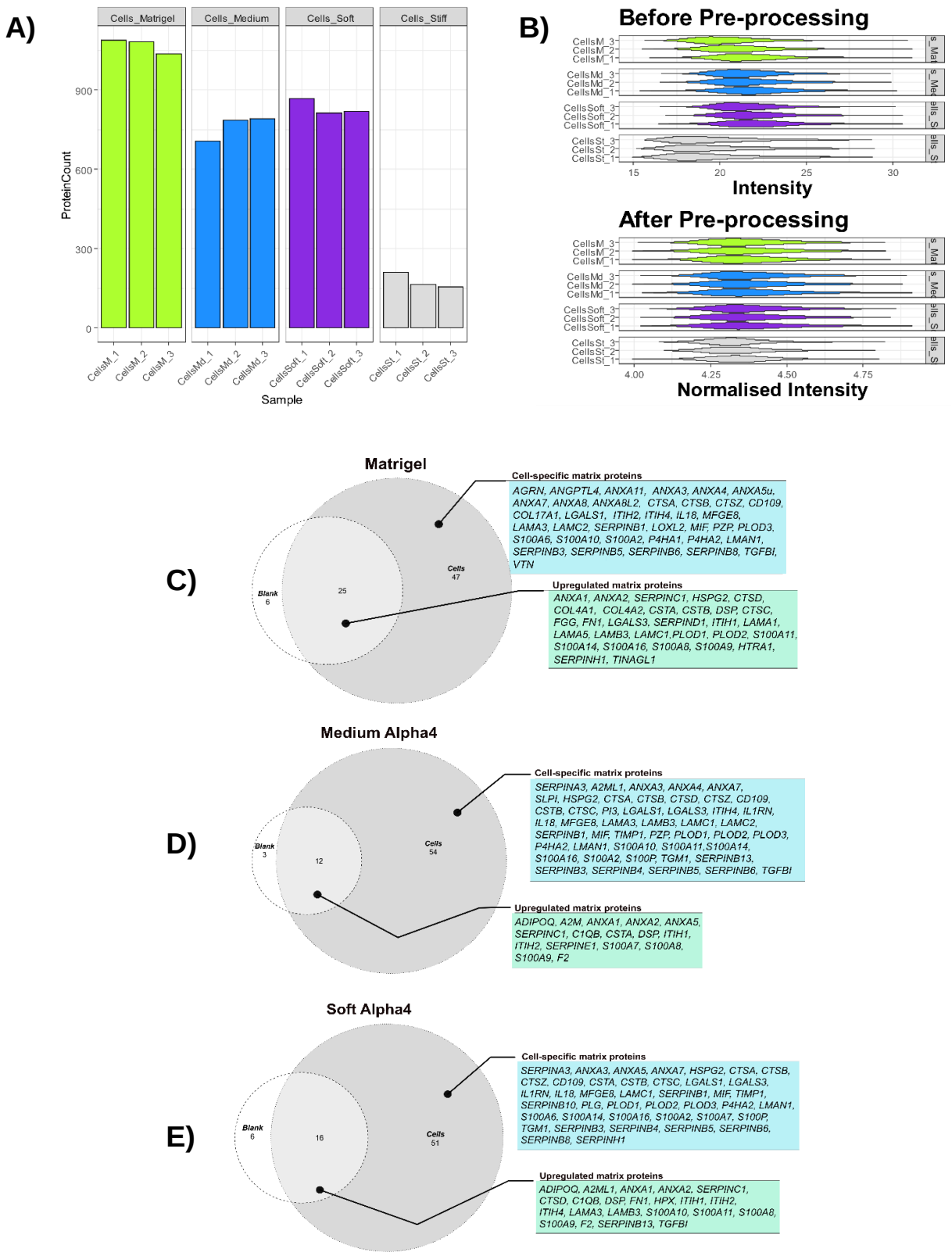

Fig. 8. MCF10a cells encapsulated in soft and medium Alpha4 hydrogels synthesise a variety of matrix proteins like those found in Matrigel-encapsulated MCF10a cells. A) Number of proteins quantified in cell-laden Matrigel and soft, medium, and stiff Alpha4 samples. B) Comparison of protein intensity for cell-laden Matrigel and soft, medium, and stiff Alpha4 samples, pre- and post-normalisation. C) Overlap analysis of matrix protein expression in cell-free and cell-laden Matrigel samples. D) Overlap analysis of matrix protein expression in cell-free and cell-laden medium Alpha4 samples. E) Overlap analysis of matrix protein expression in cell-free and cell-laden soft Alpha4 samples. Three technical repeats per condition were prepared and submitted to obtain N=3.

Oxidative stress, matrix synthesis and macromolecule biosynthesis in MCF10a cells are influenced by hydrogel composition and stiffness

Since reduced Alpha4 matrix stiffness prompts an increase in MCF10a cell viability, we asked if MCF10a cells responded to changes in Alpha4 stiffness in other ways and, if so, whether these stiffness-driven changes could be detected using proteomics. Principal component analysis of our cell-laden Matrigel, soft and medium Alpha4 samples showed clear separation between Matrigel samples and the soft and medium Alpha4 samples, which demonstrates that intrinsic differences in hydrogel properties such as matrix composition between Matrigel and Alpha4 generated changes in MCF10a protein expression (Fig. 9A). Interestingly, there was only mild separation across PC3 between medium and soft Alpha4 samples, which indicates that their mechanical properties provoke similar responses in MCF10a cells. Indeed, comparing differential protein expression using MSqRob analysis showed that only 13 cellular proteins were differentially expressed between MCF10a cells encapsulated in soft and medium Alpha4 hydrogels (Fig. 9B). Cellular proteins that were significantly upregulated in soft Alpha4 samples included vimentin, tubulin β-4B chain, calreticulin and Ras-related protein Ral-A (RALA). The four cellular proteins significantly upregulated in medium Alpha4 samples are metabolic proteins. No significant differences in matrix protein expression were found between soft and medium Alpha4 samples (Fig. 9C). These results indicate that medium and soft Alpha4 hydrogels elicit similar proteomic responses in MCF10a cells, which suggests that the difference in matrix stiffness between soft and medium Alpha4 gels is not sufficient to prompt significant changes in MCF10a behaviour. Nonetheless, expression of several proteins involved in regulating cell signalling events were significantly upregulated in response to reduced Alpha4 matrix stiffness, which suggests that the cells are detecting a change in environmental stiffness and responding to it, however minimally.

Alpha4-encapsulated MCF10a cells organise into viable organoids and synthesise matrix proteins, but they do not form polarised acini like MCF10a cells do in Matrigel. We therefore asked if we could identify changes in MCF10a cell behaviour between Matrigel samples and soft and medium Alpha4 samples by performing comparative and functional analyses on our mass spectrometry data. 252 differentially expressed cellular proteins were identified in medium Alpha4 samples when compared against Matrigel samples (Fig. 10A). Two of the most significantly downregulated cellular proteins in medium Alpha4 samples were vimentin, which has been implicated as a regulator of MEC differentiation, and nucleophosmin, a critical regulator of chromatin remodelling, apoptosis and genomic stability [106, 107] (Table S4). 31 differentially expressed matrix proteins were also identified, with basement membrane proteins such as laminins 111 and 332 and nidogen downregulated in medium Alpha4 samples when compared against Matrigel samples (Fig. 10B). These results indicate that MCF10a cells encapsulated in medium Alpha4 hydrogels do not express the proteins necessary for stimulating acinar development and express proteins that may promote behaviours such as uncontrolled growth or migration instead.

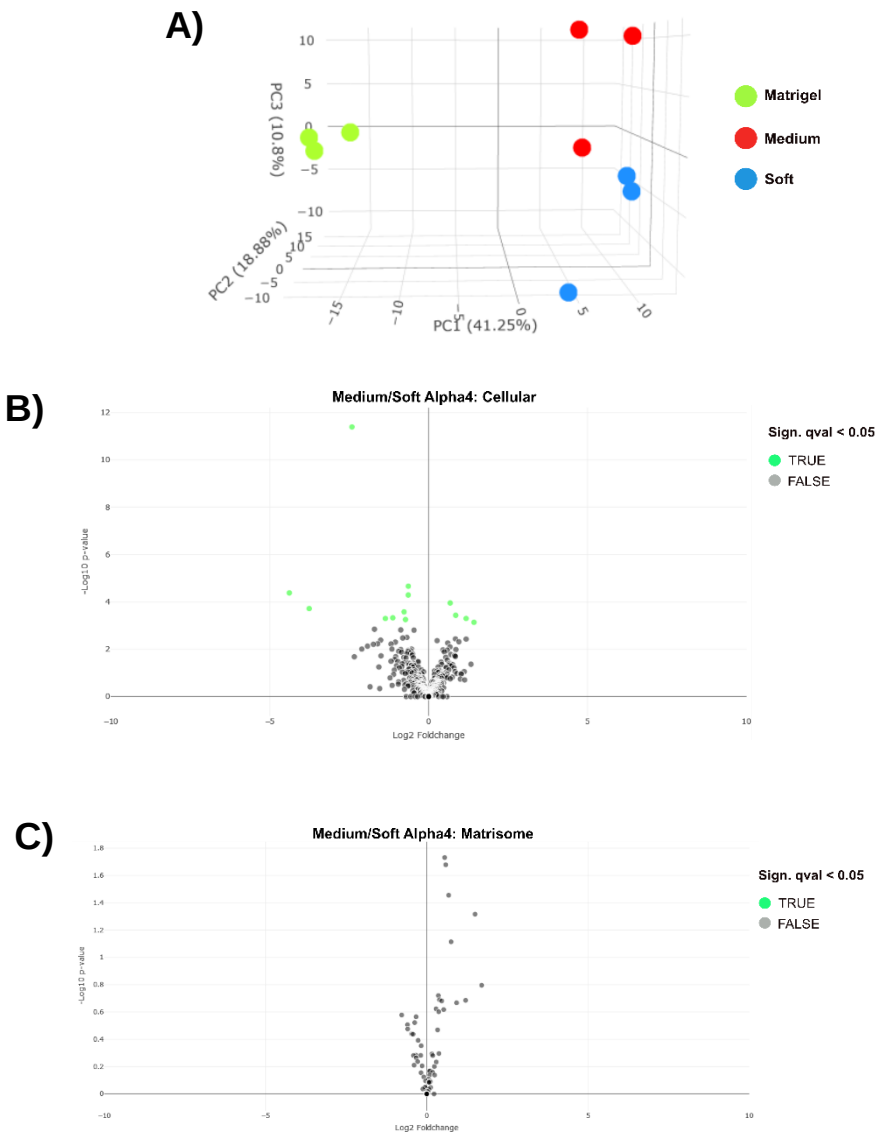

Fig. 9. Softening Alpha4 promotes limited changes in cellular protein expression. A) Principal component analysis of cell-laden Matrigel and soft and medium Alpha4 samples. B) Mean fold-change of cellular protein abundance for medium Alpha4 samples against soft Alpha4 samples. C) Mean fold-change of matrix protein abundance for medium Alpha4 samples against soft Alpha4 samples. Volcano plots depict upregulated (positive ratio) and downregulated (negative ratio) proteins in medium Alpha4 samples. P-values calculated via MSqRob from three independent replicates ($p < 0.05$).

Indeed, functional analysis of these differentially expressed cellular and matrix proteins revealed that most significantly upregulated proteins in medium Alpha4 samples were involved in positively regulating immune and inflammatory responses (Fig. 10C). Several oxidative and toxic stress responses were also upregulated in medium Alpha4 samples. Superoxide dismutase, thioredoxin and peroredoxin expression were upregulated, suggesting that the cells are accumulating reactive oxygen species (ROS) which can promote cell proliferation, migration, and survival [108]. Conversely, the most significantly downregulated biological processes in medium Alpha4 samples were protein, RNA and DNA biosynthesis (Fig. 10D). Together, these results suggest that MCF10a cells encapsulated in medium Alpha4 hydrogels are subject to increased oxidative stress, which may be preventing them from forming acini.

Comparative analysis of cellular proteins expressed in soft Alpha4 samples against Matrigel samples showed similar results to the data obtained from medium Alpha4 samples (Fig. 10E). 306 differentially expressed cellular proteins were identified, and among the significantly downregulated proteins in soft Alpha4 samples was nucleophosmin (Table S5). More matrix proteins were downregulated in soft Alpha4 samples than in medium Alpha4 samples when compared against Matrigel samples, but they were mostly basement membrane associated proteins and collagen enzymes (Fig. 10F). However, functional analysis showed that the most significantly upregulated biological processes in soft Alpha4 samples were mostly proteolytic processes, with inflammatory and immune processes appearing to occur less in soft Alpha4 samples in comparison to medium Alpha4 samples (Fig. 10G). Significantly downregulated biological processes in soft Alpha4 samples included protein and RNA biosynthesis, DNA metabolism and gene transcription and translation (Fig. 10H).

Surprisingly, we were unable to identify any significantly changed pathways in MCF10a cells between Matrigel samples and soft and medium Alpha4 samples. However, the results of our comparative and functional analyses show that MCF10a cells cultured in soft and medium hydrogels express significantly fewer matrix and matrix-associated proteins than Matrigel-encapsulated MCF10a cells. They also show that fewer biosynthetic processes occur in these cells, which could be an indicator of their reduced viability in Alpha4 hydrogels. However, these downregulated processes could also be tied to their inability to differentiate into polarised acini. Interestingly, the finding that MCF10a cells show upregulated responses to oxidative stress in medium Alpha4 hydrogels also suggests that Alpha4 provokes oxidative damage in MCF10a cells, which may also play a role in preventing MCF10a acinar differentiation. Furthermore, the comparative downregulation of inflammatory, immune and stress responses in soft Alpha4 samples in comparison to medium Alpha4 samples suggests that some of these processes may be stiffness-responsive, which would indicate that reducing Alpha4 matrix stiffness leads to reduced oxidative stress in MCF10a cells.

A)

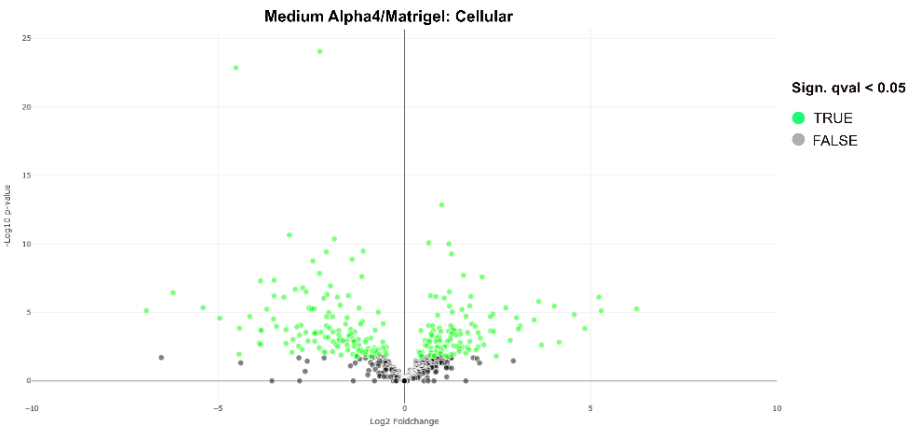

B)

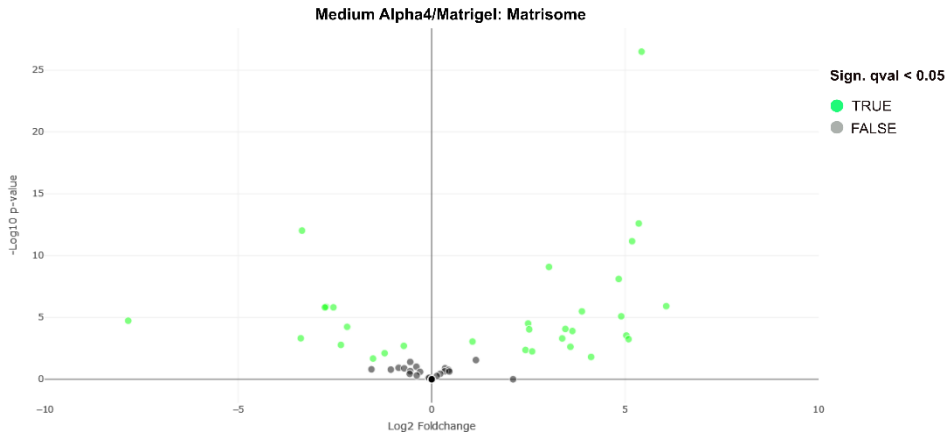
Medium Alpha4/Matrigel: Matrisome
Sign. qval < 0.05
TRUE
FALSE
−Log10 p-value
Log2 Foldchange

C)

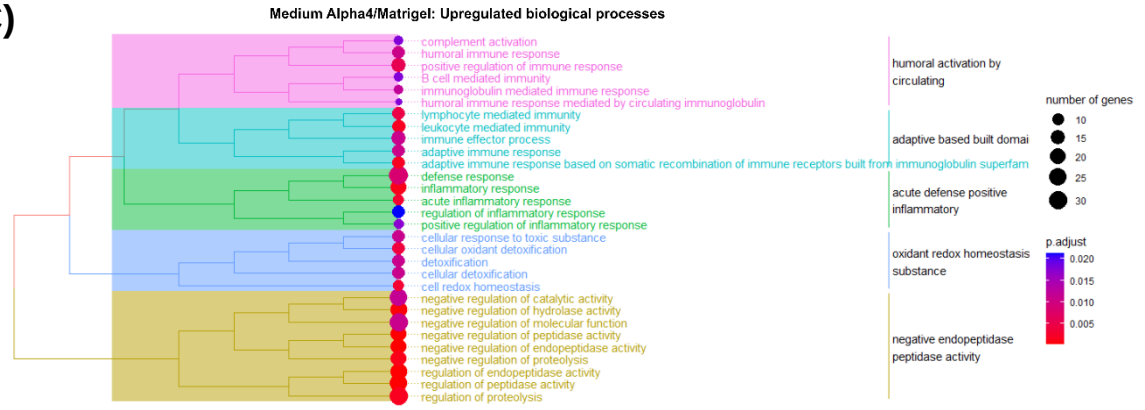
Medium Alpha4/Matrigel: Upregulated biological processes
complement activation
humoral immune response
positive regulation of immune response
B cell mediated immunity
immunoglobulin mediated immune response
humoral immune response mediated by circulating immunoglobulin
lymphocyte mediated immunity
leukocyte mediated immunity
immune effector process
adaptive immune response
adaptive immune response based on somatic recombination of immune receptors built from immunoglobulin superfam
defense response
inflammatory response
acute inflammatory response
regulation of inflammatory response
positive regulation of inflammatory response
cellular response to toxic substance
cellular oxidant detoxification
detoxification
cellular detoxification
cell redox homeostasis
negative regulation of catalytic activity
negative regulation of hydrolase activity
negative regulation of molecular function
negative regulation of peptidase activity
negative regulation of endopeptidase activity
negative regulation of proteolysis
regulation of endopeptidase activity
regulation of peptidase activity
regulation of proteolysis
humoral activation by circulating
adaptive based built domai
acute defense positive inflammatory
oxidant redox homeostasis substance
negative endopeptidase peptidase activity
number of genes
p.adjust

D)

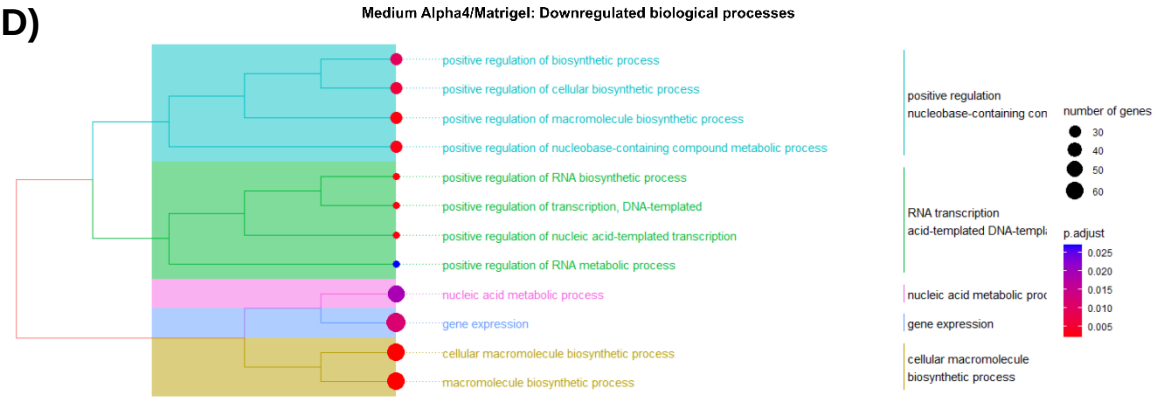
Medium Alpha4/Matrigel: Downregulated biological processes
positive regulation of biosynthetic process
positive regulation of cellular biosynthetic process
positive regulation of macromolecule biosynthetic process
positive regulation of nucleobase-containing compound metabolic process
positive regulation of RNA biosynthetic process
positive regulation of transcription, DNA-templated
positive regulation of nucleic acid-templated transcription
positive regulation of RNA metabolic process
nucleic acid metabolic process
gene expression
cellular macromolecule biosynthetic process
macromolecule biosynthetic process
positive regulation nucleobase-containing con
RNA transcription acid-templated DNA-templ
nucleic acid metabolic proc
gene expression
cellular macromolecule biosynthetic process
number of genes
p.adjust

E)

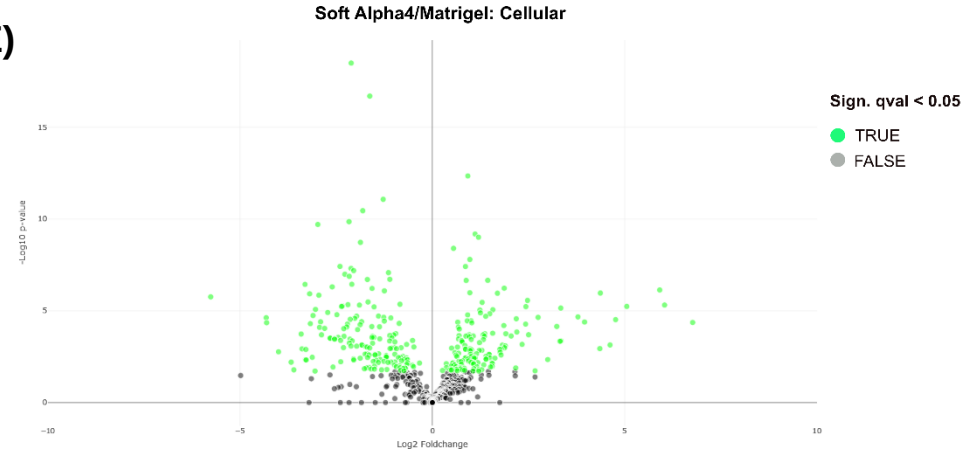
Soft Alpha4/Matrigel: Cellular
Sign. qval < 0.05
TRUE
FALSE
−Log10 p-value
Log2 Foldchange

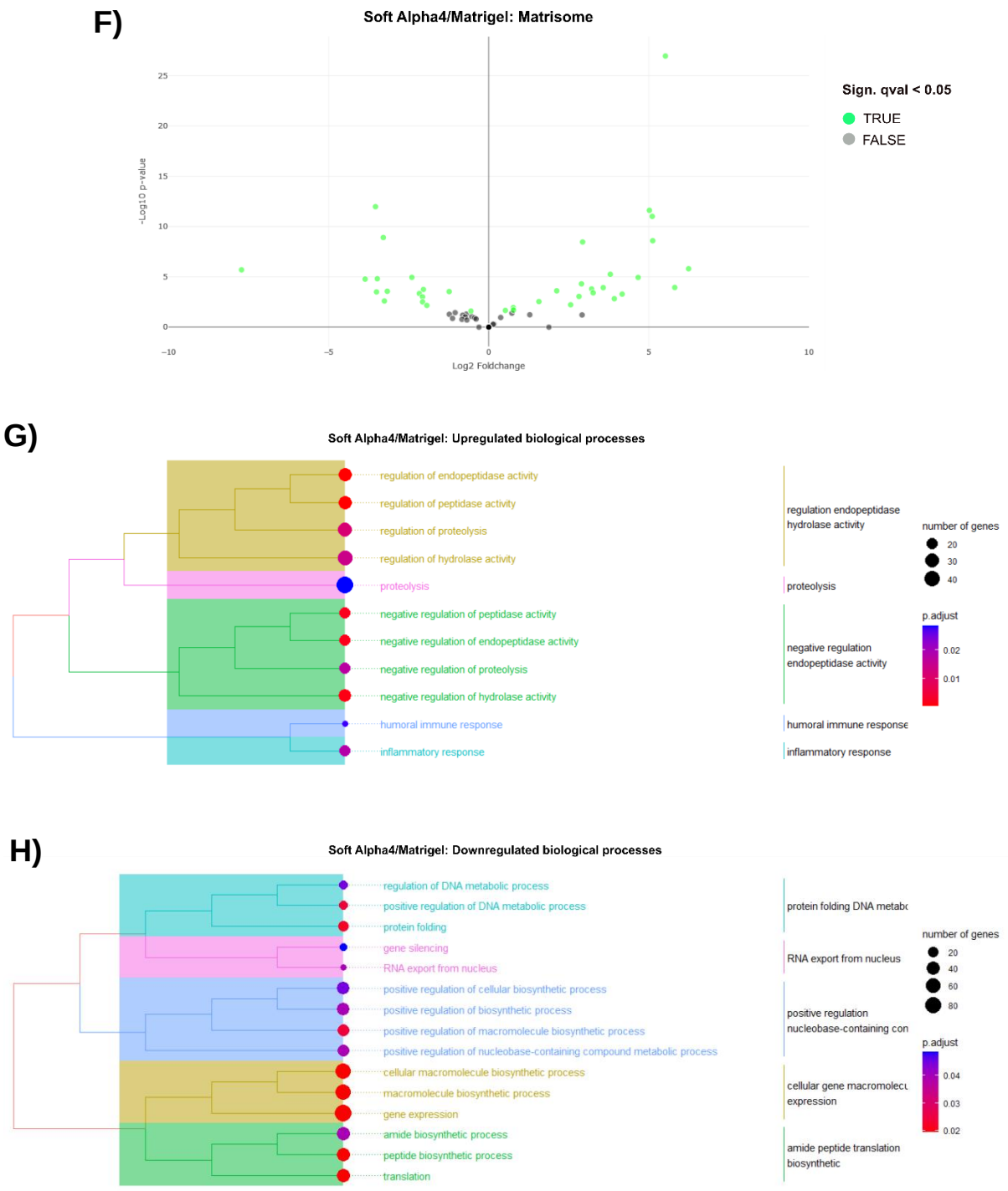

Fig. 10. Encapsulation of MCF10a cells in Alpha4 hydrogels stimulates oxidative stress and downregulates matrix production and macromolecule biosynthesis in comparison to Matrigel. A) Mean fold-change of cellular protein abundance for medium Alpha4 samples against Matrigel samples. B) Mean fold-change of matrix protein abundance for medium Alpha4 samples against Matrigel samples. C) Upregulated biological processes in medium Alpha4 samples when compared against Matrigel samples. D) Downregulated biological processes in medium Alpha4 samples when compared against Matrigel samples. E) Mean fold-change of cellular protein abundance for soft Alpha4 samples against Matrigel samples. F) Mean fold-change of matrix protein abundance for soft Alpha4 samples against Matrigel samples. G) Upregulated biological processes in soft Alpha4 samples when compared against Matrigel samples. H) Downregulated biological processes in soft Alpha4 samples when compared against Matrigel samples. Volcano plots depict upregulated (positive ratio) and downregulated (negative ratio) proteins in Alpha4 samples. P-values calculated via MSqRob and Clusterprofiler from three independent replicates ($p < 0.05$).

Discussion

Creating a well-defined and reproducible model of matrix stiffness using Matrigel is challenging due to limitations such as batch-to-batch variability, mechanical heterogeneity, resistance to mechanical modifications and poor definition [46, 50, 109-111]. In contrast, synthetic hydrogels like Alpha4 offer consistency, tuneability and definition, making Alpha4 a promising alternative to Matrigel [51, 60, 68, 112-114]. This study therefore aimed to characterise and compare Alpha4 as a MEC scaffold to Matrigel and explore Alpha4's ability to model breast matrix stiffness.

Batch-to-batch variation of matrix stiffness, growth factors and matrix proteins in Matrigel can result in inconsistent cell behaviours [115]. However, Alpha4 does not have this limitation as its simple composition of peptides and water makes it both biochemically and mechanically consistent [99]. In our study we found that Alpha4 consistently supported the organisation of MCF10a cells into organoids that deposit a laminin 332-rich basement membrane and are viable for at least 21 days. We also found that the organoids growing in Alpha4 expressed multiple matrix and matrix-associated factors, which suggests that the organoids were able to create sophisticated extracellular niches. Alpha4 has been previously shown to support viability and cluster formation in mouse MECs, which confirms that Alpha4 is supportive of MEC-characteristic behaviours observed in organic hydrogels [38, 89, 116]. These results show that Alpha4 is a consistently compatible scaffold for MEC culture.

The mechanical properties of Matrigel are also inconsistent between batches [46, 100, 110, 117]. Our findings demonstrate this as we could not replicate the stiffnesses of soft, medium, and stiff Matrigel-alginate gels made by Chaudhuri [38]. Indeed, we found our gels to be significantly softer than those previously reported. We considered whether incubating the gels in assay media prior to rheological analysis may have physically removed calcium ions from the alginate network and therefore reduced the extent of calcium crosslinking in Matrigel-alginate gels in our study. However, this does not account for the finding that Chaudhuri's 4.4 mg/mL Matrigels were stiffer than our 4.5 mg/mL Matrigels [38]. Therefore, it is likely that the difference in Matrigel-alginate stiffnesses we saw in our study were due to the inherent mechanical inconsistencies of Matrigel.

We currently cannot make any direct comparisons of our Alpha4 stiffness measurements to data in the literature as media-conditioning independently affects Alpha4 stiffness [64, 89, 90, 114, 118]. However, our findings agree with Manchester BioGEL, who reported that the stiffness of Alpha4 can be between 350 and 700 Pa depending on the media used to condition the gels [99]. Paired with the consistency of our mechanical data, this indicates that the mechanical properties of Alpha4 are consistent, more so than those of Matrigel.

A functional model of matrix stiffness requires a scaffold that can be mechanically modified to consistently simulate tissue stiffness. We have shown that the stiffness of Alpha4 is simple to modify, as dilution with PBS is sufficient to create gels that are significantly softer than undiluted Alpha4. While Matrigel can also be mechanically modified via addition of alginate and varying calcium concentrations, our inability to create soft and medium Matrigel-alginate gels with significantly

different stiffnesses demonstrates the challenges in mechanically modifying Matrigel and highlights the unreliability of using Matrigel as a model of matrix stiffness.

Using soft and medium Alpha4 hydrogels as a speculative model of matrix stiffness, we found that stiffer Alpha4 matrices promote upregulation of pro-inflammatory and immune processes and stimulates detoxification responses. *In vitro* models of matrix stiffness have previously shown that increased matrix stiffness induces inflammatory responses in various cell types [119-122]. Indeed, increased matrix stiffness in breast cancer is associated with increased tissue inflammation and immune cell infiltration [22, 27, 123-125]. Furthermore, increased matrix stiffness has been shown to induce oxidative stress in cells which can provoke cell death or, conversely, induce oncogenic cell behaviours such as apoptotic evasion, uncontrolled proliferation and metastasis [126-130]. These upregulated, malignancy-associated processes in medium Alpha4 hydrogels correlate with the tumorigenic behaviours that MCF10a cells exhibit in medium Alpha4 hydrogels, such as loss of apicobasal polarisation and growth arrest evasion [131]. However, no significant changes in the regulation of these processes were detected in soft Alpha4 samples, which could indicate that these processes are not stiffness-driven. These processes may have been upregulated in response to Alpha4's peptide matrix, since fibrillar peptide hydrogels can provoke immunogenic responses and β-sheet fibres such as amyloid fibrils can trigger inflammation, oxidative stress and immune activation [132-138]. Nonetheless, the combined upregulation of multiple inflammatory and immune processes, paired with the upregulation of antioxidant responses, in medium Alpha4 cultures suggest that its mechanical environment is provoking potentially oncogenic pro-inflammatory and oxidative events in MCF10a cells.

Interestingly, some of our findings appear to contradict supported findings from previous studies. We found that organoids continued to grow and proliferate in soft Alpha4 gels, in contrast to several studies which found that unrestricted organoid growth occurs in stiffer matrices [9, 14, 38, 39, 139, 140]. Furthermore, contrary to our expectations that softening Alpha4 would reduce tumorigenic behaviour in MCF10a cells, we detected increased expression of vimentin, calreticulin and RALA in soft Alpha4 samples, which have all been implicated as drivers and regulators of breast cancer invasion and metastasis [141-145]. The upregulation of these proteins indicates that the MCF10a cells encapsulated in soft Alpha4 hydrogels are becoming more tumorigenic, in defiance of reduced matrix stiffness. However, the increased growth and invasiveness of MCF10a cells in soft Alpha4 gels may be independent of matrix stiffness, as diluting Alpha4 may increase network porosity and compliance, and plastic and porous matrices can encourage invasiveness independent of their bulk stiffness [146, 147]. Although this indicates that we did not independently modify matrix stiffness and density in our Alpha4 hydrogels, breast matrix density and stiffness are also interconnected, which suggests that our Alpha4 hydrogels could provide a representative model of breast matrix mechanics [22, 27, 29, 30, 148]. Furthermore, Alpha4's amenability to mechanical tuning makes it likely that Alpha4 matrix stiffness can be independently modified in future studies if it has not been already.

We found that MCF10a cells did not differentiate into polarised acini in Alpha4 hydrogels. The organoids that grew in Alpha4 hydrogels consistently resemble malignant MECs as they show no signs of growth arrest or apicobasal polarisation [116, 131]. Basement membrane formation is also irregular and incomplete in Alpha4-encapsulated organoids as no signs of collagen IV production were detected, and laminin 332 deposition was irregular and not confined to the basolateral side of the organoids. Impaired basement membrane assembly and integrity are hallmarks of breast cancer as they facilitate cancer invasion, and laminin 332 shedding induces epithelial cell migration [4, 38, 149-152]. These phenotypes, paired with the elevated expression of fibronectin, metalloproteinase inhibitors and galectin-3 in Alpha4 samples, indicate that Alpha4-encapsulated organoids are tumorigenic [2, 102, 153-156]. These phenotypes do not disappear as Alpha4 stiffness is reduced, which appears to contradict multiple *in vitro* studies showing that healthy MEC behaviours are recovered in soft matrices [14, 28, 38]. This could be due to our inability to sufficiently dilute Alpha4 to provide MECs with a mechanical environment that is representative of soft breast tissues, although there is currently no consensus on the stiffness of breast tissue [29, 157-161]. Furthermore, different models of breast matrix stiffness have unique mechanical properties despite effecting similar responses in MECs, demonstrating that a combination of environmental cues regulate MEC behaviour [9, 14, 28, 35, 38, 162].

Several studies have demonstrated that mechanical cues have a limited impact on MEC behaviour when MECs are encapsulated in a laminin 111-rich matrix [38, 163]. This suggests that MECs are more responsive to biochemical cues than mechanical cues, which would explain why MCF10a cells did not exhibit more *in vivo* phenotypes in soft Alpha4 hydrogels, but a relatively minor difference in Matrigel-alginate stiffness can prompt significant changes in MCF10a behaviour. Matrigel's bioactivity is attributed to its high laminin 111 content, as laminin 111 stimulates multiple *in vivo* MEC behaviours, including acinar formation [19, 105, 140, 163-165]. Therefore, it is likely that Alpha4's inability to stimulate acinar development in MCF10a cells is not due to its inability to simulate the mechanical properties of healthy breast tissue, but because of its limited bioactivity. Previous studies have shown that SAPHs are easy to functionalise for cell culture, which suggests that supplementing Alpha4 with breast matrix proteins such as laminin 111 will create an even more representative model of breast matrix stiffness that provides the cells with appropriate mechanical and biochemical cues while remaining consistent and well-defined [140, 166, 167].

Despite Alpha4's current limitations as a model of the breast matrix, we nonetheless found that MCF10a cells exhibited several behaviours that resembled how they behave in Matrigel when encapsulated in Alpha4 hydrogels. This included the formation and viability of spheroidal organoids for at least 21 days [88]. We also found that MCF10a cells encapsulated in Alpha4 hydrogels produced matrix proteins that were also secreted by acini growing in Matrigel. MCF10a cells encapsulated in Alpha4 hydrogels consistently synthesised and secreted the epithelial cell-specific, basement membrane protein laminin 332, which has been found to maintain basement membrane integrity, control acinar organisation and maintain cell-matrix connections that regulate epithelial cell adhesion and migration [168, 169]. Therefore, our findings indicate that MCF10a organoids in Alpha4

hydrogels were assembling a basement membrane similar to what acini produce *in vivo*. Other matrix components such as the network-forming glycoprotein fibronectin and proteoglycans such as decorin, syndecans and agrin were also synthesised by Alpha4-encapsulated MCF10a cells, which are matrix factors that are either secreted by mammary acini or are already present within Matrigel and have been implicated in the regulation of MEC morphogenesis [4, 50, 102, 105, 170]. Furthermore, the expression of bioactive adhesive macromolecules that regulate various MEC behaviours such as desmoplakin, galectins and annexins, indicate that the MCF10a cells are in physical contact with their environment and are actively trying to stimulate *in vivo* MEC behaviours [2, 96, 155, 171-174]. Therefore, the morphology and behaviour of MCF10a cells encapsulated in Alpha4 hydrogels reveals that Alpha4 supports several key *in vivo* MEC phenotypes.

Dense breast tissue is correlated with increased matrix stiffness and oncogenic MEC behaviours, but the initial, mechanically driven events the stimulate MEC oncogenesis are still poorly defined and require a consistent, mechanically tuneable 3D *in vitro* model of the breast matrix to be elucidated. These results demonstrate that Alpha4 is a consistent, modifiable, and defined hydrogel that is compatible for MEC culture. While there are still limitations to this model of breast matrix stiffness, we were able to identify changes in MCF10a protein expression that were likely stimulated by the changing mechanical environment of Alpha4. These findings validate Alpha4's ability to simulate different breast matrix stiffnesses and highlight several biological processes that may play a key role in priming MEC oncogenesis in dense breast tissue.

Acknowledgements

This project was funded by the University of Manchester, the UK Regenerative Medicine Platform (UKRMP; MR/R015651/1) and Manchester BioGEL.

Matrigel-alginate gels were made by Hannah Percival, who was supported by a Manchester Cancer Research Centre studentship. Amplitude sweep experiments were performed with the help of Siyuan Dong, who was supported by the University of Manchester. Mass spectrometry data analysis was performed with the help of Craig Lawless, who was supported by the Wellcome Centre for Cell-Matrix Research (WCCMR; 203128/Z/16/Z). Joe Swift was supported by a Biotechnology and Biological Sciences Research Council (BBSRC) David Phillips Fellowship (BB/L024551/1).

In-gel digestion of lysates and proteomics was performed by the Biological Mass Spectrometry Core Facility; imaging was carried out at the Bioimaging Facility (supported by BBSRC, Wellcome and the University of Manchester Strategic Fund). We thank Drs. Ronan O'Cualain, Emma Keevil, Stacey Warwood, Julian Selley, David Knight, Steven Marsden, Roger Meadows and Peter March for Core Facility support.

Competing Interests

A. Saiani and A.F. Miller are co-founders, directors, and shareholders of Manchester BioGEL.

References

1. Bissell, M.J., et al., *The organizing principle: microenvironmental influences in the normal and malignant breast.* Differentiation, 2002. **70**(9): p. 537-546.
2. Fata, J.E., Z. Werb, and M.J. Bissell, *Regulation of mammary gland branching morphogenesis by the extracellular matrix and its remodeling enzymes.* Breast Cancer Research, 2003. **6**(1): p. 1.
3. Hu, G., L. Li, and W. Xu, *Extracellular matrix in mammary gland development and breast cancer progression.* Frontiers in Laboratory Medicine, 2017. **1**(1): p. 36-39.
4. Kass, L., et al., *Mammary epithelial cell: influence of extracellular matrix composition and organization during development and tumorigenesis.* The international journal of biochemistry & cell biology, 2007. **39**(11): p. 1987-1994.
5. Polyak, K. and R. Kalluri, *The role of the microenvironment in mammary gland development and cancer.* Cold Spring Harbor perspectives in biology, 2010. **2**(11): p. a003244-a003244.
6. Emerman, J.T. and D.R. Pitelka, *Maintenance and induction of morphological differentiation in dissociated mammary epithelium on floating collagen membranes.* 1977(0073-5655 (Print)).
7. Campbell, J.J. and C.J. Watson, *Three-dimensional culture models of mammary gland.* Organogenesis, 2009. **5**(2): p. 43-49.
8. Carter, E.P., et al., *A 3D in vitro model of the human breast duct: a method to unravel myoepithelial-luminal interactions in the progression of breast cancer.* Breast Cancer Research, 2017. **19**(1): p. 50.
9. Cavo, M., et al., *Microenvironment complexity and matrix stiffness regulate breast cancer cell activity in a 3D in vitro model.* Scientific Reports, 2016. **6**(1): p. 35367.
10. Barcellos-Hoff, M.H., et al., *Functional differentiation and alveolar morphogenesis of primary mammary cultures on reconstituted basement membrane.* Development, 1989. **105**(2): p. 223.
11. Lee, G.Y., et al., *Three-dimensional culture models of normal and malignant breast epithelial cells.* Nature methods, 2007. **4**(4): p. 359-365.
12. Aggeler, J., et al., *Cytodifferentiation of mouse mammary epithelial cells cultured on a reconstituted basement membrane reveals striking similarities to development in vivo.* Journal of Cell Science, 1991. **99**: p. 407-417
13. Brovold, M., et al., *Naturally-Derived Biomaterials for Tissue Engineering Applications.* Advances in experimental medicine and biology, 2018. **1077**: p. 421-449.
14. Paszek, M.J., et al., *Tensional homeostasis and the malignant phenotype.* Cancer Cell, 2005. **8**(3): p. 241-254.
15. Petersen, O.W., et al., *Interaction with basement membrane serves to rapidly distinguish growth and differentiation pattern of normal and malignant human breast epithelial cells.* Proceedings of the National Academy of Sciences, 1992. **89**(19): p. 9064.
16. Swamydas, M., et al., *Matrix compositions and the development of breast acini and ducts in 3D cultures.* In Vitro Cellular & Developmental Biology - Animal, 2010. **46**(8): p. 673-684.
17. Streuli, C.H. and M.J. Bissell, *Expression of extracellular matrix components is regulated by substratum.* The Journal of Cell Biology, 1990. **110**(4): p. 1405.
18. Wang, H., et al., *Rotational motion during three-dimensional morphogenesis of mammary epithelial acini relates to laminin matrix assembly.* Proceedings of the National Academy of Sciences, 2013. **110**(1): p. 163-168.
19. Xu, R., et al., *Sustained activation of STAT5 is essential for chromatin remodeling and maintenance of mammary-specific function.* Journal of Cell Biology, 2009. **184**(1): p. 57-66.
20. Li, M.L., et al., *Influence of a reconstituted basement membrane and its components on casein gene expression and secretion in mouse mammary epithelial cells.* Proceedings of the National Academy of Sciences of the United States of America, 1987. **84**(1): p. 136-140.
21. Streuli, C.H., N. Bailey, and M.J. Bissell, *Control of mammary epithelial differentiation: basement membrane induces tissue-specific gene expression in the absence of cell-cell interaction and morphological polarity.* The Journal of cell biology, 1991. **115**(5): p. 1383-1395.
22. Acerbi, I., et al., *Human breast cancer invasion and aggression correlates with ECM stiffening and immune cell infiltration.* Integrative biology : quantitative biosciences from nano to macro, 2015. **7**(10): p. 1120-1134.
23. Boyd, N.F., et al., *Mammographic Density and the Risk and Detection of Breast Cancer.* New England Journal of Medicine, 2007. **356**(3): p. 227-236.

24. Yaghjyan, L., et al., *Mammographic Breast Density and Subsequent Risk of Breast Cancer in Postmenopausal Women According to Tumor Characteristics.* JNCI: Journal of the National Cancer Institute, 2011. **103**(15): p. 1179-1189.
25. Sherratt, M.J., J.C. McConnell, and C.H. Streuli, *Raised mammographic density: causative mechanisms and biological consequences.* Breast cancer research : BCR, 2016. **18**(1): p. 45-45.
26. Chin, L., et al., *Mechanotransduction in cancer.* Current opinion in chemical engineering, 2016. **11**: p. 77-84.
27. Huo, C.W., et al., *High mammographic density is associated with an increase in stromal collagen and immune cells within the mammary epithelium.* Breast Cancer Research, 2015. **17**(1): p. 79.
28. Levental, K.R., et al., *Matrix Crosslinking Forces Tumor Progression by Enhancing Integrin Signaling.* Cell, 2009. **139**(5): p. 891-906.
29. McConnell, J.C., et al., *Increased peri-ductal collagen micro-organization may contribute to raised mammographic density.* Breast Cancer Research, 2016. **18**(1): p. 5.
30. Provenzano, P.P., et al., *Collagen density promotes mammary tumor initiation and progression.* BMC medicine, 2008. **6**: p. 11-11.
31. Mouw, J.K., et al., *Tissue mechanics modulate microRNA-dependent PTEN expression to regulate malignant progression.* Nature Medicine, 2014. **20**(4): p. 360-367.
32. Stowers, R.S., et al., *Matrix stiffness induces a tumorigenic phenotype in mammary epithelium through changes in chromatin accessibility.* Nature Biomedical Engineering, 2019.
33. Le, L.T.-N., et al., *Loss of miR-203 regulates cell shape and matrix adhesion through ROBO1/Rac/FAK in response to stiffness.* Journal of Cell Biology, 2016. **212**(6): p. 707-719.
34. Northey, J.J., et al., *Stiff stroma increases breast cancer risk by inducing the oncogene ZNF217.* The Journal of Clinical Investigation, 2020.
35. Wei, S.C., et al., *Matrix stiffness drives epithelial-mesenchymal transition and tumour metastasis through a TWIST1-G3BP2 mechanotransduction pathway.* Nature cell biology, 2015. **17**(5): p. 678-688.
36. Carey, S., K. E. Martin, and C. Reinhart-King, *Three-dimensional collagen matrix induces a mechanosensitive invasive epithelial phenotype*. Vol. 7. 2017. 42088.
37. Cavo, M., et al., *A new cell-laden 3D Alginate-Matrigel hydrogel resembles human breast cancer cell malignant morphology, spread and invasion capability observed "in vivo".* Scientific Reports, 2018. **8**(1): p. 5333.
38. Chaudhuri, O., et al., *Extracellular matrix stiffness and composition jointly regulate the induction of malignant phenotypes in mammary epithelium.* Nature Materials, 2014. **13**: p. 970.
39. Provenzano, P.P., et al., *Matrix density-induced mechanoregulation of breast cell phenotype, signaling and gene expression through a FAK–ERK linkage.* Oncogene, 2009. **28**: p. 4326.
40. Wood, A.M., et al., *Chapter 4 - Three-dimensional breast culture models: New culture models for analyzing breast development and function*, in *Organs and Organoids*, J.A. Davies and M.L. Lawrence, Editors. 2018, Academic Press. p. 73-88.
41. Anguiano, M., et al., *The use of mixed collagen-Matrigel matrices of increasing complexity recapitulates the biphasic role of cell adhesion in cancer cell migration: ECM sensing, remodeling and forces at the leading edge of cancer invasion.* PLOS ONE, 2020. **15**(1): p. e0220019.
42. Wozniak, M.A., et al., *ROCK-generated contractility regulates breast epithelial cell differentiation in response to the physical properties of a three-dimensional collagen matrix.* The Journal of Cell Biology, 2003. **163**(3): p. 583.
43. Doyle, A.D., et al., *Local 3D matrix microenvironment regulates cell migration through spatiotemporal dynamics of contractility-dependent adhesions.* Nature communications, 2015. **6**: p. 8720-8720.
44. Erikson, A., et al., *Physical and chemical modifications of collagen gels: Impact on diffusion.* Biopolymers, 2008. **89**(2): p. 135-143.
45. Taufalele, P.V., et al., *Fiber alignment drives changes in architectural and mechanical features in collagen matrices.* PLOS ONE, 2019. **14**(5): p. e0216537.
46. Aisenbrey, E.A. and W.L. Murphy, *Synthetic alternatives to Matrigel.* Nature Reviews Materials, 2020. **5**(7): p. 539-551.
47. Antoine, E.E., P.P. Vlachos, and M.N. Rylander, *Review of collagen I hydrogels for bioengineered tissue microenvironments: characterization of mechanics, structure, and transport.* Tissue engineering. Part B, Reviews, 2014. **20**(6): p. 683-696.

48. Caliari, S.R. and J.A. Burdick, *A practical guide to hydrogels for cell culture.* Nature Methods, 2016. **13**: p. 405.
49. Cruz-Acuña, R. and A.J. García, *Synthetic hydrogels mimicking basement membrane matrices to promote cell-matrix interactions.* Matrix Biology, 2017. **57-58**: p. 324-333.
50. Hughes, C.S., L.M. Postovit, and G.A. Lajoie, *Matrigel: A complex protein mixture required for optimal growth of cell culture.* PROTEOMICS, 2010. **10**(9): p. 1886-1890.
51. Gjorevski, N. and M.P. Lutolf, *Synthesis and characterization of well-defined hydrogel matrices and their application to intestinal stem cell and organoid culture.* Nature Protocols, 2017. **12**: p. 2263.
52. Jang, M., et al., *A feeder-free, defined three-dimensional polyethylene glycol-based extracellular matrix niche for culture of human embryonic stem cells.* Biomaterials, 2013. **34**(14): p. 3571-3580.
53. Leach, J.B. and C.E. Schmidt, *Characterization of protein release from photocrosslinkable hyaluronic acid-polyethylene glycol hydrogel tissue engineering scaffolds.* Biomaterials, 2005. **26**(2): p. 125-135.
54. Li, X., et al., *Functional Hydrogels With Tunable Structures and Properties for Tissue Engineering Applications.* Frontiers in Chemistry, 2018. **6**(499).
55. Norris, S.C.P., et al., *Photodegradable Polyacrylamide Gels for Dynamic Control of Cell Functions.* ACS Applied Materials & Interfaces, 2021. **13**(5): p. 5929-5944.
56. Peyton, S.R., et al., *The use of poly(ethylene glycol) hydrogels to investigate the impact of ECM chemistry and mechanics on smooth muscle cells.* Biomaterials, 2006. **27**(28): p. 4881-4893.
57. Previtera, M.L. and N.A. Langrana, *Preparation of DNA-crosslinked polyacrylamide hydrogels.* Journal of visualized experiments : JoVE, 2014(90): p. 51323.
58. Kandow, C.E., et al., *Polyacrylamide Hydrogels for Cell Mechanics: Steps Toward Optimization and Alternative Uses*, in *Methods in Cell Biology*. 2007, Academic Press. p. 29-46.
59. Zhu, J. and R.E. Marchant, *Design properties of hydrogel tissue-engineering scaffolds.* Expert review of medical devices, 2011. **8**(5): p. 607-626.
60. Ashworth, J.C., et al., *Peptide gels of fully-defined composition and mechanics for probing cell-cell and cell-matrix interactions in vitro.* Matrix Biology, 2019.
61. Black, K.A., et al., *Biocompatibility and characterization of a peptide amphiphile hydrogel for applications in peripheral nerve regeneration.* Tissue engineering. Part A, 2015. **21**(7-8): p. 1333-1342.
62. Faroni, A., et al., *Self-Assembling Peptide Hydrogel Matrices Improve the Neurotrophic Potential of Human Adipose-Derived Stem Cells.* Advanced Healthcare Materials, 2019. **8**(17): p. 1900410.
63. Gough, J.E.a.S.A.a.M.A.F., *Peptide hydrogels: mimicking the extracellular matrix.* Bioinspired, Biomimetic and Nanobiomaterials, 2012. **1**(1): p. 4-12.
64. Ligorio, C., et al., *Graphene oxide containing self-assembling peptide hybrid hydrogels as a potential 3D injectable cell delivery platform for intervertebral disc repair applications.* Acta Biomaterialia, 2019. **92**: p. 92-103.
65. Aggeli, A., et al., *Responsive gels formed by the spontaneous self-assembly of peptides into polymeric β-sheet tapes.* Nature, 1997. **386**(6622): p. 259-262.
66. Zhang, S., *Fabrication of novel biomaterials through molecular self-assembly.* Nature Biotechnology, 2003. **21**(10): p. 1171-1178.
67. Najafi, H., et al., *Recent advances in design and applications of biomimetic self-assembled peptide hydrogels for hard tissue regeneration.* Bio-Design and Manufacturing, 2021. **4**(4): p. 735-756.
68. Gao, J., et al., *Controlling Self-Assembling Peptide Hydrogel Properties through Network Topology.* Biomacromolecules, 2017. **18**(3): p. 826-834.
69. Li, J., et al., *Recent advances of self-assembling peptide-based hydrogels for biomedical applications.* Soft Matter, 2019. **15**(8): p. 1704-1715.
70. Fu, K., H. Wu, and Z. Su, *Self-assembling peptide-based hydrogels: Fabrication, properties, and applications.* Biotechnology Advances, 2021. **49**: p. 107752.
71. Yang, Z., H. Xu, and X. Zhao, *Designer Self-Assembling Peptide Hydrogels to Engineer 3D Cell Microenvironments for Cell Constructs Formation and Precise Oncology Remodeling in Ovarian Cancer.* Advanced Science, 2020. **7**(9): p. 1903718.
72. Maude, S., E. Ingham, and A. Aggeli, *Biomimetic self-assembling peptides as scaffolds for soft tissue engineering.* Nanomedicine, 2013. **8**(5): p. 823-847.

73. Horii, A., et al., *Biological Designer Self-Assembling Peptide Nanofiber Scaffolds Significantly Enhance Osteoblast Proliferation, Differentiation and 3-D Migration.* PLOS ONE, 2007. **2**(2): p. e190.
74. Jia, P., et al., *The RGD-modified self-assembling D-form peptide hydrogel enhances the therapeutic effects of mesenchymal stem cells (MSC) for hindlimb ischemia by promoting angiogenesis.* Chemical Engineering Journal, 2022. **450**: p. 138004.
75. Burgess, K.A., et al., *Functionalised peptide hydrogel for the delivery of cardiac progenitor cells.* Materials Science and Engineering: C, 2021. **119**: p. 111539.
76. Castillo Diaz, L.A., et al., *Osteogenic differentiation of human mesenchymal stem cells promotes mineralization within a biodegradable peptide hydrogel.* Journal of Tissue Engineering, 2016. **7**: p. 2041731416649789.
77. Clough, H.C., et al., *Neutrally charged self-assembling peptide hydrogel recapitulates in vitro mechanisms of breast cancer progression.* Materials Science and Engineering: C, 2021. **127**: p. 112200.
78. Hainline, K.M., et al., *Self-Assembling Peptide Gels for 3D Prostate Cancer Spheroid Culture.* Macromolecular Bioscience, 2019. **19**(1): p. 1800249.
79. Lachowski, D., et al., *Self-Assembling Polypeptide Hydrogels as a Platform to Recapitulate the Tumor Microenvironment.* Cancers, 2021. **13**(13).
80. Tyanova, S., T. Temu, and J. Cox, *The MaxQuant computational platform for mass spectrometry-based shotgun proteomics.* Nature Protocols, 2016. **11**(12): p. 2301-2319.
81. UniProt, C., *UniProt: the universal protein knowledgebase in 2021.* Nucleic acids research, 2021. **49**(D1): p. D480-D489.
82. Shao, X., et al., *MatrisomeDB: the ECM-protein knowledge database.* Nucleic Acids Research, 2020. **48**(D1): p. D1136-D1144.
83. Goeminne, L.E., K. Gevaert, and L. Clement, *Peptide-level Robust Ridge Regression Improves Estimation, Sensitivity, and Specificity in Data-dependent Quantitative Label-free Shotgun Proteomics.* Molecular & Cellular Proteomics, 2016. **15**(2): p. 657-668.
84. Wu, T., et al., *clusterProfiler 4.0: A universal enrichment tool for interpreting omics data.* The Innovation, 2021. **2**(3): p. 100141.
85. Yu, G. and Q.-Y. He, *ReactomePA: an R/Bioconductor package for reactome pathway analysis and visualization.* Molecular BioSystems, 2016. **12**(2): p. 477-479.
86. Sodunke, T.R., et al., *Micropatterns of Matrigel for three-dimensional epithelial cultures.* Biomaterials, 2007. **28**(27): p. 4006-4016.
87. Murtagh, J., et al., *Organization of mammary epithelial cells into 3D acinar structures requires glucocorticoid and JNK signaling.* The Journal of cell biology, 2004. **166**(1): p. 133-143.
88. Debnath, J., S.K. Muthuswamy, and J.S. Brugge, *Morphogenesis and oncogenesis of MCF-10A mammary epithelial acini grown in three-dimensional basement membrane cultures.* Methods, 2003. **30**(3): p. 256-268.
89. Raphael, B., et al., *3D cell bioprinting of self-assembling peptide-based hydrogels.* Materials Letters, 2017. **190**: p. 103-106.
90. Imere, A., et al., *Engineering a cell-hydrogel-fibre composite to mimic the structure and function of the tendon synovial sheath.* Acta Biomaterialia, 2021. **119**: p. 140-154.
91. Debnath, J., et al., *The Role of Apoptosis in Creating and Maintaining Luminal Space within Normal and Oncogene-Expressing Mammary Acini.* Cell, 2002. **111**(1): p. 29-40.
92. Tang, J., et al., *Phenotypic transition maps of 3D breast acini obtained by imaging-guided agent-based modeling.* Integrative biology : quantitative biosciences from nano to macro, 2011. **3**(4): p. 408-421.
93. Ween, M.P., M.K. Oehler, and C. Ricciardelli, *Transforming Growth Factor-Beta-Induced Protein (TGFBI)/(βig-H3): A Matrix Protein with Dual Functions in Ovarian Cancer.* International Journal of Molecular Sciences, 2012. **13**(8): p. 10461-10477.
94. Durán-Jara, E., T. Vera-Tobar, and L.D. Lobos-González, *Lactadherin: From a Well-Known Breast Tumor Marker to a Possible Player in Extracellular Vesicle-Mediated Cancer Progression.* International Journal of Molecular Sciences, 2022. **23**(7).
95. Douglass, S., A. Goyal, and R.V. Iozzo, *The role of perlecan and endorepellin in the control of tumor angiogenesis and endothelial cell autophagy.* Connective Tissue Research, 2015. **56**(5): p. 381-391.
96. Neill, T., L. Schaefer, and R.V. Iozzo, *Decorin: A Guardian from the Matrix.* The American Journal of Pathology, 2012. **181**(2): p. 380-387.
97. Elfenbein, A. and M. Simons, *Syndecan-4 signaling at a glance.* Journal of Cell Science, 2013. **126**(17): p. 3799-3804.

98. Chen, C.S., *Mechanotransduction – a field pulling together?* Journal of Cell Science, 2008. **121**(20): p. 3285-3292.
99. BioGEL, M. *PeptiGels for 2D and 3D Cell Culture*. 2021 [cited 06/03/2022]; Available from: https://manchesterbiogel.com/products/peptigels.
100. Alcaraz, J., et al., *Laminin and biomimetic extracellular elasticity enhance functional differentiation in mammary epithelia.* The EMBO journal, 2008. **27**(21): p. 2829-2838.
101. Wozniak, M.A. and P.J. Keely, *Use of three-dimensional collagen gels to study mechanotransduction in T47D breast epithelial cells.* Biological procedures online, 2005. **7**: p. 144-161.
102. Williams, C.M., et al., *Fibronectin expression modulates mammary epithelial cell proliferation during acinar differentiation.* Cancer research, 2008. **68**(9): p. 3185-3192.
103. Magdaleno, C., et al., *Fibronectin assembly regulates lumen formation in breast acini.* Journal of Cellular Biochemistry, 2021. **122**(5): p. 524-537.
104. Gaiko-Shcherbak, A., et al., *The Acinar Cage: Basement Membranes Determine Molecule Exchange and Mechanical Stability of Human Breast Cell Acini.* PLOS ONE, 2015. **10**(12): p. e0145174.
105. Corning. *Corning® Matrigel® Matrix: Frequently Asked Questions*. [PDF] 2021 [cited 20/02/2022]; Available from: https://www.corning.com/catalog/cls/documents/faqs/CLS-DL-CC-026.pdf.
106. Box, J.K., et al., *Nucleophosmin: from structure and function to disease development.* BMC Molecular Biology, 2016. **17**(1): p. 19.
107. Peuhu, E., et al., *Epithelial vimentin plays a functional role in mammary gland development.* Development, 2017. **144**(22): p. 4103-4113.
108. Ray, P.D., B.-W. Huang, and Y. Tsuji, *Reactive oxygen species (ROS) homeostasis and redox regulation in cellular signaling.* Cellular Signalling, 2012. **24**(5): p. 981-990.
109. Kozlowski, M.T., C.J. Crook, and H.T. Ku, *Towards organoid culture without Matrigel.* Communications Biology, 2021. **4**(1): p. 1387.
110. Soofi, S.S., et al., *The elastic modulus of Matrigel™ as determined by atomic force microscopy.* Journal of Structural Biology, 2009. **167**(3): p. 216-219.
111. Vukicevic, S., et al., *Identification of multiple active growth factors in basement membrane matrigel suggests caution in interpretation of cellular activity related to extracellular matrix components.* Experimental Cell Research, 1992. **202**(1): p. 1-8.
112. Besser, R.R., et al., *Enzymatically crosslinked gelatin–laminin hydrogels for applications in neuromuscular tissue engineering.* Biomaterials Science, 2020. **8**(2): p. 591-606.
113. Boothroyd, S., A.F. Miller, and A. Saiani, *From fibres to networks using self-assembling peptides.* Faraday Discussions, 2013. **166**(0): p. 195-207.
114. Koch, F., et al., *Mechanical characteristics of beta sheet-forming peptide hydrogels are dependent on peptide sequence, concentration and buffer composition.* Royal Society Open Science, 2018. **5**(3): p. 171562.
115. Tian, A., J. Muffat, and Y. Li, *Studying Human Neurodevelopment and Diseases Using 3D Brain Organoids.* The Journal of Neuroscience, 2020. **40**(6): p. 1186.
116. Imbalzano, K.M., et al., *Increasingly transformed MCF-10A cells have a progressively tumor-like phenotype in three-dimensional basement membrane culture.* Cancer Cell International, 2009. **9**(1): p. 7.
117. Slater, K., Partridge, J. and Nandivada, H. , *Tuning the Elastic Moduli of Corning® Matrigel®and Collagen I 3D Matrices by Varying the Protein Concentration*, in *Corning Application Note*. 2018.
118. Caplan, M.R., et al., *Self-Assembly of a β-Sheet Protein Governed by Relief of Electrostatic Repulsion Relative to van der Waals Attraction.* Biomacromolecules, 2000. **1**(4): p. 627-631.
119. Zhuang, Z., et al., *Control of Matrix Stiffness Using Methacrylate–Gelatin Hydrogels for a Macrophage-Mediated Inflammatory Response.* ACS Biomaterials Science & Engineering, 2020. **6**(5): p. 3091-3102.
120. Yao, D., et al., *Matrix stiffness regulates bone repair by modulating 12-lipoxygenase-mediated early inflammation.* Materials Science and Engineering: C, 2021. **128**: p. 112359.
121. Johnson, L.A., et al., *Matrix Stiffness Corresponding to Strictured Bowel Induces a Fibrogenic Response in Human Colonic Fibroblasts.* Inflammatory Bowel Diseases, 2013. **19**(5): p. 891-903.
122. Mambetsariev, I., et al., *Stiffness-Activated GEF-H1 Expression Exacerbates LPS-Induced Lung Inflammation.* PLOS ONE, 2014. **9**(4): p. e92670.

123. Goff, S.L. and D.N. Danforth, *The Role of Immune Cells in Breast Tissue and Immunotherapy for the Treatment of Breast Cancer.* Clinical breast cancer, 2021. **21**(1): p. e63-e73.
124. Schwertfeger, K.L., et al., *Hyaluronan, Inflammation, and Breast Cancer Progression.* Frontiers in Immunology, 2015. **6**.
125. Zhao, H., et al., *Inflammation and tumor progression: signaling pathways and targeted intervention.* Signal Transduction and Targeted Therapy, 2021. **6**(1): p. 263.
126. Lang, J., et al., *Investigating the Effect of Substrate Stiffness on the Redox State of Cardiac Fibroblasts Using Scanning Electrochemical Microscopy.* Analytical Chemistry, 2021. **93**(14): p. 5797-5804.
127. Wang, B., et al., *Mechanosensitive Ion Channel Piezo1 Activated by Matrix Stiffness Regulates Oxidative Stress-Induced Senescence and Apoptosis in Human Intervertebral Disc Degeneration.* Oxidative Medicine and Cellular Longevity, 2021. **2021**: p. 8884922.
128. Hecht, F., et al., *The role of oxidative stress on breast cancer development and therapy.* Tumor Biology, 2016. **37**(4): p. 4281-4291.
129. Sosa, V., et al., *Oxidative stress and cancer: An overview.* Ageing Research Reviews, 2013. **12**(1): p. 376-390.
130. Valko, M., et al., *Free radicals, metals and antioxidants in oxidative stress-induced cancer.* Chemico-Biological Interactions, 2006. **160**(1): p. 1-40.
131. Shaw, K.R.M., C.N. Wrobel, and J.S. Brugge, *Use of Three-Dimensional Basement Membrane Cultures to Model Oncogene-Induced Changes in Mammary Epithelial Morphogenesis.* Journal of Mammary Gland Biology and Neoplasia, 2004. **9**(4): p. 297-310.
132. Rudra, J.S., et al., *Modulating Adaptive Immune Responses to Peptide Self-Assemblies.* ACS Nano, 2012. **6**(2): p. 1557-1564.
133. Wen, Y., et al., *Switching the Immunogenicity of Peptide Assemblies Using Surface Properties.* ACS Nano, 2016. **10**(10): p. 9274-9286.
134. Wu, X., et al., *Immune Enhancement by the Tetra-Peptide Hydrogel as a Promising Adjuvant for an H7N9 Vaccine against Highly Pathogenic H7N9 Virus.* Vaccines, 2022. **10**(1): p. 130.
135. Chen, G.-f., et al., *Amyloid beta: structure, biology and structure-based therapeutic development.* Acta Pharmacologica Sinica, 2017. **38**(9): p. 1205-1235.
136. Kolev, M.V., et al., *Implication of complement system and its regulators in Alzheimer's disease.* Current neuropharmacology, 2009. **7**(1): p. 1-8.
137. Cheignon, C., et al., *Oxidative stress and the amyloid beta peptide in Alzheimer's disease.* Redox Biology, 2018. **14**: p. 450-464.
138. Gustot, A., et al., *Amyloid fibrils are the molecular trigger of inflammation in Parkinson's disease.* Biochemical Journal, 2015. **471**(3): p. 323-333.
139. Leight, J.L., et al., *Matrix rigidity regulates a switch between TGF-β1–induced apoptosis and epithelial–mesenchymal transition.* Molecular Biology of the Cell, 2012. **23**(5): p. 781-791.
140. Miroshnikova, Y.A., et al., *Engineering strategies to recapitulate epithelial morphogenesis within synthetic three-dimensional extracellular matrix with tunable mechanical properties.* Physical biology, 2011. **8**(2): p. 026013-026013.
141. Lu, Y.-C., W.-C. Weng, and H. Lee, *Functional Roles of Calreticulin in Cancer Biology.* BioMed Research International, 2015. **2015**: p. 526524.
142. Zamanian, M., et al., *Calreticulin mediates an invasive breast cancer phenotype through the transcriptional dysregulation of p53 and MAPK pathways.* Cancer Cell International, 2016. **16**(1): p. 56.
143. Chien, Y. and M.A. White, *RAL GTPases are linchpin modulators of human tumour-cell proliferation and survival.* EMBO reports, 2003. **4**(8): p. 800-806.
144. Wang, X., et al., *Vimentin plays an important role in the promotion of breast cancer cell migration and invasion by leucine aminopeptidase 3.* Cytotechnology, 2020. **72**(5): p. 639-647.
145. Ghoroghi, S., et al., *Ral GTPases promote breast cancer metastasis by controlling biogenesis and organ targeting of exosomes.* eLife, 2021. **10**: p. e61539.
146. Ehrbar, M., et al., *Elucidating the role of matrix stiffness in 3D cell migration and remodeling.* Biophysical journal, 2011. **100**(2): p. 284-293.
147. Wisdom, K.M., et al., *Matrix mechanical plasticity regulates cancer cell migration through confining microenvironments.* Nature Communications, 2018. **9**(1): p. 4144.
148. Baker, E.L., R.T. Bonnecaze, and M.H. Zaman, *Extracellular matrix stiffness and architecture govern intracellular rheology in cancer.* Biophysical journal, 2009. **97**(4): p. 1013-1021.

149. Rousselle, P. and J.Y. Scoazec, *Laminin 332 in cancer: When the extracellular matrix turns signals from cell anchorage to cell movement.* Seminars in Cancer Biology, 2020. **62**: p. 149-165.
150. Wu, X., et al., *Visualization of basement membranes in normal breast and breast cancer tissues using multiphoton microscopy.* Oncol Lett, 2016. **11**(6): p. 3785-3789.
151. Katayama, M. and K. Sekiguchi, *Laminin-5 in Epithelial Tumour Invasion.* Journal of Molecular Histology, 2004. **35**(3): p. 277-286.
152. Wiseman, B.S. and Z. Werb, *Stromal Effects on Mammary Gland Development and Breast Cancer.* Science, 2002. **296**(5570): p. 1046-1049.
153. Chang, J. and O. Chaudhuri, *Beyond proteases: Basement membrane mechanics and cancer invasion.* Journal of Cell Biology, 2019. **218**(8): p. 2456-2469.
154. Li, C.L., et al., *Fibronectin induces epithelial-mesenchymal transition in human breast cancer MCF-7 cells via activation of calpain.* Oncol Lett, 2017. **13**(5): p. 3889-3895.
155. Viguier, M., et al., *Galectins in epithelial functions.* Tissue Barriers, 2014. **2**(3): p. e29103.
156. Cardoso, A.C.F., et al., *Galectin-3 Determines Tumor Cell Adaptive Strategies in Stressed Tumor Microenvironments.* Frontiers in Oncology, 2016. **6**.
157. Butcher, D.T., T. Alliston, and V.M. Weaver, *A tense situation: forcing tumour progression.* Nature Reviews Cancer, 2009. **9**: p. 108.
158. Cheng, Q., et al., *Stiffness of the microenvironment upregulates ERBB2 expression in 3D cultures of MCF10A within the range of mammographic density.* Scientific Reports, 2016. **6**(1): p. 28987.
159. Cox, T.R. and J.T. Erler, *Remodeling and homeostasis of the extracellular matrix: implications for fibrotic diseases and cancer.* Disease models & mechanisms, 2011. **4**(2): p. 165-178.
160. McKnight, A.L., et al., *MR Elastography of Breast Cancer: Preliminary Results.* American Journal of Roentgenology, 2002. **178**(6): p. 1411-1417.
161. Lopez, J.I., et al., *In situ force mapping of mammary gland transformation.* Integrative biology : quantitative biosciences from nano to macro, 2011. **3**(9): p. 910-921.
162. Lance, A., et al., *Increased extracellular matrix density decreases MCF10A breast cell acinus formation in 3D culture conditions.* Journal of Tissue Engineering and Regenerative Medicine, 2016. **10**(1): p. 71-80.
163. Gudjonsson, T., et al., *Normal and tumor-derived myoepithelial cells differ in their ability to interact with luminal breast epithelial cells for polarity and basement membrane deposition.* Journal of cell science, 2002. **115**(Pt 1): p. 39-50.
164. Streuli, C.H., et al., *Laminin mediates tissue-specific gene expression in mammary epithelia.* The Journal of cell biology, 1995. **129**(3): p. 591-603.
165. Ekblom, P., P. Lonai, and J.F. Talts, *Expression and biological role of laminin-1.* Matrix Biology, 2003. **22**(1): p. 35-47.
166. Genové, E., et al., *Functionalized self-assembling peptide hydrogel enhance maintenance of hepatocyte activity in vitro.* Journal of Cellular and Molecular Medicine, 2009. **13**(9b): p. 3387-3397.
167. Galler, K.M., et al., *Self-assembling multidomain peptide hydrogels: designed susceptibility to enzymatic cleavage allows enhanced cell migration and spreading.* Journal of the American Chemical Society, 2010. **132**(9): p. 3217-3223.
168. Gandellini, P., et al., *miR-205 regulates basement membrane deposition in human prostate: implications for cancer development.* Cell Death & Differentiation, 2012. **19**(11): p. 1750-1760.
169. Rousselle, P. and K. Beck, *Laminin 332 processing impacts cellular behavior.* Cell Adhesion & Migration, 2013. **7**(1): p. 122-134.
170. Parry, G., et al., *Collagenous substrata regulate the nature and distribution of glycosaminoglycans produced by differentiated cultures of mouse mammary epithelial cells.* Experimental Cell Research, 1985. **156**(2): p. 487-499.
171. Basham, K.J., et al., *Chemical Genetic Screen Reveals a Role for Desmosomal Adhesion in Mammary Branching Morphogenesis* Journal of Biological Chemistry, 2013. **288**(4): p. 2261-2270.
172. Bhat, R., et al., *Nuclear repartitioning of galectin-1 by an extracellular glycan switch regulates mammary morphogenesis.* Proceedings of the National Academy of Sciences, 2016. **113**(33): p. E4820-E4827.
173. Zhang, M., et al., *Annexin A2 positively regulates milk synthesis and proliferation of bovine mammary epithelial cells through the mTOR signaling pathway.* Journal of Cellular Physiology, 2018. **233**(3): p. 2464-2475.

174. Schwartz-Albiez, R., et al., *Differential expression of annexins I and II in normal and malignant human mammary epithelial cells.* Differentiation, 1993. **52**(3): p. 229-237.

Supplementary information: Mammary epithelial organoids cultured in a self-assembling peptide hydrogel exhibit stiffness-induced remodelling

Protein names	Gene names	Intensity
Annexin A2	ANXA2	7996900000
Fibronectin	FN1	5068400000
Alpha-2-macroglobulin	A2M	4344900000
Serpin B5	SERPINB5	2104400000
Protein S100-A8	S100A8	1852300000
Annexin A1	ANXA1	1299500000
Pregnancy zone protein	PZP	1228900000
Alpha-1-antitrypsin	SERPINA1	888100000
Galectin-1	LGALS1	735720000
Laminin subunit beta-3	LAMB3	715620000
Antithrombin-III	SERPINC1	649170000
Protein S100-A9	S100A9	630280000
Protein S100	S100A6	622810000
Laminin subunit alpha-3	LAMA3	540590000
Macrophage migration inhibitory factor	MIF	474590000
Transforming growth factor-beta-induced protein ig-h3	TGFBI	361520000
Desmoplakin	DSP	349940000
Laminin subunit gamma-2	LAMC2	339300000
Inter-alpha-trypsin inhibitor heavy chain H2	ITIH2	300810000
Cathepsin D	CTSD	297350000
Inter-alpha-trypsin inhibitor heavy chain H4	ITIH4	246970000
Heparin cofactor 2	SERPIND1	222870000
Syndecan-1	SDC1	175100000
Annexin A5	ANXA5	151500000
Syndecan-4	SDC4	148510000
Vitronectin	VTN	112140000
Protein S100-A10	S100A10	111110000
Annexin A3	ANXA3	105280000
Protein S100-A16	S100A16	94774000
Serpin H1	SERPINH1	87870000
Annexin A4	ANXA4	84383000
Annexin	ANXA8	79801000
Plasminogen	PLG	76511000
Serpin B6	SERPINB6	69141000
Protein S100-A2	S100A2	63259000
Dipeptidyl peptidase 1	CTSC	57933000
Lactadherin	MFGE8	57284000
Galectin-3	LGALS3	53600000
Cathepsin B	CTSB	51104000
Thrombospondin-1	THBS1	48759000
Laminin subunit gamma-1	LAMC1	47088000
Endorepellin	HSPG2	40696000
Agrin	AGRN	37097000
Protein S100-A14	S100A14	34488000
Plasma protease C1 inhibitor	SERPING1	28501000
Annexin A11	ANXA11	26317000
Serpin B4	SERPINB4	20854000
Decorin	DCN	19804000
Mucin-1	MUC1	15309000
Collagen alpha-1(XVII) chain	COL17A1	14685000
Annexin A7	ANXA7	14188000
Protein S100-A7A	S100A7A	12051000
Adiponectin	ADIPOQ	10584000
Protein S100-P	S100P	8675300

Table S1. MCF10a cells encapsulated in Alpha4 gels express multiple matrix and matrix-associated proteins. List of matrix and matrix-associated proteins synthesised by 7-day old MCF10a cells encapsulated in Alpha4 hydrogels (seeding density was 2.5 x 10^5 cells per mL) and their intensities. Proteins are listed in descending order of peptide intensity.

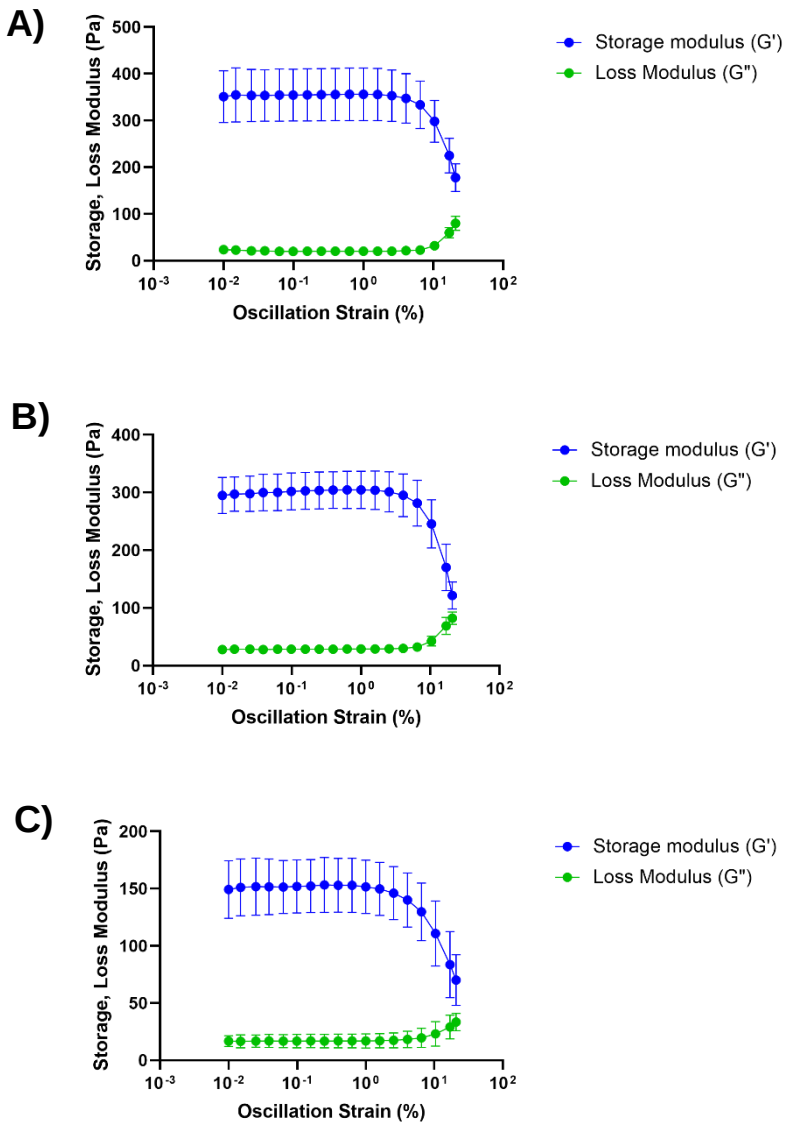

Fig. S1. Diluted Alpha4 hydrogels are elastic. A) Storage and loss moduli at 1 Hz of 90% (v/) Alpha4 hydrogels diluted with PBS. B) Storage and loss moduli at 1 Hz of 75% (v/) Alpha4 hydrogels diluted with PBS. C) Storage and loss moduli at 1 Hz of 50% (v/) Alpha4 hydrogels diluted with PBS. Data are shown as mean ± SD. All measurements were performed at least three times, but underloading of three 90% (v/v) Alpha4 samples led to their exclusion from analysis.

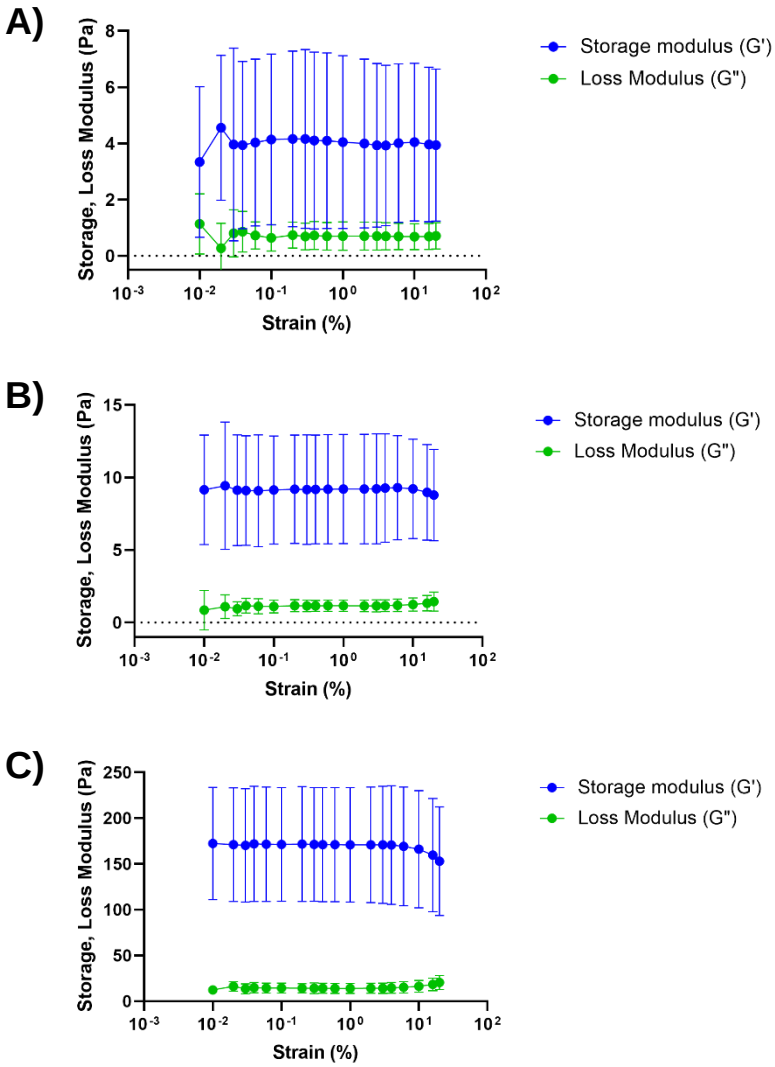

Fig. S2. Soft Matrigel-alginate gels are almost viscous. A) Storage and loss moduli at 1 Hz of Matrigel-alginate gels stiffened with 0 mM calcium sulphate ($CaSO_4$). B) Storage and loss moduli at 1 Hz of Matrigel-alginate gels stiffened with 2.4 mM calcium sulphate ($CaSO_4$). C) Storage and loss moduli at 1 Hz of Matrigel-alginate gels stiffened with 24 mM calcium sulphate ($CaSO_4$). Data are shown as mean ± SD. All measurements were performed at least three times, but underloading of five, 20 mM $CaSO_4$ Matrigel-alginate samples led to their exclusion from analysis.

Protein names	Gene names	Sample 1 Intensity	Sample 2 Intensity	Sample 3 Intensity
Alpha-1-antitrypsin	SERPINA1	10454000	9404300	4505800
Alpha-2-macroglobulin	A2M	10017000	3152300	5497600
Alpha-2-macroglobulin-like protein 1	A2ML1	110240	0	0
Annexin A1	ANXA1	422740	783680	73793
Annexin A2	ANXA2	5684400	3410800	1741200
Antithrombin-III	SERPINC1	1606000	2624700	1520900
Endorepellin	HSPG2	13126000	12013000	10747000
Carboxypeptidase	CTSA	159940	0	0
Cathepsin D	CTSD	1202300	382010	207990
Collagen alpha-1(IV) chain	Col4a1	1737100	1788800	229460
Collagen alpha-1(XVIII) chain	COL18A1	869100	671540	496760
Collagen alpha-2(IV) chain	COL4A2	1220600	1075900	466850
Complement C1q subcomponent subunit B	C1QB	0	138430	129270
Cystatin-A	CSTA	95770	0	0
Cystatin-B	CSTB	356450	0	0
Desmoplakin	DSP	20918000	15050000	12692000
Dipeptidyl peptidase 1	CTSC	75530	0	0
Fibrinogen beta chain	FGB	437320	297210	241640
Fibrinogen gamma chain	FGG	5439100	5084300	3419200
Fibronectin	FN1	1647700	1405700	1138000
Fibulin-1	FBLN1	214520	0	0
Galectin-3	LGALS3	351760	439110	252150
Galectin-7	LGALS7	288470	161720	92293
Heparin cofactor 2	SERPIND1	669530	495700	246190
Inter-alpha-trypsin inhibitor heavy chain H1	ITIH1	780950	578460	377680
Laminin subunit alpha-1	LAMA1	36936000	50887000	26038000
Laminin subunit alpha-3	LAMA3	442880	0	0
Laminin subunit alpha-5	LAMA5	112930	147550	99369
Laminin subunit beta-2	LAMB2	447870	703910	621020
Laminin subunit beta-3	LAMB3	278960	524880	233460
Laminin subunit gamma-1	LAMC1	82078000	78714000	58162000
Plasminogen	PLG	305610	592590	508220
Procollagen-lysine,2-oxoglutarate 5-dioxygenase 1	PLOD1	155160	144940	0
Procollagen-lysine,2-oxoglutarate 5-dioxygenase 2	PLOD2	393550	276470	196640
Protein S100-A11	S100A11	166050	0	0
Protein S100-A14	S100A14	381370	0	130510
Protein S100-A16	S100A16	0	574070	415810
Protein S100-A8	S100A8	1607600	427350	0
Protein S100-A9	S100A9	1198700	800500	103110
Protein-glutamine gamma-glutamyltransferase	TGM3	4243700	1108600	865730
Protein-glutamine gamma-glutamyltransferase K	TGM1	4678800	776640	419630
Serine protease HTRA1	HTRA1	485140	381140	207280
Serpin B12	SERPINB12	4850200	1989100	1678400
Serpin H1	SERPINH1	955640	808290	540280
Tubulointerstitial nephritis antigen-like	TINAGL1	0	0	326440

Table S2. Matrix proteins from Matrigel hydrogels can be detected during mass spectrometry analysis. List of matrix and matrix-associated proteins and their intensities detected in three cell-free, day 14 Matrigel lysates.

		Intensity								
		Stiff Alpha4 gels			Medium Alpha4 gels			Soft Alpha4 gels		
Protein names	**Gene names**	**Sample 1**	**Sample 2**	**Sample 3**	**Sample 1**	**Sample 2**	**Sample 3**	**Sample 1**	**Sample 2**	**Sample 3**
Adiponectin	ADIPOQ	1378900	1373200	1489600	6140500	2966600	24112000	0	0	16445000
Agrin	AGRN	8795500	0	0	0	0	0	0	0	0
Alpha-1-antitrypsin	SERPINA1	78895000	64912000	87691000	114280000	5250300	137510000	46091000	46861000	3281800
Alpha-2-macroglobulin	A2M	253270000	537380000	47775000	158130000	69720000	79327000	37844000	71377000	28892000
Alpha-2-macroglobulin-like protein 1	A2ML1	0	0	644410	0	0	0	0	0	0
Annexin A1	ANXA1	0	0	0	0	288400	0	0	154820	0
Annexin A2	ANXA2	1273100	1124200	410860	1925700	1344500	637400	1767800	1738400	1098900
Annexin A5	ANXA5	264470	176550	317900	4909000	2808200	0	0	0	0
Annexin A7	ANXA7	134530	0	0	0	0	437680	0	0	0
Antithrombin-III	SERPINC1	96799000	80219000	10858000	62748000	44675000	38131000	38992000	27167000	61926000
Endorepellin	HSPG2	0	66011	0	0	0	0	0	0	0
Carboxypeptidase	CTSA	0	0	0	598750	0	0	0	0	0
Cathepsin D	CTSD	0	0	0	0	0	0	196080	144900	0
Complement C1q subcomponent subunit B	C1QB	2300300	1758900	1915600	1980100	2196400	0	1550800	1989200	1867200
Cystatin-A	CSTA	0	0	0	0	296560	0	0	0	0
Desmoplakin	DSP	2094300	8697800	5968400	2343700	809280	2378700	6816800	4760700	2250700
Fibronectin	FN1	7762900	2971500	10853000	52964000	74091000	93725000	29571000	37492000	43300000
Galectin-3	LGALS3	0	0	152010	0	0	0	0	0	0
Galectin-7	LGALS7	0	306310	0	0	0	0	0	0	101120
Hemopexin	HPX	3635000	2600600	3873800	4716900	2622200	2731400	0	3572400	0
Heparin cofactor 2	SERPIND1	10598000	6282900	14414000	42242000	15719000	25099000	5134000	23107000	11688000
Insulin-like growth factor-binding protein complex acid labile subunit	IGFALS	543510	528050	532700	1866600	828820	936780	459020	822910	664440
Inter-alpha-trypsin inhibitor heavy chain H2	ITIH2	1673600	4544900	7822900	2871600	524350	3053400	8612400	15752000	18312000
Inter-alpha-trypsin inhibitor heavy chain H4	ITIH4	5522400	4528600	6378500	0	0	7921700	4928200	5713900	6753700
Laminin subunit alpha-1	LAMA1	790910	0	0	0	0	0	0	0	0
Laminin subunit alpha-3	LAMA3	1665800	1597000	1675300	6022800	5543300	5044800	2253900	4484800	3412000
Laminin subunit beta-3	LAMB3							0	1332000	0

Laminin subunit gamma-1	LAMC1	1005500	306740	205590	0	0	0	0	0	0
Laminin subunit gamma-2	LAMC2	2156000	190410	1888400	279980	1544800	2297000	1419400	3793500	3664600
Macrophage migration inhibitory factor	MIF	0	0	0	0	0	0	0	0	146640
Plasminogen	PLG	0	0	8387700	4596000	2278000	0	0	6455700	11879000
Pregnancy zone protein	PZP	140130000	143760000	128180000	0	218830000	201970000	88005000	232790000	191180000
Protein kinase C-binding protein NELL2	NELL2	0	686770	0	2804300	662140	1265500	252790	525390	493320
Protein S100-A10	S100A10	0	0	1243800	0	0	0	970570	0	765950
S100A11	Protein S100-A11	0	0	0	0	0	0	0	0	62910
S100A14	Protein S100-A14	0	0	0	0	0	0	117480	0	0
Protein S100-A7	S100A7;	0	0	0	915860	0	209520	0	0	0
Protein S100-A8	S100A8	57794	584550	0	0	127000	0	201610	531110	456020
Protein S100-A9	S100A9	0	612220	0	0	299330	0	108150	0	580110
Protein-glutamine gamma-glutamyltransferase E	TGM3	835960	0	0	0	0	0	0	0	0
Protein-glutamine gamma-glutamyltransferase K	TGM1	0	328680	0	0	0	0	1238400	179570	0
Prothrombin	F2	0	0	0	3177200	2918200	0	837400	1319500	710350
Serine protease HTRA1	HTRA1	4813200	5094600	5327400	0	0	3784000	2653900	5858300	5547400
Serpin B12	SERPINB12	360520	298110	449880	265810	0	0	893590	245400	161520
Serpin B13	SERPINB13	0	163140	159870	255130	170840	0	113210	0	216550
Serpin B8	SERPINB8	0	0	0	0	0	305630	0	0	0
Transforming growth factor-beta-induced protein ig-h3	TGFBI	0	0	0	3595600	367900	685950	296270	888300	848960
Vitronectin	VTN	0	251340	0	1270000	3053600	0	644240	1156800	857470

Table S3. Some matrix proteins detected in cell-free Alpha4 hydrogels may be contamination from Matrigel. List of matrix and matrix-associated proteins detected in cell-free, day 14 stiff, medium or soft Alpha4 lysates and their intensities. The hydrogels and their intensities are presented in the order that the lysates were run on the mass analyser. Three replicates were submitted for each Alpha4 gel type.

Protein names	Gene names	estimate	p-value
Elongation factor 1-gamma	EEF1G	-2.27044	8.95E-25
Clathrin heavy chain	CLTC	-4.52403	1.39E-23
Adenosylhomocysteinase	AHCY	0.996873	1.4E-13
Voltage-dependent anion-selective channel protein 3	VDAC3	-3.08601	2.23E-11
Calpain-1 catalytic subunit	CAPN1	-1.88112	4.29E-11
Transketolase	TKT	0.654572	8.45E-11
Leukotriene A-4 hydrolase	LTA4H	1.192299	9.81E-11
Voltage-dependent anion-selective channel protein 1	VDAC1	-1.10632	3.29E-10
60 kDa heat shock protein, mitochondrial	HSPD1	-2.09997	3.76E-10
Protein deglycase DJ-1	PARK7	1.262784	5.34E-10
Hexokinase-1	HK1	-1.40541	1.33E-09
Talin-1	TLN1	-2.45679	1.75E-09
Valine--tRNA ligase	VARS	-2.28169	1.41E-08
Inorganic pyrophosphatase	PPA1	1.585118	1.93E-08
Protein disulfide-isomerase A6	PDIA6	-1.14367	2.38E-08
10 kDa heat shock protein, mitochondrial	HSPE1	2.085992	2.54E-08
60S ribosomal protein L12	RPL12	-3.49734	4.46E-08
Keratin, type I cytoskeletal 18	KRT18	-3.86234	5.04E-08
Voltage-dependent anion-selective channel protein 2	VDAC2	-1.98564	1.16E-07
Ras GTPase-activating-like protein IQGAP1	IQGAP1	-2.72671	1.6E-07
Protein disulfide-isomerase A4	PDIA4	-2.93003	2.06E-07
Dihydrolipoyl dehydrogenase, mitochondrial	DLD	1.206648	3.08E-07
Interleukin enhancer-binding factor 3	ILF3	-2.64001	3.13E-07
Nidogen-1	Nid1	-6.21016	3.69E-07
Transmembrane protein 43	TMEM43	-2.07496	4.87E-07
Splicing factor, proline- and glutamine-rich	SFPQ	-1.50525	5.92E-07
Endoplasmic reticulum resident protein 44	ERP44	0.700911	6.15E-07
Poly(rC)-binding protein 1	PCBP1	-3.49736	6.18E-07
Pterin-4-alpha-carbinolamine dehydratase	PCBD1	1.781613	6.81E-07
L-lactate dehydrogenase A chain	LDHA	0.842134	6.84E-07
HLA class I histocompatibility antigen, alpha chain E	HLA-E	5.220839	7.56E-07
Erythrocyte band 7 integral membrane protein	STOM	-3.23885	7.71E-07
Spliceosome RNA helicase DDX39B	DDX39B	-1.7955	7.75E-07
Aspartate aminotransferase, mitochondrial	GOT2	1.069404	8.91E-07
Major vault protein	MVP	-2.16545	9.17E-07
ATP-dependent DNA helicase Q1	RECQL	-1.7264	2.97E-06
Nucleoside diphosphate kinase A	NME1	1.755306	3.37E-06
Complement C5	C5	4.024505	3.46E-06
Peptidyl-prolyl cis-trans isomerase FKBP1A	FKBP1A	1.206901	3.5E-06
Vimentin	VIM	-5.40455	4.52E-06
Protein deglycase DJ-1	PARK7	2.72052	4.53E-06
Exportin-2	CSE1L	-2.45793	4.74E-06
Large neutral amino acids transporter small subunit 1	SLC7A5	-2.56636	4.76E-06
UDP-glucose 6-dehydrogenase	UGDH	-1.21621	4.81E-06
Calreticulin	CALR	-2.42061	5.34E-06
Pre-mRNA-splicing factor 18	PRPF18	6.230912	5.49E-06

Integrin alpha-6	ITGA6	-2.49011	5.63E-06
Elongation factor Tu, mitochondrial	TUFM	-3.69371	5.77E-06
Myeloid-derived growth factor	MYDGF	1.544753	6.07E-06
Tubulin beta-4B chain	TUBB4B	-6.92447	7.32E-06
Structural maintenance of chromosomes protein 6	SMC6	5.278746	7.42E-06
Phosphatidylethanolamine-binding protein 1	PEBP1	1.285263	9.19E-06
Transmembrane emp24 domain-containing protein 9	TMED9	-0.70218	9.61E-06
Plectin	PLEC	-2.03067	1.03E-05
Kynureninase	KYNU	2.375832	1.31E-05
Chromatin modification-related protein MEAF6	MEAF6	4.554701	1.46E-05
Actin-related protein 2/3 complex subunit 2	ARPC2	0.890534	1.58E-05
Microtubule-associated protein	MAP4	1.650021	1.93E-05
DNA-dependent protein kinase catalytic subunit	PRKDC	-4.14982	1.98E-05
Peptidyl-prolyl cis-trans isomerase FKBP2	FKBP2	2.309859	1.99E-05
Protein LYRIC	MTDH	-1.92715	2.04E-05
Eukaryotic translation initiation factor 3 subunit F	EIF3F	-2.08792	2.05E-05
Alpha-actinin-4	ACTN4	-1.53655	2.38E-05
Galectin-3-binding protein	LGALS3BP	3.009062	2.46E-05
Putative elongation factor 1-alpha-like 3	EEF1A1P5	-4.95737	2.61E-05
Calpain small subunit 1	CAPNS1	-3.51466	3E-05
Ig gamma-3 chain C region	IGHG3	3.47832	3.6E-05
Endoplasmic reticulum-Golgi intermediate compartment protein 1	ERGIC1	-1.12655	4.72E-05
Calcyclin-binding protein	CACYBP	-0.5702	6.52E-05
Probable ATP-dependent RNA helicase DDX6	DDX6	-1.57768	6.97E-05
Cytoskeleton-associated protein 4	CKAP4	-1.17623	6.97E-05
Poly(ADP-ribose) glycohydrolase	PARG	1.805002	7.03E-05
Myosin-14	MYH14	-2.77819	8.62E-05
ADP-sugar pyrophosphatase	NUDT5	1.241162	8.86E-05
WD repeat-containing protein 1	WDR1	0.650531	9.16E-05
Electron transfer flavoprotein subunit beta	ETFB	0.752494	9.2E-05
Bifunctional glutamate/proline--tRNA ligase	EPRS	-2.09364	9.51E-05
Complement factor B	CFB	3.102579	9.87E-05
Actin-related protein 2/3 complex subunit 3	ARPC3	1.896739	0.000103
Small nuclear ribonucleoprotein Sm D3	SNRPD3	-3.4329	0.000105
40S ribosomal protein S20	RPS20	-2.88539	0.000112
Vacuolar protein sorting-associated protein 29	VPS29	1.268604	0.000116
40S ribosomal protein S16	RPS16	-2.01557	0.000135
Thioredoxin	TXN	0.939147	0.000138
Laminin subunit alpha-1	Lama1	-4.43132	0.000142
Golgin subfamily A member 1	GOLGA1	4.842776	0.000152
RNA-binding motif protein, X chromosome	RBMX	3.059115	0.000163
ATP synthase subunit gamma, mitochondrial	ATP5C1	-1.44236	0.00017
Ezrin	EZR	1.307193	0.000173
Nuclear transport factor 2	NUTF2	1.287502	0.000176
Glucosidase 2 subunit beta	PRKCSH	-3.17711	0.000182
Nascent polypeptide-associated complex subunit alpha	NACA	-3.86392	0.000192

Mitochondrial carrier homolog 2	MTCH2	-0.78916	0.000196
40S ribosomal protein S21	RPS21	0.781081	0.000204
60S ribosomal protein L15	RPL15	-3.84098	0.000207
Ubiquitin-conjugating enzyme E2 variant 1	UBE2V1	1.344942	0.000209
Ubiquitin carboxyl-terminal hydrolase	USP14	-1.76427	0.000211
Sialic acid synthase	NANS	0.440029	0.000213
10 kDa heat shock protein, mitochondrial	HSPE1	2.314722	0.000224
Transaldolase	TALDO1	1.488327	0.00023
Peroxiredoxin-1	PRDX1	0.977337	0.000242
CAD protein	CAD	1.18835	0.000244
Putative protein PTGES3L	PTGES3L	2.395194	0.000246
Histone H4	HIST1H4A	-1.33287	0.000261
Integrin beta-4	ITGB4	-1.92068	0.000262
Niban-like protein 1	FAM129B	-2.36849	0.000266
60S ribosomal protein L13	RPL13	-2.24126	0.000281
Catenin alpha-1	CTNNA1	-2.64343	0.000282
GRIP1-associated protein 1	GRIPAP1	1.692364	0.000297
Small nuclear ribonucleoprotein F	SNRPF	-2.37754	0.000328
Small nuclear ribonucleoprotein E	SNRPE	-2.41357	0.000332
Aldo-keto reductase family 1 member C3	AKR1C3	1.2557	0.000343
L-lactate dehydrogenase B chain	LDHB	0.731465	0.000346
Staphylococcal nuclease domain-containing protein 1	SND1	-1.47029	0.000352
Vesicular integral-membrane protein VIP36	LMAN2	1.275816	0.000363
T-complex protein 1 subunit alpha	TCP1	-1.42607	0.000365
Actin-related protein 2/3 complex subunit 4	ARPC4	0.716553	0.000373
Destrin	DSTN	1.498165	0.000403
26S protease regulatory subunit 6A	PSMC3	-1.75996	0.000443
ADP-sugar pyrophosphatase	NUDT5	1.394257	0.000444
Eukaryotic initiation factor 4A-I	EIF4A1	-2.81328	0.000444
Myosin-9	MYH9	-1.48888	0.000509
Omega-amidase NIT2	NIT2	0.738199	0.000523
Secretory carrier-associated membrane protein 1	SCAMP1	0.914186	0.000537
Histone deacetylase 1	HDAC1	-2.12435	0.000638
26S proteasome non-ATPase regulatory subunit 6	PSMD6	-2.05341	0.000667
Fumarylacetoacetase	FAH	1.238696	0.00068
Ras-related protein Rab-10	RAB10	0.928213	0.000703
Vesicle-associated membrane protein 8	VAMP8	2.038619	0.000743
Protein AHNAK2	AHNAK2	-0.90336	0.000745
Beta-hexosaminidase subunit beta	HEXB	0.871852	0.000746
Sodium/potassium-transporting ATPase subunit beta-3	ATP1B3	-1.73224	0.000765
Protein disulfide-isomerase A3	PDIA3	-1.38931	0.000841
Translocon-associated protein subunit gamma	SSR3	-1.23905	0.000921
RNA-binding motif protein, X chromosome	RBMX	-2.98875	0.000944
Protein RER1	RER1	-1.67501	0.000977
Non-specific lipid-transfer protein	SCP2	0.95019	0.000981
Probable aminopeptidase NPEPL1	NPEPL1	1.228865	0.001017

Vacuolar protein sorting-associated protein 26A	VPS26A	-1.75971	0.001061
Small ubiquitin-related modifier 2	SUMO2	2.838176	0.001087
Phosphoglycerate mutase 1	PGAM1	0.553503	0.001117
14-3-3 protein gamma	YWHAG	0.635475	0.001175
Vacuolar protein sorting-associated protein 35	VPS35	-1.5455	0.001186
Heat shock 70 kDa protein 4	HSPA4	0.92693	0.001189
PDZ and LIM domain protein 5	PDLIM5	-1.64737	0.001225
ATP-dependent 6-phosphofructokinase, platelet type	PFKP	-2.58975	0.00123
60S ribosomal protein L35a	RPL35A	-2.40508	0.001244
Importin-5	IPO5	-1.37646	0.001252
Glyoxylate reductase/hydroxypyruvate reductase	GRHPR	1.154002	0.001264
Syntaxin-7	STX7	0.842416	0.001267
Retinol-binding protein 4	RBP4	1.754962	0.001291
Thioredoxin domain-containing protein 5	TXNDC5	0.679627	0.001334
DnaJ homolog subfamily C member 5	DNAJC5	-1.90895	0.001343
Argininosuccinate synthase	ASS1	-1.34803	0.001347
Guanine nucleotide-binding protein G(i) subunit alpha-2	GNAI2	-1.051	0.0014
Asparagine--tRNA ligase, cytoplasmic	NARS	-0.57925	0.001437
SH3 domain-binding glutamic acid-rich-like protein 3	SH3BGRL3	4.15218	0.00147
Putative heat shock protein HSP 90-beta 2	HSP90AB2P	1.496286	0.001633
60S ribosomal protein L27	RPL27	-3.89692	0.001747
Laminin subunit beta-1	Lamb1	-3.1758	0.001829
ADP-ribosylation factor 4	ARF4	-3.85878	0.002192
40S ribosomal protein S8	RPS8	-1.83779	0.002239
Acylamino-acid-releasing enzyme	APEH	2.131241	0.002286
Hemoglobin subunit beta	HBB	3.676657	0.002357
SUN domain-containing protein 1	SUN1	-1.53822	0.002444
ATP synthase subunit a	MT-ATP6	-1.2194	0.002465
Peptidyl-prolyl cis-trans isomerase B	PPIB	0.556361	0.002482
Malate dehydrogenase, cytoplasmic	MDH1	0.604051	0.002701
Integrin alpha-V	ITGAV	1.324619	0.002703
40S ribosomal protein S20	RPS20	-2.83561	0.002885
Aspartate aminotransferase, cytoplasmic	GOT1	1.120905	0.002929
Mitochondrial 2-oxoglutarate/malate carrier protein	SLC25A11	-1.34102	0.003004
Gamma-glutamylcyclotransferase	GGCT	1.425884	0.003015
RNA-binding protein FUS	FUS	-1.78182	0.0031
60S ribosomal protein L38	RPL38	1.074388	0.003176
40S ribosomal protein S17	RPS17	1.974118	0.003249
Eukaryotic translation initiation factor 3 subunit L	EIF3L	-0.48737	0.003285
Peroxiredoxin-5, mitochondrial	PRDX5	0.879892	0.003378
Epididymal secretory protein E1	NPC2	1.54044	0.003541
Rab GDP dissociation inhibitor beta	GDI2	0.879793	0.003561
Type-1 angiotensin II receptor-associated protein	AGTRAP	-0.80374	0.003723
Aldo-keto reductase family 1 member C2	AKR1C2	1.680859	0.003738
60S ribosomal protein L34	RPL34	-2.28917	0.003799
78 kDa glucose-regulated protein	HSPA5	-0.56974	0.003833

LIM and SH3 domain protein 1	LASP1	0.974851	0.00403
Enoyl-CoA hydratase, mitochondrial	ECHS1	0.744468	0.004168
GTP-binding nuclear protein Ran	RAN	-0.9702	0.004209
Ribonuclease UK114	HRSP12	1.469942	0.004273
14-3-3 protein beta/alpha	YWHAB	0.705254	0.004339
Inositol monophosphatase 2	IMPA2	-1.21325	0.004861
Stonin-2	STON2	-2.74289	0.005067
Superoxide dismutase [Mn], mitochondrial	SOD2	1.730965	0.00508
Up-regulated during skeletal muscle growth protein 5	USMG5	1.925928	0.0053
ATP synthase subunit alpha, mitochondrial	ATP5A1	-0.78338	0.005369
Heterogeneous nuclear ribonucleoprotein A1	HNRNPA1	-0.7076	0.005411
Transmembrane emp24 domain-containing protein 10	TMED10	-1.51595	0.005509
Lysine--tRNA ligase	KARS	-1.15518	0.005769
Ras-related C3 botulinum toxin substrate 2	RAC2	-1.01403	0.005999
Amine oxidase [flavin-containing] A	MAOA	-1.21563	0.006138
T-complex protein 1 subunit alpha	TCP1	-0.75726	0.006156
Cell division control protein 42 homolog	CDC42	0.711642	0.006354
E3 ubiquitin-protein ligase MYCBP2	MYCBP2	0.997041	0.00641
Dihydropteridine reductase	QDPR	0.826748	0.006527
Malate dehydrogenase, cytoplasmic	MDH1	1.469585	0.006869
Vesicle transport protein GOT1B	GOLT1B	-0.8621	0.006898
Serine/arginine-rich splicing factor 6	SRSF6	-2.17701	0.007137
ATP synthase subunit e, mitochondrial	ATP5I	0.822531	0.007274
Adapter molecule crk	CRK	0.376348	0.007337
Core histone macro-H2A.1	H2AFY	-1.93035	0.007361
Transmembrane protein 258	TMEM258	-1.03769	0.007375
1,4-alpha-glucan-branching enzyme	GBE1	-0.51043	0.007558
Aflatoxin B1 aldehyde reductase member 2	AKR7A2	0.764874	0.007767
Tubulin--tyrosine ligase-like protein 12	TTLL12	-1.12219	0.00778
Glutathione reductase, mitochondrial	GSR	0.471482	0.007828
Mimitin, mitochondrial	NDUFAF2	0.72142	0.007984
Heat shock protein HSP 90-alpha	HSP90AA1	-3.01666	0.00811
Ras-related protein Ral-B	RALB	0.719281	0.00816
Hepatoma-derived growth factor	HDGF	0.40406	0.008264
Actin-related protein 2/3 complex subunit 4	ARPC4	0.699304	0.008677
14-3-3 protein sigma	SFN	0.946985	0.008685
Trifunctional enzyme subunit beta, mitochondrial	HADHB	-0.76102	0.008793
Thioredoxin-dependent peroxide reductase, mitochondrial	PRDX3	0.408456	0.008915
Transgelin-2	TAGLN2	0.417084	0.009137
UV excision repair protein RAD23 homolog B	RAD23B	0.725902	0.009346
Heme-binding protein 2	HEBP2	1.64518	0.009423
Aldo-keto reductase family 1 member C1	AKR1C1	0.96715	0.010479
Vesicle-associated membrane protein 8	VAMP8	1.325034	0.010964
Nucleophosmin	NPM1	-4.43476	0.011209
Coatomer subunit beta	COPB2	-1.38362	0.011441
Proteasome subunit beta type-1	PSMB1	1.257509	0.011893

7-dehydrocholesterol reductase	DHCR7	-1.04636	0.012146
Ras-related protein R-Ras2	RRAS2	-0.486	0.012631
Delta(3,5)-Delta(2,4)-dienoyl-CoA isomerase, mitochondrial	ECH1	0.72282	0.012938
Ras-related protein Rab-2A	RAB2A	0.428105	0.013027
RNA-binding protein Raly	RALY	-1.70075	0.013102
Phosphoglucomutase-2	PGM2	0.682985	0.013652
3-ketoacyl-CoA thiolase, mitochondrial	ACAA2	0.784636	0.014053
NAD(P)H dehydrogenase [quinone] 1	NQO1	1.104681	0.014147
Glutathione synthetase	GSS	0.803946	0.014404
Transferrin receptor protein 1	TFRC	-1.28157	0.014931
3-beta-hydroxysteroid-Delta(8),Delta(7)-isomerase	EBP	-1.30283	0.015242
Ras-related protein Rab-8A	RAB8A	0.458512	0.015574
T-complex protein 1 subunit gamma	CCT3	-0.9213	0.015816
Complement C3	C3	2.465354	0.0159
TATA-binding protein-associated factor 2N	TAF15	-1.27683	0.015991
Drebrin	DBN1	-0.87964	0.016112
Thymidine phosphorylase	TYMP	1.160423	0.016648

Table S4. Significant changes in cell and matrix protein expression were detected between cell-laden Matrigel and medium Alpha4 cultures. List of cellular and matrix proteins in day 14 MCF10a cells that are significantly upregulated (positive estimate values) or downregulated (negative estimate values) in medium Alpha4 hydrogels compared to cell-laden Matrigel hydrogels. ‘Estimate’ refers to the log2 fold-change of a given protein’s expression value. P-values calculated via MSqRob from three independent replicates per condition ($p < 0.05$).

Protein names	Gene names	estimate	pval
Clathrin heavy chain	CLTC	-2.11124	3.17E-19
Elongation factor 1-gamma	EEF1G	-1.6277	1.99E-17
Adenosylhomocysteinase	AHCY	0.922355	4.49E-13
Voltage-dependent anion-selective channel protein 1	VDAC1	-1.27864	8.41E-12
Programmed cell death 6-interacting protein	PDCD6IP	-1.81023	3.51E-11
60 kDa heat shock protein, mitochondrial	HSPD1	-2.167	1.39E-10
Voltage-dependent anion-selective channel protein 3	VDAC3	-2.97898	1.98E-10
Leukotriene A-4 hydrolase	LTA4H	1.110956	6.56E-10
Protein deglycase DJ-1	PARK7	1.199717	9.82E-10
Integrin beta-4	ITGB4	-1.87049	1.87E-09
Transketolase	TKT	0.550004	3.96E-09
L-lactate dehydrogenase A chain	LDHA	0.974634	1.59E-08
Ras GTPase-activating-like protein IQGAP1	IQGAP1	-2.40252	3.82E-08
Endoplasmic reticulum resident protein 44	ERP44	0.860909	3.86E-08
Arginine--tRNA ligase, cytoplasmic	RARS	-2.1156	4.9E-08
Voltage-dependent anion-selective channel protein 2	VDAC2	-2.04628	6.46E-08
Hexokinase-1	HK1	-1.14127	8.34E-08
Ras GTPase-activating-like protein IQGAP1	IQGAP1	-2.27547	1.02E-07
Transmembrane protein 43	TMEM43	-2.16215	1.31E-07
Calpain-1 catalytic subunit	CAPN1	-1.10648	1.93E-07
Dolichyl-diphosphooligosaccharide--protein glycosyltransferase subunit 1	RPN1	-1.68988	1.97E-07
Inorganic pyrophosphatase	PPA1	1.440491	2.19E-07
Transgelin-2	TAGLN2	0.879197	2.21E-07
Spliceosome RNA helicase DDX39B	DDX39B	-2.09459	3.58E-07
Keratin, type I cytoskeletal 18	KRT18	-3.31124	3.63E-07
Niban-like protein 1	FAM129B	-2.60528	4.96E-07
Myeloid-derived growth factor	MYDGF	1.86854	5.87E-07
General vesicular transport factor p115	USO1	-1.56801	6.06E-07
HLA class I histocompatibility antigen, alpha chain E	HLA-E	5.912107	7.33E-07
Endoplasmic reticulum-Golgi intermediate compartment protein 1	ERGIC1	-1.24856	8.19E-07
Proteasome subunit alpha type-5	PSMA5	0.974859	1.04E-06
Complement C5	C5	4.368843	1.08E-06
Pterin-4-alpha-carbinolamine dehydratase	PCBD1	1.692132	1.1E-06
Prelamin-A/C	LMNA	-3.19138	1.19E-06
Erythrocyte band 7 integral membrane protein	STOM	-2.9521	1.42E-06
Nidogen-1	Nid1	-5.76448	1.74E-06
Ubiquitin-conjugating enzyme E2 variant 1	UBE2V1	2.47377	2.72E-06
Talin-1	TLN1	-1.67295	3.31E-06
Peptidyl-prolyl cis-trans isomerase FKBP1A	FKBP1A	1.294484	3.49E-06
Protein disulfide-isomerase A6	PDIA6	-0.84314	4.4E-06
ATP synthase subunit gamma, mitochondrial	ATP5C1	-2.19521	4.64E-06
Pre-mRNA-splicing factor 18	PRPF18	6.038457	4.86E-06
Staphylococcal nuclease domain-containing protein 1	SND1	-1.89684	4.89E-06
Poly(rC)-binding protein 1	PCBP1	-2.34072	5.48E-06
Structural maintenance of chromosomes protein 6	SMC6	5.055265	5.79E-06

40S ribosomal protein S16	RPS16	-2.36081	5.83E-06
Protein deglycase DJ-1	PARK7	2.43113	5.94E-06
Splicing factor, proline- and glutamine-rich	SFPQ	-1.51615	6.13E-06
Galectin-3-binding protein	LGALS3BP	3.339067	7.12E-06
Eukaryotic translation initiation factor 3 subunit F	EIF3F	-3.03888	8.4E-06
Ezrin	EZR	1.572723	8.76E-06
10 kDa heat shock protein, mitochondrial	HSPE1	1.23628	9.12E-06
40S ribosomal protein S8	RPS8	-2.72118	1.23E-05
Phosphatidylethanolamine-binding protein 1	PEBP1	1.250641	1.3E-05
Nucleoside diphosphate kinase A	NME1	1.493933	1.45E-05
60S ribosomal protein L12	RPL12	-2.48385	1.63E-05
Aspartate aminotransferase, mitochondrial	GOT2	0.918027	1.67E-05
Calpain small subunit 1	CAPNS1	-3.10308	1.8E-05
Major vault protein	MVP	-1.40015	1.95E-05
Plectin	PLEC	-1.9706	1.95E-05
Vacuolar protein sorting-associated protein 29	VPS29	1.387192	2E-05
Ig gamma-3 chain C region	IGHG3	3.785783	2.15E-05
Pre-mRNA-splicing factor ATP-dependent RNA helicase DHX15	DHX15	-1.26362	2.27E-05
Integrator complex subunit 1	INTS1	2.74912	2.28E-05
40S ribosomal protein S14	RPS14	-4.32112	2.39E-05
Protein AHNAK2	AHNAK2	-1.0801	2.45E-05
Interleukin enhancer-binding factor 3	ILF3	-2.01827	2.59E-05
Peptidyl-prolyl cis-trans isomerase FKBP2	FKBP2	2.181922	2.72E-05
Integrin alpha-6	ITGA6	-2.13693	2.92E-05
RNA-binding motif protein, X chromosome	RBMX	4.765442	3.04E-05
Ras-related protein Ral-A	RALA	1.006454	3.5E-05
Actin-related protein 2/3 complex subunit 2	ARPC2	0.906746	3.53E-05
Asparagine--tRNA ligase, cytoplasmic	NARS	-1.25045	3.62E-05
Valine--tRNA ligase	VARS	-1.83996	3.92E-05
40S ribosomal protein S20	RPS20	-2.90715	3.98E-05
Chromatin modification-related protein MEAF6	MEAF6	3.957855	4.08E-05
Glyceraldehyde-3-phosphate dehydrogenase	GAPDH	0.660041	4.18E-05
Golgin subfamily A member 1	GOLGA1	6.768426	4.34E-05
Putative elongation factor 1-alpha-like 3	EEF1A1P5	-4.31035	4.45E-05
Syntaxin-7	STX7	1.024639	4.5E-05
Mitochondrial carrier homolog 2	MTCH2	-0.86366	4.87E-05
Small nuclear ribonucleoprotein Sm D3	SNRPD3	-3.1733	5.03E-05
Prostaglandin E synthase 3	PTGES3	-2.20882	5.3E-05
Filamin-A	FLNA	-1.87869	5.71E-05
Actin-related protein 2/3 complex subunit 3	ARPC3	1.858421	6.37E-05
Complement factor B	CFB	3.234657	7.14E-05
RNA-binding protein 14	RBM14	-1.57486	7.24E-05
26S protease regulatory subunit 10B	PSMC6	-2.22709	7.65E-05
WD repeat-containing protein 1	WDR1	0.67483	7.78E-05
DNA-dependent protein kinase catalytic subunit	PRKDC	-2.93458	7.99E-05
Myosin-14	MYH14	-2.80194	9.1E-05

Small nuclear ribonucleoprotein Sm D2	SNRPD2	-2.30352	9.4E-05
Phosphoglycerate mutase 1	PGAM1	0.700428	9.87E-05
Ubiquitin carboxyl-terminal hydrolase	USP14	-1.94371	0.000106
GRIP1-associated protein 1	GRIPAP1	2.196019	0.000143
Transaldolase	TALDO1	1.567898	0.000167
UDP-glucose 6-dehydrogenase	UGDH	-0.95322	0.000176
14-3-3 protein sigma	SFN	1.362689	0.000176
Kynureninase	KYNU	1.909499	0.000178
Laminin subunit beta-1	Lamb1	-3.41222	0.000185
14-3-3 protein beta/alpha	YWHAB	0.952891	0.000198
Serine/threonine-protein phosphatase PP1-beta catalytic subunit	PPP1CB	2.502679	0.000202
Catenin alpha-1	CTNNA1	-2.88355	0.000203
Nuclear transport factor 2	NUTF2	1.32082	0.000206
C-1-tetrahydrofolate synthase, cytoplasmic	MTHFD1	-1.00614	0.000206
T-complex protein 1 subunit alpha	TCP1	-1.10689	0.000222
Peptidyl-prolyl cis-trans isomerase B	PPIB	0.695003	0.000226
Proteasome subunit alpha type-1	PSMA1	0.931773	0.000226
Non-specific lipid-transfer protein	SCP2	1.063593	0.000237
Secretory carrier-associated membrane protein 1	SCAMP1	0.87131	0.000241
Coatomer subunit beta	COPB2	-1.5533	0.000244
Cell division control protein 42 homolog	CDC42	1.355946	0.000245
60S ribosomal protein L13	RPL13	-2.29766	0.000246
Peroxiredoxin-1	PRDX1	0.964016	0.00026
Heat shock protein 75 kDa, mitochondrial	TRAP1	-2.45074	0.00028
Large neutral amino acids transporter small subunit 1	SLC7A5	-1.51826	0.000282
Probable ATP-dependent RNA helicase DDX17	DDX17	-1.56949	0.000286
Alpha-actinin-4	ACTN4	-1.0571	0.0003
Calnexin	CANX	-2.66676	0.000307
Polymerase I and transcript release factor	PTRF	-2.65515	0.000311
Tubulin beta-4B chain	TUBB4B	-2.54036	0.000327
Guanine nucleotide-binding protein G(i) subunit alpha-2	GNAI2	-1.36812	0.000338
40S ribosomal protein S21	RPS21	0.679574	0.000344
ATP-dependent RNA helicase A	DHX9	-2.14363	0.000349
60S acidic ribosomal protein P0	RPLP0	-2.54367	0.000354
ADP-sugar pyrophosphatase	NUDT5	1.327078	0.000368
Ras-related protein Rab-2A	RAB2A	0.755022	0.000399
Histone deacetylase 1	HDAC1	-2.38657	0.000413
Calcyclin-binding protein	CACYBP	-0.51464	0.000415
Thioredoxin domain-containing protein 5	TXNDC5	0.766265	0.00043
Heterogeneous nuclear ribonucleoprotein M	HNRNPM	-2.08524	0.000435
Serum paraoxonase/arylesterase 1	PON1	3.346909	0.000439
Protein LYRIC	MTDH	-1.11119	0.000442
Small ubiquitin-related modifier 2	SUMO2	3.319452	0.000459
Malate dehydrogenase, cytoplasmic	MDH1	0.776224	0.000494
MICOS complex subunit MIC60	IMMT	-0.97528	0.000495
CAD protein	CAD	1.22601	0.000544

Vasodilator-stimulated phosphoprotein	VASP	-2.15827	0.000568
Amine oxidase [flavin-containing] A	MAOA	-1.55533	0.000585
40S ribosomal protein S17	RPS17	2.333028	0.000677
Eukaryotic translation initiation factor 3 subunit L	EIF3L	-0.66981	0.000682
Septin-7	SEPT7	-1.8378	0.00072
Hemoglobin subunit beta	HBB	4.620955	0.000728
Proteasome subunit beta type-1	PSMB1	1.821051	0.000738
26S proteasome non-ATPase regulatory subunit 13	PSMD13	-1.83239	0.00074
ADP-sugar pyrophosphatase	NUDT5	0.84753	0.000786
10 kDa heat shock protein, mitochondrial	HSPE1	1.897681	0.000818
Sodium/potassium-transporting ATPase subunit beta-3	ATP1B3	-2.1163	0.000832
Lysine--tRNA ligase	KARS	-1.96874	0.000845
cAMP-dependent protein kinase type II-alpha regulatory subunit	PRKAR2A	-1.73416	0.000891
Transmembrane emp24 domain-containing protein 9	TMED9	-0.48061	0.000932
Coatomer subunit alpha	COPA	-1.69941	0.000944
Actin-related protein 2/3 complex subunit 4	ARPC4	0.653508	0.000949
60S ribosomal protein L4	RPL4	-2.31135	0.001018
Type-1 angiotensin II receptor-associated protein	AGTRAP	-0.81283	0.001031
Mitochondrial 2-oxoglutarate/malate carrier protein	SLC25A11	-0.99255	0.001033
Putative protein PTGES3L	PTGES3L	1.877898	0.001036
Sideroflexin-1	SFXN1	-1.63054	0.001058
Purine nucleoside phosphorylase	PNP	0.500084	0.001083
Calreticulin	CALR	-1.05763	0.001084
Lupus La protein	SSB	-1.0989	0.001141
SH3 domain-binding glutamic acid-rich-like protein 3	SH3BGRL3	4.355159	0.00115
Probable ATP-dependent RNA helicase DDX6	DDX6	-0.9332	0.001162
Transforming protein RhoA	RHOA	0.983287	0.001169
Importin subunit beta-1	KPNB1	-3.38945	0.001185
Vesicle-associated membrane protein 8	VAMP8	1.791867	0.001196
Ras-related protein Rab-10	RAB10	0.845581	0.001196
Proteasome subunit alpha type	PSMA6	0.863263	0.001248
Heterogeneous nuclear ribonucleoprotein R	HNRNPR	1.751457	0.00127
Heat shock protein HSP 90-alpha	HSP90AA1	-3.28962	0.001276
Vesicular integral-membrane protein VIP36	LMAN2	1.017487	0.001341
Destrin	DSTN	1.28621	0.001434
Microtubule-associated protein	MAP4	1.21983	0.001443
Heat shock 70 kDa protein 4	HSPA4	0.978914	0.001465
60S ribosomal protein L11	RPL11	-4.00046	0.00172
Histone H2A.V	H2AFV	1.762157	0.00181
Omega-amidase NIT2	NIT2	0.585839	0.001882
Proteasome subunit beta type-5	PSMB5	0.682618	0.002079
Fumarylacetoacetase	FAH	1.145741	0.002197
Vacuolar protein sorting-associated protein 35	VPS35	-1.39849	0.002207
Tubulin-folding cofactor B	TBCB	-1.69544	0.00224
40S ribosomal protein S23	RPS23	-1.74882	0.002289
Cocaine esterase	CES2	1.471486	0.002323

Probable aminopeptidase NPEPL1	NPEPL1	0.993112	0.002332
Heterogeneous nuclear ribonucleoprotein F	HNRNPF	-0.97664	0.002336
Heterogeneous nuclear ribonucleoprotein D0	HNRNPD	-1.49034	0.002338
Retinol-binding protein 4	RBP4	1.478047	0.002409
Aldo-keto reductase family 1 member C2	AKR1C2	1.786392	0.002544
Polyadenylate-binding protein 1	PABPC1	-1.48868	0.00257
Vimentin	VIM	-1.64562	0.002575
L-lactate dehydrogenase B chain	LDHB	0.6149	0.002644
ATP synthase subunit a	MT-ATP6	-1.19841	0.002726
Heterogeneous nuclear ribonucleoprotein A1	HNRNPA1	-0.7637	0.003049
14-3-3 protein zeta/delta	YWHAZ	1.011686	0.003053
Gamma-glutamylcyclotransferase	GGCT	1.390487	0.003062
Beta-hexosaminidase subunit beta	HEXB	0.63684	0.003094
Peptidyl-prolyl cis-trans isomerase FKBP5	FKBP5	-1.18353	0.003258
Protein disulfide-isomerase A3	PDIA3	-1.20155	0.003293
Heterogeneous nuclear ribonucleoprotein L	HNRNPL	-3.12309	0.003424
Aspartate aminotransferase, cytoplasmic	GOT1	1.091966	0.003481
ATP synthase subunit alpha, mitochondrial	ATP5A1	-0.81891	0.00351
NHP2-like protein 1	NHP2L1	-1.68433	0.003523
26S protease regulatory subunit 6A	PSMC3	-0.88325	0.003531
Peroxiredoxin-5, mitochondrial	PRDX5	0.874086	0.003548
Cysteine and glycine-rich protein 1	CSRP1	1.493786	0.003624
Heat shock protein 105 kDa	HSPH1	-0.67256	0.003635
B-cell receptor-associated protein 31	BCAP31	0.854981	0.003775
Tumor protein D54	TPD52L2	1.115788	0.003831
Calcium-binding mitochondrial carrier protein SCaMC-1	SLC25A24	-1.87646	0.003834
Acylamino-acid-releasing enzyme	APEH	1.62453	0.003835
Uridine phosphorylase 1	UPP1	1.08153	0.003876
Dipeptidyl peptidase 2	DPP7	1.391339	0.004154
40S ribosomal protein S20	RPS20	-2.04971	0.004205
LIM and SH3 domain protein 1	LASP1	0.933519	0.00424
Epididymal secretory protein E1	NPC2	1.396549	0.004345
Stress-70 protein, mitochondrial	HSPA9	-0.72378	0.004435
Bifunctional glutamate/proline--tRNA ligase	EPRS	-1.35714	0.004485
Apolipoprotein A-I	APOA1	3.00021	0.004545
Brain-specific angiogenesis inhibitor 1-associated protein 2-like protein 1	BAIAP2L1	-0.64867	0.004596
60S ribosomal protein L7a	RPL7A	-3.3013	0.004665
Laminin subunit alpha-1	Lama1	-3.28149	0.004777
60S ribosomal protein L34	RPL34	-2.04552	0.004796
DnaJ homolog subfamily C member 5	DNAJC5	-1.46121	0.00497
Cytoskeleton-associated protein 4	CKAP4	-0.80127	0.005273
Translin	TSN	0.779503	0.005328
Integrin alpha-V	ITGAV	0.942161	0.005439
Proteasome subunit beta type-3	PSMB3	0.689926	0.005698
Filamin-B	FLNB	-1.25975	0.005708
Small nuclear ribonucleoprotein F	SNRPF	-1.53379	0.005721

Actin-related protein 2/3 complex subunit 4	ARPC4	0.74228	0.005925
40S ribosomal protein S9	RPS9	-2.38317	0.005988
Histone H4	HIST1H4A	-0.97244	0.006146
Argininosuccinate synthase	ASS1	-1.07542	0.006243
Sterol-4-alpha-carboxylate 3-dehydrogenase, decarboxylating	NSDHL	1.036158	0.006288
Nucleophosmin	NPM1	-3.67242	0.006306
E3 ubiquitin-protein ligase MYCBP2	MYCBP2	1.006443	0.006403
Drebrin	DBN1	-1.1543	0.006425
Transmembrane emp24 domain-containing protein 10	TMED10	-1.40727	0.006535
Ras-related protein Rab-8A	RAB8A	0.54496	0.006648
Synaptic vesicle membrane protein VAT-1 homolog	VAT1	1.181754	0.006699
Glucose-6-phosphate isomerase	GPI	1.546018	0.006733
1,4-alpha-glucan-branching enzyme	GBE1	-0.64398	0.006773
Glutamate dehydrogenase 1, mitochondrial	GLUD1	-0.33368	0.007068
Dihydrolipoyl dehydrogenase, mitochondrial	DLD	0.529638	0.007088
Dihydropteridine reductase	QDPR	1.073402	0.007386
Heme-binding protein 2	HEBP2	1.558598	0.007404
Adapter molecule crk	CRK	0.362514	0.007621
Tubulin beta-3 chain	TUBB3	1.071763	0.007991
14-3-3 protein eta	YWHAH	0.756202	0.008249
Aflatoxin B1 aldehyde reductase member 2	AKR7A2	0.572258	0.008374
T-complex protein 1 subunit alpha	TCP1	-0.66713	0.008411
Proteasome subunit alpha type	PSMA2	1.336313	0.008842
Proteolipid protein 2	PLP2	0.570736	0.008994
Transmembrane protein 258	TMEM258	-0.98487	0.009203
Adenylyl cyclase-associated protein 1	CAP1	-0.51683	0.009352
60S ribosomal protein L37a	RPL37A	-0.85734	0.010033
Katanin p60 ATPase-containing subunit A-like 2	KATNAL2	0.490969	0.010218
Putative protein FAM10A4	ST13	-1.50661	0.010553
GDP-L-fucose synthase	TSTA3	1.556841	0.01075
Mimitin, mitochondrial	NDUFAF2	0.613916	0.011081
78 kDa glucose-regulated protein	HSPA5	-0.48986	0.011095
Transferrin receptor protein 1	TFRC	-0.93735	0.011204
NAD(P)H dehydrogenase [quinone] 1	NQO1	1.159813	0.011409
Superoxide dismutase [Mn], mitochondrial	SOD2	1.511288	0.011509
Monocarboxylate transporter 1	SLC16A1	-2.5841	0.011569
Elongation factor 1-delta	EEF1D	-1.64376	0.012167
Ras-related protein Ral-B	RALB	0.718458	0.012242
Trifunctional enzyme subunit beta, mitochondrial	HADHB	-0.8382	0.012536
Calcium-binding protein 39	CAB39	0.365534	0.012583
Protein RER1	RER1	-0.73214	0.012691
Dystrophin	DMD	-1.71165	0.012901
Mevalonate kinase	MVK	2.167333	0.013028
Translocon-associated protein subunit gamma	SSR3	-0.68948	0.013518
Heterogeneous nuclear ribonucleoproteins A2/B1	HNRNPA2B1	-0.70912	0.013526
Dynactin subunit 1	DCTN1	0.83256	0.013635

Phosphoglucomutase-2	PGM2	0.669937	0.013875
GTP-binding nuclear protein Ran	RAN	-0.76118	0.013998
Heterogeneous nuclear ribonucleoprotein A0	HNRNPA0	-1.76711	0.014341
D-dopachrome decarboxylase	DDT	1.081134	0.014358
Proteasome subunit alpha type-1	PSMA1	0.723504	0.014422
UV excision repair protein RAD23 homolog B	RAD23B	0.731556	0.014712
60S ribosomal protein L22	RPL22	-1.59131	0.014888
ATP-dependent 6-phosphofructokinase, platelet type	PFKP	-1.50769	0.015042
Poly(ADP-ribose) glycohydrolase	PARG	0.627803	0.015213
Proteasome activator complex subunit 1	PSME1	0.51625	0.015773
RNA-binding protein FUS	FUS	-1.18364	0.01588
Malate dehydrogenase, cytoplasmic	MDH1	1.208835	0.01607
Catechol O-methyltransferase	COMT	1.284379	0.016151
Serine/threonine-protein phosphatase	PPP5C	0.4613	0.016278
Tubulin alpha-1B chain	TUBA1B	-3.6023	0.016496
Receptor protein-tyrosine kinase	EGFR	-1.32097	0.016547
Cysteine and glycine-rich protein 1	CSRP1	0.786963	0.016912
Glutathione S-transferase omega-1	GSTO1	0.493992	0.016944
Glyoxylate reductase/hydroxypyruvate reductase	GRHPR	0.838479	0.017433
Inositol monophosphatase 2	IMPA2	-0.82785	0.017626
Sialic acid synthase	NANS	0.263599	0.017914
Ras-related C3 botulinum toxin substrate 2	RAC2	-0.73761	0.018636
Eukaryotic translation initiation factor 4H	EIF4H	0.647433	0.018636
Nuclear pore membrane glycoprotein 210-like	NUP210L	2.670926	0.018695
Vesicle-associated membrane protein 8	VAMP8	1.056809	0.01899
Tubulin alpha-1C chain	TUBA1C	-3.05093	0.019314
6-phosphogluconate dehydrogenase, decarboxylating	PGD	1.205676	0.019338

Table S5. Significant changes in cell and matrix protein expression were detected between cell-laden Matrigel and soft Alpha4 cultures. List of cellular and matrix proteins in day 14 MCF10a cells that are significantly upregulated (positive estimate values) or downregulated (negative estimate values) in soft Alpha4 hydrogels compared to cell-laden Matrigel hydrogels. ‘Estimate’ refers to the log2 fold-change of a given protein’s expression value. P-values calculated via MSqRob from three independent replicates per condition ($p < 0.05$).

Lingard et al. 2022

Functionalising a negatively charged self-assembling peptide hydrogel for mammary epithelial cell culture with laminin 111

Eliana Lingard[1,2], Craig Lawless[1], Aline Miller[3,4], Marco Domingos[5,6], Joe Swift[1,7], Alberto Saiani[3,8], Andrew Gilmore[1,2]

Affiliations

[1]Wellcome Centre for Cell-Matrix Research, Oxford Road, Manchester, M13 9PT, UK.

[2]Division of Cancer Sciences, School of Medical Sciences, Faculty of Biology, Medicine and Health, Manchester Academic Health Science Centre, University of Manchester, Manchester, M13 9PL, UK.

[3]Manchester Institute of Biotechnology (MIB), The University of Manchester, Oxford Road, Manchester, UK.

[4]School of Chemical Engineering and Analytical Sciences, Faculty of Science and Engineering, The University of Manchester, Oxford Road, Manchester M13 9PL, UK.

[5]The Henry Royce Institute, Department of Materials, the University of Manchester, Manchester, UK.

[6]Department of Mechanical, Aerospace and Civil Engineering, School of Engineering, Faculty of Science and Engineering, The University of Manchester, Manchester, UK.

[7]Division of Cell Matrix Biology and Regenerative Medicine, School of Biological Sciences, Faculty of Biology, Medicine and Health, Manchester Academic Health Science Centre, University of Manchester, Manchester, M13 9PL, UK.

[8]School of Materials, Faculty of Science and Engineering, The University of Manchester, Oxford Road, Manchester, UK.

Abstract

Matrigel is an organic hydrogel that is considered the gold-standard material for *in vitro* mammary epithelial cell (MEC) culture as it can support many complex MEC behaviours owing to its numerous matrix proteins and growth factors. However, Matrigel has many limitations as a cell culture material which has prompted the development of alternative scaffolds for MEC culture. In recent years, significant progress has been made in generating synthetic hydrogels that offer researchers simple, reliable, tuneable, and biocompatible scaffolds for *in vitro* cell culture. However, creating a synthetic hydrogel that can provide MECs with tissue-specific biochemical cues is difficult, as the composition of both Matrigel and human breast tissue is poorly defined. Laminin 111, a key matrix protein in breast tissue and a major component of Matrigel, can support complex MEC behaviours. We wanted to investigate whether laminin 111 could be used to functionalise self-assembling peptide hydrogels for *in vitro* MEC culture. Our results show that a negatively charged peptide hydrogel can be supplemented with laminin 111 to create hydrogels that can support acinar formation for at least 7 days. We also found that laminin 111 directly stimulates upregulation of proteins responsible for driving cell differentiation and downregulates proliferation. These results indicate that a peptide hydrogel functionalised with laminin 111 could be a viable alternative to Matrigel, providing researchers with a simpler and more reliable hydrogel for three-dimensional (3D) breast matrix modelling.

Keywords

Matrigel // laminin 111 // self-assembling peptide hydrogels // functionalisation

Abbreviations

- MEC - mammary epithelial cell
- 3D - three-dimensional
- ECM - extracellular matrix
- rBM - reconstituted basement membrane
- EHS - Engelbreth-Holm-Swarm
- lrECM - laminin-rich extracellular matrix
- LDV - lactate dehydrogenase-elevating virus
- PEG - polyethylene-glycol
- PAM - polyacrylamide
- SAPH - self-assembling peptide hydrogel
- DMEM - Dulbecco’s modified eagle medium
- HSer - horse serum
- EGF - epidermal growth factor
- PBS - phosphate-buffered saline
- BSA - bovine serum albumin
- RPMI - Roswell Park Memorial Institute
- NaOH - sodium hydroxide

- DAPI - 4′,6-diamidino-2-phenylindole
- RIPA - radioimmunoprecipitation assay buffer
- SDS - sodium dodecyl sulphate
- W - Watts
- DTT - dithiothreitol
- LC-MS/MS - liquid chromatography-coupled tandem mass spectrometry
- SD - standard deviation
- SEM - standard error of mean
- LG - laminin globular domain
- PI3K - phosphoinositide-3 kinase
- ERK - MAP kinase 1

Introduction

Modelling human tissues *in vitro* presents a challenge for researchers due to their complex and dynamic natures. Tissue organisation and function is dictated by its cells and their surrounding extracellular matrix (ECM), which are in constant communication through intricate, tightly regulated signalling mechanisms that collectively control tissue morphology and function [1]. The ECM is remodelled by cells and matrix factors to maintain tissue homeostasis, resulting in changes to ECM composition and architecture that subsequently elicit changes in cell behaviour to promote healthy tissue function [2, 3]. Developing tissues also undergo major compositional and structural remodelling events that alter cell fate and the organisation of cells and their ECM to modify tissue structure and function [3, 4]. Abnormal ECM remodelling occurs during the development of diseases such as fibrosis and cancer, which stimulates pathological cell behaviours that reinforce aberrant ECM remodelling in a positive feedback signalling loop that drives disease progression [4, 5]. Recapitulating these complex, dynamic changes in matrix composition and organisation *in vitro* and investigating their effect on cell behaviour and fate requires that the cells are surrounded in a physiologically representative environment that they can interact with and modify.

The function of the mammary gland is to produce and secrete milk, which requires that it undergoes rapid and frequent remodelling in response to hormonal cues that arise during puberty, the menstrual cycle, pregnancy, lactation, and involution [6, 7]. The dramatic changes to cell organisation and fate that occur during these events, as well as alterations made to their environment, are the result of complex molecular events initiated by both the cells and their ECM [8-15]. Dysregulation of any part of these molecular mechanisms can drive cell malignancy [16-18]. Due to the complexity of these mechanisms, there are still many ill-defined molecular networks and interactions that occur during mammary gland development, remodelling and malignancy. These require further investigation using a modifiable MEC culture model that can simulate the key properties of the human mammary gland without being too complex, poorly defined, or difficult to reproduce.

3D models of the human mammary gland have been used for MEC culture since the 1970s [19]. An enduring hydrogel used for MEC culture is the reconstituted basement membrane (rBM) extract Matrigel, which began development in 1977 and was first used as a scaffold for MECs in 1987 [20-22]. Also called Cultrex, Engelbreth-Holm-Swarm (EHS) extract, rBM or laminin-rich ECM (lrECM), Matrigel is obtained from basement membrane-producing, murine EHS tumours [22-25]. Consequently, Matrigel is enriched in basement membrane proteins such as collagen IV, laminin 111, nidogen and perlecan, rendering it supportive of complex MEC behaviours such as their differentiation into acini and secretion of milk proteins [20, 23, 26-29]. This impressive array of cell behaviours is also encouraged by the presence of numerous growth factors in Matrigel [28, 30-33]. Matrigel's bioactivity makes it popular for MEC culture, and it remains in use today as a model of the mammary gland [24, 34-36].

Initially, Matrigel was used to characterise how MECs respond to being encapsulated in a basement membrane and to investigate how ECM components influence MEC differentiation and fate [20, 27, 36-42]. These investigations helped provide the foundation upon which subsequent research into

mammary gland development and dysfunction was based [43-49]. As our understanding of the role MECs and their surrounding ECM play in regulating mammary gland structure and function developed, the applications of Matrigel also evolved. For example, hybrid Matrigel-collagen I and Matrigel-alginate gels were developed to explore the role matrix stiffness plays in regulating MEC fate and driving cell malignancy, which has helped us to understand why dense breast tissue is a risk factor for breast cancer [43, 50-58]. Without Matrigel to provide a supportive and bioactive scaffold for MECs, it is uncertain which, if any, of these insights into MEC fate and function would have been obtained.

Although Matrigel has undoubtedly played a pivotal role in our understanding of mammary gland development and function, its applications for *in vitro* MEC culture are limited [30]. Matrigel is a notoriously complex and poorly defined substrate, containing approximately 1800 proteins and an undefined number of growth factors, any of which may independently affect cell behaviour [28, 31, 32, 59-63]. This complexity is exacerbated by variations in protein and growth factor content and concentration between batches, resulting in inconsistent cell behaviours across experiments. Matrigel's mechanical properties also suffer from batch-to-batch variation which may also independently affect cell behaviour [32, 48, 55, 64, 65]. Additionally, Matrigel is mechanically weak, and its mechanical properties are difficult to modify separately due to the interplay between matrix density and pore size with matrix stiffness [66]. Furthermore, as an EHS tumour extract, Matrigel also contains tumorigenic factors that can stimulate pro-oncogenic cell behaviours and enhance tumorigenicity in tumour models, which makes it unsuitable for modelling healthy, non-tumorigenic tissue environments [67-69]. Finally, Matrigel is also xenogenic which makes it unrepresentative of human tissues and introduces the risk of exposing cells to contaminants such as the immunogenic lactate dehydrogenase-elevating virus (LDV) [70-72]. These limitations highlight the necessity for a more consistent, defined, modifiable and contaminant-free MEC scaffold.

The limitations of Matrigel have prompted the development of synthetic cell scaffolds that offer researchers improved consistency, definition and tuneability [73]. Scaffolds that meet these criteria are often composed of synthetic polymers such as polyethylene-glycol (PEG) or polyacrylamide (PAM), which are created by reacting monomers with crosslinking agents to create hydrated, cross-linked networks [74-76]. The individual components are easy to obtain and are available in different molecular weights and with varying degrees of degradability which provides users with greater control over the final properties of the hydrogel. The simple compositions and flexible cross-linking chemistry of these synthetic hydrogels therefore makes them well-defined and amenable to modifications that functionalise them for specific cell culture applications [77-81]. While PAM cannot be used for 3D cell culture applications due to the cytotoxicity of its acrylamide monomer precursors, PEG hydrogels are compatible for 3D cell culture and have been successfully functionalised with the collagen RGD peptide motif to promote mammary cell adhesion and proliferation, and a compliant, hybridised PEG-heparin scaffold has been found to promote MEC differentiation into acinar structures [74, 82-85]. However, there are disadvantages to using these hydrogels for cell culture. Cells cannot interact with or adhere to synthetic polymers unless they have been functionalised with peptide motifs or growth

factors, which can be a time-consuming, expensive, and complex process [73, 86, 87]. Some synthetic hydrogels are also cytotoxic or contain toxic agents, which make them unsuitable for 3D cell culture applications [88-90]. These limitations can be off-putting to researchers who are unfamiliar with materials chemistry, leaving them struggling for an alternative scaffold to Matrigel.

One class of promising cell scaffolds for 3D culture are self-assembling peptide hydrogels (SAPH). These are hydrogels composed of short, synthetic, amphipathic peptides that self-assemble into fibrillar structures which entangle with each other in water to form hydrated, fibrillar scaffolds [91-93]. Like synthetic hydrogels, SAPHs are simple, well-defined, and reproducible, which makes them amenable to a variety of modifications that can specialise them for a variety of cell culture applications [94-99]. Furthermore, as a peptide-based scaffold, SAPHs are also inherently biocompatible which can prevent the need for cell-specific functionalisation, saving researchers valuable time and money [100-103]. The diversity of peptide sequences available also provides users with greater control over the final properties of the hydrogel and allows them to explore which scaffold is best suited for their cells [104-106]. SAPHs are compatible for 3D MEC culture, as they have been used to model breast tumour environments and one hydrogel has been found to support MEC viability, which makes SAPHs promising potential candidates for modelling the human mammary gland [107-109].

The soft, positively charged SAPH PeptiGel® Alpha4 (Manchester BioGEL) supports long-term MEC viability and organisation into non-differentiated organoids. However, since Alpha4 is only composed of peptides and water, it cannot support complex MEC behaviours such as acinar development. SAPHs are amenable to modifications, which makes them promising candidates for functionalisation. Here we investigated whether SAPHs can be functionalised for MEC culture by incorporating matrix proteins into the hydrogels. We found that laminin 111 was able to stimulate acinar development in MECs and functionalise a negatively charged SAPH for MEC culture.

Materials and Methods

Materials

PeptiGels® Alpha4 and Alpha7 were purchased from Manchester BioGEL (Alderley Park, UK). Matrigel and rat tail collagen I were bought from Corning (Glendale, US). High-concentration laminin 111 was purchased from Trevigen (Gaithersburg, US).

Mammary epithelial cell maintenance and passaging

Immortalised, non-tumorigenic human mammary epithelial cells (MCF10a) were sourced from ATCC and maintained in monolayer culture using Dulbecco's modified eagle medium (DMEM)-F12 media supplemented with 5% filtered horse serum (HSer) (v/v), 10 µg/mL insulin, 0.5 µg/mL hydrocortisone, 100 ng/mL cholera toxin and 20 ng/mL epidermal growth factor (EGF). The cells were passaged at 70-90% confluency using 1X trypsin/EDTA solution and the cell suspension was collected in a 15 mL falcon tube. Cells were recovered by centrifuging the suspension at 350 xg for 5 minutes to obtain a cell pellet, which was resuspended in 1 mL of resuspension media (DMEM-F12 containing 1.8% HSer (v/v), 10 µg/mL insulin, 0.5 µg/mL hydrocortisone, 100 ng/µL cholera toxin and 5 ng/mL EGF).

Mammary epithelial cell encapsulation in Matrigel

Wells of a 24-well plate were coated with a 50 µL layer of undiluted Matrigel (8.9 mg/mL) and left to set for 30 minutes at 37°C. Passaged MCF10a cells were resuspended in 1 mL of resuspension media (DMEM-F12 containing 1.8% HSer (v/v), 10 µg/mL insulin, 0.5 µg/mL hydrocortisone, 100 ng/µL cholera toxin and 5 ng/mL EGF). Appropriate volumes of cell suspension were mixed into blank DMEM to give a volume of 49.5 µL per gel. 50.6 µL of 8.9 mg/mL Matrigel was then pipetted into the cell-DMEM mixture to give a final total protein concentration of 4.5 mg/mL and a seeding density of 0.5×10^5 cells per 100 µL of gel. 100 µL of the Matrigel-cell-DMEM solution was then pipetted into each well and gently spread to ensure even coverage before being left to polymerise at 37°C (5% CO2) for 30 minutes. After the gels had polymerised, MCF10a cultures were bathed in assay media (DMEM-F12 supplemented with 2% HSer (v/v), 10 µg/mL insulin, 0.5 µg/mL hydrocortisone, 100 ng/µL cholera toxin and 5 ng/mL EGF). The gels were then incubated at 37°C (5% CO2). Media was refreshed every 2-4 days.

Mammary epithelial cell encapsulation in laminin 111 gels

Wells of a 24-well plate were coated with a 50 µL layer of undiluted, high-concentration laminin 111 (6.1 mg/mL) and left to set for 30 minutes at 37°C. Passaged MCF10a cells in resuspension media were mixed with 6.1 mg/mL laminin 111 to create gels with a seeding density of 0.5×10^5 cells per 100 µL of gel. 100 µL of laminin-cell mixture was then pipetted into each well and spread on top of the base gel layer to ensure even coverage, before being left to polymerise at 37°C (5% CO2) for 30 minutes. The gels were then bathed in assay media and incubated at 37°C (5% CO2). Media was refreshed every 2-3 days.

Mammary epithelial cell encapsulation in peptide hydrogels

PeptiGels® were pre-warmed to room temperature before 50 µL of gel was spread over the bottom surface of wells in 24-well plates. Passaged MCF10a cells were encapsulated via gentle pipetting and mixing of cell suspension, as per the manufacturer's directions, into appropriate volumes of gel and left to recover for 5 minutes. Volumes of cell suspension used were calculated to ensure a final cell density of 0.5 x 10^5 cells per mL. Following encapsulation, 100 µL aliquots of cell-laden hydrogels were pipetted into wells and carefully spread on top of the gel layer. After 5 minutes recovery, 1 mL of assay media was added to each well and the cultures were incubated at 37°C (5% CO_2). Media was changed the following day and every 2-4 days thereafter.

Preparation of hybrid Matrigel-peptide hydrogel cultures

PeptiGels® were pre-warmed to room temperature before 50 µL of gel was spread over the bottom surface of wells in 24-well plates. Passaged MCF10a cells were mixed with 18 µL of 8.9 mg/mL Matrigel and left to incubate at room temperature for 10 minutes. Following this incubation period, the cell-Matrigel mixture was then gently mixed with 75 µL of PeptiGel® following the manufacturer's directions, resulting in hybrid gels with a final Matrigel concentration of 1.6 mg/mL. Volumes of cell suspension used were calculated to ensure a final cell density of 0.5 x 10^5 cells per mL. After being left to recover for 5 minutes, 100 µL of gel was pipetted into wells and spread on top of the gel layer. The gels were then incubated at 37°C for 30 minutes before 1 mL of assay media was added to each gel. The cultures were incubated at 37°C (5% CO_2) and the media was changed the following day and every 2-4 days afterwards.

Preparation of hybrid laminin 111-peptide hydrogel cultures

PeptiGels® were pre-warmed to room temperature before 50 µL of gel was spread over the bottom surface of wells in 24-well plates. Passaged MCF10a cells were mixed with either 18 or 50 µL of 6.1 mg/mL laminin 111 and incubated at room temperature for 10 minutes. Following incubation, the 18 µL and 50 µL cell-laminin mixtures were mixed with 75 and 40 µL of PeptiGel®, respectively, following the manufacturer's directions. This created hybrid gels with a final laminin 111 concentration of 1.0 mg/mL or 3.1 mg/mL. Volumes of cell suspension used were calculated to ensure a final cell density of 0.5 x 10^5 cells per mL. The gels were left to recover for 5 minutes before 100 µL of gel was pipetted into wells and spread on top of the gel layer. The gels were left to set for 30 minutes at 37°C, after which 1 mL of assay media was added to each culture. The cultures were incubated at 37°C (5% CO_2) and the media was changed the following day and every 2-4 days afterwards.

Organoid extraction from Matrigel and peptide hydrogels

3D hydrogel cultures were washed with 1 mL of phosphate-buffered saline (PBS) following removal of media and then depolymerised using 1 mL of ice-cold cell recovery solution (Corning). After being incubated on an orbital shaker for 1 hour at 4°C, the freed well contents were resuspended and collected into falcon tubes pre-coated with 1% bovine serum albumin (BSA) in PBS (w/v) and washed

via centrifugation in PBS at 70 xg for 3 minutes at 4°C. The supernatants were discarded, and the pellets could then be resuspended for re-encapsulation or fixed for staining.

Organoid re-encapsulation in hydrogels

Organoid pellets isolated from Matrigel were resuspended in 100 µL of resuspension medium and 10 µL of suspension was added to fresh Matrigel, laminin 111, or hybrid hydrogel mix and encapsulated as described previously.

Organoid re-encapsulation in collagen I gels

200 µL collagen I gel bases with a final concentration of 1.5 mg/mL were first prepared by mixing 75 µL of 3.98 mg/mL collagen I with 104 µL DMEM and 20 µL 10X Roswell Park Memorial Institute (RPMI) media. This mixture was neutralised by adding 3 µL of 1M sodium hydroxide (NaOH), before being spread over the bottom surfaces of wells in 24-well plates and left to set for 30 minutes at 37°C (5% CO_2). Cell-laden, 200 µL1.5 mg/mL collagen I gels were then prepared by mixing 75 µL 3.98 mg/mL collagen I with 54 µL DMEM and 20 µL 10X RPMI media and then neutralising the gels with 3 µL of 1M NaOH. Pelleted organoids were resuspended in 100 µL of resuspension media and 50 µL organoid suspension was then added to this mixture before the gels were deposited into wells on top of the base layer. The gels were incubated for 30 minutes at 37°C (5% CO_2) before being bathed in 1 mL of assay MCF10a media and incubated at 37°C (5% CO_2). Media was refreshed every 2-4 days.

Immunofluorescent staining of extracted organoids

Extracted organoids were fixed for 45 minutes in 4% formaldehyde in PBS (v/v) at room temperature. The fixative was then diluted with 10 mL of PBS and the suspension was centrifuged at 70 xg for 3 minutes at 4°C. After discarding the supernatants, pellets were resuspended in 1 mL of organoid wash buffer (PBS containing 0.1% Triton-X-100 and 0.2% BSA), transferred to pre-coated, low adherent 24-well plates (Greiner Bio-One, UK) and left to block at room temperature for 15 minutes. After blocking, excess buffer was carefully removed to leave 200 µL of liquid in each well and the clusters were incubated with 2X primary antibodies (Table 1) in organoid wash buffer overnight on an orbital shaker (100 RPM) at 4°C. The plates were retrieved, and after being left to settle at room temperature for 10 minutes, the organoids were washed three times in 1 mL of organoid wash buffer for 1 hour each time on an orbital shaker at 4°C. After removing the excess buffer to leave 200 µL of liquid in each well, the clusters were incubated with 2X secondary antibody (Table 2) solutions in organoid wash buffer overnight on an orbital shaker at 4°C. The organoids were then left to settle at room temperature for 10 minutes before excess liquid was removed to leave 200 µL of liquid per well. The organoids were then incubated with 200 µL of 2 µg/mL 4′,6-diamidino-2-phenylindole (DAPI) in PBS for 10 minutes on an orbital shaker at 4°C before being washed 3 times with organoid wash buffer for 1 hour each time, as described above. Following the final wash, the organoids were diluted in PBS and transferred to 6-well plates.

Antigen	Host	Source	Catalogue number	Dilution
Active caspase-3	Rabbit	R&D Systems	AF835	1:200
Laminin α3 chain	Mouse	R&D Systems	MAB21441	1:200
Collagen IV	Rabbit	Abcam	ab6586	1:200
β-catenin	Mouse	BD Biosciences	610154	1:200

Table 1. Primary antibodies for immunofluorescence.

Antigen	Conjugate dye	Host	Source	Catalogue number	Dilution
Anti-mouse	AlexaFluor 594	Donkey	Invitrogen	A21203	1:250
Anti-rabbit	AlexaFluor 488	Donkey	Invitrogen	A21206	1:250

Table 2. Secondary antibodies for immunofluorescence.

Fluorescent microscope imaging

Confocal images were collected on a Leica TCS SP8 AOBS upright confocal using a 63x/0.90 water immersion objective. The confocal settings were as follows, pinhole 1 airy unit, scan speed 400 Hz unidirectional, format 1024 x 1024. Images were collected using hybrid and photomultiplier detectors with the following detection mirror settings; DAPI 410-475 nm; Alexa-488 507-580 nm; Alexa-594 605-750 nm using the 405 nm (50%), 490 nm (30%) and 590 nm (30%) laser lines respectively. When it was not possible to eliminate crosstalk between channels, the images were collected sequentially. The acquired images were processed in ImageJ.

Brightfield microscope imaging

Brightfield images were collected on a Leica DMIL LED inverted brightfield microscope connected to a xiQ USB3.0 Vision camera using a 20x objective. The acquired images were processed using ImageJ.

Organoid analysis in Matrigel and laminin hydrogels

To assess organoid area and circularity, 20x brightfield images of organoids encapsulated in Matrigel and laminin 111 hydrogels were analysed in ImageJ. Clusters in focus were traced around their periphery using the freehand tool (to measure circularity) or the freehand line tool (to measure area). The tracing was done by hand using a Wacom One drawing tablet and pen. Measurements were exported to GraphPad Prism.

To assess organoid density, Matrigel- and laminin 111-encapsulated MCF10a organoids were prepared in triplicate in 96-well plates, following the techniques described above. The gels were cultured for a maximum of 21 days and fixed with 4% formaldehyde in PBS for 30 minutes at room temperature. The fixative was washed out using PBS and then permeabilised for 5 minutes with 0.5% Triton-X-100. After being washed with 3D IF wash buffer (PBS containing 0.1% BSA, 0.2% Triton-X-100 and 0.05% Tween-20) for 30 minutes, the clusters were blocked in 10% HSer in 3D IF wash

buffer for 90 minutes. The clusters were then stained with 1 µg/mL DAPI in PBS for 10 minutes before being washed with 3D IF wash buffer for 10 minutes and then double-distilled water overnight.

Fluorescent images of DAPI-stained clusters grown in Matrigel and laminin 111 were collected as Z-stacks on the EVOS M7000 Imaging system (Thermo Fisher Scientific, MA) using a 4x objective. 50% of each well area was imaged and 12 Z-planes were collected each time. Images were collected using the DAPI light source channel. The acquired images were processed in QuPath v0.2.3 by manually counting fluorescent nuclei. Measurements were exported to GraphPad Prism.

Protein extraction from peptide hydrogels for mass spectrometry analysis

Peptide hydrogel-encapsulated cells were washed for 15 minutes in 1X PBS and then lysed in 100 µL of 1X radioimmunoprecipitation assay buffer (RIPA) (50 mM Tris-HCL (pH 7.4), 150 mM sodium chloride, 1% IGEPAL, 0.1% (w/v) sodium dodecyl sulphate (SDS), 1% sodium deoxycholate, 20 mM sodium fluoride, 2 mM sodium orthovanadate, 1X protease inhibitor cocktail). Following 15 minutes incubation on ice, the samples were sonicated for 180 seconds at 10 Watts (W) using a Covaris S220 ultrasonicator before being centrifuged at 3220 xg for 5 minutes at 4°C. Lysates were stored at 20°C prior to use.

In-gel digestion of lysates

Lysates were mixed with 4X Laemmli buffer (Bio-Rad, CA) and heated at 95°C for 5 minutes. The samples were then allowed to migrate past the wells of a pre-cast 4-20% polyacrylamide gel (Bio-Rad) before being stained with InstantBlue for 1 hour. The samples were then left to de-stain in de-ionised water overnight. Following de-staining, the sample bands were excised from the gel and dehydrated using acetonitrile before being subjected to vacuum centrifugation. The dried samples were reduced with 10 mM dithiothreitol (DTT) and alkylated using 55 mM iodoacetamide and then washed with 25 mM ammonium bicarbonate and then acetonitrile twice. The samples were dried again using vacuum centrifugation and digested in trypsin overnight at 37°C.

Liquid chromatography-coupled tandem mass spectrometry

Digested samples were analysed by liquid chromatography-coupled tandem mass spectrometry (LC-MS/MS) using an UltiMate® 3000 Rapid Separation LC (Dionex Corporation, CA) coupled to a QExactive HF mass spectrometer (Thermo Fisher Scientific, MA) or Orbitrap Elite (Thermo Fisher Scientific, MA) mass spectrometer.

Using the QExactive HF mass spectrometer, mobile phase A was 0.1% formic acid in water and mobile phase B was 0.1% formic acid in acetonitrile and the column used was a 75 mm x 250 µm i.d. 1.7 mM CSH C18, analytical column (Waters). 1 µL sample aliquots were transferred to a 5 µL loop and loaded onto the column at a flow rate of 300nl/min for 5 minutes at 5% B. The loop was then taken out of line and the flow was reduced from 300nl/min to 200nl/min over 30 seconds. Peptides were then separated using a 5% to 18% B gradient over 34.5 minutes, then a 18% to 27% B gradient

over 8 minutes and finally a 27% to 60% B gradient in 1 minute. The column was then washed at 60% B for 3 minutes before being re-equilibrated to 5% B in 1 minute. At 55 minutes, the flow was increased to 300nl/min until the end of the run was reached at 60 minutes.

Using the Orbitrap Elite mass spectrometer, peptide mixtures were separated using a gradient from 92% A (0.1% formic acid in water) and 8% B (0.1% formic acid in acetonitrile) to 33% B, in 44 min at 300 nL min^{-1}, using a 75 mm x 250 µm i.d. 1.7 mM BEH C18 analytical column (Waters). Peptides were selected for fragmentation automatically by data dependant analysis.

Liquid chromatography-coupled tandem mass spectrometry data acquisition

Mass spectrometry data was acquired in a data-directed manner for 60 minutes in positive mode, where peptides were selected for fragmentation automatically by data-dependent analysis on a basis of the top 12 peptides with m/z between 300 to 1750 Th and a charge state of 2, 3 or 4 with a dynamic exclusion set at 15 seconds. The MS Resolution was set at 120,000 with an AGC target of 3e6 and a maximum fill time set at 20 ms. The MS2 Resolution was set to 30,000, with an AGC target of 2e5, a maximum fill time of 45 ms, an isolation window of 1.3 Th and a collision energy of 28. The resulting data were searched using Mascot (Matrix Science, UK), against the Swissprot and Trembl databases with human taxonomy selected. The data were validated using Scaffold (Proteome Software, OR).

MaxQuant processing of raw peptide data

All raw data files were processed in MaxQuant (v2.0.1.0, [110]). Spectra were searched against the Human (Homo Sapiens) reference proteome obtained from Uniprot (June 2021, [111]). This proteome was modified to include the three murine laminin 111 subunits LAMA1_MOUSE, LAMB1_MOUSE, LAMC1_MOUSE peptide sequences obtained from the Mouse (Mus musculus) reference proteome (July 2021). Methionine oxidation and N-terminal acetylation were set as variable modifications and cysteine carbamidomethylation was set as a fixed modification. Fast label-free quantification was enabled, with a minimum label ratio of 2 selected. A minimum of 3 and an average of six sample neighbours were also set. Precursor tolerance for the first and main searches was set at 20 ppm and 4.5 ppm, respectively. MS/MS tolerance was set at 20 ppm, with a maximum of two missed cleavages allowed. The false discovery rate of PSM and protein were set at 0.01 and “Match between runs” was enabled.

Analysis of mass spectrometry data

Differential expression was performed in R (release 4.1.2) using the MSqRob package (v0.7.7, [112], using a false discovery rate of 0.05 for significantly changing proteins. Functional analysis was performed using the packages ClusterProfiler (v4.2.2, [113]) and ReactomePA (v1.38.0, [114]), with significantly over-represented functional terms taken at adjusted p-value < 0.05. Significant functional terms were visualised using enrichplot (v1.14.2).

Statistical analysis

All data were analysed in GraphPad Prism v9.4.1. Quantitative values are presented as mean ± standard deviation (SD) or mean ± standard error of mean (SEM). Parametric data were analysed using one-way or two-way analysis of variance (ANOVA). Four levels of significance (p-value <0.05 (*), p-value <0.01 (**), p-value <0.001 (***), and p-value <0.0001 (****)) were used.

Results

MCF10a cells need sustained contact with a laminin 111-rich matrix to form polarised acinar structures

Acini recapitulate the key features of *in vivo* mammary alveoli as they are hollow, polarised spheroidal structures that produce a laminin 332- and collagen IV-rich basement membrane; hence their development *in vitro* indicates that their environment sufficiently simulates the native breast microenvironment (Fig. 1A) [26]. Previous studies have shown that the differentiation of MECs into polarised acini requires the presence of breast matrix proteins such as collagen I or laminin 111 within a soft scaffold [19, 27, 42, 55, 115-117]. SAPHs are 3D, hydrated and biocompatible hydrogels that have previously supported osteoblastic differentiation and kidney organoid differentiation without requiring the incorporation of exogenous matrix proteins [118, 119]. Therefore, we theorised that SAPHs with similar bulk stiffnesses to established MEC scaffolds could provide MECs with environmental cues that stimulate acinar development. To investigate whether MECs form acini in SAPHs, we encapsulated non-malignant, human MECs (MCF10a cells) in two soft SAPHs: Alpha4 (positively charged) and Alpha7 (negatively charged). MCF10a cells were also encapsulated within Matrigel to provide a positive control as Matrigel is enriched in breast matrix proteins and consequently supports MCF10a acinar development [26, 28]. After 7 days, brightfield imaging was used to examine MCF10a morphology and viability before the cells were extracted from the SAPH and Matrigel cultures and probed with antibodies raised against key markers of acinar development: active caspase-3, laminin 332, collagen IV and β-catenin. We found that polarised acini were developing in Matrigel (Fig. 1B). However, no polarised acini were found in Alpha4 and Alpha7 cultures. In Matrigel, acinar structures were easily identified by the organisation of cells around a hollow centre and the deposition of collagen IV and laminin 332 around the periphery of the structures. In Alpha4, the cells organised into unpolarised clusters which did not undergo luminal apoptosis and some structures also lacked a laminin 332-rich basement membrane. While MCF10a cells were viable in Alpha7, the majority remained as single cells throughout the 7-day culture period, with only some cells appearing to organise together into small, immature clusters. These results show that the soft, biocompatible, 3D and hydrated fibrillar scaffold that SAPHs provide for MCF10a cells is not sufficient to stimulate acinar development.

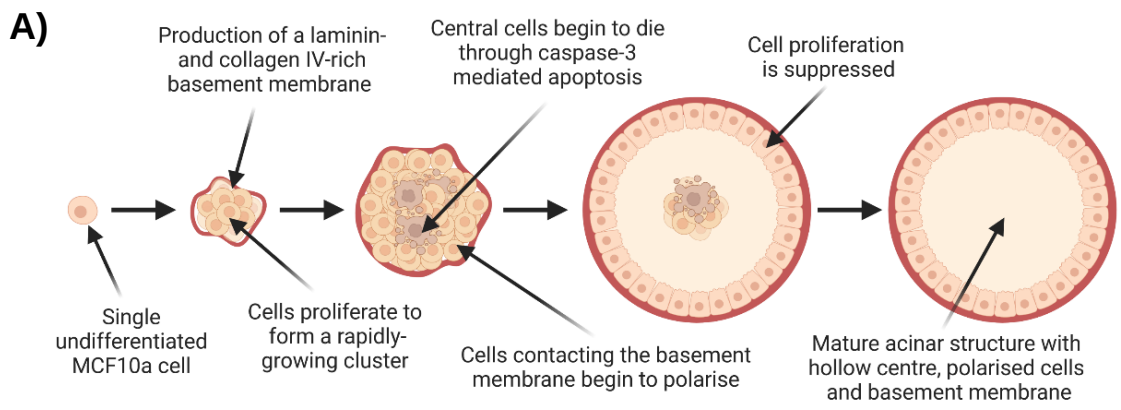

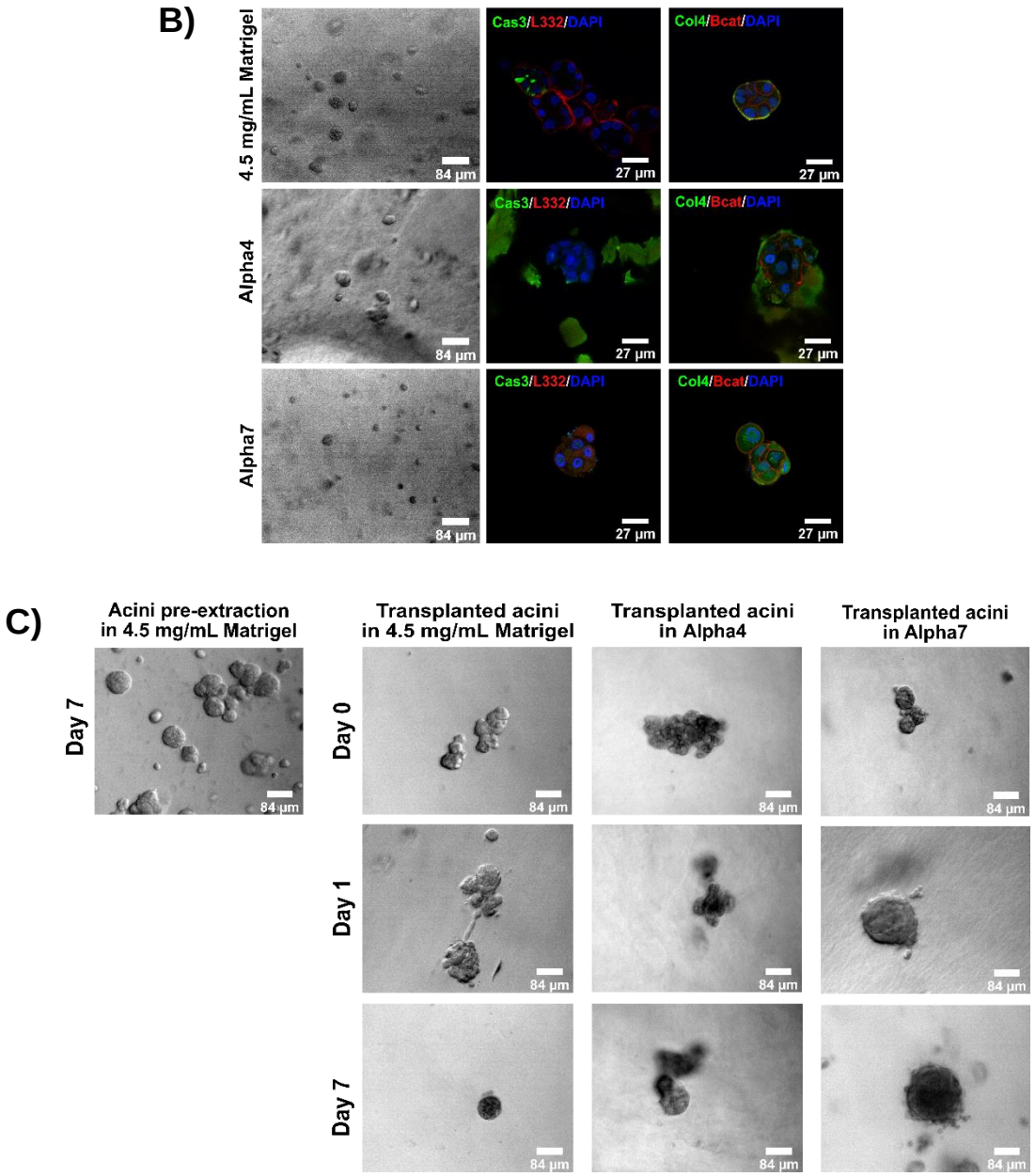

Fig. 1. Developing acini need to be in constant contact with a bioactive matrix to continue differentiating into acini. A) Diagram showing the biological events that occur during MCF10a acinar development. Single MCF10a cells proliferate into immature acini which produce a laminin 332- and collagen IV-rich basement membrane. As the immature acini grow, cells closest to the basement membrane begin to polarise, which gradually creates two cell populations within the acini: cells with apicobasal polarity that are in direct contact with the basement membrane and disorganised cells within the structure that do not contact the matrix. The inner population of cells begin to die via caspase-3 mediated apoptosis. The acini eventually become growth-arrested, and the centre of the structures become hollow as the remaining centralised cells die, creating mature acini. Adapted from [26]. Created with BioRender.com. B) Brightfield and IF images of MCF10a cells encapsulated in Matrigel, Alpha4 or Alpha7 gels which were maintained in culture for 7 days. The cells were subsequently extracted and stained with acinar markers: active caspase-3 (Cas3), laminin 332 (L332), collagen IV (Col4) and β-catenin (Bcat). Nuclei were stained with DAPI. C) Brightfield images of MCF10a acini that were grown in Matrigel for 7 days before being transplanted into Matrigel, Alpha4 or Alpha7 hydrogels. The transplanted acini were maintained for 7 days.

The acinar basement membrane forms early on during acinar development and regulates the differentiation of MECs into acinar structures by controlling cell polarisation and proliferation, primarily via integrin signalling [15, 26, 46, 120-124]. Indeed, Matrigel's ability to support acinar development is

attributed to the fact that it is enriched in key basement membrane proteins such as laminin 111, nidogen and collagen IV [23, 27, 125, 126]. Therefore, we theorised that the acinar basement membrane is all that is required to maintain acinar differentiation *in vitro* once it has assembled, and that SAPHs could provide a supportive 3D environment for developing acini to completely differentiate into mature acini. If so, this would eliminate the need to introduce exogenous biological factors into SAPHs to promote acinar differentiation. To investigate whether the acinar basement membrane drives acinar differentiation and therefore supports acinar development in SAPHs, we grew acinar structures from single MCF10a cells in Matrigel for 7 days before extracting the acini and transplanting them into Alpha4, Alpha7 or Matrigel hydrogels. The architecture of extracted and re-encapsulated acinar structures was preserved at day 0, which indicates that the extraction process did not disrupt acinar integrity (Fig. 1C). However, the acinar structures transferred to Alpha4 and Alpha7 hydrogels started to lose their differentiated phenotypes after just 1 day in culture. In these SAPHs, the cells within the structures were no longer polarised and luminal filling had occurred. In contrast, acini that had been transplanted into Matrigel hydrogels remained differentiated, as cells within the structures appeared to remain polarised around hollow lumens 7 days later. These results indicate that the basement membranes produced by MCF10a acini are not responsible for driving and maintaining acinar development and suggest that MCF10a cells require constant contact with an appropriate, bioactive ECM to differentiate into acini. Since the extracellular signals that MECs need to differentiate into acini are present in the native breast matrix and organic hydrogels such as Matrigel, identifying their key components may highlight the matrix factors responsible for driving acinar development.

We next wanted to investigate whether specific matrix proteins are required to maintain acinar development. The interstitial matrix protein collagen I and the basement membrane protein laminin 111 were selected for investigation because they are breast matrix proteins that can stimulate acinar development *in vitro* [3, 115, 117, 127-130]. Additionally, Matrigel consistently supports acinar development and is approximately 60% laminin 111, which led us to predict that laminin 111 can stimulate acinar development [28, 131]. We grew MCF10a acini in Matrigel for 7 days before we extracted them and transplanted them into either collagen I or laminin 111 hydrogels and asked whether acinar structures could remain differentiated in them. We found that acinar structures lost their organisation and became progressively more invasive when embedded in collagen I gels, whereas in laminin 111 gels the acini remained differentiated during the 7-day culture period (Fig. 2A). This indicates that laminin 111 alone can maintain acinar differentiation, which suggests that laminin 111 may be able to promote acinar development in non-differentiated MCF10a cells.

To determine whether laminin 111 can stimulate the formation of acini from single, non-differentiated MCF10a cells, we first encapsulated single MCF10a cells in laminin 111 or Matrigel hydrogels and compared their growth and organisation within the two hydrogels over 21 days. Brightfield images taken of the encapsulated MCF10a cells at days 1, 7, 12 and 21 showed that single MCF10a cells encapsulated in laminin 111 gels developed into spheroidal organoids that resembled the acini growing in Matrigel (Fig. 2B). This suggests that acini were growing in laminin 111 hydrogels.

Interestingly, we also found that some of the organoids growing in laminin 111 were clustering together around elongated MCF10a cells that were organised into duct-like structures. These structures in laminin 111 resembled the ductal-alveolar units that develop in the human mammary gland, which suggests that laminin 111 supports MCF10a differentiation into both acini and ducts [132, 133].

We then compared the growth rate of organoids grown from single MCF10a cells in Matrigel and laminin 111 gels. To quantify the number of MCF10a organoids growing within Matrigel and laminin 111 gels, MCF10a cells were encapsulated in Matrigel or laminin 111 hydrogels and maintained for 21 days. Organoids were stained with DAPI on days 7, 14 and 21 of culture and organoids with fluorescent nuclei were quantified. We found that Matrigel consistently supported the development of more organoids than laminin 111 at each time interval (Fig. 2C). Although the organoid population gradually declined over the 21-day culture period in both hydrogels, 1000 ± 100 organoids were counted in Matrigel at day 7 in contrast to the 500 ± 100 organoids counted in laminin 111, which is a 2-fold difference in organoid population. At day 14, the number of organoids growing in Matrigel and laminin 111 had declined, but there was still a noticeable difference in organoid population between the two hydrogels as 500 ± 100 organoids were counted in Matrigel while laminin 111 contained 200 ± 0 organoids. By day 21, Matrigel contained 400 ± 100 organoids whereas only 100 ± 0 organoids were counted in laminin 111. These results suggest that laminin 111 supports MCF10a acinar development but does not stimulate the development of as many acini as Matrigel does, which suggests that other extracellular factors present in Matrigel, such as growth factors, encourage acinar development.

A key hallmark of acinar development is their growth arrest at approximately 14 days, which results in the formation of relatively uniform, spheroidal acini that do not exceed 10,000 μm^2 in size [26, 55]. To investigate whether laminin 111 supports the development of growth arrested, spheroidal acini, we compared the size and shape of organoids grown from MCF10a cells in Matrigel or laminin 111 hydrogels at days 7, 14 and 21. Brightfield images of organoids encapsulated in Matrigel and laminin 111 were taken at these time intervals, and organoid area and circularity were subsequently measured. We found that there was no significant difference in organoid area between Matrigel and laminin 111 gels, except on day 14 (Fig. 2D). Between days 7 and 14, organoid area significantly increased in both Matrigel and laminin 111 hydrogels, which indicates that MCF10a cells within the organoids were proliferating as they do in developing acini. At day 14, the organoids growing in laminin 111 gels were found to be significantly larger than the organoids growing in Matrigel, although they did not exceed 10,000 μm^2 in size which suggests that these organoids were still acini. By day 21, organoids grown in Matrigel showed no significant change in area which indicates that they underwent growth arrest between days 14 and 21. There was a significant decrease in organoid area between days 14 and 21 in laminin 111 hydrogels and no significant difference in organoid area between day 21 Matrigel and laminin 111 cultures, which suggests that the organoids growing in laminin 111 also underwent growth arrest between days 14 and 21. These results indicate that laminin 111 supports the development of growth arrested acini. Comparison of organoid circularity

between Matrigel and laminin 111 cultures supported this theory, as no significant difference in organoid shape was found between Matrigel and laminin 111 cultures at any time point (Fig. 2E). Furthermore, organoid shape in both Matrigel and laminin 111 was consistently spherical throughout the 21-day culture period as a consistently high circularity score of 0.9 ± 0.01 was calculated for organoids in both hydrogels at each time interval. Together, these results indicate that laminin 111 supports the development of growth arrested, spheroidal acini.

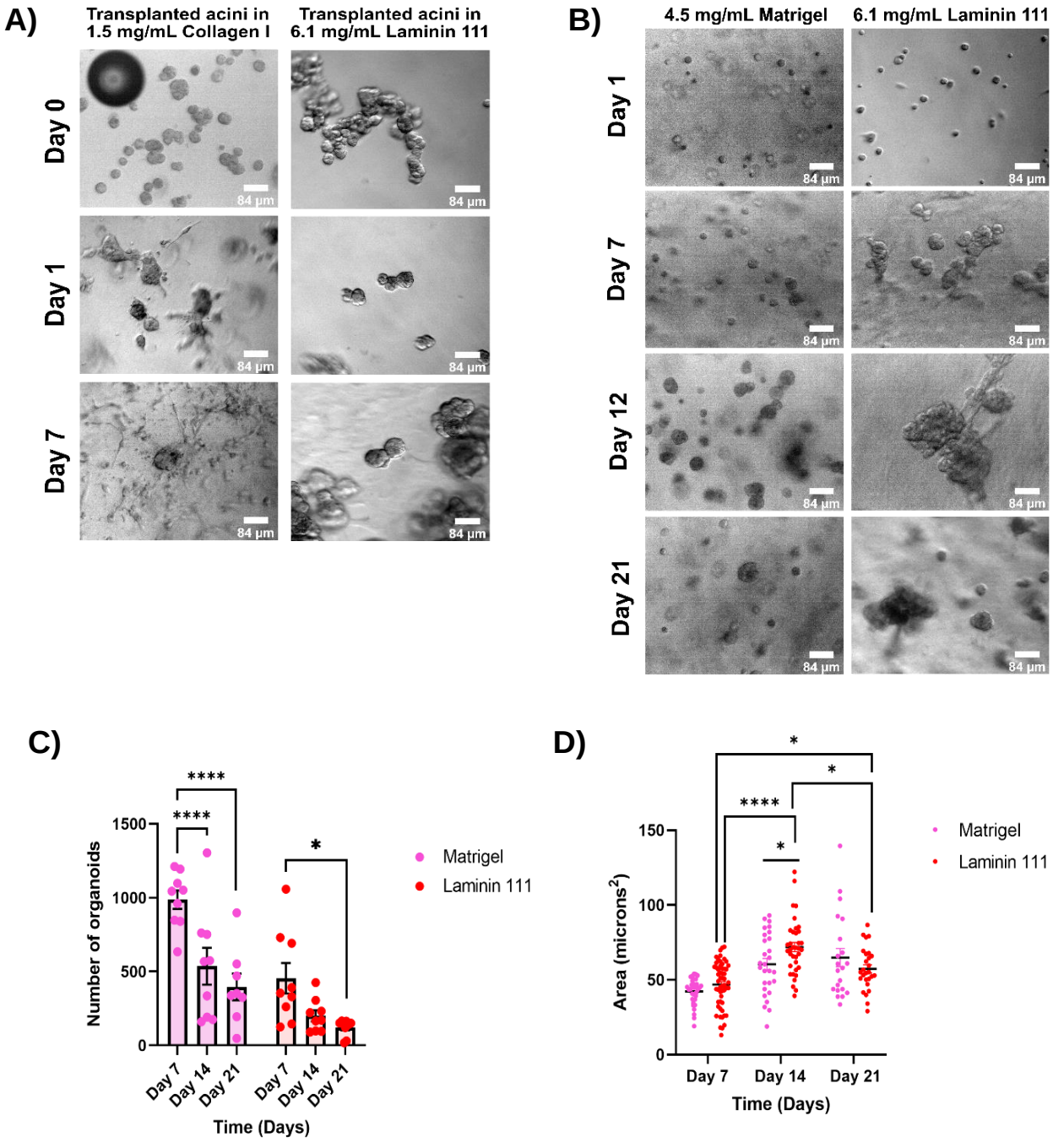

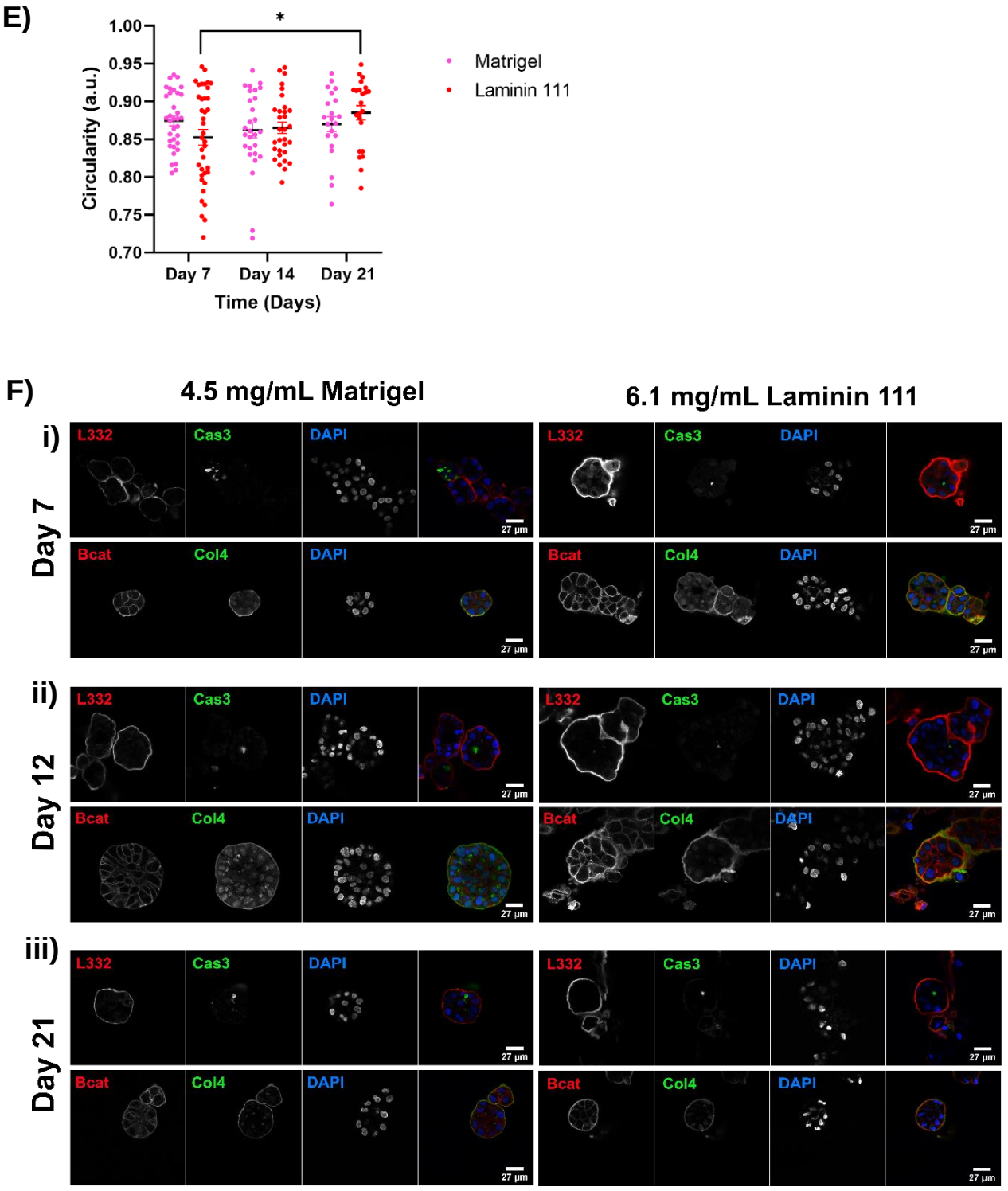

Fig. 2. Laminin 111 promotes and maintains the development of polarised acini. A) Brightfield images of MCF10a acini that were grown in Matrigel for 7 days before being transplanted into collagen I or laminin 111 hydrogels. The transplanted acini were maintained for 7 days. B) Brightfield images of MCF10a cells that were grown in Matrigel or laminin 111 hydrogels for 21 days. C) Number of organoids counted in Matrigel or laminin 111 hydrogels at days 7, 14 and 21. D) Area measurements of organoids cultured in Matrigel or laminin 111 hydrogels at days 7, 14 and 21. E) Circularity measurements of organoids grown in Matrigel or laminin 111 hydrogels at days 7, 14 and 21. All measurements were performed at least 3 times. (Data are shown as mean ± SEM; * p-value <0.05, ** p-value <0.01, *** p-value <0.001, **** p-value <0.0001). F) IF images of organoids that were grown from MCF10a cells in either Matrigel or laminin 111 hydrogels. At days 7 (i), 12 (ii) and 21 (iii), the organoids were extracted from the hydrogels and stained with acinar markers: active caspase-3 (Cas3), laminin 332 (L332), collagen IV (Col4) and β-catenin (Bcat). Nuclei were stained with DAPI. 20 (day 7), 10 (day 12) and 11 (day 21) organoids were quantified for positive laminin 332 staining in Matrigel. 19 (day 7), 19 (day 12) and 30 (day 21) organoids were quantified for positive laminin 332 staining in laminin 111 gels.

To confirm whether laminin 111 stimulates acinar development, we grew organoids in Matrigel or laminin 111 gels from single MCF10a cells. At days 7, 12 and 21, organoids were extracted from the hydrogels and probed for markers of acinar development using antibodies raised against active caspase-3, laminin 332, collagen IV and β-catenin. We found that acini form in laminin 111 gels (Fig. 2F). At day 7, 100% of developing acini with laminin 332- and collagen IV-rich basement membranes had begun to form in both Matrigel and laminin 111 gels (Fig. 2F-i). The acini had outer polarised layers of cells and were also beginning to undergo luminal, caspase-3 mediated apoptosis. At day 12, newer acini were still developing in both Matrigel and laminin 111 gels while some acini appeared to be fully mature with hollow lumens (Fig. 2F-ii). All observed acini had laminin 332-rich basement membranes. New acini were still developing in Matrigel and laminin 111 hydrogels by day 21. 100% of acini in Matrigel and 93% of acini in laminin 111 had a laminin 332-rich basement membrane, which indicates that Matrigel and laminin 111 constantly provide signals to MCF10a cells that stimulate acinar development (Fig. 2F-iii).

Taken together, these results show that laminin 111 can substitute for most functions of Matrigel such as acinar formation. Laminin 111 lacks the growth factors and other basement membrane proteins such as nidogen and collagen IV that are abundant in Matrigel, yet it stimulates and maintains acinar development in MCF10a cells which suggests that Matrigel's ability to support acinar development is primarily due to its high laminin 111 content. Furthermore, laminin 111 also supports the development of *in vivo*-like ductal-alveolar structures, which suggests that laminin 111 recapitulates the native breast microenvironment better than Matrigel.

Laminin 111 can functionalise self-assembling peptide hydrogels for mammary acinar development

Unlike organic hydrogels such as Matrigel, the SAPHs Alpha4 and Alpha7 are well-defined, reproducible, and tuneable cell scaffolds. This makes them desirable as 3D models of the breast matrix as their biochemical, physical, and mechanical properties can be independently modified to recapitulate the breast matrix at different stages of mammary gland development and disease progression. However, Alpha4 and Alpha7 do not support crucial *in vivo* MEC behaviours such as acinar development, which are necessary for a functional, representative model of the breast matrix. Since laminin 111 promotes *in vivo* MEC behaviours such as acinar formation and SAPHs are amenable to modifications that enhance their ability to support *in vivo* cell behaviours, we next investigated whether we could use laminin 111 to functionalise SAPHs for MEC culture.

To determine whether SAPHs can be functionalised for MEC culture by incorporating bioactive matrix proteins into the gels, we first attempted to functionalise Alpha4 with Matrigel by mixing undiluted Matrigel into Alpha4. Within 7 days, MCF10a cells that were encapsulated in these Matrigel-Alpha4 hydrogels developed into acini (Fig. 3A). This indicates that SAPHs can be functionalised to stimulate acinar development when a bioactive mixture of basement membrane proteins and growth factors is incorporated into the hydrogel. We next attempted to functionalise Alpha4 with laminin 111 by mixing as much laminin 111 as possible into the hydrogel. When we encapsulated MCF10a cells within the laminin 111-Alpha4 hydrogels, no acinar structures developed by day 7 (Fig. 3B). However, we found

that encapsulating MCF10a cells into laminin 111 hydrogels with the same final concentration as our laminin 111-Alpha4 hydrogels did promote acinar formation within 7 days (Fig. 3C). Since the final concentration of laminin 111 that was present in the laminin 111-Alpha4 hydrogels was shown to be a sufficient concentration for stimulating acinar development, our results suggested that some physical property of Alpha4 was preventing laminin 111 from providing differentiation cues to MCF10a cells.

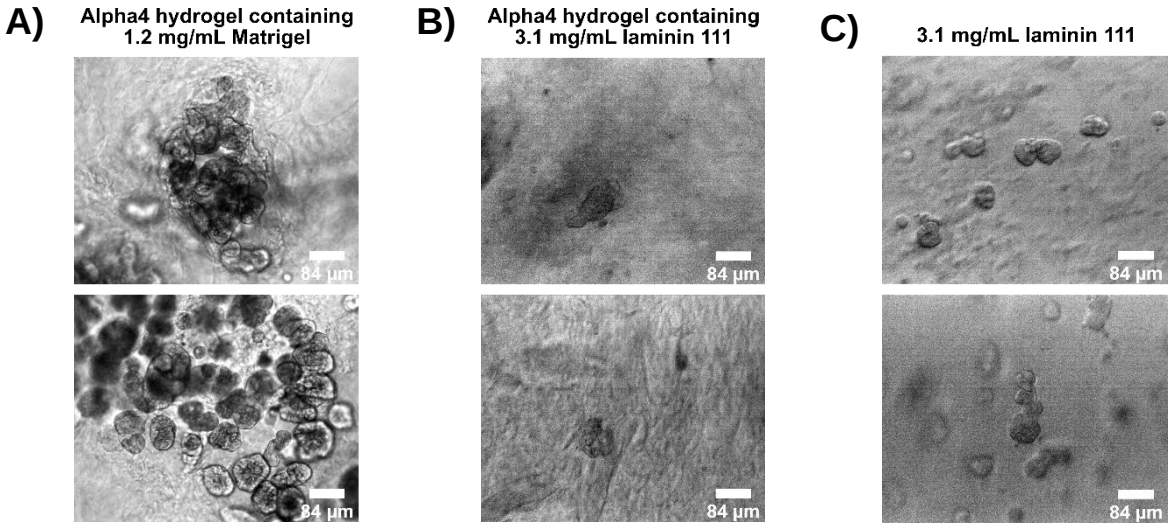

Fig. 3. Mixing laminin 111 into Alpha4 hydrogels does not stimulate acinar development. A) Brightfield images of day 7 MCF10a acini that were grown in either A) Alpha4 hydrogels containing 1.2 mg/mL Matrigel (final concentration), B) Alpha4 hydrogels containing 3.1 mg/mL laminin 111 (final concentration) or C) Laminin 111 hydrogels with a final concentration of 3.1 mg/mL.

To provide cells with complex biological cues that promote acinar differentiation, laminin 111 needs to self-assemble into an ordered network that binds to cell-surface receptors, which requires laminin to be localised to the cell surface so that binding interactions between the globular domains of laminin 111 (LG domains) and cell-surface moieties such as β1 integrins, dystroglycans, and sulphated glycolipids can occur [134-136]. Cells encapsulated in laminin-rich, organic hydrogels are provided with a polymerised laminin 111 scaffold that interacts with cell-surface receptors to direct cell behaviour, hence MECs encapsulated in a laminin 111 hydrogel can form acini. However, when laminin 111 is added into another hydrogel, it is possible that the laminin 111 monomers are dispersed throughout the hydrogel which could prevent them from polymerising into a bioactive network since the local laminin concentration within any given region of the hydrogel would be relatively low. Therefore, encapsulated MECs would be unable to receive the necessary cues for acinar differentiation. Since MECs need to have sustained, direct contact with a laminin 111-rich scaffold, we asked if it was possible to promote acinar development in Alpha4 hydrogels by providing MCF10a cells with the opportunity to bind to a laminin 111-rich matrix before encapsulating them within the SAPH.

To investigate this, we encapsulated MCF10a cells within 50 µL of concentrated laminin 111 (final laminin 111 concentration 3.1 mg/mL) or 18 µL of Matrigel (final Matrigel concentration 1.6 mg/mL) and incubated the mixtures at room temperature for 10 minutes before encapsulating the cell-matrix mixtures into separate Alpha4 hydrogels. After 7 days, the laminin 111-Alpha4 and Matrigel-Alpha4

hydrogels were imaged using brightfield microscopy before the organoids were extracted from the hydrogels and probed for markers of acinar development using antibodies raised against active caspase-3, laminin 332, collagen IV and β-catenin. We found that coating MCF10a cells with laminin 111 did not promote acinar development in Alpha4 hydrogels as the organoids were large, irregularly shaped and did not produce a collagen IV-rich basement membrane (Fig. 4A). Interestingly, some of the organoids appeared to be polarised and some organoids also appeared to have lumens, and all the organoids deposited laminin 332 into their immediate environment. This suggests that some laminin 111-coated MCF10a cells encapsulated within Alpha4 hydrogels received some cues from laminin 111. In contrast, Alpha4 hydrogels functionalised with Matrigel supported the development of polarised, spheroidal organoids with laminin 332- and collagen-rich basement membranes. These organoids also developed lumens through caspase-3 mediated apoptosis, which confirms that these structures were acini. These results indicate that incubating MCF10a cells with laminin 111 before encapsulating the cells in Alpha4 does enhance laminin 111 bioactivity as acinar phenotypes such as cell polarisation and lumen formation were observed in some organoids. Since MCF10a organoids grown in non-functionalised Alpha4 hydrogels or Alpha4 hydrogels that were mixed with laminin 111 did not polarise or form lumens, these results suggest that MCF10a cells incubated in laminin 111 were able to form contacts with the laminin and stimulate laminin 111 network assembly, which subsequently enhanced laminin 111's ability to direct MCF10a cell differentiation. However, the inability of laminin 111-coated MCF10a cells to fully differentiate into acini when they were encapsulated in Alpha4 hydrogels suggests that Alpha4 interferes with laminin 111 signalling.

Since acini require sustained contact with a laminin 111 network to remain differentiated, we next asked whether laminin 111-MCF10a cell contacts could be disrupted when laminin 111-coated acini are encapsulated in Alpha4. To investigate this, we grew acinar structures from MCF10a cells in Matrigel for 7 days before extracting the acini. Some acini were immediately transplanted into Matrigel hydrogels to provide a positive control. Remaining extracted acini were encapsulated in 50 µL of concentrated laminin 111 and incubated at room temperature for 10 minutes. Following incubation, the laminin 111-coated acini were then transplanted into Alpha4 hydrogels. Acinar integrity was maintained throughout the extraction and transplantation processes as polarised acini were found within the Matrigel and laminin 111-Alpha4 hydrogels immediately after their transplantation (Fig. 4B). Acini that were transplanted in Matrigel remained differentiated after 7 days in culture. In contrast, acini that were encapsulated in laminin 111 and then embedded in Alpha4 hydrogels became unpolarised after day 1. The acinar lumens filled with cells and some organoids became flattened and developed protrusions. These results indicate that the laminin 111-coated acini encapsulated within Alpha4 hydrogels do not have contact with a polymerised laminin 111 network as they were unable to remain differentiated over 7 days. However, the acini remained differentiated for 1 day after encapsulation, which suggests that they were briefly receiving signals to remain polarised acini in Alpha4. Together, these results suggest that encapsulation of MCF10a cells in laminin 111 promotes the assembly of a functional laminin 111 network but the subsequent encapsulation of the laminin 111-coated MCF10a cells within Alpha4 disrupts vital cell-laminin 111 interactions, which halts acinar development and leads to the MCF10a cells losing their differentiated phenotypes.

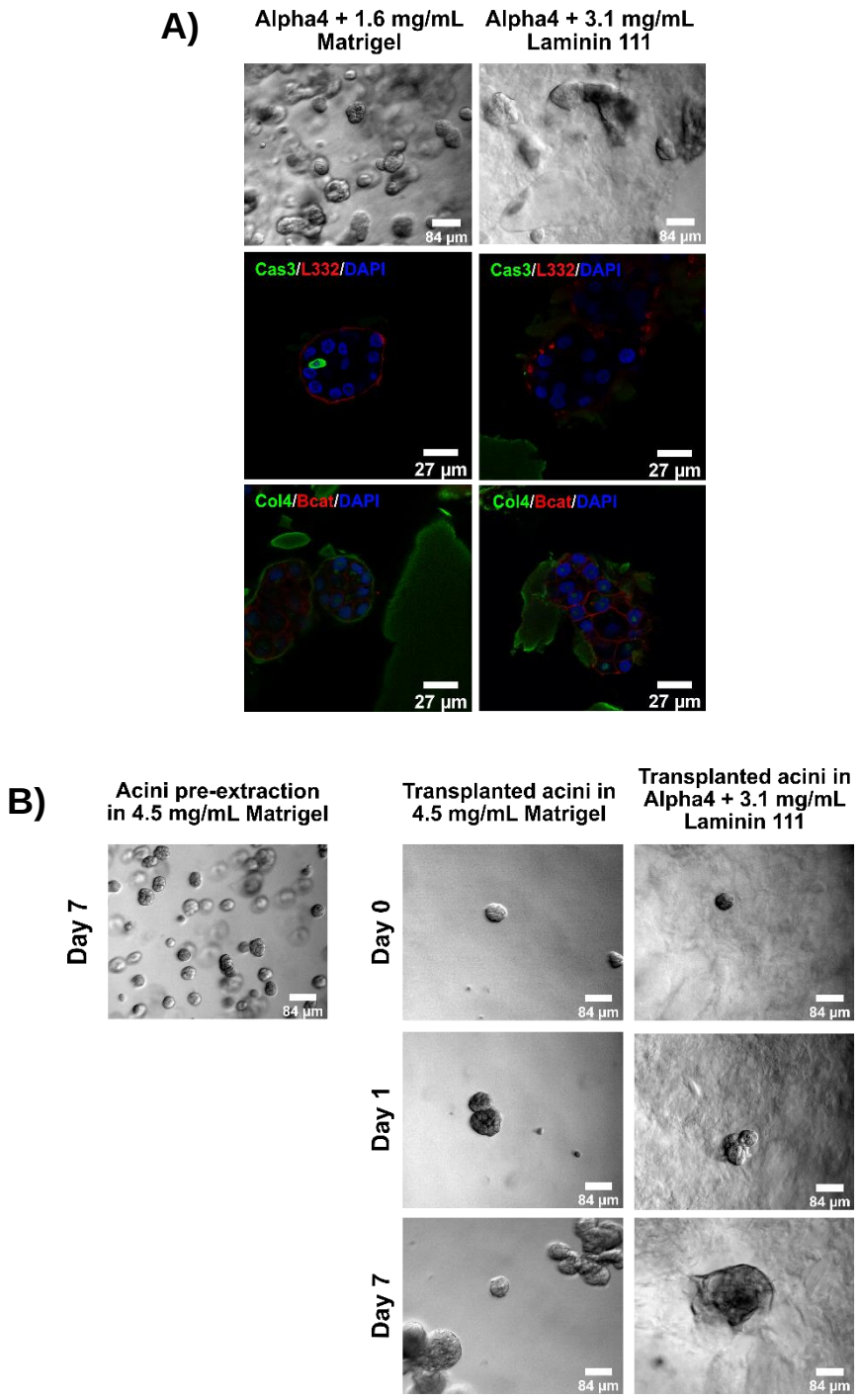

Fig. 4. Alpha4 cannot be functionalised with laminin 111 to promote acinar development. A) Brightfield and IF images of day 7 MCF10a cells encapsulated in laminin 111- (final concentration 3.1 mg/mL) or Matrigel-functionalised (final concentration1.6 mg/mL) Alpha4 hydrogels. To promote the assembly of a functional laminin 111 polymer network, MCF10a cells were incubated in either laminin 111 or Matrigel for 10 minutes at room temperature before being encapsulated in Alpha4. After being maintained for 7 days, the cells were extracted and stained with acinar markers: active caspase-3 (Cas3), laminin 332 (L332), collagen IV (Col4) and β-catenin (Bcat). Nuclei were stained with DAPI. 11 organoids were quantified for positive laminin 332 staining in laminin 111-functionalised Alpha4 gels. 13 organoids were quantified for positive laminin 332 staining in Matrigel-functionalised Alpha4 gels. B) Brightfield images of MCF10a acini that were grown in Matrigel for 7 days before being transplanted into Matrigel or incubated in laminin 111 for 10 minutes at room temperature. Incubated laminin 111-MCF10a mixtures were subsequently encapsulated into Alpha4. The transplanted acini were maintained for 7 days.

The successful functionalisation of Alpha4 for MEC culture with Matrigel, but not laminin 111, suggests that Alpha4's physical properties inhibit laminin 111's ability to attach to MCF10a cells and stimulate their development into acini. Previous studies have shown that laminin 111 network assembly at the cell surface is initiated by laminin anchorage to sulphated glycolipids in the outer leaflet of the cell membrane [135, 137]. Sulphated glycolipids bear an extracellular, negatively charged sulphate group which binds to positively charged regions within the LG4 domain of laminin 111 [138-141]. Since charge-driven interactions between laminin 111 and cells promote laminin 111 network assembly and signalling, we hypothesised that the positively charged peptide network of Alpha4 disrupts these crucial interactions and asked if MCF10a cells coated with laminin 111 could form acini in the negatively charged SAPH Alpha7.

To investigate this, we encapsulated MCF10a cells in either 50 µL of concentrated laminin 111 or 18 µL of Matrigel and incubated the cell-matrix mixtures as described above before encapsulating them into separate, negatively charged Alpha7 hydrogels. After 7 days in culture, MCF10a organoid morphology in the laminin 111-Alpha7 and Matrigel-Alpha7 hydrogels was examined using brightfield microscopy before the organoids were extracted from the hydrogels and probed for markers of acinar development using antibodies raised against active caspase-3, laminin 332, collagen IV and β-catenin. Both Matrigel-coated and laminin 111-coated MCF10a cells formed acini in Alpha7 hydrogels (Fig. 5A). 100% of the acini growing in Matrigel-Alpha7 and 93% of the acini growing in laminin 111-Alpha7 gels deposited a laminin 332- and collagen IV-rich basement membrane. The acini were also beginning to polarise and centralised, caspase-3 mediated apoptosis was occurring within some of the acini which indicated that they were forming lumens. We also found that acini developing within the Matrigel- and laminin 111-Alpha7 hydrogels were often surrounded by branched networks of elongated MCF10a cells that resembled the ductal structures growing in laminin 111 hydrogels. These results show that laminin 111 can promote *in vivo* MEC behaviours such as acinar development and, potentially, ductal organisation in MCF10a cells that are encapsulated within a negatively charged SAPH, which indicates that the net charge of SAPHs affects the ability of laminin 111 to bind to MECs and promote acinar formation.

We also wanted to see whether laminin 111-coated acini would remain differentiated when they were grown in Alpha7 hydrogels. To investigate this, we grew acini from MCF10a cells in Matrigel for 7 days before extracting the acini. Acini were either immediately transplanted into Matrigel hydrogels or they were incubated in 50 µL of concentrated laminin 111 for 10 minutes before being transplanted into Alpha7 hydrogels. Brightfield imaging confirmed that acinar integrity was maintained throughout the extraction and transplantation procedures and showed that acini encapsulated in Matrigel hydrogels remained differentiated after 7 days in culture (Fig. 5B). Laminin 111-coated acini that were transplanted into Alpha7 hydrogels also remained polarised and developed lumens over the 7-day culture period, which indicates that they were still differentiated acini. These results indicate that laminin 111-coated acini remain in contact with a functional laminin 111 network when they are encapsulated in a negatively charged SAPH, which suggests that the negatively charged peptide network of Alpha7 does not disrupt or inhibit binding interactions between laminin 111 and MECs.

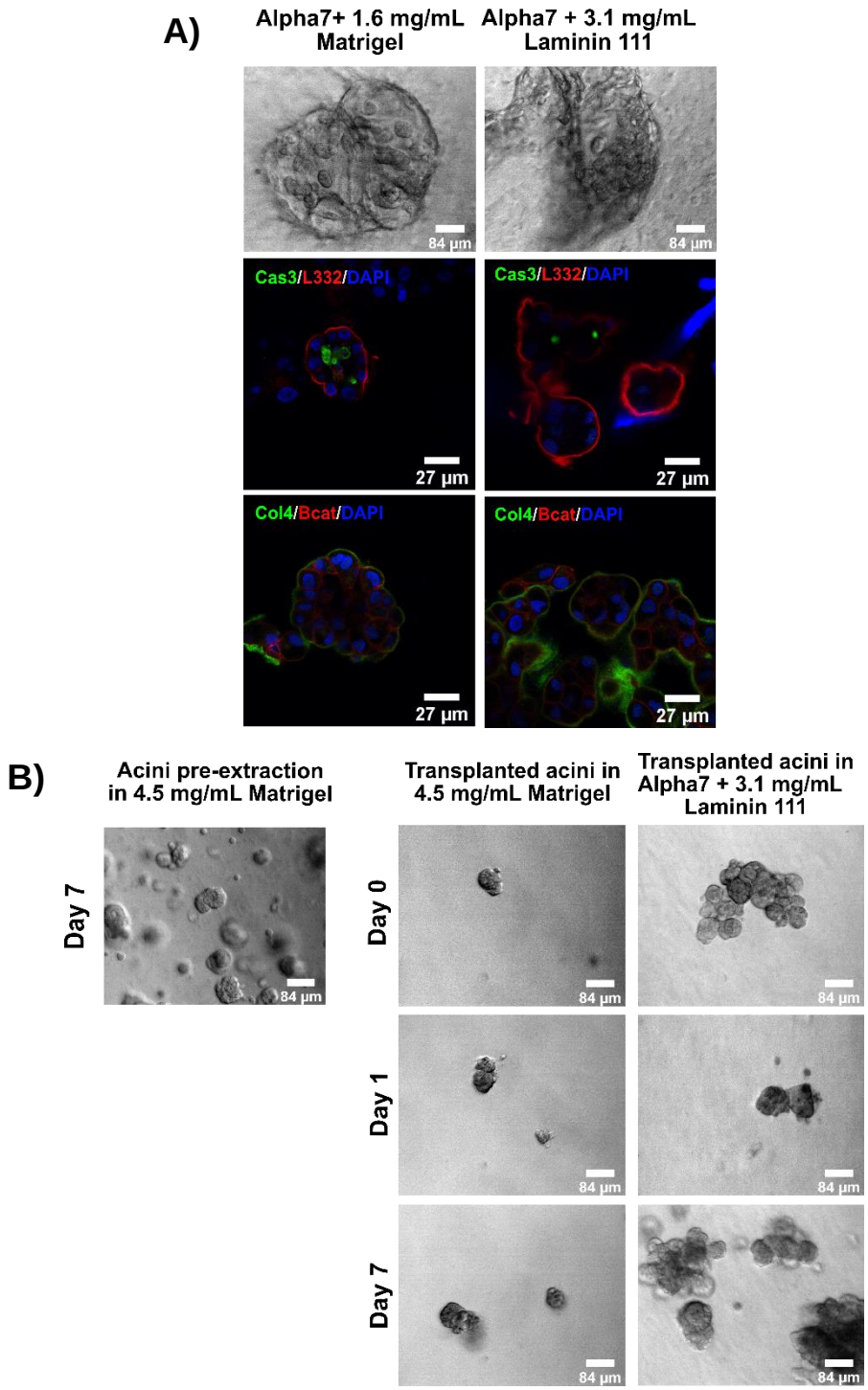

Fig. 5. Alpha7 can be functionalised with laminin 111 to support acinar development. A) Brightfield and IF images of day 7 MCF10a cells encapsulated in laminin 111- (final concentration 3.1 mg/mL) or Matrigel-functionalised (final concentration1.6 mg/mL) Alpha7 hydrogels. To promote the assembly of a functional laminin 111 polymer network, MCF10a cells were incubated in either laminin 111 or Matrigel for 10 minutes at room temperature before being encapsulated in Alpha7. After being maintained for 7 days, the cells were extracted and stained with acinar markers: active caspase-3 (Cas3), laminin 332 (L332), collagen IV (Col4) and β-catenin (Bcat). Nuclei were stained with DAPI. 15 organoids were quantified for positive laminin 332 staining in laminin 111-functionalised Alpha7 gels. 14 organoids were quantified for positive laminin 332 staining in Matrigel-functionalised Alpha7 gels. B) Brightfield images of MCF10a acini that were grown in Matrigel for 7 days before being transplanted into Matrigel or incubated in laminin 111 for 10 minutes at room temperature. Incubated laminin 111-MCF10a mixtures were subsequently encapsulated into Alpha7. The transplanted acini were maintained for 7 days.

Previous studies using Matrigel- and collagen I-based breast matrix models have identified downstream effectors of acinar differentiation and lactation that are stimulated in response to laminin 111-receptor binding events [116, 142-146]. However, these models are limited in their ability to accurately and consistently recapitulate the microenvironment that surrounds acini in healthy human breast tissue and therefore may stimulate non-physiological signalling cascades in MECs or independently affect their behaviour. Laminin 111-functionalised Alpha7 could substitute these established scaffolds to investigate laminin 111 signalling targets as it is a more defined and consistent scaffold that supports acinar development in human MECs. We encapsulated non-coated and laminin 111-coated MCF10a cells into separate Alpha7 hydrogels and asked if we could identify downstream intracellular effectors of acinar morphogenesis in Alpha7-encapsulated MCF10a cells using proteomics. Here, laminin 111-coated MCF10a cells were encapsulated in 18 µL of concentrated laminin 111 (final laminin concentration 1.0 mg/mL), which we found was sufficient to promote acinar formation (Fig. S1). After 7 days, we obtained lysates from these cultures and submitted them for LC-MS/MS to obtain global qualitative and quantitative proteomic data.

To control for proteins within the cell culture medium and for the addition of laminin 111 into functionalised Alpha7 hydrogels, we also submitted cell-free Alpha7 and laminin 111-Alpha7 lysates that were conditioned in cell culture medium for 7 days. Over 150 proteins were detected in the cell-free lysates, with laminin 111-functionalised lysates containing the greatest number of proteins (Fig. 6A). While we did not anticipate that our cell-free lysates would contain so many proteins, we theorised that most of the proteins detected in these samples could be attributed to contamination from sample handling and from samples that were previously run on the mass analyser. We expected to find that cell-free laminin 111-Alpha7 lysates contained laminin 111. Indeed, differential protein expression analysis of the proteins detected in the cell-free lysates showed that laminin 111-Alpha7 gels were significantly enriched in laminin 111 (Fig. 6B). However, other proteins such as the basement membrane protein nidogen-1 were also enriched in laminin 111-Alpha7 hydrogels (Table S1). Since the laminin 111 used to functionalise Alpha7 was purified from the basement membrane of EHS tumours, and nidogen-1 has high binding affinity for laminin 111, this suggests that the detected nidogen-1 was bound to the purified laminin 111 that was used to functionalise Alpha7. Nidogen-1 has been found to augment laminin 111 signalling in MECs and studies have indicated that nidogen-1 indirectly regulates tissue development by altering basement membrane organisation and establishing morphogenic gradients [147, 148]. Together, these results indicate that functionalising SAPHs with tissue-derived proteins such as laminin 111 can introduce other bioactive factors into the scaffold that may independently influence cell behaviour, affecting scaffold definition and reproducibility.

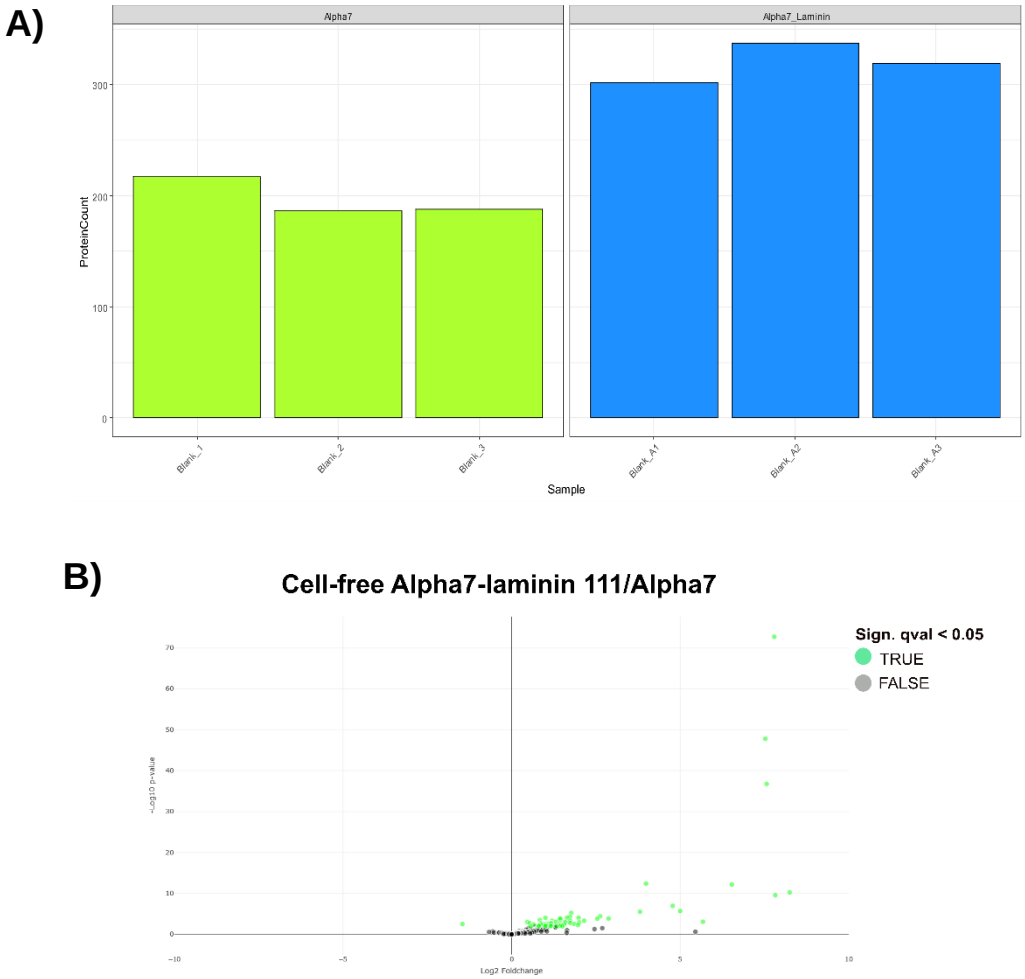

Fig. 6. Adding EHS-purified laminin 111 into Alpha7 reduces scaffold definition. A) Number of proteins quantified in cell-free Alpha7 and laminin 111-Alpha7 hydrogels. Three technical repeats per condition were prepared and submitted to obtain N=3. B) Mean fold-change of cellular protein abundance for cell-free laminin 111-Alpha7 samples against Alpha7 samples. The plot depicts upregulated (positive ratio) and downregulated (negative ratio) proteins in laminin 111-Alpha7 samples. P-values calculated via MSqRob from three independent replicates (p <0.05). EHS, Engelbreth-Holm-Swarm.

Significantly more proteins were detected in the cell-laden lysates than the cell-free lysates, which indicates that we were able to extract and detect many cellular proteins from Alpha7-encapsulated MCF10a cells (Fig. 7A). Principal component analysis of the cell-laden Alpha7 and laminin 111-Alpha7 lysates showed that there was strong separation between the lysates obtained from non-functionalised and laminin 111-functionalised samples (Fig. 7B). This suggests that functionalising Alpha7 with laminin 111 drives major changes in MCF10a protein expression. Differential protein expression analysis of the cell-laden samples confirmed this, as 438 proteins were found to be differentially expressed between MCF10a cells encapsulated in non-functionalised and laminin 111-functionalised Alpha7 hydrogels (Fig. 7C). Overlap comparison of significantly upregulated proteins in cell-free and cell-laden samples revealed that there were no proteins with the same log-fold change across cell-free and cell-laden samples, which indicated that all the significant changes in protein expression between non-functionalised and laminin 111-functionalised Alpha7 samples were due to changes in endogenous protein expression (Fig. S2). Proteins that were significantly upregulated in laminin 111-functionalised Alpha7 samples included basement membrane proteins such as agrin and

the α5, α1, β1 and γ 1 laminin subunits, which suggests that both laminin 511 and laminin 111 were being produced by MCF10a cells (Table S2). Cell adhesion proteins such as desmoplakin, β-catenin and δ-catenin were also upregulated in laminin 111-functionalised Alpha7 samples, indicating that the encapsulated MCF10a cells were forming cell adhesions such as desmosomes, which have been implicated as crucial mediators of MEC organisation and polarity during acinar development [149]. Proteins involved in intracellular signalling cascades such as protein tyrosine kinase beta and Ras GTPase-activating-like protein IQGAP1 were also enriched in laminin 111-functionalised Alpha7 samples. In contrast, many significantly downregulated proteins appeared to be proteins involved in maintaining cell functions such as DNA replication and repair, protein folding and metabolism. Together, these results indicate that laminin 111 stimulates basement membrane production and desmosome formation in MCF10a cells, which subsequently help drive acinar development.

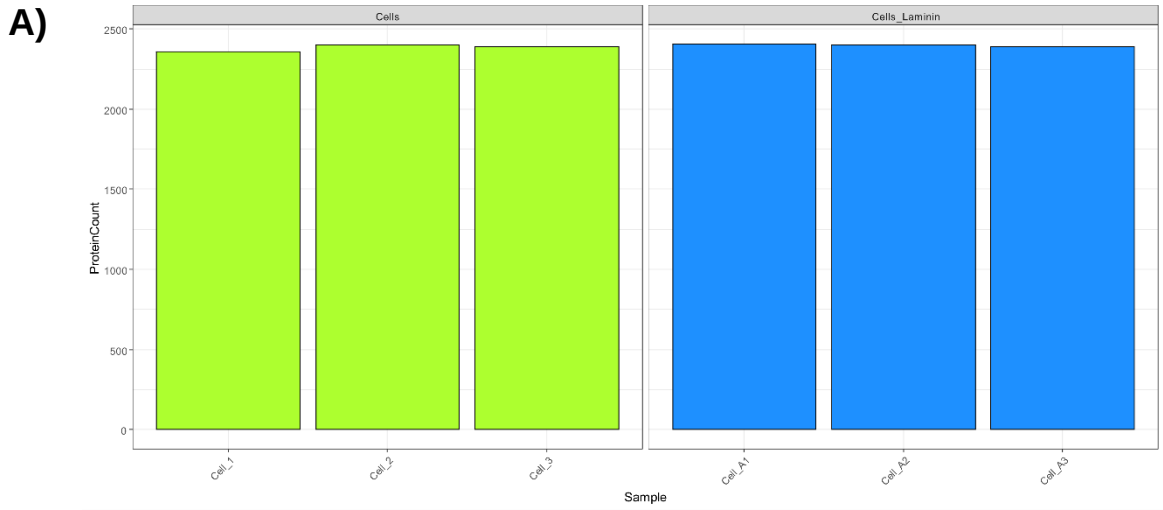

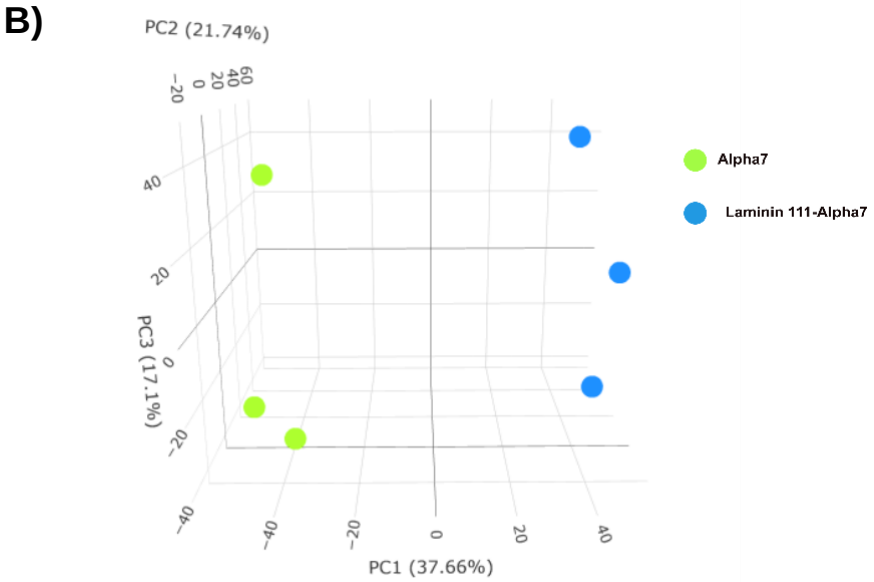

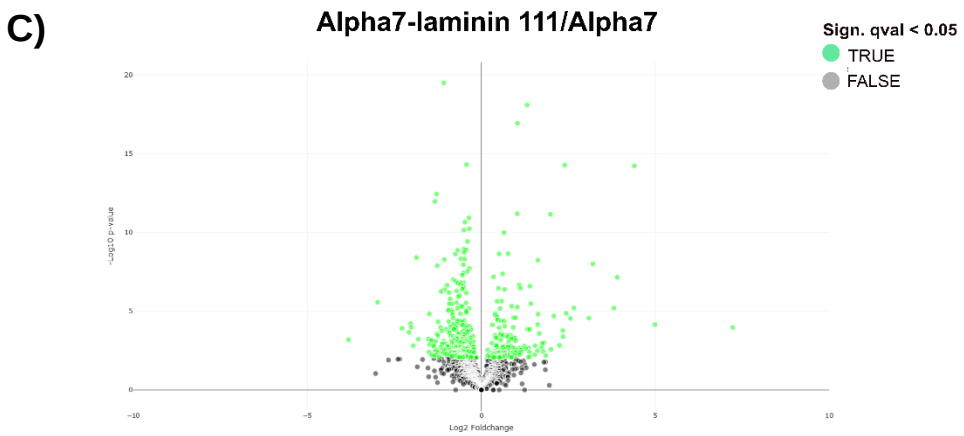

Fig. 7. Laminin 111 stimulates significant changes in MCF10a protein expression. A) Number of proteins quantified in cell-laden non-functionalised and laminin 111-functionalised Alpha7 samples. B) Principal component analysis of cell-laden non-functionalised and laminin 111-functionalised Alpha7 samples. C) Mean fold-change in protein expression for cell-laden laminin 111-functionalised Alpha7 samples. The volcano plot depicts upregulated (positive ratio) and downregulated (negative ratio) proteins in laminin 111-functionalised Alpha7 samples. P-values calculated via MSqRob from three independent replicates ($p < 0.05$).

Functional analysis showed that the most significantly upregulated biological processes in laminin 111-functionalised Alpha7 samples included epithelial cell differentiation and cytoskeletal reorganisation (Fig. 8A). We also found that cell junction assembly and organisation and cellular organisation were biological processes that were upregulated in 111-functionalised Alpha7 samples. All these processes occur during acinar development. In contrast, biological processes that were downregulated in laminin 111-functionalised Alpha7 samples were involved in DNA repair and replication as well as mitosis and protein synthesis (Fig. 8B). These results support our findings that laminin 111 stimulates acinar morphogenesis and suggest that laminin 111 suppresses proliferation.

Pathway analysis showed that the only significantly upregulated pathways detected in laminin 111-functionalised Alpha7 were involved in driving keratinisation, formation of a cornified envelope and nucleobase catabolism (Fig. 8C). Keratinisation and cornified envelope formation appeared to be enriched due to the upregulation of proteins involved in desmosome formation such as desmoplakin, envoplakin, plakoglobin, periplakin and plakophilin, which are all expressed in MECs [150]. Significantly downregulated pathways that were identified in laminin 111-functionalised Alpha7 were involved in pushing cells towards dividing, such as DNA elongation, replication, and mitosis (Fig. 8D). Expression of mitotic spindle-forming tubulins and lamin B1 were reduced in laminin 111-functionalised Alpha7 samples, suggesting that laminin 111 controls and downregulates MEC proliferation, which supports the findings of our functional analysis.

A)

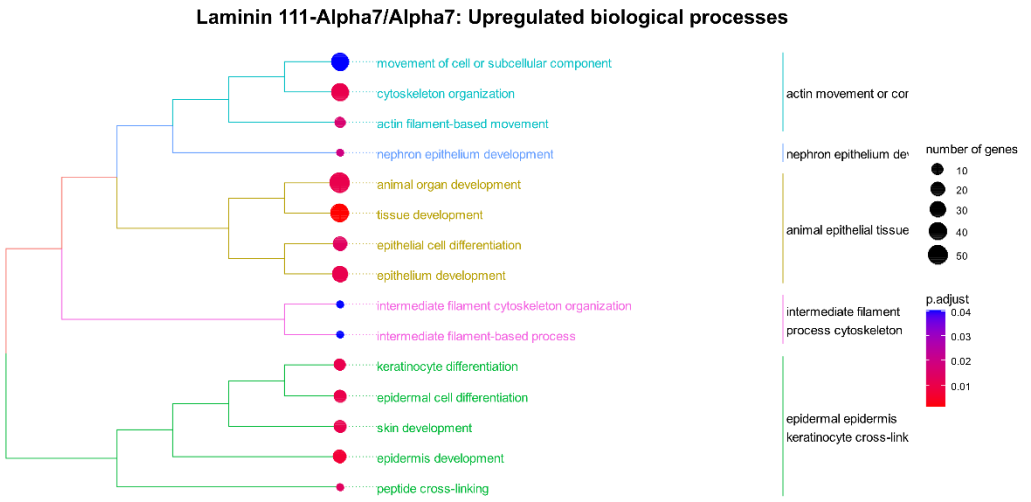
Laminin 111-Alpha7/Alpha7: Upregulated biological processes
movement of cell or subcellular component
cytoskeleton organization
actin filament-based movement
nephron epithelium development
animal organ development
tissue development
epithelial cell differentiation
epithelium development
intermediate filament cytoskeleton organization
intermediate filament-based process
keratinocyte differentiation
epidermal cell differentiation
skin development
epidermis development
peptide cross-linking
actin movement or cor
nephron epithelium de
animal epithelial tissue
intermediate filament
process cytoskeleton
epidermal epidermis
keratinocyte cross-link
number of genes
10
20
30
40
50
p.adjust
0.04
0.03
0.02
0.01

B)

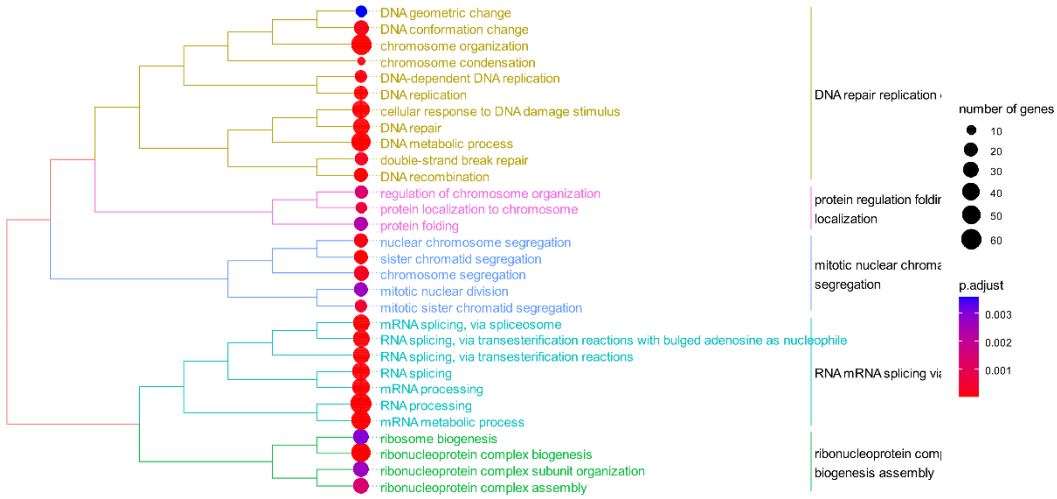
Laminin 111-Alpha7/Alpha7: Downregulated biological processes
DNA geometric change
DNA conformation change
chromosome organization
chromosome condensation
DNA-dependent DNA replication
DNA replication
cellular response to DNA damage stimulus
DNA repair
DNA metabolic process
double-strand break repair
DNA recombination
regulation of chromosome organization
protein localization to chromosome
protein folding
nuclear chromosome segregation
sister chromatid segregation
chromosome segregation
mitotic nuclear division
mitotic sister chromatid segregation
mRNA splicing, via spliceosome
RNA splicing, via transesterification reactions with bulged adenosine as nucleophile
RNA splicing, via transesterification reactions
RNA splicing
mRNA processing
RNA processing
mRNA metabolic process
ribosome biogenesis
ribonucleoprotein complex biogenesis
ribonucleoprotein complex subunit organization
ribonucleoprotein complex assembly
DNA repair replication
protein regulation foldir
localization
mitotic nuclear chroma
segregation
RNA mRNA splicing via
ribonucleoprotein com
biogenesis assembly
number of genes
10
20
30
40
50
60
p.adjust
0.003
0.002
0.001

C)

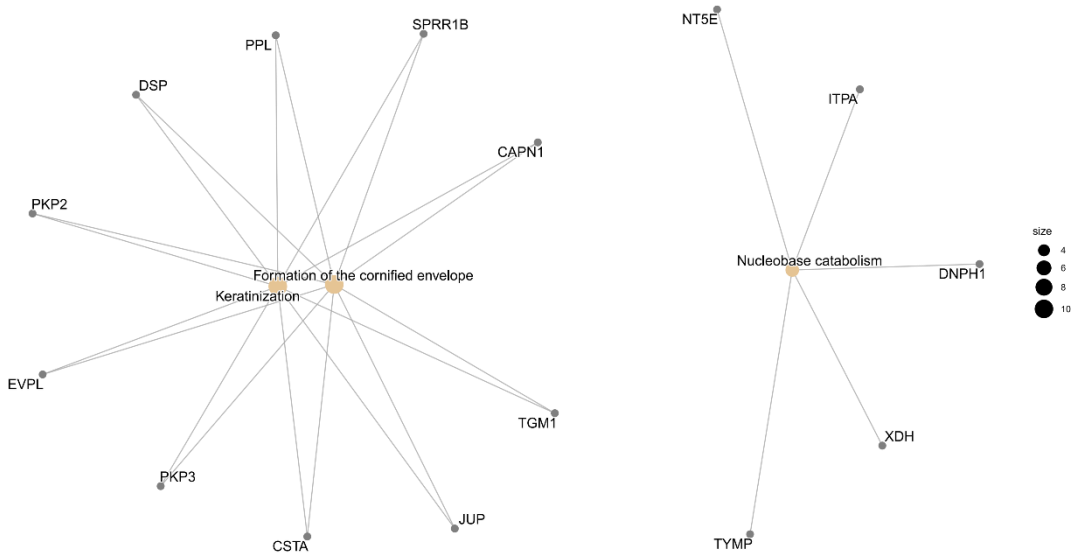
SPRR1B
PPL
DSP
CAPN1
PKP2
Formation of the cornified envelope
Keratinization
EVPL
TGM1
PKP3
JUP
CSTA
NT5E
ITPA
Nucleobase catabolism
DNPH1
XDH
TYMP
size
4
6
8
10

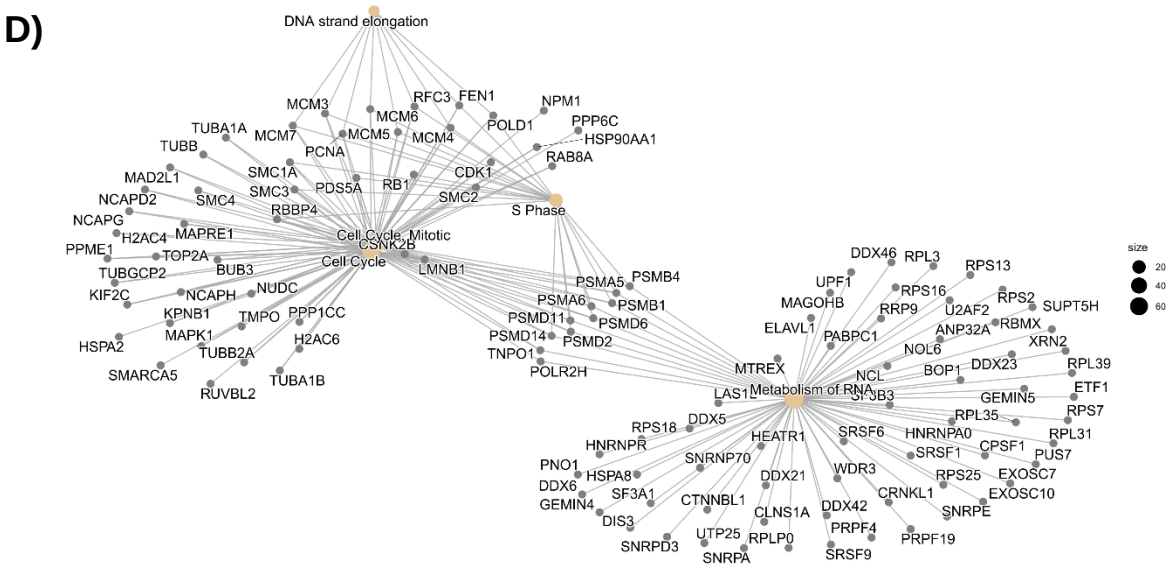

Fig. 8. Laminin 111 stimulates epithelial cell differentiation and suppresses proliferation. A) Upregulated biological processes in laminin 111-functionalised Alpha7 samples when compared against non-functionalised Alpha7 samples. B) Downregulated biological processes in laminin 111-functionalised Alpha7 samples when compared against non-functionalised Alpha7 samples. C) Upregulated pathways in laminin 111-functionalised Alpha7 samples when compared against non-functionalised Alpha7 samples. D) Downregulated pathways in laminin 111-functionalised Alpha7 samples when compared against non-functionalised Alpha7 samples. P-values calculated via Clusterprofiler from three independent replicates ($p < 0.05$).

Taken together, these results indicate that we can identify laminin 111-stimulated changes in global MCF10a protein expression using proteomics and connect these changes in protein expression to biological processes such as cell proliferation, adhesion, and organisation. The data we collected confirm that laminin 111-functionalised Alpha7 hydrogels support MCF10a acinar formation and indicate that laminin 111 promotes acinar morphogenesis by stimulating the formation of cell-cell adhesions and basement membrane production. Our results also suggest that laminin 111 suppresses MCF10a cell proliferation by inhibiting mitotic spindle formation and downregulating lamin B1 expression. Overall, these results show that laminin 111 can functionalise a negatively charged SAPH to stimulate *in vivo* MEC behaviours such as acinar development, creating a reproducible and defined scaffold that can substitute established models of the breast matrix.

Discussion

Matrigel is complex, inconsistent, poorly defined, difficult to modify and introduces xenogeneic and tumorigenic factors to cells [31, 60, 61, 67, 72]. However, Matrigel remains a popular substrate for MEC culture because it is relatively easy to use, versatile and widely available [30]. Furthermore, there are few alternative MEC scaffolds that are reproducible, tuneable and defined that can also substitute for the bioactivity of Matrigel [73]. There is therefore a need for a synthetic, simple, well-defined, and consistent hydrogel that can support complex cell behaviours. Here we have shown that we can stimulate MEC differentiation in a synthetic peptide hydrogel using the matrix glycoprotein laminin 111, allowing us to culture mammary organoids in a relatively consistent and defined 3D scaffold.

Consideration of the individual properties of SAPHs is an essential aspect of model development. Laminin 111 has been shown to stimulate *in vivo* cell behaviours such as cell differentiation within negatively and neutrally charged synthetic hydrogels [151-155]. We found that laminin 111 stimulated acinar formation in negatively charged Alpha7 hydrogels but not in positively charged Alpha4 hydrogels. Since acinar development was not stimulated in the positively charged Alpha4 hydrogel, this suggests that laminin 111 signalling can be influenced by the electrostatic properties of the hydrogel network. Indeed, electrostatic binding interactions between cationic lysine residues within the globular domains of laminin 111 and anionic cell-surface moieties such as sulphated glycolipids and dystroglycans are crucial for anchoring laminin 111 to the cell surface and initiating the assembly of a laminin 111 network that interacts with other cell-surface receptors such as integrins [122, 134, 135, 138, 141, 156-162]. Through these interactions with cell surface moieties, the laminin 111 network can regulate cell survival, adhesion, proliferation, polarisation, and basement membrane assembly [135, 163-168]. Laminin 111's inability to stimulate and maintain acinar differentiation in positively charged Alpha4 hydrogels suggests that Alpha4's cationic peptide network displaces existing electrostatic interactions between laminin 111 and anionic cell surface moieties and sequesters the anionic moieties from laminin 111. This would compromise the integrity of any pre-formed laminin 111 networks that managed to assemble around the MECs during the incubation period and stop laminin 111 monomers from adhering to dystroglycans and sulphated glycolipids, thus preventing laminin 111 from binding to cell-surface receptors and initiating acinar differentiation in MECs. The merit of this theory could be assessed by monitoring the accumulation of fluorescently labelled laminin 111 around MECs encapsulated within SAPHs with different net charges [168]. Nonetheless, studies have found that positively charged scaffolds form electrostatic interactions with negatively charged surfaces on cells and have also shown that they can sequester negatively charged proteins, demonstrating that the peptide sequence of SAPHs plays a critical role in dictating how cells and macromolecules will interact within, and with, the hydrogel [169-172].

We identified laminin 111 as the matrix protein responsible for driving and maintaining acinar development in MCF10a cells. Laminin 111 is a key basement membrane protein in the mammary gland that is responsible for promoting acinar differentiation in a variety of non-malignant MECs, and numerous studies have examined the mechanisms by which laminin 111 promotes and maintains

such a complex developmental process [42-44, 116, 120, 124]. Laminin 111 has been shown to drive MEC polarisation and promote milk production, and MECs cultured on laminin 111-rich scaffolds such as Matrigel form polarised, hollow acini that can secrete milk in response to lactogenic stimulation [115, 163, 166, 173-176]. Knockout studies in mice and rats have highlighted laminin 111 as the matrix protein responsible for driving basement membrane assembly during embryogenesis and Schwann cell formation, which could also be the case for mammary acinar development given our finding that laminin 111 alone is sufficient for stimulating MCF10a acinar development and, consequently, basement membrane formation [177-180].

Interestingly, we found that the basement membrane produced by MCF10a acini was unable to support acinar differentiation on its own. This suggests that MCF10a cells do not produce enough laminin 111 to drive their own differentiation into acini. Indeed, Gudjonsson et al. found that primary luminal MECs, which MCF10a cells resemble, produce laminins 332 and 511 but depend on their surrounding myoepithelial cells to produce laminin 111 as they cannot make it [115, 181]. Laminins 332 and 511 are also key mammary basement membrane proteins, although their roles in driving or maintaining mammary acinar development are less well-defined than laminin 111's. Studies have indicated that laminin 332 suppresses proliferation and keeps MECs anchored to the basement membrane, which suggests that laminin 332 promotes MEC survival and helps maintain acinar polarity [142, 182-185]. Laminin 511, unlike laminin 111 and laminin 332, is commonly overexpressed by tumorigenic MECs where it promotes tumour survival, proliferation, adhesion, and invasion which indicates that it regulates these same behaviours in non-tumorigenic MECs [186-188]. Of these laminins, only laminin 111 has been shown to stimulate acinar development as well as maintain it, which suggests that laminin 111 is the driver of acinar development in MECs while laminins 332 and 511 help maintain MEC differentiation [115, 163, 168, 175]. While we did find proteomic evidence to suggest that MCF10a cells produce some laminin 111, altogether our findings indicate that the amount they produce is not enough to maintain their own differentiation, hence they require an external source of laminin 111 to form acini.

We found that we could grow acini within a synthetic SAPH by mixing MCF10a cells directly with laminin 111 before encapsulating them in the negatively charged SAPH Alpha7. A similar outcome was also observed in a study conducted by Miroshnikova's group, where MCF10a cells were suspended in laminin 111 prior to encapsulation in the neutrally-charged PuraMatrix® SAPH RAD16-I [151]. They found that acini growing in RAD16-I gels mixed with laminin 111 could be maintained for 18 days, whereas we found that our Alpha7 cultures could not be maintained for more than 7 days due to the instability of the Alpha7 peptide network. Whether this instability could be resolved by increasing the peptide concentration or incorporating crosslinkers into the scaffold warrants investigation [189-193]. Miroshnikova also found that MCF10a cells can form acini following incubation with 100 µg/mL laminin 111, which is a significantly lower concentration of laminin 111 than was used in our investigations [151]. *In vitro* studies have indicated that there is no minimum laminin 111 concentration required to initiate laminin 111 polymerisation at cell surfaces, presumably because electrostatic bonds between laminin and anionic cell surface moieties enhance laminin polymerisation

by increasing the local concentration of laminin at the cell surface and potentially triggering conformational changes that stimulate polymerisation [194, 195]. Therefore, it is possible that Alpha7 hydrogels could be functionalised for MEC culture using a lower concentration of laminin 111. Indeed, many laminin 111-functionalised hydrogels have shown that laminin can stimulate *in vivo* cell behaviours when provided at low concentrations [153-155, 196, 197]. For example, hybrid gelatin-PEG hydrogels that presented immobilised laminin 111 (10 µg/mL) to mesenchymal stem cells and endothelial cells promoted vascular development and osteogenic differentiation, creating a vascularised and mineralised model of vascular bone tissue [198]. Interestingly, non-functionalised gelatin-PEG hydrogels also promoted osteogenic differentiation and vascular growth, although the vascular structures were found to be smaller than those grown in laminin 111-functionalised gelatin-PEG gels. This suggests that laminin 111 simply enhanced existing *in vivo* behaviours, which could be because the laminin 111 was presented to cells as monomers rather than as a multifunctional polymerised network. Alternatively, laminin 111's relatively limited functionality in these hydrogels could be because it is not native to bone tissue and thus may not stimulate osteogenic behaviours, highlighting the importance of providing cells with tissue-specific cues when modelling tissues in vitro [199, 200].

We obtained mass spectrometry data which confirms that laminin 111 stimulates MEC differentiation in MCF10a cells. While we found that functionalising Alpha7 with EHS-derived laminin 111 introduced other factors such as nidogen-1 into the scaffold, their lower expression levels relative to laminin 111 led us to decide that it was unlikely that they significantly influenced MEC behaviour. Our results showed that laminin 111 stimulated the expression of basement membrane proteins such as agrin and laminin 511, which are produced by mammary acini [115]. The increased production of polarity markers such as desmoplakins and catenins in laminin 111-functionalised Alpha7 gels and upregulation of processes involved in cytoskeletal reorganisation and cell junction assembly also indicates that laminin 111 drives apicobasal polarisation [149, 201-203]. This supports the findings of Gudjonsson et al., who showed that laminin 111 established apicobasal polarity in MECs embedded within collagen I gels [115]. We also found that biological events involved in pushing cells towards mitosis were downregulated in laminin 111-functionalised Alpha7 hydrogels, which indicates that laminin 111 suppresses MEC proliferation. While it is possible that these processes were downregulated because cells within laminin 111-functionalised Alpha7 gels were being released from mitosis, laminin 111 has been shown to suppress MEC growth and proliferation by inhibiting phosphoinositide-3 kinase (PI3K) activity and stimulating nuclear actin export into the cytoplasm [44, 146]. The suppression of proliferation via laminin 111-mediated actin export was linked other aspects of MEC differentiation, as knocking down the actin exporter exportin-6 in MECs disrupted their apical polarity and resulted in proliferative clusters with filled lumens [44]. Furthermore, disruption of laminin 111 binding to dystroglycans has been shown to enhance MEC proliferation by pushing cells into entering the S-phase of the cell cycle [168]. This stage of the cell cycle is where DNA replication occurs, and our data do suggest that proteins involved in driving DNA replication, such as minichromosome maintenance proteins and lamin B1, are downregulated in response to laminin 111 signalling [204, 205]. Whether laminin 111-mediated inhibition of proliferation is regulated through

nuclear actin transport or by another mechanism remains unknown, although it is possible that the downregulation of MAP kinase 1 (ERK) in laminin 111-functionalised Alpha7 gels may be responsible given its role in promoting proliferative and oncogenic behaviours in various MECs [176, 206, 207].

Our results highlighted several potential laminin 111-driven regulators of MEC differentiation, including Stat6, maspin and interferon regulatory factor 6, which have previously been implicated as regulators of MEC acinar differentiation [208-213]. While our understanding of their roles as regulators of MEC differentiation are limited, there is evidence to suggest that they mediate cell polarity, sensitise cells to apoptosis and regulate MEC entry into the cell cycle [209, 214]. These findings demonstrate that we can identify potential downstream effectors of laminin 111 that stimulate mammary acinar morphogenesis in our functionalised SAPH using mass spectrometry.

The results of our study show that Alpha7 can be functionalised for MEC culture by mixing the cells with laminin 111 prior to encapsulation, creating a scaffold that is relatively defined, simple and still potentially modifiable. We have shown that electrostatic interactions between the hydrogel network, cells, and laminin 111 can determine the efficacy of bioactive groups added into the scaffold. Using microscopy and mass spectrometry, we were able to confirm that laminin 111-functionalised Alpha7 hydrogels support MCF10a acinar differentiation and identified proteins that appear to be directly regulated by laminin 111, opening potential avenues of future research into MEC differentiation and its dysregulation during breast cancer development. We used EHS-derived laminin 111 to functionalise Alpha7 due to its availability and high concentration, creating a semi-synthetic, relatively defined scaffold that supported acinar formation. This functional model of the breast matrix offers researchers a more defined, consistent, and tuneable alternative to Matrigel that has strong potential to be functionalised with synthetic laminin 111 or its cell binding fragments to create a fully synthetic model of the breast matrix that is functionalised for MEC culture.

Acknowledgements

This project was funded by the University of Manchester, the UK Regenerative Medicine Platform (UKRMP; MR/R015651/1) and Manchester BioGEL.

Collagen gels were made by Alice Hales, who was supported by a Manchester Cancer Research Centre studentship. Mass spectrometry data analysis was carried out with the help of Craig Lawless, who was supported by the Wellcome Centre for Cell-Matrix Research (WCCMR; 203128/Z/16/Z).

In-gel digestion of lysates and proteomics was performed by the Biological Mass Spectrometry Core Facility; imaging was carried out at the Bioimaging Facility (supported by BBSRC, Wellcome and the University of Manchester Strategic Fund). We thank Drs. Ronan O'Cualain, Emma Keevil, Stacey Warwood, Julian Selley, David Knight, Steven Marsden, Roger Meadows and Peter March for Core Facility support.

Competing Interests

A. Saiani and A.F. Miller are co-founders, directors, and shareholders of Manchester BioGEL.

References

1. Frantz, C., K.M. Stewart, and V.M. Weaver, *The extracellular matrix at a glance.* Journal of Cell Science, 2010. **123**(24): p. 4195.
2. Pinet, K. and K.A. McLaughlin, *Mechanisms of physiological tissue remodeling in animals: Manipulating tissue, organ, and organism morphology.* Developmental Biology, 2019. **451**(2): p. 134-145.
3. Bonnans, C., J. Chou, and Z. Werb, *Remodelling the extracellular matrix in development and disease.* Nature reviews. Molecular cell biology, 2014. **15**(12): p. 786-801.
4. Lu, P., et al., *Extracellular matrix degradation and remodeling in development and disease.* Cold Spring Harbor perspectives in biology, 2011. **3**(12): p. 10.1101/cshperspect.a005058 a005058.
5. Karsdal, M.A., et al., *Extracellular Matrix Remodeling: The Common Denominator in Connective Tissue Diseases - Possibilities for Evaluation and Current Understanding of the Matrix as More Than a Passive Architecture, but a Key Player in Tissue Failure.* ASSAY and Drug Development Technologies, 2012. **11**(2): p. 70-92.
6. Inman, J.L., et al., *Mammary gland development: cell fate specification, stem cells and the microenvironment.* Development, 2015. **142**(6): p. 1028.
7. Slepicka, P.F., A.V.H. Somasundara, and C.O. dos Santos, *The molecular basis of mammary gland development and epithelial differentiation.* Seminars in Cell & Developmental Biology, 2021. **114**: p. 93-112.
8. Sternlicht, M.D., *Key stages in mammary gland development: The cues that regulate ductal branching morphogenesis.* Breast Cancer Research, 2005. **8**(1): p. 201.
9. Akhtar, N., et al., *Rac1 Controls Both the Secretory Function of the Mammary Gland and Its Remodeling for Successive Gestations.* Developmental Cell, 2016. **38**(5): p. 522-535.
10. Oakes, S.R., H.N. Hilton, and C.J. Ormandy, *Key stages in mammary gland development - The alveolar switch: coordinating the proliferative cues and cell fate decisions that drive the formation of lobuloalveoli from ductal epithelium.* Breast Cancer Research, 2006. **8**(2): p. 207.
11. Watson, C.J., *Key stages in mammary gland development - Involution: apoptosis and tissue remodelling that convert the mammary gland from milk factory to a quiescent organ.* Breast Cancer Research, 2006. **8**(2): p. 203.
12. Strange, R., et al., *Apoptotic cell death and tissue remodelling during mouse mammary gland involution.* Development, 1992. **115**(1): p. 49-58.
13. Fata, J.E., Z. Werb, and M.J. Bissell, *Regulation of mammary gland branching morphogenesis by the extracellular matrix and its remodeling enzymes.* Breast Cancer Research, 2003. **6**(1): p. 1.
14. Wicha, M.S., et al., *Effects of inhibition of basement membrane collagen deposition on rat mammary gland development.* Developmental Biology, 1980. **80**(2): p. 253-266.
15. Muschler, J. and C.H. Streuli, *Cell-matrix interactions in mammary gland development and breast cancer.* Cold Spring Harbor perspectives in biology, 2010. **2**(10): p. a003202-a003202.
16. Callens, C., et al., *Molecular features of untreated breast cancer and initial metastatic event inform clinical decision-making and predict outcome: long-term results of ESOPE, a single-arm prospective multicenter study.* Genome Medicine, 2021. **13**(1): p. 44.
17. Huo, Y., et al., *Analysis of Breast Cancer Based on the Dysregulated Network.* Frontiers in Genetics, 2022. **13**.
18. Feng, Y., et al., *Breast cancer development and progression: Risk factors, cancer stem cells, signaling pathways, genomics, and molecular pathogenesis.* Genes & diseases, 2018. **5**(2): p. 77-106.
19. Emerman, J.T. and D.R. Pitelka, *Maintenance and induction of morphological differentiation in dissociated mammary epithelium on floating collagen membranes.* In Vitro, 1977. **13**(5): p. 316-328.
20. Li, M.L., et al., *Influence of a reconstituted basement membrane and its components on casein gene expression and secretion in mouse mammary epithelial cells.* Proceedings of the National Academy of Sciences of the United States of America, 1987. **84**(1): p. 136-140.
21. Kleinman, H.K., et al., *Basement membrane complexes with biological activity.* Biochemistry, 1986. **25**(2): p. 312-318.
22. Orkin, R.W., et al., *A murine tumor producing a matrix of basement membrane.* The Journal of experimental medicine, 1977. **145**(1): p. 204-220.
23. Kleinman, H.K. and G.R. Martin, *Matrigel: Basement membrane matrix with biological activity.* Seminars in Cancer Biology, 2005. **15**(5): p. 378-386.

24. Lee, G.Y., et al., *Three-dimensional culture models of normal and malignant breast epithelial cells.* Nature methods, 2007. **4**(4): p. 359-365.
25. Rosenbluth, J.M., et al., *Organoid cultures from normal and cancer-prone human breast tissues preserve complex epithelial lineages.* Nature Communications, 2020. **11**(1): p. 1711.
26. Debnath, J., S.K. Muthuswamy, and J.S. Brugge, *Morphogenesis and oncogenesis of MCF-10A mammary epithelial acini grown in three-dimensional basement membrane cultures.* Methods, 2003. **30**(3): p. 256-268.
27. Petersen, O.W., et al., *Interaction with basement membrane serves to rapidly distinguish growth and differentiation pattern of normal and malignant human breast epithelial cells.* Proceedings of the National Academy of Sciences, 1992. **89**(19): p. 9064.
28. Corning. *Corning® Matrigel® Matrix: Frequently Asked Questions*. [PDF] 2021 [cited 20/02/2022]; Available from: https://www.corning.com/catalog/cls/documents/faqs/CLS-DL-CC-026.pdf.
29. Kleinman, H.K., et al., *Isolation and characterization of type IV procollagen, laminin, and heparan sulfate proteoglycan from the EHS sarcoma.* Biochemistry, 1982. **21**(24): p. 6188-6193.
30. Aisenbrey, E.A. and W.L. Murphy, *Synthetic alternatives to Matrigel.* Nature Reviews Materials, 2020. **5**(7): p. 539-551.
31. Vukicevic, S., et al., *Identification of multiple active growth factors in basement membrane matrigel suggests caution in interpretation of cellular activity related to extracellular matrix components.* Experimental Cell Research, 1992. **202**(1): p. 1-8.
32. Talbot, N.C. and T.J. Caperna, *Proteome array identification of bioactive soluble proteins/peptides in Matrigel: relevance to stem cell responses.* Cytotechnology, 2015. **67**(5): p. 873-883.
33. Benton, G., et al., *Matrigel: From discovery and ECM mimicry to assays and models for cancer research.* Advanced Drug Delivery Reviews, 2014. **79-80**: p. 3-18.
34. Niklander, J. and L. Paasonen, *Breast Cancer Cell Line MCF7 3D Culture Demonstrated in GrowDex ® and Matrigel*. UPM Biomedicals 2019.
35. Walker, S., et al., *Oncogenic activation of FAK drives apoptosis suppression in a 3D-culture model of breast cancer initiation.* Oncotarget, 2016. **7**(43): p. 70336-70352.
36. Aggeler, J., et al., *Cytodifferentiation of mouse mammary epithelial cells cultured on a reconstituted basement membrane reveals striking similarities to development in vivo.* Journal of Cell Science, 1991. **99**: p. 407-417
37. Schmeichel, K.L., V.M. Weaver, and M.J. Bissell, *Structural cues from the tissue microenvironment are essential determinants of the human mammary epithelial cell phenotype.* Journal of mammary gland biology and neoplasia, 1998. **3**(2): p. 201-213.
38. Weaver, V.M., et al., *Reversion of the malignant phenotype of human breast cells in three-dimensional culture and in vivo by integrin blocking antibodies.* The Journal of cell biology, 1997. **137**(1): p. 231-245.
39. Weaver, V.M., et al., *beta4 integrin-dependent formation of polarized three-dimensional architecture confers resistance to apoptosis in normal and malignant mammary epithelium.* Cancer cell, 2002. **2**(3): p. 205-216.
40. Bissell, M.J., et al., *Tissue structure, nuclear organization, and gene expression in normal and malignant breast.* 1999(0008-5472 (Print)).
41. Streuli, C.H., N. Bailey, and M.J. Bissell, *Control of mammary epithelial differentiation: basement membrane induces tissue-specific gene expression in the absence of cell-cell interaction and morphological polarity.* The Journal of cell biology, 1991. **115**(5): p. 1383-1395.
42. Barcellos-Hoff, M.H., et al., *Functional differentiation and alveolar morphogenesis of primary mammary cultures on reconstituted basement membrane.* Development, 1989. **105**(2): p. 223.
43. Swamydas, M., et al., *Matrix compositions and the development of breast acini and ducts in 3D cultures.* In Vitro Cellular & Developmental Biology - Animal, 2010. **46**(8): p. 673-684.
44. Fiore, A.P.Z.P., et al., *Laminin-111 and the Level of Nuclear Actin Regulate Epithelial Quiescence via Exportin-6.* Cell Reports, 2017. **19**(10): p. 2102-2115.
45. Sodunke, T.R., et al., *Micropatterns of Matrigel for three-dimensional epithelial cultures.* Biomaterials, 2007. **28**(27): p. 4006-4016.
46. Debnath, J., et al., *The Role of Apoptosis in Creating and Maintaining Luminal Space within Normal and Oncogene-Expressing Mammary Acini.* Cell, 2002. **111**(1): p. 29-40.

47. Muthuswamy, S.K., et al., *ErbB2, but not ErbB1, reinitiates proliferation and induces luminal repopulation in epithelial acini.* Nature cell biology, 2001. **3**(9): p. 785-792.
48. Alcaraz, J., et al., *Laminin and biomimetic extracellular elasticity enhance functional differentiation in mammary epithelia.* The EMBO journal, 2008. **27**(21): p. 2829-2838.
49. Sumbal, J., et al., *Primary Mammary Organoid Model of Lactation and Involution.* Frontiers in Cell and Developmental Biology, 2020. **8**: p. 68.
50. Paszek, M.J., et al., *Tensional homeostasis and the malignant phenotype.* Cancer Cell, 2005. **8**(3): p. 241-254.
51. Lance, A., et al., *Increased extracellular matrix density decreases MCF10A breast cell acinus formation in 3D culture conditions.* Journal of Tissue Engineering and Regenerative Medicine, 2016. **10**(1): p. 71-80.
52. Lee, J.Y., et al., *YAP-independent mechanotransduction drives breast cancer progression.* Nature Communications, 2019. **10**(1): p. 1848.
53. Nguyen-Ngoc, K.V. and A.J. Ewald, *Mammary ductal elongation and myoepithelial migration are regulated by the composition of the extracellular matrix.* Journal of Microscopy, 2013. **251**(3): p. 212-223.
54. Anguiano, M., et al., *The use of mixed collagen-Matrigel matrices of increasing complexity recapitulates the biphasic role of cell adhesion in cancer cell migration: ECM sensing, remodeling and forces at the leading edge of cancer invasion.* PLOS ONE, 2020. **15**(1): p. e0220019.
55. Chaudhuri, O., et al., *Extracellular matrix stiffness and composition jointly regulate the induction of malignant phenotypes in mammary epithelium.* Nature Materials, 2014. **13**: p. 970.
56. Cavo, M., et al., *A new cell-laden 3D Alginate-Matrigel hydrogel resembles human breast cancer cell malignant morphology, spread and invasion capability observed "in vivo".* Scientific Reports, 2018. **8**(1): p. 5333.
57. Stowers, R.S., et al., *Matrix stiffness induces a tumorigenic phenotype in mammary epithelium through changes in chromatin accessibility.* Nature Biomedical Engineering, 2019.
58. Wood, A., et al., *Increased microenvironment stiffness leads to altered aldehyde metabolism and DNA damage in mammary epithelial cells through a RhoA-dependent mechanism.* bioRxiv, 2020: p. 2020.10.06.327726.
59. Polykandriotis, E., et al., *To matrigel or not to matrigel.* The American journal of pathology, 2008. **172**(5): p. 1441-1442.
60. Vaillant, F., G.J. Lindeman, and J.E. Visvader, *Jekyll or Hyde: does Matrigel provide a more or less physiological environment in mammary repopulating assays?* Breast Cancer Research, 2011. **13**(3): p. 108.
61. Hughes, C.S., L.M. Postovit, and G.A. Lajoie, *Matrigel: A complex protein mixture required for optimal growth of cell culture.* PROTEOMICS, 2010. **10**(9): p. 1886-1890.
62. Gillette, K.M., I. Forbes K Fau - Sehgal, and I. Sehgal, *Detection of matrix metalloproteinases (MMP), tissue inhibitor of metalloproteinase-2, urokinase and plasminogen activator inhibitor-1 within matrigel and growth factor-reduced matrigel basement membrane.* 2003(0300-8916 (Print)).
63. Hansen, K.C., et al., *An in-solution ultrasonication-assisted digestion method for improved extracellular matrix proteome coverage.* Molecular & cellular proteomics : MCP, 2009. **8**(7): p. 1648-1657.
64. Soofi, S.S., et al., *The elastic modulus of Matrigel™ as determined by atomic force microscopy.* Journal of Structural Biology, 2009. **167**(3): p. 216-219.
65. Reed, J., et al., *In Situ Mechanical Interferometry of Matrigel Films.* Langmuir, 2009. **25**(1): p. 36-39.
66. Slater, K., Partridge, J. and Nandivada, H. , *Tuning the Elastic Moduli of Corning® Matrigel® and Collagen I 3D Matrices by Varying the Protein Concentration*, in *Corning Application Note*. 2018.
67. Prokhorova, T.A., et al., *Teratoma Formation by Human Embryonic Stem Cells Is Site Dependent and Enhanced by the Presence of Matrigel.* Stem Cells and Development, 2008. **18**(1): p. 47-54.
68. Mehta, R.R., et al., *Growth and metastasis of human breast carcinomas with Matrigel in athymic mice.* 1993(0167-6806 (Print)).
69. Mullen, P., et al., *Effect of matrigel on the tumorigenicity of human breast and ovarian carcinoma cell lines.* International Journal of Cancer, 1996. **67**(6): p. 816-820.

70. Liu, H., et al., *Removal of lactate dehydrogenase-elevating virus from human-in-mouse breast tumor xenografts by cell-sorting.* Journal of Virological Methods, 2011. **173**(2): p. 266-270.
71. Riley, V., et al., *The LDH Virus: An Interfering Biological Contaminant.* Science, 1978. **200**(4338): p. 124-126.
72. Peterson, N.C., *From Bench to Cageside: Risk Assessment for Rodent Pathogen Contamination of Cells and Biologics.* ILAR Journal, 2008. **49**(3): p. 310-315.
73. Kozlowski, M.T., C.J. Crook, and H.T. Ku, *Towards organoid culture without Matrigel.* Communications Biology, 2021. **4**(1): p. 1387.
74. Caliari, S.R. and J.A. Burdick, *A practical guide to hydrogels for cell culture.* Nature Methods, 2016. **13**: p. 405.
75. Sawhney, A.S., C.P. Pathak, and J.A. Hubbell, *Bioerodible hydrogels based on photopolymerized poly(ethylene glycol)-co-poly(.alpha.-hydroxy acid) diacrylate macromers.* Macromolecules, 1993. **26**(4): p. 581-587.
76. Díaz-Bello, B., et al., *Method for the Direct Fabrication of Polyacrylamide Hydrogels with Controlled Stiffness in Polystyrene Multiwell Plates for Mechanobiology Assays.* ACS Biomaterials Science & Engineering, 2019. **5**(9): p. 4219-4227.
77. Tse, J.R. and A.J. Engler, *Preparation of Hydrogel Substrates with Tunable Mechanical Properties.* Current Protocols in Cell Biology, 2010. **47**(1): p. 10.16.1-10.16.16.
78. Pelham Robert, J. and Y.-l. Wang, *Cell locomotion and focal adhesions are regulated by substrate flexibility.* Proceedings of the National Academy of Sciences, 1997. **94**(25): p. 13661-13665.
79. Appel, E.A., et al., *Supramolecular polymeric hydrogels.* Chemical Society Reviews, 2012. **41**(18): p. 6195-6214.
80. Li, X., et al., *Functional Hydrogels With Tunable Structures and Properties for Tissue Engineering Applications.* Frontiers in Chemistry, 2018. **6**(499).
81. Zustiak, S.P. and J.B. Leach, *Hydrolytically Degradable Poly(Ethylene Glycol) Hydrogel Scaffolds with Tunable Degradation and Mechanical Properties.* Biomacromolecules, 2010. **11**(5): p. 1348-1357.
82. Smithmyer, M.E., L.A. Sawicki, and A.M. Kloxin, *Hydrogel scaffolds as in vitro models to study fibroblast activation in wound healing and disease.* Biomaterials Science, 2014. **2**(5): p. 634-650.
83. Duval, K., et al., *Modeling Physiological Events in 2D vs. 3D Cell Culture.* Physiology, 2017. **32**(4): p. 266-277.
84. Nowak, M., et al., *Modular GAG-matrices to promote mammary epithelial morphogenesis in vitro.* Biomaterials, 2017. **112**: p. 20-30.
85. Livingston, M.K., et al., *Evaluation of PEG-based hydrogel influence on estrogen receptor driven responses in MCF7 breast cancer cells.* ACS biomaterials science & engineering, 2019. **5**(11): p. 6089-6098.
86. Drury, J.L. and D.J. Mooney, *Hydrogels for tissue engineering: scaffold design variables and applications.* Biomaterials, 2003. **24**(24): p. 4337-4351.
87. Hubbell, J.A., *Bioactive biomaterials.* Current Opinion in Biotechnology, 1999. **10**(2): p. 123-129.
88. Liu, V.A. and S.N. Bhatia, *Three-Dimensional Photopatterning of Hydrogels Containing Living Cells.* Biomedical Microdevices, 2002. **4**(4): p. 257-266.
89. Lowe, A.B., *Thiol-ene "click" reactions and recent applications in polymer and materials synthesis.* Polymer Chemistry, 2010. **1**(1): p. 17-36.
90. Vihola, H., et al., *Cytotoxicity of thermosensitive polymers poly(N-isopropylacrylamide), poly(N-vinylcaprolactam) and amphiphilically modified poly(N-vinylcaprolactam).* Biomaterials, 2005. **26**(16): p. 3055-3064.
91. Zhang, S., et al., *Unusually stable β-sheet formation in an ionic self-complementary oligopeptide.* Biopolymers, 1994. **34**(5): p. 663-672.
92. Caplan, M.R., et al., *Control of self-assembling oligopeptide matrix formation through systematic variation of amino acid sequence.* Biomaterials, 2002. **23**(1): p. 219-227.
93. Boothroyd, S., A.F. Miller, and A. Saiani, *From fibres to networks using self-assembling peptides.* Faraday Discussions, 2013. **166**(0): p. 195-207.
94. Roberts, D., et al., *Effect of Peptide and Guest Charge on the Structural, Mechanical and Release Properties of β-Sheet Forming Peptides.* Langmuir, 2012. **28**(46): p. 16196-16206.
95. Burgess, K.A., et al., *Functionalised peptide hydrogel for the delivery of cardiac progenitor cells.* Materials Science and Engineering: C, 2021. **119**: p. 111539.

96. Ligorio, C., et al., *TGF-β3-loaded graphene oxide - self-assembling peptide hybrid hydrogels as functional 3D scaffolds for the regeneration of the nucleus pulposus.* Acta Biomaterialia, 2021. **127**: p. 116-130.
97. Gao, J., et al., *Controlling Self-Assembling Peptide Hydrogel Properties through Network Topology.* Biomacromolecules, 2017. **18**(3): p. 826-834.
98. Scelsi, A., et al., *Tuning of hydrogel stiffness using a two-component peptide system for mammalian cell culture.* Journal of Biomedical Materials Research Part A, 2019. **107**(3): p. 535-544.
99. Lachowski, D., et al., *Self-Assembling Polypeptide Hydrogels as a Platform to Recapitulate the Tumor Microenvironment.* Cancers, 2021. **13**(13).
100. Mujeeb, A., et al., *Self-assembled octapeptide scaffolds for in vitro chondrocyte culture.* Acta Biomaterialia, 2013. **9**(1): p. 4609-4617.
101. Wan, S., et al., *Self-assembling peptide hydrogel for intervertebral disc tissue engineering.* Acta Biomaterialia, 2016. **46**: p. 29-40.
102. Kumar, D., et al., *Peptide Hydrogels—A Tissue Engineering Strategy for the Prevention of Oesophageal Strictures.* Advanced Functional Materials, 2017. **27**(38): p. 1702424.
103. Faroni, A., et al., *Self-Assembling Peptide Hydrogel Matrices Improve the Neurotrophic Potential of Human Adipose-Derived Stem Cells.* Advanced Healthcare Materials, 2019. **8**(17): p. 1900410.
104. BioGEL, M. *PeptiGels for 2D and 3D Cell Culture*. 2021 [cited 06/03/2022]; Available from: https://manchesterbiogel.com/products/peptigels.
105. Worthington, P., D.J. Pochan, and S.A. Langhans, *Peptide Hydrogels - Versatile Matrices for 3D Cell Culture in Cancer Medicine.* Frontiers in oncology, 2015. **5**: p. 92-92.
106. Ashworth, J.C., et al., *Preparation of a User-Defined Peptide Gel for Controlled 3D Culture Models of Cancer and Disease.* JoVE, 2020(166): p. e61710.
107. Mi, K., et al., *Influence of a Self-Assembling Peptide, RADA16, Compared with Collagen I and Matrigel on the Malignant Phenotype of Human Breast-Cancer Cells in 3D Cultures and in vivo.* Macromolecular Bioscience, 2009. **9**(5): p. 437-443.
108. Clough, H.C., et al., *Neutrally charged self-assembling peptide hydrogel recapitulates in vitro mechanisms of breast cancer progression.* Materials Science and Engineering: C, 2021. **127**: p. 112200.
109. Raphael, B., et al., *3D cell bioprinting of self-assembling peptide-based hydrogels.* Materials Letters, 2017. **190**: p. 103-106.
110. Tyanova, S., T. Temu, and J. Cox, *The MaxQuant computational platform for mass spectrometry-based shotgun proteomics.* Nature Protocols, 2016. **11**(12): p. 2301-2319.
111. UniProt, C., *UniProt: the universal protein knowledgebase in 2021.* Nucleic acids research, 2021. **49**(D1): p. D480-D489.
112. Goeminne, L.E., K. Gevaert, and L. Clement, *Peptide-level Robust Ridge Regression Improves Estimation, Sensitivity, and Specificity in Data-dependent Quantitative Label-free Shotgun Proteomics.* Molecular & Cellular Proteomics, 2016. **15**(2): p. 657-668.
113. Wu, T., et al., *clusterProfiler 4.0: A universal enrichment tool for interpreting omics data.* The Innovation, 2021. **2**(3): p. 100141.
114. Yu, G. and Q.-Y. He, *ReactomePA: an R/Bioconductor package for reactome pathway analysis and visualization.* Molecular BioSystems, 2016. **12**(2): p. 477-479.
115. Gudjonsson, T., et al., *Normal and tumor-derived myoepithelial cells differ in their ability to interact with luminal breast epithelial cells for polarity and basement membrane deposition.* Journal of cell science, 2002. **115**(Pt 1): p. 39-50.
116. Streuli, C.H., et al., *Laminin mediates tissue-specific gene expression in mammary epithelia.* The Journal of cell biology, 1995. **129**(3): p. 591-603.
117. Dhimolea, E., et al., *The role of collagen reorganization on mammary epithelial morphogenesis in a 3D culture model.* Biomaterials, 2010. **31**(13): p. 3622-3630.
118. Treacy, N.J., et al., *Growth and differentiation of human induced pluripotent stem cell (hiPSC)-derived kidney organoids using fully synthetic peptide hydrogels.* Bioactive Materials, 2022. **21**: p. 142-156.
119. Castillo Diaz, L.A., et al., *Osteogenic differentiation of human mesenchymal stem cells promotes mineralization within a biodegradable peptide hydrogel.* Journal of Tissue Engineering, 2016. **7**: p. 2041731416649789.
120. Klinowska, T.C.M., et al., *Laminin and β1 Integrins Are Crucial for Normal Mammary Gland Development in the Mouse.* Developmental Biology, 1999. **215**(1): p. 13-32.

121. Streuli, C.H., *Preface: Cell Adhesion in Mammary Gland Biology and Neoplasia.* Journal of Mammary Gland Biology and Neoplasia, 2003. **8**(4): p. 375-381.
122. Yurchenco, P.D. and B.L. Patton, *Developmental and pathogenic mechanisms of basement membrane assembly.* Current pharmaceutical design, 2009. **15**(12): p. 1277-1294.
123. Gaiko-Shcherbak, A., et al., *The Acinar Cage: Basement Membranes Determine Molecule Exchange and Mechanical Stability of Human Breast Cell Acini.* PLOS ONE, 2015. **10**(12): p. e0145174.
124. Murtagh, J., et al., *Organization of mammary epithelial cells into 3D acinar structures requires glucocorticoid and JNK signaling.* The Journal of cell biology, 2004. **166**(1): p. 133-143.
125. Kibbey, M.C., *Maintenance of the EHS sarcoma and Matrigel preparation.* Journal of tissue culture methods, 1994. **16**(3): p. 227-230.
126. Howlett, A.R. and M.J. Bissell, *Regulation of mammary epithelial cell function: a role for stromal and basement membrane matrices.* Protoplasma, 1990. **159**(2): p. 85-95.
127. Brownfield, Douglas G., et al., *Patterned Collagen Fibers Orient Branching Mammary Epithelium through Distinct Signaling Modules.* Current Biology, 2013. **23**(8): p. 703-709.
128. Hu, G., L. Li, and W. Xu, *Extracellular matrix in mammary gland development and breast cancer progression.* Frontiers in Laboratory Medicine, 2017. **1**(1): p. 36-39.
129. Ingman, W.V., et al., *Macrophages promote collagen fibrillogenesis around terminal end buds of the developing mammary gland.* Developmental Dynamics, 2006. **235**(12): p. 3222-3229.
130. LeBleu, V.S., B. MacDonald, and R. Kalluri, *Structure and Function of Basement Membranes.* Experimental Biology and Medicine, 2007. **232**(9): p. 1121-1129.
131. Uriel, S., et al., *Extraction and Assembly of Tissue-Derived Gels for Cell Culture and Tissue Engineering.* Tissue Engineering Part C: Methods, 2008. **15**(3): p. 309-321.
132. Cristea, S. and K. Polyak, *Dissecting the mammary gland one cell at a time.* Nature Communications, 2018. **9**(1): p. 2473.
133. Carter, E.P., et al., *A 3D in vitro model of the human breast duct: a method to unravel myoepithelial-luminal interactions in the progression of breast cancer.* Breast Cancer Research, 2017. **19**(1): p. 50.
134. Hohenester, E. and P.D. Yurchenco, *Laminins in basement membrane assembly.* Cell adhesion & migration, 2013. **7**(1): p. 56-63.
135. Li, S., et al., *Laminin-sulfatide binding initiates basement membrane assembly and enables receptor signaling in Schwann cells and fibroblasts.* The Journal of cell biology, 2005. **169**(1): p. 179-189.
136. McKee, K.K., et al., *Role of Laminin Terminal Globular Domains in Basement Membrane Assembly.* Journal of Biological Chemistry, 2007. **282**(29): p. 21437-21447.
137. McKee, K.K., S. Capizzi, and P.D. Yurchenco, *Scaffold-forming and Adhesive Contributions of Synthetic Laminin-binding Proteins to Basement Membrane Assembly.* Journal of Biological Chemistry, 2009. **284**(13): p. 8984-8994.
138. Compostella, F., L. Panza, and F. Ronchetti, *The mammalian sulfated glycolipid sulfatide: Synthesis and biological implications.* Comptes Rendus Chimie, 2012. **15**(1): p. 37-45.
139. Talts, J.F., et al., *Binding of the G domains of laminin α1 and α2 chains and perlecan to heparin, sulfatides, α-dystroglycan and several extracellular matrix proteins.* The EMBO Journal, 1999. **18**(4): p. 863-870.
140. Andac, Z., et al., *Analysis of heparin, α-dystroglycan and sulfatide binding to the G domain of the laminin α1 chain by site-directed mutagenesis11Edited by A. R. Fersht.* Journal of Molecular Biology, 1999. **287**(2): p. 253-264.
141. Harrison, D., et al., *Crystal structure and cell surface anchorage sites of laminin alpha1LG4-5.* The Journal of biological chemistry, 2007. **282**(15): p. 11573-11581.
142. Furuta, S., et al., *Laminin signals initiate the reciprocal loop that informs breast-specific gene expression and homeostasis by activating NO, p53 and microRNAs.* eLife, 2018. **7**: p. e26148.
143. Akhtar, N. and C.H. Streuli, *Rac1 links integrin-mediated adhesion to the control of lactational differentiation in mammary epithelia.* The Journal of cell biology, 2006. **173**(5): p. 781-793.
144. Xu, R., V.A. Spencer, and M.J. Bissell, *Extracellular matrix-regulated gene expression requires cooperation of SWI/SNF and transcription factors.* The Journal of biological chemistry, 2007. **282**(20): p. 14992-14999.
145. Novaro, V., C.D. Roskelley, and M.J. Bissell, *Collagen-IV and laminin-1 regulate estrogen receptor alpha expression and function in mouse mammary epithelial cells.* Journal of cell science, 2003. **116**(Pt 14): p. 2975-2986.

146. Spencer, V.A., et al., *Depletion of nuclear actin is a key mediator of quiescence in epithelial cells.* Journal of cell science, 2011. **124**(Pt 1): p. 123-132.
147. Pujuguet, P., et al., *Nidogen-1 regulates laminin-1-dependent mammary-specific gene expression.* Journal of cell science, 2000. **113 (Pt 5)**(Pt 5): p. 849-858.
148. Zhou, S., et al., *Nidogen: A matrix protein with potential roles in musculoskeletal tissue regeneration.* Genes & Diseases, 2022. **9**(3): p. 598-609.
149. Runswick, S., et al., *Desmosomal adhesion regulates epithelial morphogenesis and cell positioning.* Nature Cell Biology, 2001. **3**: p. 823-830.
150. DiColandrea, T., et al., *Subcellular Distribution of Envoplakin and Periplakin: Insights into Their Role as Precursors of the Epidermal Cornified Envelope.* Journal of Cell Biology, 2000. **151**(3): p. 573-586.
151. Miroshnikova, Y.A., et al., *Engineering strategies to recapitulate epithelial morphogenesis within synthetic three-dimensional extracellular matrix with tunable mechanical properties.* Physical biology, 2011. **8**(2): p. 026013-026013.
152. Dobre, O., et al., *A Hydrogel Platform that Incorporates Laminin Isoforms for Efficient Presentation of Growth Factors – Neural Growth and Osteogenesis.* Advanced Functional Materials, 2021. **31**(21): p. 2010225.
153. Barros, D., et al., *Engineering hydrogels with affinity-bound laminin as 3D neural stem cell culture systems.* Biomaterials science, 2019. **7**(12): p. 5338-5349.
154. Francisco, A.T., et al., *Photocrosslinkable laminin-functionalized polyethylene glycol hydrogel for intervertebral disc regeneration.* Acta biomaterialia, 2014. **10**(3): p. 1102-1111.
155. Ziemkiewicz, N., et al., *Laminin-111 functionalized polyethylene glycol hydrogels support myogenic activity in vitro.* Biomedical Materials, 2018. **13**(6): p. 065007.
156. Yoshida-Moriguchi, T., et al., *O-mannosyl phosphorylation of alpha-dystroglycan is required for laminin binding.* Science (New York, N.Y.), 2010. **327**(5961): p. 88-92.
157. Hohenester, E., *Laminin G-like domains: dystroglycan-specific lectins.* Current opinion in structural biology, 2019. **56**: p. 56-63.
158. Combs, A.C. and J.M. Ervasti, *Enhanced laminin binding by alpha-dystroglycan after enzymatic deglycosylation.* The Biochemical journal, 2005. **390**(Pt 1): p. 303-309.
159. Xiao, S., C.V. Finkielstein, and D.G.S. Capelluto, *The Enigmatic Role of Sulfatides: New Insights into Cellular Functions and Mechanisms of Protein Recognition*, in *Lipid-mediated Protein Signaling*, D.G.S. Capelluto, Editor. 2013, Springer Netherlands: Dordrecht. p. 27-40.
160. Bosshard, H.R., D.N. Marti, and I. Jelesarov, *Protein stabilization by salt bridges: concepts, experimental approaches and clarification of some misunderstandings.* Journal of Molecular Recognition, 2004. **17**(1): p. 1-16.
161. Moore, C.J. and S.J. Winder, *Dystroglycan versatility in cell adhesion: a tale of multiple motifs.* Cell Communication and Signaling, 2010. **8**(1): p. 3.
162. Roberts, D.D., et al., *Laminin binds specifically to sulfated glycolipids.* Proceedings of the National Academy of Sciences of the United States of America, 1985. **82**(5): p. 1306-1310.
163. Weir, M.L., et al., *Dystroglycan loss disrupts polarity and beta-casein induction in mammary epithelial cells by perturbing laminin anchoring.* Journal of cell science, 2006. **119**(Pt 19): p. 4047-4058.
164. Durbeej, M., et al., *Dystroglycan binding to laminin α1LG4 module influences epithelial morphogenesis of salivary gland and lung in vitro.* Differentiation, 2001. **69**(2): p. 121-134.
165. Henry, M.D. and K.P. Campbell, *A Role for Dystroglycan in Basement Membrane Assembly.* Cell, 1998. **95**(6): p. 859-870.
166. Kent, A.J., et al., *The microstructure of laminin-111 compensates for dystroglycan loss in mammary epithelial cells in downstream expression of milk proteins.* Biomaterials, 2019. **218**: p. 119337-119337.
167. Li, S., et al., *The Role of Laminin in Embryonic Cell Polarization and Tissue Organization.* Developmental Cell, 2003. **4**(5): p. 613-624.
168. Akhavan, A., et al., *Loss of cell-surface laminin anchoring promotes tumor growth and is associated with poor clinical outcomes.* Cancer research, 2012. **72**(10): p. 2578-2588.
169. Branco, M.C., et al., *The effect of protein structure on their controlled release from an injectable peptide hydrogel.* Biomaterials, 2010. **31**(36): p. 9527-9534.
170. Schulz, A., et al., *Poly(amidoamine)-alginate hydrogels: directing the behavior of mesenchymal stem cells with charged hydrogel surfaces.* Journal of Materials Science: Materials in Medicine, 2018. **29**(7): p. 105.
171. Schneider, G.B., et al., *The effect of hydrogel charge density on cell attachment.* Biomaterials, 2004. **25**(15): p. 3023-3028.

172. Nagayasu, A., et al., *Efficacy of Self-assembled Hydrogels Composed of Positively or Negatively Charged Peptides as Scaffolds for Cell Culture.* Journal of Biomaterials Applications, 2010. **26**(6): p. 651-665.
173. Slade, M.J., et al., *The Human Mammary Gland Basement Membrane Is Integral to the Polarity of Luminal Epithelial Cells.* Experimental Cell Research, 1999. **247**(1): p. 267-278.
174. Beliveau, A., et al., *Raf-induced MMP9 disrupts tissue architecture of human breast cells in three-dimensional culture and is necessary for tumor growth in vivo.* Genes & development, 2010. **24**(24): p. 2800-2811.
175. Xu, R., et al., *Sustained activation of STAT5 is essential for chromatin remodeling and maintenance of mammary-specific function.* Journal of Cell Biology, 2009. **184**(1): p. 57-66.
176. Debnath, J. and J.S. Brugge, *Modelling glandular epithelial cancers in three-dimensional cultures.* Nature Reviews Cancer, 2005. **5**(9): p. 675-688.
177. Smyth, N., et al., *Absence of basement membranes after targeting the LAMC1 gene results in embryonic lethality due to failure of endoderm differentiation.* The Journal of cell biology, 1999. **144**(1): p. 151-160.
178. Chen, Z.-L. and S. Strickland, *Laminin gamma1 is critical for Schwann cell differentiation, axon myelination, and regeneration in the peripheral nerve.* The Journal of cell biology, 2003. **163**(4): p. 889-899.
179. Miner, J.H., et al., *Compositional and structural requirements for laminin and basement membranes during mouse embryo implantation and gastrulation.* Development, 2004. **131**(10): p. 2247-2256.
180. Aumailley, M., et al., *Altered synthesis of laminin 1 and absence of basement membrane component deposition in (beta)1 integrin-deficient embryoid bodies.* Journal of Cell Science, 2000. **113**(2): p. 259-268.
181. Qu, Y., et al., *Evaluation of MCF10A as a Reliable Model for Normal Human Mammary Epithelial Cells.* PLOS ONE, 2015. **10**(7): p. e0131285.
182. Borradori, L. and A. Sonnenberg, *Hemidesmosomes: roles in adhesion, signaling and human diseases.* Current Opinion in Cell Biology, 1996. **8**(5): p. 647-656.
183. Martin, K.J., et al., *Down-regulation of laminin-5 in breast carcinoma cells. Molecular medicine*, 1998. **4**(9): p. 602–613.
184. Prince, J.M., et al., *Cell–matrix interactions during development and apoptosis of the mouse mammary gland in vivo.* Developmental Dynamics, 2002. **223**(4): p. 497-516.
185. Englund, J.I., et al., *Laminin alpha 5 is Necessary for Mammary Epithelial Growth and Function by Maintaining Luminal Epithelial Cell Identity.* bioRxiv, 2019: p. 2019.12.27.889451.
186. Pouliot, N. and N. Kusuma, *Laminin-511.* Cell Adhesion & Migration, 2013. **7**(1): p. 142-149.
187. Chang, C., et al., *A laminin 511 matrix is regulated by TAZ and functions as the ligand for the α6Bβ1 integrin to sustain breast cancer stem cells.* Genes & Development, 2015. **29**(1): p. 1-6.
188. Chia, J., et al., *Evidence for a Role of Tumor-Derived Laminin-511 in the Metastatic Progression of Breast Cancer.* The American Journal of Pathology, 2007. **170**(6): p. 2135-2148.
189. Fathi, A., et al., *Enhancing the mechanical properties and physical stability of biomimetic polymer hydrogels for micro-patterning and tissue engineering applications.* European Polymer Journal, 2014. **59**: p. 161-170.
190. Pugliese, R., et al., *Self-assembling peptides cross-linked with genipin: resilient hydrogels and self-standing electrospun scaffolds for tissue engineering applications.* Biomaterials Science, 2019. **7**(1): p. 76-91.
191. Bakota, E.L., et al., *Enzymatic Cross-Linking of a Nanofibrous Peptide Hydrogel.* Biomacromolecules, 2011. **12**(1): p. 82-87.
192. Zhao, Y., et al., *Self-Assembled pH-Responsive Hydrogels Composed of the RATEA16 Peptide.* Biomacromolecules, 2008. **9**(6): p. 1511-1518.
193. Aggeli, A., et al., *Hierarchical self-assembly of chiral rod-like molecules as a model for peptide beta -sheet tapes, ribbons, fibrils, and fibers.* Proceedings of the National Academy of Sciences of the United States of America, 2001. **98**(21): p. 11857-11862.
194. Freire, E. and T. Coelho-Sampaio, *Self-assembly of Laminin Induced by Acidic pH.* Journal of Biological Chemistry, 2000. **275**(2): p. 817-822.
195. Kalb, E. and J. Engel, *Binding and calcium-induced aggregation of laminin onto lipid bilayers.* Journal of Biological Chemistry, 1991. **266**(28): p. 19047-19052.
196. Besser, R.R., et al., *Enzymatically crosslinked gelatin–laminin hydrogels for applications in neuromuscular tissue engineering.* Biomaterials Science, 2020. **8**(2): p. 591-606.

197. Nam, K., et al., *Laminin-111 Peptides Conjugated to Fibrin Hydrogels Promote Formation of Lumen Containing Parotid Gland Cell Clusters.* Biomacromolecules, 2016. **17**(6): p. 2293-2301.
198. Klotz, B.J., et al., *A Versatile Biosynthetic Hydrogel Platform for Engineering of Tissue Analogues.* Advanced Healthcare Materials, 2019. **8**(19): p. 1900979.
199. Gu, Y., et al., *Characterization of Bone Marrow Laminins and Identification of α5-Containing Laminins as Adhesive Proteins for Multipotent Hematopoietic FDCP-Mix Cells.* Blood, 1999. **93**(8): p. 2533-2542.
200. Susek, K.H., et al., *Bone marrow laminins influence hematopoietic stem and progenitor cell cycling and homing to the bone marrow.* Matrix Biology, 2018. **67**: p. 47-62.
201. Bissell, M.J. and D. Bilder, *Polarity determination in breast tissue: desmosomal adhesion, myoepithelial cells, and laminin 1.* Breast cancer research : BCR, 2003. **5**(2): p. 117-119.
202. Nelson, W.J., *Adaptation of core mechanisms to generate cell polarity.* Nature, 2003. **422**(6933): p. 766-774.
203. Roignot, J., X. Peng, and K. Mostov, *Polarity in Mammalian Epithelial Morphogenesis.* Cold Spring Harbor Perspectives in Biology, 2013. **5**(2).
204. Dreesen, O., et al., *Lamin B1 fluctuations have differential effects on cellular proliferation and senescence.* Journal of Cell Biology, 2013. **200**(5): p. 605-617.
205. Forsburg, S.L., *Eukaryotic MCM Proteins: Beyond Replication Initiation.* Microbiology and Molecular Biology Reviews, 2004. **68**(1): p. 109-131.
206. Whyte, J., et al., *Key signalling nodes in mammary gland development and cancer. Mitogen-activated protein kinase signalling in experimental models of breast cancer progression and in mammary gland development.* Breast cancer research : BCR, 2009. **11**(5): p. 209-209.
207. Nolan, M.E., et al., *The polarity protein Par6 induces cell proliferation and is overexpressed in breast cancer.* Cancer research, 2008. **68**(20): p. 8201-8209.
208. Khaled, W.T., et al., *The IL-4/IL-13/Stat6 signalling pathway promotes luminal mammary epithelial cell development.* Development, 2007. **134**(15): p. 2739-2750.
209. Bailey, C.M. and M.J.C. Hendrix, *IRF6 in development and disease: a mediator of quiescence and differentiation.* Cell cycle (Georgetown, Tex.), 2008. **7**(13): p. 1925-1930.
210. Khan, I.A., et al., *ErbB2-driven downregulation of the transcription factor Irf6 in breast epithelial cells is required for their 3D growth.* Breast Cancer Research, 2018. **20**(1): p. 151.
211. Bailey, C.M., et al., *Temporal and spatial expression patterns for the tumor suppressor Maspin and its binding partner interferon regulatory factor 6 during breast development.* Development, growth & differentiation, 2009. **51**(5): p. 473-481.
212. Teoh, S.S.Y., J.C. Whisstock, and P.I. Bird, *Maspin (SERPINB5) Is an Obligate Intracellular Serpin.* Journal of Biological Chemistry, 2010. **285**(14): p. 10862-10869.
213. Zhang, M., et al., *Maspin Plays an Important Role in Mammary Gland Development.* Developmental Biology, 1999. **215**(2): p. 278-287.
214. Bailey, C.M., et al., *Biological functions of maspin.* Journal of Cellular Physiology, 2006. **209**(3): p. 617-624.

Supplementary information: Functionalising a negatively charged self-assembling peptide hydrogel for mammary epithelial cell culture with laminin 111

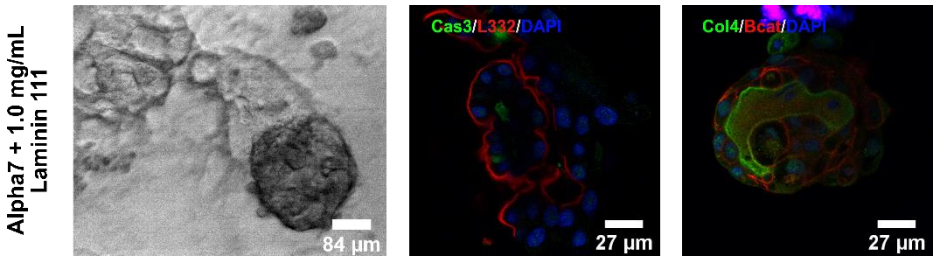

Fig. S1. Alpha7 hydrogels functionalised with a lower concentration of laminin 111 support acinar development. Brightfield and IF images of day 7 MCF10a cells encapsulated in laminin 111-functionalised Alpha7 hydrogels (final concentration 1.0 mg/mL). To promote the assembly of a functional laminin 111 polymer network, MCF10a cells were incubated in laminin 111 for 10 minutes at room temperature before being encapsulated in Alpha7. After being maintained for 7 days, the cells were extracted and stained with acinar markers: active caspase-3 (Cas3), laminin 332 (L332), collagen IV (Col4) and β-catenin (Bcat). Nuclei were stained with DAPI.

Protein names	Gene names	estimate	pval
Laminin subunit alpha-1	Lama1	7.786974	1.91E-73
Laminin subunit gamma-1	Lamc1	7.522227	1.63E-48
Laminin subunit beta-1	Lamb1	7.560795	1.75E-37
Myosin-9	MYH9	3.984209	3.9E-13
Histone H4	HIST1H4A	6.528041	6.8E-13
Nidogen-1	NID1	8.245021	5.57E-11
Laminin subunit gamma-1	LAMC1	7.816543	2.71E-10
Heat shock cognate 71 kDa protein	HSPA8	4.776187	1.1E-07
Histone H3	HIST2H3PS2	4.995099	2E-06
Heat shock 70 kDa protein 6	HSPA6	3.806883	3.1E-06
Coagulation factor V	F5	1.767729	5.86E-06
Heat shock protein HSP 90-alpha	HSP90AA1	2.624855	3.89E-05
Eukaryotic translation initiation factor 3 subunit D	EIF3D	1.72728	4.85E-05
14-3-3 protein sigma	SFN	1.643881	8.34E-05
Fructose-bisphosphate aldolase A	ALDOA	1.984846	8.76E-05
Antithrombin-III	SERPINC1	1.003393	9.19E-05
Alpha-enolase	ENO1	1.436237	0.000132
E3 ubiquitin-protein ligase NEDD4	NEDD4	2.873286	0.000135
Actin, cytoplasmic 1	ACTB	2.540292	0.000145
Ig kappa chain V-III region POM	IGKV3OR2-268	1.440324	0.000161
Adenosylhomocysteinase	AHCY	0.836625	0.000327
Myosin-10	MYH10	1.736823	0.000476
Golgi-associated plant pathogenesis-related protein 1	GLIPR2	2.150719	0.000477
Complement component C8 alpha chain	C8A	1.196135	0.000504
Actin, alpha skeletal muscle	ACTA1	5.673958	0.000841
HLA class I histocompatibility antigen, Cw-7 alpha chain	HLA-C	1.310201	0.00086
Alpha-2-macroglobulin	A2M	0.462458	0.001038
Complement component C8 gamma chain	C8G	1.548526	0.00107
Glutathione peroxidase	GPX3	2.003998	0.001165
Ras-related protein Rab-27B	RAB27B	1.598616	0.001244
Rho GTPase-activating protein 21	ARHGAP21	1.14275	0.001506
Fibrinogen alpha chain	FGA	1.17197	0.001628
Adenylyl cyclase-associated protein 1	CAP1	1.739269	0.001721
Complement component C8 beta chain	C8B	1.440406	0.001805
Ig kappa chain V-III region B6		0.871561	0.001841
Apolipoprotein A-I	APOA1	0.531345	0.001874
Retinol-binding protein 4	RBP4	1.037594	0.002534
Heat shock 70 kDa protein 14	HSPA14	1.171855	0.00254
L-lactate dehydrogenase A chain	LDHA	1.853378	0.002757
Proteoglycan 4	PRG4	0.939171	0.002894
Exportin-2	CSE1L	-1.45945	0.002982
Adiponectin	ADIPOQ	0.971639	0.003679
Sodium/potassium-transporting ATPase subunit alpha-1	ATP1A1	1.484346	0.003769
Pigment epithelium-derived factor	SERPINF1	1.006374	0.003846
Heparin cofactor 2	SERPIND1	0.866461	0.003981

Phospholipid transfer protein	PLTP	0.649497	0.004108
Glyceraldehyde-3-phosphate dehydrogenase	GAPDH	1.556458	0.004429
Pyruvate kinase PKM	PKM	1.968545	0.005212
Acetyl-CoA acetyltransferase, cytosolic	ACAT2	0.802224	0.006473
Unconventional myosin-XVIIIa	MYO18A	1.456668	0.006616
Vitronectin	VTN	1.02481	0.007341
Polymerase delta-interacting protein 2	POLDIP2	1.186273	0.007498
Angio-associated migratory cell protein	AAMP	1.426813	0.008625
Pericentrin	PCNT	1.156047	0.009386
Serum paraoxonase/arylesterase 1	PON1	1.332191	0.009716
Serine/arginine repetitive matrix protein 2	SRRM2	0.80712	0.01048
Tubulin beta-4B chain	TUBB4B	1.50766	0.010505
Aspartate aminotransferase, cytoplasmic	GOT1	0.561126	0.010967
Ferritin heavy chain	FTH1	0.994652	0.011372

Table S1. Addition of laminin 111 into Alpha7 gels introduces multiple exogenous proteins. List of proteins that are significantly upregulated (positive estimate values) or downregulated (negative estimate values) in cell-free Alpha7 gels supplemented with laminin 111 compared to cell-free Alpha7 gels. 'Estimate' refers to the log2 fold-change of a given protein's expression value. P-values calculated via MSqRob from three independent replicates per condition ($p < 0.05$).

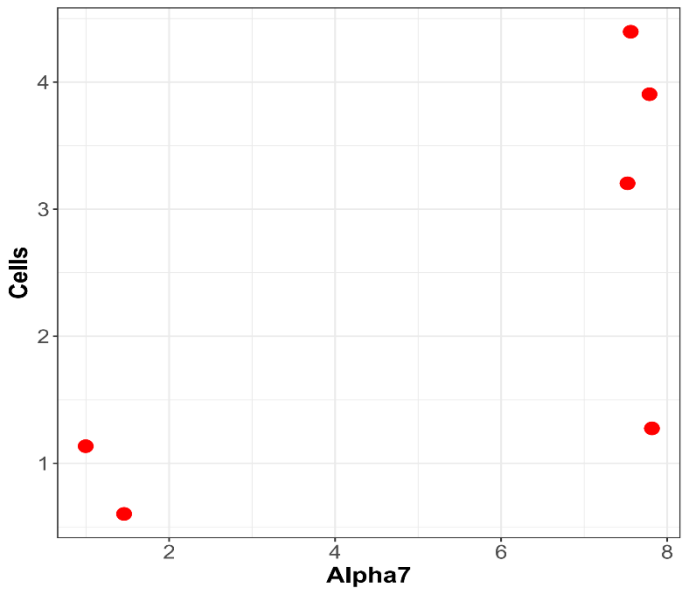

Fig. S2. Significantly upregulated proteins detected in both cell-laden and cell-free lysates did not exhibit the same log-fold changes in expression. Significant overlap analysis showing log-fold values of proteins (red dots) upregulated in both cell-free (Alpha7) and cell-laden (Cells) samples. P-values calculated via MSqRob from three independent replicates ($p < 0.05$).

Protein names	Gene names	estimate	pval
Transferrin receptor protein 1	TFRC	-1.08029	3.27E-20
Serpin B5	SERPINB5	1.318554	8.13E-19
Glycogen phosphorylase, brain form	PYGB	1.037111	1.18E-17
Gem-associated protein 5	GEMIN5	-0.42636	4.94E-15
Endorepellin	HSPG2	2.394767	5.35E-15
Laminin subunit beta-1	Lamb1	4.396045	5.89E-15
DNA replication licensing factor MCM6	MCM6	-1.28758	3.63E-13
DNA replication licensing factor MCM3	MCM3	-1.33446	1.08E-12
182 kDa tankyrase-1-binding protein	TNKS1BP1	1.031928	6.52E-12
Protein-glutamine gamma-glutamyltransferase K	TGM1	1.982692	7.1E-12
T-complex protein 1 subunit delta	CCT4	-0.35812	1.2E-11
Eukaryotic translation initiation factor 3 subunit L	EIF3L	-0.47137	2.23E-11
Staphylococcal nuclease domain-containing protein 1	SND1	-0.34561	5.82E-11
Elongation factor 1-gamma	EEF1G	-0.4988	7.08E-11
General vesicular transport factor p115	USO1	0.647077	1.03E-10
X-ray repair cross-complementing protein 5	XRCC5	-0.40005	3.75E-10
Ornithine aminotransferase, mitochondrial	OAT	-0.49775	1.13E-09
Threonine--tRNA ligase, cytoplasmic	TARS	-0.44082	1.27E-09
Splicing factor, proline- and glutamine-rich	SFPQ	-0.68245	1.37E-09
RuvB-like 2	RUVBL2	-0.49878	1.82E-09
Xanthine dehydrogenase/oxidase	XDH	0.76578	2.25E-09
CD109 antigen	CD109	0.510319	2.3E-09
Nicotinamide N-methyltransferase	NNMT	-0.74843	2.36E-09
Heterogeneous nuclear ribonucleoprotein R	HNRNPR	-1.86607	4.02E-09
Lamin-B2	LMNB2	-0.58972	4.73E-09
Superkiller viralicidic activity 2-like 2	SKIV2L2	-0.47753	4.93E-09
DnaJ homolog subfamily A member 1	DNAJA1	-1.06474	5.28E-09
Amine oxidase [flavin-containing] A	MAOA	1.622542	5.8E-09
Laminin subunit gamma-1	Lamc1	3.203483	9.94E-09
T-complex protein 1 subunit theta	CCT8	-0.51764	1.13E-08
DNA replication licensing factor MCM5	MCM5	-1.26893	1.29E-08
Structural maintenance of chromosomes protein 3	SMC3	-0.34411	1.95E-08
Dihydropyrimidinase-related protein 2	DPYSL2	-0.40675	3.06E-08
Microtubule-associated protein RP/EB family member 1	MAPRE1	-0.51493	3.76E-08
Prelamin-A/C;Lamin-A/C	LMNA	0.611572	4.26E-08
Catalase	CAT	-0.54946	5.05E-08
Programmed cell death 6-interacting protein	PDCD6IP	0.350823	6.53E-08
Laminin subunit alpha-1	Lama1	3.904449	7.04E-08
ATP-dependent RNA helicase DDX42	DDX42	-0.80341	9.6E-08
Protein phosphatase 1G	PPM1G	-0.74013	1.29E-07
Heat shock protein HSP 90-alpha	HSP90AA1	-0.5081	1.52E-07
FACT complex subunit SSRP1	SSRP1	-0.58909	1.54E-07
Eukaryotic peptide chain release factor subunit 1	ETF1	-0.68103	1.68E-07
Heterogeneous nuclear ribonucleoprotein A0	HNRNPA0	-0.60041	1.97E-07
Agrin	AGRN	1.085882	2.16E-07
Serine/arginine-rich splicing factor 6	SRSF6	-0.98768	2.27E-07

Putative ATP-dependent RNA helicase DHX30	DHX30	-0.52976	2.53E-07
Leukocyte elastase inhibitor	SERPINB1	1.399051	2.57E-07
5-3 exoribonuclease 2	XRN2	-0.50859	3.35E-07
Glycerol-3-phosphate dehydrogenase, mitochondrial	GPD2	0.487547	3.48E-07
Leucine-rich repeat transmembrane protein FLRT3	FLRT3	1.12479	3.51E-07
ELAV-like protein 1	ELAVL1	-0.54867	3.98E-07
Calpain-1 catalytic subunit	CAPN1	0.667868	4.13E-07
DNA replication licensing factor MCM7	MCM7	-1.05682	4.3E-07
Calcyclin-binding protein	CACYBP	-0.70847	5.28E-07
Solute carrier family 43 member 3	SLC43A3	-1.1553	5.62E-07
Transferrin receptor protein 1	TFRC	-0.93239	6.51E-07
Eukaryotic translation initiation factor 3 subunit D	EIF3D	-0.43253	6.99E-07
Pre-mRNA-processing factor 19	PRPF19	-0.62055	9.69E-07
Plasminogen activator inhibitor 1 RNA-binding protein	SERBP1	-0.66137	1.19E-06
Monofunctional C1-tetrahydrofolate synthase, mitochondrial	MTHFD1L	-0.8981	1.66E-06
Nck-associated protein 1	NCKAP1	0.582926	2.29E-06
Trifunctional enzyme subunit alpha, mitochondrial	HADHA	0.450286	2.35E-06
Beta-enolase	ENO3	-2.98189	2.73E-06
Eukaryotic translation initiation factor 3 subunit H	EIF3H	-0.71592	2.91E-06
Rab GDP dissociation inhibitor beta	GDI2	-0.438	2.96E-06
Gem-associated protein 4	GEMIN4	-0.84245	3.32E-06
Metalloreductase STEAP3	STEAP3	1.423213	3.33E-06
Lamina-associated polypeptide 2, isoforms beta/gamma	TMPO	-0.92409	3.38E-06
Heterogeneous nuclear ribonucleoprotein D-like	HNRNPDL	-0.59596	4.49E-06
Plakophilin-3	PKP3	0.870333	4.76E-06
Eukaryotic translation initiation factor 2A	EIF2A	-0.55566	5.03E-06
Envoplakin	EVPL	1.033381	5.44E-06
Cornifin-B	SPRR1B	2.657719	6.16E-06
Cellular retinoic acid-binding protein 2	CRABP2	3.808483	6.36E-06
Mitotic checkpoint protein BUB3	BUB3	-0.68554	6.58E-06
Hexokinase-1	HK1	0.535943	6.69E-06
Peroxiredoxin-6	PRDX6	-0.35795	6.82E-06
Structural maintenance of chromosomes protein 2	SMC2	-0.94035	7.86E-06
Mini-chromosome maintenance complex-binding protein	MCMBP	-0.85499	8.51E-06
Structural maintenance of chromosomes protein	SMC4	-0.94232	8.91E-06
Importin-5	IPO5	-0.43526	9.15E-06
FACT complex subunit SPT16	SUPT16H	-0.43516	9.58E-06
Serine/arginine-rich splicing factor 9	SRSF9	-0.83275	1.11E-05
Exportin-2	CSE1L	-0.4293	1.2E-05
Nuclear factor NF-kappa-B p100 subunit	NFKB2	0.398662	1.39E-05
Histone H1.5	HIST1H1B	-0.60609	1.45E-05
Condensin complex subunit 3	NCAPG	-1.49766	1.5E-05
Thymidine phosphorylase	TYMP	1.627936	1.54E-05
Inosine-5-monophosphate dehydrogenase	IMPDH1	-0.83223	1.64E-05
Annexin A1	ANXA1	0.395735	1.75E-05
Protein S100-A8	S100A8	2.084783	2.02E-05

Rab3 GTPase-activating protein catalytic subunit	RAB3GAP1	0.446195	2.26E-05
Translocator protein	TSPO	0.923484	2.55E-05
Protein S100-A10	S100A10	0.98503	2.62E-05
Ras-related protein Rab-8A	RAB8A	-0.80804	2.7E-05
Alpha-2-macroglobulin-like protein 1	A2ML1	3.08996	2.75E-05
Serpin B3	SERPINB3	2.563106	2.87E-05
Dynamin-1-like protein	DNM1L	0.45002	3.47E-05
AP-2 complex subunit alpha-1	AP2A1	0.476118	3.53E-05
Probable ATP-dependent RNA helicase DDX46	DDX46	-0.50077	3.73E-05
SEC23-interacting protein	SEC23IP	0.563598	4.02E-05
Suppressor of G2 allele of SKP1 homolog	SUGT1	-0.65067	4.07E-05
Multifunctional protein ADE2	PAICS	-0.62067	4.09E-05
Activated RNA polymerase II transcriptional coactivator p15	SUB1	-0.69894	4.14E-05
Protein S100-A11	S100A11	0.648459	4.17E-05
DNA-directed RNA polymerases I, II, and III subunit RPABC3	POLR2H	-0.93602	4.58E-05
Condensin complex subunit 1	NCAPD2	-1.24573	4.62E-05
Serine-threonine kinase receptor-associated protein	STRAP	-0.54171	4.72E-05
DNA replication licensing factor MCM4	MCM4	-2.03495	6.11E-05
Complement component 1 Q subcomponent-binding protein, mitochondrial	C1QBP	-0.8087	6.24E-05
HEAT repeat-containing protein 1	HEATR1	-0.69648	6.41E-05
Lysophospholipid acyltransferase 2	MBOAT2	1.615746	7E-05
RNA-binding protein 40	RNPC3	4.991174	7.08E-05
Obg-like ATPase 1	OLA1	-0.46915	7.18E-05
26S protease regulatory subunit 7	PSMC2	0.317251	7.31E-05
Crooked neck-like protein 1	CRNKL1	-0.57174	7.58E-05
Gamma-tubulin complex component 2	TUBGCP2	-0.53344	7.6E-05
Condensin complex subunit 2	NCAPH	-0.80164	7.76E-05
Far upstream element-binding protein 1	FUBP1	-0.34544	8.57E-05
Tubulin beta-2A chain	TUBB2A	0.668425	8.87E-05
26S proteasome non-ATPase regulatory subunit 11	PSMD11	-0.75738	9.35E-05
Chromobox protein homolog 3	CBX3	-0.88906	9.71E-05
Protein phosphatase methylesterase 1	PPME1	-0.38434	9.75E-05
Actin-binding protein anillin	ANLN	-2.0202	0.000103
Peroxiredoxin-5, mitochondrial	PRDX5	0.913112	0.000105
DNA mismatch repair protein Msh2	MSH2	-1.17319	0.000105
40S ribosomal protein S11	RPS11	7.22495	0.000107
Sister chromatid cohesion protein PDS5 homolog A	PDS5A	-0.4442	0.00011
Unconventional myosin-Ib	MYO1B	0.509841	0.000111
RNA-binding protein Raly	RALY	-0.72845	0.000115
Alpha-enolase	ENO1	-0.29794	0.000122
Proliferating cell nuclear antigen	PCNA	-2.28122	0.000122
Nardilysin	NRD1	-0.78712	0.000134
Nuclear migration protein nudC	NUDC	-0.78475	0.000139
Sideroflexin-3	SFXN3	1.328101	0.000139
D-3-phosphoglycerate dehydrogenase	PHGDH	-1.01105	0.00014
Dipeptidyl peptidase 1	CTSC	1.389954	0.000143

Interleukin enhancer-binding factor 2	ILF2	-0.45319	0.000151
Proliferation-associated protein 2G4	PA2G4	-0.30349	0.000155
WD40 repeat-containing protein SMU1	SMU1	-0.36762	0.000166
Acetyl-CoA acetyltransferase, mitochondrial	ACAT1	2.340213	0.000169
Elongation of very long chain fatty acids protein	ELOVL5	-1.13886	0.000176
Lamin-B1	LMNB1	-0.52884	0.000178
Cytosol aminopeptidase	LAP3	-0.37567	0.000184
Kinesin-like protein KIF14	KIF14	-0.92867	0.000194
40S ribosomal protein S16	RPS16	-0.41361	0.000196
Polyadenylate-binding protein 1	PABPC1	-0.67968	0.000218
Caldesmon	CALD1	-0.55825	0.000219
Perilipin-3	PLIN3	-2.08247	0.000222
Nucleophosmin	NPM1	-0.91509	0.000239
Testin	TES	0.586281	0.000249
Heat shock protein 105 kDa	HSPH1	-0.54586	0.000256
Lactadherin	MFGE8	1.662023	0.000264
Nuclear autoantigenic sperm protein	NASP	-1.27478	0.000276
DnaJ homolog subfamily A member 2	DNAJA2	-0.65557	0.000281
NADH dehydrogenase [ubiquinone] 1 alpha subcomplex subunit 7	NDUFA7	0.534474	0.000284
SWI/SNF-related matrix-associated actin-dependent regulator of chromatin subfamily A member 5	SMARCA5	-0.41871	0.000286
Large neutral amino acids transporter small subunit 1	SLC7A5	-0.52106	0.000305
Transcription elongation factor SPT5	SUPT5H	-0.4813	0.000306
SH3 domain-binding glutamic acid-rich-like protein 3	SH3BGRL3	0.558237	0.000322
Protein lifeguard 3	TMBIM1	0.844734	0.000333
CD59 glycoprotein	CD59	0.75452	0.000335
Glutamate dehydrogenase 1, mitochondrial	GLUD1	0.619052	0.000344
26S protease regulatory subunit 10B	PSMC6	0.395055	0.000344
DNA topoisomerase 2-alpha	TOP2A	-1.24942	0.000354
Sterol O-acyltransferase 1	SOAT1	-0.88508	0.000359
Regulator of nonsense transcripts 1	UPF1	-0.23782	0.000387
Glucose-6-phosphate 1-dehydrogenase	G6PD	-0.80669	0.000389
Very-long-chain (3R)-3-hydroxyacyl-CoA dehydratase 2	HACD2	2.347305	0.000413
Peroxisomal membrane protein 11B	PEX11B	0.755532	0.000426
Splicing factor U2AF 65 kDa subunit	U2AF2	-0.70245	0.000436
Pachytene checkpoint protein 2 homolog	TRIP13	-0.51098	0.000443
Catenin delta-1	CTNND1	0.456515	0.000459
Carbonic anhydrase 2	CA2	0.927119	0.00046
10 kDa heat shock protein, mitochondrial	HSPE1	-0.74925	0.000466
Gelsolin	GSN	0.860099	0.000483
60S ribosomal protein L3	RPL3	-0.33369	0.000485
26S proteasome non-ATPase regulatory subunit 14	PSMD14	-0.30559	0.000491
Acetyl-coenzyme A synthetase, cytoplasmic	ACSS2	0.420665	0.000496
Isochorismatase domain-containing protein 1	ISOC1	-0.70216	0.000498
Quinone oxidoreductase PIG3	TP53I3	0.956357	0.000507
Transcription elongation regulator 1	TCERG1	-0.72123	0.000539
Protein FAM83H	FAM83H	0.864088	0.000563

Probable ATP-dependent RNA helicase DDX23	DDX23	-0.43564	0.000564
Serum deprivation-response protein	SDPR	-0.70188	0.000567
U4/U6 small nuclear ribonucleoprotein Prp4	PRPF4	-0.55094	0.000572
Antigen KI-67	MKI67	-1.51939	0.00058
Cyclin-dependent kinase 1	CDC2	-1.81233	0.000604
Proteasome subunit beta type-1	PSMB1	-0.45773	0.000605
Ovostatin homolog 2	OVOS2	-3.8219	0.000638
Clathrin heavy chain	CLTC	0.555922	0.000643
Eukaryotic translation initiation factor 1A, X-chromosomal	EIF1AX	-0.82651	0.00065
Luc7-like protein 3	LUC7L3	-0.77521	0.000667
T-complex protein 1 subunit alpha	TCP1	-0.31181	0.000672
Thioredoxin reductase 1, cytoplasmic	TXNRD1	-1.43354	0.00069
Cleavage and polyadenylation specificity factor subunit 1	CPSF1	-0.45153	0.000706
Lanosterol 14-alpha demethylase	CYP51A1	-1.43195	0.00072
Translocon-associated protein subunit delta	SSR4	-0.54874	0.00073
Periplakin	PPL	0.987417	0.000742
Structural maintenance of chromosomes protein 1A	SMC1A	-1.08524	0.000782
U1 small nuclear ribonucleoprotein 70 kDa	SNRNP70	-0.46304	0.000814
Proteasome assembly chaperone 1	PSMG1	-1.31559	0.000822
Adenosylhomocysteinase	AHCY	-0.21499	0.000828
Beta-catenin-like protein 1	CTNNBL1	-0.72628	0.000845
RNA-binding protein PNO1	PNO1	-0.85801	0.000849
Ras-related protein Rab-9A	RAB9A	0.781746	0.000867
Protein THEM6	THEM6	-0.66086	0.000878
Exosome component 10	EXOSC10	-0.35122	0.000879
Tubulin beta chain	TUBB	-0.44311	0.000918
Asparagine--tRNA ligase, cytoplasmic	NARS	-0.23549	0.000922
Probable ATP-dependent RNA helicase DDX6	DDX6	-0.36987	0.00093
Structural maintenance of chromosomes protein 1A	SMC1A	-0.54543	0.000978
Proteasome subunit beta type-4	PSMB4	-0.59588	0.000995
5-nucleotidase	NT5E	1.800237	0.001005
Myosin regulatory light chain 12A	MYL12A	-0.82353	0.001021
2-deoxynucleoside 5-phosphate N-hydrolase 1	DNPH1	0.303725	0.001062
Splicing factor 3B subunit 3	SF3B3	-0.26547	0.001067
T-complex protein 1 subunit gamma	CCT3	-0.32661	0.001078
Exportin-7	XPO7	1.747212	0.001108
Protein mago nashi homolog 2	MAGOHB	-1.05874	0.001134
Peptidyl-tRNA hydrolase 2, mitochondrial	PTRH2	-0.48638	0.001147
Guanine nucleotide-binding protein subunit beta-2-like 1	GNB2L1	-1.01787	0.0012
Long-chain-fatty-acid--CoA ligase 4	ACSL4	-0.48979	0.001209
Nucleolar RNA helicase 2	DDX21	-1.1371	0.00122
Helicase SKI2W	SKIV2L	0.457998	0.001262
Replication factor C subunit 3	RFC3	-0.78342	0.001267
Kinesin-like protein KIF2C	KIF2C	-1.49147	0.001279
Digestive organ expansion factor homolog	DIEXF	-0.71486	0.001314
Coiled-coil domain-containing protein 47	CCDC47	-0.33831	0.001317

Heat shock 70 kDa protein 4L	HSPA4L	-0.42414	0.001363
Very long-chain specific acyl-CoA dehydrogenase, mitochondrial	ACADVL	0.43841	0.001399
Acyl-coenzyme A thioesterase 11	ACOT11	0.730827	0.001462
Fatty acid desaturase 2	FADS2	-1.38827	0.001465
SUN domain-containing protein 1	SUN1	0.418357	0.001485
Fumarate hydratase, mitochondrial	FH	-0.22169	0.001487
Estradiol 17-beta-dehydrogenase 2	HSD17B2	2.243241	0.001489
Exosome complex exonuclease RRP44	DIS3	-0.93835	0.001513
Protein FAM50A	FAM50A	-0.9835	0.001527
DNA replication licensing factor MCM4	MCM4	-1.96222	0.001531
Cystatin-B	CSTB	1.545827	0.001532
Paraspeckle component 1	PSPC1	-0.72384	0.001551
Tripartite motif-containing protein 16	TRIM16	0.666547	0.001555
Casein kinase II subunit beta	CSNK2B-LY6G5B-1181	-0.734	0.001562
Midasin	MDN1	-0.74255	0.001589
Methionine aminopeptidase 2	METAP2	-0.40717	0.001603
Protein-tyrosine kinase 2-beta	PTK2B	1.237421	0.001616
Heat shock cognate 71 kDa protein	HSPA8	-1.36006	0.001641
Delta(3,5)-Delta(2,4)-dienoyl-CoA isomerase, mitochondrial	ECH1	0.436767	0.001665
Polymerase delta-interacting protein 2	POLDIP2	-0.46314	0.001686
Wiskott-Aldrich syndrome protein family member 2	WASF2	0.85116	0.001691
DNA-directed RNA polymerase	POLR1A	-0.62242	0.001707
Eukaryotic translation initiation factor 3 subunit E	EIF3E	-0.42775	0.00171
GMP synthase [glutamine-hydrolyzing]	GMPS	-0.21511	0.001731
Non-specific protein-tyrosine kinase	YES1	0.763289	0.00174
40S ribosomal protein S25	RPS25	-0.44734	0.001763
Transmembrane emp24 domain-containing protein 7	TMED7-TICAM2	-0.40968	0.001782
S-adenosylmethionine synthase isoform type-2	MAT2A	-0.93552	0.001796
Syndecan-4	SDC4	-0.76948	0.001799
Small nuclear ribonucleoprotein E	SNRPE	-0.97617	0.001817
Protein AHNAK2	AHNAK2	0.697989	0.001836
Tubulin-folding cofactor B	TBCB	-0.42522	0.00184
26S proteasome non-ATPase regulatory subunit 2	PSMD2	-0.22568	0.001841
ATP-dependent RNA helicase DDX3X	DDX3X	-1.15808	0.001885
Unconventional myosin-XVIIIa	MYO18A	0.602158	0.001887
D-beta-hydroxybutyrate dehydrogenase, mitochondrial	BDH1	0.772973	0.00189
Proteasome subunit alpha type-5	PSMA5	-0.51661	0.001905
Laminin subunit alpha-5	LAMA5	0.624102	0.001914
Eukaryotic translation initiation factor 5	EIF5	-0.61914	0.001918
Heat shock cognate 71 kDa protein	HSPA8	-0.74187	0.00192
Nucleolin	NCL	-0.73247	0.001946
Ataxin-10	ATXN10	-0.4075	0.001962
HLA class I histocompatibility antigen, alpha chain E	HLA-E	1.734081	0.001995
Cathepsin B	CTSB	0.93218	0.00201
Ferritin heavy chain	FTH1	1.135064	0.002016
Coactosin-like protein	COTL1	-0.45466	0.002113

Syntenin-2	SDCBP2	1.357165	0.002135
Protein phosphatase Slingshot homolog 3	SSH3	0.909129	0.002148
Rho guanine nucleotide exchange factor 7	ARHGEF7	1.087306	0.002221
Methylosome subunit pICln	CLNS1A	-0.8367	0.002275
Peptidyl-prolyl cis-trans isomerase FKBP4	FKBP4	-0.45335	0.00233
Flap endonuclease 1	FEN1	-1.08322	0.002333
Bifunctional 3-phosphoadenosine 5-phosphosulfate synthase 1	PAPSS1	-0.46086	0.002354
General transcription factor II-I	GTF2I	-0.39401	0.002391
Laminin subunit gamma-1	LAMC1	1.275231	0.002417
ATP-dependent RNA helicase DDX24	DDX24	-0.74175	0.002429
Small nuclear ribonucleoprotein Sm D3	SNRPD3	-0.54437	0.002508
Macrophage-capping protein	CAPG	0.961931	0.002523
26S proteasome non-ATPase regulatory subunit 6	PSMD6	-0.20665	0.002532
High mobility group protein B2	HMGB2	-0.51488	0.002561
Probable ATP-dependent RNA helicase DDX5	DDX5	-1.11658	0.002591
Prohibitin-2	PHB2	-1.04677	0.002604
Protein S100-A9	S100A9	1.998688	0.002657
Tubulin alpha-1B chain	TUBA1B	-1.27563	0.002769
Coatomer subunit beta	COPB2	-0.22216	0.002784
Clustered mitochondria protein homolog	CLUH	-0.9053	0.002787
Desmoplakin	DSP	0.678237	0.002792
Protein S100-P	S100P	1.140158	0.002796
Interferon regulatory factor 6	IRF6	1.020534	0.002824
Dynactin subunit 1	DCTN1	0.485476	0.00283
Epiplakin	EPPK1	0.182807	0.002875
DNA polymerase	POLD1	-1.06057	0.002915
40S ribosomal protein S18	RPS18	-0.59288	0.002933
Antileukoproteinase	SLPI	1.130088	0.002956
Cold shock domain-containing protein E1	CSDE1	-1.30374	0.002979
Histone H1.2	HIST1H1C	-0.56891	0.003022
Pseudouridylate synthase 7 homolog	PUS7	-0.8705	0.003074
Bleomycin hydrolase	BLMH	-0.72605	0.003116
Tricarboxylate transport protein, mitochondrial	SLC25A1	0.771392	0.003161
Importin subunit beta-1	KPNB1	-0.33846	0.003168
Splicing factor 3A subunit 1	SF3A1	-0.57293	0.0032
Ubiquilin-1	UBQLN1	-0.64762	0.003212
Ubiquitin-conjugating enzyme E2 D3	UBE2D3	-0.75633	0.003217
Serine/arginine-rich splicing factor 1	SRSF1	-0.80728	0.003233
Inosine triphosphate pyrophosphatase	ITPA	1.610349	0.003251
40S ribosomal protein S13	RPS13	-0.78962	0.00333
Mitogen-activated protein kinase 1	MAPK1	-0.52204	0.003403
Serine/threonine-protein phosphatase 6 catalytic subunit	PPP6C	-0.39105	0.003441
Type-1 angiotensin II receptor-associated protein	AGTRAP	0.36789	0.003487
Proteasome subunit alpha type	PSMA6	-0.36267	0.003503
HIG1 domain family member 1A, mitochondrial	HIGD1A	-0.68561	0.003505
Microtubule-associated serine/threonine-protein kinase 4	MAST4	1.778142	0.003609

Ribosomal L1 domain-containing protein 1	RSL1D1	-1.08739	0.003615
Tissue factor	F3	-1.32315	0.00362
Ribosome biogenesis protein BOP1	BOP1	-0.68583	0.003636
NADH-cytochrome b5 reductase 1	CYB5R1	0.945373	0.00367
Growth hormone-inducible transmembrane protein	GHITM	0.510305	0.003742
ADP-sugar pyrophosphatase	NUDT5	-0.77429	0.003756
Eukaryotic translation initiation factor 4H	EIF4H	-0.69103	0.003824
Heterogeneous nuclear ribonucleoprotein H2	HNRNPH2	0.689329	0.00383
Protein FAM3C	FAM3C	-0.86673	0.003847
Thioredoxin domain-containing protein 5	TXNDC5	-0.2528	0.00386
Calcium-binding protein 39	CAB39	-0.40666	0.003871
Ubiquitin-fold modifier 1	UFM1	-0.67457	0.003886
Cold shock domain-containing protein E1	CSDE1	-0.75219	0.00391
Laminin subunit gamma-2	LAMC2	1.149455	0.003933
Angiopoietin-related protein 4	ANGPTL4	-1.50526	0.003945
Plakophilin-2	PKP2	0.675773	0.00397
Cocaine esterase	CES2	1.377561	0.003992
Nucleolar protein 6	NOL6	-0.62527	0.004013
Junction plakoglobin	JUP	1.012401	0.004045
Mitotic spindle assembly checkpoint protein MAD2A	MAD2L1	-1.24787	0.004055
Amidophosphoribosyltransferase	PPAT	-0.50343	0.004075
T-complex protein 1 subunit eta	CCT7	-0.29356	0.004076
60S acidic ribosomal protein P0	RPLP0	-0.85598	0.004085
ATP synthase subunit O, mitochondrial	ATP5O	0.495915	0.004114
26S protease regulatory subunit 6B	PSMC4	0.270219	0.004134
Oligoribonuclease, mitochondrial	REXO2	-0.78708	0.004162
40S ribosomal protein S2	RPS2	-0.20873	0.004164
Cytochrome c oxidase subunit 6C	COX6C	1.085163	0.004192
2-oxoglutarate dehydrogenase, mitochondrial	OGDH	0.647111	0.004207
A-kinase anchor protein 13	AKAP13	0.965381	0.004229
Syntaxin-binding protein 5	STXBP5	0.601834	0.004232
60S ribosomal protein L24	RPL24	0.264682	0.004302
Putative 60S ribosomal protein L39-like 5	RPL39P5	-0.76459	0.004391
Sorting nexin-9	SNX9	0.342578	0.004411
Exocyst complex component 4	EXOC4	0.402437	0.004417
Cysteine and histidine-rich domain-containing protein 1	CHORDC1	-0.60534	0.004418
Catenin beta-1	CTNNB1	0.865037	0.004532
Vacuolar protein sorting-associated protein 13C	VPS13C	0.495693	0.004548
N-acylneuraminate cytidylyltransferase	CMAS	0.678196	0.004589
Acidic leucine-rich nuclear phosphoprotein 32 family member A	ANP32A	-1.10039	0.004629
Arginine--tRNA ligase, cytoplasmic	RARS	0.312082	0.004777
Embryonic stem cell-specific 5-hydroxymethylcytosine-binding protein	HMCES	-1.03028	0.004791
Transportin-1	TNPO1	-0.57793	0.005012
Supervillin	SVIL	0.34246	0.005074
Methionine aminopeptidase 2	METAP2	-0.67281	0.005207
60S ribosomal protein L31	RPL31	-0.99937	0.005355

Guanine nucleotide-binding protein subunit alpha-11	GNA11	-0.45892	0.005522
SUMO-activating enzyme subunit 1	SAE1	-0.90513	0.005628
Transforming growth factor-beta-induced protein ig-h3	TGFBI	1.540662	0.005716
Guanine nucleotide-binding protein subunit alpha-13	GNA13	-0.56099	0.005748
High mobility group protein HMG-I/HMG-Y	HMGA1	-1.37999	0.005758
Heat shock protein beta-1	HSPB1	1.094381	0.005773
General transcription factor 3C polypeptide 5	GTF3C5	-0.68706	0.005805
Mitochondrial glutamate carrier 1	SLC25A22	0.710612	0.005905
Thioredoxin domain-containing protein 9	TXNDC9	-1.43151	0.006004
Retinoblastoma-associated protein	RB1	-1.28862	0.006044
Thioredoxin-related transmembrane protein 1	TMX1	-0.58166	0.006051
Protein S100-A16	S100A16	0.410255	0.00608
Chitobiosyldiphosphodolichol beta-mannosyltransferase	ALG1	-0.76202	0.006082
Peroxiredoxin-4	PRDX4	0.787804	0.006146
Absent in melanoma 1 protein	AIM1	0.202485	0.00621
Histone H2A type 1-C	HIST1H2AC	-0.71343	0.006214
Tetraspanin	CD82	0.953973	0.006253
Succinate dehydrogenase [ubiquinone] flavoprotein subunit, mitochondrial	SDHA	0.535655	0.006373
Coatomer subunit beta	COPB1	0.300485	0.006388
Protein S100-A2	S100A2	0.615175	0.006475
Sterile alpha motif domain-containing protein 9	SAMD9	0.677995	0.006486
Tumor-associated calcium signal transducer 2	TACSTD2	1.848302	0.006532
E3 ubiquitin-protein ligase UBR5	UBR5	-0.61258	0.006539
Histone-binding protein RBBP4	RBBP4	-0.83407	0.006546
Lamina-associated polypeptide 2, isoforms beta/gamma	TMPO	-0.44683	0.006585
U3 small nucleolar RNA-interacting protein 2	RRP9	-0.45305	0.006645
Serine/threonine-protein phosphatase	PPP1CC	-1.34648	0.00665
WD repeat-containing protein 3	WDR3	-0.74147	0.006713
SRSF protein kinase 1	SRPK1	-0.54464	0.006728
Nardilysin	NRD1	-0.60005	0.006745
Ras GTPase-activating-like protein IQGAP1	IQGAP1	0.175955	0.006841
UTP--glucose-1-phosphate uridylyltransferase	UGP2	0.595498	0.006933
Protein MAL2	MAL2	0.607268	0.007258
Ral GTPase-activating protein subunit beta	RALGAPB	1.390602	0.007343
U1 small nuclear ribonucleoprotein A	SNRPA	-0.51597	0.007391
LIM and SH3 domain protein 1	LASP1	-0.32011	0.007504
40S ribosomal protein S7	RPS7	-0.84767	0.00752
Calpastatin	CAST	0.618854	0.007567
Mitofusin-2	MFN2	0.418022	0.007593
Farnesyl pyrophosphate synthase	FDPS	0.532558	0.007594
Protein transport protein Sec24C	SEC24C	0.557638	0.007637
Ribosomal biogenesis protein LAS1L	LAS1L	-0.52536	0.007649
Elongation factor Tu, mitochondrial	TUFM	0.23842	0.007717
60S ribosomal protein L35	RPL35	-0.59363	0.007771
Putative protein FAM10A4	ST13	-0.66278	0.007836
Bifunctional purine biosynthesis protein PURH	ATIC	-0.27542	0.007843

Unconventional myosin-Ic	MYO1C	0.499378	0.007897
RNA-binding motif protein, X chromosome	RBMX	-0.58887	0.007943
Probable E3 ubiquitin-protein ligase HERC4	HERC4	0.312281	0.007949
DNA (cytosine-5)-methyltransferase 1	DNMT1	-1.21627	0.008012
X-ray repair cross-complementing protein 6	XRCC6	-0.62628	0.008226
Signal transducer and activator of transcription 6	STAT6	0.441691	0.008325
Cystatin-A	CSTA	1.35225	0.008342
Lysine--tRNA ligase	KARS	-0.13937	0.008385
ATP-dependent Clp protease proteolytic subunit	CLPP	0.368285	0.008421
Non-POU domain-containing octamer-binding protein	NONO	-0.29856	0.008435
N-acetylgalactosamine kinase	GALK2	0.887406	0.008437
Complement decay-accelerating factor	CD55	0.86045	0.008537
Septin-8	SEPT8	0.35378	0.008655
Proteasome subunit alpha type-6	PSMA6	-0.62651	0.008675
DnaJ homolog subfamily C member 11	DNAJC11	0.506267	0.00868
Exosome complex component RRP42	EXOSC7	-0.54166	0.008695
Early endosome antigen 1	EEA1	0.532834	0.008766

Table S2. Laminin 111 signalling stimulates significant changes in protein expression in Alpha7-encapsulated MCF10a cells. List of proteins that are significantly upregulated (positive estimate values) or downregulated (negative estimate values) in day 7 MCF10a cell-laden Alpha7 gels supplemented with laminin 111 compared to cell-laden Alpha7 gels. ‘Estimate’ refers to the log2 fold-change of a given protein’s expression value. P-values calculated via MSqRob from three independent replicates per condition ($p < 0.05$).

Lingard et al. 2022

Optimising experimental procedures for self-assembling peptide hydrogels

Eliana Lingard[1,2], Siyuan Dong[3,4], Aline Miller[4,5], Marco Domingos[6,7], Joe Swift[1,8], Alberto Saiani[3,4], Andrew Gilmore[1,2]

Affiliations

[1]Wellcome Centre for Cell-Matrix Research, Oxford Road, Manchester, UK.

[2]Division of Cancer Sciences, School of Medical Sciences, Faculty of Biology, Medicine and Health, Manchester Academic Health Science Centre, University of Manchester, Manchester, UK.

[3]School of Materials, Faculty of Science and Engineering, The University of Manchester, Oxford Road, Manchester, UK.

[4]Manchester Institute of Biotechnology, The University of Manchester, Oxford Road, Manchester, UK.

[5]School of Chemical Engineering and Analytical Sciences, Faculty of Science and Engineering, The University of Manchester, Oxford Road, Manchester M13 9PL, UK.

[6]The Henry Royce Institute, Department of Materials, the University of Manchester, Manchester, UK.

[7]Department of Mechanical, Aerospace and Civil Engineering, School of Engineering, Faculty of Science and Engineering, The University of Manchester, Manchester, UK.

[8]Division of Cell Matrix Biology and Regenerative Medicine, School of Biological Sciences, Faculty of Biology, Medicine and Health, Manchester Academic Health Science Centre, University of Manchester, Manchester, UK.

Abstract

Self-assembling peptide hydrogels (SAPH) provide defined, consistent, and tuneable three-dimensional (3D) scaffolds for a variety of cell culture applications. However, these novel biomaterials present some challenges when using established protocols for protein isolation, immunofluorescence (IF) staining, and force microscopy due to interactions between the hydrogel network and charged moieties. Optimising these methods for 3D SAPH cultures is necessary to obtain clear and accurate information on how cells respond to their environment. Here, we describe our efforts to optimise methods for IF staining and protein analysis of cells encapsulated in SAPHs. These approaches require physically disrupting the peptide matrix to extract the cells and their proteins for analysis. We demonstrate that cell and organoid architecture is preserved following extraction and show that the standard immunoblotting method is compatible with lysates obtained from 3D SAPH cultures. We also show that the choice of charged slide is imperative to prevent sample loss during atomic force measurement analysis. These adjustments significantly improved the accuracy of data obtained from SAPHs, allowing us to evaluate their potential as 3D tissue models.

Keywords

Self-assembling peptide hydrogels // analytical technique optimisation // immunofluorescence staining // western blot analysis // atomic force microscopy

Abbreviations

- SAPH - self-assembling peptide hydrogel
- 3D - three-dimensional
- IF - immunofluorescence
- ECM - extracellular matrix
- MEC - mammary epithelial cell
- AFM - atomic force microscopy
- DMEM - Dulbecco’s modified eagle medium
- HSer - horse serum
- EGF - epidermal growth factor
- FBS - foetal bovine serum
- PBS - phosphate-buffered saline
- PEG - polyethylene-glycol
- FACS - fluorescence-activated cell sorting
- GFP - green fluorescent protein
- RFP - red fluorescent protein
- BSA - bovine serum albumin
- DAPI - 4′,6-diamidino-2-phenylindole
- $CaSO_4$ - calcium sulphate
- RIPA – radioimmunoprecipitation assay buffer
- SDS - sodium dodecyl sulphate

- DTT - dithiothreitol
- W - Watts
- SD - standard deviation
- H2B - histone 2B
- kDa – kilodaltons
- kPa - kilopascal

Introduction

Much work has gone into developing 3D cell scaffolds that recapitulate the extracellular matrix (ECM). A popular class of materials for this purpose are hydrogels, which are hydrated, fibrillar polymer networks that possess key properties of the ECM [1-4]. Organic hydrogels such as Matrigel and collagen gels have been used to mimic various tissue matrices since the 1970s due to their biocompatibility and ability to support a variety of behaviours and processes in cells [5-9]. However, the past three decades have seen the emergence of hydrogels composed of self-assembling peptides, which are more consistent and modifiable than organic hydrogels due to their synthetic origin [10-17]. Various peptides with unique gelation triggers have been developed [18-21]. One of the most enduring SAPH designs are β-sheet forming peptides [22-26]. β-sheet forming peptides are typically 4-30 amino acids long and contain alternating hydrophobic and hydrophilic residues, which drive their self-assembly into antiparallel β-sheets that entangle to form a hydrated, 3D scaffold when above their critical gelation concentration in solvent [27, 28]. SAPHs have already shown considerable promise for cell culture and tissue engineering applications, guaranteeing their future as desirable 3D cell scaffolds [29-32].

3D tissue models are used to investigate how cells respond to environmental cues *in vivo*. Various techniques can be employed to examine how cells are affected by their environment, such as IF staining, western blotting, and mass spectrometry. These techniques require that the proteins produced by cells are made accessible for identification, which is typically achieved by permeabilising the cell membrane, or by breaking the cells apart (lysis) and releasing the proteins into solution. IF staining is primarily used to label cellular proteins *in situ*, which requires that the cells are fixed to preserve their structures and contents [33, 34]. This is often done by cross-linking the cell proteins using chemicals such as aldehydes. Since fixation often reduces cell membrane permeability and thus hinders fluorescent antibody penetration, the cells are also permeabilised with organic solvents or non-ionic detergents to allow antibodies access to the proteins of interest [33, 35, 36]. Conversely, proteomics techniques such as western blot and mass spectrometry analysis are performed to identify and quantify multiple proteins, which requires that as many proteins as possible are extracted from cells to ensure that proteins of interest have the greatest chance of being detected [37]. The choice of lysis buffer used depends on the proteins of interest, downstream experiments, and the cell environment, but typically the buffer will contain a detergent (non-ionic or ionic depending on the sample type), reducing agents, salts, buffering agents and protease and phosphatase inhibitors [38-41]. However, standard protocols for these techniques are often designed for 2D cell culture models, while cells encapsulated in a 3D matrix are surrounded in an environment that may interfere with reagents and probes, requiring optimisation to obtain accurate results.

Cell behaviour is also regulated by the physical properties of SAPHs, such as stiffness and porosity [42-44]. Therefore, characterising these properties is also important. Techniques such as shear rheology provide quantitative bulk stiffness measurements of hydrogels and characterise their viscoelasticity, but atomic force microscopy (AFM) can measure local mechanical forces that cells directly sense with high resolution [45-48]. However, the accuracy of the force measurement data

depends on several factors including probe size and geometry, as well as sample stiffness and composition [49-51]. Additionally, there are limitations when analysing soft biomaterials using AFM as most force measurement techniques and equipment are designed for stiffer substrates [52-56]. For example, the viscoelastic properties of compliant hydrogels can reduce measurement accuracy, keeping samples hydrated during indentation is challenging, and existing data analysis models are primarily designed to account for the mechanical properties of elastic (solid) materials which have high moduli, instantaneously respond to deformation, and do not adhere to the probe. However, optimisation of existing AFM techniques and equipment for biomaterials has previously been shown to be successful, allowing researchers to determine the nanomechanical forces experienced by cells encapsulated in β-sheet forming SAPHs [50].

Typically, protocols adapted for 3D biomaterials are specific to organic matrices, where enzymes are used to cleave the biological polymers, isolating cells or proteins of interest from the matrix [57-59]. Synthetic hydrogels such as SAPHs cannot be digested using biological enzymes unless they are specifically functionalised with cleavage motifs, and therefore the cells must be isolated from SAPHs using other methods, such as solubilising the peptide network with urea [41, 60-62]. Previous studies have shown that protocol optimisation is necessary for isolating cells from 3D β-sheet forming SAPH scaffolds as the peptide matrix entraps the cells and its contents, hindering their detection downstream [41, 63]. This sequestration appears to be due in part to electrostatic interactions between the peptide matrix and biological macromolecules, where the net charge of the peptide network dictates whether ionic bonds are formed between the peptide network and charged macromolecules such as RNA [63]. The net charge of the SAPH network can be changed by altering hydrogel pH, but as cells are sensitive to pH, this is rarely a viable method [50]. Therefore, due to the unique physical and charge properties of SAPHs, there is strong likelihood that protocols must be optimised for 3D SAPH cultures.

Here, we investigated and optimised several analytical techniques for cells encapsulated in the β-sheet forming SAPH PeptiGel® Alpha4. We found that established protocols for 3D IF staining, protein extraction and AFM did not provide accurate and reliable data. We found that it was necessary to extract cells from 3D Alpha4 hydrogels before performing IF staining and western blotting techniques to reliably probe cellular proteins with fluorescent antibodies and to isolate the proteins for western blotting analysis. We also found that the net positive charge of Alpha4 affects its adhesion to charged slides, which can affect the accuracy of data collected during AFM experiments. These results demonstrate that the physical properties of SAPHs and their interactions with biological units can be reliably and accurately characterised.

Materials and Methods

Materials

PeptiGel® Alpha4 was purchased from Manchester BioGEL (Alderley Park, UK). Sterile alginate was purchased from Novamatrix (Sandvika, Norway). Matrigel was bought from Corning (Glendale, US).

Cell maintenance and passaging

Immortalised, non-tumorigenic human mammary epithelial cells (MCF10a) and human kidney epithelial cells (HEK-293T) were sourced from ATCC. MCF10a cells were maintained in monolayer culture using Dulbecco's modified eagle medium (DMEM)-F12 media supplemented with 5% filtered horse serum (HSer) (v/v), 10 µg/mL insulin, 0.5 µg/mL hydrocortisone, 100 ng/mL cholera toxin and 20 ng/mL epidermal growth factor (EGF). HEK-293T cells were maintained in monolayer culture using DMEM supplemented with 10% foetal bovine serum (FBS) (v/v). The cells were passaged at 70-90% confluency using 1X trypsin/EDTA solution and the cell suspension was collected in a 15 mL falcon tube. Cells were recovered by centrifuging the suspension at 350 xg for 5 minutes to obtain a cell pellet. MCF10a cells were resuspended in 1 mL of resuspension media (DMEM-F12 containing 1.8% HSer (v/v), 10 µg/mL insulin, 0.5 µg/mL hydrocortisone, 100 ng/µL cholera toxin and 5 ng/mL EGF) while HEK-293T cells were resuspended in growth media.

Lentiviral generation of stable MCF10A cells

Lentiviruses were generated using HEK-293T cells. On day 0, HEK-293T cells were seeded into two flasks at 70% confluency. On day 1, the media was replaced with 5 mL of growth media and the cells were transfected with 12 µg of pCDH vector, 9 µg of packaging vector psPax2 and 6 µg packaging vector MD2.G. These plasmids were incubated in blank DMEM for 2 minutes at room temperature before being mixed with 500 µL DMEM containing 54 µL 1X PEI. This mixture was incubated at room temperature for 30 minutes before being added to the cells. The cells were treated 24 hour later with 10 mM sodium butyrate for 6 hours before being given fresh medium overnight. The media was collected 72 hours post transfection and filtered through a 0.45 µm filter. 5 mL of chilled, 5X polyethylene-glycol (PEG) was added to the media which was left to incubate for 12 hours at 4°C. The media was then concentrated via centrifugation at 1500 xg for 30 minutes at 4°C, with the remaining supernatant being re-centrifuged for another 5 minutes to obtain residual virus. The resulting pellets were resuspended in 100 µL of cold phosphate-buffered saline (PBS) before being aliquoted into cryovials and stored at -80°C.

MCF10a cells were seeded at 1 x 10^5 cell density in 6-well plates 24 hours before transduction. The cells were then bathed in 1 mL complete growth medium containing 10 µg/mL Polybrene and 50 µL of virus was added dropwise to the cells. The virus was left for 48 hours at 37°C (5% CO_2) before the media was replaced with fresh complete growth medium. The cells were passaged as required for 2 weeks before being submitted for fluorescence-activated cell sorting (FACS).

Confluent fluorescent MCF10a cells were trypsinised and resuspended in complete growth medium before being spun for 5 minutes at 350 xg. The pellet was resuspended in 1 mL of sorting media (DMEM F12 containing 1% PS (v/v) and 25 mM HEPES). The cells were counted and 10 x 10^6 cells per mL were filtered through a 50 µm Filcon cup filter and stored on ice. Cells were sorted on the BD Aria-Fusion Cell Sorter (Beckton Dickinson, UK) using either a 488 or 561 nm laser excitation. Cells were identified over debris and aggregates using forward and side scatter and single cells were identified by virtue of the pulse height and pulse area signal. Green fluorescent protein (GFP) emission was collected following excitation with a 200 mW 488 nm laser through a 525/50 nm bandpass filter. Red fluorescent protein (RFP) emission was collected following excitation with a 200 mW 561 nm laser through a 610/20 bandpass filter. Cells were sorted on a 'Purity' sort mask and collected into 15 mL tubes containing 3 mL of complete media.

Cell encapsulation in Matrigel

MCF10a cells were resuspended in 1 mL of resuspension media (DMEM-F12 containing 1.8% HSer (v/v), 10 µg/mL insulin, 0.5 µg/mL hydrocortisone, 100 ng/µL cholera toxin and 5 ng/mL EGF). Appropriate volumes of cell suspension were mixed into blank DMEM to give a volume of 49.5 µL per gel. 50.6 µL of 8.9 mg/mL Matrigel was then pipetted into the cell-DMEM mixture to give a final total protein concentration of 4.5 mg/mL and a seeding density of 0.5 x 10^5 cells per 100 µL of gel. Wells of a 24-well plate were coated with a 50 µL layer of undiluted Matrigel before 100 µL of the Matrigel-cell-DMEM solution was then pipetted into each well and gently spread to ensure even coverage before being left to polymerise at 37°C (5% CO_2) for 30 minutes. After the gels had polymerised, MCF10a cultures were bathed in assay media (DMEM-F12 supplemented with 2% HSer (v/v), 10 µg/mL insulin, 0.5 µg/mL hydrocortisone, 100 ng/µL cholera toxin and 5 ng/mL EGF). The gels were then incubated at 37°C (5% CO_2). Media was refreshed every 2-4 days.

Cell encapsulation in peptide hydrogels

PeptiGels® were pre-warmed to room temperature before 50 µL of gel was spread over the bottom surface of wells in 24-well plates. MCF10a cells were encapsulated via gentle pipetting and mixing of cell suspension, as per the manufacturer's directions, into appropriate volumes of gel. Volumes of cell suspension used were calculated to ensure final cell densities ranging from 0.25 x 10^5 to 2.5 x 10^5 cells per mL. Following encapsulation, 100 µL aliquots of cell-laden hydrogels were pipetted into wells and carefully spread on top of the gel layer. After 5 minutes recovery, 1 mL of assay media was added to each well and the cultures were incubated at 37°C (5% CO_2). Media was changed the following day and every 3-4 days thereafter.

Organoid extraction from Matrigel and peptide hydrogels

Matrigel and peptide hydrogel cultures were washed with 1 mL of PBS following removal of media and then depolymerised using 1 mL of ice-cold cell recovery solution (Corning). After being incubated on an orbital shaker for 1 hour at 4°C, the freed well contents were resuspended and collected into

falcon tubes pre-coated with 1% bovine serum albumin (BSA) in PBS (w/v) and washed via centrifugation in PBS at 70 xg for 3 minutes at 4°C. The supernatants were discarded, and the pellets could then be resuspended for re-encapsulation or fixed for staining.

Organoid re-encapsulation in hydrogels

Organoid pellets isolated from Matrigel were resuspended in 1 mL of resuspension medium. 50 µL of suspension was added to fresh Matrigel and peptide hydrogels and encapsulated as previously described.

Matrigel and peptide hydrogels prepared for 37°C staining experiments were pipetted into ThinCert well inserts (Greiner Bio-One, UK). Matrigels were left to polymerise for 30 minutes at 37°C (5% CO_2) while peptide hydrogels were left to recover for 5 minutes before 900 µL of assay media was added into the wells. Following 5 minutes recovery, 100 µL of assay media was added to each insert and the gels were maintained as previously described.

Organoid re-encapsulation in alginate hydrogels

Organoid re-encapsulation in alginate gels was performed by mixing 30 µL of resuspended organoids with 50 µL of 25 mg/mL alginate. 20 µL of 40 mM calcium sulphate ($CaSO_4$) solution in blank DMEM was added to the mixture to give a final alginate concentration of 12.5 mg/mL and final $CaSO_4$ concentration of 8 mM. The gels were then spread on top of coverslips and left to set for 30 minutes at 37°C (5% CO_2). Following polymerisation, the gels were bathed in 1 mL of assay MCF10a media and incubated at 37°C (5% CO_2) for 30 minutes before being fixed and stained.

Immunofluorescent staining of extracted organoids

Extracted organoids were fixed for 45 minutes in 4% formaldehyde in PBS (v/v) at room temperature. The fixative was then diluted with 10 mL of PBS and the suspension was centrifuged at 70 xg for 3 minutes at 4°C. After discarding the supernatants, pellets were resuspended in 1 mL of organoid wash buffer (PBS containing 0.1% Triton-X-100 and 0.2% BSA), transferred to pre-coated, low adherent 24-well plates (Greiner Bio-One) and left to block at room temperature for 15 minutes. After blocking, excess buffer was carefully removed to leave 200 µL of liquid in each well and the clusters were incubated with 2X primary antibodies (Table 1) in organoid wash buffer overnight on an orbital shaker (100 RPM) at 4°C. The plates were retrieved, and after being left to settle at room temperature for 10 minutes, the organoids were washed three times in 1 mL of organoid wash buffer for 1 hour each time on an orbital shaker at 4°C. After removing the excess buffer to leave 200 µL of liquid in each well, the clusters were incubated with 2X secondary antibodies (Table 2) in organoid wash buffer overnight on an orbital shaker at 4°C. The organoids were then left to settle at room temperature for 10 minutes before excess liquid was removed to leave 200 µL of liquid per well. The organoids were then incubated with 200 µL of 2 µg/mL 4′,6-diamidino-2-phenylindole (DAPI) in PBS for 10 minutes on an orbital shaker at 4°C before being washed 3 times with organoid wash buffer for

1 hour each time, as described above. Following the final wash, the organoids were diluted in PBS and transferred to 6-well plates.

Antigen	Host	Source	Catalogue number	Dilution
Active caspase-3	Rabbit	R&D Systems	AF835	1:200
Laminin α3 chain	Mouse	R&D Systems	MAB21441	1:200
Collagen IV	Rabbit	Abcam	ab6586	1:200
E-cadherin	Mouse	BD Transduction Laboratories	610181	1:200

Table 1. Primary antibodies for suspension immunofluorescence.

Antigen	Conjugate dye	Host	Source	Catalogue number	Dilution
Anti-mouse	AlexaFluor 594	Donkey	Invitrogen	A21203	1:250
Anti-rabbit	AlexaFluor 488	Donkey	Invitrogen	A21206	1:250

Table 2. Secondary antibodies for suspension immunofluorescence.

Immunofluorescent staining of organoids in 3D hydrogels

Hydrogels prepared in inserts were transferred to 30 mm dishes. Hydrogels were washed with PBS for 15 minutes and fixed with 4% formaldehyde in PBS for 30 minutes at room temperature. The fixative was washed out using PBS for 15 minutes. Hydrogels were permeabilised with 0.5% Triton-X-100 for either 5 minutes at room temperature or for 30 minutes at 37°C. The hydrogels were then washed with 3D IF wash buffer (PBS containing 0.1% BSA, 0.2% Triton-X-100 and 0.05% Tween-20) for 30 minutes before being blocked in 10% HSer in 3D IF wash buffer for either 90 minutes at room temperature or an hour at 37°C. The hydrogels were stained with primary antibodies (Table 3) diluted in 5% HSer in 3D IF wash buffer overnight at either 4°C or 37°C. Following primary antibody incubation, the gels were washed for 50 minutes using 3D IF wash buffer and then incubated with secondary antibodies (Table 4) diluted in 5% HSer in 3D IF wash buffer for an hour at either room temperature or 37°C. The gels were then washed for another 50 minutes before being stained with 1 µg/mL DAPI in PBS for 10 minutes at either room temperature or 37°C. The gels were then washed with 3D IF wash buffer for either 10 minutes or 30 minutes and left to wash in deionised water overnight. Hydrogels prepared on coverslips were dried and mounted onto slides.

Antigen	Host	Source	Catalogue number	Dilution
Active caspase-3	Rabbit	R&D Systems	AF835	1:400
Laminin α3 chain	Mouse	R&D Systems	MAB21441	1:400
Collagen IV	Rabbit	Abcam	ab6586	1:400
E-cadherin	Mouse	BD Transduction Laboratories	610181	1:400
β-catenin	Mouse	BD Biosciences	610154	1:400

Table 3. Primary antibodies for immunofluorescence.

Antigen	Conjugate dye	Host	Source	Catalogue number	Dilution
Anti-mouse	AlexaFluor 594	Donkey	Invitrogen	A21203	1:500
Anti-rabbit	AlexaFluor 488	Donkey	Invitrogen	A21206	1:500

Table 4. Secondary antibodies for immunofluorescence.

Fluorescent microscope imaging

Confocal images were collected on either a Leica TCS SP8 AOBS upright confocal using a 63x/1.40 oil or 63x/0.90 water immersion objective, or a Leica SP8x inverted confocal using a 20x/0.75 APO objective. The confocal settings were as follows, pinhole 1 airy unit, scan speed 400 Hz unidirectional, format 1024 x 1024. Images were collected using hybrid and photomultiplier detectors with the following detection mirror settings; DAPI 410-475 nm; Alexa-488 507-580 nm; Alexa-594 605-750 nm using the 405 nm (50%), 490 nm (30%) and 590 nm (30%) laser lines respectively. When it was not possible to eliminate crosstalk between channels, the images were collected sequentially. The acquired images were processed using ImageJ.

Images of fluorescent MCF10a clusters encapsulated in Matrigel and peptide hydrogels were collected as single images on the EVOS M7000 Imaging system (Thermo Fisher Scientific, MA) using a 20x objective. Images were collected using the GFP and RFP light source channels. The acquired images were processed in ImageJ.

Brightfield microscope imaging

Brightfield images were collected on a Leica DMIL LED inverted brightfield microscope connected to a xiQ USB3.0 Vision camera using a 20x objective. The acquired images were processed using ImageJ.

Protein extraction from 2D cultures

Following media removal, cells were washed for 15 minutes in 1X PBS and then lysed in 100 µL of lysis buffer, either 1X radioimmunoprecipitation assay buffer (RIPA) (50 mM Tris-HCL (pH 7.4), 150 mM sodium chloride, 1% IGEPAL, 0.1% (w/v) sodium dodecyl sulphate (SDS), 1% sodium deoxycholate, 20 mM sodium fluoride, 2 mM sodium orthovanadate, 1X mM protease inhibitor cocktail) or urea buffer (100 mM Tris-HCL (pH 8.0), 8 M urea, 2 M thiourea, 5 mM dithiothreitol (DTT)). The samples were incubated on ice for 15 minutes before being sonicated for 180 seconds at 10 Watts (W) using a Covaris S220 ultrasonicator before being centrifuged at 3220 xg for 5 minutes at 4°C. Lysates were stored at 20°C.

Protein extraction from peptide hydrogels

Following media removal, all gels were washed in 1X PBS for 15 minutes. Undiluted peptide hydrogels were diluted with either 50, 75 or 100 µL of PBS. Hydrogel-encapsulated cells were then

lysed by mixing the gels with 100 µL of lysis buffer, either 1X RIPA or urea buffer, and then incubated, ultrasonicated and centrifuged as described above.

Western blot analysis

RIPA lysates were mixed with 5X Laemmli buffer (250 mM Tris-HCL (pH 6.8), 50% glycerol (v/v), 10% SDS (w/v), 0.1% Bromophenol blue, 500 mM DTT) and heated at 95°C for 5 minutes. Urea lysates were mixed with Laemmli buffer but were not heated. The samples were then separated alongside a broad range (11-250 kDa) stained protein ladder (New England Biolabs, UK) by 12% SDS-PAGE for 1.5 hours at 35 mA and 200 V. The proteins were then transferred to 0.45 µm nitrocellulose membranes (Fisher Scientific, MA) for 1 hour at 2 A and 100 V before being blocked in 1X casein blocking buffer (Sigma Aldrich, MO) for 30 minutes. Following this, the proteins were incubated with primary antibodies (Table 5) diluted in blocking buffer overnight at 4°C. The proteins were then washed in 1X TBS-T (137 mM NaCl, 2.7 mM KCl, 19 mM Tris, 1 % Tween (v/v)) for 45 minutes before being incubated with secondary antibodies (Table 6) diluted in blocking buffer for 1 hour. The proteins were then washed in TBS-T for at least 45 minutes before the protein bands were detected using the Odyssey CLx (Li-Cor, NE).

Antigen	Host	Source	Catalogue Number	Dilution
Paxillin Y113	Rabbit	Abcam	ab32084	1:1000
Phospho-paxillin Y31	Rabbit	Invitrogen	44-720G	1:1000
Phospho-p130cas Y410	Rabbit	Cell Signalling	4011S	1:1000
β-actin	Mouse	Abcam	ab8224	1:1000

Table 5. Primary antibodies for western blotting.

Antigen	Conjugate dye	Host	Source	Catalogue Number	Dilution
Anti-mouse	680CW	Donkey	Li-Cor	926-32212	1:10,000
Anti-rabbit	800CW	Donkey	Li-Cor	926-32213	1:10,000

Table 6. Secondary antibodies for western blotting.

Atomic force microscopy

The elastic moduli of re-hydrated peptide hydrogels were measured in water using a Hysitron BioSoft In-situ Indenter (Bruker, MN), with Tribo iQ™ software (Bruker) and a Hysitron (Bruker) 400 µm sapphire sphere probe. The probe was brought into contact with the gel and allowed to equilibrate for 5 minutes before force relaxation measurements were taken, where 25 µm of gel was displaced for 50 seconds each time. Non-linear regression was used to fit the force curves.

Oscillatory shear rheometry

The storage modulus of gels was investigated using a Discovery HR-2 hybrid rheometer (TA Instruments, US) with a 20 mm parallel plate and a gap size of 500 µm. Samples were prepared by aliquoting 180 µL of gel into ThinCert well inserts (1 µm pore size, Greiner Bio-One). Following 5

minutes recovery time, 900 µL of assay media was added into the wells. After another 5 minutes recovery time, 100 µL of assay media was added to each insert and the gels were incubated at 37°C (5% CO_2) for at least 30 minutes prior to testing. Samples were removed from the inserts by peeling off the bottom membrane of the insert and transferred onto the rheometer plate as described by Ligorio et al. [64]. The upper rheometer head was then lowered to the gap size and samples were equilibrated for 3 minutes at 37°C. Oscillatory amplitude experiments were performed at 1 Hz frequency and within the linear viscoelastic region in the strain range: 0.01 to 20%. The mean storage modulus values described in the results section were obtained at 0.2% oscillation strain.

Statistical analysis

All data were analysed in GraphPad Prism v9.4.1. Quantitative values are presented as mean ± standard deviation (SD).

Results and discussion

IF labelling of Alpha4-encapsulated cells yields severe background staining and inconsistent labelling

With the right choice and concentration of reagents and antibodies and optimised incubation times, good-quality fluorescent images of hydrogel-encapsulated cells can be obtained that improve our understanding of mammary epithelial cell (MEC) differentiation and the factors that affect it [42, 65-71]. For example, studies have established that non-malignant, human MECs such as MCF10a cells form polarised acini when they are encapsulated in a laminin 111-rich hydrogel such as Matrigel [68, 72, 73]. Acini display apicobasal polarisation, assemble a laminin 332- and collagen IV-rich basement membrane and develop lumens through caspase-3-mediated apoptosis, which can all be visualised in 3D Matrigel cultures using 3D IF staining. To establish a baseline for the image quality of IF-labelled acini embedded within 3D Matrigel hydrogels that we can use to evaluate IF data obtained from SAPHs, we encapsulated MCF10a cells in Matrigel for 5, 12 or 21 days before immunostaining them for markers of acinar formation. In brief, MCF10a cells embedded within Matrigel hydrogels were fixed with 4% formalin for 30 minutes and permeabilised with the non-ionic detergent Triton-X-100 for 5 minutes. After blocking, the cells were incubated with primary antibodies raised against active caspase-3 and laminin 332 overnight at 4°C. Incubation with fluorescent secondary antibodies was performed for one hour. The cells were counterstained with DAPI and mounted onto slips. We found that Matrigel-embedded acini were consistently labelled for key markers of apoptosis (Fig. 1A). By day 5, acini were producing a laminin 332-rich basement membrane. Some acini were polarised and hollow, which shows that they had fully matured. At day 12, more polarised acini were found, with many undergoing centralised, caspase-3-mediated apoptosis to form lumens. Since acinar structures continuously form in Matrigel, some organoids still showed signs of maturing by day 21 and therefore displayed clear signs of centralised caspase-3 activity as luminal clearance took place. These markers of acinar formation were easily and consistently identified in the Matrigel cultures at each time point, demonstrating the efficacy of this IF labelling method for 3D Matrigel cultures.

There is limited published information regarding Alpha4's suitability as a 3D MEC scaffold [74]. Therefore, IF labelling could be used to explore how MECs respond to encapsulation in Alpha4. However, the correct IF staining protocol must be selected to provide us with consistent and accurate images. To investigate whether Alpha4-encapsulated MECs could be immunolabelled using the standard 3D IF staining technique used for 3D Matrigel cultures, we immunostained day 5, 12 and 21 Alpha4-encapsulated MCF10a cells with antibodies raised against active caspase-3 and laminin 332 following the 3D IF staining protocol described above. The quality of IF labelling in 3D Alpha4 cultures was found to be far lower than the quality of images obtained from 3D Matrigel cultures (Fig. 1B). Background fluorescence was relatively high in comparison, which made it difficult to distinguish between nuclei and the gel. The relatively low contrast between the gel and nuclei also made it challenging to identify whether the cells were polarising. However, images with lower background fluorescence helped us confirm that the cells did not polarise over the 21-day culture period. Caspase-3 activity was easy to identify within clusters at each timepoint, which indicates that with this

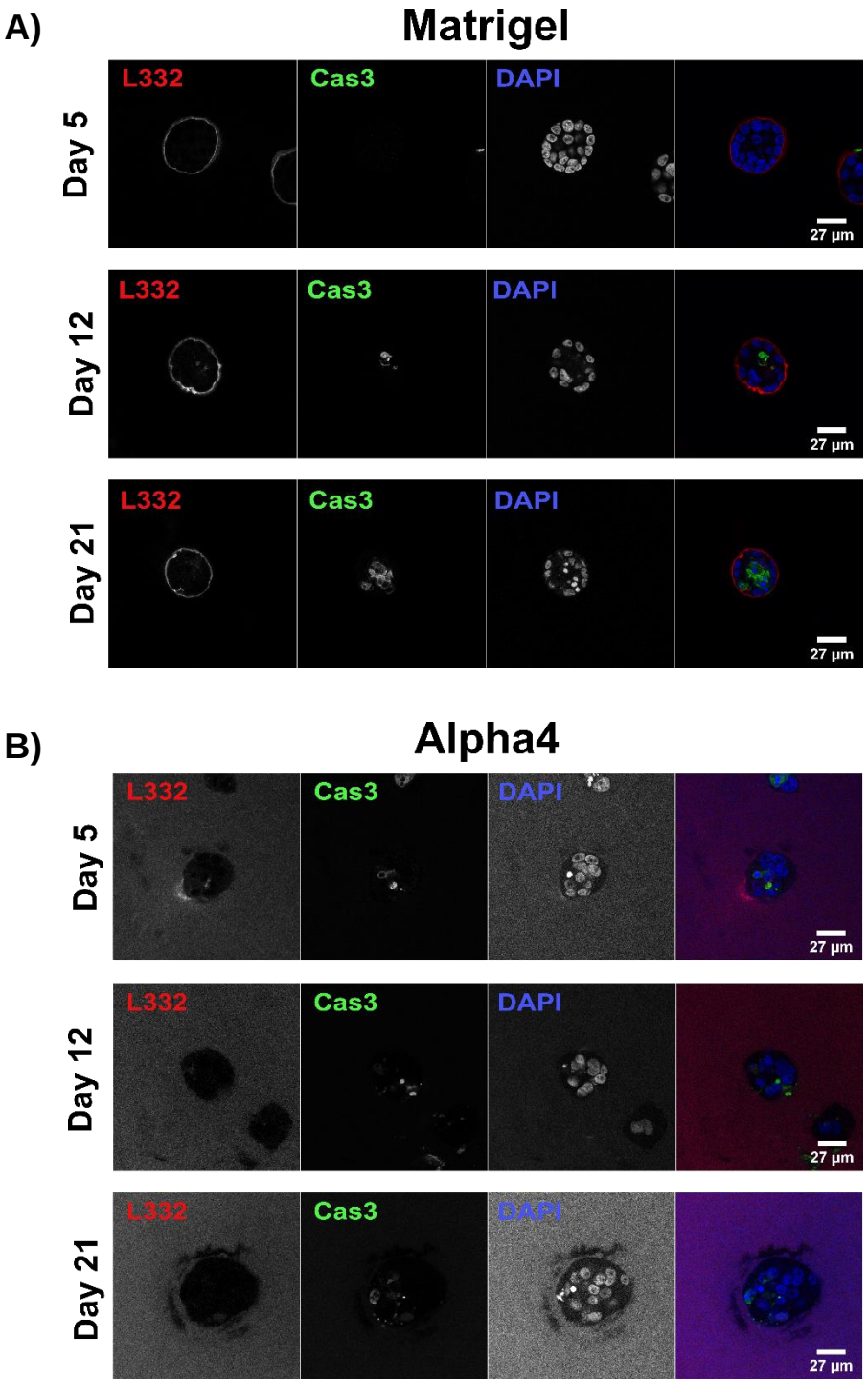

Fig. 1. 3D Alpha4 hydrogels display high background staining and inconsistent protein labelling when stained with IF antibodies. A) IF images of MCF10a acini encapsulated in Matrigel. At days 5, 12 and 21, the organoids were stained with antibodies raised against acinar markers: active caspase-3 (Cas3) and laminin 332 (L332). Nuclei were stained using DAPI. B) IF images of MCF10a organoids encapsulated in Alpha4. At days 5, 12 and 21, the organoids were stained with antibodies raised against acinar markers: active caspase-3 (Cas3) and laminin 332 (L332). Nuclei were stained with DAPI.

IF staining protocol, the active caspase-3 antibody can penetrate the SAPH and enter permeabilised, encapsulated MCF10a cells to bind its antigen. Since caspase-3 activation was not restricted to the centre of clusters, these images suggest that MCF10a cells encapsulated in Alpha4 gels do not form the same acinar structures as in Matrigel. Laminin 332 staining was occasionally detected within 3D

Alpha4 hydrogels, which made it unclear as to whether the organoids were producing basement membranes. While these results indicate that only some Alpha4- encapsulated organoids can produce a basement membrane, they also suggest that the antibody raised against laminin 332 cannot consistently access its target when it is introduced into Alpha4 hydrogels. This could be caused by aldehyde-induced cross-links between laminin 332 and Alpha4's peptide network, as aldehyde cross-linking in fixed proteins has been shown to induce conformational changes in proteins and form steric barriers that block antibody access to binding sites [33]. It is also possible that the antibody cannot penetrate the hydrogel, preventing it from accessing its target. If antibodies cannot access their targets in Alpha4, this labelling technique would not be a reliable or accurate method for probing proteins within 3D Alpha4 cultures. The high background fluorescence present in Alpha4 hydrogels also indicates that this 3D IF labelling technique is not suitable for Alpha4. Indeed, this fluorescence may be an intrinsic property of the hydrogel since aromatic residues present in its peptide network are known to autofluoresce at near-UV wavelengths and therefore cannot be removed or quenched [75, 76]. Together, these results suggest that alternative approaches to fluorescent antibody labelling are required if we are to obtain consistently good-quality images of cells embedded in Alpha4 gels.

The optically dense peptide matrix of Alpha4 reduces image resolution and quality

Heat-induced epitope retrieval (HIER) is a technique used to improve staining results by inducing conformational changes in cellular proteins with heated buffers, which reduces protein cross-linking during fixation and thus promotes complementary antigen binding [77]. Increasing the antibody incubation temperature to 37°C has been shown to increase the quality of fluorescent immunolabelling of thick tissue sections [78, 79]. We therefore examined whether it was possible to improve the quality of IF images obtained from 3D Alpha4 gels by performing the key steps of the 3D IF staining protocol at 37°C. To investigate this, acini were cultured in Matrigel for 7 days before being extracted and transplanted into either Matrigel or Alpha4 hydrogels. The gels were washed and fixed with formalin before being permeabilised for 30 minutes at 37°C. Blocking, antibody incubations, and DAPI staining were also performed at 37°C. Primary antibodies raised against collagen IV and β-catenin were used to probe the encapsulated acini. We consistently found acini that displayed peripheral collagen IV staining within Matrigel hydrogels (Fig. 2A). β-catenin expression and localisation were harder to distinguish but it was shown to be expressed between cell boundaries. In contrast, organoids were difficult to identify within Alpha4 as the high background fluorescence obscured the stained nuclei, which was consistent across low (20x) and high (63x) magnifications (Fig. 2B). Collagen IV staining was difficult to distinguish, and β-catenin staining was negligible in all Alpha4-encapsulated acini. The poor quality of the IF images obtained from 3D Alpha4 gels suggest some incompatibility of this staining technique with 3D Alpha4 cultures. Although increasing incubation temperatures during staining has helped improve antibody binding and detection in 3D tissues, finding the right combination of buffers, incubation temperatures and times is necessary to achieve such an outcome [80]. It is possible that this staining method could produce consistent IF images with good antibodies. However, given that the major issue with staining in Alpha4 is the

resulting high background, it is unlikely that further efforts to optimise this method will significantly improve staining quality in Alpha4 hydrogels.

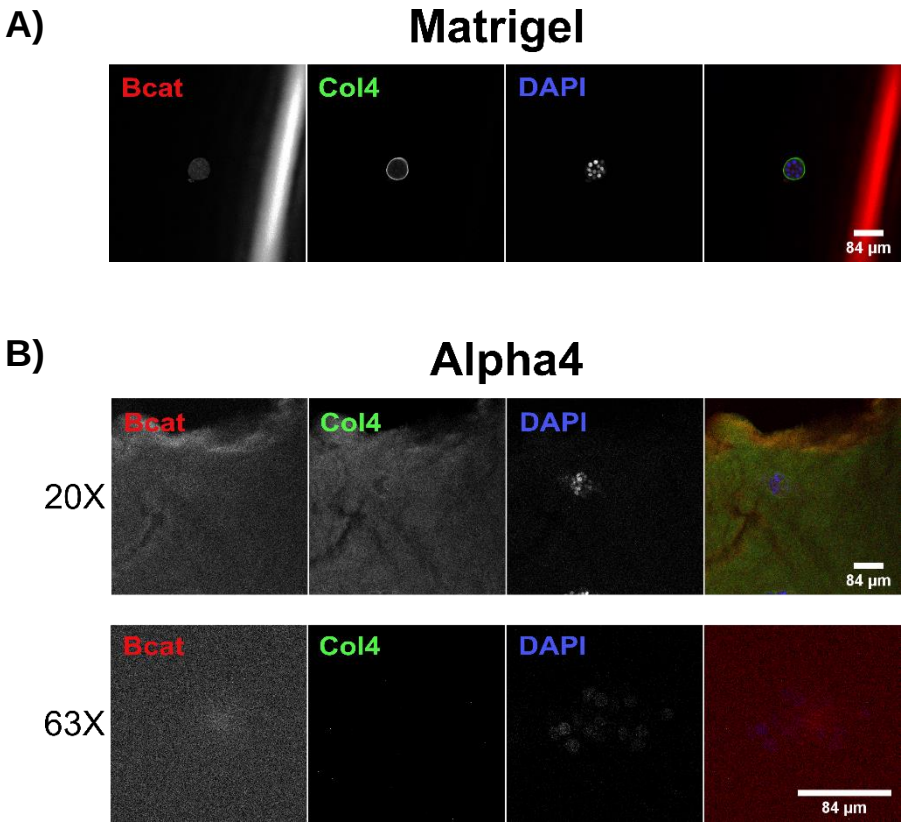

Fig. 2. Increasing incubation temperatures to 37°C does not improve the quality of antibody staining in 3D Alpha4 gels. A) 20x IF images of MCF10a acini that were grown in Matrigel for 7 days before being transplanted into fresh Matrigel hydrogels. Following transplantation, the encapsulated acini were stained with antibodies raised against acinar markers: collagen IV (Col4) and β-catenin (Bcat). Nuclei were stained with DAPI. The blocking, antibody incubation and DAPI staining steps were performed at 37°C. B) 20x and 63x IF images of MCF10a acini that were grown in Matrigel for 7 days before being transplanted into Alpha4 hydrogels. Following transplantation, the encapsulated acini were stained with antibodies raised against acinar markers: collagen IV (Col4) and β-catenin (Bcat). Nuclei were stained with DAPI. The blocking, antibody incubation and DAPI staining steps were performed at 37°C.

To investigate whether the high background fluorescence observed in 3D Alpha4 hydrogels is caused by Alpha4's peptide network or non-specific antibody binding, we encapsulated fluorescent MCF10a cells within Matrigel or Alpha4 hydrogels and asked whether we could observe background fluorescence in the hydrogels. Fluorescent cells have been modified to express proteins that fluoresce when excited at specific light wavelengths, eliminating the need for fluorescent antibodies. Since antibodies are not required to label the proteins, we can determine whether the high fluorescent background seen in antibody labelled Alpha4 gels is caused by its peptide network. Two stable fluorescent cell lines were generated for this investigation: MCF10a cells expressing Venus-vinculin (green, cytosolic) or histone 2B (H2B)-RFP (red, nuclear). Both cell lines were seeded together into the Matrigel and Alpha4 hydrogels at equal cell densities and were cultured for 7 days prior to imaging. We found that we could clearly identify fluorescent acini within Matrigel hydrogels (Fig. 3A). While crosstalk between the GFP and RFP channels made it harder to identify whether acini were composed of H2B-RFP or Venus-vinculin MCF10a cells, the transparency of the Matrigel hydrogels

made them relatively easy to distinguish. In contrast, we found it challenging to identify fluorescent organoids in Alpha4 hydrogels as they were obscured by the cloudy appearance of the hydrogel, which was exacerbated by the crosstalk between the GFP and RFP channels. These results indicate that the high fluorescent background of Alpha4 is caused by its peptide network and suggest that Alpha4 is an optically dense SAPH, as it is near-opaque when examined using fluorescence microscopy which indicates that the peptide network is absorbing light emitted by the microscope.

We asked whether we could reduce the opacity of Alpha4 by reducing its peptide concentration to obtain better quality fluorescent images. To investigate this, we prepared 75% and 50% (v/v) Alpha4 hydrogels by diluting them with different volumes of PBS and encapsulated Venus-vinculin and H2B-RFP MCF10a cells within them as described above. We found that the diluted Alpha4 hydrogels were less cloudy than the undiluted Alpha4 hydrogels, which made it easier to identify fluorescent organoids (Fig. 3B). These results show that reducing Alpha4's peptide concentration reduces the gel background, which demonstrates that Alpha4's peptide network is optically dense.

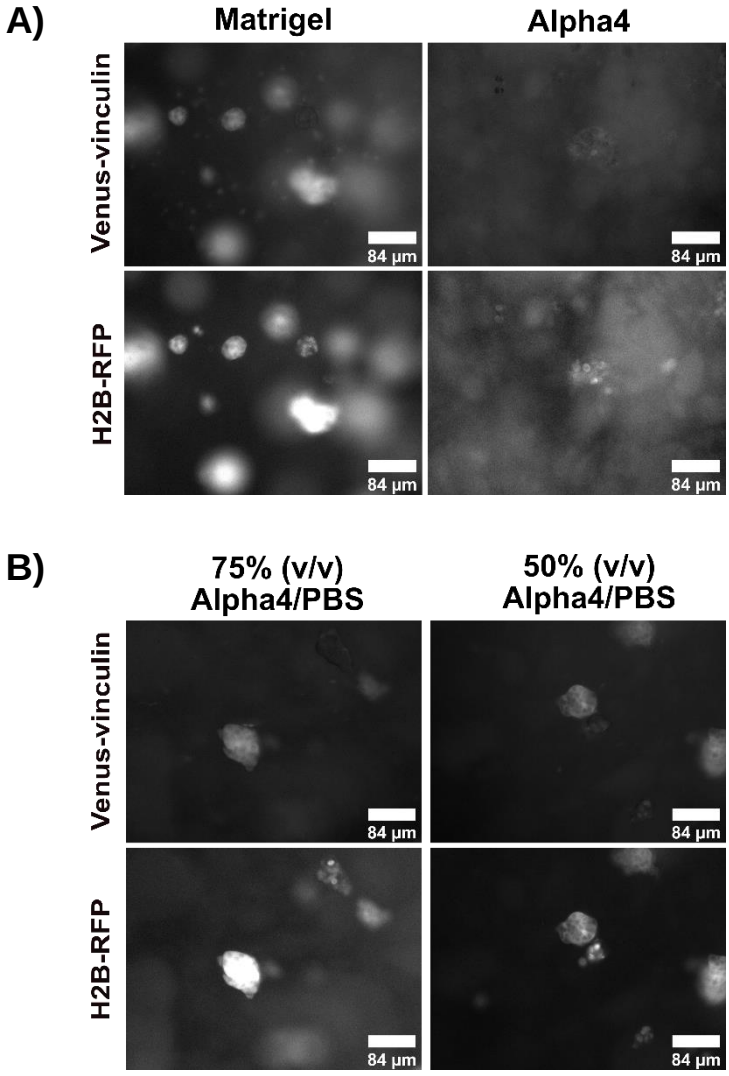

Fig. 3. The peptide network of Alpha4 is optically dense. Fluorescent images of day 7 Venus-vinculin (cytosolic) and H2B-RFP (nuclear) fluorescent MCF10a cells encapsulated within A) Matrigel or Alpha4 hydrogels, or B) Alpha4 hydrogels diluted with PBS. H2B, histone 2B; RFP, red fluorescent protein.

While these results indicate that the peptide network absorbs light, it remains unclear whether it emits fluorescent light and thus autofluoresces. However, studies have shown that β-sheet enriched proteins such as amyloid fibrils are autofluorescent at near-UV excitation wavelengths as hydrogen bonds within β-sheet facilitate proton transfer between fibril N- and C-termini, which reduces electron excitation energy [81-85]. These findings suggest that the β-sheet forming peptide network of Alpha4 is intrinsically fluorescent, which could be clarified using fluorescence spectroscopy analysis in a future study. Taken together, these results show that Alpha4 hydrogels are optically dense when exposed to near-UV wavelengths of light that are required to excite DAPI- and GFP-fluorophores [86-88]. The difficulties in obtaining good quality images of Alpha4 cultures was exacerbated by the crosstalk between the GFP and RFP channels. However, while crosstalk can potentially be eliminated, these results confirmed that Alpha4 gels are optically dense when exposed to fluorescent light, which makes it unlikely that high quality fluorescent images of organoids can be obtained while they remain encapsulated within Alpha4.

Poor antibody penetration and high background fluorescence in Alpha4 gels are mitigated by extracting organoids from Alpha4 and staining them in suspension

The results of our imaging experiments have shown that 3D Alpha4 gels, particularly undiluted Alpha4 gels, are almost optically opaque. This makes it challenging to obtain high-quality fluorescent images of Alpha4-encapsulated cells. It also appears that antibodies have trouble accessing their targets within the Alpha4 matrix, resulting in inconsistent staining results across experiments. To investigate whether Alpha4 hinders antibody penetration, we compared the labelling consistency and intensity of immunolabelled acini encapsulated within Matrigel, alginate or Alpha4 hydrogels. MCF10a acini were grown in Matrigel hydrogels for 7 days before extracting the acini from the Matrigel hydrogels using ice-cold Corning® cell recovery solution. The recovered acini were transplanted into either Matrigel, alginate or Alpha4 hydrogels and were fixed and stained within the hydrogels. The acini were immunostained with antibodies to activated caspase-3, laminin 332, collagen IV and E-cadherin. Acini stained in 3D Matrigel hydrogels were clearly and consistently immunolabelled with all four markers of acinar development, confirming that the structures and their morphology are preserved throughout extraction and re-encapsulation (Fig. 4A). Caspase-3 activity was restricted to the lumen of the organoids. E-cadherin was concentrated at cell junctions and laminin 332 deposition was also clearly labelled around the periphery of the organoids. Collagen IV staining was harder to detect, which suggested that most of the collagen IV was lost to the cell recovery solution, but traces were found around the periphery of acini, showing that it was localised to the basement membrane. Similarly, acini that were stained in alginate hydrogels showed consistent labelling for all four acinar markers (Fig. 4B). Laminin 332 and collagen IV were clearly labelled around the periphery of acini and E-cadherin expression was clearly labelled at cell junctions. Caspase-3 activity was mostly restricted to the organoid lumens. In contrast, the acini encapsulated within Alpha4 hydrogels were inconsistently immunolabelled (Fig. 4C). Laminin 332 and collagen IV production were not detected in most acini. Luminally restricted capase-3 activity and E-cadherin expression at cell junctions were detected at relatively lower intensities in comparison to Matrigel- and alginate-encapsulated acini. These

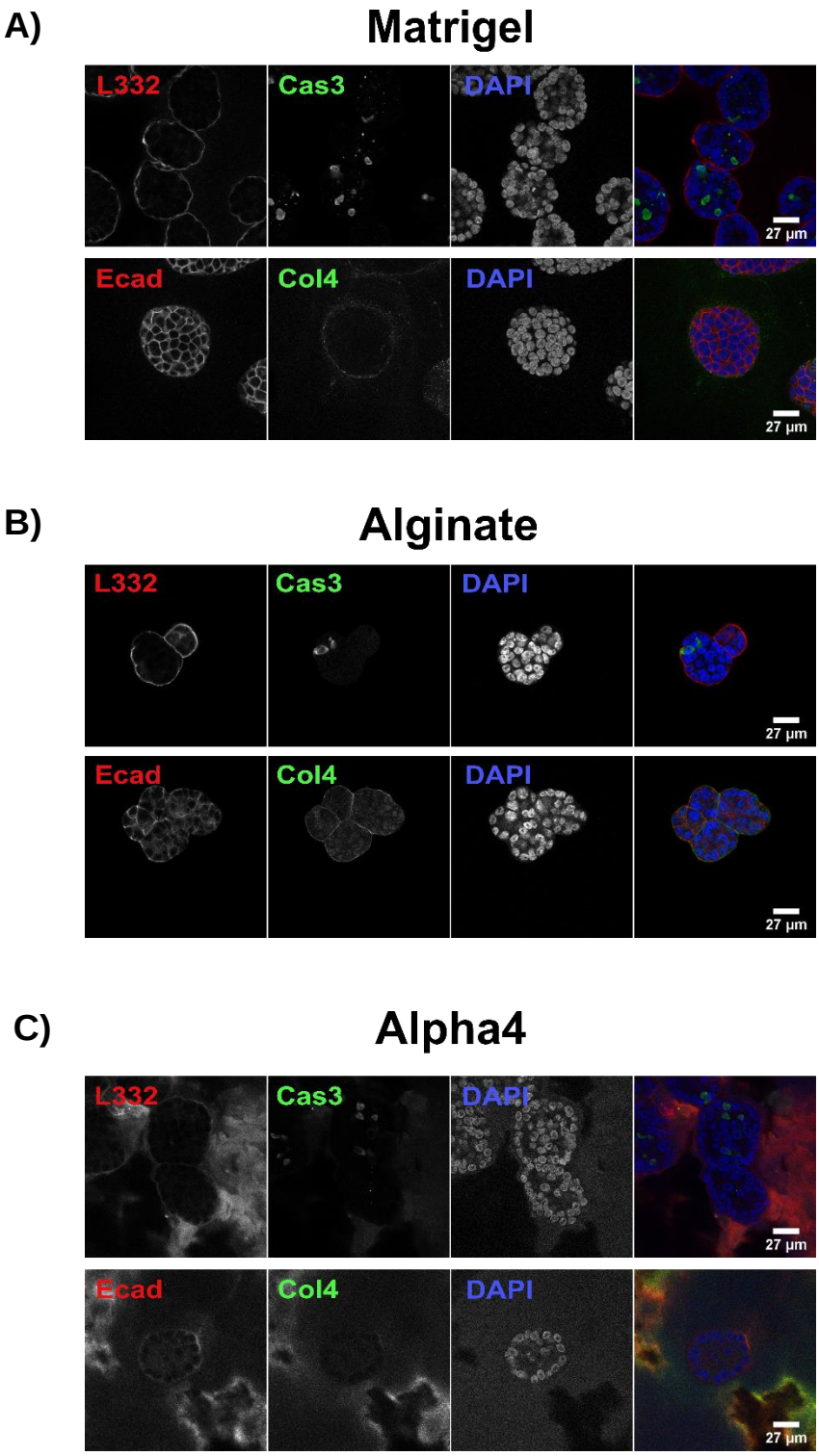

Fig. 4. Alpha4 hydrogels hinder antibody penetration. IF images of day 7 MCF10a acini immunolabelled with antibodies raised against active caspase-3 (Cas3), laminin 332 (L332), collagen IV (Col4) and E-cadherin (Ecad). Nuclei were stained with DAPI. The acini were grown in Matrigel before being transplanted into A) Matrigel, B) alginate, or C) Alpha4 hydrogels, and immunolabelled.

challenges in identifying immunolabelled acinar markers within Alpha4 hydrogels were exacerbated by the optical density of Alpha4. While it is unclear whether aldehyde-generated cross-links between matrix proteins and Alpha4's peptide network contribute, these results show that Alpha4 hydrogels

limit antibody penetration and confirm that staining organoids encapsulated within 3D Alpha4 gels is not a viable option.

Previous studies exploring cell behaviour within PeptiGels® have found it necessary to stain thin (<20 µm) gel sections to enhance antibody and stain penetration [30, 89]. However, using sections of gels would preclude the observation of 3D organisation within organoids, a significant limitation. These limitations prompted us to explore whether we could obtain clear IF images of organoids grown in Alpha4 by extracting and staining them in suspension, as extracting organoids from 3D matrices prior to preparing them for fluorescent imaging has been shown to be effective for obtaining high-resolution fluorescent images [71, 90]. Acini can be recovered from 3D Matrigel cultures by depolymerising them at 4°C using ion chelators such as EDTA or Corning® cell recovery solution [59, 71]. While Alpha4 does not depolymerise at low temperatures, its peptide matrix is stabilised by media-derived ions. This suggests that we could recover organoids from Alpha4 gels by destabilising the peptide network with an ion chelator and disrupting the gels via dilution to release the organoids. To investigate this, we grew MCF10a cells within Matrigel or Alpha4 gels and extracted the organoids after 7 days. The gels were incubated in cell recovery solution for 1 hour before being mixed with the solution and diluted in PBS. The mixtures were then centrifuged to isolate the organoids and the recovered acini were fixed, washed, blocked, and stained in suspension with antibodies against active caspase-3, laminin 332, collagen IV and E-cadherin. As these acini were suspended in 200 µL buffer, antibody and DAPI concentrations were doubled to ensure their concentrations remained optimal. Organoids recovered from Matrigel were positively labelled for all four acinar markers, showing that their extraction and transplantation did not disrupt the structural integrity of the acini (Fig. 5A). Collagen IV and laminin 332 production was clearly labelled around the acini and caspase-3 activity was restricted to the lumens. E-cadherin expression was concentrated at cell junctions, confirming that acini can be consistently immunolabelled in suspension. We also found that organoids were successfully extracted from the Alpha4 hydrogels using this method (Fig. 5B). These organoids consistently displayed clear staining for active caspase-3 and E-cadherin and multiple organoids were also labelled for laminin 332. This reveals that organoids grown in Alpha4 gels produce a basement membrane, confirming that staining Alpha4-embedded organoids yields misleading IF data.

Alpha4's optically dense peptide network obscures signs of matrix production and hinders antibody penetration, which means that removal of the hydrogel must be prioritised for IF imaging experiments. Removing the organoids from Alpha4 reduced background fluorescence and made them easier to label and identify. However, some background fluorescence remained in the Alpha4 suspensions as some gel fragments remained following centrifugation, which may obscure labelled matrix proteins and cause uncertainty. We were unsure if collagen IV was produced by Alpha4-grown organoids as the green fluorescence could be caused by bound hydrogel fragments. We found that we could not resolve this issue by increasing the centrifugal force used to separate organoids from the gel, but whether the gel fragments could be removed physically via filtration, enzymatic digestion, or charge-separation is currently unknown and warrants investigation. Nonetheless, we observed a marked improvement in the quality and consistency of IF labelling in suspension-stained organoids recovered

from Alpha4 hydrogels compared to previously investigated techniques, which demonstrates that this is the most effective method for immunolabelling organoids grown in Alpha4 hydrogels.

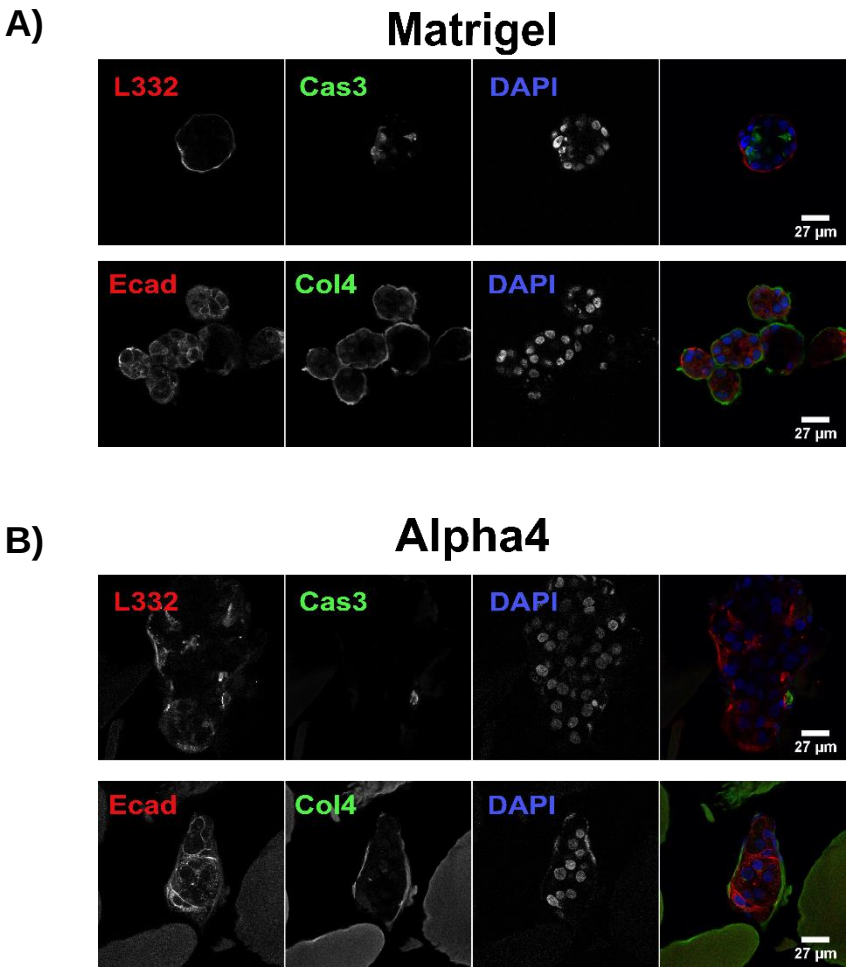

Fig. 5. Extracting organoids from Alpha4 and immunolabelling them in suspension improves labelling quality and consistency. IF images of day 7 MCF10a organoids in suspension that are immunolabelled with antibodies raised against active caspase-3 (Cas3), laminin 332 (L332), collagen IV (Col4) and E-cadherin (Ecad). Nuclei were stained with DAPI. The organoids were grown from MCF10a cells in, and extracted from, A) Matrigel, or B) Alpha4 hydrogels.

Disrupting Alpha4's peptide network facilitates the extraction of cellular proteins for western blotting

Western blot analysis permits identification and quantification of cellular proteins, but recovering the proteins for analysis from synthetic 3D environments is challenging as synthetic polymers cannot be broken down using conventional enzymes [38]. Burgess et al. found that cellular proteins could be extracted from 3D, neutrally charged PeptiGel® cultures once the peptide matrix was completely solubilised with urea buffer [41]. Urea is a chaotropic agent that weakens hydrophobic interactions between peptides by forming hydrogen bonds with water, reducing its entropy and therefore making hydrophobic interactions between peptides less energetically favourable, and by directly interacting with peptides, which destabilises proteins [27, 91-94]. As PeptiGels® are composed of peptides whose self-assembly into β-sheets is driven by hydrophobic interactions, urea can promote the

dissolution of the fibrils' hydrophobic cores, dissolving the hydrogel and making cells and their proteins readily accessible for western blot analysis.

To investigate whether we could obtain cellular proteins from 3D Alpha4 cultures using urea, we encapsulated MCF10a cells in Alpha4 hydrogels and cultured them for 7 days before adding either RIPA or urea buffer to the hydrogels, which were subsequently sonicated and centrifuged. Any supernatant was collected into separate tubes. 2D MCF10a cultures and cell-free Alpha4 hydrogels were also prepared and lysed to provide positive and negative controls, respectively. The lysates were immunoblotted with antibodies to β-actin (~42 kilodaltons (kDa)) and paxillin (~63 kDa). RIPA- and urea-treated 2D cell lysates were completely solubilised following sonication. However, RIPA-treated 3D lysates displayed prominent pellets following centrifugation, which were not disrupted through two further cycles of buffer addition, sonication, and centrifugation (Fig. 6A). In contrast, urea-treated 3D lysates were completely solubilised after two cycles (Fig. 6B). These results agreed with the findings of Burgess et al., as they found that 2-3 sonication cycles were required to completely solubilise urea-treated 3D lysates, while RIPA-treated lysates failed to completely solubilise after multiple rounds of buffer addition and sonication [41]. However, our western blot analysis showed that β-actin and paxillin were detected in RIPA- and urea-treated 2D controls, but not in the RIPA- or urea-treated 3D cell lysates (Fig. 6C). Neither β-actin or paxillin were detected in any cell-free 3D lysates. These results indicate that urea solubilised the peptide network of 3D Alpha4 gels, but our inability to detect cell proteins in the resulting lysates suggests that either urea failed to solubilise cell proteins or that the solubilised cell proteins were inaccessible to the antibodies.

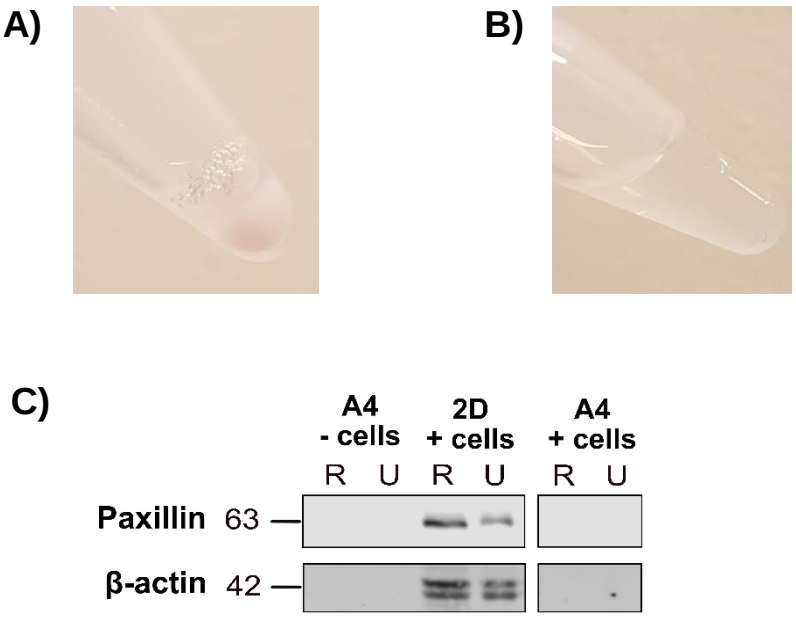

Fig. 6. Cell proteins cannot be detected in urea solubilised Alpha4 cell lysates. A) Image of a cell-laden Alpha4 hydrogel following three sonication-centrifugation cycles with 1X RIPA lysis buffer. B) Image of a cell-laden Alpha4 hydrogel following two sonication-centrifugation cycles with 8 M urea lysis buffer. C) Western blot analysis of MCF10a lysates obtained from 3D Alpha4 hydrogels and 2D cultures to detect the cellular proteins β-actin (~42 kDa) and paxillin (~63 kDa).

Alpha4's peptide concentration is greater than the peptide concentration of the PeptiGel® used by Burgess et al. in their study [41]. Therefore, it is possible that the concentration of urea we used in this study was unable to solubilise both Alpha4's peptide network and cell proteins. However, as we previously established that Alpha4's dense peptide matrix hinders antibody penetration, we hypothesised that the peptide matrix within sol Alpha4 gels makes cells less accessible to the antibodies. Since Alpha4's peptide network can be disrupted to make cells more accessible for IF antibodies, we asked whether we could disrupt Alpha4's peptide matrix via dilution to make proteins more accessible to western blot antibodies. To investigate this, we encapsulated MCF10a cells in either undiluted Alpha4 gels (100% (v/v)) or PBS-diluted (50% (v/v)) Alpha4 gels for 7 days and obtained RIPA and urea lysates from the cultures following the method described above. The lysates were then immunoblotted with antibodies to β-actin and paxillin. 2D MCF10a cultures were also prepared as a positive control. Paxillin and β-actin were detected in RIPA- and urea-treated lysates obtained from diluted Alpha4 gels and the 2D cultures (Fig. 7A). No proteins were detected in RIPA- and urea-treated undiluted Alpha4 lysates. More protein was detected in the RIPA-treated Alpha4 cell lysates than the urea-treated cell lysates which suggests that more proteins were extracted from Alpha4 with RIPA buffer. These results show that diluting Alpha4 makes cell proteins accessible for immunoblotting, which indicates that Alpha4's peptide matrix prevents cell proteins from being accessible to antibodies. Indeed, Burgess et al. found that cell proteins could be recovered from the gel pellets of RIPA-treated SAPH lysates, which indicates that the gel matrix was trapping the proteins [41]. This suggests that diluting Alpha4 fragments its peptide matrix which allows proteins to be separated from the gel with centrifugation, making them accessible to western blot antibodies.

We developed a new lysis protocol for Alpha4-encapsulated cells wherein undiluted Alpha4 hydrogels are diluted with PBS to disrupt Alpha4's peptide matrix, and asked if we could immunoblot cell proteins using this method (Fig. 7B). To investigate this, we encapsulated MCF10a cells in undiluted (100% (v/v)) and diluted (50% (v/v)) Alpha4 gels and maintained them for 7 days. 2D MCF10a cultures and cell-free hydrogels were also prepared as controls. Undiluted Alpha4 cultures were first diluted with either 50, 75 or 100 µL of PBS to investigate whether there is a minimum dilution threshold to disrupt the Alpha4 peptide network. All cultures were then lysed with RIPA buffer, sonicated, and then centrifuged to separate the proteins from the gel matrix. The lysates were immunoblotted with antibodies to β-actin and paxillin. Paxillin and β-actin were detected in all the Alpha4 cell lysates, but not the cell-free lysates (Fig. 7C). Paxillin and β-actin were also detected in the 2D lysate. We found that less paxillin and β-actin were present in cell lysates that were obtained from undiluted Alpha4 gels when compared to the 2D and diluted Alpha4 cell lysates. Additionally, less β-actin was detected in Alpha4 cell lysates that were diluted with higher volumes of PBS. These results indicate that diluting Alpha4 with PBS prior to lysis disrupts Alpha4's peptide matrix and makes cell proteins more accessible to antibodies. They also suggest that disrupting the peptide matrix with PBS decreases the protein concentration of the lysate, hence the volume of PBS used should be no more than 50 µL. Together, these results show that antibodies can access proteins from Alpha4-encapsulated cells when Alpha4's peptide matrix is disrupted and separated from the proteins and demonstrate that we can obtain cell lysates from 3D Alpha4 cultures for western blot analysis.

Protein phosphorylation is a major, reversible modification that helps cells to regulate and coordinate most cell functions such as metabolism, apoptosis, and differentiation [95]. Protein phosphorylation is a key mechanism in signalling cascades and western blot analysis can be used to identify protein phosphorylation events within cells, allowing researchers to determine which signalling proteins are involved in driving specific cell behaviours [96, 97]. However, protein phosphorylation is labile and can be reversed during cell lysis, which can make phosphorylation events difficult to detect during western blot analysis [98]. We asked whether we could use our lysis protocol to investigate phospho-signalling events within Alpha4-encapsulated cells. Briefly, diluted (75% and 50% (v/v) Alpha4) and undiluted (100% (v/v)) Alpha4 hydrogels were prepared with or without cells and maintained for 7 days before being lysed with RIPA buffer and prepared for immunoblotting as previously described. 100% (v/v) Alpha4 cultures were mixed with 50 µL of PBS prior to addition of lysis buffer. The lysates were immunoblotted with an antibody to phospho-paxillin Y31 (phosphorylated at tyrosine 31, ~68 kDa). Paxillin Y31 was detected in all the cell lysates (Fig. 7D). However, less paxillin Y31 was detected in the 75% (v/v) and 100% (v/v) cell lysates, indicating that less paxillin Y31 was present in these lysates. Additional, lower molecular-weight bands within the lysates also indicate protease or phosphatase activity, which could be minimised by incubating the cells with phosphatase inhibitors before lysis or by increasing their concentration [99].

We also examined phosphorylation of p130CAS. Phospho-p130CAS Y410 (phosphorylated at tyrosine 410, ~130 kDa) was detected in all the Alpha4 cell lysates (Fig. 7E). The presence of multiple, higher molecular-weight bands within the lysates suggests multiple phosphorylation events, which is consistent with the finding that p130CAS has multiple phosphorylation sites [100]. Again, less p130CAS Y410 was detected in the 75% (v/v) and 100% (v/v) cell lysates, which indicates that less p130CAS Y410 was present in these lysates. Whether the comparatively low detection of paxillin Y31 and p130CAS Y410 in 75% (v/v) and 100% (v/v) Alpha4 cell lysates is because cells were less accessible to the antibodies, or because cell density was lower in these gels, is unclear. Since phosphorylation sites on p130CAS are exposed in response to increased matrix stiffness, it is unlikely that the difference in phospho-protein expression observed between the 100%, 75% and 50% (v/v) Alpha4 cell lysates is due to altered matrix stiffness [101, 102]. Nonetheless, these results show that phospho-proteins can be extracted from 3D Alpha4 cultures for western blot analysis by diluting the gels with PBS to disrupt Alpha4's peptide matrix.

Alpha4's peptide network makes cell proteins inaccessible to antibodies during western blot analysis, which means that they must be extracted from the matrix. Disrupting Alpha4's peptide network by diluting it with PBS allowed us to separate the proteins from the gel during centrifugation and subsequently detect cell proteins in western blot analyses. However, less protein was consistently detected in lysates obtained from Alpha4 hydrogels that were diluted with lower volumes of PBS. We were unsure if this was because the proteins were less accessible to antibodies or because the cells behaved differently within the gels. Whether we could detect more proteins within lysates obtained from less-diluted Alpha4 cultures by increasing matrix disruption using larger volumes of PBS and concentrating the lysates or using higher SDS concentrations in the RIPA buffer merits investigation

[41, 103]. Ensuring that the protein concentrations of different lysates are the same could also help us determine whether differences in protein intensity are due to changes in cell behaviour [37].

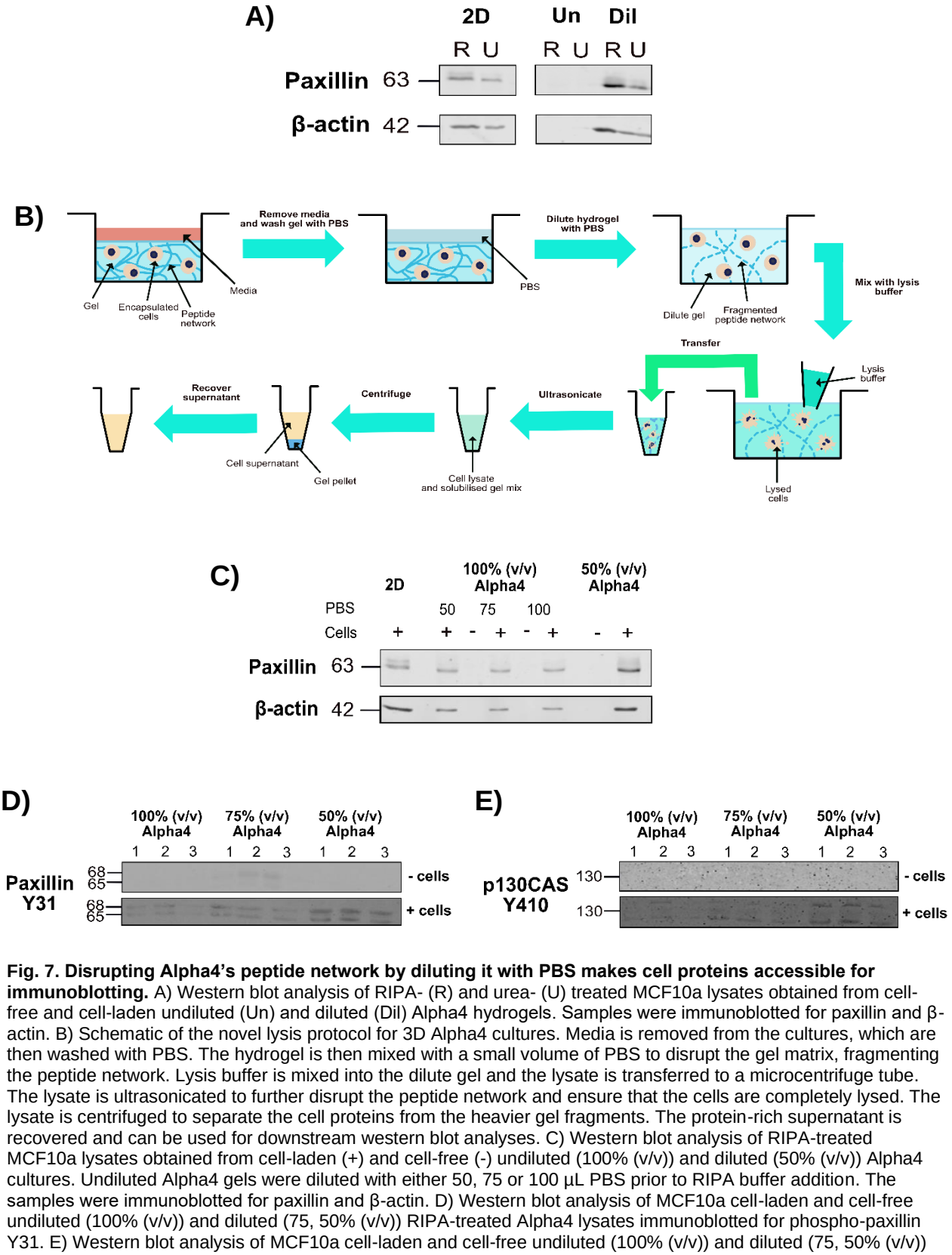

Fig. 7. Disrupting Alpha4's peptide network by diluting it with PBS makes cell proteins accessible for immunoblotting. A) Western blot analysis of RIPA- (R) and urea- (U) treated MCF10a lysates obtained from cell-free and cell-laden undiluted (Un) and diluted (Dil) Alpha4 hydrogels. Samples were immunoblotted for paxillin and β-actin. B) Schematic of the novel lysis protocol for 3D Alpha4 cultures. Media is removed from the cultures, which are then washed with PBS. The hydrogel is then mixed with a small volume of PBS to disrupt the gel matrix, fragmenting the peptide network. Lysis buffer is mixed into the dilute gel and the lysate is transferred to a microcentrifuge tube. The lysate is ultrasonicated to further disrupt the peptide network and ensure that the cells are completely lysed. The lysate is centrifuged to separate the cell proteins from the heavier gel fragments. The protein-rich supernatant is recovered and can be used for downstream western blot analyses. C) Western blot analysis of RIPA-treated MCF10a lysates obtained from cell-laden (+) and cell-free (-) undiluted (100% (v/v)) and diluted (50% (v/v)) Alpha4 cultures. Undiluted Alpha4 gels were diluted with either 50, 75 or 100 µL PBS prior to RIPA buffer addition. The samples were immunoblotted for paxillin and β-actin. D) Western blot analysis of MCF10a cell-laden and cell-free undiluted (100% (v/v)) and diluted (75, 50% (v/v)) RIPA-treated Alpha4 lysates immunoblotted for phospho-paxillin Y31. E) Western blot analysis of MCF10a cell-laden and cell-free undiluted (100% (v/v)) and diluted (75, 50% (v/v)) RIPA-treated Alpha4 lysates immunoblotted for phospho-p130CAS Y410.

Nonetheless, we found that we could consistently identify cell proteins, including phospho-proteins, within diluted Alpha4 lysates which shows that this is an effective method for extracting cellular proteins from Alpha4 hydrogels.

Consistent force measurement data can be obtained from Alpha4 hydrogels that are prepared on mica

The mechanical properties of hydrogels and tissues influence cell motility, viability, metabolism, proliferative ability, and differentiation [104-106]. Characterising the mechanical properties that are applied to cells encapsulated within hydrogels is therefore essential to assess the suitability of a hydrogel for 3D culture. Using shear oscillatory rheology and the equation below, we found that the shear modulus of Alpha4 gels is approximately 0.4 kilopascals (kPa) (Fig. 8A):

$$G = \sqrt{G'^2 + G''^2}$$

Where *G* is the shear modulus, *G'* is the storage modulus and *G"* is the loss modulus.

However, cells sense and respond to local forces that are often orders of magnitude lower than the forces that macroscopic organisms primarily sense and interact with, which makes it important to quantify the nano- and micro-scale mechanical properties of hydrogels and tissues [56, 107]. Since cells encapsulated within Alpha4 will be subject to mechanical cues transmitted via the peptide network of the hydrogel, AFM can be used to characterise the compressive and tensile forces generated by the peptide fibrils [50, 108, 109]. However, accurate measurements are subject to variations in sample preparation. Samples must be adhered to a flat, solid substrate such as glass, mica or plastic to help them withstand lateral forces exerted by the probe [110]. Depending on the properties of the sample, different substrates may be more or less effective at securing the sample due to factors such as hydrophobicity, size and charge. Ensuring that the sample is secure is vital, as the probe must be positioned manually before indentation which requires that the sample is always kept in one fixed location on the substrate. We initially prepared our Alpha4 hydrogels for AFM by leaving 250 µL of gel to air-dry onto a polylysine-coated slide before rehydrating and probing it in deionised water, but we found that we could not obtain accurate or consistent measurements using this preparation technique (Fig. 8B). Alpha4 hydrogels prepared on polylysine were found to have an elastic modulus of 300 ± 700 kPa. Using the equation below and assuming a Poisson's ratio of 0.5, we calculated the shear modulus of Alpha4:

$$E = 2G(1 + v)$$

Where *E* is the Young's modulus, *G* is the shear modulus and *v* is the Poisson ratio of the material.

The calculated shear modulus of Alpha4 was 100 kPa, which is a significantly different shear modulus value from the one calculated from our oscillatory rheology data. A previous study established that the shear modulus of Alpha4 is approximately 0.7 kPa [30]. Alpha4 is a soft hydrogel, so its elastic modulus is expected to be closer to the elastic modulus of Matrigel or collagen I, having a Young's modulus of 0.1 and 0.3 kPa respectively [111]. The Young's modulus value of 300 kPa that we

obtained puts the nanomechanical properties of Alpha4 closer to tendons [112]. This discrepancy indicates that the elastic modulus values obtained during these tests are likely to be inaccurate. This, paired with the inconsistency of the individual values, led us to conclude that the probe was not in contact with the samples and therefore not providing us with elastic modulus measurements of Alpha4. This was confirmed when we removed the water surrounding the samples, as we found that the hydrogels had detached from the substrate and were freely floating in the water. Therefore, the measurements obtained from these tests were not representative of the elastic modulus of Alpha4 but the environment the gels were surrounded by, namely the polylysine substrate and the water.

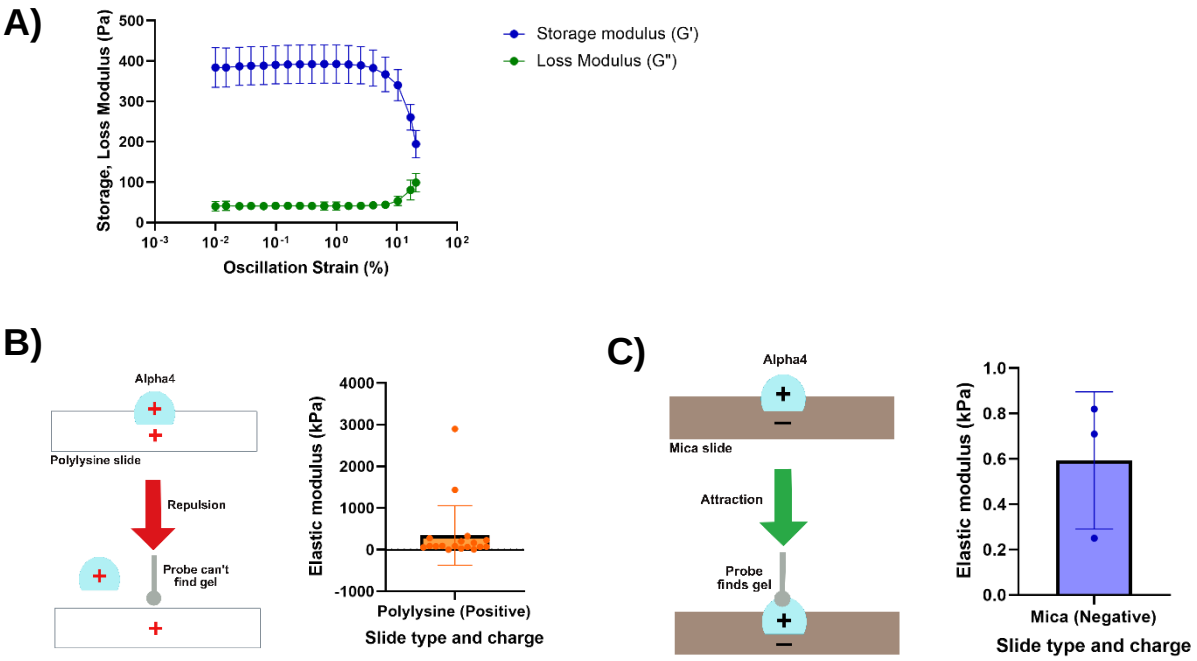

Fig. 8. Preparing Alpha4 on a negatively charged substrate improves the accuracy and consistency of elastic modulus measurements. A) Storage (G') and loss (G") moduli of Alpha4 hydrogels at 37°C. B) Young's (Elastic) moduli of Alpha4 hydrogels prepared on polylysine (positively charged substrate) at 25°C. C) Young's (Elastic) moduli of Alpha4 hydrogels prepared on mica (negatively charged substrate) at 25°C.

Since Alpha4 and polylysine are positively charged, we hypothesised that Alpha4 disengaged from the polylysine-coated slides due to charge repulsion [113]. To confirm this, we prepared Alpha4 gels on mica slides, ensuring that the top layer of the mica was removed to provide a clean, negatively charged surface for Alpha4 to adhere to via electrostatic attraction [110, 114]. We found that Alpha4 gels did not detach from the mica slides, which allowed us to obtain consistent elastic modulus measurements which put the elastic modulus of Alpha4 at approximately 0.6 ± 0.3 kPa (Fig. 8C). The calculated shear modulus of these gels was found to be 0.2 kPa, which is 2-fold softer than the shear modulus of Alpha4 gels measured using shear oscillatory rheology. This discrepancy between the data obtained from AFM and shear oscillatory rheology suggests that further adjustments to sample preparation or force measurement analysis need to be made. For example, Alpha4 hydrogels subjected to shear rheology were kept at 37°C throughout the test, whereas AFM tests were performed at room temperature. Keeping the temperature of the gels and their immediate environment constant across experiments is pertinent, as peptide hydrogels are temperature sensitive

and are often stiffer at higher temperatures [16, 115-117]. The accuracy of the values obtained from Alpha4 gels prepared on mica may also be limited by the low number of measurements, and further testing could yield more reliable data that may agree with our rheology data. Mica has been confirmed as a suitable substrate for Alpha4 indentation studies, which indicates that if further optimisation of the AFM protocol is needed, it should be focused on indentation and analysis procedures [30, 118]. While these results are preliminary, they indicate that consistent force measurement data can be obtained from Alpha4 hydrogels.

Conclusions

Here we examined the compatibility of several established experimental techniques with 3D Alpha4 cultures: IF staining, western blot analysis and AFM analysis. We found that these techniques needed to be adapted to obtain reliable data from SAPHs. It was not feasible to stain organoids with fluorescent antibodies while they remained embedded in the hydrogel as it obstructed several of the antibodies from reaching their target proteins. Furthermore, the SAPH's optically dense peptide matrix made it impossible to obtain clear images of the embedded organoids. We found that staining the organoids in suspension after removing them from the SAPH yielded clear and consistently labelled images. Our western blot data showed that a similar approach was required to isolate proteins from SAPH-encapsulated cells. Diluting the gels with PBS before lysing the cells ensured that the SAPH's peptide matrix was disrupted, making the cell proteins more accessible to antibodies. Our attempts to perform AFM analysis also revealed that the net charge of SAPHs can affect their ability to adhere to charged substrates. We could only collect accurate and consistent data once the positively charged gels were prepared on negatively charged mica as electrostatic attraction kept the gel adhered to the mica. The findings we have presented here show that by understanding the unique physical properties of SAPHs, we can optimise and use established analytical methods to characterise them and investigate their capabilities as 3D cell scaffolds.

Acknowledgements

This project was funded by the University of Manchester, the UK Regenerative Medicine Platform (UKRMP; MR/R015651/1) and Manchester BioGEL.

Fluorescent cell lines were generated by Alis Hales and Isobel Taylor-Hearn, who were supported by a Manchester Cancer Research Centre studentship and a Wellcome Trust Quantitative and Biophysical Biology studentship, respectively. Amplitude sweep experiments were performed with the help of Siyuan Dong, who was supported by the University of Manchester.

Imaging and atomic force microscopy were carried out at the Bioimaging Facility (supported by BBSRC, Wellcome, Walgreen Boots Alliance and the University of Manchester Strategic Fund); cell sorting was performed by the Flow Cytometry Core Facility (supported by the Medical Research Council and the University of Manchester Strategic Fund). We thank Drs. Nigel Hodson, Craig Williams, Gareth Howell, Steven Marsden, Roger Meadows and Peter March for Core Facility support.

Competing Interests

A. Saiani and A.F. Miller are co-founders, directors, and shareholders of Manchester BioGEL.

References

1. Tibbitt, M.W. and K.S. Anseth, *Hydrogels as extracellular matrix mimics for 3D cell culture.* Biotechnology and Bioengineering, 2009. **103**(4): p. 655-663.
2. Caliari, S.R. and J.A. Burdick, *A practical guide to hydrogels for cell culture.* Nature Methods, 2016. **13**: p. 405.
3. Geckil, H., et al., *Engineering hydrogels as extracellular matrix mimics.* Nanomedicine (London, England), 2010. **5**(3): p. 469-484.
4. Peppas, N.A., et al., *Hydrogels in Biology and Medicine: From Molecular Principles to Bionanotechnology.* Advanced Materials, 2006. **18**(11): p. 1345-1360.
5. Anguiano, M., et al., *The use of mixed collagen-Matrigel matrices of increasing complexity recapitulates the biphasic role of cell adhesion in cancer cell migration: ECM sensing, remodeling and forces at the leading edge of cancer invasion.* PLOS ONE, 2020. **15**(1): p. e0220019.
6. Branco da Cunha, C., et al., *Influence of the stiffness of three-dimensional alginate/collagen-I interpenetrating networks on fibroblast biology.* Biomaterials, 2014. **35**(32): p. 8927-8936.
7. Brovold, M., et al., *Naturally-Derived Biomaterials for Tissue Engineering Applications.* Advances in experimental medicine and biology, 2018. **1077**: p. 421-449.
8. Barcellos-Hoff, M.H., et al., *Functional differentiation and alveolar morphogenesis of primary mammary cultures on reconstituted basement membrane.* Development, 1989. **105**(2): p. 223.
9. Jun, D.-Y., et al., *Tubular organotypic culture model of human kidney.* PloS one, 2018. **13**(10): p. e0206447-e0206447.
10. Ahmed, E.M., *Hydrogel: Preparation, characterization, and applications: A review.* Journal of Advanced Research, 2015. **6**(2): p. 105-121.
11. Talbot, N.C. and T.J. Caperna, *Proteome array identification of bioactive soluble proteins/peptides in Matrigel: relevance to stem cell responses.* Cytotechnology, 2015. **67**(5): p. 873-883.
12. Antoine, E.E., P.P. Vlachos, and M.N. Rylander, *Review of collagen I hydrogels for bioengineered tissue microenvironments: characterization of mechanics, structure, and transport.* Tissue engineering. Part B, Reviews, 2014. **20**(6): p. 683-696.
13. Aisenbrey, E.A. and W.L. Murphy, *Synthetic alternatives to Matrigel.* Nature Reviews Materials, 2020. **5**(7): p. 539-551.
14. Ashworth, J.C., et al., *Peptide gels of fully-defined composition and mechanics for probing cell-cell and cell-matrix interactions in vitro.* Matrix Biology, 2019.
15. Ashworth, J.C., et al., *Preparation of a User-Defined Peptide Gel for Controlled 3D Culture Models of Cancer and Disease.* JoVE, 2020(166): p. e61710.
16. Gao, J., et al., *Controlling Self-Assembling Peptide Hydrogel Properties through Network Topology.* Biomacromolecules, 2017. **18**(3): p. 826-834.
17. Bakota, E.L., et al., *Enzymatic Cross-Linking of a Nanofibrous Peptide Hydrogel.* Biomacromolecules, 2011. **12**(1): p. 82-87.
18. Li, L., et al., *Self-Assembly Dipeptide Hydrogel: The Structures and Properties.* Frontiers in Chemistry, 2021. **9**.
19. Lopez-Silva, T.L., et al., *Self-Assembling Multidomain Peptides: Design and Characterization of Neutral Peptide-Based Materials with pH and Ionic Strength Independent Self-Assembly.* ACS Biomaterials Science & Engineering, 2019. **5**(2): p. 977-985.
20. Carvalho, A., et al., *Magnetic Dehydrodipeptide-Based Self-Assembled Hydrogels for Theragnostic Applications.* Nanomaterials, 2019. **9**(4).
21. Haines-Butterick, L., et al., *Controlling hydrogelation kinetics by peptide design for three-dimensional encapsulation and injectable delivery of cells.* Proceedings of the National Academy of Sciences of the United States of America, 2007. **104**(19): p. 7791-7796.
22. Zhang, S., et al., *Unusually stable β-sheet formation in an ionic self-complementary oligopeptide.* Biopolymers, 1994. **34**(5): p. 663-672.
23. Collier, J.H., et al., *Thermally and Photochemically Triggered Self-Assembly of Peptide Hydrogels.* Journal of the American Chemical Society, 2001. **123**(38): p. 9463-9464.
24. Hartgerink, J.D., E. Beniash, and S.I. Stupp, *Self-Assembly and Mineralization of Peptide-Amphiphile Nanofibers.* Science, 2001. **294**(5547): p. 1684-1688.
25. Lachowski, D., et al., *Self-Assembling Polypeptide Hydrogels as a Platform to Recapitulate the Tumor Microenvironment.* Cancers, 2021. **13**(13).
26. Arosio, P., et al., *End-to-End Self-Assembly of RADA 16-I Nanofibrils in Aqueous Solutions.* Biophysical Journal, 2012. **102**(7): p. 1617-1626.

27. Caplan, M.R., et al., *Self-Assembly of a β-Sheet Protein Governed by Relief of Electrostatic Repulsion Relative to van der Waals Attraction.* Biomacromolecules, 2000. **1**(4): p. 627-631.
28. Wychowaniec, J.K., et al., *Role of Sheet-Edge Interactions in β-sheet Self-Assembling Peptide Hydrogels.* Biomacromolecules, 2020. **21**(6): p. 2285-2297.
29. Ligorio, C., et al., *TGF-β3-loaded graphene oxide - self-assembling peptide hybrid hydrogels as functional 3D scaffolds for the regeneration of the nucleus pulposus.* Acta Biomaterialia, 2021. **127**: p. 116-130.
30. Imere, A., et al., *Engineering a cell-hydrogel-fibre composite to mimic the structure and function of the tendon synovial sheath.* Acta Biomaterialia, 2021. **119**: p. 140-154.
31. Mujeeb, A., et al., *Self-assembled octapeptide scaffolds for in vitro chondrocyte culture.* Acta Biomaterialia, 2013. **9**(1): p. 4609-4617.
32. Miroshnikova, Y.A., et al., *Engineering strategies to recapitulate epithelial morphogenesis within synthetic three-dimensional extracellular matrix with tunable mechanical properties.* Physical biology, 2011. **8**(2): p. 026013-026013.
33. Melan, M.A., *Overview of Cell Fixation and Permeabilization*, in *Immunocytochemical Methods and Protocols*, L.C. Javois, Editor. 1995, Humana Press: Totowa, NJ. p. 55-66.
34. Alvarado-Kristensson, M., *A simple and fast method for fixation of cultured cell lines that preserves cellular structures containing gamma-tubulin.* MethodsX, 2018. **5**: p. 227-233.
35. Jamur, M.C. and C. Oliver, *Permeabilization of Cell Membranes*, in *Immunocytochemical Methods and Protocols*, C. Oliver and M.C. Jamur, Editors. 2010, Humana Press: Totowa, NJ. p. 63-66.
36. Donaldson, J.G., *Immunofluorescence Staining.* Current Protocols in Cell Biology, 2015. **69**(1): p. 4.3.1-4.3.7.
37. Mahmood, T. and P.-C. Yang, *Western blot: technique, theory, and trouble shooting.* North American journal of medical sciences, 2012. **4**(9): p. 429-434.
38. Bass, J.J., et al., *An overview of technical considerations for Western blotting applications to physiological research.* Scandinavian Journal of Medicine & Science in Sports, 2017. **27**(1): p. 4-25.
39. Glatter, T., E. Ahrné, and A. Schmidt, *Comparison of Different Sample Preparation Protocols Reveals Lysis Buffer-Specific Extraction Biases in Gram-Negative Bacteria and Human Cells.* Journal of Proteome Research, 2015. **14**(11): p. 4472-4485.
40. Shen, K., et al., *Comparison of Different Buffers for Protein Extraction from Formalin-Fixed and Paraffin-Embedded Tissue Specimens.* PLOS ONE, 2015. **10**(11): p. e0142650.
41. Burgess, K., et al., *Western blot analysis of cells encapsulated in self-assembling peptide hydrogels.* BioTechniques, 2017. **63**.
42. Chaudhuri, O., et al., *Extracellular matrix stiffness and composition jointly regulate the induction of malignant phenotypes in mammary epithelium.* Nature Materials, 2014. **13**: p. 970.
43. Paszek, M.J., et al., *Tensional homeostasis and the malignant phenotype.* Cancer Cell, 2005. **8**(3): p. 241-254.
44. Lin, S., et al., *Influence of Physical Properties of Biomaterials on Cellular Behavior.* Pharmaceutical Research, 2011. **28**(6): p. 1422-1430.
45. Alonso, J.L. and W.H. Goldmann, *Feeling the forces: atomic force microscopy in cell biology.* Life Sciences, 2003. **72**(23): p. 2553-2560.
46. Haase, K. and A.E. Pelling, *Investigating cell mechanics with atomic force microscopy.* Journal of The Royal Society Interface, 2015. **12**(104): p. 20140970.
47. Yan, C. and D.J. Pochan, *Rheological properties of peptide-based hydrogels for biomedical and other applications.* Chemical Society reviews, 2010. **39**(9): p. 3528-3540.
48. Staunton, J.R., et al., *Correlating confocal microscopy and atomic force indentation reveals metastatic cancer cells stiffen during invasion into collagen I matrices.* Scientific Reports, 2016. **6**(1): p. 19686.
49. Chyasnavichyus, M., et al., *Probing elastic properties of soft materials with AFM: Data analysis for different tip geometries.* Polymer, 2016. **102**: p. 317-325.
50. Wychowaniec, J.K., J. Moffat, and A. Saiani, *Quantitative nanomechanical properties evaluation of a family of β-sheet peptide fibres using rapid bimodal AFM.* Journal of the Mechanical Behavior of Biomedical Materials, 2021. **124**: p. 104776.
51. Lee, J.S., et al., *Multifunctional hydrogel nano-probes for atomic force microscopy.* Nature communications, 2016. **7**: p. 11566-11566.
52. Qian, L. and H. Zhao, *Nanoindentation of Soft Biological Materials.* Micromachines, 2018. **9**(12): p. 654.

53. Kurland, N.E., Z. Drira, and V.K. Yadavalli, *Measurement of nanomechanical properties of biomolecules using atomic force microscopy.* Micron, 2012. **43**(2): p. 116-128.
54. Khan, M.K., Q.Y. Wang, and M.E. Fitzpatrick, *1 - Atomic force microscopy (AFM) for materials characterization*, in *Materials Characterization Using Nondestructive Evaluation (NDE) Methods*, G. Hübschen, et al., Editors. 2016, Woodhead Publishing. p. 1-16.
55. Garcia, R., *Nanomechanical mapping of soft materials with the atomic force microscope: methods, theory and applications.* Chemical Society Reviews, 2020. **49**(16): p. 5850-5884.
56. Megone, W., N. Roohpour, and J.E. Gautrot, *Impact of surface adhesion and sample heterogeneity on the multiscale mechanical characterisation of soft biomaterials.* Scientific Reports, 2018. **8**(1): p. 6780.
57. Burdick, J.A. and G.D. Prestwich, *Hyaluronic Acid Hydrogels for Biomedical Applications.* Advanced Materials, 2011. **23**(12): p. H41-H56.
58. Huang, F., Q. Shen, and J. Zhao, *Growth and differentiation of neural stem cells in a three-dimensional collagen gel scaffold.* Neural regeneration research, 2013. **8**(4): p. 313-319.
59. Wang, M., et al., *In-Depth Comparison of Matrigel Dissolving Methods on Proteomic Profiling of Organoids.* Molecular & Cellular Proteomics, 2022. **21**(1): p. 100181.
60. Patterson, J. and J.A. Hubbell, *Enhanced proteolytic degradation of molecularly engineered PEG hydrogels in response to MMP-1 and MMP-2.* Biomaterials, 2010. **31**(30): p. 7836-7845.
61. Ehrbar, M., et al., *Biomolecular Hydrogels Formed and Degraded via Site-Specific Enzymatic Reactions.* Biomacromolecules, 2007. **8**(10): p. 3000-3007.
62. Lutolf, M.P., et al., *Synthetic matrix metalloproteinase-sensitive hydrogels for the conduction of tissue regeneration: Engineering cell-invasion characteristics.* Proceedings of the National Academy of Sciences, 2003. **100**(9): p. 5413-5418.
63. Burgess, K.A., et al., *RNA extraction from self-assembling peptide hydrogels to allow qPCR analysis of encapsulated cells.* PLOS ONE, 2018. **13**(6): p. e0197517.
64. Ligorio, C., et al., *Graphene oxide containing self-assembling peptide hybrid hydrogels as a potential 3D injectable cell delivery platform for intervertebral disc repair applications.* Acta Biomaterialia, 2019. **92**: p. 92-103.
65. Akhtar, N. and C.H. Streuli, *Rac1 links integrin-mediated adhesion to the control of lactational differentiation in mammary epithelia.* The Journal of cell biology, 2006. **173**(5): p. 781-793.
66. Lee, J.Y., et al., *YAP-independent mechanotransduction drives breast cancer progression.* Nature Communications, 2019. **10**(1): p. 1848.
67. Muthuswamy, S.K., et al., *ErbB2, but not ErbB1, reinitiates proliferation and induces luminal repopulation in epithelial acini.* Nature cell biology, 2001. **3**(9): p. 785-792.
68. Petersen, O.W., et al., *Interaction with basement membrane serves to rapidly distinguish growth and differentiation pattern of normal and malignant human breast epithelial cells.* Proceedings of the National Academy of Sciences, 1992. **89**(19): p. 9064.
69. Wang, P., et al., *Vinculins interaction with talin is essential for mammary epithelial differentiation.* Scientific Reports, 2019. **9**(1): p. 18400.
70. Bergdorf, K.N., et al., *Immunofluorescent staining of cancer spheroids and fine-needle aspiration-derived organoids.* STAR Protocols, 2021. **2**(2): p. 100578.
71. Lee, G.Y., et al., *Three-dimensional culture models of normal and malignant breast epithelial cells.* Nature methods, 2007. **4**(4): p. 359-365.
72. Debnath, J., S.K. Muthuswamy, and J.S. Brugge, *Morphogenesis and oncogenesis of MCF-10A mammary epithelial acini grown in three-dimensional basement membrane cultures.* Methods, 2003. **30**(3): p. 256-268.
73. Sodunke, T.R., et al., *Micropatterns of Matrigel for three-dimensional epithelial cultures.* Biomaterials, 2007. **28**(27): p. 4006-4016.
74. Raphael, B., et al., *3D cell bioprinting of self-assembling peptide-based hydrogels.* Materials Letters, 2017. **190**: p. 103-106.
75. Xiong, Y., et al., *A review on recent advances in amino acid and peptide-based fluorescence and its potential applications.* New Journal of Chemistry, 2021. **45**(34): p. 15180-15194.
76. Niyangoda, C., et al., *Carbonyl-based blue autofluorescence of proteins and amino acids.* PLOS ONE, 2017. **12**(5): p. e0176983.
77. Myers, J. *Overview of Heat-Induced Epitope Retrieval (HIER) Techniques and Devices*. 2011 [cited 16/05/2022]; Available from: http://www.ihcworld.com/_protocols/epitope_retrieval/overview.htm.
78. Xiao, X., et al., *Antibody incubation at 37°C improves fluorescent immunolabeling in free-floating thick tissue sections.* BioTechniques, 2017. **62**(3): p. 115-122.

79. Gleave, J.A., et al., *A Method for 3D Immunostaining and Optical Imaging of the Mouse Brain Demonstrated in Neural Progenitor Cells.* PLOS ONE, 2013. **8**(8): p. e72039.
80. Krenacs, L., et al., *Heat-induced antigen retrieval for immunohistochemical reactions in routinely processed paraffin sections.* Methods in molecular biology (Clifton, N.J.), 2010. **588**: p. 103-119.
81. Pinotsi, D., et al., *Proton Transfer and Structure-Specific Fluorescence in Hydrogen Bond-Rich Protein Structures.* Journal of the American Chemical Society, 2016. **138**(9): p. 3046-3057.
82. Sirangelo, I., et al., *Intrinsic blue-green fluorescence in amyloyd fibrils.* AIMS Biophysics, 2018. **5**(2): p. 155-165.
83. Giansante, C., et al., *White-Light-Emitting Self-Assembled NanoFibers and Their Evidence by Microspectroscopy of Individual Objects.* Journal of the American Chemical Society, 2011. **133**(2): p. 316-325.
84. Grelich-Mucha, M., et al., *Autofluorescence of Amyloids Determined by Enantiomeric Composition of Peptides.* The Journal of Physical Chemistry B, 2021. **125**(21): p. 5502-5510.
85. Johansson, P.K. and P. Koelsch, *Label-free imaging of amyloids using their intrinsic linear and nonlinear optical properties.* Biomedical Optics Express, 2017. **8**(2): p. 743-756.
86. Croce, A.C. and G. Bottiroli, *Autofluorescence spectroscopy and imaging: a tool for biomedical research and diagnosis.* European journal of histochemistry, 2014. **58**(4).
87. Siik, S., et al., *Lens autofluorescence and light scatter in relation to the lens opacities classification system, LOCS III.* Acta Ophthalmologica Scandinavica, 1999. **77**(5): p. 509-514.
88. Piatkevich, K.D. and V.V. Verkhusha, *Chapter 17 - Guide to Red Fluorescent Proteins and Biosensors for Flow Cytometry*, in *Methods in Cell Biology*, Z. Darzynkiewicz, et al., Editors. 2011, Academic Press. p. 431-461.
89. Clough, H.C., et al., *Neutrally charged self-assembling peptide hydrogel recapitulates in vitro mechanisms of breast cancer progression.* Materials Science and Engineering: C, 2021. **127**: p. 112200.
90. Dekkers, J.F., et al., *High-resolution 3D imaging of fixed and cleared organoids.* Nature Protocols, 2019. **14**(6): p. 1756-1771.
91. Zangi, R., R. Zhou, and B.J. Berne, *Urea's Action on Hydrophobic Interactions.* Journal of the American Chemical Society, 2009. **131**(4): p. 1535-1541.
92. Lim Woon, K., J. Rösgen, and S.W. Englander, *Urea, but not guanidinium, destabilizes proteins by forming hydrogen bonds to the peptide group.* Proceedings of the National Academy of Sciences, 2009. **106**(8): p. 2595-2600.
93. Mihajlovic, M., H.M. Wyss, and R.P. Sijbesma, *Effects of Surfactant and Urea on Dynamics and Viscoelastic Properties of Hydrophobically Assembled Supramolecular Hydrogel.* Macromolecules, 2018. **51**(13): p. 4813-4820.
94. Peach, M., N. Marsh, and D.J. MacPhee, *Protein Solubilization: Attend to the Choice of Lysis Buffer*, in *Protein Electrophoresis: Methods and Protocols*, B.T. Kurien and R.H. Scofield, Editors. 2012, Humana Press: Totowa, NJ. p. 37-47.
95. Ardito, F., et al., *The crucial role of protein phosphorylation in cell signaling and its use as targeted therapy (Review).* International journal of molecular medicine, 2017. **40**(2): p. 271-280.
96. Horinouchi, T., et al., *Using Phos-Tag in Western Blotting Analysis to Evaluate Protein Phosphorylation*, in *Kidney Research: Experimental Protocols*, T.D. Hewitson, E.R. Smith, and S.G. Holt, Editors. 2016, Springer New York: New York, NY. p. 267-277.
97. Woods, A., et al., *LKB1 Is the Upstream Kinase in the AMP-Activated Protein Kinase Cascade.* Current Biology, 2003. **13**(22): p. 2004-2008.
98. O'Donoghue, L. and A. Smolenski, *Analysis of protein phosphorylation using Phos-tag gels.* Journal of Proteomics, 2022. **259**: p. 104558.
99. Schroeder, M.J., et al., *Methods for the Detection of Paxillin Post-translational Modifications and Interacting Proteins by Mass Spectrometry.* Journal of Proteome Research, 2005. **4**(5): p. 1832-1841.
100. Defilippi, P., P. Di Stefano, and S. Cabodi, *p130Cas: a versatile scaffold in signaling networks.* Trends in Cell Biology, 2006. **16**(5): p. 257-263.
101. Sawada, Y., et al., *Force sensing by mechanical extension of the Src family kinase substrate p130Cas.* Cell, 2006. **127**(5): p. 1015-1026.
102. Goldmann, W.H., *Vinculin-p130Cas interaction is critical for focal adhesion dynamics and mechano-transduction.* Cell Biology International, 2014. **38**(3): p. 283-286.

103. Nielsen, M.M., et al., *Unfolding of beta-sheet proteins in SDS.* Biophysical journal, 2007. **92**(10): p. 3674-3685.
104. Ge, H., et al., *Extracellular Matrix Stiffness: New Areas Affecting Cell Metabolism.* Frontiers in Oncology, 2021. **11**.
105. Handorf, A.M., et al., *Tissue stiffness dictates development, homeostasis, and disease progression.* Organogenesis, 2015. **11**(1): p. 1-15.
106. Leight, J.L., et al., *Matrix rigidity regulates a switch between TGF-β1–induced apoptosis and epithelial–mesenchymal transition.* Molecular Biology of the Cell, 2012. **23**(5): p. 781-791.
107. Yusko, E.C. and C.L. Asbury, *Force is a signal that cells cannot ignore.* Molecular Biology of the Cell, 2014. **25**(23): p. 3717-3725.
108. Guo, S. and B.B. Akhremitchev, *Packing Density and Structural Heterogeneity of Insulin Amyloid Fibrils Measured by AFM Nanoindentation.* Biomacromolecules, 2006. **7**(5): p. 1630-1636.
109. Liao, H.-S., et al., *Self-assembly mechanisms of nanofibers from peptide amphiphiles in solution and on substrate surfaces.* Nanoscale, 2016. **8**(31): p. 14814-14820.
110. El Kirat, K., et al., *Sample preparation procedures for biological atomic force microscopy.* Journal of Microscopy, 2005. **218**(3): p. 199-207.
111. Alcaraz, J., et al., *Laminin and biomimetic extracellular elasticity enhance functional differentiation in mammary epithelia.* The EMBO journal, 2008. **27**(21): p. 2829-2838.
112. Liu, J., et al., *Hydrogels for Engineering of Perfusable Vascular Networks.* International Journal of Molecular Sciences, 2015. **16**(7).
113. Morsin, M., et al., *The role of positively charge poly-L-lysine in the formation of high yield gold nanoplates on the surface for plasmonic sensing application.* PLOS ONE, 2021. **16**(11): p. e0259730.
114. Bailey, S., *Micas*. Reviews in Mineralogy & Geochemistry. Vol. 13. 1984, Berlin, Boston: De Gruyter.
115. Jaspers, M., et al., *Ultra-responsive soft matter from strain-stiffening hydrogels.* Nature Communications, 2014. **5**(1): p. 5808.
116. Rombouts, W.H., et al., *Reversible Temperature-Switching of Hydrogel Stiffness of Coassembled, Silk-Collagen-Like Hydrogels.* Biomacromolecules, 2015. **16**(8): p. 2506-2513.
117. Sun, L. and X. Zhao, *A self-assembling peptide RADA16-I integrated with spider fibroin uncrystalline motifs.* International journal of nanomedicine, 2012. **7**: p. 571-580.
118. Norman, M.D.A., et al., *Measuring the elastic modulus of soft culture surfaces and three-dimensional hydrogels using atomic force microscopy.* Nature Protocols, 2021. **16**(5): p. 2418-2449.

Final discussion and future work

The extracellular matrix (ECM) provides cells with dynamic biophysical and biochemical cues that regulate their survival, growth, proliferation, adhesion, migration, and differentiation [1-4]. Dysregulated signalling events between cells and their ECM can trigger aberrant cell behaviours and pathological changes in matrix composition and organisation which cause disease [5-7]. Increased breast matrix stiffness has been shown to promote malignant cell behaviours and breast cancer progression, but the mechanosignalling mechanisms responsible for driving these events are poorly defined [8-10]. Established three-dimensional (3D) organoid models of breast matrix stiffness such as Matrigel-alginate and collagen I gels cannot consistently and accurately recapitulate the key biophysical and biochemical properties of human breast matrix due to their batch-to-batch variability, poor definition, xenogenicity and limited tuneability [11-13]. Despite these long-established limitations, there remains a need for a consistent, defined, biocompatible model of the breast matrix that can be mechanically modified to interrogate the stiffness-driven mechanisms that drive oncogenic behaviours in mammary epithelial cells (MEC).

In this thesis, I have shown that a synthetic, positively charged self-assembling peptide hydrogel (SAPH) consistently supports MEC viability and organisation into organoids that produce a basement membrane. I have also shown that laminin 111 can be incorporated into a negatively charged SAPH to functionalise it for MEC culture. I present novel mass spectrometry studies performed in 3D SAPH cultures, to examine how matrix stiffness and composition direct MEC behaviour. My results suggest that increased matrix stiffness upregulates the presence of reactive oxygen species (ROS) and indicate that laminin 111 drives acinar development by establishing apicobasal polarity through cell junction formation and by regulating proliferation. I obtained these data by optimising immunofluorescence (IF) staining and protein extraction protocols for 3D SAPH cultures. I found that disrupting the peptide network of SAPHs through dilution made it easier to obtain clear and consistent qualitative and quantitative data from 3D SAPH cultures. Together, these results support my hypothesis that SAPHs can be used to create reproducible, mechanically tuneable models of breast matrix stiffness and demonstrate that molecular events within SAPH-encapsuled MECs can be interrogated using techniques such as IF staining and mass spectrometry.

The physical properties of synthetic peptide hydrogels dictate how they interact with cells and substrates

Appreciating the physical properties of SAPHs is essential if we want to optimise them for cell culture applications and obtain good quality data. I found that MECs must be extracted from the positively charged SAPH Alpha4 to obtain reliable IF and western blot data as Alpha4's peptide network hinders antibody penetration. Additionally, Alpha4's peptide network is optically dense and potentially autofluoresces when exposed to fluorescent wavelengths of light, which means that organoids must be extracted from 3D Alpha4 gels to obtain high-quality IF images. Furthermore, electrostatic interactions between Alpha4's positively charged peptide network and other charged materials affect their functionality. Alpha4 must be fixed on negatively charged substrates such as mica for atomic

force microscopy (AFM) analysis, and my findings also suggest that Alpha4's positively charged peptide network stops laminin 111 from binding to negatively charged cell surface moieties, which prevents MECs from receiving laminin 111-directed cues to differentiate into acini. These findings allowed me to obtain reliable qualitative and quantitative data from 3D SAPH cultures and understand how SAPHs can be functionalised for MEC culture.

Matrix stiffness might elevate oxidative stress in mammary epithelial cells

Alpha4 consistently supported the development of MCF10a cells into organoids that produced a laminin 332-rich basement membrane. However, Alpha4 was unable to stimulate acinar formation as the organoids were unpolarised and did not undergo growth arrest or produce the basement membrane protein collagen IV. Although studies have shown that acini develop in soft scaffolds, reducing the stiffness of Alpha4 did not encourage acinar development in MCF10a cells [8, 14]. However, I did find evidence to suggest that MECs encapsulated in a stiff environment undergo oxidative stress, as stiffer Alpha4 hydrogels appeared to promote upregulation of antioxidant proteins such as superoxide dismutase, thioredoxin and peroredoxins. Increased microenvironmental stiffness has been shown to increase ROS production [15, 16]. Reactive species created by ROS can damage DNA and interfere with cell signalling events, which can promote pro-oncogenic cell behaviours [17-19]. Cells upregulate antioxidants to neutralise ROS and maintain homeostasis, but this response is also upregulated in malignant cells to help them evade ROS-mediated apoptosis [15, 20, 21]. Therefore, these findings suggest that increased matrix stiffness elevates ROS levels within MECs, which may prime the cells to become oncogenic if they accumulate enough insults such as DNA damage. This indicates that this model of matrix stiffness can be used to identify potential mechanistic pathways that drive breast cancer development *in vivo*.

Laminin 111 may stimulate and maintain acinar morphogenesis in breast tissue

Studies have indicated that matrix composition drives acinar morphogenesis [14, 22]. Indeed, I showed that laminin 111 stimulates MCF10a acinar formation, as acini could grow in the soft, negatively charged SAPH Alpha7 once it had been functionalised with laminin 111. The results of my mass spectrometry analysis indicate that laminin 111 drives acinar basement membrane formation and apicobasal polarity by upregulating production of basement membrane proteins and cell adhesion proteins, respectively. The mass spectrometry data also suggest that laminin 111 negatively regulates MEC proliferation by inhibiting entry into the S-phase of the cell cycle. These results agree with previous studies that have shown laminin 111 to be a key component of *in vivo* mammary acinar basement membranes and, subsequently, a critical regulator of acinar polarity and cell proliferation that drives the formation of hollow, polarised acini [22-29]. Interestingly, some studies have suggested that laminin 111 signalling hinders MECs from responding to increased matrix stiffness [14, 30]. Since the *in vivo* mammary acinar basement membrane shields MECs from the underlying interstitial matrix, this apparent mechanosignalling-dampening mechanism of laminin 111 may help MECs maintain their differentiated, healthy phenotypes when they are surrounded by stiff interstitial collagen [31, 32]. These findings therefore suggest that the assembly of a laminin 111-rich basement membrane around MECs drives and maintains acinar morphogenesis *in vivo*.

Evaluation of laminin 111-functionalised Alpha7 hydrogels as a model of the breast matrix

Here I functionalised Alpha7 for MEC culture using laminin 111 to create a semi-synthetic scaffold that consistently supports acinar development. Compared with established, organic models of the breast matrix such as Matrigel, laminin 111-functionalised Alpha7 hydrogels support the same key MEC behaviours while being more defined and consistent [33-36]. Alpha7-based hydrogels can also be easily modified in various ways to alter their biochemical, physical, and mechanical properties independently of one another, unlike organic hydrogels [37-41]. Additionally, the biocompatible nature of Alpha7 means that it intrinsically supports cell viability in both 2D and 3D cultures without requiring any functionalisation, in contrast to synthetic hydrogels such as polyacrylamide (PAM), which is composed of cytotoxic monomers, or polyethylene-glycol (PEG), which often needs to be modified with biological factors to support crucial cell functions such as survival, proliferation and adhesion [42, 43]. Although Alpha7 is more expensive than most hydrogels, it is provided as a ready-to-use hydrogel that is easy to handle and does not need to be formulated from scratch or polymerised under specific environmental conditions [44]. This makes Alpha7 accessible to researchers who are unfamiliar with biomaterials. Manchester BioGEL also has technical advice and protocols for several analytical techniques readily available on their site, which makes it relatively easy to troubleshoot technical and analytical issues with Alpha7 [45].

However, laminin 111-functionalised Alpha7 hydrogels suffer from some limitations. Alpha7 is an unstable hydrogel that cannot last for more than seven days following media-conditioning, which limits the applicability of Alpha7-based hydrogels as long-term scaffolds for cell culture and increases the risk of losing cells and acini during media changes and wash steps. Since acini can take over 14 days to mature, researchers may not be able to examine how environmental changes affect MEC behaviour at later stages of acinar development using this model of the breast matrix [46]. Alpha7 is also a novel biomaterial whose negatively charged peptide matrix may interact with other materials such as ions, matrix factors, antibodies, and cells in unexpected ways. Troubleshooting and optimising functionalisation and analytical techniques can be time-consuming and expensive, which may put off researchers who would prefer to use established biomaterials and protocols. Furthermore, functionalising Alpha7 with laminin 111 purified from murine Engelbreth-Holm-Swarm (EHS) sarcomas introduces a xenogenic protein into Alpha7 that prevents it from accurately modelling human breast matrix. I also found that using EHS-purified laminin 111 introduces other xenogenic and potentially tumorigenic factors into Alpha7, reducing its definition and consistency and rendering it less reliable than fully synthetic hydrogels that could be used to model the breast matrix.

Altogether, these strengths and limitations of laminin 111-functionalised Alpha7 hydrogels show that it currently has some limitations as a model of human breast matrix. However, Alpha7's synthetic and tuneable nature makes it probable that with some adjustments, a more accurate, consistent, and stable model of the human breast matrix could be created using Alpha7.

Discussion of limitations

Laminin 111-functionalised Alpha7 hydrogels are limited in their ability to model the breast matrix for long term cell culture applications. Given the amenability of SAPHs to physical and mechanical modifications, it is possible that Alpha7 can be stabilised by increasing its peptide concentration or by cross-linking the network, which would allow researchers to use this model for longer-term experiments [38, 41, 47]. For example, incorporating positively charged β-sheet forming peptides within Alpha7 could generate electrostatic cross-links between the oppositely charged fibrils and stabilise the hydrogel, as a previous study showed that two oppositely charged peptides could be layered on top of one another to create a stable and resilient peptide hydrogel [48]. This would have the benefit of avoiding the use of chemicals, ultraviolet light, or extreme temperatures to create cross-links as these processes can damage cells [49].

In this study I functionalised Alpha7 for MEC culture using EHS-purified laminin 111, which made the scaffold xenogenic and introduced other undefined factors into the scaffold that could have independently affected MEC behaviour. There are several functionalisation strategies that could be employed in future studies with Alpha7 to avoid this. Firstly, recombinant, full-length laminin 111 could be used to functionalise Alpha7 for MEC culture as it is synthetic and therefore would create a non-xenogenic, non-tumorigenic, defined and consistent model of the breast matrix [50]. Recombinant laminin 111 could also help maintain the functionality of our current model of the breast matrix as they are full length proteins and therefore can likely assemble into functional signalling networks around MECs and direct acinar formation [51, 52]. Secondly, bioactive laminin 111 peptides such IKVAV and YIGSR could be incorporated into or conjugated to Alpha7's peptide network to functionalise it for MEC culture, which would keep the gel synthetic, defined and consistent [53-56]. However, studies have shown that stimulating complicated processes such as acinar morphogenesis *in vitro* requires functionalising hydrogels with multiple peptides, as discrete laminin domains communicate with specific cell surface receptors to direct specific behaviours such as adhesion, proliferation, survival, and polarisation [57-61]. Therefore, functionalising Alpha7 using laminin 111 peptides could be time-consuming and expensive as multiple peptide formulations would need to be trialled to optimise peptide density and combinations. Another option is to co-culture luminal or non-differentiated MECs like MCF10a cells with myoepithelial cells, as studies have demonstrated that *in vivo*, myoepithelial cells localised to the basal side of mammary acini are responsible for producing laminin 111 [22, 62, 63]. Therefore, co-culturing MCF10a cells with myoepithelial cells in Alpha7 gels may stimulate acinar formation and provide a more representative model of the breast matrix that recapitulates the bi-layered organisation and functionality of *in vivo* mammary acini.

Another limitation of laminin 111-functionalised Alpha7 hydrogels, and indeed most established models of the breast matrix, is that they do not recapitulate the organisation of breast tissue as they encapsulate MECs in a relatively homogenous matrix. *In vivo*, human mammary acini are separated from the collagen-rich interstitial breast matrix by a laminin 111-rich basement membrane [63]. As non-myoepithelial MECs do not produce much laminin 111, acini grown from mono-cultures in established models of the breast matrix or functionalised Alpha7 gels likely do not form a fully

functional basement membrane that can sufficiently modulate biochemical or mechanical cues from the interstitial matrix like *in vivo* basement membranes do [22, 28-30, 64-66]. 3D bioprinting could instead be used to create reproducible, spatially defined SAPH constructs that provide MECs with a more physiologically representative environment [48, 67-69]. For example, MECs could be encapsulated in laminin 111-functionalised Alpha7 gels and then deposited into a collagen mimetic SAPH to recapitulate the organisation of the human mammary gland and provide the cells with an *in vivo*-like laminin 111-rich microenvironment that separates them from the stiffer collagen-like matrix, allowing researchers to decipher how the acinar microenvironment and its surrounding interstitial matrix regulate MEC fate *in vivo* [70].

I reduced the storage modulus of Alpha4 by diluting it with phosphate-buffered saline (PBS), creating gels with reduced bulk stiffness. However, MECs predominantly sense and respond to local nanoscale mechanical forces generated by each other and their microenvironment, which cannot be characterised with bulk measurements [65, 71, 72]. Furthermore, my approach to mechanically modifying Alpha4 may have also altered Alpha4's matrix density, which has been shown to independently affect cell morphology, proliferation and matrix production and organisation [73-77]. Although previous studies have shown that introducing cross-links into or changing the concentration of a hydrogel does not always change the gel architecture, I did not investigate whether this was the case for diluted Alpha4 gels [14, 78]. Therefore, I cannot rule out the possibility that altered Alpha4 matrix density, not stiffness, could have helped drive the changes in oxidative stress and inflammatory processes that were observed between soft and medium Alpha4 hydrogels. These limitations could be easily addressed in future investigations. First, nanomechanical data that accurately and precisely describe forces that MECs sense and exert within SAPHs could be obtained using AFM or traction force microscopy [79, 80]. I have already shown that it is possible to obtain consistent elastic modulus measurements from Alpha4 hydrogels using AFM, and recent advances in stiffness mapping and data modelling for viscoelastic materials could help researchers obtain accurate force data from SAPHs in the future [81]. SAPH matrix density could be characterised using scanning electron microscopy or by tracking the diffusion of molecules through the hydrogel [14, 73].

Future directions

I have shown that a laminin 111-functionalised, Alpha7-based model of the breast matrix recapitulates the functionality of the breast microenvironment, and I have highlighted potential ways in which its stability, definition, accuracy, and consistency could be improved. Another important step forward would be to investigate whether the mechanical properties of this model could be independently modified to recapitulate different breast matrix stiffnesses, which could be accomplished by altering peptide concentration, altering the ionic strength of the gel or by cross-linking the peptide matrix [37, 82, 83]. The bulk and nanoscale mechanical properties of these mechanically modified Alpha7 hydrogels could be compared against mechanical data obtained from breast tissue explants using the same techniques to determine whether this novel, mechanically modifiable Alpha7-based model of the breast matrix can recapitulate the key mechanical properties of healthy, pre-tumorigenic and

tumorigenic breast tissue. If so, this novel model of the breast matrix could be used to investigate how ECM stiffness regulates MEC fate.

We could use this novel model to ask mechanistic questions that would help us identify pro-oncogenic mechanotransduction mechanisms in breast tissue. For example, we could investigate whether stiffening the matrix of laminin 111-functionalised Alpha7 hydrogels increases the production of reactive species, such as oxidised lipids, using commercial assay kits that quantify lipid peroxidation levels [84]. To assess whether stiffness-driven oxidative stress causes DNA damage, we could quantify and compare DNA damage in MECs grown in soft and stiff matrices by immunostaining markers of DNA damage or DNA repair complexes [17, 85-87]. We could also use this model to investigate how intracellular protein-protein interactions change when MECs are cultured on soft and stiff matrices using proximity-dependent biotin labelling (BioID) and mass spectrometry analysis [88, 89]. Such experiments could help us understand how poorly defined regulators of acinar development such as maspin and Stat6 direct MEC behaviour and investigate whether they are involved in mechanosensitive signalling events in breast tissue.

Conclusion

In this thesis, I demonstrated that qualitative and quantitative analytical techniques can be optimised to obtain accurate and consistent data from 3D SAPH-based cultures. From these data I found that SAPHs can be mechanically modified to stimulate changes in MEC behaviour and identified increased oxidative stress as a potential driver of mechanically driven oncogenesis in MECs. I also showed that a negatively charged SAPH can be functionalised for MEC culture using the breast matrix protein laminin 111 and revealed that the physical properties of SAPHs can affect the efficacy of biological factors. While my SAPH-based, *in vitro* model of the breast matrix currently has its limitations, my findings demonstrate the potential of SAPHs to create a defined, consistent, tuneable, and functional model of breast matrix stiffness that can be used to investigate normal and pro-oncogenic mechanistic pathways in breast tissue.

References

1. Baker, B.M. and C.S. Chen, *Deconstructing the third dimension: how 3D culture microenvironments alter cellular cues.* Journal of cell science, 2012. **125**(Pt 13): p. 3015-3024.
2. Frantz, C., K.M. Stewart, and V.M. Weaver, *The extracellular matrix at a glance.* Journal of Cell Science, 2010. **123**(24): p. 4195.
3. Hynes, R.O., *The Extracellular Matrix: Not Just Pretty Fibrils.* Science, 2009. **326**(5957): p. 1216.
4. Muncie, J.M. and V.M. Weaver, *Chapter One - The Physical and Biochemical Properties of the Extracellular Matrix Regulate Cell Fate*, in *Current Topics in Developmental Biology*, E.S. Litscher and P.M. Wassarman, Editors. 2018, Academic Press. p. 1-37.
5. Lu, P., et al., *Extracellular matrix degradation and remodeling in development and disease.* Cold Spring Harbor perspectives in biology, 2011. **3**(12): p. 10.1101/cshperspect.a005058 a005058.
6. Egeblad, M., M.G. Rasch, and V.M. Weaver, *Dynamic interplay between the collagen scaffold and tumor evolution.* Current Opinion in Cell Biology, 2010. **22**(5): p. 697-706.
7. Theocharis, A.D., D. Manou, and N.K. Karamanos, *The extracellular matrix as a multitasking player in disease.* The FEBS Journal, 2019. **286**(15): p. 2830-2869.
8. Paszek, M.J., et al., *Tensional homeostasis and the malignant phenotype.* Cancer Cell, 2005. **8**(3): p. 241-254.
9. Acerbi, I., et al., *Human breast cancer invasion and aggression correlates with ECM stiffening and immune cell infiltration.* Integrative biology : quantitative biosciences from nano to macro, 2015. **7**(10): p. 1120-1134.
10. Provenzano, P.P., et al., *Collagen density promotes mammary tumor initiation and progression.* BMC medicine, 2008. **6**: p. 11-11.
11. Aisenbrey, E.A. and W.L. Murphy, *Synthetic alternatives to Matrigel.* Nature Reviews Materials, 2020. **5**(7): p. 539-551.
12. Kozlowski, M.T., C.J. Crook, and H.T. Ku, *Towards organoid culture without Matrigel.* Communications Biology, 2021. **4**(1): p. 1387.
13. Caliari, S.R. and J.A. Burdick, *A practical guide to hydrogels for cell culture.* Nature Methods, 2016. **13**: p. 405.
14. Chaudhuri, O., et al., *Extracellular matrix stiffness and composition jointly regulate the induction of malignant phenotypes in mammary epithelium.* Nature Materials, 2014. **13**: p. 970.
15. Tharp, K.M., et al., *Adhesion-mediated mechanosignaling forces mitohormesis.* Cell Metabolism, 2021. **33**(7): p. 1322-1341.e13.
16. Voulgaridou, G.-P., et al., *DNA damage induced by endogenous aldehydes: Current state of knowledge.* Mutation Research/Fundamental and Molecular Mechanisms of Mutagenesis, 2011. **711**(1): p. 13-27.
17. Wood, A., et al., *Increased microenvironment stiffness leads to altered aldehyde metabolism and DNA damage in mammary epithelial cells through a RhoA-dependent mechanism.* bioRxiv, 2020: p. 2020.10.06.327726.
18. Ray, P.D., B.-W. Huang, and Y. Tsuji, *Reactive oxygen species (ROS) homeostasis and redox regulation in cellular signaling.* Cellular Signalling, 2012. **24**(5): p. 981-990.
19. Martins, S.G., et al., *Linking Oxidative Stress and DNA Damage to Changes in the Expression of Extracellular Matrix Components.* Frontiers in Genetics, 2021. **12**.
20. Kumari, S., et al., *Reactive Oxygen Species: A Key Constituent in Cancer Survival.* Biomarker Insights, 2018. **13**: p. 1177271918755391.
21. Tochhawng, L., et al., *Redox regulation of cancer cell migration and invasion.* Mitochondrion, 2013. **13**(3): p. 246-253.
22. Gudjonsson, T., et al., *Normal and tumor-derived myoepithelial cells differ in their ability to interact with luminal breast epithelial cells for polarity and basement membrane deposition.* Journal of cell science, 2002. **115**(Pt 1): p. 39-50.
23. Klinowska, T.C.M., et al., *Laminin and β1 Integrins Are Crucial for Normal Mammary Gland Development in the Mouse.* Developmental Biology, 1999. **215**(1): p. 13-32.
24. Kent, A.J., et al., *The microstructure of laminin-111 compensates for dystroglycan loss in mammary epithelial cells in downstream expression of milk proteins.* Biomaterials, 2019. **218**: p. 119337-119337.
25. Wang, P., et al., *Vinculins interaction with talin is essential for mammary epithelial differentiation.* Scientific Reports, 2019. **9**(1): p. 18400.

26. Debnath, J., et al., *The Role of Apoptosis in Creating and Maintaining Luminal Space within Normal and Oncogene-Expressing Mammary Acini.* Cell, 2002. **111**(1): p. 29-40.
27. Fiore, A.P.Z.P., et al., *Laminin-111 and the Level of Nuclear Actin Regulate Epithelial Quiescence via Exportin-6.* Cell Reports, 2017. **19**(10): p. 2102-2115.
28. Akhavan, A., et al., *Loss of cell-surface laminin anchoring promotes tumor growth and is associated with poor clinical outcomes.* Cancer research, 2012. **72**(10): p. 2578-2588.
29. Beliveau, A., et al., *Raf-induced MMP9 disrupts tissue architecture of human breast cells in three-dimensional culture and is necessary for tumor growth in vivo.* Genes & development, 2010. **24**(24): p. 2800-2811.
30. Kechagia, Z., et al., *The laminin-keratin link shields the nucleus from mechanical deformation and signalling.* bioRxiv, 2022: p. 2022.03.01.482474.
31. Bissell, M.J. and W.C. Hines, *Why don't we get more cancer? A proposed role of the microenvironment in restraining cancer progression.* Nature medicine, 2011. **17**(3): p. 320-329.
32. Carey, S., K. E. Martin, and C. Reinhart-King, *Three-dimensional collagen matrix induces a mechanosensitive invasive epithelial phenotype*. Vol. 7. 2017. 42088.
33. Hughes, C.S., L.M. Postovit, and G.A. Lajoie, *Matrigel: A complex protein mixture required for optimal growth of cell culture.* PROTEOMICS, 2010. **10**(9): p. 1886-1890.
34. Petersen, O.W., et al., *Interaction with basement membrane serves to rapidly distinguish growth and differentiation pattern of normal and malignant human breast epithelial cells.* Proceedings of the National Academy of Sciences, 1992. **89**(19): p. 9064.
35. Talbot, N.C. and T.J. Caperna, *Proteome array identification of bioactive soluble proteins/peptides in Matrigel: relevance to stem cell responses.* Cytotechnology, 2015. **67**(5): p. 873-883.
36. Soofi, S.S., et al., *The elastic modulus of Matrigel™ as determined by atomic force microscopy.* Journal of Structural Biology, 2009. **167**(3): p. 216-219.
37. Li, R., et al., *Tuning the mechanical and morphological properties of self-assembled peptide hydrogels via control over the gelation mechanism through regulation of ionic strength and the rate of pH change.* RSC Advances, 2015. **5**(1): p. 301-307.
38. Bairagi, D., et al., *Self-Assembling Peptide-Based Hydrogel: Regulation of Mechanical Stiffness and Thermal Stability and 3D Cell Culture of Fibroblasts.* ACS Applied Bio Materials, 2019. **2**(12): p. 5235-5244.
39. Engler, A., et al., *Substrate compliance versus ligand density in cell on gel responses.* Biophysical journal, 2004. **86**(1 Pt 1): p. 617-628.
40. Liu, X., et al., *In vivo studies on angiogenic activity of two designer self-assembling peptide scaffold hydrogels in the chicken embryo chorioallantoic membrane.* Nanoscale, 2012. **4**(8): p. 2720-2727.
41. Bakota, E.L., et al., *Enzymatic Cross-Linking of a Nanofibrous Peptide Hydrogel.* Biomacromolecules, 2011. **12**(1): p. 82-87.
42. Zhu, J., *Bioactive modification of poly(ethylene glycol) hydrogels for tissue engineering.* Biomaterials, 2010. **31**(17): p. 4639-4656.
43. Duval, K., et al., *Modeling Physiological Events in 2D vs. 3D Cell Culture.* Physiology, 2017. **32**(4): p. 266-277.
44. BioGEL, M. *PeptiGels for 2D and 3D Cell Culture*. 2021 [cited 06/03/2022]; Available from: https://manchesterbiogel.com/products/peptigels.
45. BioGEL, M. *Technical Resources*. 2022 [cited 17/09/2022]; Available from: https://manchesterbiogel.com/resources/.
46. Debnath, J., S.K. Muthuswamy, and J.S. Brugge, *Morphogenesis and oncogenesis of MCF-10A mammary epithelial acini grown in three-dimensional basement membrane cultures.* Methods, 2003. **30**(3): p. 256-268.
47. Zhang, J., et al., *Physically Associated Synthetic Hydrogels with Long-Term Covalent Stabilization for Cell Culture and Stem Cell Transplantation.* Advanced Materials, 2011. **23**(43): p. 5098-5103.
48. Jian, H., et al., *Dipeptide Self-Assembled Hydrogels with Tunable Mechanical Properties and Degradability for 3D Bioprinting.* ACS Applied Materials & Interfaces, 2019. **11**(50): p. 46419-46426.
49. GhavamiNejad, A., et al., *Crosslinking Strategies for 3D Bioprinting of Polymeric Hydrogels.* Small, 2020. **16**(35): p. 2002931.
50. BioLamina. *Biolaminin 111 LN (LN111)*. 2021 [cited 15/04/2022]; Available from: https://biolamina.com/products/biolaminin-111-ln/.

51. Barroso, M.M.S.A., et al., *Artificial Laminin Polymers Assembled in Acidic pH Mimic Basement Membrane Organization.* Journal of Biological Chemistry, 2008. **283**(17): p. 11714-11720.
52. BioLamina. *Instructions 001: Coating cell cultureware with Biolaminin substrates*. Resources and Instructions 2020 [cited 17/09/2022]; Available from: https://biolamina.com/news-resources/resources-instructions/?_sft_area_of_interest=laminins.
53. Nam, K., et al., *Laminin-111 Peptides Conjugated to Fibrin Hydrogels Promote Formation of Lumen Containing Parotid Gland Cell Clusters.* Biomacromolecules, 2016. **17**(6): p. 2293-2301.
54. Hayashi, H., et al., *Biological activities of laminin-111-derived peptide-chitosan matrices in a primary culture of rat cortical neurons.* Archives of Biochemistry and Biophysics, 2018. **648**: p. 53-59.
55. Nomizu, M., et al., *Identification of Cell Binding Sites in the Laminin a1 Chain Carboxyl-terminal Globular Domain by Systematic Screening of Synthetic Peptides* Journal of Biological Chemistry, 1995. **270**(35): p. 20583-20590.
56. Kuratomi, Y., et al., *Laminin γ1 chain peptide, C-16 (KAFDITYVRLKF), promotes migration, MMP-9 secretion, and pulmonary metastasis of B16–F10 mouse melanoma cells.* British Journal of Cancer, 2002. **86**(7): p. 1169-1173.
57. Speer, J.E., et al., *Development of a library of laminin-mimetic peptide hydrogels for control of nucleus pulposus cell behaviors.* Journal of Tissue Engineering, 2021. **12**: p. 20417314211021220.
58. Hoffman, M.P., et al., *Laminin-1 and Laminin-2 G-domain Synthetic Peptides Bind Syndecan-1 and Are Involved in Acinar Formation of a Human Submandibular Gland Cell Line.* Journal of Biological Chemistry, 1998. **273**: p. 28633-28641.
59. Balaoing, L.R., et al., *Laminin Peptide-Immobilized Hydrogels Modulate Valve Endothelial Cell Hemostatic Regulation.* PLOS ONE, 2015. **10**(6): p. e0130749.
60. Horejs, C.-M., et al., *Biologically-active laminin-111 fragment that modulates the epithelial-to-mesenchymal transition in embryonic stem cells.* Proceedings of the National Academy of Sciences, 2014. **111**(16): p. 5908-5913.
61. Aumailley, M., *The laminin family.* Cell adhesion & migration, 2013. **7**(1): p. 48-55.
62. Warburton, M.J., et al., *Distribution of myoepithelial cells and basement membrane proteins in the resting, pregnant, lactating, and involuting rat mammary gland.* Journal of Histochemistry & Cytochemistry, 1982. **30**(7): p. 667-676.
63. Adriance, M.C., et al., *Myoepithelial cells: good fences make good neighbors.* Breast Cancer Research, 2005. **7**(5): p. 190.
64. Ronnov-Jessen, L., O.W. Petersen, and M.J. Bissell, *Cellular changes involved in conversion of normal to malignant breast: importance of the stromal reaction.* Physiological Reviews, 1996. **76**(1): p. 69-125.
65. Gaiko-Shcherbak, A., et al., *The Acinar Cage: Basement Membranes Determine Molecule Exchange and Mechanical Stability of Human Breast Cell Acini.* PLOS ONE, 2015. **10**(12): p. e0145174.
66. Muschler, J. and C.H. Streuli, *Cell-matrix interactions in mammary gland development and breast cancer.* Cold Spring Harbor perspectives in biology, 2010. **2**(10): p. a003202-a003202.
67. Yao, B., et al., *Biochemical and structural cues of 3D-printed matrix synergistically direct MSC differentiation for functional sweat gland regeneration.* Science Advances, 2020. **6**(10): p. eaaz1094.
68. Bishop, E., et al., *3-D bioprinting technologies in tissue engineering and regenerative medicine: Current and future trends* Genes and Diseases, 2017. **4**(4): p. 185-195.
69. Langer, E.M., et al., *Modeling Tumor Phenotypes In Vitro with Three-Dimensional Bioprinting.* Cell Reports, 2019. **26**(3): p. 608-623.e6.
70. O'Leary, L.E.R., et al., *Multi-hierarchical self-assembly of a collagen mimetic peptide from triple helix to nanofibre and hydrogel.* Nature Chemistry, 2011. **3**(10): p. 821-828.
71. Butcher, D.T., T. Alliston, and V.M. Weaver, *A tense situation: forcing tumour progression.* Nature Reviews Cancer, 2009. **9**: p. 108.
72. Evans, N.D. and E. Gentleman, *The role of material structure and mechanical properties in cell–matrix interactions.* Journal of Materials Chemistry B, 2014. **2**(17): p. 2345-2356.
73. Lin, S., et al., *Influence of Physical Properties of Biomaterials on Cellular Behavior.* Pharmaceutical Research, 2011. **28**(6): p. 1422-1430.
74. Ehrbar, M., et al., *Elucidating the role of matrix stiffness in 3D cell migration and remodeling.* Biophysical journal, 2011. **100**(2): p. 284-293.

75. Bryant, S.J., et al., *Crosslinking Density Influences Chondrocyte Metabolism in Dynamically Loaded Photocrosslinked Poly(ethylene glycol) Hydrogels.* Annals of Biomedical Engineering, 2004. **32**(3): p. 407-417.
76. Villanueva, I., et al., *Cross-linking density alters early metabolic activities in chondrocytes encapsulated in poly(ethylene glycol) hydrogels and cultured in the rotating wall vessel.* Biotechnology and Bioengineering, 2009. **102**(4): p. 1242-1250.
77. Ramanujan, S., et al., *Diffusion and Convection in Collagen Gels: Implications for Transport in the Tumor Interstitium.* Biophysical Journal, 2002. **83**(3): p. 1650-1660.
78. Miroshnikova, Y.A., et al., *Engineering strategies to recapitulate epithelial morphogenesis within synthetic three-dimensional extracellular matrix with tunable mechanical properties.* Physical biology, 2011. **8**(2): p. 026013-026013.
79. Reinhart-King, C.A., M. Dembo, and D.A. Hammer, *Endothelial Cell Traction Forces on RGD-Derivatized Polyacrylamide Substrata.* Langmuir, 2003. **19**(5): p. 1573-1579.
80. Haase, K. and A.E. Pelling, *Investigating cell mechanics with atomic force microscopy.* Journal of The Royal Society Interface, 2015. **12**(104): p. 20140970.
81. Norman, M.D.A., et al., *Measuring the elastic modulus of soft culture surfaces and three-dimensional hydrogels using atomic force microscopy.* Nature Protocols, 2021. **16**(5): p. 2418-2449.
82. Jung, J.P., et al., *Modulating the mechanical properties of self-assembled peptide hydrogels via native chemical ligation.* Biomaterials, 2008. **29**(13): p. 2143-2151.
83. Li, X., et al., *Functional Hydrogels With Tunable Structures and Properties for Tissue Engineering Applications.* Frontiers in Chemistry, 2018. **6**(499).
84. Wood, A.M., *Mechanotransduction in Mammary Epithelial Cells and Breast Cancer Risk*. 2017. PhD Thesis, The University of Manchester: Manchester. p. 203.
85. Sharma, A., K. Singh, and A. Almasan, *Histone H2AX Phosphorylation: A Marker for DNA Damage*, in *DNA Repair Protocols*, L. Bjergbæk, Editor. 2012, Humana Press: Totowa, NJ. p. 613-626.
86. Lopez-Martinez, D., C.-C. Liang, and M.A. Cohn, *Cellular response to DNA interstrand crosslinks: the Fanconi anemia pathway.* Cellular and Molecular Life Sciences, 2016. **73**(16): p. 3097-3114.
87. Willers, H., et al., *Biomarkers and Mechanisms of FANCD2 Function.* Journal of Biomedicine and Biotechnology, 2008. **2008**: p. 821529.
88. Dong, J.-M., et al., *Proximity biotinylation provides insight into the molecular composition of focal adhesions at the nanometer scale.* Science Signaling, 2016. **9**(432): p. rs4-rs4.
89. Roux, K.J., et al., *A promiscuous biotin ligase fusion protein identifies proximal and interacting proteins in mammalian cells.* Journal of Cell Biology, 2012. **196**(6): p. 801-810.